Charles University

Faculty of Science

Department of Experimental Plant Biology

Mgr. Katarína Kulichová

Unravelling essential function of stored mRNAs in the male gametophyte

Doctoral thesis

Prague, 2025

SUPERVISOR

Said S. Hafidh, PhD.

CONSULTANT

prof. RNDr. David Honys, PhD.

DECLARATIONS

I declare that I wrote this thesis autonomously, using data from my own research and those I have actively participated in. This work is not submitted as candidature for any other degree. All sources of information were properly cited.

Katarína Kulichová, date, České Budějovice

On behalf of the co-authors of the papers published, I hereby confirm the agreement with the inclusion of the papers below into the dissertation thesis of Katarína Kulichová. The papers were produced as a teamwork and the particular contribution of Katarína Kulichová is specified at the beginning of relevant chapters of the thesis.

Said Hafidh, date, Prague

ACKNOWLEDGEMENT

First and foremost, I need to thank my supervisor Dr. Said Hafidh. I wouldn't be writing these words without his help, wisdom, perseverance and enthusiasm. Said has guided me through my PhD. studies and believed in me, even when I stopped believing in myself. I am grateful that I found not only a great supervisor, but also a very good friend. I am grateful to prof. David Honys for the opportunity to work in his laboratory and present my research in multiple conferences.

My big thank you goes to my family, my parents, my husband Ivan and my children Nela and Viliam. My parents must have seen my enthusiasm and love for plants and nature from my early childhood, when I filled every empty space in our flat and balcony with planted pots. I am grateful that they let me choose my path and I want to thank them for love and support. I wish that my mom Soňa could still be with us and see that I have not given up on finishing my studies and withheld the promise I gave her before she recently passed away. I want to thank my husband Ivan for his love and patience and the chance to come back to the laboratory after maternity leave. Our family is a driving force for everything I do.

I am grateful for all my classmates, colleagues and friends from all the places I studied and worked at. Your support, friendship and companionship mean a lot and have made this journey bearable and enjoyable.

I also wish to acknowledge the financial support from the grant agencies:

Czech Science Foundation (P501/11/P321, P501/11/1462, 522/09/0858, 21-15856S, 22-29717S, 17-23203S, 18-02448S, 19-01723S)

Ministry of Education, Youth and Sports of the Czech Republic (OC10054, LD11018, LTAIN19030, LTC20028, LTAUSA18115)

European Regional Development Fund project 'Centre for Experimental Plant Biology' (CZ. 02.1.01/0.0/0.0/16_019/0000738)

ABSTRACT

Pollen grains and pollen tubes are highly specialised organs with a strict developmental program. Pollen grain needs to synthesise a plethora of enzymes, structural and storage components and must be able to quickly react to its environment to sense the perfect timing and conditions for its germination. Its sole purpose is to be the fastest and deliver the sperm cells that are needed for successful fertilisation. The concept of RNA storage is not exclusive to pollen, it is often found also in seeds and mammalian oocytes, both of which have a similar fate and purpose as the pollen and pollen tube: preparation for a quick response. Previous research in the Laboratory of Pollen Biology led to the identification of specialised mRNA-storage particles, termed EPP (EDTA/puromycin-resistant particles) that were later revised as stalled monosomes fraction (Honys, Reňák et al. 2009, Hafidh et al. 2018). RNA distribution between translated and stored sub-cellular fractions was initially studied in *Nicotiana tabacum* (Hafidh et al. 2012a, 2012b) and was later extended into Arabidopsis (Klodová et al. 2023). The tobacco microarray data thus served as a starting point for of my PhD project that led to the identification of three candidate genes whose transcripts are stored even after 24hrs of *in vitro* pollen tube growth) and are featured in this thesis. They include EMB2036/ Ankyrin repeat protein AKRP, EMB1441/AtNEMF and a short suspensor protein (SUS2/ PRP8a). The embryo-related annotations of these genes were intriguing, as they hinted at a possible role of pollen-stored transcripts post fertilisation. We formulated the following question as the central objective of this thesis: Are pollen late-stored transcripts still functional in the very late stages of pollen tube growth, during the male-female crosstalk and fertilisation, or do they even promote early embryogenesis? Taken together, results from this thesis identified that late pollen stored transcripts encodes enzymes and structural proteins with function in cell-cell signalling, organelles differentiation and early embryo patterning. I have structured this thesis as introduction, five published articles of which two are first author articles, two unpublished chapters and a discussion and conclusions chapter.

Brief historical perspective of the work conducted in this thesis

I started my experiments with the selection of Arabidopsis homologs and their respective mutant T-DNA lines. We focused on the description of morphological defects both in the male and female gametophytes and unsurprisingly also found malformed and arrested embryos as

their gene annotations suggested. Viability assays, transmission analyses, crosses with cell-fate markers, cloning for expression, localisation and complementation were done at the same time for all three genes of interest, as we were unsure whether we would find a suitable candidate to answer all of our questions. However, such an amount of material has proven to be too extensive and time consuming, so we gradually decided to focus more on PRP8a and AKRP. EMB1441/AtNEMF remains as a chapter of unpublished results in this thesis. EMB2036/AKRP study has demonstrated its importance in the development of the pollen plastids, with a significant role also in the female gametophyte and the developing embryo (Kulichová et al. 2022). The most promising candidate has turned out to be SUS2/PRP8a. Initially only described as an embryo-lethal mutant with a prolonged suspensor and with unknown function (Schwartz et al. 1994), now described as an essential protein in the heart of the spliceosome (Kulichová et al. 2020). It functions at the very core of the splicing machinery, which is essential for proper assembly of every spliced mRNA, but still has specific targets and functions in the development of the gametophytic and embryonic tissues. When combined with its paralog, PRP8b, its impact on both the female and the male are even more evident, resulting in severe issues with targeting, cross-talk and fertilisation (Kulichová et al. 2020). However, none of our experiments were able to answer what is the origin of the all the observed embryonic phenotypes in our candidate genes/mutants. Whether the defects in the zygote and globular embryo are a result of a faulty mRNA inherited through the male (which should not be theoretically possible due to a membrane barrier), or a result of a faulty protein being made after the onset of the zygotic translation. Even though we have shown that pollen-derived PRP8a-GFP RNA is delivered to the zygote 1-2 days after pollination and that the *prp8a* mutation affects splicing of a subset of embryo-specific patterning genes, these results have been repeatedly rejected by reviewers as insufficient to prove the RNA inheritance hypothesis and thus remain as an unpublished chapter in this PhD. thesis.

AIMS AND HYPOTHESIS

Building on the concept of RNA storage in reproductive organs, we hypothesise that pollen and pollen tubes in flowering plants store a diverse array of mRNAs. These transcripts encode proteins with functions spanning enzymatic activity, structural integrity, molecular processing, signalling, and developmental regulation, and are maintained in a translationally repressed state. The primary aim of this thesis is to unveil the roles of selected candidate genes whose transcripts persist in pollen tubes even after 24 hours of in vitro germination. To achieve this, I employed a combination of genetic, genomic, bioinformatic, molecular, cytological, and advanced microscopic techniques to uncover their underlying mechanisms.

ABSTRAKT

Pylová zrna a pylové láčky jsou vysoce specializované orgány se striktním vývojovým programem. Pylové zrno potřebuje nasyntetizovat množství enzymů, strukturních a úložních komponentů a musí být schopné rychle reagovat na okolní prostředí, aby vycítilo ideální čas a podmínky pro vyklíčení. Jeho jediným cílem je být nejrychlejší a doručit spermatické buňky, které jsou potřeba pro úspěšné oplození. Koncept skladovaní RNA není exkluzivní pro pyl, často se nachází také v semenech a savčích oocytech. Oba mají podobný osud a účel jako pyl a pylová láčka: příprava na rachlou reakci. Předešlý výzkum v Laboratoři biologie pylu vedl k objevu a popisu specifických částic pro uložení mRNA, nazvaných EPP (EDTA/puromycin-resistentní částice), později anotovanými jako zabrzděné/uskladněné monosomy (Honys, Reňák et al. 2009, Hafidh et al. 2018). Distribuce RNA mezi translatovanými a uloženými / netranslatovanými subcelulárními frakcemi byl původně studován na tabáku (*Nicotiana tabacum*, Hafidh et al. 2012a, 2012b), později byl rozšířený také na huseníček *Arabidopsis* (Klodová et al. 2023). Microarray data z tabáku posloužily jako startovací bod pro můj PhD projekt, který vedl k identifikaci tří kandidátních genů (s prodlouženým uskladnením až 24 hodin *in vitro* růstu pylových láček). Patří mezi ně EMB2036/AKRP, EMB1441/AtNEMF a SUS2/PRP8a. Anotace těchto genů ukazující na embryonální defekty byla zajímavá z důvodu, že poukazovaly na možnou roli skladovaných transkriptů také po oplození. Hlavní otázka, kterou jsme se snažili zodpovědět byly formulována nasledovně: Jsou transktipty skladované po dlouhou dobu pořád schopny plnit své role i v pozdních stádiích růstu pylové láčky, počas komunikace samčího a samičího gametofytu, nebo také počas formování samotného embrya? Výsledky této disertace dokazují, že dlouhodobě skladované pylové transkripty mají funkce v buněčné signalizaci, diferenciaci organel a ve formování embrya. Tuto disertaci jsem strukturovala jako literární přehled, výsledky v podobě pěti publikovaných článků (z toho dvou prvoautorvých publikací) a dvou nepublikovaných kapitol, diskusi a závěr.

Stručný historický přehled práce presentované v této disertaci

Své experimenty jsem začínala výběrem homologů v Arabidopsis a jejich mutantních T-DNA linií. Následně jsme se soustředili na popis morfologických defektů v samčím i samičím gametofytu a objevili jsme i popsané deformovaná a zakrnělá embrya, jak jejich genová anotace naznačovala. Prováděny byly také testy na životaschopnost, transmisní analýzy,

křížení s vývojovými markery, klonovány byly konstrukty pro studium exprese, lokalizace a komplementace. Všechny experimenty byly prováděny zároveň pro všechyn tři vybrané geny, protože jsme si nebyli jisti zda nalezneme vhodného kandidáta na zodpovědení všech našich otázek. Nakonec se ukázalo takovéto množství materiálu a práce příliš extenzivní a časově náročné, takže jsme se nakonec rozhodli soustředit zejména na PRP8a a AKRP. EMB1441/ AtNEMF zůstává jenom jako kapitola nepublikovaných výsledků v této disertaci. Studium EMB2026/AKRP demonstrovalo důležitost vývoje plastidů v pylu, spolu s esenciální funkcí také v samičím gametofytu a ve vyvíjejícím se embryu (Kulichová et al. 2022). Nejzajímavějším kandidátem se ukázal být SUS2/PRP8A. Na počátku popisován jen jako embryo-defektní mutant s prodlouženým suspensorem a neznámou funkcí (Schwartz et al. 1994), nyní námi popsán jako esenciální protein v srdci spliceosomu (Kulichová et al. 2020). Funguje v samém centru splicingové mašinérie, která je esenciální pro správné poskládání každé zestříhané mRNA, ale stejně má specifické cíle a funkce ve vývoji gametofytu a embryonálních pletiv. Když jej skombinujeme s jeho paralogem, PRP8b, jeho impakt na samčí a samičí gametofyt jsou ještě výraznější, což je možné vidět na problémech s targetingem, cross-talkem nezi gametofyty a oplozením (Kulichová et al. 2020). Bohužel, žádný z našich experimentů nebyl schopný zodpovědět otázku jaký je původ všech pozorovaných embronálních defetů v našich kandidátních genech/mutantech. Jestli jsou defekty v zygotě a globulárním embryu výsledkem vadné mRNA zděděné z otce/saměího gametofytu (což by teoreticky nemělo být možné kvůli membráně bránící průniku), nebo jsou výsledkem vadného proteinu vyrobeného po nastartování zygotické translace. I když jsme ukázali, že RNA PRP8a-GFP, odvozená z pylu, je doručená do zygoty 1-2 dny po opylení a že prp8a mutace specificky ovlivňuje splicing vybrané části embro-specifických genů, tak tyto výsledky nebyly oponenty článků považovány za dostatečné a proto tato kapitola zůstává jako nepublikovaná část této disertace.

CÍLE A HYPOTÉZA

Na základě konceptu skladováni RNA v reproduktivních orgánech jsme postulovali hypotézu, že pyl a pylové láčky dokáží dlouhodobě skladovat různé mRNA. Tyto skladované a nepřekládané transkripty kódují proteiny s funkcemi zahrňujícími enzymatickou aktivitu, strukturální integritu, molekulární processing, signalizaci a vývojovou regulaci. Primárním cílem této práce je odhalit role vybraných kandidátních genů, kterých transkripty jsou skladovány v pylových láčkách i po 24 hodinách od vyklíčení *in vitro*. K dosažení tohoto cíle jsem použila kombinaci genetických, genomických, bioinformatických, molekulárních, cytologických a pokročilých mikroskopických technik.

ABBREVIATIONS

ALTA/AA	alternative splice acceptor
ALTD/AD	alternative splice donor
AS	alternative splicing
BCP	bicellular pollen
BPS	branch point sequence
CC	central cell
CCN	central cell nuclei
CRP	cysteine rich proteins
DAP	days after pollination
EC	egg cell
ECN	egg cell nuclei
EMB	embryo defective mutants
EPP	EDTA-puromycin resistant particles
ER	endoplasmic reticulum
ES	exon skipping
FG	female gametophyte
GC	generative cell
HAP	hours after pollination
IR	intron retention
MG	male gametophyte
MGU	male germ unit
MPG	mature pollen grain
MMC	megaspore mother cell
MS	microspore
mRNA	messenger RNA
NMD	nonsense-mediated decay
ORF	open reading frame
PB	processing bodies
PCD	programmed cell death

PMI	pollen mitosis I
PMII	pollen mitosis II
PT	pollen tube
PPT	polypyrimidine tract
RAM	root apical meristem
RBP	RNA binding proteins
RNAi	RNA interference
RNA-seq	RNA sequencing
RT-PCR	reverse transcription polymerase chain reaction
SAM	shoot apical meristem
SC	sperm cell
SCN/SN	sperm cell nucleus
SG	stress granules
SF	splicing factor
siRNA	small interfering RNA
snRNP	small ribonucleoprotein particles
TCP	tricellular pollen
TF	transcription factor
UNM	unicellular microspore
UTR	untranslated region
VC	vegetative cell
VN	vegetative nucleus
WT	wild type
ZGA	zygotic gene activation
3’ss	3’splice site
5’ss	5’ splice site

TABLE OF CONTENTS

ACKNOWLEDGEMENT 2

ABSTRACT 3

AIMS AND HYPOTHESIS 5

ABSTRAKT 6

CÍLE A HYPOTÉZA 8

ABBREVIATIONS 9

TABLE OF CONTENTS 11

1. INTRODUCTION 14

1.1. Gametophyte Life Cycle 14

1.1.1. The Female Gametophyte 14

1.1.2. The Male Gametophyte 19

1.2. Pollen Tube Guidance and Male-Female Interactions 24

1.2.1. The Female Gametophyte Attractants 24

1.2.2. Pollen Tube Guidance 25

1.2.3. Pollen Tube Reception and Sperm Cell Release 26

1.2.4. Fertilisation Recovery 29

1.2.5. Gamete Activation and Fusion 30

1.3. Embryogenesis 34

1.3.1. Developmental Stages of Embryogenesis 34

1.3.2. Embryo patterning 36

1.3.3. Zygotic Genome Activation and Inheritance of Transcripts 38

1.3.4. Embryo-defective mutants 39

1.4. RNA Biosynthesis and Regulation in the Gametophyte 42

1.4.1. Male Gametophyte Transcriptome Specifics 42

1.4.2. Post-transcriptional regulation 45

1.4.2.1. RNA Splicing 45

1.4.2.2. Splicing Factors and Mechanism 48

1.4.2.3. Splicing mutants of the gametophyte development and embryo patterning 51

1.4.2.4. Alternative Splicing in Plants 53

1.4.3. Translational regulation 55

1.4.3.1. RNA Binding Proteins (RBP) 56

1.4.3.2. mRNA Storage 57

1.4.3.3. RNA Storage in Pollen 60

2. RESULTS 63

2.1. Comprehensive analysis of tobacco pollen transcriptome unveils common pathways in polar cell expansion and underlying heterochronic shift during spermatogenesis 63

2.2. De novo post-pollen mitosis II tobacco pollen tube transcriptome 64

2.3. A Plastid-Bound Ankyrin Repeat Protein Controls Gametophyte and Early Embryo Development in Arabidopsis thaliana 65

2.4. PRP8A and PRP8B spliceosome subunits act coordinately to control pollen tube attraction in Arabidopsis thaliana 66

2.5. Unpublished chapter: Disruption of Arabidopsis Pre-mRNA Processing Factor PRP8a Affects Suspensor Cell Fate Specification and Embryogenesis 68

2.6. Unpublished chapter: EMB1441/AtNEMF has long-term stored transcripts in pollen and functions during embryogenesis 97

2.7. LARP6C orchestrates posttranscriptional reprogramming of gene expression during hydration to promote pollen tube guidance 111

3. DISCUSSION 112

3.1. AnKyrin Repeat Protein (AKRP) 113

3.2. Pre-mRNA Processing Protein 8 (PRP8) 115

3.3. RNA inheritance 119

4. CONCLUSIONS 121

5. LITERATURE 124

1. INTRODUCTION

1.1. Gametophyte Life Cycle

1.1.1. The Female Gametophyte

The flowering plants that dominate our landscapes and agriculture alternate between a diploid sporophytic stage, which is the main body of the plant, and a reduced haploid gametophytic stage, which is a reproductive part of the plant containing the male and female flower organs. The pollen grain comprises the mature male gametophyte and bears two sperm cells, known as the male gametes. The female gametophyte, also referred to as the embryo sac, is responsible for producing the female gametes and is often concealed within the maternal, sporophytic ovule (Skinner and Sundaresan 2018).

The female gametophyte (FG) generates the egg cell alongside three other cell types and separates distinct fertilisation functions both temporally and spatially. Processes regulated by the various types of FG cells comprise the generation of a molecular platform promoting cell-cell interaction, the initiation of interaction with the male fertilisation partner, establishing a recognition system to differentiate between beneficial and harmful contacts, capability to terminate systems when dispensable, integrity control mechanisms, and the development of strategies for repairing or compensating developmental errors (Hater et al. 2020).

In *Arabidopsis thaliana*, as in most angiosperms, the establishment of the egg-forming FG can be traced back to a single subepidermal cell in the apical part of the ovule primordium (Figure 1). This archesporial cell differentiates into the megaspore mother cell (MMC). The MMC undergoes meiosis, leading to the production of four haploid spores. This process is commonly known as megasporogenesis, which has been extensively reviewed (Drews and Koltunow 2011, Nakajima 2018). Among the four spores, the three apical ones degenerate while the remaining functional megaspore undergoes four incomplete mitotic divisions. The resulting syncytium comprises eight nuclei that are integrated into the seven-cell female gametophyte: three antipodal cells at the chalazal end and the egg cell, along with two synergids at the micropylar pole surrounding the central cell. The central cell bears two haploid nuclei that subsequently merge into a diploid nucleus (Hater et al. 2020). The central

cell and the egg cell both function as gametes and are fertilised by the two sperm cells transported by a single pollen tube. The antipodal cells of Arabidopsis undergo programmed cell death (PCD) during fertilisation (Kagi et al. 2010, Song et al. 2014). Synergid cells play a critical role in controlling pollen tube attraction (Higashiyama et al., 2001) and serve as the communication interface with approaching pollen tubes (Higashiyama and Yang 2017).

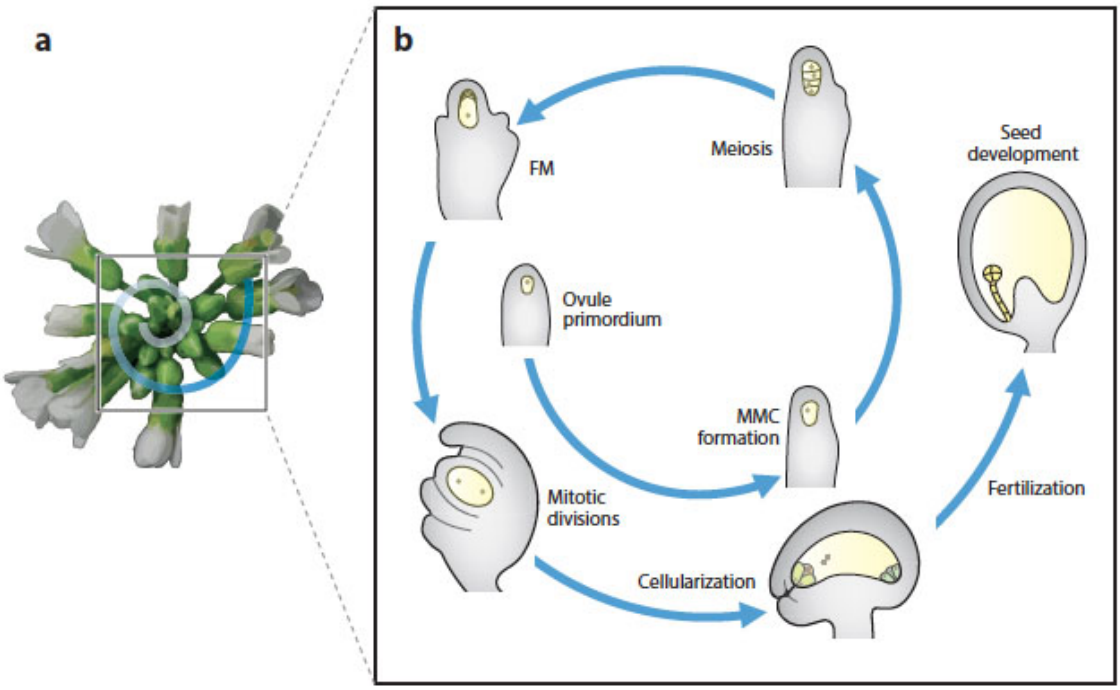

Figure 1. Development of the female germline. a) New flower buds develop in a spiral growth pattern, b) Inside the forming gynoeceum of the flower buds, ovule primordia develop. First, a diploid nucellar cell differentiates into the MMC. After meiosis, four spores are formed. The three apical spores degenerate, while the basal one differentiates into the functional megaspore. Three rounds of nuclear division give rise to an eight-nucleate syncytium, which, following cellularisation, develops into a seven-celled FG. Both the egg and the central cell of the FG are fertilised, giving rise to an embryo and endosperm, respectively. Abbreviations: FG, female gametophyte; MMC, megaspore mother cell (Hater et al. 2020).

The transition from the meiotic phase during FG formation to the mitotic development of the gametophyte is a crucial stage in plant reproduction. Moreover, the functional megaspore signifies the onset of a developmental phase wherein detrimental recessive loci are exposed due to the lack of a second functional allele. It is essential to note that the heterozygous history of a mutant embryo sac can significantly conceal gene functions. This is mainly because mutants' defects are anticipated to manifest with a delay, contingent on the quantity and turnover of functional protein conveyed from the MMC to the functional megaspore (Hater et al. 2020).

Given the polarity of the female gametophyte and the surrounding sporophytic tissue, the nuclei's positioning within the developing FG's syncytium may take a decisive role in FG patterning (Sprunck and Gross-Hardt 2011). During the two-nucleate stage in Arabidopsis, both nuclei position themselves at opposing ends of the developing syncytium, separated by a central vacuole (Christensen et al. 1997, Schneitz et al. 1995). During the second round of mitosis, the nuclei from both poles divide, resulting in two nuclei being positioned at each pole in a transverse orientation to the longitudinal axis of the FG. Afterwards, at the four-nucleate stage's end, the nuclei shift and are oriented parallel to the longitudinal axis of the FG (Christensen et al. 1997, Schneitz et al. 1995, Sprunck and Gross-Hardt 2011). The third mitotic division gives rise to four nuclei. The two nuclei positioned adjacent to the central vacuole on both poles of the FG move toward each other. This process results in the formation of the polar nuclei of the central cell, while cytokinesis leads to the emergence of synergid, egg and antipodal cells. (Christensen et al. 1997, Schneitz et al. 1995). After cellularisation, the polar nuclei fuse in Arabidopsis, whereas in grasses like maize they remain unfused (Evans and Grossniklaus 2008). The homodiploid nucleus of the central cell in Arabidopsis is located at the micropylar side of the central cell, adjacent to the egg cell (Christensen et al. 1997, Schneitz et al. 1995). To establish and maintain different cellular functions in the mature female gametophyte, it is essential to compartmentalise through cellularisation (reviewed by Hater et al. 2020).

An FG-specific factor, MYB98, has been identified among MYB transcription factors related to the feminiser MpFGMYB in *Marchantia polymorpha* (Hisanaga et al. 2019). MYB98 is expressed specifically in synergids and its loss of function has an impact on filiform apparatus

formation and the pollen tube guidance (Kasahara et al. 2005, Punwani et al. 2008). The micropylar side of the synergid cell displays a fingerlike cell wall protrusion referred to as the filiform apparatus (Huang and Russell 1992, Willemse and van Went 1984). This apparatus is deemed a likely secretion site for guidance cues that direct pollen tube attraction (Punwani et al. 2008). MYB98 acts upstream of a gene regulatory network of proteins that ultimately leads to the secretion of guidance cues into the micropylar region of the FG (Punwani et al. 2008). One of the downstream targets is *DD2/CRP810_1.2/LURE1.2*, which acts as a powerful pollen tube attractant (Takeuchi and Higashiyama 2012). Central cell development is regulated by the transcription factor AGAMOUS LIKE 80 (AGL80) and its hetero-dimeric interaction partner AGL61 (Bemer et al. 2008, Portereiko et al. 2006, Steffen et al. 2008). For the egg cell, *RWP-RK domain-containing transcription factors* (*RKD*) *1* and *RKD2* have been reported to initiate an egg cell–like transcriptome profile, even when expressed in sporophytic tissues (Koszegi et al. 2011). However, defects in *RKD1* and *RKD2* (Koszegi et al. 2011, Tedeschi et al. 2017) suggest that additional factors contribute to the specification of egg cells. A known gene downstream of *RKD1* and *RKD2* is *ARGONAUTE8* (*AGO8*) (Koszegi et al. 2011), suggesting a link to RNA interference pathways (Hernandez-Lagana et al. 2016). In *Marchantia polymorpha*, *RKD* function appears to be largely conserved. Down-regulation of *MpRKD* has been shown to cause defects in egg cell differentiation (Rövekamp et al. 2016) or egg cell arrest (Koi et al. 2016), respectively.

Several mutants have been identified which form ectopic egg cells located at the position of synergids including *eostre*, *lachesis* (*lis*), *clotho* (*clo*), and *atropos* (*ato*), as well as in the central cell (*lis* and *clo*) (Gross-Hardt et al. 2007, Moll et al. 2008, Pagnussat and Sundaresan 2007). The mutants *lis*, *ato*, and *clo* are caused by loss-of-function mutations and all encode putative core components of the splicing machinery (Gross-Hardt et al. 2007, Moll et al. 2008). The gametic competence of all FG cells aligns with the notion that egg cell identity is the default state. RNAi-based approaches by Völz et al. (2012) suggest the presence of a LIS-dependent mobile factor that originates from the egg cell and restricts gametic fate in accessory cells via lateral inhibition. Additionally, laser ablation studies have demonstrated that accessory cells acquire gametic fate when the egg cell is absent (Lawit et al. 2013, Susaki et al. 2015). Remarkably, *lis*, *clo*, and *ato* indicate a hierarchical order of the FG cells along the micropylar-chalazal axis in terms of gametic potential. Alongside morphological

characteristics such as nucleus placement and cell size, there is an observable progression from the synergid cell to the egg cell, the central cell to the egg cell, and the antipodal cell to the central cell (Gross-Hardt et al. 2007). This gametic potential serves as a backup mechanism in the event of gametic failure which ultimately strengthens the robustness of the FG (Gross-Hardt et al. 2007, Lituiev and Grossniklaus 2014, reviewed in Hater et al. 2020).

While reproduction is inherently associated with the formation of new life, FG maturation and fertilisation is a catastrophic event to accessory cells (Heydlauff and Gross-Hardt 2014). During the final stage of FG maturation, antipodal cells begin to degenerate. Notably, in emasculated FGs, antipodals disappear three days after emasculation, a time point when fertilised ovules of the same age are in the four-to-eight-nucleate endosperm stage, indicating that antipodal PCD is fertilisation- independent (Kägi et al. 2010, Murgia et al. 1993, Song et al. 2014). In contrast to antipodal cells, synergids disintegrate sequentially in a fertilisation-dependent manner (Beale et al. 2012, Leydon et al. 2015, Maruyama et al. 2013, Maruyama et al. 2015, Sandaklie-Nikolova et al. 2007, Völz et al. 2013), with the first degeneration occurring upon contact of the first pollen tube with the receptive synergid. The exact trigger for PCD of the receptive synergid seems to vary among different species. In *Arabidopsis* and *Torrenia fournieri,* degeneration of the receptive synergid was observed only upon pollen tube arrival (Sandaklie-Nikolova et al. 2007). Interestingly, the non-receptive synergid disintegrates in a two-step process after successful double fertilisation by rapid fusion with the endosperm and degeneration of the nucleus (Beale et al. 2012, Maruyama et al. 2013, Maruyama et al. 2015). The persistent synergid nucleus has been shown to undergo molecular assimilation by the endosperm and contributes to the syncytial nuclear division regime (reviewed in Skinner and Sundaresan 2018 and Hater et al. 2020).

1.1.2. The Male Gametophyte

Formation of the male gametophyte (MG) in flowering plants takes place within specialised male reproductive organs called the stamens and consists of two distinct sequential phases, microsporogenesis and microgametogenesis (Figure 2.). During microsporogenesis, inside the anther loculi lined up with a layer of tapetal cells, diploid pollen mother cells undergo meiotic division to produce tetrads of haploid microspores. This stage is completed when distinct unicellular microspores are released from the tetrad by the activity of a mixture of enzymes secreted by the tapetum, the inner nutritive layer of the stamen (Scott et al. 2004).

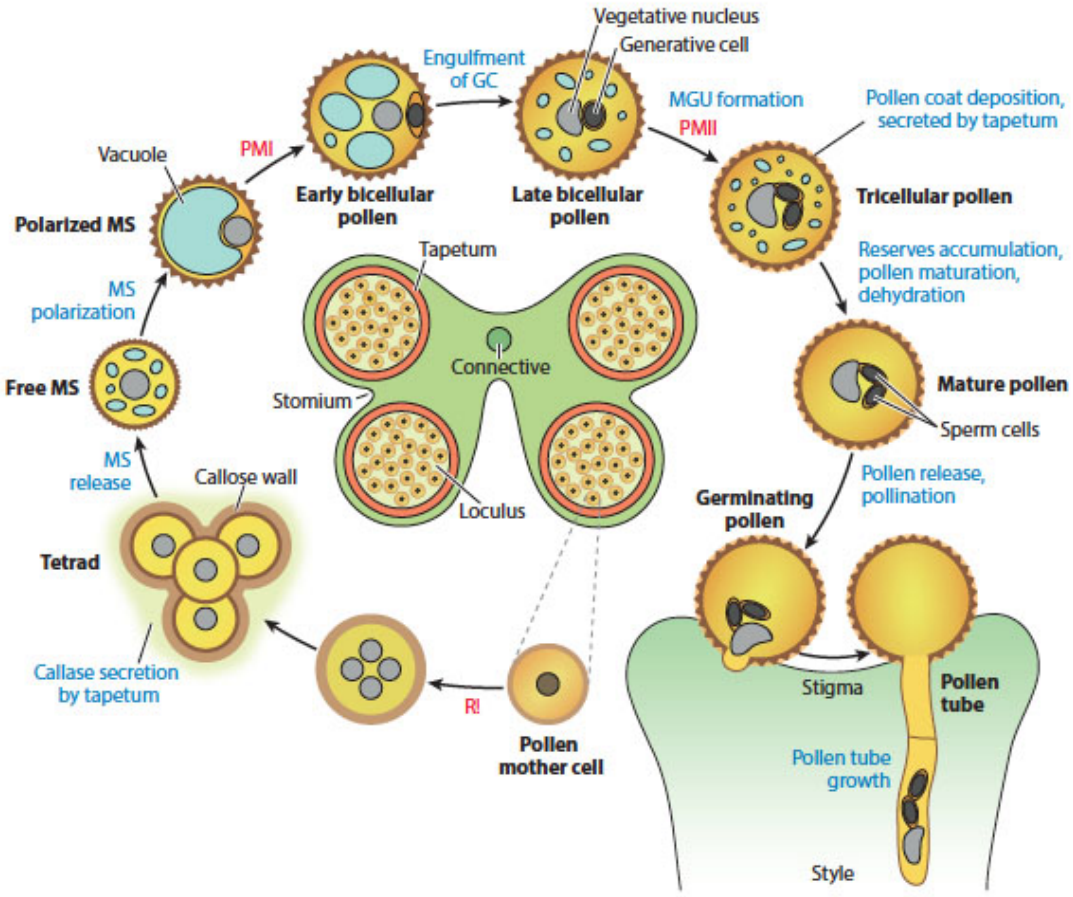

Figure 2. Pollen development and maturation within an anther. During microsporogenesis, the diploid pollen mother cell (microsporocyte) undergoes two meiotic divisions to produce a tetrad of four haploid microspores (MS). During microgametogenesis, MSs polarize and undergo highly

asymmetric division, PMI, resulting in the formation of two unequal daughter cells with distinct cell fates: a large vegetative cell (VC) and a small generative cell (GC). The GC migrates into the vegetative cell to form a unique cell-within-a-cell structure. The GC undergoes one more cell division, PMII, to produce two male gametes, the sperm cells. Abbreviations: GC, generative cell; MGU, male germ unit; MS, microspore; PMI, pollen mitosis I; PMII, pollen mitosis II; R!, meiosis (Hafidh and Honys 2021).

During microgametogenesis, the released microspores enlarge and a single large vacuole is formed (Owen and Makaroff 1995). This is accompanied by migration of the microspore nucleus to a peripheral position against the cell wall. The microspore then undergoes an asymmetric cell division known as Pollen Mitosis I (PMI). The small germ/generative cell (GC), representing the male germline, is subsequently engulfed within the cytoplasm of the larger vegetative cell (VC) to form a new cell-within-a-cell structure. This engulfment process involves degradation of the hemispherical callose wall that separates the newly formed vegetative and germ cells (reviewed in Borg et al. 2009). After PMI, the large vegetative cell has dispersed nuclear chromatin and exits the cell cycle in G1. The vegetative cell nourishes the developing germ cell and gives rise to the pollen tube after successful pollination. This pollen tube grows through the stylar tissue of the gynoeceum to deliver twin sperm cells (SC) to the embryo sac. The smaller germ cell has condensed nuclear chromatin and continues through a further round of mitosis, called Pollen Mitosis II (PMII), to produce twin sperm cells (reviewed in Borg et al. 2009 and Hafidh and Honys 2021).

The second meiotic division is followed by the synthesis of callose walls around and between the individual microspores within the tetrad. Callose, chemically β-1,3-glucan synthesized by callose synthase, is secreted by the microsporocytes and later by the microspores themselves (reviewed in Hafidh and Honys 2021). The pollen wall isolates and protects the MG and mediates its communication with the stigma surface (Scott et al. 2004). The pollen wall consists of inner intine, outer exine, and pollen coat/tryphine layers, with the latter two being predominantly of a lipidic nature (Zhang et al. 2016). The pollen wall is of mixed sporophytic and gametophytic origins since tapetum contributes to the biosynthesis of the exine and pollen coat, and the pollen grain contributes to the intine (Ariizumi and Toriyama 2011). After the

emergence of the partially formed exine, microspores are released from tetrads following callose degradation by callase (β-1,3-glucanase).

Meiosis also represents an important developmental transition from the sporophytic to gametophytic developmental program, and it is associated with global transcriptome reprogramming (Nelms and Walbot 2019) and cytoplasmic remodelling. It involves the elimination of a significant part of the ribosome complement early in the meiotic prophase and its subsequent restoration during late prophase (Dickinson and Heslop-Harrison 1977) that may represent a mechanism for the elimination of transcripts persisting from the diploid phase.

In species that shed tricellular pollen, such as *Arabidopsis thaliana*, PMII takes place inside the pollen grain before anthesis. This is in contrast to the majority of species that shed their pollen in a bicellular state, such as *Lilium longiflorum*, where PMII occurs in the growing pollen tube. Following PMII, a physical link is established between the sperm cells and the vegetative nucleus, termed as the male germ unit (MGU) (reviewed in Borg et al. 2009). It plays a vital role not only in the delivery of sperm cells to the female gametophyte, but especially in their direct communication (McCue et al. 2011). The functional phase starts by pollen activation on the stigma. Pollen grain rehydrates and germinates into a long pollen tube (PT). It grows toward the ovule, where its growth ends with double fertilisation. This phase involves the mutual activation of PT and pistil tissues, PT guidance, and the communication between the two gametophytes (reviewed in Hafidh and Honys 2021).

A recent review by Huang et al. (2021) provides evidence supporting the predominant roles of the vegetative cell for the pollen tube to be guided and to deliver the sperm cells for double fertilisation. In tobacco, ablation of the VC by cell-specific expression of DIPHTHERIA TOXIN A resulted in failure of the generative cell to migrate from the pollen grain wall into the VC cytoplasm and ultimately in loss of viability (Twell 1995). Similar approach was used to damage PMII, which resulted in the defective pollen tube containing a vegetative nucleus (VN) and a sperm-like cell. However, this pollen tube was still capable of fertilisation in Arabidopsis (Frank and Johnson 2009). The results discussed above suggested that the VC is more important for pollen tube responses to female cues. The ultimate evidence for a passive role of the VC in pollen tube delivery was provided by the loss-of-function *drop1 drop2*

mutant (Zhang et al. 2017). The absence of the basic helix-loop-helix transcription factors DROP1 and DROP2 resulted in the absence of sperm cells (SCs) in pollen, but normal guided tube growth towards the ovule. It is concluded that the SCs are a passive cargo, while the vegetative tube cell acts as a vehicle. Consistently, another study genetically blocked the initial unequal division of the microspore to produce pollen containing a single VC. Interestingly, these defective pollen tubes, like the wild type, were able to travel through female tissues and complete the entire journey in the pistil (Glöckle et al. 2018). These studies provided evidence that the VC/pollen tube represents a cell that has evolved specifically to transport SCs to the ovule for fertilisation in angiosperms. Consistently, some recent studies have revealed that signals from the pollen tube, but not from the two SCs, can induce initial endosperm enlargement (Zhong et al. 2017) and seed coat formation (Liu et al. 2019) in plant reproduction (reviewed in Huang et al. 2021).

The pollen tube (PT) phase comprises the post-pollination period, during which dehydrated pollen hydrates on the stigmatic papillae and germinates, forming a PT transporting sperm cells to an ovule. The stigmatic papillae are equipped with female-specific membrane receptors which detect ligand molecules deposited on the pollen coat to distinguish between self and non-self-pollen, initiating the reception or rejection pathway of a pollen grain. At this stage, the successful delivery of a sperm cell relies on the performance of pollen. Pollen grains are subjected to inter-pollen competition during germination, a compatibility test, transmitting tract penetration, and an inter-pollen tube race in response to signals of ovule attraction (Williams and Reese 2019). To facilitate all of these processes, pollen fitness and success in fertilising the female gametophyte are dependent on the mobilisation of resources and the ability to utilise resources deposited by the female (reviewed in Hafidh and Honys 2021). Pollen tubes face the physical hurdle of navigating through ovarian tissues in the solid-type style or the hollow-type style of the extracellular matrix. The perception of compressive forces during tip growth is critical for all plant cells (Chehab et al. 2009). Consequently, PTs growing inside the pistil must overcome the external mechanical hindrances of the transmitting tract and exert adequate penetrative force while reconfiguring their growth behaviour (Burri et al. 2018). The advancing PT apex senses physical barriers and adjusts its growth rate using mechanoresponse signalling. This phenomenon is known as durotropic growth (Reimann et al. 2020). Therefore, PTs need to overcome physical obstacles as a

further compatibility check, and the solid matrices function as a filter for nonfit PTs (reviewed in Hafidh and Honys 2021).

A compatible pollen grain hydrates and starts to germinate, allowing it to enter the papillae cell. The site of PT emergence is identified and marked by the rapid influx of Ca2+ at the active site (Iwano et al. 2004), presumably through targeted secretion involving ROP, ROP-INTERACTIVE PARTNER 1 (RIP1), and exocyst subunit SEC3A (Li et al. 2008, Li et al. 2017). To prevent the initiated PT from rupturing due to hypoosmotic shock, it is crucial to tightly regulate aquaporins and sphingolipid signalling, as well as to utilise sensors for mechanical stress (Iwano et al. 2004, Pérez di Giorgio et al. 2016).

The sperm cells' first-come-first-served strategy propels the pollen tubes towards an ovule to deliver their cargo. The speed of pollen tube extension relies on stored nutrient reserves and varies between bicellular and tricellular pollen species (Williams and Reese 2019). The tip growth of a PT is accomplished through cytoskeleton organisation, vesicular trafficking, small GTPase signalling, and ion gradient formation, all fuelling cell wall extension while maintaining communication with the surrounding female tissues (Palanivelu and Preuss 2000). The tip zone (extension zone) of the PT appears transparent due to a lack of amyloplasts and is further divided into apical and subapical zones. The apical zone is characterised by its inverted cone shape, in which secretory vesicles accumulate. The subapical region houses the endoplasmic reticulum, Golgi apparatus, and mitochondria (Lancelle and Hepler 1992). Positioned behind the subapical region are actin filaments arranged in parallel bundles, serving as highways for myosin-transported vesicles (Staiger et al., 2010). The cortical filaments transport vesicles towards the tip, while the central filaments are dedicated to basipetal vesicular transport, resulting in a reversed fountain flow (Hafidh et al. 2016). In contrast, microtubules are thought to operate in mitochondria (Romagnoli et al. 2007) and vesicular transport (Onelli et al. 2015), and could potentially function as docking sites for RNA storage particles (Honys et al. 2009), (reviewed in Hafidh and Honys 2021).

1.2. Pollen Tube Guidance and Male-Female Interactions

1.2.1. The Female Gametophyte Attractants

A recent review by Hater et al. (2020) provides an in-depth description of female gametophyte development, alongside the interactions between male and female gametophytes that lead to successful fertilisation. The precise and targeted attraction of pollen tubes towards female tissue has been the focus of numerous studies, sparking much speculation around the underlying mechanics of this growth pattern (Higashiyama et al. 1998)**.** In their paper, Higashiyama et al. employed single and combined laser cell ablations in *Torrenia fournieri* in order to investigate the crucial role of synergids in pollen tube attraction. Their results demonstrate that the loss of both synergids led to complete abolishment of pollen tube attraction, while ablation of the egg and central cells did not produce a statistically significant decrease in pollen tube-ovule interactions (Higashiyama et al. 2001). The attraction between pollen tube and ovule in *T. fournieri* relies upon the presence of small, cysteine-rich proteins (CRPs). These CRPs were named LURE proteins and are highly abundant in synergids (Okuda et al. 2009). LUREs contain a predicted cleavable signal peptide and localize to the filiform apparatus, from which they get secreted to the micropylar tissue (Okuda et al. 2009, Takeuchi and Higashiyama 2016).

Apart from the synergids, both the central cell and the egg cell have been implicated in pollen tube guidance in Arabidopsis and maize, respectively. In the Arabidopsis central cell, the CENTRAL CELL GUIDANCE (CCG) protein is expressed. *ccg* mutants fail to attract pollen tubes, a defect that can be rescued by central cell–specific restoration of CCG function (Chen et al. 2007).

EGG APPARATUS1 (*ZmEA1*) from *Zea mays* encodes a small peptide that is secreted toward the micropylar region of the ovule. RNAi-mediated knockdown unveiled a crucial function of *ZmEA1* in micropylar pollen tube guidance and fertility. Along with its prevalence in the synergids, *ZmEA1* expression has been detected in the egg cells, leading some researchers to suggest that egg cells in maize play a role in attracting the pollen tube towards the ovule (Martón et al. 2005).

1.2.2. Pollen Tube Guidance

The current understanding of pollen tube guidance indicates a clearly marked path through different maternal fields containing gradually dispersed guidance cues (Figure 3.) (Hater et al. 2020). These signals can signify entrances like the micropyle or intersections such as the septum-funiculus transition. The guidance of the pollen tube (PT) in the pre-ovular transmitting tract is not unidirectional and does not require the female gametophyte for growth towards the ovule (Mizuta and Higashiyama 2018). During this phase, PTs are believed to be guided by the physical barriers of the transmitting tissues, adhesin proteins, and chemotropic signals (Chebli and Geitmann 2007). PT progression along the style is accompanied by programmed cell death (PCD) in the transmitting tract. Researchers Zhong and Qu (2019) have reexamined previously identified Arabidopsis LUREs and found that their function begins well upstream of micropylar guidance. AtLURE1 peptides facilitate the penetration of the septum when pollen tubes transit from the transmitting tract to the funicular surface. Interestingly, AtLURE1 accelerates the pollen of its own species, giving it a competitive edge over unrelated pollen tubes. Conversely, the four CRPs XIUQIU1–4 aid in the pollen tube attraction in a species-independent manner, exemplified by their ability to lure pollen tubes from various Arabidopsis species (Zhong and Qu 2019).

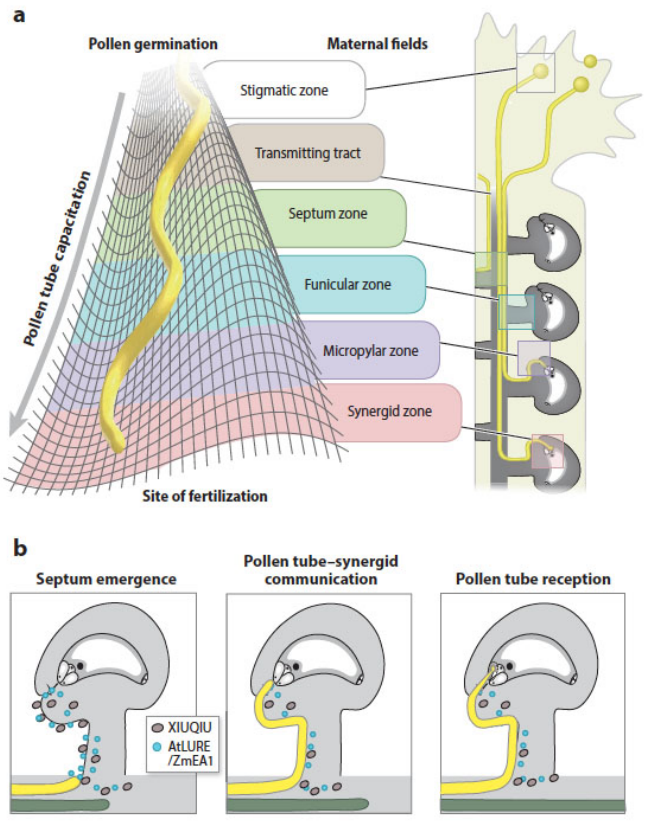

Figure 3. The pollen tube travels through distinct maternal fields. a) Maternal fields (*center*) corresponding to inlets highlighted in a gynoeceum indicate the distinct checkpoints that pollen tubes pass on their way to the female gametes. b) Transmitting tract emergence is regulated by XIUQIU, ZmEA1, and AtLURE peptides, with the latter promoting kin selection. Abbreviations: AtLURE, *Arabidopsis thaliana* LURE; ZmEA1, *Zea mays* EGG APPARATUS1 (Hater et al.2020).

Close to the ovule, ovular guidance assumes control of the reorientation of the PT from the transmitting tract towards the entry at the micropyle. The guidance process has two phases: funicular and micropylar. There are no apparent factors that exclusively impact funicular guidance; nevertheless, the mutation of two mitogen-activated protein kinases, *mpk3 mpk6*, leads to critical flaws within the funicular guidance (Guan et al. 2014). In contrast, micropylar guidance has undergone extensive analysis and several ligand-receptor mechanisms have been elaborated. At first, an R2R3-MYB TF, MYB98, specifically expressed in synergids, switches on the expression and eventual secretion of different groups of cysteine-rich proteins (Punwani et al. 2008). Of these proteins, LURE1 and LURE3, which are synergid-specific, display PT attraction activities (Okuda et al. 2009). To perceive signals of attraction by LURE1, Leucine-rich repeat receptor-like protein kinases (LRR-RLKs) are present on the plasma membrane of PT (Figure 4.). These include PRK6, MALE DISCOVERER 1 (MDIS1) and MDIS2, and MIDS-INTERACTING RLK 1 (MIK1) and MIK2, and they directly interact with LURE1 peptides (Takeuchi and Higashiyama 2016). Additionally, Arabidopsis central cell and maize egg apparatus also participate in micropylar control of PT attraction. Arabidopsis CENTRAL CELL GUIDANCE (CCG) interacts with CCG BINDING PROTEIN 1 (CBP1) and regulates the expression of synergid- and various central cell-expressed CRPs to facilitate pollen tube micropylar guidance (Chen et al. 2007, Li et al. 2015). This suggests a presence of a mobile signal coordinating central cell- and synergid-mediated PT attraction activities. On successful PT attraction and micropyle penetration, the PT reception module becomes a checkpoint for the species-specific pre-hybridisation barrier of the gametophyte (reviewed in Hafidh and Honys 2021).

1.2.3. Pollen Tube Reception and Sperm Cell Release

In their initial growth phase while approaching ovules, pollen tubes have to resist internal turgor pressure to promote cell elongation. In contrast, the final phase occurring in the ovule is marked by the rupture of the pollen tube, which enables the release of sperm cells (Johnson et al. 2019, Michard et al. 2017, Zheng et al. 2019). Pollen tube viability and elongation are mutually dependent processes, governed by a sophisticated signalling mechanism, and reliant on the monitoring and maintenance of the cell wall (Scheible and McCubbin 2019).

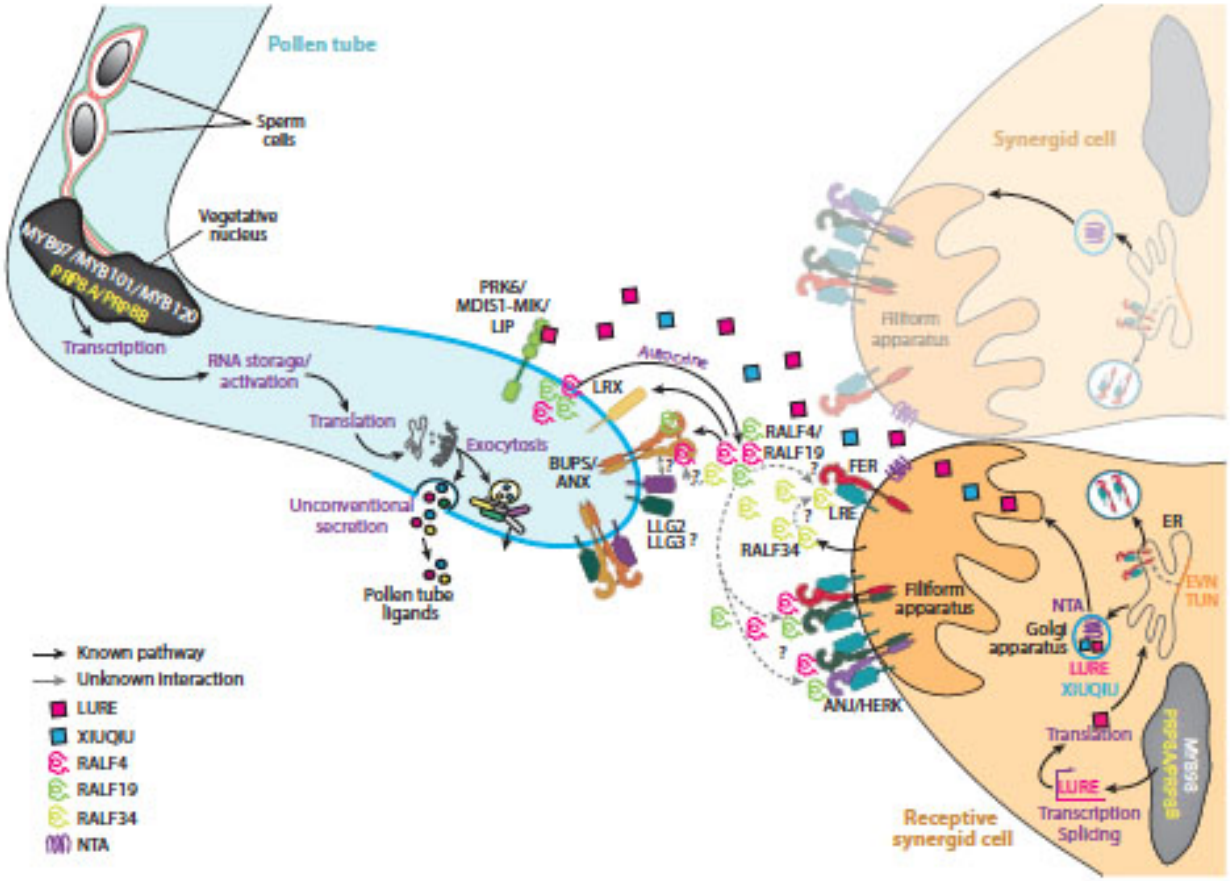

Figure 4. Pollen tube ovular guidance and attraction by the receptive synergid cell. MYB98 TF and PRP8 splicing factors promote the expression of PT-attracting CRPs. ER-localized EVN and TUN are likely involved in the *N*-glycosylation of synergid-secreted proteins. To exit the transmitting tract, species-non-specific CRPs, XIUQIUs, attract the PT to emerge from the septum into the funiculus. Once emerged, species-specific CRPs, LUREs, function as a gametophytic barrier and attract only PTs of the same species. LUREs are perceived by PT PRK6/MDIS1-MIK/LIP receptors. As the PT approaches, the FER-LRE-ANJ/HERK1 complex functions as a coreceptor to perceive a yet-unknown ligand. The putative ligands could be the synergid-secreted RALFs, RALF34 or others. LRE-FER signalling induced by a PT-derived ligand promotes the relocalisation of NTA from the synergid endomembrane into its plasma membrane. In the PT, MYB97, MYB101, MYB120, and PRP8 prime the PT reception by the synergid cell. To prevent PT premature bursting, the RALF14/RALF19/ANX/ BUPS complex, LRXs, and MSL8 impose an autocrine homeostasis control over the PT cell wall. Once correctly received by the receptive synergid cell, synergid-secreted RALF34 outcompetes RALF4/RALF19 to induce PT burst and sperm cell release inside the receptive synergid cell at the proximity of the egg cell and the central cell for gamete fusion. Thicker blue line indicates the membrane lipid bilayer at the active fusion site. Abbreviations: ANJ, ANJEA; ANX, ANXUR; BUPS,

BUDDHA'S PAPER SEAL; CRP, cysteine-rich protein; ER, endoplasmic reticulum; EVN, EVAN; FER, FERONIA; HERK, HERCULES; LIP, LOST IN POLLEN TUBE GUIDANCE; LLG, LORELEI-LIKE GPI-ANCHORED PROTEIN; LRE, LORELEI; LRX, LEUCINE-RICH REPEAT EXTENSIN; MDIS1, MALE DISCOVERER 1; MIK, MDIS1-INTERACTING RECEPTOR-LIKE KINASE; MSL8, MECHANOSENSITIVE-LIKE CHANNEL 8; NTA, NORTIA; PRK6, POLLEN RECEPTOR-LIKE KINASE 6; PT, pollen tube; RALF, RAPID ALKALINIZATION FACTOR; TF, transcription factor; TUN, TURAN (Hafidh and Honys, 2021).

The control of cell wall integrity in *Catharanthus roseus* is exercised by several receptor-like kinases (CrRLKs) which are situated at the tip of the pollen tube (Figure 4., Li et al. 2016). These kinases include ANXUR1, ANXUR2 (Boisson-Dernier et al. 2009, Miyazaki et al. 2009), BUDDHA'S PAPER SEAL1 (BUPS1) and BUPS2 (Ge et al. 2017), and ERULUS (Haruta et al. 2014, Schoenaers et al. 2018). It has recently been shown that small rapid alkalisation factors (RALFs) can act as ligands for the CrRLK receptors (Haruta et al. 2014). A family of cysteine-rich proteins (CRPs), RAPID ALKALINIZATION FACTORS (RALFs), and their receptors from the RLK1-LIKE (CrRLK1L) family play a vital role in perceiving pollen tubes (Ge et al. 2019, Li et al. 2016, Liang and Zhou 2018). FERONIA (FER)/ SIRENE, as the first female receptor from the CrRLK1L family, detects PT arrival (Escobar-Restrepo et al. 2007, Huck et al. 2003). FER localises at the filiform apparatus, and *fer* ovules exhibit PT overgrowth, suggesting that FER is critical for PT growth arrest (Rotman et al. 2003). The small GPI-anchored protein LORELEI (LRE) mediates the relocalisation of FER to the filiform apparatus (Capron et al. 2008, Li et al. 2016).

Downstream signalling involves the mildew resistance locus O protein NORTIA that is necessary for Ca^{2+} spiking (Kessler et al. 2010, Ngo et al. 2014). NORTIA function is dependent on relocalisation from Golgi- associated compartments to the synergid filiform apparatus upon pollen tube arrival (Jones et al. 2017). RALFs act as FER ligands, and the RALF-FER complex has been inferred to be involved in several regulatory processes. RALF1 regulates root expansion (Haruta et al. 2014), whereas fungus-secreted RALF23 controls plant immune signalling after fungal infection (Stegmann et al. 2017) (reviewed in Hater et al. 2020 and Hafidh and Honys 2021).

Fluorescence resonance energy transfer–based Ca^{2+} probes that allow for live cell imaging helped establish that female and male Ca^{2+} signatures dynamically change upon arrival of the pollen tube (Denninger et al. 2014, Hamamura et al. 2014, Iwano et al. 2012, Ngo et al. 2014). Depending on their role in fertilisation, the two synergids exhibit varying responses to the arrival of pollen tubes. The receptive synergid shows stronger but less persistent Ca^{2+} oscillations compared to its counterpart (Denninger et al. 2014, Iwano et al. 2012, Ngo et al. 2014).

After physically interacting with the synergid, the pollen tube accelerates, passes through the filiform apparatus (Leshem et al. 2013), and grows parallel to the axis of the synergid (Denninger et al. 2014, Ngo et al. 2014). Interestingly, as the pollen tube advances towards the chalazal zone of the synergid, the highest Ca^{2+} amplitudes within the synergids follow the tip region of the pollen tube. This suggests that extensive regions of the synergid may have the ability to sense and potentially direct the pollen tube (Denninger et al. 2014). The explosive release of sperm cells is cytologically followed by a quick shrinking of the receptive synergid (Ngo et al. 2014). The rapid contraction of the receptive synergid can be observed cytologically after the energetic release of sperm cells (Ngo et al. 2014). Receptive synergid degeneration begins at an earlier stage and is not solely caused by pollen tube discharge, demonstrated by the fact that FGs with a mutation in pollen tube rupture can prompt synergid degeneration (Leydon et al. 2015), as reviewed in Hater et al. (2020).

1.2.4. Fertilisation Recovery

Following pollen tube rupture within the female gametophyte, the sperm cells must reach distinct female gametes in order to attach and fuse with both the egg and the central cell. Ensuring successful fertilisation not only establishes the foundation for the next generation but also stimulates the breakdown of the pollen tube attraction machinery, preventing the attraction of supernumerary pollen tubes. Commonly, only one pollen tube reaches the synergids (Beale et al. 2012), which indicates the presence of a pollen tube block that limits the quantity of sperm cells targeting female gametes. Intriguingly, when incomplete fertilisation of the egg cell or the central cell occurs, it stimulates receptivity for additional

pollen tubes (Kasahara et al. 2012). This mechanism for fertilisation recovery salvages individual fertilised ovules that would otherwise have aborted and proposes a correlation between the integrity of the synergid and fertilisation status. Significantly, the programmed cell death of the receptive synergid initiates upon pollen tube reception, the disintegration of the second synergid requires successful fertilisation (Beale et al. 2012, Kasahara et al. 2012, Völz et al. 2013).

1.2.5. Gamete Activation and Fusion

Upon successful pollen tube (PT) reception, the PT ruptures adjacent to the receptive synergid, releasing two sperm cells in close proximity to the female gametes. The sperm cell release activates various fertilisation processes. Employing fusion-defective *gcs1* mutant sperm, Kasahara et al. (2016) demonstrated that the content of pollen tube induces ovule enlargement and initiates seed coat development. This suggests that regardless of successful fertilisation, the content of the pollen tube has a proliferative impact on the central cell and ovule. Additionally, a brief wave of Ca^{2+} is detected in both the egg and central cells, indicating activation of the female gamete (Denninger et al. 2014, Hamamura et al. 2014).

Once sperm cells are ejected, two mechanisms are proposed to lead to the repositioning of sperm cells prior to their activation and fusion. Each individual sperm cell can fertilise either of the female gametes (Hamamura et al. 2011). Minutes after their discharge, each sperm cell adheres to one female gamete and assembles and relocalises the cell fusion machinery into close proximity to the plasma membrane (Johnson et al. 2019). If two sperm cells become associated with the same female gamete by chance, their positions are readjusted, implying an adhesion-induced communication between the pairs of sperm cells and the trio of sperm-egg-central cell (Huang et al. 2015, Sprunck 2020). Preferentially, sperm–egg plasmogamy takes place first (Hamamura et al. 2011). Successful gamete fusion triggers the degeneration of the second synergid to prevent polytubey (Johnson et al. 2019). Arabinogalactan protein 4, JAGGER (Pereira et al. 2016) is implicated in this process. If one or both gamete fusions fail, the remaining synergid attracts a second PT for the delivery of additional sperm cells, referred to as fertilisation recovery or hetero-fertilisation (Kasahara et al. 2012).

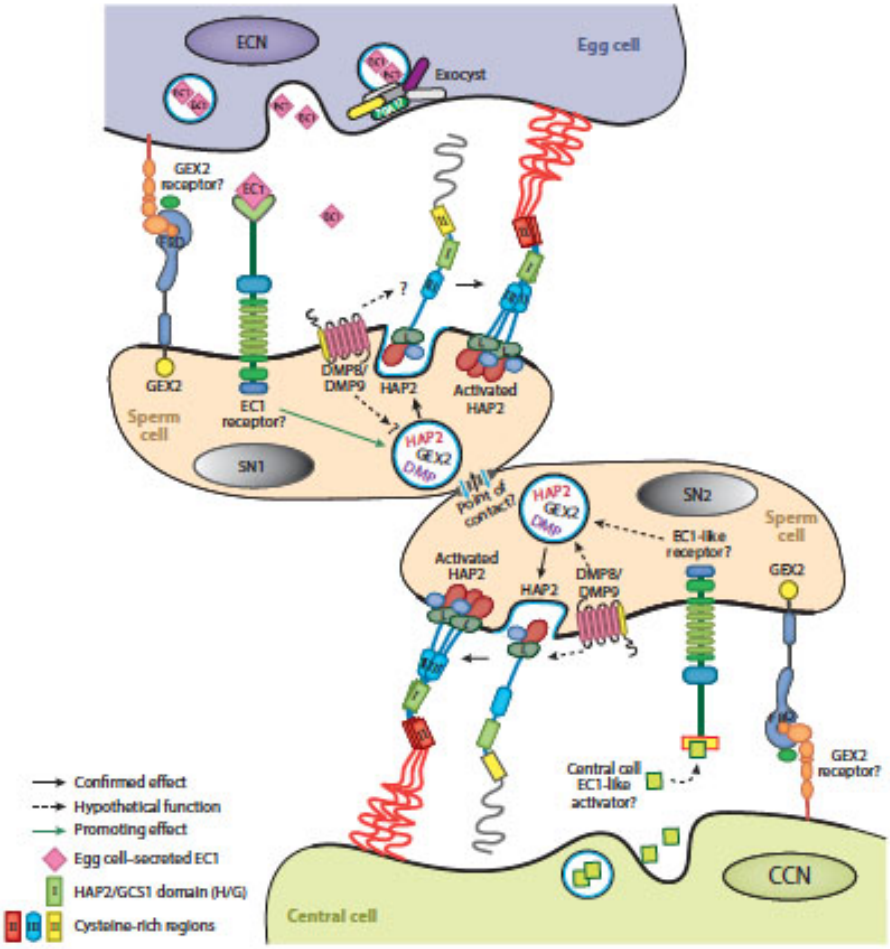

Figure 5. Gamete double fertilisation in *Arabidopsis*. Once ejected by the pollen tube, the sperm cell pair reside at the egg–central cell interphase and make membrane contact. Sperm cell arrival triggers exocytosis of EC1 peptides from the egg cell perceived by an unknown EC1 sperm cell receptor. Sperm-specific GEX2 then makes membrane contact and promotes membrane adhesion via an unknown egg cell receptor. These events coincide with the further relocalisation of an evolutionarily conserved fusogen HAP2 protein from the endomembrane to the sperm cell plasma membrane (peri-germ cell membrane, Sugi et al. 2024). To facilitate gamete fusion, DMP8 and DMP9 likely assist with efficient HAP2 plasma membrane localisation, activation (homotrimerisation), and possible selection of an HAP2 docking site as a membrane fusion–competent site. In the central cell, a similar EC1-like peptide likely triggers a second fusion cycle of sperm–central cell plasma membranes. Readjustment of sperm cell positioning upon association with only one female gamete suggests a contact-induced communication between the two sperm cells. A membrane connection between the sperm cell pair might allow this symplastic communication to coordinate gamete fusions. Thicker lines indicate membrane lipid bilayers at active fusion sites. Abbreviations: CCN, central cell nuclei; EC1, EGG CELL 1; ECN, egg cell nuclei; FRD, two filamin repeat domains; GEX2, GAMETE

EXPRESSED 2; HAP2, HAPLESS 2; L, HAP2 linker stretch; SN, sperm cell nucleus (Hafidh and Honys 2021).

Around the time of pollen tube rupture, the egg cell secretes vesicles that contain CRPs from the EGG CELL1 (EC1) family (Figure 5.). These vesicles then merge with sperm cells, causing the fusogen GENERATIVE CELL-SPECIFIC1-HAPLESS2 (GCS1-HAP2) to relocate from the sperm transmembrane system to the plasma membrane (Sprunck et al. 2012). The first molecular player to be identified in flowering plants which is involved in sperm cell adhesion was GENERATIVE EXPRESSED2 (GEX2). Sperm cell attachment to female gametes is partially compromised in *gex2* mutants (Mori et al. 2014). Furthermore, sperm adhesion is also compromised in *ec1* gametes, pointing towards a dual functionality of EC1 proteins during the male gamete activation process. Specifically, these proteins mediate the recruitment of unknown sperm adhesion factors and the relocalisation of HAP2 that is vital for membrane fusion (Cyprys et al. 2019). HAPLESS 2 (HAP2), also recognised as GENERATIVE CELL-SPECIFIC 1 (GCS1) (von Besser et al. 2006), is a transmembrane protein that is highly conserved and localises to the sperm plasma membrane (Mori et al. 2006, von Besser et al. 2006), where it forms a trimer. The subsequent apical amphipathic helix integrates into the female gamete plasma membrane, facilitating the fusion of the two gametes (being a fusogen) (Fédry et al. 2017). This suggests that HAP2 operates independently and does not require a female binding partner. This implies that further mechanisms are necessary to prevent non-specific fusion of sperm cells with each other or with somatic cells (Johnson et al. 2019). DMP8 and DMP9, two other sperm cell-specific DUF679 membrane fusogen proteins, were recently discovered to aid gamete fusion. They have a greater impact on sperm-egg fusion than on sperm-central cell fusion (Cyprys et al. 2019).

In summary, successful double fertilisation requires multiple processes and relies on specific gametophytic cell types. Pollen tube guidance is provided primarily by the synergids but also the central cell while pollen tube entry occurs through the synergid cells. Sperm cell fusion with the two female gametes requires factors provided by the egg cell; finally, suppression of the pollen tube attraction signal occurs by fusion of the central cell with the persistent synergid cell. Thus, successful double fertilisation to produce a seed is an orchestrated process

involving multiple interactions of the synergid cells, the egg cell, and the central cell (Skinner and Sundaresan 2018).

1.3. Embryogenesis

The seed is produced by a double fertilisation event, where one sperm cell fuses with the diploid central cell to create the triploid endosperm, and the second sperm cell fuses with the egg cell to produce the diploid zygote. The resulting embryo and endosperm continue to develop within the seed coat, which is derived from the maternal tissues of the ovule. The diploid embryo has one maternal and one paternal genome, the triploid endosperm has two maternal genomes and one paternal genome, and the diploid seed coat is derived entirely from diploid maternal tissue, without undergoing meiosis (Reiser and Fischer 1993).

1.3.1. Developmental Stages of Embryogenesis

After fertilisation in *Arabidopsis thaliana*, the nucleus of the zygote moves to the apical pole and the zygote divides asymmetrically to produce a small apical cell that will generate the entire embryo, with the exception of the suspensor, hypophysis, and root cap, which are derived from the larger basal cell. Cell division in these two lineages produces the 2- to 4-cell-stage embryo at 48 h after pollination (HAP), the 8-cell embryo at 60 HAP, the 16-cell dermatogen embryo at 66 HAP, the 32-cell globular embryo at 72 HAP, and the 500-cell heart-stage embryo 120 HAP (Jurgens et al. 1995). The specification of the epidermal lineage occurs during the dermatogen stage. The ground and vascular tissue lineages, alongside the shoot apical meristem (SAM) and root apical meristem (RAM), are produced during the globular stage. Cotyledons (embryonic leaves, the first lateral organs) are produced at the heart stage, when all major pattern elements of the Arabidopsis embryo have been established. After pattern formation, the embryo undergoes a period of morphogenesis where growth of the organs that were established by the heart stage lead to an embryo with fully organised SAM and RAM, hypocotyl (embryonic stem), and elongated cotyledons which fold over as the embryo grows inside the seed coat. Following pattern formation and morphogenesis, embryos of Arabidopsis and closely related oilseed crops undergo maturation, ultimately resulting in the desiccated seed (reviewed in Armenta-Medina et al. 2021). The mother plant coordinates seed development by supplying auxin to the early embryo from the integuments of the ovule. Auxin response increases in ovules after fertilisation, due to up-regulated auxin biosynthesis in the integuments, and this maternally produced auxin is required for correct

embryo development (Robert et al. 2018). Auxin allows proper polarity and patterning of the developing embryo through its distribution, which is maintained by a local auxin production together with well-coordinated transport. The auxin signalling pathway interprets these auxin maxima into proper developmental programs (for detailed review see Verma et al. 2021).

Maturation stages comprise the mid-heart, torpedo, bent cotyledon, mature green, and dry seed stages (Figure 6.). The initial stage, or 'seed filling', is characterised by swift cellular growth and expansion of the embryos, which subsequently turn green at the mid-heart stage whilst producing and accumulating seed storage proteins (cruciferins/12S globulins and arabins/2S albumins). At the early torpedo stage, the oils and waxes that form the cuticle of the epidermis are synthesised. The storage of lipids, carbohydrates and fatty acids during late embryogenesis is essential for meeting the energy requirements needed for germination (Baud and Lepiniec 2010). Additionally, late maturation involves desiccation resulting in water loss and the establishment of seed dormancy (Leprince et al. 2017).

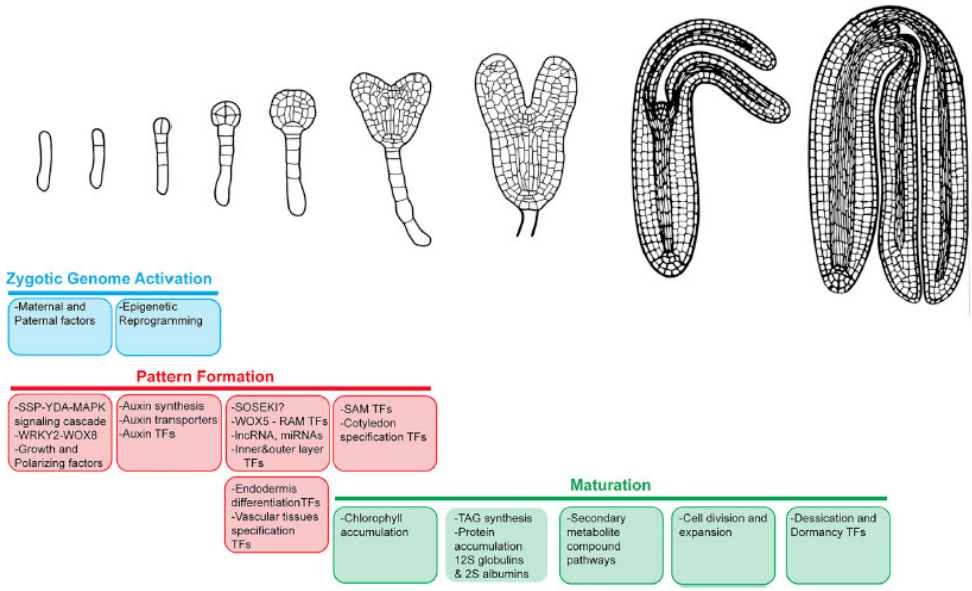

Figure 6. Embryogenesis. The activation of the zygotic genome in early phases involves several genetic processes described in blue, while in red are the processes that participate in the formation of the embryo pattern setting and specification of the primary plant tissues. The maturation processes are highlighted in green and include the last steps of embryonic development (Armenta-Medina et al. 2021).

Coincident with the development of the embryo, the endosperm is initially a coenocyte formed by nuclear division and migration of the nuclei from the micropylar region (surrounding the embryo) toward the opposite (chalazal) end of the seed. The endosperm of Arabidopsis has three regions that become distinct as the seed grows: the micropylar endosperm that surrounds the embryo, the peripheral endosperm in the central region, and the chalazal endosperm. From about 5 days after pollination (DAP), cellularisation occurs in the endosperm during the embryonic heart stage. Similarly to many dicots, the Arabidopsis endosperm is consumed during seed maturation, leaving behind only a peripheral aleurone-like cell layer next to the seed coat, surrounding the fully developed embryo (Olsen 2004).

Importantly, the end point of embryogenesis—the mature embryo—does not generate the body architecture of the adult organism in most land plants. Rather, embryogenesis serves only to establish a blueprint for post-embryonic development. The stem cells found in meristems perpetuate growth and expansion of pre-existing organs, form novel ones post-embryonically and shape the adult body plan. Although the embryo is not just a miniature edition of the adult plant, numerous morphogenetic processes that operate throughout plant development are an integral part of embryo development. These processes include cell polarisation, oriented- and asymmetric cell divisions, and differential cell identity specification (reviewed in Radoeva et al. 2019).

1.3.2. Embryo patterning

One of the initial events in patterning post-fertilisation is the establishment of the apical-basal axis of the zygote. Although the egg cell in Arabidopsis is polarised, fertilisation leads to a transient loss of its polarity (Ueda et al. 2011). After this, the zygote undergoes elongation and repolarisation, with its nucleus positioned near the apical tip and the large vacuoles towards the basal end. This polarised state is indicative of the first asymmetric division. The position of the zygotic nucleus coincides with the division plane, resulting in a small apical cell and a larger basal cell. Recent research has indicated that the cytoskeletal components, including actin filaments and microtubules, undergo dynamic rearrangement during fertilisation to establish the essential pattern for proper asymmetric zygote division (reviewed in Radoeva et al. 2019)

Microscopic examination of cellular remodelling has facilitated the description of the cellular processes responsible for asymmetry. Nonetheless, what prompts the asymmetric division remains a crucial question. It seems that the embryo's parents exert at least two non-genetic, trans-generational influences.

Firstly, synthesis of the plant hormone auxin is activated in the integument cells surrounding the zygote in the ovule following fertilisation. Maternal auxin is transported into the embryo, accumulating in the apical cell, and contributing to normal development after the initial zygotic division. Polar auxin transport from the suspensor is mediated by the auxin efflux transporter PIN7, which is expressed in the basal cell lineage. Later in embryo development, other auxin transporters, such as PIN1, are expressed in the apical proembryo (Friml et al. 2003). Auxin regulates pattern formation in embryos, and thus defects in auxin response, auxin biosynthesis, and auxin transport affect embryonic development (Robert et al. 2018).

Additionally, functional and molecular studies have identified signalling pathways and transcription factors (TFs) that regulate the first divisions of the zygote, leading to the first cell fate differentiation events in the embryo. The WOX TF family genes WOX2 and WOX8 are co-expressed in the zygote. After the first asymmetric division, WOX2 is expressed in the apical daughter cell and WOX8 is specifically expressed in the basal daughter cells of the zygote (Haecker et al. 2004). The elongation of the zygote and its first asymmetric division are regulated through the YODA (YDA) mitogen-activated protein kinase kinase kinase (MAPKKK), which acts through the MAP kinase kinases, MPK3/ MPK6, to phosphorylate and activate the WRKY2 TF (Ueda et al.,2017). Subsequently, WOX8 transcription in the zygote is promoted by WRKY2 (Ueda et al. 2017). In the zygote, the YDA-MAP signalling cascade is activated initially by paternal SHORT SUSPENSOR (SSP) (Bayer et al. 2009). This is a membrane-associated pseudokinase that is delivered from the sperm cell. Additionally, a maternal contribution is required for the YDA-MAPK cascade. Reciprocal crosses between wild-type and MAPKKK mutants showed only a maternal effect on asymmetric division and cell elongation (Zhang et al. 2017). The HOMEODOMAIN GLABROUS11/12 (HDG11/12) transcription factors, expressed maternally, cooperate with WRKY2 to regulate WOX8 transcription, as reported by Ueda et al. in 2017. Subsequently,

the embryonic apical cell establishes and generates the majority of the mature embryo via well-defined division sequences (reviewed by Armenta-Medina et al. 2021).

1.3.3. Zygotic Genome Activation and Inheritance of Transcripts

The maternal to zygotic transition denotes the period when control of development transfers from the maternal to zygotic genome. This transition includes two individual events: the concerted degradation of maternal mRNAs and the initiation of zygotic transcription, better known as zygotic genome activation (ZGA). Transcript profiling in early plant embryos has posed difficulties in distinguishing between maternal transcripts of gametophytic origin, originating from egg or sperm, and those of zygotic origin, resulting from transcription in the zygote. Additionally, there is the challenge of isolating zygotic tissue without containing maternal sporophytic transcripts leading to contamination of zygotic transcripts. These challenges, as well as possible inherent differences in ZGA between plant species, have contributed to a lack of resolution in the literature on two basic questions: (a) whether large-scale zygotic transcription begins within the first few hours after fertilisation, or up to several days later; and (b) whether the onset of zygotic transcription occurs in a bi-allelelic manner, or with an initial maternal bias where paternal alleles show variable degrees of silencing (Del Toro de Leon et al. 2016).

Contrasting outcomes were found in transcriptome analysis of transcription from maternal and paternal genomes in early Arabidopsis embryos (Nodine and Bartel 2012, Autran et al. 2011). Genetic analysis indicates a dominant involvement of maternal gene copies during early embryonic development (Del Toro-De León et al. 2014). However, whether this conveys differential parental transcript contributions after fertilisation remains to be established. Conversely, it is generally agreed upon that ZGA occurs at the zygote stage soon after fertilisation in monocot embryos (Anderson et al. 2017, Chen et al. 2017). In rice, the contributions of the maternal and paternal genomes to ZGA are highly uneven. The majority of all transcriptional output, fundamental processes operating in the cell, is provided by the maternal genome (Anderson et al. 2017). Conversely, the paternal genome predominantly contributes genes encoding putative pluripotency factors, which are necessary to initiate embryo development (Anderson et al. 2017).

Despite the ongoing debate about the contribution of paternal and maternal genomes to zygotic genome activation in Arabidopsis (Del Toro-De Leon et al. 2016, Armenta-Medina and Gillmor 2019), there is a consensus for the importance of early zygotic transcriptional activity, because inhibition of RNA polymerase II in the zygote caused a delay or arrest of cell divisions of Arabidopsis zygotes (Pillot et al. 2010, Kao and Nodine 2019, Zhao et al. 2019). *De novo* transcripts are detectable in the zygote after fertilisation (Zhao et al. 2019), yet it is also true that the majority of transcripts found in the plant zygote are already present in the egg cell (Zhao et al. 2019), which suggests transcript carryover representing maternal origin from the egg cell to the zygote. A few examples of paternal inheritance exist, for instance TREE1 and DAZ3 (Cheng et al. 2023). Both genes are absent in egg cells and are expressed exclusively in sperm cells. Fluorescence detection and qRT-PCR measurements after reciprocal crosses with GFP-labelled constructs driven by native promoters both confirmed presence of paternally-inherited transcripts and proteins in the embryos up to octant stage (Cheng et al. 2023). Despite presenting no evident defects in sperm development and fertilisation, *tree1 daz3* unexpectedly led to aberrant differentiation of the embryo root stem cell niche. TREE1 and DAZ3 function by suppression of maternal *RKD2* transcription, thus mitigating the detrimental maternal effects from RKD2 on root stem cell niche (Cheng et al. 2023).

1.3.4. Embryo-defective mutants

Many years of systematic developmental and genetic studies have resulted in identification of more than 500 for embryo-defective (*emb*) mutants. EMB genes are broadly defined as necessary genes for embryogenesis, comprising of mutants that play a role in cell-type differentiation, the transformation of suspensor cell mutants, meristem differentiation mutants, maturation program mutants, and genes necessary for critical cellular functions. The loss of these genes leads to the lethality of the embryo or seedling. The defining feature of recessive embryo-defective mutants is that siliques of selfed heterozygotes segregate mutant seeds with abnormal embryos. Mutants with altered seed pigmentation but normal embryo morphology are typically excluded. The frequency of mutant seeds in heterozygous siliques is

usually about 25% but can range from 5% to 50%, depending on the locus and allele involved. In some cases, both embryo and gametophyte development are disrupted. In other cases, mutant embryos can germinate to produce defective seedlings (extensively reviewed in Meinke et al. 2020).

On the paternal side, there are instances where the embryo phenotype is solely determined by the pollen genotype. In other words, 50% defective seeds are produced when WT plants are crossed with pollen from heterozygotes. With knockouts of CDC2A (Iwakawa et al. 2006, Nowack et al.,2006), FBL17 (Kim et al. 2008, Gusti et al. 2009), DUO3 (Brownfield et al. 2009), and XRI1 (Dean et al. 2009), the underlying cause is the formation of pollen with a single sperm cell. Aborted seeds are produced irrespective of maternal genotype due to the compromised double fertilisation. These genes are included in the EMB dataset, despite the initial defect being gametophytic in nature, because limited fertilisation is still achievable. Knockouts of KPL demonstrate a propensity for single fertilisation of either the embryo or endosperm, despite the presence of two sperm cells. This highlights a distinct underlying mechanism and presents a novel case of natural regulation via cis-antisense siRNA involving a nearby gene (Ron et al. 2010). A different mechanism of paternal inheritance is observed in knockouts of SSP, which encodes a receptor-associated protein kinase. In this case, transcripts produced in pollen are not translated until delivery to the zygote, where they function to activate the YODA protein kinase that regulates the first cell division (Bayer et al. 2009). The NIMNA gene exhibits a weaker paternal effect in which heterozygous embryos with a paternal mutant allele are defective in embryo development, though to a lesser degree than homozygotes (Babu et al. 2013).

The spectrum of mutants with gametophytic maternal effects is even more diverse (Ngo et al. 2012, Armenta-Medina and Gillmor 2019). The most notable cases involve the knockout of five extensively researched genes (MEA, FIE1, FIS2, MSI1 and DME) that are essential for Polycomb Repressive Complex 2 (PRC2) to function during reproductive development. Heterozygous plants, regardless of their pollen genotype, generate 50% faulty seeds with a unique phenotype characterised by over-proliferation of the endosperm and arrest of the embryo at the heart stage. Paternal alleles of MEA, FIS2, and FIE were reported to be inactive early in seed development, consistent with the observed maternal effect (Kinoshita et

al. 1999, Luo et al. 2000, Yadegari et al. 2000). By contrast, the paternal allele of MSI1 is expressed, but at levels insufficient to rescue mutant embryos lacking functional protein in female gametophytes (Leroy et al. 2007). DME function is required for DNA hypomethylation in the central cell of the female gametophyte and maternal MEA function in the endosperm (Choi et al. 2002).

1.4. RNA Biosynthesis and Regulation in the Gametophyte

1.4.1. Male Gametophyte Transcriptome Specifics

The *Arabidopsis thaliana* mature pollen and isolated sperm cell transcriptomes have been analysed using microarray and serial analysis of gene expression (SAGE) methods (Becker et al. 2003, Honys and Twell 2003, 2004, Lee and Lee 2003, Pina et al. 2005, Borges et al. 2008). Microarray studies estimated the complexity of the Arabidopsis pollen transcriptome to be about 6,000 genes, with about 10% pollen-specific genes (Twell et al. 2006). A landmark study using Affymetrix ATH1 genome arrays identified 13,977 Arabidopsis male gametophyte-expressed mRNAs, of which 9.7% were considered to be male gametophyte-specific (Honys and Twell 2004). Additional transcriptome analyses were conducted on pollen and SCs from other flowering species, including rice (Anderson et al. 2013), maize (Chen et al. 2017), tomato (Liu et al. 2018), and tobacco (Hafidh et al. 2012). RNA sequencing (RNA-seq) has yielded more comprehensive understanding of the pollen transcriptome in Arabidopsis and other species (Loraine et al. 2013, Borg et al. 2020, Julca et al. 2021, Nelms and Walbot 2022, Misra et al. 2023, Klodová et al. 2023).

Thanks to high-throughput sequencing technologies, it has been observed that the male gametophyte in higher plants exhibits distinctly different transcriptomes in comparison to other plant tissues (as reviewed in Huang et al. 2021). For instance, in both *Arabidopsis thaliana* and rice (*Oryza sativa*), nearly one fifth of total transcripts were identified to be enriched specifically in sperm cells (SCs) while absent in seedlings (Hackenberg and Twell 2019). A closer analysis of the transcriptomes of vegetative cells (VC) and SC in rice demonstrated significant differences in gene expression patterns, with less than 43% transcript overlap (Anderson et al. 2013). Furthermore, a comprehensive comparison of 31 different tissues in rice revealed that gene expression in SCs is more divergent from sporophyte or VC (Russell and Jones 2015). The GO terms for SC-specific transcripts were mostly enriched in the processes of DNA repair, ubiquitin-mediated protein degradation and the cell cycle, all of which appear to be consistent with the essential maintenance of germline integrity in the SC (Borges et al. 2008). A recent paper by Misra et al. (2023) found considerable overlap in the Arabidopsis sperm cell, vegetative cell and egg cell transcriptomes, while also identifying

specific transcript sets for each cell type, which may encode proteins performing specific functions for the respective cell type.

The pollen's developmental transcriptome undergoes a shift in transcript abundance, marked by a decline in early transcripts and a simultaneous increase in late transcripts. These trends coincide with a reduction in cellular activity and the favouring of specific transcript sets during late development (Honys and Twell 2003). The data additionally substantiate a general partition of developmental gene expression between an earlier, more comparable to sporophyte phase and a later, more specific to gametophyte phase (Mascarenhas 1990). The transcriptome dynamics of developing pollen affect numerous biological processes, with major changes occurring during the phase transition from early to late stages (Figure 7.). In the early stages, there is an increase in gene transcription for proteins involved in translation, mRNA and protein processing, as well as cell division. During the later phase, there is indication of preparation for pollen desiccation through increased transcription of stress-related genes. This is followed by preparation for pollen activation and pollen tube growth, which is facilitated by the accumulation and storage of transcripts related to vesicle transport, energy metabolism and pollen tube growth. (Klodová et al. 2023).

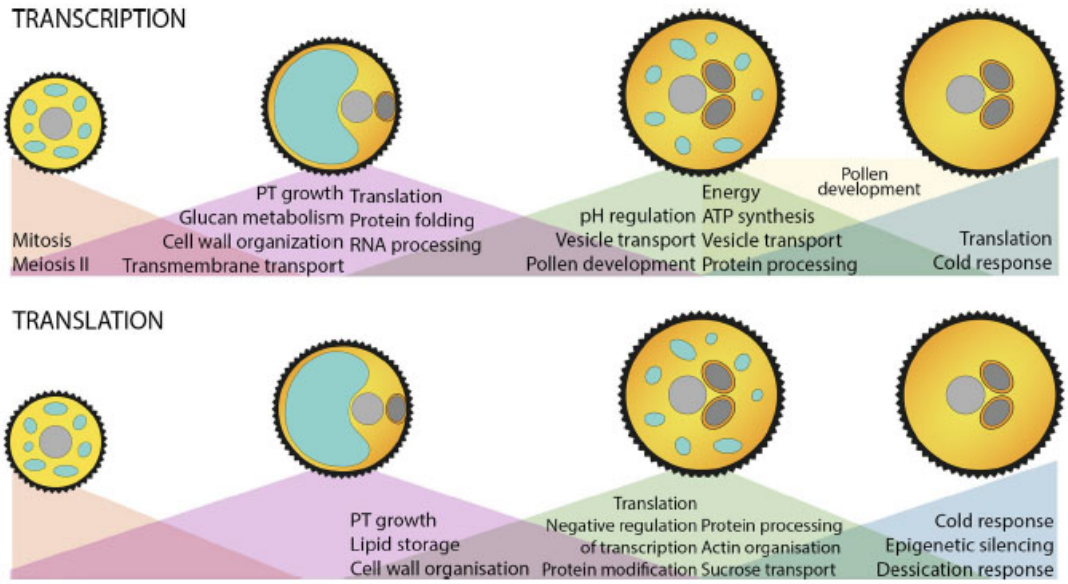

Figure 7. Summary of major changes in biological processes in developing Arabidopsis pollen. GO terms reflect the analysis of differential gene expression based on transcriptomic and proteomic data at four developmental stages. Coloured triangles indicate increased expression (left) or decreasing expression (right) of GO processes during stage transitions (Klodová et al. 2023).

Several transcriptomic shifts were identified during Arabidopsis pollen development (Klodová et al. 2023). During UNM-BCP (unicellular microspore - bicellular pollen) transition, 115 positively enriched GO categories were up-regulated in UNM. These included terms linked with mitotic events such as cyclin-dependent protein phosphorylation, phase transition control and spindle organisation, indicating the preparation of microspores for cell division. Transcripts elevated in BCP were primarily linked to glucan metabolism and transmembrane transport, which included transcripts associated with the cell wall. A major transcriptomic shift was associated also with the BCP-TCP (bicellular pollen - tricellular pollen) transition. The BCP stage was defined by up-regulated transcripts related to translation, from tRNA and ribosome biogenesis to mRNA maturation and protein folding. From the TCP stage, there was a significant reduction in the enrichment of GO categories related to translation, and an increase in transcripts related to pollination, pollen germination and pollen tube growth. BCP-TCP transition was also characterised by up-regulation of transcripts connected to vesicle transport including both exocytosis and clathrin-dependent endocytosis, while the signalling terms activation of GTPase activity, Rab protein signalling and Ras protein signalling were also enriched along with glycerophospholipid metabolic process. The final developmental phase from TCP to MPG showed fewer changes compared with BCP-TCP transition. The GO categories up-regulated in TCP were enriched for energy and biosynthetic processes including ATP synthesis coupled proton transport and electron transport chain. The expression of these gradually declined from UNM to MPG, similar to those coding for vesicle transport- and exocytosis-related proteins. Transcripts connected to pollen, pollen tube germination and pollen development were up-regulated in TCP, while transcripts up-regulated in MPG were involved in pollen tube growth regulation and microgametogenesis. Moreover, some transcripts were enriched in the response to cold and abscisic acid. Of the 3,087 annotated DEGs (differential gene expression) up-regulated in MPG, 26% were linked to stress response. Compared to other stages, an increase in stress response transcripts was noticeable. The list comprises of gene groups that are responsive to salt, radiation, heat, cold, desiccation, and chemical stimuli. Additionally, genes responsible for DNA repair, protein oxidation, signalling, transport, and response to biotic stress were identified (Klodová et al. 2023).

1.4.2. Post-transcriptional regulation

Post-transcriptional regulation of the eukaryotic transcriptome can occur at any step of the RNA "life cycle" including maturation (e.g. splicing, polyadenylation, etc.); transport from the nucleus; localisation within subcellular compartments; molecule stability; as well as the initiation, elongation, and termination of protein translation. Numerous *cis*- and *trans*-acting features and factors are integral to all of these regulatory processes (Silverman et al. 2013).

1.4.2.1. RNA Splicing

Complex multicellular organisms generate a myriad of highly specialised cell and tissue types during their lifetime. In addition, they must respond swiftly and effectively to an extensive range of external stresses, both abiotic (e.g., high temperature or salinity) and biotic (e.g., bacterial infections), all requiring unique and highly coordinated molecular responses. Remarkably, all this is achieved by differentially regulating a single genome sequence to generate specific transcriptomes and proteomes for each environmental condition and cell or tissue type (Martin et al. 2021).

Environmental signals can regulate the transcription of thousands of genes while also affecting other aspects of gene expression other than transcription initiation, such as 5′ end capping, splicing, 3′ end processing, export, translation, and RNA stability/ degradation. These regulatory mechanisms can be directly related to transcription, that is, being co-transcriptional or post-transcriptional. Moreover, changes in chromatin (epigenomic) and/or modifications in RNA bases (epitranscriptomic) may significantly impact the processing and stability of RNA molecules (Martin et al. 2021, Xu et al. 2022, Tognacca et al. 2023).

Alternative splicing (AS) is a co-transcriptional mechanism that produces more than one mRNA isoform from a single gene (reviewed in Martin et al. 2021, Tognacca et al. 2023). It plays multiple roles in plant responses by integrating endogenous developmental and exogenous environmental signals (Lee et al. 2013, Posé et al. 2013), and is the most important contributor to transcriptome diversification in both plants and animals. RNA splicing is one of the steps in RNA processing that involves the removal of some regions (introns) while joining others (exons). This process requires more than 200 proteins and five small RNAs, which are

associated with the spliceosome complex (Wahl et al. 2009). The genes undergoing alternative splicing encode proteins with regulatory functions, and this mechanism impacts on protein functions such as binding properties, enzymatic activity, intracellular localisation, post-translational modification, or protein stability (Zhu et al. 2017). Alternative splicing can serve two main molecular functions. Firstly, it can increase proteome complexity by producing two or more unique protein isoforms, some of which can exhibit significantly diverse functional properties (Kelemen et al. 2013). Alternatively, AS can lead to a down-regulation in gene expression by disrupting the primary open reading frame (ORF) of the target gene. This occurs through the production of truncated protein isoforms, which may function as dominant negatives (Kelemen et al. 2013), or by inducing nonsense-mediated decay mRNA (NMD) (Lewis et al. 2003). Given the different proportions of AS types in each lineage, a higher relevance has been given to proteomic expansion associated with exon skipping (ES) in animals (Irimia and Blencowe 2012), whereas in plants the focus has been put mainly into the regulation of gene expression by intron retention (IR) coupled to NMD (Kalyna et al. 2012, Drechsel et al. 2013, Wang and Brendel 2006).

An intron-containing gene has the potential to generate multiple different isoforms, depending on the intron–exon structure/composition (Figure 8.). The most common types of alternative splicing are: (a) exon skipping (an exon is alternatively skipped and results in a shorter mature mRNA), (b) alternative 5′ splice site (5'ss) (the spliceosome may recognise an alternative 5′ss, within an exon, thereby producing a shorter transcript), (c) alternative 3′ splice site (3’ss, a 3′ss within an exon is recognised by the spliceosome), (d) intron retention (the spliceosome retains a full intron in the mature mRNA), (e) exitron splicing (alternatively spliced internal regions of protein-coding exons. Transcripts with retained exitrons exit the nucleus for translation into different proteins in a tissue-specific manner; Marquez et al. 2015), and (f) mutually exclusive exons (an exon-skipping-derived mechanism where an exon is included and another exon is excluded, so the mature mRNAs never contain both exons) (Tognacca et al. 2023).

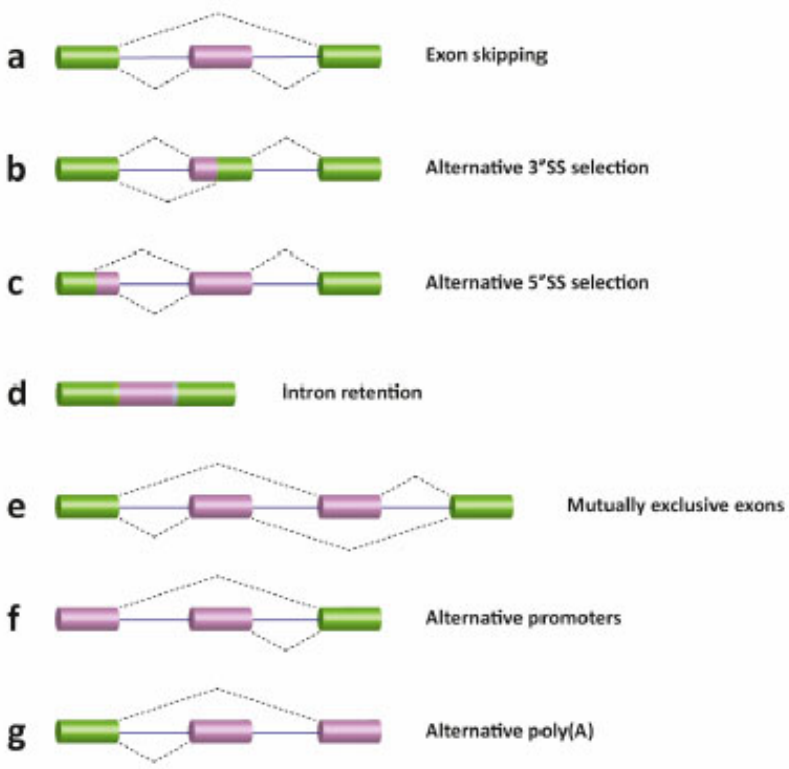

Figure 8. Schematic representation of different types of alternative transcriptional or splicing events, with exons (boxes) and introns (lines). Constitutive exons are shown in green and alternatively spliced exons in purple. Dashed lines indicate the AS event. Exon skipping (a); alternative 3'ss (b) and 5'ss selection (c); intron retention (d); mutually exclusive exons (e); alternative promoter usage (f); and alternative polyadenylation (g) events are shown. Like alternative splicing (AS), usage of alternative promoter and polyadenylation sites allow a single gene to encode multiple mRNA transcripts (Suñé-Pou et al. 2017).

In addition to the exclusion or inclusion of exons/introns, alternative start or termination sites further contribute to the complexity of alternative isoforms (reviewed in Erdem et al. 2023). The transcription start sites are primarily determined by the dynamic interactions between RNA Polymerase II and the various promoter elements (Yu et al., 2016). In contrast, the 3′-ends of mRNAs are determined by the cleavage and polyadenylation reactions. Firstly, a multi-subunit protein complex identifies the hexameric polyadenylation signal and its adjacent sequences (Shi and Manley, 2015). Subsequently, the mRNA is cleaved at the polyadenylation site, which is typically located 10–30 nucleotides downstream of the signal sequence. Subsequently, a poly(A) tail is added to the 3′-end of the mRNA (Neve et al., 2017). Hence, the 3′-end of the mRNA is primarily dependent on where the polyadenylation and other conserved sequences are. In addition to changes to the 3′-UTR lengths, a significant portion of human genes (~20%) have one or more polyadenylation sites within introns (Tian et al. 2007). Activation of proximal intronic polyadenylation sites can generate mRNA isoforms that lack a significant portion of the 3′-end of the gene. These mRNAs can subsequently lead to the production of C-terminus truncated proteins.

In addition to alternative mRNA isoforms, small RNA sequencing methods have revealed the existence of additional miRNAs and isomiRs that differ from the canonical mature miRNA sequences (Morin et al. 2008). IsomiRs may exhibit shorter or longer 5′- and/or 3′-ends. The observed heterogeneity at the ends of isomiRs is likely to result from variations in the activity of the enzymes Drosha and Dicer during the maturation process, or through their interactions with RNA-binding proteins such as LIN28 and HNRNPA1 (Michlewski and Cáceres, 2019).

Trans-splicing of RNA joins exons from different pre-mRNAs to generate a chimeric transcript without a chromosomal rearrangement (reviewed in Erdem et al. 2023). Initially identified in trypanosomes, trans-splicing events were also reported in viruses, bacteriophages, prokaryotes, lower eukaryotes, *Caenorhabditis elegans* and, albeit less frequently, vertebrates (Hong et al. 2020). A chimeric transcript may have a continuous reading frame translated into a fusion protein, or the downstream frame might shift. Alternatively, chimeric RNAs may act as competing endogenous RNAs. Termination of RNA Pol II transcription is a critical step of gene expression. If RNA Pol II elongates beyond the defined transcription-termination site and into the adjacent gene, read-through transcripts are generated. Stress, viral infections and disease states may induce read-through transcription (reviewed in Erdem et al. 2023) .

1.4.2.2. Splicing Factors and Mechanism

The splicing machinery and mechanisms are shared across all eukaryotic phyla to some extent, such as the RNA sequences that define exon/intron boundaries, spliceosome components, and splicing factors, which are conserved across all eukaryotes (Reddy 2007, McGuire et al. 2008, Ling et al. 2019). Splicing is carried out by the spliceosome complex, comprising of five small nuclear ribonucleoprotein particles (snRNPs) labelled U1, U2, U4, U5, and U6 and additional spliceosome-associated non-snRNP proteins (Will and Lührmann 2011, Matera and Wang 2014, reviewed in Chaudhary et al. 2019).

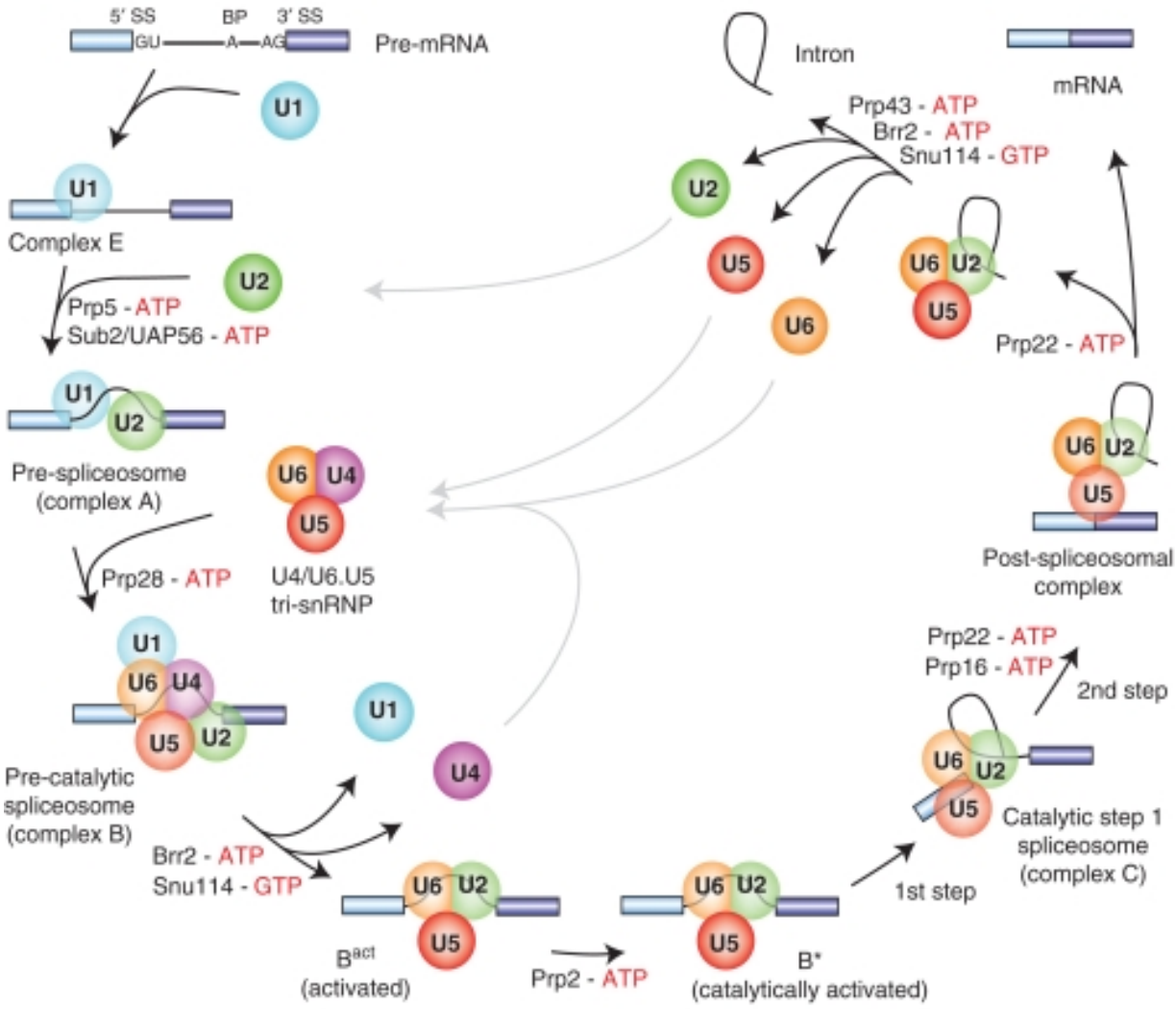

Figure 9. Pre-mRNA splicing by the U2-type spliceosome. In the first step of the splicing process, the 5'splice site (GU, 5'ss) is bound by the U1 snRNP, and the splicing factors SF1/BBP and U2AF cooperatively recognize the branch point sequence (BPS), the polypyrimidine (Py) tract, and the 3'ss splice site (AG, 3'ss) to assemble complex E. The binding of the U2 snRNP to the BPS results in the pre-spliceosomal complex A. Subsequent steps lead to the binding of the U4/U5–U6 tri-snRNP and the formation of complex B. Complex C is assembled after rearrangements that detach the U1 and U4 snRNPs to generate activated complex B. Complex C is responsible for the two trans-esterification reactions at the SS. Additional rearrangements result in the excision of the intron, which is removed as a lariat RNA, and ligation of the exons. The U2, U5, and U6 snRNPs are then released from the complex and recycled for subsequent rounds of splicing. The various spliceosomal complexes are named according to the metazoan nomenclature. Exon and intron sequences are indicated by boxes and lines, respectively. The stages at which the evolutionarily conserved DExH/D-box RNA ATPases/

helicases Prp5, Sub2/UAP56, Prp28, Brr2, Prp2, Prp16, Prp22 and Prp43, or the GTPase Snu114, act to facilitate conformational changes are indicated (Will a Luhrmann, 2011).

The *cis*-regulatory elements found on pre-mRNA include 5' splice sites (5’ ss), 3' splice sites (3’ss), polypyrimidine tracts (PPT) and branch point sequences (BPS), which are recognized by the *trans*-acting factors such as splicing factors (SFs), predominantly serine/arginine-rich (SR) proteins and hnRNPs. The *trans*-acting SFs and *cis*-regulatory elements guide and modulate the spliceosome to recognize differential splice sites present on pre-mRNA (Koncz et al. 2012, Reddy et al. 2013).

The co-transcriptional behavior of splicing means that the splicing process is significantly impacted by the chromatin environment, including factors such as methylation status, histone modifications, nucleosome occupancy and RNA Polymerase II (RNAPII) processivity (Listerman et al. 2006, Jabre et al. 2019).

Spliceosome assembly occurs by the ordered interaction of the spliceosomal snRNPs and numerous other splicing factors. In the event that an intron does not exceed 200–250 nts, the spliceosome initially assembles across the intron. In the earliest cross-intron spliceosomal complex (i.e., the E complex), the U1 snRNP is recruited to the 5′ ss and non-snRNP factors such as SF1/mBBP and U2AF interact with the BPS and PPT, respectively. In a subsequent step, the U2 snRNP stably associates with the BS, forming the A complex (also denoted pre-spliceosome). The U4/U6.U5 tri-snRNP, which is pre-assembled from the U5 and U4/U6 snRNPs, is then recruited, generating the precatalytic B complex. Major rearrangements in RNA–RNA and RNA–protein interactions, leading to the destabilisation of the U1 and U4 snRNPs, give rise to the activated spliceosome (i.e., the Bact complex). Subsequent catalytic activation by the DEAH-box RNA helicase Prp2, generates the B∗ complex, which catalyses the first of the two steps of splicing. This yields the C complex, which in turn catalyses the second step. The spliceosome then dissociates and, after additional remodelling, the released snRNPs take part in additional rounds of splicing (reviewed in Will and Luhrmann, 2011). A few proteins remain as core components of the tri-snRNP complex, including Snu114, Brr2 and PRP8. PRP8A interacts with a preformed U4/ U6.U5 tri-snRNP complex to form a larger catalytically active spliceosomal B complex (Maeder et al. 2009, Bartels et al. 2002).

Recently, a glycine rich RNA-binding protein GRP20 has been identified as a regulatory protein for micro- (less than 51 nt) and small- (51-100 nt) exon splicing (Wang et al. 2024). GRP20 interacts with the U5 subunit of the spliceosome, specifically with the Prp18 protein. The interaction between GRP20 and the spliceosome is required for flower organ patterning and RNA splicing of floral regulatory genes (Wang et al. 2024).

1.4.2.3. Splicing mutants of the gametophyte development and embryo patterning

During a screen for regulators of egg-cell fate, three mutants were isolated, *lachesis (lis), clotho* (*clo*) and *atropos* (*ato*), respectively. In the case of *lis* mutants, which are defective for the splicing factor PRP4, accessory cells are observed to differentiate into gametic cells. It has been demonstrated that CLO/GAMETOPHYTIC FACTOR 1 (CLO/GFA1) is a requisite factor for the restricted expression of egg- and central-cell fate. CLO/GFA1 encodes the Arabidopsis homologue of Snu114, which is an essential component of the spliceosome. ATO encodes the Arabidopsis homologue of SF3a60, a protein that has been implicated in pre-spliceosome formation. The restriction of gametic cell fate is specifically coupled to the function of various core spliceosomal components (Moll et al. 2008).

Another protein involved in RNA biogenesis and exhibiting mutant embryo-lethal phenotype and diminished female gametophyte development at stage FG5 is GAMETOPHYTIC FACTOR 1 (GFA1). Homologs of the GFA1 gene in yeast and humans have been shown to encode putative U5 snRNP-specific proteins that are essential for the splicing of pre-mRNA. GFA1 has been demonstrated to physically interact with AtBrr2 and AtPrp8, the U5 snRNP components of Arabidopsis (Liu et al., 2009).

Sasaki et al. (2015) identified a novel protein in Arabidopsis, RTF2 (AtRTF2). RTF2 is a previously uncharacterised, evolutionarily conserved protein containing a replication termination factor 2 (Rtf2) domain. A homozygous null mutation in AtRTF2 is embryo lethal. The results of quantitative RT-PCR demonstrated that impaired expression of GFP in *atrtf2* and *prp8* mutants is due to inefficient splicing of the GFP pre-mRNA. A genome-wide analysis using RNA sequencing indicated that 13–16% of total introns were retained to a significant degree in *atrtf2* mutants (Sasaki et al. 2015).

The yeast Bud13p (bud-site selection protein 13) has been demonstrated to regulate the budding pattern and pre-mRNA splicing in yeast cells. However, no Bud13p homologs have been identified in plants. Xiong et al. (2019) isolated two mutants that carry T-DNA insertions at the At1g31870 locus, which were observed to exhibit early embryo lethality and seed abortion. The At1g31870 gene encodes an Arabidopsis homolog of the yeast Bud13p protein, designated AtBUD13. AtBUD13 is expressed throughout the plant life cycle, including during embryogenesis. In Arabidopsis, AtBUD13 proteins are localised to the nucleus. The results of the RNA-seq analysis indicated that the AtBUD13 mutation predominantly resulted in intron retention, particularly for shorter introns (≤100 bases). The results demonstrate that AtBUD13 plays a critical role in early embryo development, affecting pre-mRNA splicing (Xiong et al., 2019).

The activated splicing complex B-act is comprised of the three snRNP complexes U2, U5 and U6, as well as the so-called NineTeen complex (NTC), which plays a crucial role in spliceosomal activation. CWC15 is an integral component of the NTC in humans and has been demonstrated to be associated with the NTC in other species. The Arabidopsis orthologue of yeast CWC15 has been observed to associate with the core components of the Arabidopsis NTC, and its loss leads to inefficient splicing. Consistent with the central role of CWC15 in RNA splicing, cwc15 mutants are embryo lethal and additionally display strong defects in the female haploid phase. Interestingly, the haploid male gametophyte or pollen in Arabidopsis, on the other hand, can cope without functional CWC15, suggesting that developing pollen may exhibit greater tolerance to CWC15-mediated defects in splicing than either the embryo or female gametophyte (Slane et al. 2020).

The plant hormone auxin is a fundamental regulator of organ patterning and development that regulates gene expression via the canonical AUXIN RESPONSE FACTOR (ARF) and AUXIN/INDOLE-3-ACETIC ACID (Aux/IAA) combinatorial system. ARF and Aux/IAA factors interact, but at high auxin concentrations, the Aux/IAA transcriptional repressor is degraded, allowing ARF-containing complexes to activate gene expression. ARF5/ MONOPTEROS (MP) is an important integrator of auxin signalling in Arabidopsis development and activates gene transcription in cells with elevated auxin levels. Cucinotta et al. (2021) show that in ovules, MP is expressed in cells with low levels of auxin and can

activate the expression of direct target genes. They identified and characterised a splice variant of MP that encodes a biologically functional isoform that lacks the Aux/IAA interaction domain. This MP11ir isoform was able to complement inflorescence, floral, and ovule developmental defects in *mp* mutants, suggesting that it was fully functional. The present study describes a previously unidentified scenario in which ARF post-transcriptional regulation controls the formation of an isoform that can function as a transcriptional activator in regions of sub-threshold auxin concentration (Cucinotta et al. 2021).

1.4.2.4. Alternative Splicing in Plants

When comparing alternative splicing (AS) studies in plants and animals, it is clear that information on tissue-specific AS is relatively sparse in plants. Furthermore, the relative proportions and frequencies of different types of AS events differ between plants and animals (Chaudhary et al. 2019, Timofeyenko et al. 2023). The differential usage of transcript isoforms is common in plants, with around 22% of AS events resulting in changes to protein sequences in Arabidopsis (Vaneechoutte et al. 2017). Among AS events, intron retention was previously reported as the most frequent, but AS can also result in protein sub-functionalisation (Ner-Gaon et al. 2004, Keller et al. 2017). Intron retention (IR) was also reported to be the predominant AS mechanism in developing pollen of *Brassica rapa* (Golicz et al. 2021). According to the high-throughput transcriptomic dataset for Arabidopsis, IR was the most common alternative splicing event (40%), followed by alternative 3′ ss, alternative 5′ ss, exon skipping, and mutually exclusive exons (Zhang et al. 2017). Isoform usage was reported to be similar between mature Arabidopsis pollen and seedlings, with few pollen-specific changes, mostly related to transcripts involved in splicing, suggesting a possible autonomous regulation of the spliceosome complex (Loraine et al. 2013). The distribution of alternative splicing events was similar across all three Arabidopsis pollen stage transitions (UNM-BCP, BCP-TCP, TCP-MPG). The most common types of AS events were alternative transcription start sites and alternative transcription termination sites, followed by alternative 3’ splice site and intron retention. Multiple exon skipping resulting from isoform switches was rare (Klodová et al. 2023).

Martin et al. (2021) estimated that 62.2% of Arabidopsis multi-exonic genes were alternatively spliced through at least one AS event across developmental and tissue samples. Consistent with previous studies (Grau-Bove et al. 2018, Ner-Gaon et al. 2004, Marquez et al. 2012, Filichkin et al. 2015), IR was the most prevalent type of AS genome-wide (Martin et al. 2021). The study revealed that exon skipping (ES), alternative splice acceptor (ALTA), and alternative splice donor (ALTD) AS types were overrepresented compared to IR in most of the categories of regulated AS events, which are more likely to be functional. These categories included AS events that were differentially regulated upon multiple stresses, among tissues, or that were broadly alternatively spliced across conditions (PanAS events). Additionally, ALTA events were found to be particularly prevalent in Arabidopsis when compared to metazoans. The results suggest that the functional significance of non-IR AS events in the dynamic remodelling of plant transcriptomes may have been underestimated (Martin et al. 2021).

The authors Misra et al. (2023) recently analysed the alternative splicing landscape in the germ cells of Arabidopsis. They determined the cell-specific pattern in sperm cells (SCs), vegetative nuclei (VN), and egg cells (ECs) and classified the splicing events into four types: intron retention (IR), exon skipping (ES), alternative acceptor (AA), and alternative donor (AD). The most prevalent AS event in all three cell types was the alternative acceptor type, followed by intron retention in the VN and EC. In SCs, the second most prevalent form of splicing events was alternative donor. Exon skipping was the least abundant splicing event in all three cell types (Misra et al. 2023). The AS landscape in the sperms, VN, and ECs of monocot species rice and maize (Anderson et al. 2013; Chen et al. 2017) differed from the dicot datasets. Exon skipping was the most predominant form of splicing event in maize ECs and the second most prevalent in SCs, in contrast to both rice and Arabidopsis. Intron retention was the most predominant form of splicing event in the rice male germline, however alternative acceptor was the most predominant form of splicing event in ECs of rice, similar to what was observed in Arabidopsis (Misra et al. 2023).

Transcriptomic studies have demonstrated that a substantial number of splice isoforms show differential expression in various cell types (Klepikova et al. 2016, Li et al. 2016, Martín et al. 2021). One of the most noticeable features of AS is the capability to change the sub-cellular

localisation of the protein. The *RADIATION SENSITIVE 52* (*RAD52-1)* gene, required for the homology-dependent DNA double-strand break repair, encodes a *RAD52-1A* isoform with the last intron retained. RAD52-1A was shown to be localised to the nucleoplasm, while the full-length RAD52-1B isoform is targeted to mitochondria. The concurrent event in the near *RAD52-2* paralog gives rise to the RAD52-2A variant, present in both nucleoplasm and chloroplast, and RAD52-2B, detected exclusively in chloroplasts. Thus, AS controls the delivery of the RAD52 proteins (and DNA repair) between semiautonomous organelles and nuclei. The truncated alternative isoforms commonly show the ability to interfere with the canonical proteins. This has been particularly explored on transcription factors, which tend to form homo- or heterodimers (Seo et al. 2011a). CONSTANS or B-BOX DOMAIN PROTEIN 1 (CO or BBX1) is a transcription factor that regulates photoperiodic flowering by controlling the integrator gene *FLOWERING LOCUS T* (*FT*). Due to the retention of the only intron and premature stop codon presence, the alternative COβ variant lacks the *C*-terminal CCT domain responsible for binding DNA. COβ heterodimerises with the full-length COα isoform and prevents it from binding DNA. A high number of studies illustrate how minor truncated isoforms can interfere with the activity of the full-length proteins. This mode of action seems to be common in most eukaryotes (Jangi and Sharp 2014, Seo et al. 2011a). Removal of protein domains by AS typically reduces the number of interaction partners at least in half in animal systems (Rodriguez et al. 2020, Yang et al. 2016). Mathematical models of regulatory network motifs indicate that gene expression systems containing dominant-negative factors (here alternative isoforms) show faster response times following the signal stimulus. It can thereby represent a potent adaptation to the changing external or developmental cues (Alon 2007, Jangi and Sharp 2014). Numerous RNA-binding factors show the ability to bind their own transcript to induce AS, leading to the production of the variants that apparently remain untranslated, thus turning off their own expression (Schöning et al. 2008, Hartmann et al. 2018, Quesada et al. 2003). (reviewed in Kashkan et al. 2022).

1.4.3. Translational regulation

Translational regulation enables cells to quickly and reversibly modify gene expression in response to developmental and environmental signals. Translation can be regulated globally or at the gene-specific level. In plants, several mechanisms, such as the phosphorylation of

poly-A-binding proteins (PABPs) or specific eukaryotic initiation factors (eIFs), can globally enhance or repress translation (as reviewed by Browning and Bailey-Serres 2015). This is a common occurrence under severe stress conditions such as high salt (Matsuura et al. 2010), hypoxia (Juntawong et al. 2014, Sorenson and Bailey-Serres 2015), drought (Lei et al. 2015), heat stress (Matsuura et al. 2010, Merret et al. 2015, Matsuura et al. 2013), reactive oxygen species (Benina et al. 2015), and cold stress (Wang et al. 2017). In contrast, gene-specific translational regulation could be controlled by trans factors like RNA-binding proteins (RBPs), small RNAs, and metabolites or specific translation factors that recognise sequence or structure-based cis regulatory elements in their target mRNA (Ray et al. 2013, reviewed in Saajev et al. 2019).

1.4.3.1. RNA Binding Proteins (RBP)

DNA is the genetic blueprint for all organisms, controlling all life processes through intermediate RNA molecules that dictate the types and levels of proteins produced in cells. RNA molecules are associated with many proteins throughout their biogenesis to degradation. RNA-binding proteins (RBPs) are a diverse class of proteins that interact with RNAs. They are characterised by the presence of one or more RNA binding domains, usually alongside other catalytic or functional domains (Burjoski and Reddy 2021). During RNA synthesis, maturation, export to the cytosol, and translation, all RNAs are tightly bound and controlled by diverse RNA-binding proteins (RBPs). This allows RBPs to serve as master regulators of RNA fate (Cho et al. 2019). RNA-binding proteins interact with mRNAs to form dynamic multi-component ribonucleoprotein (mRNP) complexes, which regulate the functionality, processing, and production of proteins in eukaryotic cells. Proper formation of these complexes is crucial for precise regulation of transcripts in plant cells (Silverman et al. 2013). RNA-binding proteins interact with mRNA through a series of canonical RNA-binding domains, including the RNA recognition motif (RRM), which is one of the most abundant domains in eukaryotes (Juntawong et al. 2014). Other domains include the pentatricopeptide repeat (PPR) motif (Cruz and Westhof 2009), the K homology (KH) domain, zinc fingers, DEAD box helicase domains (Glisovic et al. 2008), and the Pumilio p-homology and Fem-3 mRNA binding factor (PUF) domain (Cho et al. 2019, Koster et al. 2022).

In Arabidopsis, it has been reported that nucleo-cytosolic RBPs are present and significant for post-transcriptional regulation. However, only a subset of these RBPs has been functionally characterised, with roles in flowering time, hormonal responses, pathogen defense, circadian timekeeping, and abiotic stress responses. As a result, plant RBP mutants may experience severe phenotypes or lethality. Several proteins play a role in pre-mRNA processing, including alternative splicing, 3'-end formation, pri-microRNA processing, and mRNA export (Koster et al. 2022).

1.4.3.2. mRNA Storage

Contrary to common expectations, functional mRNA is not necessarily recruited immediately into polysomes for translation, nor is it immediately degraded after leaving polysomes. Instead, it may remain elsewhere, waiting to be translated or re-translated. Several sets of data, using a wide array of tissues, have shown that less than 50% of the translatable mRNA is in the polysome fraction, indicating that the majority is not in polysomes (as reviewed in Davies et al. 2012).

Recruitment of different mRNAs into polysomes does not guarantee equal translation. Polysomes can be found in four cytoplasmic locations: free, membrane-bound, cytoskeleton-bound, or cytoskeleton-membrane-bound (Abe and Davies 1995, Davies and Abe 1995). The sub-cellular location of the polysome is a crucial factor in determining the eventual destination of the protein. Free polysomes primarily synthesise cytoplasmic proteins, while membrane-bound polysomes synthesise proteins for organelles or export. Cytoskeleton-bound polysomes synthesise cytoskeleton-associated (and other) proteins, and cytoskeletal membrane-bound polysomes synthesise storage (and other) proteins (reviewed in Davies et al. 2012).

Cytoplasmic mRNPs are classified into two categories: stored mRNPs or as polyribosomal-associated mRNPs (Minich and Obchinnikov 1992). The presence of stored, untranslated mRNAs is a common feature of animal embryo development (Li et al. 2010) as well as seed maturation and germination (Nakabayashi et al. 2005). Translationally active mRNPs are complexed with the 80S ribosome and associated RNA-binding proteins such as P1, P2 and

P3. Hundreds of RNA-binding proteins have been identified in plants capable of forming cytoplasmic mRNPs (Bailey-Serres et al. 2009).

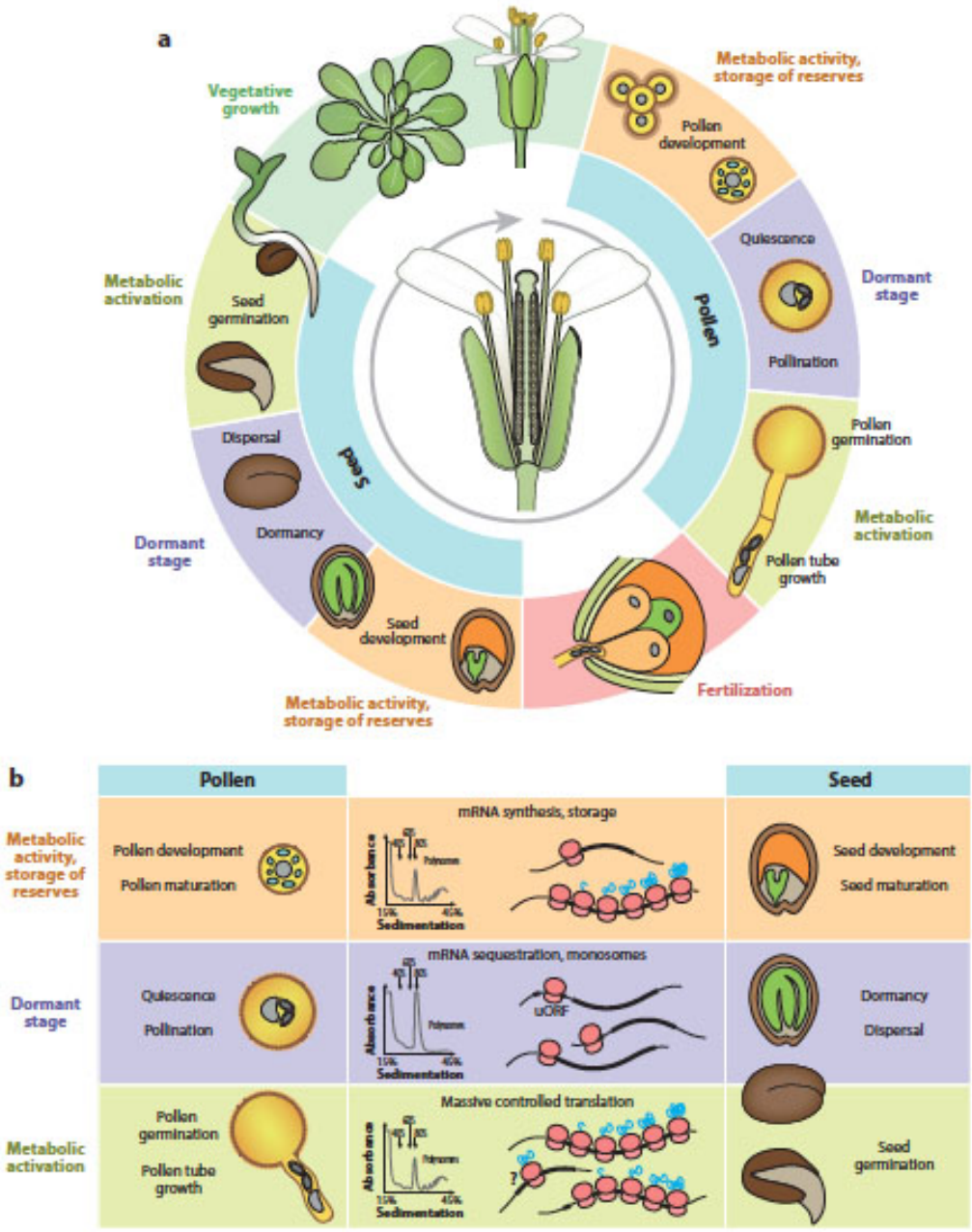

Figure 10. Translational and post-translational regulation in the seed and the male gametophyte. a) Simplified angiosperm life cycle highlighting the similar phases of pollen and seed development, including development, quiescence/dormancy, and activation, that are reflected in the accumulation, storage, and activation of mRNA reserves. b) Transcriptome and proteome analyses revealed that pollen and the pollen tube sequestrome comprised diverse mRNA populations that are highly dynamic between the actively translating polysomes and the sequestered monosome sub-fractions.

Abbreviations: mRNA, messenger RNA; RBP, RNA-binding protein; uORF, upstream open reading frame; UTR, untranslated region (Hafidh and Honys, 2021).

Stored/Long-lived mRNAs were first identified in cotton seeds in 1965 by Dure and Waters. These mRNAs accumulate during seed maturation and are known for their ability to remain translatable over extended periods of time, even under stress conditions. They are found in most angiosperms and are believed to be crucial for protein synthesis during seed germination (Galland et al. 2014, Kuligowski et al. 1991, Ishibashi et al. 1990). Stored mRNAs are important for protein synthesis not only in the early stages of germination but also in later stages, indicating their role in both early and late seed germination (Figure 10., Nakabayashi et al. 2005, Sano et al. 2012).

mRNP complexes, such as processing bodies (P-bodies, PBs) and stress granules (SGs), may act as protective shields for mRNAs in dry seeds. P-bodies and SGs are cytoplasmic molecular assemblies where mRNAs are either degraded or temporarily stored in response to internal or external stimuli (for reviews see Chantarachot and Bailey-Serres 2018, Davies et al. 2012, Weber et al. 2008). Translational repression leads to polysome disassembly, which causes mRNAs to be sequestered into translationally inactive mRNPs. Stress granules are one type of mRNPs that form in response to stress-induced inhibition of translation initiation. They act as triage centers for mRNA sorting to PBs to protect them from degradation (Protter and Parker 2016). These heterogeneous complexes are physically, compositionally, and functionally linked to processing bodies (Buchan and Parker 2009). mRNAs stored in SGs are usually capable of translation and can be reutilised once released (Chantarrachot and Bailey-Serres 2018). The P-bodies contain mRNA decay machinery and could serve as the degradation site for mRNAs remaining from the maturation program that are no longer required for germination (reviewed in Saajev et al. 2019).

Polysome profiling has demonstrated that mRNAs exhibit increased translation activity during germination in sunflower seeds, highlighting the significance of translation in this process (Layat et al. 2014). Additionally, Bai et al. (2017) recently discovered extensive transcript-specific translational control during seed germination. Polysome profiling revealed that thousands of mRNAs exhibit changes in ribosome association during two specific temporal phases of seed germination (Bai et al. 2017). These phases correspond to two

significant developmental transitions during seed germination: the hydration translational shift and the germination translational shift. The hydration translational shift is when the seed transitions from a quiescent dry state to a fully active metabolic state. The germination translational shift is when the seed commits to germination and reaches a point of no return in its developmental program. The most dominant gene groups under strong translational control belonged to the categories of seed storage, late embryogenesis, stress response, heat-shock protein, ABA- and auxin-response genes, cell-wall-related genes, ribosomal proteins, and metabolic genes (Bai et al. 2017, reviewed in Saajev et al. 2019).

1.4.3.3. RNA Storage in Pollen

The half-lives of different RNA messages within the same cell can range from less than 30 min to more than 1 day (Sachs 1993), implying that features of the mRNA contribute to stability. In animal reproductive cells, long-lived mRNAs are common. For example, in mammalian sperm and *Xenopus* oocytes, transcription stops before development is completed. Thus, many mRNAs must be pre-synthesised, but they are protected from degradation and premature translation because they are masked by proteins containing Y-box motifs (Tafuri et al. 1993, Wolffe 1994). Developmental cues or fertilisation subsequently leads to dramatic increases in protein synthesis due to recruitment of these masked mRNAs onto polysomes. In tobacco pollen, Ylstra and McCormick (1999) found many pollen-expressed mRNAs that were long-lived (more that 1 day), but they also identified some mRNAs undergoing decay during pollen maturation. Thus, they conclude that there is no overall cytoplasmic condition in pollen that stabilises mRNAs and specific mRNA turnover mechanisms must exist (Ylstra and McCormick 1999).

A number of pollen mRNAs were shown to accumulate in pollen-stored ribonucleoprotein (RNP) particles, which remain intact even in a buffer comprising strong detergents. This class of detergent-resistant RNP particles was annotated as EDTA/puromycin-resistant particles or EPPs (Honys et al. 2000). The identification of the EPPs in the tobacco male gametophyte highlighted the presence of germ cell-like granules in flowering plants. Honys, Reňák et al. (2009) isolated and characterised the proteome of EPPs and proposed that, during pollen maturation, the storage EPPs represent preloaded complex machinery devoted to mRNA

processing, transport, sub-cellular localisation, and protein synthesis. The discovery of the EPPs also supported the long-hypothesised presence of stored mRNP particles in developing tobacco male gametophytes (Honys et al. 2000, 2009). The physiological advantage of EPPs is that they are composed of mRNA sets that are stored and translationally silenced at earlier stages of development. This enables an immediate activation of translation of selected mRNAs during germination of the pollen grain and subsequent pollen tube growth (Honys et al. 2009, reviewed in Hafidh et al. 2018).

Hafidh et al. 2018 have reported that pollen and the pollen tube sequestrome constitute diverse mRNA populations that are highly dynamic between polysome and EPP sub-fractions in the course of pollen development and pollen tube growth. The distribution of a given mRNA in the polysomal profile can be used to assess its translation efficiency at a particular developmental stage. In general, higher translation rates can be expected as the transcript shifts from monosomal to polysomal fractions. Stalled 80S couples at the initiating AUG codon on various mRNAs represent a different class of fully assembled monosomes and may serve as a means of translational control (Hafidh et al. 2018). The authors analysed the mRNAs associated with polysomes and monosomes to measure translation efficiency (Hafidh et al. 2018). The results showed that mature pollen grains were dominated by monosomes, with very few polysomes present. However, after 4 hours of *in vitro* pollen tube growth, there was a significant increase in polysomal fractions at the expense of monosomes. This illustrates a rapid change from a nonactive to an active translational status that must inevitably occur in the growing pollen tubes. As pollen matures, the complexity of the transcriptome and translatome decreases, but there is an increased abundance of transcripts forming the sequestrome. The sequesterome reached its highest level in mature pollen. This observation is consistent with the general concept of reduced translation activity during this quiescent stage, accompanied by the storage of presynthesised transcripts (Mascarenhas 1993, Štorchová et al. 1994, Honys et al. 2000). According to Hafidh et al. (2018), the isolated EPPs are monosomes stalled on late-encoded transcripts in a translationally quiescent state.

Transcript sequestration and mRNA storage, regardless of the repression mechanism, do not completely block mRNA translation. Instead, they are post-transcriptional mechanisms that enable the modulation of protein abundance and long-term transcript storage to facilitate

immediate translation, particularly in tip growth. Stored transcripts are highly dynamic between sub-cellular compartments in both the long and short term, and their half-life within storage granules varies during development. In pollen tubes, EPPs likely facilitate immediate translation during tip growth and protect transcripts with late function from cytosolic 5′ to 3′ and 3′ to 5′ exonuclease activities (Łabno et al. 2016).

Transcript profiling in late stages of pollen tube growth revealed that approximately 6% of the EPP -stored transcripts at the 24-hr *in vitro* grown pollen tubes time point (a more than halfway growth of tobacco pollen tube toward the ovule) were expressed in sperm cells and some were sperm cell specific. It is likely that not all transcripts associated with sperm cells are utilised for sperm cell-related cellular activities before fertilisation. Some of these stored transcripts may be inherited and involved in embryogenesis. The inheritance of RNA via gametes in plants and its significance is still poorly understood; however, recent studies have shed light on its importance (view chapter on transcript inheritance and zygotic gene activation No. 4.3.).

Recently, studies of Arabidopsis seed translatomes have also revealed and characterised non-translating monosomes as the actual sites of mRNA storage in seeds (Bai et al. 2020, Basbouss-Serhal et al. 2015). Although the evolutionary origin and biological functions of pollen and seeds differ, both serve as dispersal units and share similarities in their biology, including an alternate desiccated dormant phase followed by rapid metabolic activation (Figure 10.). Pollen tube growth and seed germination are complex processes that require reserve mobilisation, protein synthesis, and the formation of new structures. One mechanism that facilitates these processes is the regulation of mRNA storage and the activation of massive translation upon hydration (as reviewed by Hafidh and Honys 2021).

2. RESULTS

2.1. Comprehensive analysis of tobacco pollen transcriptome unveils common pathways in polar cell expansion and underlying heterochronic shift during spermatogenesis

Said Hafidh, Katarína Breznenová, Petr Růžička, Jana Feciková, Věra Čapková and David Honys

BMC Plant Biology 2012, 12:24, doi: 10.1186/1471-2229-12-24

My contribution: When I started working in the Laboratory of Pollen Biology, newly obtained microarray data from tobacco mature pollen and in 4 hrs *in vitro*-grown pollen tubes were available. The focus was to identify and compare genes and their profiles in EPP (mRNA storage) granules vs. in actively translating monosomes after sub-cellular fractionation. I was given the task to find out the time-frame for second pollen mitosis (PMII), which occurs in tobacco after the pollen germination and during the pollen tube growth. Timed PT cultivation and microscopy led me to the finding that PMII occurs 10 hrs (+/- 2 hrs) after pollen germination (Fig. 1). Pollen tubes grown *in vitro* for extended time (13hrs, 24 hrs and 48 hrs, respectively) were then collected to extend the scope of study even after PMII. Multiple candidate genes were selected based on their transcription profiles in the studied microarray categories and I helped to verify these results using qRT-PCR (Fig. 2, Fig. 5). Based on these results, we decided to extend the microarray dataset with the 24-hrs grown *in vitro* tobacco pollen tubes and published the obtained results in Hafidh et al. 2012b. Both of these publications served as a starting point for the selection of my genes of interest that I present in this thesis.

BMC Plant Biology

RESEARCH ARTICLE Open Access

Comprehensive analysis of tobacco pollen transcriptome unveils common pathways in polar cell expansion and underlying heterochronic shift during spermatogenesis

Said Hafidh[1], Katarína Breznenová[1], Petr Růžička[1], Jana Feciková[1], Věra Čapková[1] and David Honys[1,2*]

Abstract

Background: Many flowering plants produce bicellular pollen. The two cells of the pollen grain are destined for separate fates in the male gametophyte, which provides a unique opportunity to study genetic interactions that govern guided single-cell polar expansion of the growing pollen tube and the coordinated control of germ cell division and sperm cell fate specification. We applied the Agilent 44 K tobacco gene chip to conduct the first transcriptomic analysis of the tobacco male gametophyte. In addition, we performed a comparative study of the Arabidopsis root-hair trichoblast transcriptome to evaluate genetic factors and common pathways involved in polarized cell-tip expansion.

Results: Progression of pollen grains from freshly dehisced anthers to pollen tubes 4 h after germination is accompanied with > 5,161 (14.9%) gametophyte-specific expressed probes active in at least one of the developmental stages. In contrast, > 18,821 (54.4%) probes were preferentially expressed in the sporophyte. Our comparative approach identified a subset of 104 pollen tube-expressed genes that overlap with root-hair trichoblasts. Reverse genetic analysis of selected candidates demonstrated that Cu/Zn superoxide dismutase 1 (CSD1), a WD-40 containing protein (BP130384), and Replication factor C1 (NtRFC1) are among the central regulators of pollen-tube tip growth. Extension of our analysis beyond the second haploid mitosis enabled identification of an opposing-dynamic accumulation of core regulators of cell proliferation and cell fate determinants in accordance with the progression of the germ cell cycle.

Conclusions: The current study provides a foundation to isolate conserved regulators of cell tip expansion and those that are unique for pollen tube growth to the female gametophyte. A transcriptomic data set is presented as a benchmark for future functional studies using developing pollen as a model. Our results demonstrated previously unknown functions of certain genes in pollen-tube tip growth. In addition, we highlighted the molecular dynamics of core cell-cycle regulators in the male gametophyte and postulated the first genetic model to account for the differential timing of spermatogenesis among angiosperms and its coordination with female gametogenesis.

Background

Polarized extension of the pollen tube to deliver twin sperm cells to the female gametophyte is a fundamental process required for successful sexual reproduction and preservation of the floristic dominance of flowering plants. Understanding sexual reproduction is at the forefront of plant research and has benefited immensely from the development of genomic, transcriptomic and proteomics techniques in recent decades. Advances in microarray technology and development of gene chips for Arabidopsis, rice and other species have allowed studies on large-scale transcriptional profiling from diverse tissues, which has emerged as a key tool for identification of novel targets for functional genomics.

As in other angiosperms, the tobacco (*Nicotiana tabacum*) male gametophyte is formed within the anthers following meiotic division of the archesporial

* Correspondence: honys@ueb.cas.cz
[1]Laboratory of Pollen Biology, Institute of Experimental Botany, Academy of Sciences of the Czech Republic, Rozvojová 263, 165 02 Praha 6, Czech Republic
Full list of author information is available at the end of the article

BioMed Central

© 2012 Hafidh et al; licensee BioMed Central Ltd. This is an Open Access article distributed under the terms of the Creative Commons Attribution License (http://creativecommons.org/licenses/by/2.0), which permits unrestricted use, distribution, and reproduction in any medium, provided the original work is properly cited.

sporophytic cells to produce haploid microspores [1]. Thereafter, only two mitotic divisions occur. The first pollen mitosis (PMI) involves division of the haploid microspore to produce a gametic germ cell and a vegetative cell. These two cell types differ not only in the quantity and diversity of expressed transcripts [2,3], but also, crucially, in their fate. Whereas after pollen tube germination the germ cell undergoes a second mitotic division (PMII) to produce two male gametes (sperm cells), the vegetative cell adopts a different fate and acquires the critical task of ensuring growth of the pollen tube. At the stigma surface, the pollen tube germinates and penetrates the female stylar tissues to deliver the two sperm cells to the proximity of the egg and central cell for double fertilization. Among flowering plants, the production of sperm cells after pollen germination represents the ancestral pattern. However, over 30% of angiosperms, including *Arabidopsis thaliana*, complete the second division before pollen maturation [4,5]. No explanation has been proposed for the mechanisms that have imposed this regulon prompting differential timing in sperm cell proliferation in the male gametophyte of seed plants, nor have the evolutionary benefits of early gamete production been elucidated. Independent analysis of sperm cell DNA content revealed five patterns of sperm-cell development that differ with respect to relative timing of sperm-cell formation and maturation prior to fusion with the female gametes [5,6].

Pollen-tube germination represents a unique cellular phenomenon. The pollen tube grows through the female tissues in a polarized fashion similar to root-hair outgrowth, trichome specification, hyphal growth in fungi and extension of neuronal dendrites in the animal nervous system [7,8]. Thus, common factors are likely to be involved in the raw molecular cascades that initiate and control the single cell-tip expansion and morphogenesis, which are subsequently modulated by cell- or tissue-specific morphological demands. Studies using pollen tubes and root hairs as model systems have revealed a number of signaling molecules and regulatory pathways that promote and maintain the tip-growth characteristic. Recently, a study by Qin et al. [9] revealed a specific subset of genes that are induced in pollen tubes during growth through the pistil, but not when grown in vitro. Among this set of genes are potential receptor proteins that may respond to female cues for guidance of the pollen-tube tip growth. Collectively, these experiments demonstrated the direct dependence of cell-tip expansion on polarized exocytosis of vesicles at the apical growth region of the cell. Vesicular trafficking to the tip region is a structural requirement for tip growth and plays a significant role in feedback regulation of the tip-localized signaling to maintain the apical cell expansion [10].

Until recently, no major studies had analyzed the bicellular pollen transcriptome, with the sole exception of soybean (*Glycine max*) [11]. A first glimpse into the tobacco pollen transcriptome was reported by Xin and co-workers [12], who constructed an EST library from isolated tobacco sperm cells. This project aimed to identify proteins involved in sperm-egg recognition and fusion and identified over 1,864 EST sequences distributed in more than 1,050 clusters. This analysis discovered paternal candidate genes that could play a role during fertilization and in the early stages of embryogenesis. However, the sperm cell transcriptome alone represents only a small proportion of the total pollen-expressed transcripts and, although EST sequencing is sensitive, it provides only a limited list of expressed genes and thus minimizes comprehensive functional downstream analyses [3,12-14].

In the present study, we capitalized on the recent development of the Agilent 44 K tobacco microarray to present the first insight into tobacco pollen and pollen-tube transcriptomes, which represents a contrary experimental model from the tricellular pollen of Arabidopsis to a bicellular model of scientific, medical and commercial interest. In addition to broad-spectrum gene expression profiling, we performed a comparative analysis of the transcriptomes of tobacco pollen tubes and Arabidopsis root-hair trichoblasts [15-17] to uncover common pathways involved in polar cell expansion. To investigate their potential role in tobacco pollen-tube growth, we used gene ontology (GO) tools to allocate their biological roles, and applied an antisense-transfection approach to verify the function of selected candidate genes.

We further explored our data set to elucidate the control of male germ-cell proliferation and sperm-cell formation from a molecular perspective. In angiosperms, heterochronic alterations in cell cycle activity led to the developmental shift in the timing of germ-cell division and resulted in diversified patterns of spermatogenesis and gamete fusion during fertilization [4-6]. To elucidate the genetic network responsible for this shift among angiosperms, we investigated the expression of core cell-cycle repressors and activators at five stages of pollen development–namely, mature pollen and in vitro-germinated pollen tubes grown for 4, 13, 24 and 48 h - following completion of the germ cell mitotic division. On the basis of these results, we postulated a genetic model in which the male germ cell-cycle progression is coordinated with 'time to fertilization'.

The tobacco pollen and pollen-tube gene expression profiles generated in this study together with our analyses provide an ideal platform for future research into aspects of polarized cell expansion and control of spermatogenesis. In addition, cataloguing the expressed

genes will provide an opportunity for development of gametophytic fluorescent markers with which cell behaviour and cell fate can be studied. The present study represents a step towards a comprehensive understanding of male gametogenesis, knowledge of which will provide an effective framework to improve current farming and breeding programs to sustain food requirements and for investigation of tobacco health implications.

Results

Application of the Agilent 44 k tobacco microarray to the *Nicotiana tabacum* male gametophyte transcriptome

In an effort to understand the diversity of gene expression accompanying bicellular tobacco pollen maturation and transcriptional changes with progamic phase induction, we applied tobacco microarray technology (imaGenes, Berlin, Germany) and performed comparative microarray analysis at two time points of male gametophyte development: mature pollen grains (MPG), and in vitro-germinated pollen tubes grown for 4 h (PT4). Tobacco mature pollen is bicellular when shed (Figure 1a), and is predicted to have a unique set of transcripts that are over- and under-represented in reference to phylogenetically advanced tricellular pollen. Pollen tubes grown for 4 to 48 h in vitro were used to verify the microarray expression by real-time quantitative RT-PCR (qRT-PCR) and to establish expression patterns of core cell-cycle regulators (Figure 1b, c). Two other tissue samples - leaves (L) and roots with substantial root-hair outgrowth (R) - were used as sporophytic references. The pollen grains were collected from tobacco plants grown in an outdoor greenhouse, so we investigated the possible effect of variable weather conditions on pollen-tube germination. Overall, no significant variation in pollen-tube germination rate or length throughout the harvesting period was observed (Figure 1d).

Normalized expression values (see Materials and Methods, Additional files 1 and 2: Figure S1a and Table S1) were used to perform cross-tissue comparisons for identification of preferentially expressed genes. To test the quality of the arrays, we stringently assessed our data sets to justify their reproducibility among replicates, and thus provide a feasible comparison between individual tissues. We used principal component analysis (PCA) and independently applied hierarchical clustering to visualize the relationship among the tissues as well as between biological replicates. The uniqueness of gametophyte versus sporophyte gene expression profiles was verified, together with the reproducibility between sample replicates (Additional file 1: Figure S1b). Scatterplots were used to visualize the distribution of p-values for individual probes relative to each other and in relation to the mean expression values. A close relationship between replicates and among tissues of similar origin was observed, whereas great variability in relation to disparate tissues was verified (Additional file 1: Figure S1c). Intensity-dependent-ratio (MvA) -derived values of array-array intensity independently supported the intra- and inter-relationships observed. Overall, the obtained normalized expression arrays were confirmed as being of good quality for downstream comparison.

We selected nine candidate genes to verify their microarray expression profiles by real-time qRT-PCR at the two developmental stages used for microarray analysis (MPG and PT4) and extended the analysis to three developmental stages post-PMII (13, 24 and 48 h after in vitro pollen germination). For all genes tested, with the exception of RAB GTPase and WD40 motif-containing protein (BP130384), qRT-PCR profiles corresponded to those of the microarray (Figure 2). The extended analysis of post-PMII stages provided additional information not obtained by microarrays to understand gene expression and mRNA stability in relation to gene function in the course of pollen-tube extension.

Comparative analysis of the tobacco male gametophyte and sporophyte transcriptomes

Soma-derived tissues constitute a transcriptome that is distinct from that of gametophytes, and thus provide a good reference point to classify genes that are preferentially expressed in the male gametophyte. For systematic comparison of the four tissue samples, only a subset of reliably expressed genes were considered for analysis (see Materials and Methods). On the basis of this criterion, 13,966 probes from MPG (40.3% of expressed genes), 14,100 from PT4 (40.7%), 27,869 from L (80.5%) and 27,589 from R (79.7%) were selected and classified as reliably expressed. A previous analysis of the tobacco transcriptome that utilized 40 k custom-designed Affymetrix microarrays reported reliable expression of 76% of the probe sets in 19 different tobacco tissues, including leaves and roots [19]. We examined the extent of overlap between individual arrays. As anticipated, MPG shared the greatest number of expressed genes with PT4 in comparison with leaves or roots (Figure 3a). The inverse was true between the sporophytic tissues, with > 16,566 (56%) transcripts being exclusive to the sporophyte and shared between leaves and roots (Figure 3a). A detailed examination at the biological significance of these co-expressed genes is discussed below.

When the average of the eight arrays were combined into sporophyte and gametophyte 'master lists' of expressed genes, the reduced complexity of the gametophyte was apparent, with 5,161 probes (14.9% of expressed transcripts) putatively male gametophyte-specific and active in at least one developmental stage. This was significantly less than the analogous value for genes exclusive to sporophytes (18,821 probes, 54.4% of expressed transcripts). The contribution of both MPG and PT4 to the

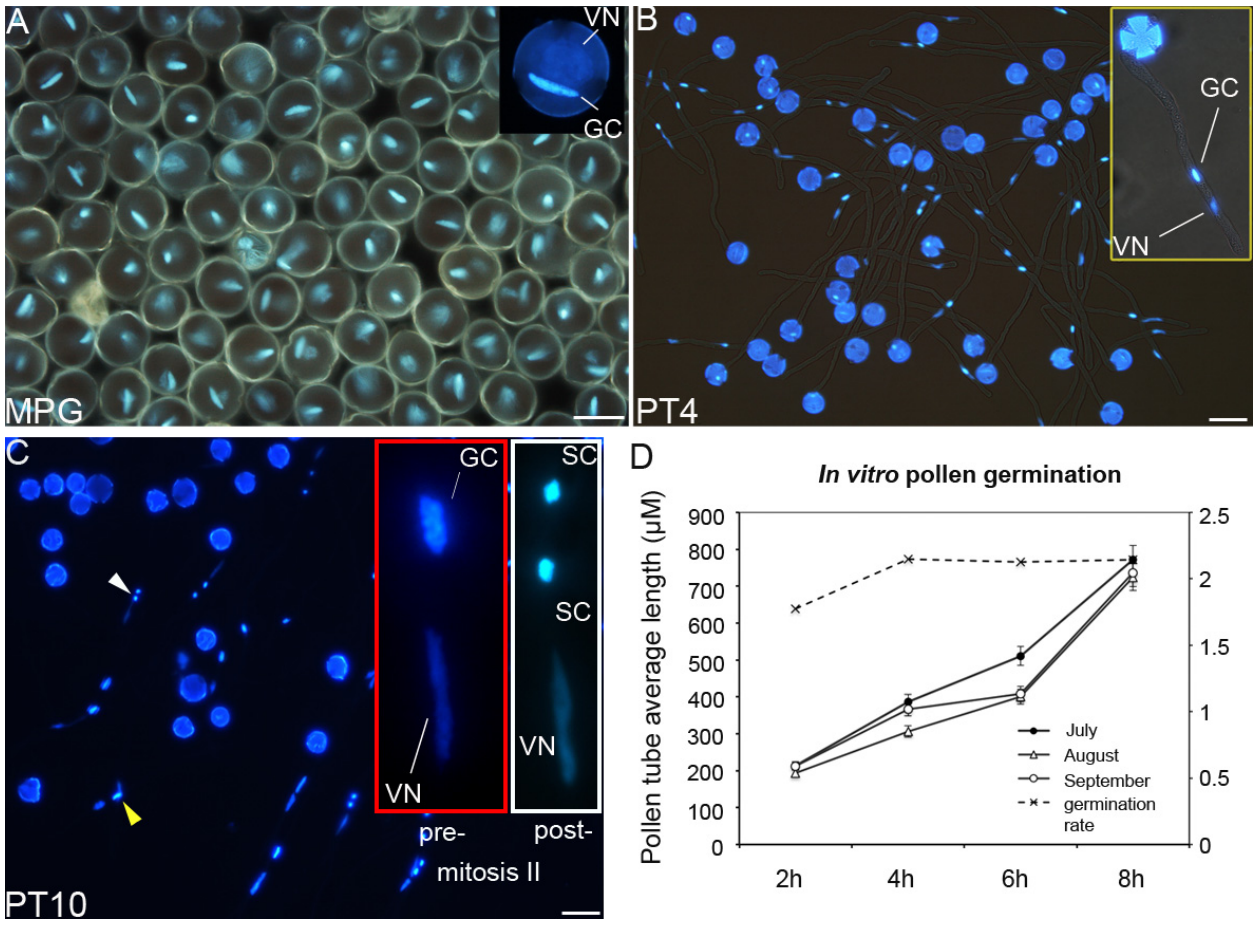

Figure 1 Tobacco pollen and pollen tubes used for comparative transcriptomic analyses. (**a**) Pollen from stage six of male gametophyte development [18], representing mature bicellular pollen with fully elongated germ cell (GC) alongside vegetative nucleus (VN), inset. Scale bar = 40 μM. (**b**) Pollen tubes cultivated in vitro for 4 h still at the bicellular stage. Scale bar = 60 μM. (**c**) Pollen tubes cultivated in vitro for 10 h with mixed population of premitotic germ cells (red inset) and those with newly formed sperm cells, SC (white inset). Scale bar = 60 μM. (**d**) Analysis of pollen-tube germination rate and length of pollen grains used in this study that were harvested at different times during the summer period. No significant differences in pollen fitness were observed, irrespective of time of collection.

male gametophyte-specific subset was similar, with only 544 and 630 probes exclusive to MPG and PT4, respectively (Figure 3a and Additional file 3: Table S2). This marginal, but significant, change in the pollen-tube transcriptome signified a subtle difference with respect to the diversity of the two transcriptomes and a less significant induction of newly transcribed genes on initiation of the progamic phase. Our results coincide with changes in gene expression observed in Arabidopsis pollen and pollen-tube transcriptomes [9,13], which emphasized that regulation of overall gene expression is similar in species with bicellular and tricellular pollen.

Gene enrichment analysis provides valuable information for prediction of biological functions of gene subsets and dominant pathways imposed in the tissue of interest. We applied a statistical *t*-test on the quantile-normalized $\log_2$-transformed array data and selected only genes that fulfilled the following criteria: for a gene to have undergone a significant change in expression, a probe must have (1) a *p*-value ≤ 0.05; (2) passed a false discovery rate (FDR) correction to minimize the FDR [20]; (3) an absolute expression signal (fold change) of ≥ 3 (up- or down-regulated); and (4) expression levels of > 100 (arbitrary cut-off). A moderate number of genes (830; 5.3% of male-gametophytic genes) had undergone a significant change in expression between MPG and PT4 (Figure 3b, c and Additional file 4: Table S3). Interestingly, the MPG transcriptome was 11.2% and 10.9% less diverse than the PT4 transcriptome with respect to changes in gene expression when compared with leaves and roots, respectively (Figure 3b, c). For other pairwise analyses, see Additional files 5: Table S4, Additional files 6: Table S5, Additional files 7: Table S6, Additional files 8: Table S7, Additional files 9: Table S8.

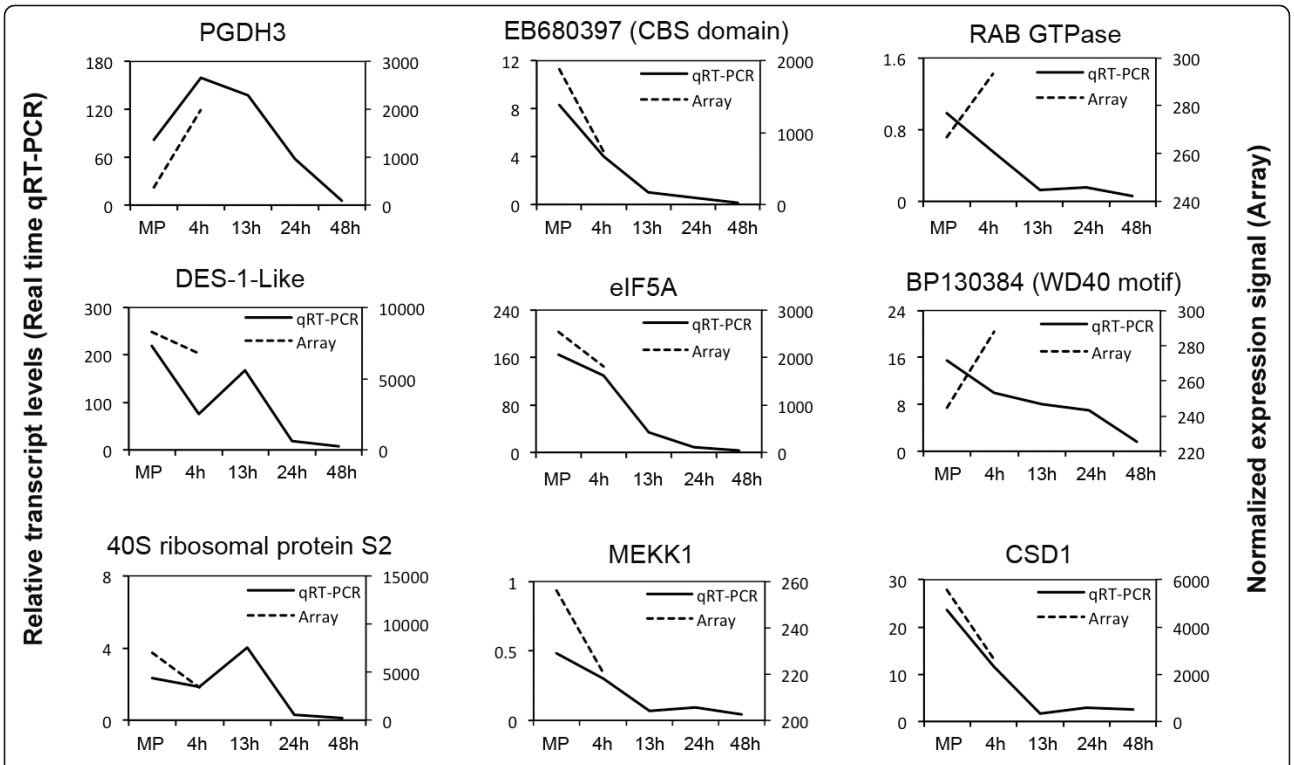

Figure 2 Quantitative RT-PCR validation of microarray gene expression. Relative expression levels of selected genes determined at mature pollen (MP) and at four stages of pollen-tube growth (4, 13, 24 and 48 h of cultivation). On the secondary axis, corresponding normalized expression signal at two pollen stages (MP and PT4) derived from microarray chip hybridization. The tobacco 18S RNA gene was used to normalize obtained Ct values to compute relative expression levels at each stage of the pollen gametophyte development.

We determined whether any GO terms were significantly over-represented among the gametophytic preferentially expressed genes compared with those of the sporophytes. The over-represented GO terms in the gametophyte included those related to localization (GO biological process, p = 2.3e-11), transporter and structural molecule activities (GO molecular function, p = 1.2e-06 and p = 4.4e-16, respectively), as well as membrane-enclosed lumen (GO cellular component, p = 9.4e-06) (Figure 3d). The GO categories related to transporter activities (GO molecular function, p = 0.0016), calmodulin binding (GO molecular function, p = 0.019) and the macromolecular complex (GO cellular component, p = 5.4e-4) were among the most over-represented in mature pollen compared with pollen tubes (Figure 3e). Over-representation of these categories in mature pollen, particularly calmodulin protein binding [21,22], may facilitate pollen competence in preparation for initial phases of pollen-tube germination.

Pollen-tube transcriptome shares a distinct set of genes with roots and root hairs

The characteristic tip growth of a pollen tube shows a common physiology with other polar-growing tissues such as root hairs, trichomes and neuronal axons in animals [23]. We investigated the extent of overlap with the list of genes from Arabidopsis that were either functionally verified to be critical for root-hair development or conferred putative root-hair-specific *cis*-elements (RHE) within their promoters [11,15,16], and references therein]. These motifs were defined by combination of *in silico* (Patmatch Analysis Tool, http://www.arabidopsis.org/cgi-bin/patmatch/nph-patmatch.pl;) and experimental screens that produced an initial list of 904 genes with the consensus RHE element [15]. Although this list was derived from a root-hair-specific transcriptome, the role of the identified genes was not necessarily confined to root-hair morphogenesis. We extended our analysis with the compilation of Cvrčková et al. [16], who gathered a list of genes that had either a root-hair-defective phenotype, root-hair-specific expression and/or were known to have a role in pollen-tube tip growth. This accounted for 73 genes in total [16].

First, we identified genes that overlapped between PT4 and the root transcriptomes of the present study and compiled a set of 9,812 genes (denoted PT4R, Additional file 10: Table S9). To obtain a meaningful and direct evaluation of common pathways involved in tip growth, the PT4R list was filtered further to leave genes with closest Arabidopsis homologs only (e = < 10^{-10}

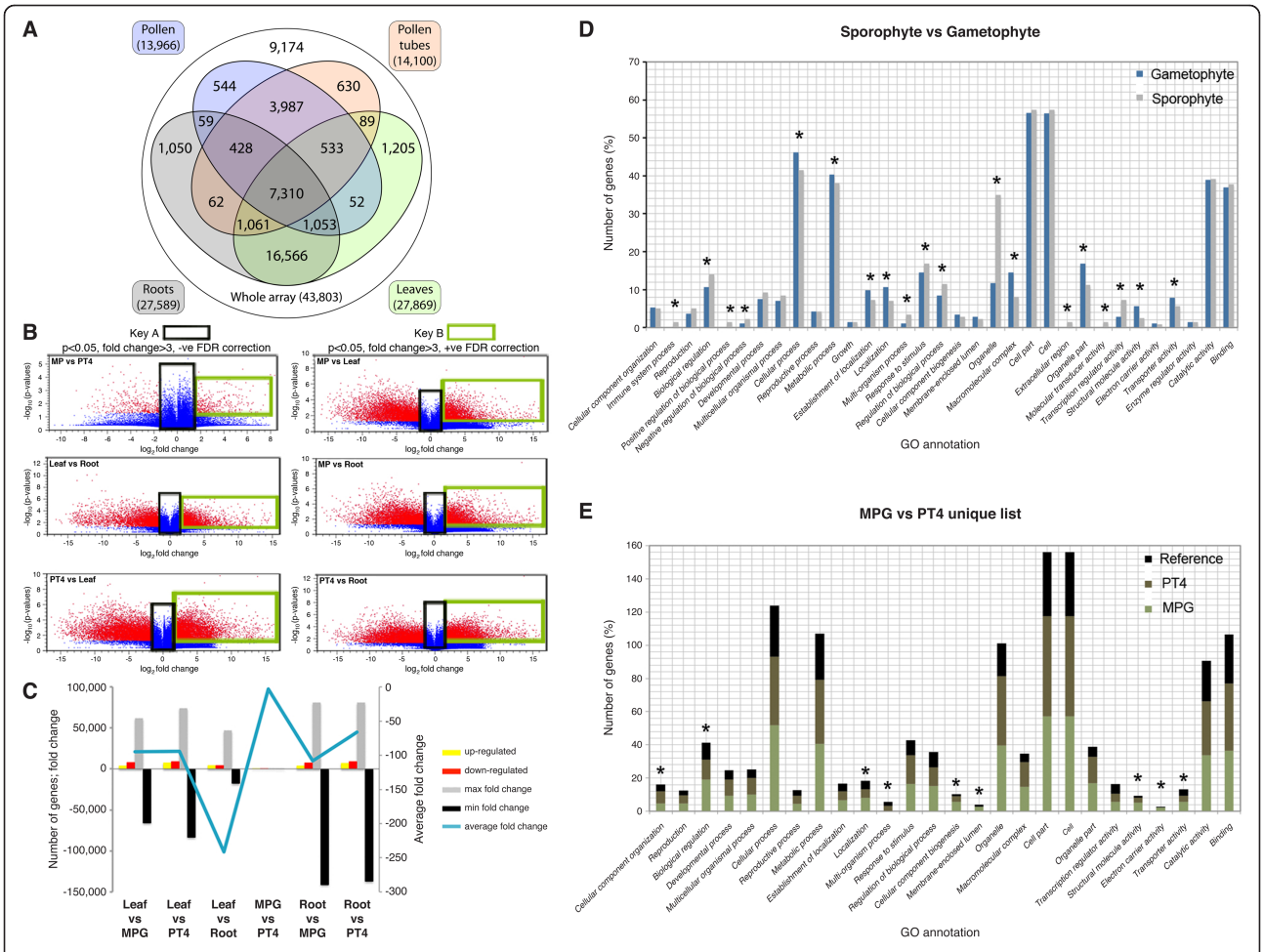

Figure 3 Differential gene expression and over-represented GO terms between the gametophyte and the sporophyte transcriptomes. (**a**) Quantification of gametophytic-gametophytic, gametophytic-sporophytic and sporophytic-sporophytic overlaps of transcriptome profiles. Four-way Venn diagram showing all 15 possible overlaps between four independent transcriptome datasets. For each sample, the total number of expressed genes is given in parentheses, together with the total number of unique probes harboured on the array (Whole array). The 9,174 probes were not reliably expressed in any tissue. (**b**) Volcano plot showing pairwise analysis of differentially expressed genes computed through statistical *t*-test of the normalized data. The plot shows differences between the means of the two analysed samples on the x-axis and -$\log_{10}$ *p*-values on the y-axis. Probe sets that passed the set criteria (see Materials and Methods section) are highlighted in red (differentially expressed genes), and blue spots represent total probe population. (**c**) Summary of differentially expressed genes following two-way comparison. (**d**) Relative percentage of genes of selected GO categories that were significantly over-represented between the sporophyte and gametophyte transcriptomes. (**e**) Over-represented GO terms of MPG- and PT4-enriched genes not expressed in any sporophytic tissue analyzed. Asterisks indicate GO categories that were significantly different ($p < 0.05$).

[19]) (3,264 genes). We designated this subset as PT4R_ATH (Additional file 11: Table S10).

The PT4R_ATH subset was used to screen for overlap with the root-hair transcriptome and proteome [15,16]. We detected 78 genes (8.6%) from the 904 RHE-patched genes that overlapped with the tobacco PT4R_ATH transcriptome, and an additional 26 genes (35.6%) from the list of Cvrčková et al. Collectively, this represented 104 genes (Additional file 12: Table S11). Additional genes with a known function in tip growth were manually selected either without a significant Arabidopsis homolog and/or their expression was confined to 4 h pollen tubes (not reliable in root and root-hair transcriptomes) (Additional file 12: Table S11). Our approach led to identification of genes with a known function in pollen-tube and/or root-hair-cell expansion, as well as novel targets that potentially could play a significant role in polarized cell growth. Several specific targets emerged including: a WD-40 repeat family protein; a RAC GTPase activating protein; a microtubule motor protein; a CBS domain-containing protein; translation initiation factor 5A (eIF-5A); replication factor C1 (AtRFC1); members of the VILLIN and FIBRIN protein families; and copper/zinc superoxide dismutase 1 (CSD1).

To emphasize molecular networks that facilitate polar cell expansion, we investigated GO categories over- or under-represented in the subset of 104 pollen-tube/root-hair overlapping genes. We identified 18 over-represented GO terms, including those associated with transport, cellular component organization, response to stimulus, and nutrient reservoir activity, whereas the GO term 'binding' (ion binding) was under-represented (Additional file 13: Table S12). Highly over-represented subcategories included those associated with chromatin modification (p = 0.01, n = 4), translation (p = 0.03, n = 4), protein transport and turnover (p = 0.013, n = 3), *cis*- and *trans*-Golgi networks, retrograde vesicle-mediated transport, and genes associated with GTPase activities (p = 0.003, n = 3), signal transduction (p = 0.004, n = 9), microtubule and cytoskeleton organization (p = 0.014, n = 3), and cell fate and cell morphogenesis (p = 4.15e-05, n = 5). Several of the identified GO terms have been implicated in pollen-tube and root-hair polarized growth [9,13]. In particular, genes involved in chromatin remodeling and transcription, signal transduction and transport previously were reported to be over-represented in pollen tubes that had grown semi-in vivo through the pistil and could thus mediate pollen-tube growth and guidance through the style [9].

Functional verification of pollen-tube and root-hair overlapping candidate genes using a reverse genetic approach

Five candidate proteins were selected for functional analysis on the basis of their expression profile, GO category, relevance and novelty. Three candidates were identified among GO categories over-represented in the overlap between the pollen-tube and root-hair transcriptomes: Cu/Zn superoxide dismutase 1 (CSD1; GO reactive oxygen species metabolic processes); replication factor C1 (NtRFC1; GO binding); and WD-40 containing protein PD40 (GO intracellular processes, subcategory CUL4-RING ubiquitin ligase complex). The fourth candidate, NTP303 (SKU5-like putative copper oxidase; GO oxidoreductase activities [24]), was selected as the most abundant tobacco pollen-tube wall glycoprotein [25] that is massively translated throughout pollen-tube growth [26] and with predicted important function(s). Finally, eukaryotic translation initiation factor eIF5A (GO primary metabolic processes) was selected as a constitutively expressed protein and a component of the translation machinery during pollen-tube growth.

We used the transfection reagent Cytofectin [27,28] to feed growing pollen tubes with antisense oligonucleotides designed against a target gene. Transfection techniques and microinjection for the introduction of antisense oligonucleotides as well as siRNAs mimic the transfection of *C. elegans* and mammalian cell lines with RNA interference (RNAi) sequences [29,30]. The techniques have been used to demonstrate gene function in tobacco and lily pollen tubes [31,32].

Transfection with anti-eIF5A and anti-NTP303 does not impair pollen-tube growth

Eukaryotic translation initiation and elongation factors have been implemented in various cellular processes, including cell division, cell growth and cell death [33], as well as in plant response to iron deficiency [34]; eIF5A served as a general, non-specific control. No significant difference in pollen-tube length or morphology was observed between wild-type sense- or antisense-transfected pollen tubes after 4 h of pollen-tube cultivation (n = 254, two-tailed Wilcoxon Mann-Whitney U test [U test hereafter], $p > 0.05$, U = 2932, Figure 4b). With reference to pollen germination dependency on translation [35], we propose a likely redundancy with other translation initiation factors.

The rapid extension of the growing pollen tube is predetermined by the biosynthesis and delivery of pollen tube wall material. NTP303 encodes a 69-kDa glycoprotein [37] assigned a putative function as copper ion oxidoreductase (UniProtKB/TrEMBL, accession B6U720) with predicted localization in the vacuole and chloroplast (WoLFPSORT score = 5 and 4), with a probability of being extracellular (SubLoc RI = 1, Accuracy = 56%). Our attempt to deplete NTP303 gene expression with antisense oligonucleotide transfection resulted in no apparent perturbation of pollen-tube growth or any pleiotropic morphological defects (n = 151, U test, $p > 0.05$, U = 309) (Figure 4b).

Anti-PD40 induced knockdown displayed severe pollen-tube growth arrest

We investigated the putative role of BP130384 (Arabidopsis homolog AT5G67320), here annotated as PD40 (**P**ollen tube **D**efective WD-**40**), a WD-40 containing protein with predicted nuclear localization (WoLFPSORT score = 8; SubLoc RI = 1, Accuracy = 56%). WD-40 domain-containing proteins are known to be involved in protein-protein interactions that facilitate key developmental processes [38]. Transfection of germinating pollen grains with PD40-antisense oligonucleotides severely perturbed pollen-tube growth (Figure 4c). On average, 36% of PD40 antisense-treated pollen tubes were significantly shorter (n = 252, U test, $p < 0.001$, U = 4694.5) than the average length of the wild-type or sense-treated pollen tubes (Figure 4c, d). Apart from stunted growth, no other morphological abnormalities were observed. Recently, the role of WD-40 proteins as substrate receptors for CUL4-RING E3 ubiquitin ligases has been demonstrated in Arabidopsis and rice [39]. To date, a stand-alone model that involves WD-40 proteins is that of root-hair and trichome specification composed of a WD-40 protein TRANSPARENT TESTA

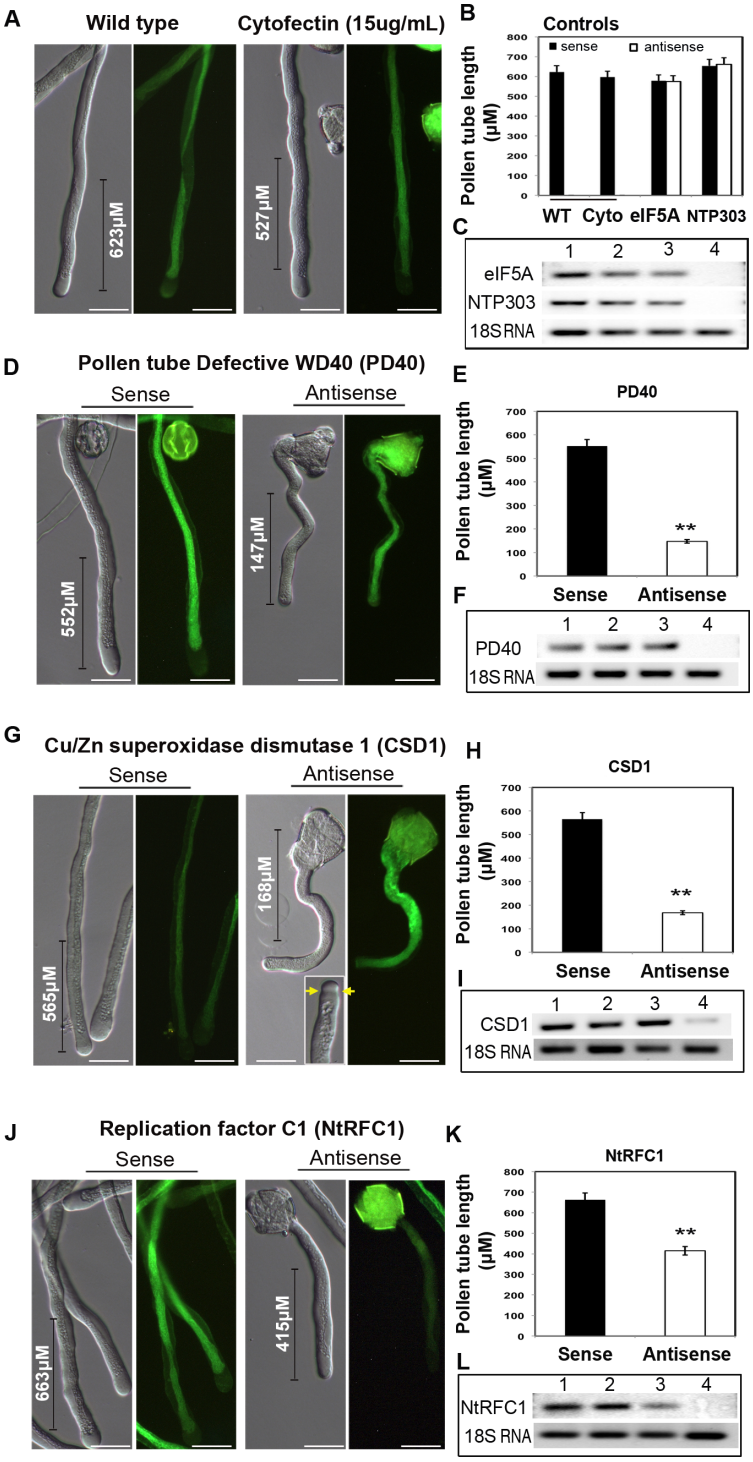

Figure 4 Antisense knockdown of candidate genes with putative role in polarized pollen-tube tip expansion. All samples were observed with differential interference contrast (DIC, left panel) and fluorescence microscopy (right panel). The NtpSF3-Lim2a:GFP construct, an actin-cytoskeleton marker [36], was used to monitor possible defects in cytoskeleton organization. (a) Wild-type control and cytofectin-treated pollen tubes. (b) Quantitative analysis of mean pollen-tube length (± SEM) from NTP303 and eIF5A control. Lower panel; semi-quantitative RT-PCR analysis was used to determine transcript levels in each treatment. 1: wild-type control 2: cytofectin-treated pollen tubes; 3: sense-transfected pollen tubes; 4: antisense-transfected pollen tubes. The same numbers key is used for panels (d), (f) and (h). (c, d) Aberrant pollen-tube growth following PD40 knockdown with significant reduction in pollen-tube length ($p < 0.001$), however with no evident defect in cytoskeleton biogenesis or organization. (e, f) Severe pollen-tube growth defects and occasional abnormal tip morphology (inset, yellow arrows) following CSD1 knockdown. Pollen tubes were significantly shorter ($p < 0.001$), with 'hook-like' morphology generated immediately after the initiation of germination. (g, h) Less severe but significant ($p < 0.01$) reduction in NtRFC1-depleted pollen-tube growth. Moderate reduction in transcripts levels were also observed in sense-treated pollen tubes, although this was not reflected by alterations in the pollen-tube phenotype. Scale bar = 20 µM.

GLABRA1 (TTG1), bHLH transcription factor GLABRA3 (GL3) and two MYB proteins, WEREWOLF (WER) and CAPRICE (CPC), that together impose position-dependent patterning of root-hair specification [40-42]. Our observation places an emphasis on the significance of protein turnover and recycling during polarized cell growth.

CSD1 deficiency exhibits a complete block of pollen-tube extension as well as pollen-tube tip morphology

To determine whether our overlapping candidates with predicted role in the regulation of reactive oxygen species (ROS) also play a role in tip growth, we investigated CSD1, an apoprotein of Cu-Zn superoxide dismutase with a known function in ROS detoxification [43]. Recently, CSD1 was demonstrated to be regulated by miR398 at the transcription and translation levels in response to copper availability [44]. We established that CSD1 is cytosol-localized (WoLFPSORT score = 14; SubLoc RI = 3, Accuracy = 84%). Antisense knockdown of CSD1 resulted in stunted pollen tubes with an average length of 168 μM, which was significantly shorter than that of control samples (n = 251, *U* test, $p < 0.001$, U = 4511) (Figure 4e). Approximately 33% of the population displayed the aberrant pollen-tube phenotype (Figure 4f). A small proportion of the pollen tubes (3.4%, n = 91) showed abnormal swollen tips that were not observed in CSD1-sense transfected pollen tubes nor in wild-type pollen tubes (Figure 4e inset). The influence of ROS dynamics on pollen-tube tip morphology has been demonstrated repeatedly and has conclusively highlighted the function of ROS at the apical dome of the germinating pollen tube [10,17]. Our discovery that depletion of CSD1 compromises pollen-tube growth further extends our knowledge of polar cell expansion, and it is likely to have a similar role during root-hair specification and morphogenesis.

NtRFC1 knockdown induces partial block of pollen-tube germination

The DNA replication factor C1, NtRFC1 (*Nicotiana tabacum* NCBI accession DW003643, Arabidopsis homolog AT5G22010) mediates genomic stability and transcriptional gene silencing in Arabidopsis [45]. NtRFC1 was predicted to localize in the nucleus (WoLFPSORT score = 12; SubLoc RI = 5, Accuracy = 94%). Pollen germination in the presence of NtRFC1-antisense oligonucleotides for 4 h resulted in pollen-tube extension defects in which 51.7% of the total population had an average length of 415 μM, which was significantly on the dwarf side (n = 191, *U* test, $p < 0.001$, U = 1485) (Figure 4g, h). In the most severe scenario, 6.2% (n = 188) of the pollen tubes showed almost complete arrest in germination. Interestingly, the proportion of defective pollen tubes was enhanced at a higher concentration of NtRFC1-antisense oligonucleotides (data not shown).

The remaining candidates are of considerable interest for further functional analysis to understand the molecular basis that governs pollen-tube tip growth, pollen tube-pistil interaction, signaling and guidance.

Genes with a demonstrated or potential role in cell-cycle repression are dominant in mature pollen and 4 h pollen tubes

We used MAPMAN software http://mapman.gabipd.org/web/guest/mapman[46] to extract a cluster of genes classified as regulators of cell division and cell-cycle progression. We limited our analysis to genes reliably detected in both replicates and with expression levels well above the background. Thirty-seven genes were grouped with a role in cell-cycle progression, whereas 25 genes were annotated to participate in some aspects of cell division (Additional file 14: Table S13). We used semi-quantitative RT-PCR to validate the expression of selected target genes and to extend the analysis post-PMII after 13, 24 and 48 h of pollen-tube growth (Figure 1c, Figure 5). The sample selection allowed us to establish the expression dynamics of these key cell-cycle regulators pre- and post-PMII in angiosperms with bicellular pollen.

Reduced accumulation of cell-cycle repressors implies derepression and mitotic entry of the germ cell

Quantification of DNA content in bicellular pollen indicated that the progression of the germ cells requires cell-cycle arrest or slow progression through the S-phase immediately after the first haploid division of the microspore until the entry into PMII, 8-12 h after pollen germination [5,6]. Our analysis revealed a dominant presence of known cell-cycle inhibitors at the mature pollen stage that persisted into 4 h pollen tubes (Figure 5, Additional file 14: Table S13). These inhibitors included a RETINOBLASTOMA protein 1 (RBR1), two inhibitory kinases of cyclin-dependent kinases–namely, Kip-related proteins 1 and 3 (KRP1, KRP3)–as well as DEL3 and PAS2. We previously demonstrated the essential role of RBR1 in blocking S-phase entry of the vegetative-cell nucleus and linked this later role with an earlier function of specifying cell fate of the vegetative cell and the germ cell in the Arabidopsis male gametophyte [49]. Our present results showed that RBR1 transcripts are highly abundant at the mature pollen stage. Its expression is reduced after 4 h pollen-tube growth and remained at steady-state levels up to 48 h pollen tubes (Figure 5). Similarly, KRP6/7 are known inhibitors of germ-cell-cycle progression in Arabidopsis and their repression activities are suppressed by an F-box protein, FBL17 [50]. In the

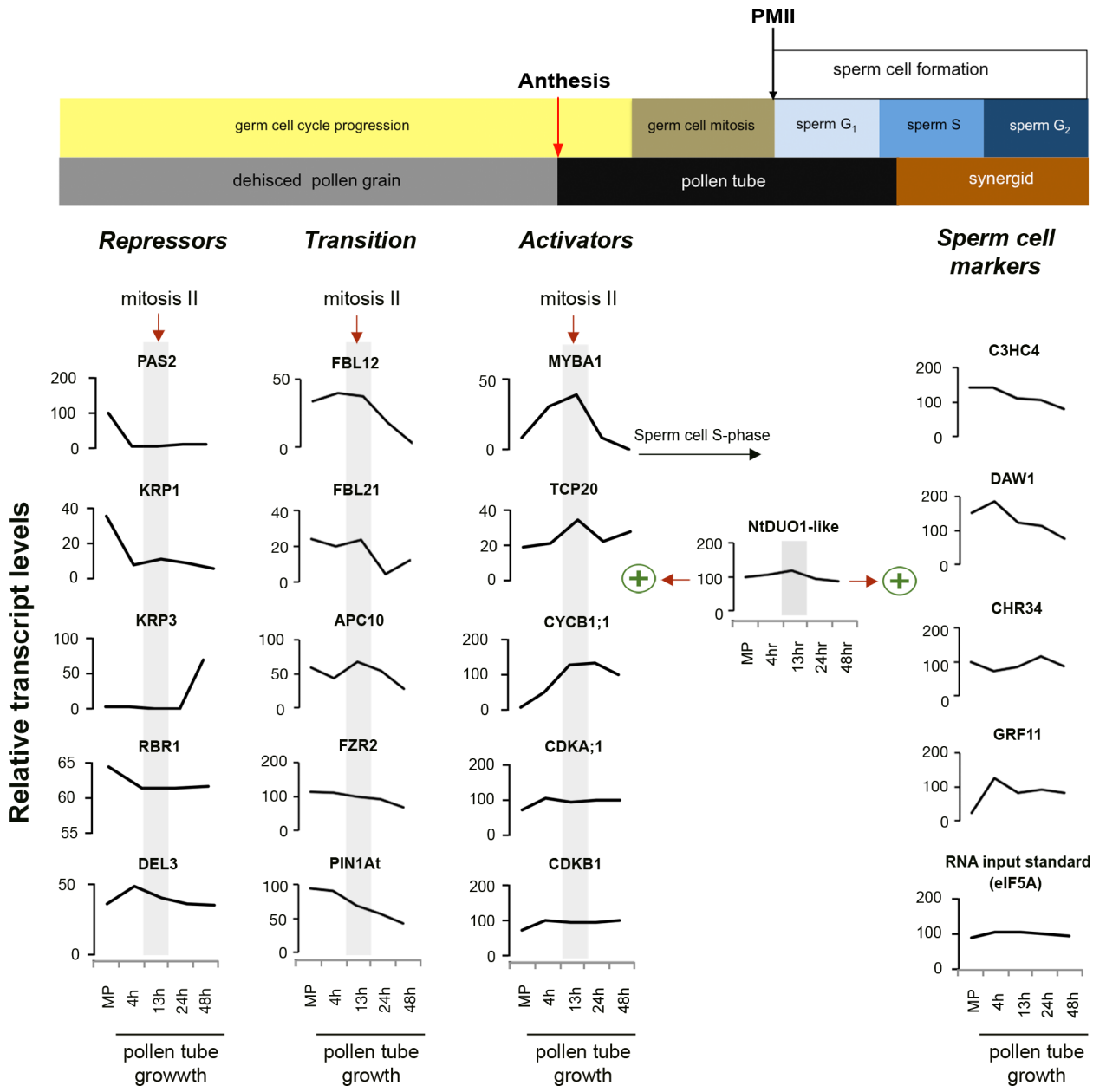

Figure 5 Expression profiles of core cell-cycle regulators and sperm cell specification markers pre- and post-mitotis of the germ cell. Schematic representation of tobacco germ cell-cycle progression during pollen-tube growth until near plasmogamy, depicted with reference to DNA content measurements of *Nicotiana tabacum* germ and sperm cells cycle [6]. mRNA expression levels were determined by semi-quantitative RT-PCR with RNA isolated from mature bicellular pollen grains (MPG) and at four stages of pollen-tube growth: 4 h, 13 h, 24 h and 48 h, both pre- and post-PMII. Signal intensities were quantified using Image J software Java 1.6.0 (National Institutes of Health, USA) and normalized against the background signal to obtain relative intensities expressed as relative transcript levels. Genes were classified as *repressors* of G1/S transition; as *transition*, for those that counteract repressors; or as *activators* of G2/M transition and progression. NtDUO1-like is regarded as an integrator of germ cell cycle mitotic progression and sperm cell fate specification, with functional evidence from the Arabidopsis male gametophyte [47]. Sperm cell fate markers are also reliably expressed pre and post germ cell mitosis to near karyogamy. Note: RBR1 levels are never minimal, accentuating the primary role of RBR1 in maintaining the vegetative cell nucleus at G_0 [48].

present study we detected two members from the KRP family, KRP1 and KRP3, with opposed expression profiles. Whereas KRP1 showed high abundance in mature pollen that dramatically declined thereafter up to the 48 h time point of pollen-tube growth (Figure 5), KRP3 showed very low expression throughout development before significantly peaking in 24 h pollen tubes (Figure 5).

Transition to cell-cycle progression is achieved by blocking the activities of the cell-cycle repressors. A family of F-box proteins, components of the SKP1-CUL1-F-box protein complex (SCF), is known to counteract the repression of CDKA induced by KRP proteins. We detected the expression of five F-box-like genes (Additional file 14: Table S13). Semi-quantitative RT-PCR analysis showed that the expression of FBL12 and FBL21 peaked at the 'division window' followed by a rapid decline post-PMII (Figure 5). We also detected expression of APC10, a component of the anaphase-promoting complex (APC/C) involved in the turnover of cyclin subunits through ubiquitin-mediated proteolysis of cyclin proteins to prevent premature entry and to promote exit from the mitotic cycle. Recent genetic characterization of another APC/C component, *APC8*, has linked APC activities to the transcriptional repression of CycB1;1 by activation of a repressor of DUO POLLEN 1, miR159 [51]. Our analysis showed that APC10 expression levels were reduced until PT4, and then increased significantly to maximum levels at the 13 h time point (Figure 5). This observation points to the dual role of APC/C in the germ cell cycle, in which CyclinB1 transcriptional repression is coupled with ubiquitin-mediated degradation in the male gametophyte.

A significant peak of G2/M factors marks transition to activation and germ-cell mitotic division

The dormant state of the mitotic cell cycle in 4 h pollen tubes was further emphasized by the under-representation of known cell-cycle activators. A G2/M master regulator, CycB1;1, was only unreliably detected in mature pollen and 4 h pollen tubes (Additional file 14: Table S13). Inversely, at the transition to the second mitotic division of the germ cell (~10-13 h after in vitro pollen germination), CycB1;1 expression was specifically and dramatically enhanced at the 'division window' (cca ~10-13 h after in vitro pollen germination) and maintained its status before gradually decreasing thereafter (Figure 5). We also detected two MYB transcription activators of CycB1;1 expression: NtMybA1, and a putative tobacco ortholog of Arabidopsis DUO POLLEN1 (DUO1), here annotated as NtDUO1-like (NCBI blastp accession AB032537 (Q8H0H3) [52], e-value of 1e-78). The tobacco NtmybA1 is a R1R2R3 MYB transcription factor similar to animal c-Myb proteins that induce CycB1;1 expression specifically at the G2/M phase of the cell cycle [53,54]. The role of NtmybA1 in the activation of CycB1;1 is enhanced specifically at G2/M by TCP20, a teosinte-branched cycloidea PCNA factor, through binding on enhancer elements (GCCCR) within CycB1;1 promoter sequences [55]. DUO1, on the other hand, is an R2R3 MYB transcription factor that we previously demonstrated to be a dual regulator of germ-cell division and sperm cell fate differentiation [47,56]. All three factors, NtMYBA1, NtDUO1-like and TCP20, were gradually enhanced, and simultaneously peaked at the 'division window', which mirrored the profile of their target (CycB1;1) and the cell-cycle status of the germ cell (Figure 5). Remarkably, the expression of these mitotic entry gate-keepers reached a maximum level at the 13 h time point, by which time > 80% of the germ cells are in the transition through mitosis or had completed mitotic division to produce the two sperm cells (Figure 1c, inset).

The stable presence of other key positive regulators, such as CDKA;1, CDKB1;1 (which counteracts KRPs activities on CDKs [57]), and CDKB2;2 (a partner of CycD3 that promotes S-phase entry and progression), appears to provide a positive balance and a molecular switch preset to enter and progress through the cell division cycle (Figure 5, Additional file 14: Table S13). We observed a marginal increase in expression of CDKA;1 and CDKB1;1 from mature pollen to PT4 preceding the strong expression of CYCB1;1 (Figure 5). Their expression was stabilized thereafter throughout the progression of the progamic phase.

Sperm cell fate specification markers continuously accumulate pre- and post-division of the germ cell

The coupling of the germ-cell mitotic division with sperm cell fate specification is designated by the overlapping expression of known cell fate differentiation markers within the germ cell that progresses to the newly formed sperm cells. We showed previously that DUO1 integrated both events, which enabled germ-cell division and regulation of the transcription of a repertoire of sperm-cell differentiation markers [47,56]. In this study, we detected 29 tobacco homologs of Arabidopsis DUO1-induced targets including two verified targets (Additional file 15: Table S14 [56]). Among these homologs is a chromatin remodelling protein (CHR34), WD-40 CUL4-RING ubiquitin ligase (DAW1), a zinc finger family protein (C3HC4-type RING finger), DUO1 Activated Unknown protein (DAU1), a NAC domain-containing protein 74 (anac074), a sugar transporter (AT5G26250), and a heavy-metal-associated domain-containing protein (AT1G51090). Given the demonstrated role of DUO1, these genes are also likely to be regulators of sperm cell fate specification in tobacco. We verified expression of four candidates and established that C3HC4, CHR34 and GRF11 showed similar abundance and expression profiles, whereas DAW1 peaked at PT4 and dropped to comparable levels thereafter (Figure 5, Additional file 15: Table S14). Additional target genes are almost certainly expressed in the tobacco male gametophyte and might play a more conserved role to that in Arabidopsis, including the determination of sperm cell fate and function.

In summary, our analysis of male gametophyte development pre- and post-second haploid mitosis uncovered an alternating accumulation of conserved regulators of cell proliferation and cell fate determinants in synchrony with the progression of the germ cell cycle. Their activities are the likely cause of the heterochronic shift that has led to diversified patterns of spermatogenesis and gamete fusion among angiosperms.

Discussion

With continuous improvement in gene annotation and the availability of functional analysis tools, *Nicotiana tabacum* has emerged as a'practical' experimental model for investigation of gene function, particularly of genes involved in pollen-tube growth and fertilization. Thus, our data set offers new opportunities for cross-species functional studies - for example, extended studies of lily GCS1 [58,59] in organisms with advanced genomic information available, such as Arabidopsis and rice. Although markedly improved, incomplete genome annotation in Solanaceae species has remained a drawback for research on these plants.

Comparative analysis of pollen-tube and root-hair transcriptomes provides insight into the genetic network of cell tip expansion and morphogenesis

We identified a suite of genes from a global-comparative analysis of pollen-tube and root-hair transcriptomes, with the implication of uncovering the genetic network involved in the control of tip-growth morphogenesis. Of the genes identified (~104), 18 GO categories were classified as highly over-represented ($p < 0.05$), which included those associated with chromatin modification, transcription and translation, protein transport and turnover, *cis*- and *trans*-Golgi networks, retrograde vesicle-mediated transport, signal transduction, microtubule and cytoskeleton organization, cell fate and cell morphogenesis, and cell and cell-wall metabolic processes. Several genes emerged from the identified GO categories were functionally characterized previously. These include two transcription factors - NPR1-like protein 3 (TRAF family) and RAP2.12 (AP2-EREBP family) - that are implicated in defence responses and enhanced ADH1 transcription and enzyme activities [60], respectively. Using the pollen tube as a model for functional tests, we verified the function of three candidate genes and illustrated their role in pollen-tube tip growth (Additional file 13: Table S12). Our results demonstrated that copper metabolism (CSD1), chromatin remodelling (AtRFC1), and regulated ubiquitin-mediated proteolysis (PD40) are essential processes during pollen-tube extension. Similarly, recently published analyses of F-box proteins SKIP2 (Arabidopsis SCF-type F-box and leucine rich repeat-containing E3 ubiquitin ligase, VFB-4) and LSK1-LSK3 (closest lily homologs of Arabidopsis ASK1) also demonstrated the importance of 26S proteasome-mediated proteolysis during pollen-tube extension [61]. Furthermore, expression 'late genes' is known to persist at a certain rate during pollen germination [13,62,63]. NtRFC1 has been implemented in maintaining genome stability and transcriptional gene silencing [45], and thus could function to repress the expression of germ-cell genes within the vegetative cell and simultaneously to regulate the tobacco germ-cell chromatin status. The concept of the two cell types sharing resources and regulatory molecules through cytoplasmic bridging potentially to implement synchronized control during maturation is increasingly apparent, although it has yet to be demonstrated at the molecular level [64,65]. In the present study, we demonstrated the essential role of NtRFC1 as a component of the gene expression network in association with pollen-tube tip expansion.

We acknowledge that our approach could have been too stringent on selection criteria and resulted in potential candidate losses. For instance, three genes - JACKDAW (JKD), CTR1 and AXR2 - are essential components of the genetic network that regulates root-hair-cell specification and extension [41,66,48], but their expression in our data set was classified as unreliable, most likely because of their low expression levels. On the other hand, the identification of genes such as GNOM-like 1 (NtGNL1), a key component of pollen-tube tip-defining growth [67] in the tobacco pollen-tube transcriptome, further endorsed our selection criteria. We simultaneously detected Cyclophilin 5 (CYP5), DV999409, which is known to interact with GNOM in vitro [48]. Moreover, our identification was not only limited to cell-fate-specification genes, but also included genes required for the proper expansion of most cell types, such as members of the root-hair defective 3 GTP-binding (RHD3) protein family (Additional file 12: Table S11) [67,68]. Our data offer further extension to investigate the control of tip specification, initiation and expansion, and provide a platform by which microarray-directed reverse genetic analysis can be used to enhance our understanding of polarized cell expansion.

The key question remains how these genes reprogram pollen-grain polarity in response to hydration to mediate the point of progamic phase initiation and pollen-tube growth through its multiple phases within the female transmitting tissues. This comparative approach supports the idea that, by investigation of the genetic overlap between polarized pollen tubes and roots/root hairs, it is more than likely to uncover universal mechanisms employed to promote tip expansion in order to achieve the intended morphological structure and cell function.

Lack of phenotypic defects following *NTP303* knockdown suggests existence of robust backup for key regulators of pollen-tube growth

The NTP303 glycoprotein is the most abundant protein in 4 h pollen tubes [37] and is a major component of the pollen tube wall [25]. Previous attempts to knockdown *NTP303* expression *in planta* using an RNAi vector did not alter pollen development or pollen-tube growth. However, targeting NTP303 family members (*ntp101*, *201*, *302* and *ntp805*) simultaneously produced male-sterile plants that showed pollen-tube growth defects in vivo but not in vitro [69]. This observation led to the hypothesis that NTP303 could (1) facilitate pollen-tube growth through the style, and hence the effect could only be observed in vivo, although NTP303 protein was not detected in transmitting tissues; and/or (2) participate in pollen-tube wall formation, and thus its knockdown could only result in weak cell-wall formation that is not evident in vitro. *In planta* and in vitro studies using amino acid microsequencing and immunolocalization approaches reported NTP303 protein detection (1) on vegetative plasma membranes surrounding the vegetative cell, generative cell and sperm cells of pollen and pollen tubes; (2) in the pollen-tube cell wall and callose plugs; and (3) in pollen-tube pellet fractions after 1 h of pollen tube growth and in cytosol after 8 h of pollen tube growth [69]. These results strongly suggested that NTP303 is translocated to the pollen-tube cell wall/membranes possibly by vesicular trafficking [69]. However, NTP303 was not detected at the tip of the growing pollen tubes, and thus it is unlikely to be involved in direct signal transduction. On the other hand, it could be part of the intracellular signalling system, because both the GTP-binding site and several possible phosphorylation sites are predicted in addition to transit peptide [70]. NTP303 is homologous to Arabidopsis SKU5 (SKS12, AT1G55570), a member of the small SKS family (SKS11, 12, 13 and 14) that possesses an ascorbate oxidase motif and encodes an extracellular glycosyl phosphatidylinositol-anchored glycoprotein [71]. This motif is required for tobacco BY2 cell expansion, and a *sku5* mutant displayed growth defects in directional root growth [71]. Our observation of the lack of pollen-tube defects after transfection with NTP303-antisense oligoneucleotides repeated and independently verified previous observations [69]. Given that NTP303 is the most abundant component of the pollen tube, NTP303 mRNA distribution into storage compartments [62] (Hafidh, Čapková and Honys, unpublished data) and its regulation at the transcription and translation level [72,73], together with its expression and functional overlap with other family members, might provide a robust 'back-up' to bypass an effect from a 'defective member' and ensure pollen germination and successful fertilization. Our current attempt to manipulate NTP303 at the protein level appears to be more effective, and thus might be more informative for elucidation of the precise function of NTP303 (Čapková, personal communication).

Determining the conserved pathway of germ cell division and sperm cell differentiation in angiosperms; a genetic model from a cell cycle perspective

Limited studies of sperm-cell DNA content in developing pollen and in the pollen tube from inception through entry into the embryo sac have been frequently used as the basis for predictions of the expression of cell-cycle-related genes, specifically CDKs and cyclins [5,52,74]. Transition through cell cycle phases in plants is primarily controlled, as in yeast and mammals, by the interactions of CDKs with the regulatory cyclins subunit. CDKA genes are constitutively expressed throughout the cell cycle, and they interact with several cyclin proteins to regulate transition through phases of the cell cycle, including the germ cell cycle in Arabidopsis [75]. Plants bearing the *cdka;1* mutation are occasionally defective in germ-cell division, and thus fail to produce the two sperm cells necessary for the double fertilization [74,76-78]. We recently showed that the *cdka;1* single sperm cell is not impaired in the expression of sperm cell fate markers, which is indicative of the competence of the sperm cell produced [47]. Interestingly, the single sperm cell produced is able to fertilize either of the female gametes and produces equal proportions of seeds with either a single endosperm or single embryo [74]. Despite the occurrence of double fertilization in the presence of *cdka;1* sperm cells, the central cells do not undergo karyogamy, which results in impaired endosperm development and eventual seed abortion [74]. This lack of nuclear fusion might potentially be because of lack of cell-cycle synchrony between the central cells and the *cdka;1* sperm cell at the time of karyogamy. Cell-cycle checkpoints (together with the rate of cell-cycle progression) are maintained by a repertoire of repressor proteins, including Retinoblastoma-related protein (RBR), Kip-related proteins (KRPs), and inhibitors of CDKs activities (ICKs). RBR1 plays an essential role in the specification of vegetative cell and germ cells and in the control of cell proliferation and differentiation [49], and has an extended function in the regulation of Polycomb Repressive Complex 2 (PRC2) and METHYLTRANSFERASE 1 (MET1) in male and female gametophytes [70]. Activity of these proteins is post-translationally modulated by either phosphorylation or protein turnover, by the ubiquitin-mediated proteolysis complexes, SCF and APC. Interestingly, *apc8* mutation inhibits germ cell division, whereas *apc8*/*apc10* hypermorphic lines showed endoreduplication in rosette

leaves of *Arabidopsis thaliana* and pleiotropic morphological defects, including small siliques, curled leaves and abnormal phylotaxy [79]. Our GO annotation of cell cycle genes (Additional file 14: Table S13) and semi-quantitative RT-PCR analyses (Figure 5) combined with previous knowledge on germ cell-cycle control [80] enabled us to propose a hypothetical genetic model from a tobacco male germ cell-cycle perspective. The proposed model is reminiscent of a biological 'clock' by which male and female gametes synchronize cell-cycle progression and coordinate gametogenesis events for successful fertilization (Figure 6). It not only provides a foundation to understand the molecular basis of the evolution of pollen tricellularity, but also acts as an informative 'genetic map' for experimental models to produce apomorphic tricellular pollen and to inspire current in vitro fertilization protocols to produce hybrid plant species. Thus understanding of this regulon could provide a useful tool for plant breeders and conservationists to utilize, either to avoid hybridization or to promote crossing of distantly related plant species that are otherwise separated because of hybrid infertility.

Conclusions

In this study we generated and verified transcriptomic profiles for *Nicotiana tabacum* mature pollen and growing pollen tubes. We functionally demonstrated the role of three pollen-tube-expressed genes in the flawless progression of the progamic phase. We further defined a gene subset, the expression of which overlaps between two tissues characterized by polarised tip growth–namely, pollen tubes and root hairs. We provided additional evidence that knockdown of the tobacco pollen-specific protein NTP303 does not cause apparent phenotypic defects and that its function is sufficiently backed up by its related family members. In addition, we demonstrated expression profiles of known cell-cycle regulators in the tobacco male gametophyte and proposed a genetic model that underlines the regulation of cell-cycle progression during haploid pollen mitosis II as a basis of pollen bicellularity in *Nicotiana tabacum*.

By making the tobacco pollen transcriptomic data publicly accessible, we offer a solid reference benchmark for future transcriptome-based functional studies. The generated transcriptomic data sets have the potential, together with other already available gene expression profiling resources, to provide the foundation for future studies of the evolution of pollen tricellularity, which has occurred independently in several angiosperm lineages. The data sets also inspire development and improvement of current in vitro fertilization protocols that are of great interest not only to plant researchers but also to breeders and conservationists. Successful protocols will offer an opportunity to cross and generate hybrid lines that otherwise face cross-compatibility barriers.

Methods

Plant materials and growth conditions

Wild-type tobacco plants (*Nicotiana tabacum* cv. Samsun) were used for the collection of tissue samples for all downstream studies. Seeds were sown in a greenhouse under short-day conditions at 22-25°C. Adult plants with a fully developed root system were transplanted to an outdoors greenhouse on ground compost and grown under the natural day-night photoperiod in spring and summer. Pollen grains were collected throughout the season and their germination rate was monitored (Figure 1)

Collection of pollen and in vitro pollen-tube cultivation

Mature pollen was isolated aseptically as described previously [81]. Flowers were collected 1 day before anthesis. Stamens were removed from the flowers into a Petri dish to dehisce in a fume-hood overnight at room temperature. Dry pollen grains were then filtered through a nylon mesh (Miracloth, pore size 50 μm), weighed and stored at-20°C. Over 80% of the collected pollen grains could successfully germinated and give rise to a pollen tube, irrespective of the collection date (Figure 1).

For in vitro pollen tube germination, approximately 10 mg/10 mL pollen was resuspended in pollen germination media (SMM: 0.3 M sucrose, 1.6 mM H_3BO_3, 3 mM $Ca(NO_3)_2$ $4H_2O$, 0.8 mM $MgSO_4.7H_2O$, 1 mM KNO_3) and aliquoted into conical flasks. The 24 h and 48 h pollen tubes were cultivated with SMM medium supplemented with casein (1 mg/mL). Cultures were incubated in a water-bath shaker at 140 rpm for 2 h and then slowed down to 90 rpm for the remaining cultivation time at 26°C in the dark. Similar procedures were followed for other pollen-tube cultures (13 h, 24 h and 48 h cultivation), though under sterile conditions. Aliquots of the samples were stained with aniline blue and 4',6-diamidino-2 phenylindole (DAPI) staining, and analyzed under a light microscope (Figure 1). Pollen tubes were vacuum-filtered, flash frozen in liquid nitrogen and stored at -80°C prior to RNA extraction. Sporophytic tissues (leaf discs and roots) were collected from juvenile plants and also from excavated adult plants. Collected samples were immediately frozen in liquid nitrogen.

RNA extraction, probe preparation and microarray hybridization

Total RNA was isolated using the Qiagen RNeasy Plant Kit in accordance with the manufacturer's instructions (Qiagen, Valencia, CA) and treated with DNaseI

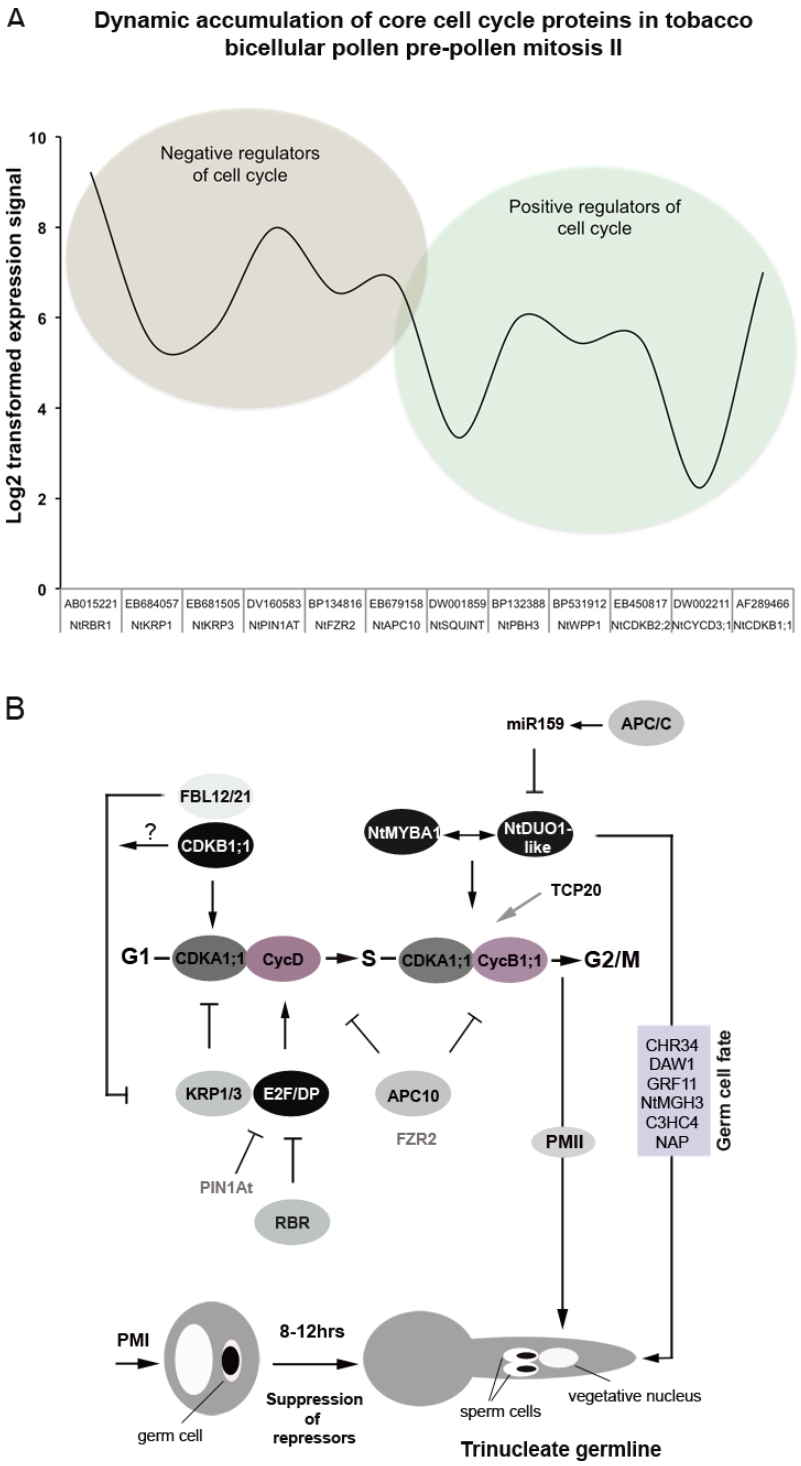

Figure 6 Putative core cell-cycle model Imposed the heterochronic shift during angiosperm spermatogenesis and fertilization. (**a**) Representative dynamic expression of cell-cycle genes at the time of anthesis of tobacco bicellular pollen as derived from transcriptomic data. The relative abundances between negative and positive regulators gives a snapshot of the cell-cycle status of germ cell and vegetative cell. Increased expression of positive regulators and post-translational inhibition of the repressors signifies the progression of the germ cell cycle to enter PMII for sperm cells production. This progression is in parallel with the expression of germ-cell fate determinants integrated by the NtDUO1-like Myb transcription factor and in synchrony with pollen-tube growth rate through the female pistil, with the effect of synchronizing the gametes cell-cycle progression for successful karyogamy. (**b**) Depicted model of core cell-cycle regulatory network likely to account for the heterochronic shift in spermatogenesis among flowering plants. The model was derived on the basis of the combined expression analysis presented herein. Key other proteins and family members are also expected to be involved in this network. Note: the hierarchical relationship between R2R3 NtDUO1-like and NtMYBA1 (both activators of CycB1;1 transcription) is yet to be established, together with that of three other R1R2R3 plant Myb transcription factors.

(Promega. Madison, WI). RNA was quantified using NanoDrop (Thermo Scientific, Wilmington, USA). Prior to shipment, five replicates from each sample were tested using semi-quantitative RT-PCR with two marker genes, Nt-eIF5A and a constitutive 18S rRNA, for reproducibility. RNA concentration, purity and integrity (RIN) were assessed using an Agilent 2100 Bioanalyzer (Agilent Technologies, Boblingen, Germany) at ImaGenes (Berlin, Germany). Biotinylated target cRNA was prepared from 50 ng of reverse-transcribed total RNA (One-Cycle Target labelling and control reagents; Agilent Technologies). Labeled cRNA was fragmented and 15 μg were used for Agilent 44 K tobacco microarray hybridization. Hybridized chips were scanned on an Agilent High Resolution Microarray Scanner.

Bioinformatics and statistical analysis of Agilent 44 K tobacco genome array data

All transcriptomic data sets were normalized using freely available dChip 1.3 software http://www.dchip.org. The reliability and reproducibility of the analyses were ensured by the use of duplicates in each experiment, the normalization of all arrays to the median probe intensity level, and the use of normalized intensities of all arrays for the calculation of model-based gene-expression values based on the Perfect Match-only model [82]. For each sample, only probes with the detection call of 'present' and an expression value detection level of 'well above background' (Boolean flag, two-sided *t*-test) in both replicates were considered to be expressed.

To determine the quality of the quantile-normalized data set and the correlation between arrays, CLC Genomics Workbench version 4.5.1 (CLC bio, Aarhus, Denmark) was used to compute mean expression values and corresponding *p*-values of the $\log_2$-transformed data. The output of this analysis was used to assess the correlation between samples using PCA, as well as independently using hierarchical clustering. To observe the variance of the distribution of the mean expression levels, scatterplots were used for pairwise comparison between samples.

Genes differentially expressed between arrays were statistically determined using the following criteria: for all filtered quantile-normalized datasets, (1) probes must have *p*-values of < 0.05; (2) the *p*-values must pass FDR correction to minimize false discovery rate; (3) they should have an absolute expression value (fold change) of ± > 3; (4) and they must have expression levels of > 100, well above background. All genes that passed the above test from pairwise comparisons are reported in Additional file 4: Table S3, Additional file 5: Table S4, Additional file 6: Table S5, Additional file 7: Table S6, Additional file 8: Table S7, Additional file 9: Table S8, together with the results from the statistical analysis.

Gene ontology analysis for PT4R overlapping genes and the gametophyte-specific subset

Gene ontology term enrichment analysis was performed using the g:Profiler http://biit.cs.ut.ee/gprofiler/ and GoToolBox http://gin.univ-mrs.fr/GOToolBox, gene ontology databases, essentially as described in [83,84], together with application of the hypergeometric distribution test, and Benjamini and Honchberg corrected *p*-value cut off < 0.05 [20]. GO terms from the categories 'biological processes', 'molecular function' and 'cellular activities' with an adjusted *p*-value of < 0.05 were considered over-represented in a subset of genes analyzed. For gametophyte and sporophyte preferentially expressed genes, enriched GO terms are shown in Figures 3d and 3e. PT4R over-represented GO categories are provided in Additional file 12: Table S11.

Real-time quantitative RT-PCR and semi-quantitative RT-PCR analysis

Independent verification of the expression profiles predicted by microarray was conducted using the same pool of RNA with qRT-PCR and semi-RT-PCR. For each replicate, 500 ng of total RNA was treated with DNAseI (Promega), and 50 ng was reverse-transcribed with ImProm-II reverse transcriptase (Promega). Real-time RT-PCR was performed using the LightCycler 480 SYBR Green I Master Kit (Roche Diagnostics, Mannheim, Germany) in a 480 LightCycler system (Roche Diagnostics). The gene encoding 18S rRNA was used to normalize the expression of all genes examined. For semi-RT-PCR of the cell-cycle and cell-fate genes, 1/10 dilution of the cDNA generated was used as a template for a 30-cycle PCR reaction. The thermocycler program was as follows: 2 min at 95°C; 45 cycles of 30 s at 95°C; 30 s at 55°C; 30 s at 72°C; and 5 min at 72°C. eIF5a was used as a standard control for RNA input. All primers used in these experiments were designed using primer 3 software http://frodo.wi.mit.edu/primer3/, and the sequences are available for download as Additional file 16: Table S15.

Antisense-mediated knockdown of selected target genes

NCBI-derived sequences of all selected tobacco target genes were used to design corresponding antisense and sense oligodeoxynucleotides for functional analysis. Antisense oligonucleotides can interfere with gene function through RNase H-mediated mRNA degradation, translation repression or alteration of splicing [85]. cDNA sequences of each target gene were submitted to Integrated DNA Technology (IDT, http://eu.idtdna.com/home/home.aspx) and Soligo S-fold software http://sfold.wadsworth.org/cgi-bin/index.pl to compute optimal antisense oligonucleotides and predict the most accessible target sites based on Matveeva rule set and Soligo

algorithms, respectively. Two pairs were designed for each gene. 21-mer oligonucleotides corresponding to antisense and sense (control) were synthesized with 5'-3' phosphorothiote modification (three bases from each end, Generi-Biotech, Hradec Králové, Czech Republic). All oligonucleotides were OPC-purified (Oligonucleotide purification cartridge). The sequences of the antisense oligonucleotides used were as follows: PD40 (NCBI; BP130384), sense: 5'-ACTCCACACACACAGAGCCT-3', antisense: 5'-AGGCTCTGTGTGTGTGGAGT-3', NTP303 (NCBI; X69440), sense: 5'-CACCCAAT-GAAATTAGTCGA-3', antisense: 5'-TCGACTAATTT-CATTGGGTG-3', ATRFC1 (NCBI; DW003643), sense: 5'-ACGAGTTACGATCAGTCGAC-3', antisense: 5'-GTCGACTGATCGTAACTCGT-3', eIF5a (NCBI; CV021663), sense: 5'-ACTACATTCGAAGCTCTAGC-3', antisense: 5'-GCTAGAGCTTCGAATGTAGT-3', Cu/Zn superoxide dismutase 1, CSD1 (NCBI; EB439640), sense: 5'-AACGGGACCACATTATAATC-3', antisense: 5'-GATTATAATGTGGTCCCGTT-3'.

Pollen-tube deoxyoligonucleotide transfection

For each pair of sense and antisense oligonucleotides, 15, 30 and 50 μM were mixed with Cytofectin (Genlantis, San Diego, CA) according to Moutinho et al. [27], to a final volume of 100 μL. A concentration of 30 μM was determined to be sufficient for most genes, with the exception of ATRFC1. Pollen tubes were transfected and germinated on a microtitre plate under constant shaking (140 rpm) at 27°C in the dark. Initial screening for phenotype was done in the microtitre plate; thereafter, an aliquot from each sample was taken for further microscopic analysis. For each gene tested, including controls, pollen tubes were cultivated with and without the cytofectin/deoxyoligonucleotide mixture for 4 h in vitro and then fixed with 4% formaldehyde prior to length measurements. Two biological and three technical replicates were performed for each experiment, and mean values are presented.

Microscopy

For nuclear visualization, DAPI staining solution (0.1 M sodium phosphate, pH 7; 1 mM EDTA, 0.1% (v/v) Triton X-100, 0.8 mg/ml DAPI) was used to stain dry mature pollen grains and germinated pollen tubes [86]. For the knockdown experiments, pollen tubes were first fixed with 4% paraformaldehyde, 50 mM PIPES and 10% sucrose, vacuum infiltrated for 5 min and incubated for 1 h. Pollen tubes were then washed three times with 50 mM PIPES (pH 6.9). Light and fluorescence microscopy was carried out with a Nikon TE2000-E fluorescent microscope (Nikon, Japan) using DAPI and GFP filter sets. Image capturing and processing was carried out and pollen-tube length measurements were taken using NIS-Elements AR3.0 software (Nikon instruments, Melville, USA) and Adobe Photoshop http://www.adobe.com.

Additional files

The following additional data are available with the online version of this paper. Additional data file 1 is a table of complete data set generated in this study with mean normalized expression derived from two biological replicates and with expression levels 'well above background'. Additional file 2: Table S1 is a table gametophyte specific expressed genes. Additional files 3: Table S2, Additional files 4: Table S3, Additional files 5: Table S4, Additional files 6: Table S5, Additional files 7: Table S6, Additional files 8: Table S7 are tables of differentially expressed genes between [1] MPGvsPT4 [2] leaves vs MPG [3] roots/root-hairs vs MPG [4] leaves vs PT4 [5] roots/root-hairs vs PT4 and [6] leaves vs roots/root-hairs, respectively. Additional file 9: Table S8 is a list of PT4-root/root-hairs overlapping subset of genes (PT4R). Additional file 10 Table S9 is a similar list as that of Additional file 9: Table S8 with identified Arabidopsis closest homologs (PT4R_ATH). Additional file 11 is a list of PT4R_ATH genes that were identified to overlap with Arabidopsis root-hair trichoblast and virtual proteome. Additional file 12: Table S11 is a list of overrepresented GO terms for genes that showed overlapping expression between PT4R_ATH and Arabidopsis root-hair trichoblast. Additional file 13: Table S12 is a list of identified cell-cycle genes expressed in the MPG and PT4 pollen stages. Additional file 14: Table S13 is a table of DUO1 target genes that were detected in our pollen and pollen tube transcriptomes. Additional file 15: Table S14 is a list of all primers used in this study.

Additional material

Additional file 1: Figure S1 Data normalization and analysis of replica reproducibility. (**a**) Box plot of the raw hybridization signal from the four samples, highlighting systematic differences between samples. The inset shows the same data after the normalization. (**b**) Output of the first and second principal component (PCA) analysis of the log_2-transformed data sets. The largest and second-largest principal component (variability projection 1 and 2, respectively) are displayed in orthogonal directions, assessing the overall homogeneity between replicates and variability between samples of different tissue types as reflected in their grouping. The inset shows hierarchical clustering of the same data set grouped according to array similarities and differences. Since both methods produced identical grouping patterns, the quality of the dataset was considered reliable and useful for comparative analysis. (**c**) Scatterplots of log_2-transformed microarray data showing a correlation between tissue arrays. A wider symmetrical scattering of the spots from the 'trendline' implicates higher variability between the tissues, with less dependency between variance and mean expression values, as compared with more tightly packed spots (MPG vs PT4) reflecting a closer relationship between the data sets.

Additional file 3: Table S2 Probe sest with expression confined to 4 hr pollen tubes classified according to detection call of the two replicates.

Additional file 4: Table S3 Complete list of differentially expressed genes between dehisced mature pollen and 4 hr pollen tubes.

Additional file 5: Table S4 Complete list of differentially expressed genes between leaf and mature pollen grains.

Additional file 6: Table S5 Complete list of differentially expressed genes between roots/root-hairs and mature pollen grains.

Additional file 7: Table S6 Complete list of differentially expressed genes between leaf and 4 hr pollen tubes.

Additional file 8: Table S7 Complete list of differentially expressed genes between roots/root-hairs and 4 hr pollen tubes.

Additional file 9: Table S8. Complete list of differentially expressed genes between leaf and roots/root-hairs.

Additional file 10: Table S9 List of genes that showed overlapped expression between 4 hr pollen tubes and root/root-hairs tobacco transcriptomes.

Additional file 11: Table S10 Missing file.

Additional file 12: Table S11 A list of tobacco acessions with significant Arabidopsis homologs that had reliable microarray expression in PT4, root/root hairs and overlapped with Arabidopsis root-hair specific transcriptome and virtual proteome.

Additional file 13: Table S12 List of significant Gene Ontology (GO) annotation of genes that showed overlap expression between PT4 and roots/root-hairs with significant arabidopsis homologs using gProfiler software [83].

Additional file 14: Table S13 A list of cell cycle regulators (annotated according to MAPMAN GO terms) with a potential role of maintaining the bicelluar status of the 70% known angiosperms that shed bicellular pollen at anthesis.

Additional file 15: Table S14. Comparative transcriptome of some putative sperm cell differentiation markers between bicellular and tricellular angiosperms that were induced by Arabidopsis DUO POLLEN 1 [68] and detected in our gametophyte transcriptomes.

Additional file 16: Table S15 List of primers used in this experiment.

Additional file 2: Table S1 Mean normalized expression of tobacco probe sets with associated detection calls computed from two biological replicates with expression levels "well above background".

Abbreviations

MPG: dehisced mature pollen grain; PT: pollen tube; oligo: soligonucleotides; FDR: false discovery rate; GO term gene ontology.

Acknowledgements

The authors thank CLC genomic staff for technical assistance with CLC genomic workbench software for microarray data analysis, Prof. Alice Cheung (Department of Biochemistry and Molecular Biology, University of Massachusetts at Amherst, MA, USA) for the kind gift of the pSF3-Lim2aGFP expressed line, Dr. Martin Potocký (Laboratory of Cell Biology, Institute of Experimental Botany ASCR, Prague, Czech Republic) for providing the transfection reagent (Cytofectin), Dr. Karel Müller (Laboratory of Plant Reproduction, Institute of Experimental Botany ASCR, Prague, Czech Republic) for assistance with real-time quantitative RT-PCR, Prof. Sheila McCormick (Department of Plant and Microbial Biology, Plant Gene Expression Center, University of California-Berkeley, Albany, USA) for constructive discussions, and Dr. Amanda Woods for critical reading of the manuscript and language corrections. This work was supported by the Czech Science Foundation (P501/11/P321; P501/11/1462) and the Ministry of Education, Youth and Sports of the Czech Republic (OC10054).

Author details

[1]Laboratory of Pollen Biology, Institute of Experimental Botany, Academy of Sciences of the Czech Republic, Rozvojová 263, 165 02 Praha 6, Czech Republic. [2]Department of Plant Experimental Biology, Faculty of Science, Charles University in Prague, Viničná 5, 128 44 Praha 2, Czech Republic.

Authors' contributions

SH and DH designed the study. SH, KB, PR, JF and VC performed the experiments. SH and DH analysed the data. SH wrote the manuscript, which was further edited by SH, VC, KB and DH. All authors read and approved the final manuscript.

Received: 22 September 2011 Accepted: 16 February 2012
Published: 16 February 2012

References

1. McCormick S: *The Plant Cell Online* 2004, **16(Supplement 1)**:S142.
2. Honys D, Twell D: **Comparative analysis of the Arabidopsis pollen transcriptome.** *Plant Physiol* 2003, **132(2)**:640.
3. Borges F, Gomes G, Gardner R, Moreno N, McCormick S, Feijó JA, Becker JD: **Comparative transcriptomics of Arabidopsis sperm cells.** *Plant Physiol* 2008, **148(2)**:1168.
4. Brewbaker JR: **The distribution and phylogenetic significance of binucleate and trinucleate pollen grains in the angiosperms.** *Am J Bot* 1967, **54(9)**:1069-1083.
5. Friedman WE: **Expression of the cell cycle in sperm of Arabidopsis: implications for understanding patterns of gametogenesis and fertilization in plants and other eukaryotes.** *Development* 1999, **126(5)**:1065.
6. Tian HQ, Yuan T, Russell SD: **Relationship between double fertilization and the cell cycle in male and female gametes of tobacco.** *Sexual Plant Reprod* 2005, **17(5)**:243-252.
7. Larkin JC, Marks MD, Nadeau J, Sack F: **Epidermal cell fate and patterning in leaves.** *Plant Cell* 1997, **9(7)**:1109.
8. Gibson DA, Ma L: **Developmental regulation of axon branching in the vertebrate nervous system.** *Development* 2011, **138(2)**:183.
9. Qin Y, Leydon AR, Manziello A, Pandey R, Mount D, Denic S, Vasic B, Johnson MA, Palanivelu R: **Penetration of the stigma and style elicits a novel transcriptome in pollen tubes, pointing to genes critical for growth in a pistil.** *PLoS Genet* 2009, **5(8)**:e1000621.
10. Lee YJ, Yang Z: **Tip growth: signaling in the apical dome.** *Curr Opin Plant Biol* 2008, **11(6)**:662-671.
11. Haerizadeh F, Wong C, Bhalla P, Gresshoff P, Singh M: **Genomic expression profiling of mature soybean (Glycine max) pollen.** *BMC Plant Biology* 2009, **9(1)**:25.
12. Xin HP, Peng XB, Ning J, Yan TT, Ma LG, Sun MX: **Expressed sequence-tag analysis of tobacco sperm cells reveals a unique transcriptional profile and selective persistence of paternal transcripts after fertilization.** *Sexual Plant Reprod* 2011, **24(1)**:37-46.
13. Wang Y, Zhang WZ, Song LF, Zou JJ, Su Z, Wu WH: **Transcriptome analyses show changes in gene expression to accompany pollen germination and tube growth in Arabidopsis.** *Plant Physiol* 2008, **148(3)**:1201.
14. Honys D, Twell D: **Transcriptome analysis of haploid male gametophyte development in Arabidopsis.** *Genome Biol* 2004, **5(11)**:R85.
15. Won SK, Lee YJ, Lee HY, Heo YK, Cho M, Cho HT: **Cis-element-and transcriptome-based screening of root hair-specific genes and their functional characterization in Arabidopsis.** *Plant Physiol* 2009, **150(3)**:1459.
16. Cvrčková F, Bezvoda R, Žárský V: **Computational identification of root hair-specific genes in Arabidopsis.** *Plant Signaling & Behavior* 2010, **5(11)**:1407.
17. Kanaoka MM, Torii KU: **FERONIA as an upstream receptor kinase for polar cell growth in plants.** *Proc National Acad Sci* 2010, **107(41)**:17461.
18. Tupý J, Süss J, Hrabětová E, Říhová L: **Developmental changes in gene expression during pollen differentiation and maturation in Nicotiana tabacum L.** *Biol Plant* 1983, **25(3)**:231-237.
19. Edwards K, Bombarely A, Story G, Allen F, Mueller L, Coates S, Jones L: **TobEA: an atlas of tobacco gene expression from seed to senescence.** *BMC Genomics* 2010, **11(1)**:142.
20. Benjamini Y, Hochberg Y: **Controlling the false discovery rate: a practical and powerful approach to multiple testing.** *J R Stat Soc Series B (Methodological)* 1995, **57(1)**:289-300.
21. Snedden WA, Fromm H: **Calmodulin, calmodulin-related proteins and plant responses to the environment.** *Trends Plant Sci* 1998, **3(8)**:299-304.
22. Zhang L, Lu YT: **Calmodulin-binding protein kinases in plants.** *Trends Plant Sci* 2003, **8(3)**:123-127.
23. Baluška F: **Recent surprising similarities between plant cells and neurons.** *Plant Signaling & Behavior* 2010, **5(2)**:87.

24. Weterings K, Reijnen W, Aarssen R, Kortstee A, Spijkers J, Herpen M, Schrauwen J, Wullems G: **Characterization of a pollen-specific cDNA clone from Nicotiana tabacum expressed during microgametogenesis and germination.** *Plant Mol Biol* 1992, **18(6)**:1101-1111.
25. Wittink FRA, Knuiman B, Derksen J, Čapková V, Twell D, Schrauwen JAM, Wullems GJ: **The pollen-specific gene Ntp303 encodes a 69-kDa glycoprotein associated with the vegetative membranes and the cell wall.** *Sexual Plant Reprod* 2000, **12(5)**:276-284.
26. Čapková V, Hrabětová E, Tupý J: **Protein changes in tobacco pollen culture; a newly synthesized protein related to pollen tube growth.** *J Plant Physiol* 1987, **130(4-5)**:307-314.
27. Moutinho A, Camacho L, Haley A, Pais MS, Trewavas A, Malhó R: **Antisense perturbation of protein function in living pollen tubes.** *Sexual Plant Reprod* 2001, **14(1)**:101-104.
28. Sun C, Ghebramedhin H, Höglund AS, Jansson C: **Antisense oligodeoxynucleotide inhibition as a potent diagnostic tool for gene function in plant biology.** *Plant Signaling & Behavior* 2008, **3(5)**:328.
29. Gönczy P, Echeverri C, Oegema K, Coulson A, Jones SJM, Copley RR, Duperon J, Oegema J, Brehm M, Cassin E: **Functional genomic analysis of cell division in C. elegans using RNAi of genes on chromosome III.** *Nature* 2000, **408(6810)**:331-336.
30. Ui-Tei K, Naito Y, Takahashi F, Haraguchi T, Ohki-Hamazaki H, Juni A, Ueda R, Saigo K: **Guidelines for the selection of highly effective siRNA sequences for mammalian and chick RNA interference.** *Nucleic Acids Res* 2004, **32(3)**:936.
31. Potocký M, Jones MA, Bezvoda R, Smirnoff N, Žárský V: **Reactive oxygen species produced by NADPH oxidase are involved in pollen tube growth.** *New Phytol* 2007, **174(4)**:742-751.
32. Wang H, Tse YC, Law AHY, Sun SSM, Sun YB, Xu ZF, Hillmer S, Robinson DG, Jiang L: **Vacuolar sorting receptors (VSRs) and secretory carrier membrane proteins (SCAMPs) are essential for pollen tube growth.** *The Plant J* 2010, **61(5)**:826-838.
33. Feng H, Chen Q, Feng J, Zhang J, Yang X, Zuo J: **Functional characterization of the Arabidopsis eukaryotic translation initiation factor 5A-2 that plays a crucial role in plant growth and development by regulating cell division, cell growth, and cell death.** *Plant Physiol* 2007, **144(3)**:1531.
34. Lan P, Schmidt W: **The enigma of eIF5A in the iron deficiency response of Arabidopsis.** *Plant Signal Behav* 2011, **6(4)**:528-530.
35. Čapková V, Hrabětová E, Tupý J: **Effects of Cycloheximide on Pollen of *Nicotiana tabacu* in Culture.** *Biochem Physiol Pflanzen* 1980, **175**:412-420.
36. Cheung AY, Duan QH, Costa SS, de Graaf B, Di Stilio VS, Feijo J, Wu HM: **The dynamic pollen tube cytoskeleton: Live cell studies using actin-binding and microtubule-binding reporter proteins.** *Molecular Plant* 2008, **1(4)**:686-702.
37. Čapková V, Zbrožek J, Tupý J: **Protein synthesis in tobacco pollen tubes: preferential synthesis of cell-wall 69-kDa and 66-kDa glycoproteins.** *Sexual Plant Reprod* 1994, **7(1)**:57-66.
38. Ramsay NA, Glover BJ: **MYB-bHLH-WD40 protein complex and the evolution of cellular diversity.** *Trends Plant Sci* 2005, **10(2)**:63-70.
39. Lee JH, Terzaghi W, Gusmaroli G, Charron JBF, Yoon HJ, Chen H, He YJ, Xiong Y, Deng XW: **Characterization of Arabidopsis and rice DWD proteins and their roles as substrate receptors for CUL4-RING E3 ubiquitin ligases.** *The Plant Cell Online* 2008, **20(1)**:152.
40. Berger F, Linstead P, Dolan L, Haseloff J: **Stomata patterning on the hypocotyl of Arabidopsis thaliana is controlled by genes involved in the control of root epidermis patterning.** *Dev Biol* 1998, **194(2)**:226-234.
41. Schiefelbein JW: **Constructing a plant cell. The genetic control of root hair development.** *Plant Physiol* 2000, **124(4)**:1525.
42. Schiefelbein J, Kwak SH, Wieckowski Y, Barron C, Bruex A: **The gene regulatory network for root epidermal cell-type pattern formation in Arabidopsis.** *J Exp Bot* 2009, **60(5)**:1515.
43. Kliebenstein DJ, Monde RA, Last RL: **Superoxide dismutase in Arabidopsis: an eclectic enzyme family with disparate regulation and protein localization.** *Plant Physiol* 1998, **118(2)**:637.
44. Beauclair L, Yu A, Bouché N: **microRNA- directed cleavage and translational repression of the copper chaperone for superoxide dismutase mRNA in Arabidopsis.** *The Plant J* 2010, **62(3)**:454-462.
45. Liu Q, Wang J, Miki D, Xia Ran, Yu W, He J, Zheng Z, Zhu JK, Gong Z: **DNA replication factor C1 mediates genomic stability and transcriptional gene silencing in *Arabidopsis*.** *The Plant Cell* 2010, **22**:2336-2352.
46. Thimm O, Bläsing O, Gibon Y, Nagel A, Meyer S, Krüger P, Selbig J, Müller LA, Rhee SY, Stitt M: **mapman: a user-driven tool to display genomics data sets onto diagrams of metabolic pathways and other biological processes.** *The Plant J* 2004, **37(6)**:914-939.
47. Brownfield L, Hafidh S, Borg M, Sidorova A, Mori T, Twell D: **A plant germline-specific integrator of sperm specification and cell cycle progression.** *PLoS Genet* 2009, **5(3)**:e1000430.
48. Hassan H, Scheres B, Blilou I: **JACKDAW controls epidermal patterning in the Arabidopsis root meristem through a non-cell-autonomous mechanism.** *Development* 2010, **137(9)**:1523.
49. Chen Z, Hafidh S, Poh SH, Twell D, Berger F: **Proliferation and cell fate establishment during Arabidopsis male gametogenesis depends on the Retinoblastoma protein.** *Proc National Acad Sci* 2009, **106(17)**:7257.
50. Kim HJ, Oh SA, Brownfield L, Hong SH, Ryu H, Hwang I, Twell D, Nam HG: **Control of plant germline proliferation by SCFFBL17 degradation of cell cycle inhibitors.** *Nature* 2008, **455(7216)**:1134-1137.
51. Zheng B, Chen X, McCormick S: **The anaphase-promoting complex is a dual integrator that regulates both MicroRNA-mediated transcriptional regulation of Cyclin B1 and degradation of Cyclin B1 during Arabidopsis male gametophyte development.** *The Plant Cell Online* 2011, **23(3)**:1033.
52. Durbarry A, Vizir I, Twell D: **Male germ line development in Arabidopsis. duo pollen mutants reveal gametophytic regulators of generative cell cycle progression.** *Plant Physiol* 2005, **137(1)**:297.
53. Ito M, Araki S, Matsunaga S, Itoh T, Nishihama R, Machida Y, Doonan JH, Watanabe A: **G2/M-phase-specific transcription during the plant cell cycle is mediated by c-Myb-like transcription factors.** *Plant Cell* 2001, **13(8)**:1891.
54. Haga N, Kato K, Murase M, Araki S, Kubo M, Demura T, Suzuki K, Müller I, Voß U, Jürgens G: **R1R2R3-Myb proteins positively regulate cytokinesis through activation of KNOLLE transcription in Arabidopsis thaliana.** *Development* 2007, **134(6)**:1101.
55. Li C, Potuschak T, Colón-Carmona A, Gutiérrez RA, Doerner P: **Arabidopsis TCP20 links regulation of growth and cell division control pathways.** *Proc Natl Acad Sci USA* 2005, **102(36)**:12978.
56. Borg M, Brownfield L, Khatab H, Sidorova A, Lingaya M, Twell D: **The R2R3 MYB transcription Factor DUO1 activates a male germline-specific regulon Essential for sperm cell differentiation in Arabidopsis.** *The Plant Cell Online* 2011, **23(2)**:534.
57. Verkest A, Weinl C, Inzé D, De Veylder L, Schnittger A: **Switching the cell cycle. Kip-related proteins in plant cell cycle control.** *Plant Physiol* 2005, **139(3)**:1099.
58. Gou X, Yuan T, Wei X, Russell SD: **Gene expression in the dimorphic sperm cells of Plumbago zeylanica: transcript profiling, diversity, and relationship to cell type.** *The Plant J* 2009, **60(1)**:33-47.
59. Mori T, Kuroiwa H, Higashiyama T, Kuroiwa T: **GENERATIVE CELL SPECIFIC 1 is essential for angiosperm fertilization.** *Nat Cell Biol* 2005, **8(1)**:64-71.
60. Zhang Y, Cheng YT, Qu N, Zhao Q, Bi D, Li X: **Negative regulation of defense responses in Arabidopsis by two NPR1 paralogs.** *The Plant J* 2006, **48(5)**:647-656.
61. Papdi C, Ábrahám E, Joseph MP, Popescu C, Koncz C, Szabados L: **Functional identification of Arabidopsis stress regulatory genes using the controlled cDNA overexpression system.** *Plant Physiol* 2008, **147(2)**:528.
62. Honys D, Reňák D, Feciková J, Jedelský PL, Nebesářová J, Dobrev P, Čapková V: **Cytoskeleton-associated large RNP complexes in tobacco male gametophyte (EPPs) are associated with ribosomes and are involved in protein synthesis, processing, and localization.** *J Proteome Res* 2009, **8(4)**:2015-2031.
63. Hafidh S, Honys D, Čapková V: **Safe keeping of the messages; RNP complexes tweaking after transcription.** In *RNA Infrastructure and Networks, Advances in medicine and Biology, Intelligence Unit.*. 722 edition. Edited by: Lesley JC. New Zealand: Landes Bioscience/Springer Science, Madame Curie Bioscience Database; 2010:118-133.
64. Slotkin RK, Vaughn M, Borges F, Tanurdzic M, Becker JD, Feijó JA, Martienssen RA: **Epigenetic reprogramming and small RNA silencing of transposable elements in pollen.** *Cell* 2009, **136(3)**:461-472.
65. McCue AD, Cresti M, Feijó JA, Slotkin RK: **Cytoplasmic connection of sperm cells to the pollen vegetative cell nucleus: potential roles of the male germ unit revisited.** *J Exp Bot* 2011, **62(5)**:1621.

66. Chang LC, Guo CL, Lin YS, Fu H, Wang CS, Jauh GY: **Pollen-specific SKP1-like proteins are components of functional SCF complexes and essential for lily pollen tube elongation.** *Plant and Cell Physiologys* 2009, **50(8)**:1558.
67. Wang L, Liao FL, Zhu L, Peng XB, Sun MX: **NtGNL1 is involved in embryonic cell division patterning, root elongation, and pollen tube growth in tobacco.** *New Phytol* 2008, **179(1)**:81-93.
68. Wang H, Lockwood SK, Hoeltzel MF, Schiefelbein JW: **The ROOT HAIR DEFECTIVE3 gene encodes an evolutionarily conserved protein with GTP-binding motifs and is required for regulated cell enlargement in Arabidopsis.** *Genes Dev* 1997, **11(6)**:799.
69. de Groot P, Weterings K, de Been M, Wittink F, Hulzink R, Custers J, van Herpen M, Wullems G: **Silencing of the pollen-specific gene NTP303 and its family members in tobacco affects in vivo pollen tube growth and results in male sterile plants.** *Plant Mol Biol* 2004, **55(5)**:715-726.
70. Guitton A, Berger F: **Control of reproduction by Polycomb Group complexes in animals and plants.** *Int J Dev Biol* 2005, **49(5/6)**:707.
71. Ryan E, Grierson CS, Cavell A, Steer M, Dolan L: **TIP1 is required for both tip growth and non-tip growth in Arabidopsis.** *New Phytol* 1998, **138(1)**:49-58.
72. Sedbrook JC, Carroll KL, Hung KF, Masson PH, Somerville CR: **The Arabidopsis SKU5 gene encodes an extracellular glycosyl phosphatidylinositol-anchored glycoprotein involved in directional root growth.** *The Plant Cell Online* 2002, **14(7)**:1635.
73. Hulzink RJM, de Groot PFM, Croes AF, Quaedvlieg W, Twell D, Wullems GJ, van Herpen M: **The 5'-untranslated region of the ntp303 gene strongly enhances translation during pollen tube growth, but not during pollen maturation.** *Plant Physiol* 2002, **129(1)**:342.
74. Aw SJ, Hamamura Y, Chen Z, Schnittger A, Berger F: **Sperm entry is sufficient to trigger division of the central cell but the paternal genome is required for endosperm development in *Arabidopsi*.** *Development* 2010, **137(16)**:2683-2690.
75. Brodersen P, Sakvarelidze-Achard L, Bruun-Rasmussen M, Dunoyer P, Yamamoto YY, Sieburth L, Voinnet O: **Widespread translational inhibition by plant miRNAs and siRNAs.** *Science* 2008, **320(5880)**:1185.
76. Nowack MK, Grini PE, Jakoby MJ, Lafos M, Koncz C, Schnittger A: **A positive signal from the fertilization of the egg cell sets off endosperm proliferation in angiosperm embryogenesis.** *Nat Genet* 2006, **38(1)**:63-67.
77. Iwakawa H, Shinmyo A, Sekine M: **Arabidopsis CDKA; 1, a cdc2 homologue, controls proliferation of generative cells in male gametogenesis.** *The Plant J* 2006, **45(5)**:819-831.
78. Dissmeyer N, Nowack MK, Pusch S, Stals H, Inze D, Grini PE, Schnittger A: **T-loop phosphorylation of Arabidopsis CDKA; 1 is required for its function and can be partially substituted by an aspartate residue.** *Plant Cell* 2007, **19(3)**:972.
79. Marrocco K, Thomann A, Parmentier Y, Genschik P, Criqui MC: **The APC/C E3 ligase remains active in most post-mitotic Arabidopsis cells and is required for proper vasculature development and organization.** *Development* 2009, **136(9)**:1475.
80. Twell D: **Male gametogenesis and germline specification in flowering plants.** *Sexual Plant Reprod* 2011, **24(2)**:149-160.
81. Petrů E, Hrabětová E, Tupý J: **The technique of obtaining germinating pollen without microbial contamination.** *Biol Plant* 1964, **6(1)**:68-69.
82. Li C, Wong WH: **Model-based analysis of oligonucleotide arrays: expression index computation and outlier detection.** *Proc National Acad Sci* 2001, **98(1)**:31.
83. Reimand J, Arak T, Vilo J: **g:Profiler–a web server for functional interpretation of gene lists (2011 update).** *Nucleic Acids Res* 2011, **39(suppl 2)**:W307.
84. Martin D, Brun C, Remy E, Mouren P, Thieffry D, Jacq B: **GOToolBox: functional analysis of gene datasets based on Gene Ontology.** *Genome Biol* 2004, **5(12)**:R101.
85. Aartsma-Rus A, Van Vliet L, Hirschi M, Janson AAM, Heemskerk H, De Winter CL, De Kimpe S, Van Deutekom JCT, AC't Hoen P, van Ommen GJB: **Guidelines for antisense oligonucleotide design and insight into splice-modulating mechanisms.** *Mol Therapy* 2008, **17(3)**:548-553.
86. Park SK, Howden R, Twell D: **The Arabidopsis thaliana gametophytic mutation gemini pollen1 disrupts microspore polarity, division asymmetry and pollen cell fate.** *Development* 1998, **125(19)**:3789.

doi:10.1186/1471-2229-12-24
Cite this article as: Hafidh *et al.*: Comprehensive analysis of tobacco pollen transcriptome unveils common pathways in polar cell expansion and underlying heterochronic shift during spermatogenesis. *BMC Plant Biology* 2012 **12**:24.

Submit your next manuscript to BioMed Central and take full advantage of:

- **Convenient online submission**
- **Thorough peer review**
- **No space constraints or color figure charges**
- **Immediate publication on acceptance**
- **Inclusion in PubMed, CAS, Scopus and Google Scholar**
- **Research which is freely available for redistribution**

Submit your manuscript at
www.biomedcentral.com/submit

BioMed Central

2.2. De novo post-pollen mitosis II tobacco pollen tube transcriptome

Said Hafidh, Katarína Breznenová Kulichová, David Honys

Plant Signaling & Behavior 2012, 7(8):918-21, doi: 10.4161/psb.20745

My contribution: I have helped with the tobacco pollen tube cultivation and collection, together with tissue grinding and RNA extraction and preparation for Affymetrix microarray measurements.

Plant Signaling & Behavior 7:8, 1-4; August 2012; © 2012 Landes Bioscience

De novo post-pollen mitosis II tobacco pollen tube transcriptome

Said Hafidh, Katarína Breznenová and David Honys*

Laboratory of Pollen Biology; Institute of Experimental Botany; Academy of Sciences of the Czech Republic; Praha, Czech Republic

Keywords: male gametophyte development, de novo pollen tube transcriptome, pollen tube growth, transcriptomics, www.pollenbiology.cz

In our previous study we applied the Agilent 44K tobacco gene chip to introduce and analyze the tobacco male gametophyte transcriptome in mature pollen and 4 h pollen tubes. Here we extended our analysis post-pollen mitosis II (PMII) by including a new data set obtained from more advanced stage of the ongoing progamic phase—pollen tubes cultivated in vitro for 24 h. Pollen mitosis II marks key events in the control of male gametophyte development, the production of two sperm cells. In bicellular species covering cca 70% of angiosperms including *Nicotiana tabacum*, PMII takes place after pollen germination in growing pollen tube. We showed the stable and even slightly increasing complexity of tobacco male gametophyte transcriptome over long period of progamic phase—24 h of pollen tube growth. We also demonstrated the ongoing transcription activity and de novo transcript accumulation in post-PMII pollen tubes cultivated in vitro. In all, we have identified 320 genes (2.2%) that were newly transcribed at least after 4 h of pollen tube cultivation in vitro. Further, 699 genes (4.8%) showed over 5-fold increased accumulation after the 24 h of cultivation.

This manuscript has been published online, prior to printing. Once the issue is complete and page numbers have been assigned, the citation will change accordingly.

In our original work,[1] we applied the Agilent 44K tobacco gene chip to conduct the first thorough transcriptomic analysis of the tobacco male gametophyte development and the dynamics of gene expression in the first four hours of pollen germination and tube growth. We presented four independent data sets—two male gametophytic mature pollen (MPG) and 4 h pollen tubes (PT4) and two sporophytic leaves (L) and roots (R) as a reference. In the meantime of the publication process of the original article, we extended our analyses and supplement with a data set from more advanced stage of the ongoing progamic phase—pollen tubes cultivated in vitro for 24 h (PT24). This extension allowed us to compare pollen tube transcriptomes pre- and post-pollen mitosis II (PMII). In tobacco, PMII occurs at the time window between 10–12 h of cultivation and is associated with changes in male germ unit (MGU) organization and pollen tube growth characteristics (ref. 1 and Breznenová K, Capková V, Hafidh S and Honys D, unpublished data).

Mature pollen was isolated according to Petru et al. and pollen tubes were in vitro germinated as described previously in reference 2. RNA extraction, probe preparation and microarray hybridization were described in the original article[1] as well as the microarray data normalization and analyses by freely available dChip 1.3 software[4] and CLC Genomic Workbench v. 4.5.1 (CLC bio, Aarhus, Denmark). As before, two biological replicates were characterized.

Principal component analysis (**Fig. 1**) confirmed the position of the new 24 h pollen tube transcriptome in the close vicinity to PT4 within the unique cluster of male gametophytic data sets clearly distinguished from sporophytic samples. Scatterplots were used to further visualize the distribution of p-values for individual probes. A close relationship between tissues of similar origin was confirmed as well as a great variability in relation to disparate tissues (**Fig. 2**).

Of the 43,803 probes present on the array, 35,129 (80%) were reliably expressed (present call "well-above-background" in both replicates) in at least one tissue (**Fig. 3**). In the original article, we already demonstrated the reduced complexity of tobacco male gametophyte transcriptome in comparison to sporophytic tissues. In this respect tobacco followed the trend shown for plant species with more advanced tricellular pollen—Arabidopsis and rice.[5-7] Here, the complexity of 24 h pollen tube transcriptome was shown to be similar, though slightly higher than that of earlier male gametophytic data sets. There were 14,420 genes (41% of expressed genes) reliably expressed in 24 h pollen tubes (**Table S1**), only 320 genes more than in 4 h pollen tubes and 454 more than in mature pollen. Thus there is moderate but significant increase in transcription during pollen tube growth, particularly after PMII. Interestingly, this increase in transcriptional activity was reflected not only by an increase in the number of expressed genes but also in continuous accumulation of their respective transcripts. Of the 14,420 transcripts present in PT24, 6,934 (48.1% of genes active in PT24) have their expression signal in PT24 stronger than in other two male gametophytic data sets. Moreover, as many as 699 genes

*Correspondence to: David Honys; Email: david@ueb.cas.cz
Submitted: 03/27/12; Accepted: 05/14/12
http://dx.doi.org/10.4161/psb.

(4.8%) have their relative expression signal 5-fold higher than both MPG and PT4. In contrast to generally stable and relatively low proportion of male gametophyte-specific genes across various plant species,[5-7] high proportion of these upregulated genes (227 genes, 32.5%) were putatively male gametophyte-specific. These results confirmed the ongoing high transcription activity and specific transcript accumulation in tobacco pollen tubes after PMII. Our finding also supplements results of a recent study by Qin et al. that revealed a specific subset of genes in Arabidopsis (semi-in-vivo (SIV)-enriched and SIV-exclusive) to be induced in pollen tubes grown through the pistil but not when grown in vitro. We rectify that among the SIV-enriched list (140 genes), we have identified at least eight tobacco homologs (47% of the total identified homologs) that had showed significant increase in accumulation, as much as 15-fold (**Fig. S1 and Table S2**) after 24 h of in vitro pollen tube cultivation. We supplement the previous findings in Arabidopsis that at least some of the identified SIV-enriched genes are continuously accumulating through the late progamic transcription program rather than as a response to the interaction with the pistil. However, the later still may have an influence on their expression. Among this set of genes there are potential receptor proteins that may respond to female cues for guidance of the pollen-tube tip growth. In the light of recent identification and biochemical characterization of long-term RNA-storage and transport of EPP particles,[3,9] it is likely that these newly synthesized and accumulated transcripts are stored within these particles.

Taking together, here we present the extended tobacco male gametophytic transcriptomic data set that is now available to the scientific community. Moreover, we showed ongoing transcription activity and de novo transcript accumulation in post-PMII pollen tubes cultivated in vitro.

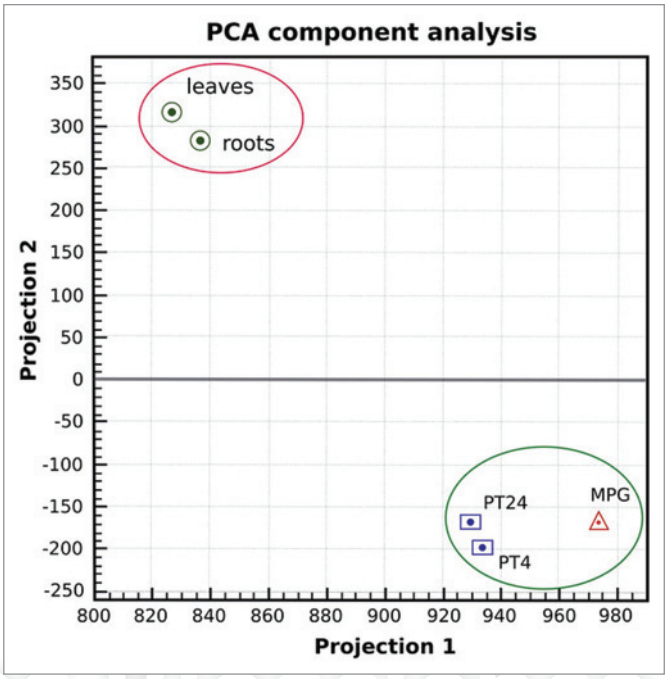

Figure 1. Output of the first and second principal component (PCA) analysis of the $\log_2$-transformed data sets. The largest and second-largest principal component (variability projection 1 and 2, respectively) are displayed in orthogonal directions, assessing the overall homogeneity between replicates and variability between samples of different tissue types as reflected in their grouping.

©2012 Landes Bioscience. Do not distribute.

Acknowledgments

The authors gratefully acknowledge the financial support from Czech Science Foundation (Grants No. P501/11/P321 and 522/09/0858) and Ministry of Education, Youth and Sports of the Czech Republic (Grant No. LD11018).

Note

Supplemental material may be found here: http://www.landesbioscience.com/journals/psb/article/20745/

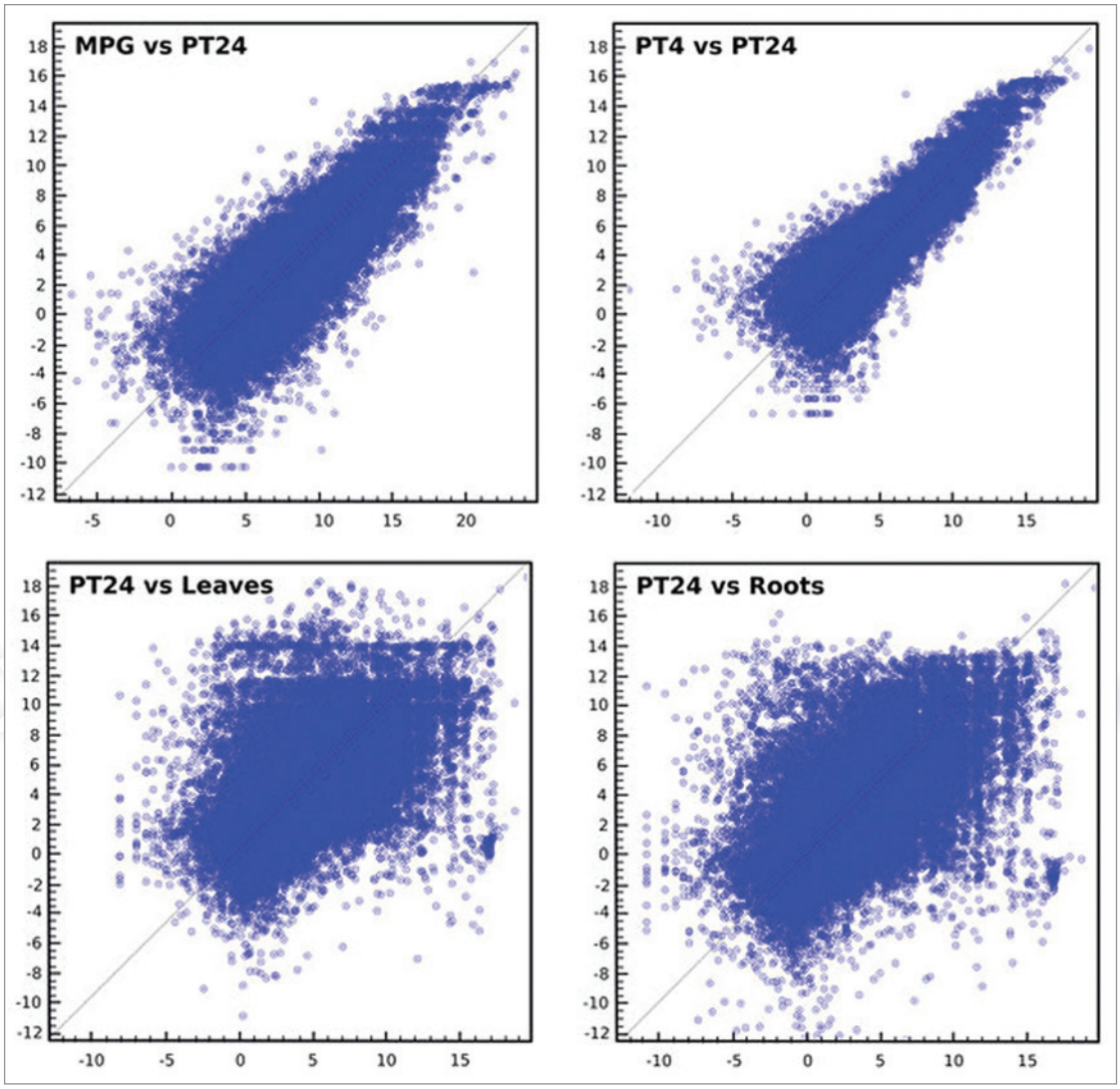

Figure 2. Scatterplots of $\log_2$-transformed quantile normalized tmicroarray data showing a correlation of 24 h data set with other tissue arrays. A wider symmetrical scattering of the probes from the 'trendline' implicates higher variability between the tissues, with less dependency between variance and mean expression values, as compared with more tightly packed male gametophytic spots reflecting a closer relationship between these data sets.

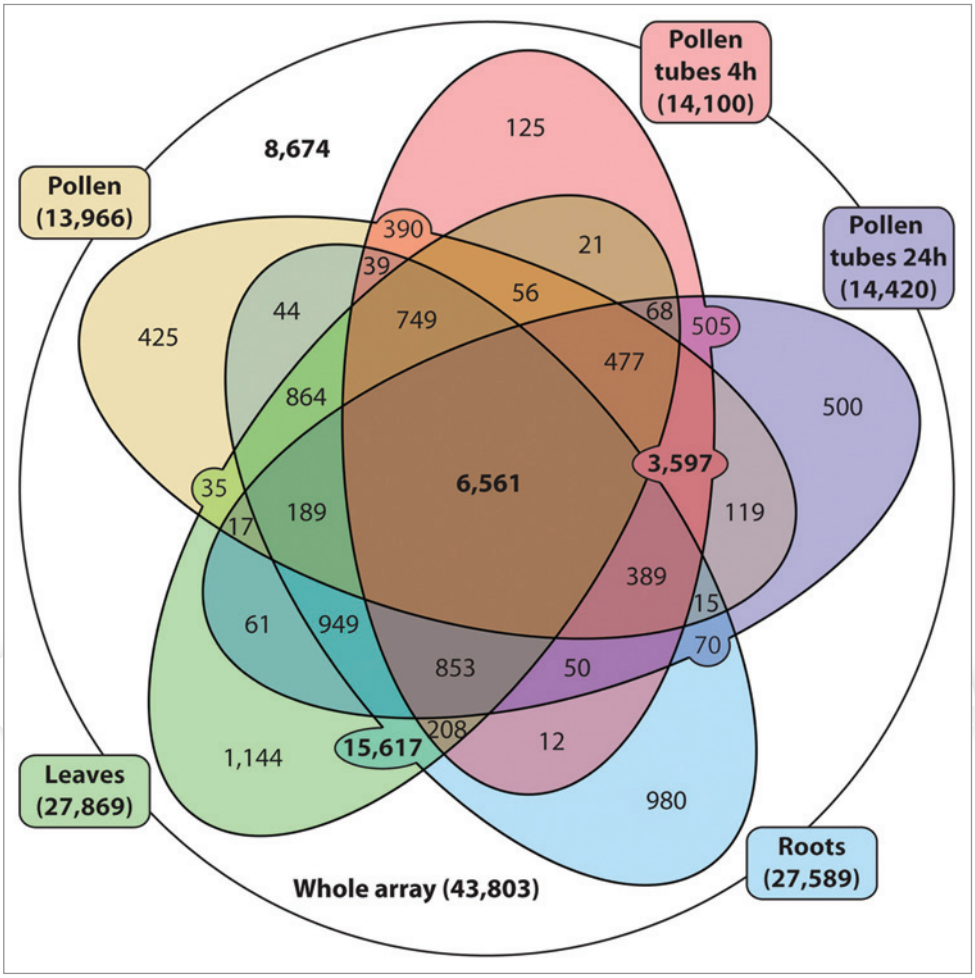

Figure 3. Five-way Venn diagram showing the quantification of all possible overlaps of all reliably expressed probes between three male gametophytic and two sporophytic data sets.

References

1. Hafidh S, Breznenová K, Růžička P, Feciková J, Čapková V, Honys D. Comprehensive analysis of tobacco pollen transcriptome unveils common pathways in polar cell expansion and underlying heterochronic shift during spermatogenesis. BMC Plant Biol 2012; 12:24; PMID:22340370; http://dx.doi.org/10.1186/1471-2229-12-24.
2. Petrů E, Hrabětová E, Tupý J. The technique of obtaining germinating pollen without microbial contamination. Biol Plant 1964; 6:68-9; http://dx.doi.org/10.1007/BF02930799.
3. Honys D, Reňák D, Feciková J, Jedelský PL, Nebesářová J, Dobrev P, et al. Cytoskeleton-associated large RNP complexes in tobacco male gametophyte (EPPs) are associated with ribosomes and are involved in protein synthesis, processing and localization. J Proteome Res 2009; 8:2015-31; PMID:19714881; http://dx.doi.org/10.1021/pr8009897.
4. Li C, Wong WH. Model-based analysis of oligonucleotide arrays: expression index computation and outlier detection. Proc Natl Acad Sci USA 2001; 98:31-6; PMID:11134512; http://dx.doi.org/10.1073/pnas.011404098.
5. Honys D, Twell D. Transcriptome analysis of haploid male gametophyte development in Arabidopsis. Genome Biol 2004; 5:85; PMID:15535861; http://dx.doi.org/10.1186/gb-2004-5-11-r85.
6. Pina C, Pinto F, Feijó JA, Becker JD. Gene family analysis of the Arabidopsis pollen transcriptome reveals biological implications for cell growth, division control and gene expression regulation. Plant Physiol 2005; 138:744-56; PMID:15908605; http://dx.doi.org/10.1104/pp.104.057935.
7. Wei LQ, Xu WY, Deng ZY, Su Z, Xue Y, Wang T. Genome-scale analysis and comparison of gene expression profiles in developing and germinated pollen in *Oryza sativa*. BMC Genomics 2010; 11:338; PMID:20507633; http://dx.doi.org/10.1186/1471-2164-11-338.
8. Qin Y, Leydon AR, Manziello A, Pandey R, Mount D, Denic S, et al. Penetration of the stigma and style elicits a novel transcriptome in pollen tubes, pointing to genes critical for growth in a pistil. PLoS Genet 2009; 5:1000621; PMID:19714218; http://dx.doi.org/10.1371/journal.pgen.1000621.
9. Hafidh S, Čapková V, Honys D. Safe keeping the message: mRNP complexes tweaking after transcription. Adv Exp Med Biol 2011; 722:118-36; PMID:21915786; http://dx.doi.org/10.1007/978-1-4614-0332-6_8.

View publication stats

2.3. A Plastid-Bound Ankyrin Repeat Protein Controls Gametophyte and Early Embryo Development in Arabidopsis thaliana

Katarína Kulichová, Janto Pieters, Vinod Kumar, David Honys and Said Hafidh

Front. Plant Sci., 08 March 2022, Sec. Plant Development and EvoDevo, doi: 10.3389/fpls.2022.767339

My contribution: The starting point for all three candidate genes (EMB2036/AKRP, EMB1441/AtNEMF and SUS2/PRP8a) was the same: the gene was selected from the tobacco pollen and pollen tube transcriptomic data published by our laboratory (Hafidh et al. 2012a, 2012b) based on its profile in the translated and non-translated/stored fractions. The Arabidopsis homolog was identified based on sequence homology with tobacco and multiple T-DNA lines were screened for defective phenotypes. In accordance with previous publications about EMB2036/AKRP, I identified malformed embryos (Fig. 4). On top of embryo lethal phenotypes, I also found gametophytic defects both in the female and the male (Fig. 1). Under the supervision of Said Hafidh and David Honys, I performed all the phenotypic screens and viability tests (Fig. S3, Fig. S4). I also crossed the used T-DNA line into multiple cell fate markers and performed all the initial screens. Some experiments needed to be extended during my maternity leave and were performed by colleagues credited in the manuscript (part of Fig. 2 and Fig. 3). I cloned the AKRP promoter for expression studies and the native protein for localisation purposes (Fig. S2). Due to native promoter weakness, I cloned AKRP under various other tissue-specific promoters not only for localisation, but also complementation purposes (Fig. 6, Fig. S5). The pollen-specific promoter showed beautiful expression in pollen proplastids (Fig. 5), confirmed by co-localisation with a plastid-specific marker (Fig. S6). The various constructs I cloned showed variable and often limited ability to complement the defective phenotypes, often leading to partial rescue of either gametophytic or sporophytic malformations (Fig. 6, Fig. S5). This shows that AKRP plays a specific and precisely timed role in the development of plastids and that perhaps the two annotated isoforms play different roles that we were able to detect with our experiments.

frontiers in Plant Science

ORIGINAL RESEARCH
published: 08 March 2022
doi: 10.3389/fpls.2022.767339

A Plastid-Bound Ankyrin Repeat Protein Controls Gametophyte and Early Embryo Development in *Arabidopsis thaliana*

Katarína Kulichová[1†‡], Janto Pieters[1], Vinod Kumar[1], David Honys[1,2†] and Said Hafidh[1†‡]*

[1] Laboratory of Pollen Biology, Institute of Experimental Botany of the Czech Academy of Sciences, Prague, Czechia,
[2] Department of Plant Experimental Biology, Faculty of Science, Charles University, Prague, Czechia

OPEN ACCESS

Edited by:
Paloma Moncaleán,
Neiker-Tecnalia, Spain

Reviewed by:
Gabriela Carolina Pagnussat,
National University of Mar del Plata, Argentina
Silvia Vieira Coimbra,
University of Porto, Portugal
Daisuke Kurihara,
Nagoya University, Japan

***Correspondence:**
Said Hafidh
hafidh@ueb.cas.cz

†ORCID:
Katarína Kulichová
orcid.org/0000-0002-1115-9899
David Honys
orcid.org/0000-0002-6848-4887
Said Hafidh
orcid.org/0000-0002-3970-713X

‡These authors have contributed equally to this work

Specialty section:
This article was submitted to Plant Development and EvoDevo, a section of the journal Frontiers in Plant Science

Received: 30 August 2021
Accepted: 10 January 2022
Published: 08 March 2022

Citation:
Kulichová K, Pieters J, Kumar V, Honys D and Hafidh S (2022) A Plastid-Bound Ankyrin Repeat Protein Controls Gametophyte and Early Embryo Development in Arabidopsis thaliana. Front. Plant Sci. 13:767339. doi: 10.3389/fpls.2022.767339

Proplastids are essential precursors for multi-fate plastid biogenesis, including chloroplast differentiation, a powerhouse for photosynthesis in plants. Arabidopsis ankyrin repeat protein (AKRP, AT5G66055) is a plastid-localized protein with a putative function in plastid differentiation and morphogenesis. Loss of function of *akrp* leads to embryo developmental arrest. Whether AKRP is critical pre-fertilization has remained unresolved. Here, using reverse genetics, we report a new allele, *akrp-3*, that exhibited a reduced frequency of mutant embryos (<13%) compared to previously reported alleles. *akrp-3* affected both male and female gametophytes resulting in reduced viability, incompetence in pollen tube attraction, altered gametic cell fate, and embryo arrest that were depleted of chlorophyll. AKRP is widely expressed, and the AKRP-GFP fusion localized to plastids of both gametophytes, in isolated chloroplast and co-localized with a plastid marker in pollen and pollen tubes. Cell-type-specific complementation of *akrp-3* hinted at the developmental timing at which AKRP might play an essential role. Our findings provide a plausible insight into the crucial role of AKRP in the differentiation of both gametophytes and coupling embryo development with chlorophyll synthesis.

Keywords: proplastid, pollen, embryo development, pollen tube reception, fertilization

INTRODUCTION

Proplastids are essential organelles for plant life cycle; they provide nutrients and monomers for energy, act as a precursor for chloroplast differentiation, and function in biosynthesis and storage of pigments, hormones, starch, fats, proteins, and terpenes. During embryo development, proplastids differentiate into chloroplasts from the globular stage, and later, during seed maturation, differentiate into storage plastids, elaioplasts (Demarsy et al., 2012; Allorent et al., 2013; reviewed in Liebers et al., 2017). Many plastid genes are, thus, critical for early plant development, and mutations often result in embryo lethality (Tzafrir et al., 2004; Meinke et al., 2008; Ajjawi et al., 2010; Myouga et al., 2010, 2013; Bryant et al., 2011). Defects in plastid function might also manifest prior to embryo development in the male or female gametophyte. Energy production in mature pollen and growing pollen tubes (PTs) is mainly supplied from mitochondrial respiration and ATP production; nevertheless, glycolysis within plastids is also a contributing source of energy (reviewed in Selinski and Scheibe, 2014). Accumulation of starch during pollen maturation is, therefore, critical, as it serves later as an energy source. Knockout mutants in enzymes catalyzing the regeneration of NAD + during glycolysis, *gapcp1* and *gapcp2*, are sterile males

(Muñoz-Bertomeu et al., 2010). The double mutant genes, *gapcp1* and *gapcp2,* exhibit defects in pollen morphology and viability in addition to having a disorganized tapetal layer. Several other mutants involved in glycolytic processes and maintaining redox homeostasis with defects in gametophyte and embryo development have been described (Prabhakar et al., 2010; Chen et al., 2011; Zhao and Assmann, 2011; reviewed in Selinski and Scheibe, 2014).

Almost all types of plastids are present during pollen development in several layers of the microsporangium and are essential in the formation of functional male gametophytes (Clément and Pacini, 2001; Hafidh and Honys, 2021). They play a supportive function to other cells as in the case of tapetum and the vegetative cell, but proplastids in sperm cells play a direct role in reproductive events through biparental cytoplasmic inheritance to the newly formed zygote. In angiosperms, only proplastids and amyloplasts are present from meiocytes to pollen maturity. Amyloplasts differentiated from proplastids in microspores are preceded by vacuolization as pollen matures (Pacini, 1994). In contrast, proplastids from tapetum undergo division during the early stages of microsporogenesis and differentiate into elaioplasts (Dickinson, 1973; Pacini and Juniper, 1979). Both tapetosomes and elaioplasts generate tapetal lipids that are secreted into the locule to form tryphine when the tapetal plasma membrane breaks down (Dickinson and Lewis, 1973). They also constitute oleosins and triacylglycerols, which later reach the coat of pollen and form a major lipid component (Ting et al., 1998).

Arabidopsis *EMB2036*, an ankyrin repeat protein (AKRP), is a single copy gene with five ankyrin repeats (Zhang et al., 1992). Ankyrin repeat-containing domains (ANK) are described as protein-protein interaction domains found in viruses, archea, bacteria, and eukaryotes. Ankyrin repeats have been found in numerous proteins with functions, such as cell signaling, cytoskeleton integrity, transcription and cell–cycle regulation, inflammatory response, development, and various transport pathways. No enzymatic function has been detected in any ankyrin repeat-containing proteins (reviewed in Mosavi et al., 2004). In Arabidopsis, there are 105 ANK-containing proteins, but only a few were described functionally (reviewed in Becerra et al., 2004). Two ankyrin repeat-containing plastid-targeted proteins, NPR1-like protein 3 and NPR1-like protein 4, are receptors for salicylic acid and are important for basal defense against pathogens (reviewed in Kuai et al., 2015). A mitochondrial protein, ANK6, is an example with function in gametophyte development and male-female gamete recognition during double fertilization (Yu et al., 2010). An *AKRP* expression was reported to be developmentally and lightly regulated. Plants transformed with sense or antisense constructs exhibited a chlorotic phenotype caused by a loss of chloroplast ultrastructure and lower amounts of chlorophylls and carotenoids (Zhang et al., 1992). Interestingly, the expression of selected photosynthesis-related genes was not affected in AKRP-deficient plants (Zhang et al., 1994). An AKRP interacted through ankyrin domains with a sequentially and functionally similar protein, EMB506 (Albert et al., 1999). Two predicted splice isoforms of *AKRP* were experimentally confirmed to be expressed (Garcion et al., 2006). Based on the observed mutant phenotype, AKRP was predicted to function in plastid differentiation. A recent study described a mechanistic role of AKRP (STT2) and EMB506 (STT1) as essential in the sorting of chloroplast twin-arginine translocation (cpTat) pathway proteins to thylakoid membranes (Ouyang et al., 2020). In this study, we have characterized a previously unknown gametophytic defect identified in a new T-DNA insertion allele of *akrp-3* that was absent in other reported *emb2036* alleles. Using gametophytic promoters, we provide a potential time window for AKRP function, pre- and post-fertilization.

RESULTS

Isolation of Novel *akrp* Allele

Two previous embryo-lethal alleles of *AKRP*, *emb2036-1* and *emb2036-2*, were reported to show 25% of pale mutant homozygous seeds containing embryos arrested at globular stage but exhibited no gametophytic defects (Garcion et al., 2006; Meinke et al., 2008). Public RNA-seq data suggest that AKRP transcripts are higher in microspores but are drastically reduced by pollen maturity, and were detected in isolated egg cell of Arabidopsis thaliana (Julca et al., 2021). As a single copy gene, the lack of gametophytic defect was puzzling. We, therefore, performed RT-qPCR measurements and verified that AKRP is broadly expressed and exhibits variation in abundance among sporophytic and gametophytic tissues with the highest expression in reproductive tissues (**Figure 1A**). Two splice variants are predicted to arise from alternative splicing of an *AKRP* single locus, with the shorter isoform lacking the last two ankyrin repeats (**Figure 1B** and **Supplementary Figure S1**). The RT-qPCR revealed that, on average, the longer isoform is >2.5-fold more abundant in both sporophytic and reproductive tissues (**Figure 1A**). We fused a 997bp putative AKRP promoter fragment with a beta-glucuronidase enzyme (GUS) and detected a promoter activity throughout development, with the strongest GUS staining specifically in the early stages of pollen development in ovules and the embryo, as well as in mature seeds (**Supplementary Figure S2**). Therefore, we screened numerous Gabi-kat T-DNA collections ([1]Kleinboelting et al., 2012) with putative insertion in the *AKRP* locus and isolated a new allele, *akrp-3* (Gk_0876D05), which exhibited both pollen and female gametophytic defects as well as a similar embryo-lethal phenotype but in a reduced frequency. We confirmed the position of insertion by Sanger sequencing, which revealed T-DNA insertion between 609 and 624 bp of exon 1 (**Figure 1B**). No homozygous individuals were recovered, confirming a gametophytic or embryo lethality. However, among segregating heterozygous individuals, some contained the canonical wild type and a mutant T-DNA band (Ht22), and others had an extra band (Ht3 and HT15) that we confirmed by sequencing as a back-to-back T-DNA inserted 6 bp away from the first insertion (**Figures 1B,C**). Both types originated from a common parent stock; therefore, we assumed that they were identified and merged as a single event at the stock center. No significant phenotypic variations

[1]https://www.gabi-kat.de

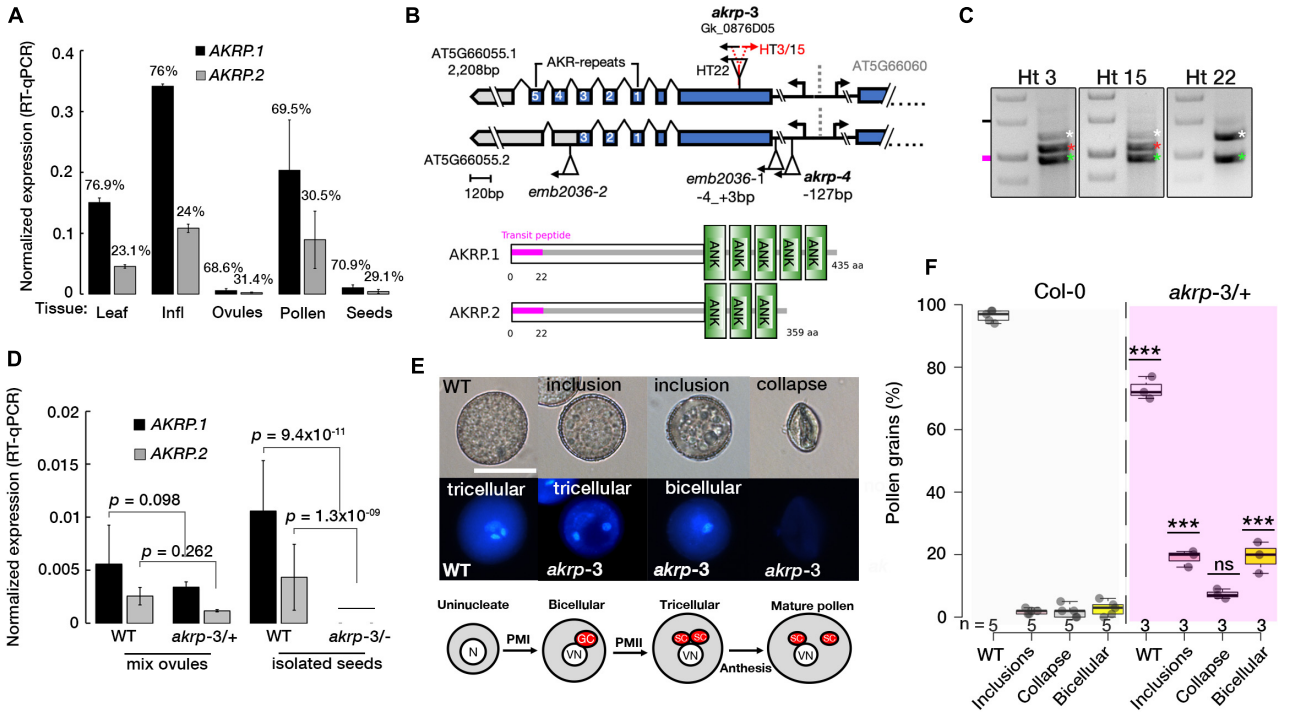

FIGURE 1 | The *akrp-3* allele exhibits abnormal pollen maturation and loss of gametic cell fate. **(A)** Quantification of AKRP splice isoform expression by RT-qPCR. Percentages represent the relative abundance of each isoform in respective tissues. **(B)** Gene and protein models of two AKRP isoforms with the position of *akrp* T-DNA insertions and ankyrin repeats (ANK). Alignment of the isoforms is presented in **Supplementary Figure S1**. **(C)** PCR genotyping of *akrp*-3 (Gk_0876D05) revealed two groups of segregating heterozygous; with three bands (HT3/15) and those with two bands (HT22), wild-type band (white asterisks), mutant (green asterisks) and a second T-DNA band (red asterisks) 6 bp apart. **(D)** Estimation of knockdown of both isoforms in *akrp*-3 mixed ovules and isolated homozygous *akrp*-3 seeds. **(E)** Abnormal pollen development observed in *akrp-3/* + includes segregant WT pollen, reduced size pollen grains with cytoplasmic inclusion bodies with a single undivided generative nucleus (binucleate pollen) or with two sperm cells, and totally collapsed pollen grains with no DNA content. Below, a schematic of a normal pollen maturation. The N/VN are nuclei of the microspore and vegetative cell, GC/SC are the products of pollen mitosis I and II, the generative and the sperm cells, respectively. **(F)** Frequency of pollen phenotype observed in panel **(E)**. Statistical evaluation was performed using one-way ANOVA with Tukey's multiple comparisons test, with "n"-representing individual M3 plants assessed. ***$p < 0.0001$, ns, not significant. N = 12,463 pollen grains, scale bar = 20 μm.

were observed between plants with single T-DNA or those with back-to-back T-DNA insertion genotypes, however, were possible we present both types separately. We quantified the expression of both *AKRP* isoforms by RT-qPCR and verified their downregulation in *akrp-3/+* heterozygous ovules and complete knockout in isolated *akrp-3* homozygous mutant seeds (**Figure 1D**).

Loss of Function of *akrp* Produced Abnormally Developed Pollen Without Gametic Cell Fate

In pollen, multiple aberrant phenotypes were identified *akrp-3/+* plants. Among the aberrant pollen phenotype they include underdeveloped smaller pollen grains with cytoplasmic inclusion bodies, bi-nucleate pollen that failed to undergo the second pollen mitotic division (PMII) of the generative cell to produce two sperm cells, and the most severe was the appearance of aborted pollen grains (**Figure 1E**). No similar phenotypes were observed in segregating wild-type progenies or in screening of the original *emb*2036-1 allele (**Figure 1B**). The screening of an independent allele, *akrp-4*, with an insertion at *AKRP5*′UTR, did not exhibit any aberrant phenotypes. To rule out a T-DNA effect on a neighboring gene, AT5G66060, we screened three T-DNA alleles belonging to the AT5G66060 locus. None of the AT5G66060 alleles recapitulated the *akrp*-3 phenotype, which strongly supports that the observed phenotype is linked to *akrp*-3 loss of function.

To better understand the nature of the *akrp-3/+* gametophytic defect, multiple assays were performed to assess viability and pollen fitness. Alexander staining revealed fully viable pollen grains alongside partially stained pollen grains containing cytoplasmic inclusion bodies, whereas *in vitro* germination showed slight reduction in *akrp*-3/+ pollen germination (**Supplementary Figures S3a–c**). The PT length appeared similar whether *in vivo*, semi-*in vivo* or *in vitro* (**Supplementary Figures S3d,e**). However, *akrp*-3 PT length perturbation could be masked by the mixture with wild-type PTs, as they are not phenotypically differentiated. The failure of *akrp*-3 generative cell to undergo PMII and appearance of inclusion bodies in the *akrp*-3 pollen implied possible pollen developmental perturbation. We therefore investigated if *akrp* gametic cell fate

is correctly specified. We crossed multiple gametophyte cell-specific markers into *akrp-3*/+ plants. These included an egg cell marker (pEC1.1-H2B-mRFP), a sperm cell marker (pHTR10-HTR10:RFP), and vegetative cell markers (pLat52-GFP and pLat52-GUS). The screening of *akrp-3*/+ plants homozygous for cell fate markers revealed that pEC1.1-H2B-mRFP egg cell expression was reduced to half of the ovules compared to that of wild-type control (35.9%, n = 1733), indicative of an effect on *akrp*-3 ovule egg cell differentiation (**Supplementary Figures S3f,g**). Similarly, the expressions of pLat52-GFP, pLat52-GUS, and pHTR10-HTR10:RFP in the vegetative cell and sperm cells were respectively reduced by 78 (n = 1,885), 47 (n = 2,211), and 60% (n = 3,889) on the *akrp-3*/+ background (**Supplementary Figures S3f,g**), indicative of *akrp*-3 pollen effect on vegetative and sperm cell differentiation. Rarely, some of the *akrp*-3 bi-cellular pollen or those containing cytoplasmic inclusions expressed both vegetative and sperm cell markers (**Supplementary Figures S3f,g**). When germinated *in vitro*, only a small population of bicellular PTs was observed, and its growth appeared retarded, with no or rare expression of cell fate markers (**Supplementary Figures S3f,g**). Collectively, these results suggest that the *akrp-3* loss of function mutant failed to correctly differentiate the male and female gametic cell fates. However, selfed *akrp*-3/+ heterozygous plants did not show significant segregation distortion, whereas reciprocal test crosses showed a decreased transmission only through the female (78% TE), but not through the male gametophyte (97% TE) (**Supplementary Figures S4a,b**).

Arabidopsis Ankyrin Repeat Protein in Ovules Is Required for Pollen Tube Attraction

In *akrp*-3/+ siliques, a high percentage of seed gaps appeared, indicating a likely fertilization defect. To establish whether untargeted ovules resulting in collapse ovules are those with *akrp-3* loss of function, we conducted a live cell imaging to visualize a correct PT reception (PT arrest, burst, and sperm cell release in the receptive synergid cell) in a*krp-3*/+ pistils. Flowers were emasculated and pollinated with a homozygous double marker for sperm cells (pHTR10-HTR10:RFP) and vegetative cell (pLat52-GFP) (**Figures 2A,B**). Twenty-four hours after pollination, ovules in pollinated pistils were exposed by dissecting the carpel walls, and confocal live-cell imaging was performed to visualize the position of GFP-labeled pollen tubes and HTR10-RFP-labeled sperm cells in wild-type and *akrp-3* ovules. On average, 43.1% (n = 250) of the ovules in *akrp*-3/+ pistil did not attract any PTs and, thus, were not fertilized (**Figures 2B,C**). In some infrequent events, mutant *akrp*-3 ovules attracted multiple PTs containing sperm cells, a phenomenon termed polytubey (Beale et al., 2012; Maruyama et al., 2013). However, none of the PTs appeared to enter the mutant *akr* ovules and burst to release sperm cells (**Figure 2C**). An independent analysis using a blue dot assay with Lat52-GUS pollen unveiled a reduced PT targeting in the *akrp*-3/+ pistil, where nearly 46% (n = 264) of the ovules were not targeted by the Lat52-GUS-expressing PT (**Supplementary Figure S4c**). These data support the live-cell imaging observations and, together, imply that *akrp*-3 ovules are incompetent in PT attraction for fertilization.

A Fraction of Targeted *akrp* Ovules Exhibits a Range of Pollen Tube Reception Defects and Fails to Develop an Embryo

The tendency of *akrp*-3 ovules we observed in live cell imaging not to attract PTs or attract multiple PTs without PT burst prompted us to investigate the frequency of PT attraction by *akrp*-3 ovules. We additionally questioned whether *akrp*-3 attracted PT experience PT reception defects and/or fertilization blockage. Since pollen tube reception and fertilization improve with longer hours after pollination (HAP) (Grossniklaus, 2017; Johnson et al., 2019; Nagahara et al., 2021), we manually crossed Col-0 × Col-0 and compared with *akrp*-3/+ × Col-0 24-to-48 HAP. Callose staining of in-pistil PTs revealed a similar *akrp*-3 untargeted event 24 HAP to that observed by live-cell imaging and the blue dot assay as the predominant phenotype (**Figure 3a**). However, a careful look unveiled that the tendency of *akrp*-3 PT attraction, polytubey attraction, as well as PT reception defects (PT overgrowth), increased at the 48 HAP time point (**Figures 3b,c**). We noticed, on average, that about 2% (n = 28) of *akrp*-3 ovules are targeted and arrested PT at micropylar entry, although without clear pollen tube burst (**Figure 3b**, scene 2). Another 1.5% (n = 19) also showed polytubey without clear PT entry, and majority of *akrp*-3-targeted ovules (3.2%, n = 23) showed a PT overgrowth, indicating a PT reception defect (**Figure 3b**, scenes 3 and 4 respectively). Nevertheless, this suggests that if given time, some of the *akrp*-3 ovules (up to 6.5%, n = 70 pistils) can eventually at least attract PTs or be targeted by a PT (**Figure 3c**). But, do these *akrp*-3-targeted ovules undergo fertilization? Whether targeted by a PT or not, mutant *akrp*-3 ovules lag behind in development, as they are clearly distinguishable by their small size at the 48 HAP time point (**Figure 3a**). Dissection of these retarded ovules revealed no presence of initiated embryos in *akrp*-3 ovules and the female gametic cells remained clearly visible and unfertilized 48 HAP (**Figure 3d**). At this time point, the wild-type targeted ovules are at the minimum 32-cell embryo stage (**Figure 3d**). We, therefore, conclude that although a fraction of *akrp*-3 ovules is successfully targeted, they likely exhibit later PT reception incompetence, as seen in PT overgrowth or the inability to induce PT burst, and, therefore, do not undergo fertilization. Forty-eight hours after pollination, on average, 55.8% (n = 44 pistils) of the ovules (corresponding to wild-type ovules) were correctly targeted in *akrp*-3/+ pistils pollinated by Col-0 pollen compared to 92.5% (n = 14 pistils) targeted ovules in Col-0 pistils also pollinated by Col-0 (**Figure 3e**). To support the observation that the majority of *akrp*-3 ovules do not proceed with fertilization and embryo development, we measured seed area 24 and 48 HAP in Col-0 and *akrp*-3/+ pistils pollinated with Col-0 pollen. Our analysis identified two distinguishable populations at 48 HAP in the *akrp*-3/+ pistils but not in the Col-0 pistils, supporting lack of fertilization and

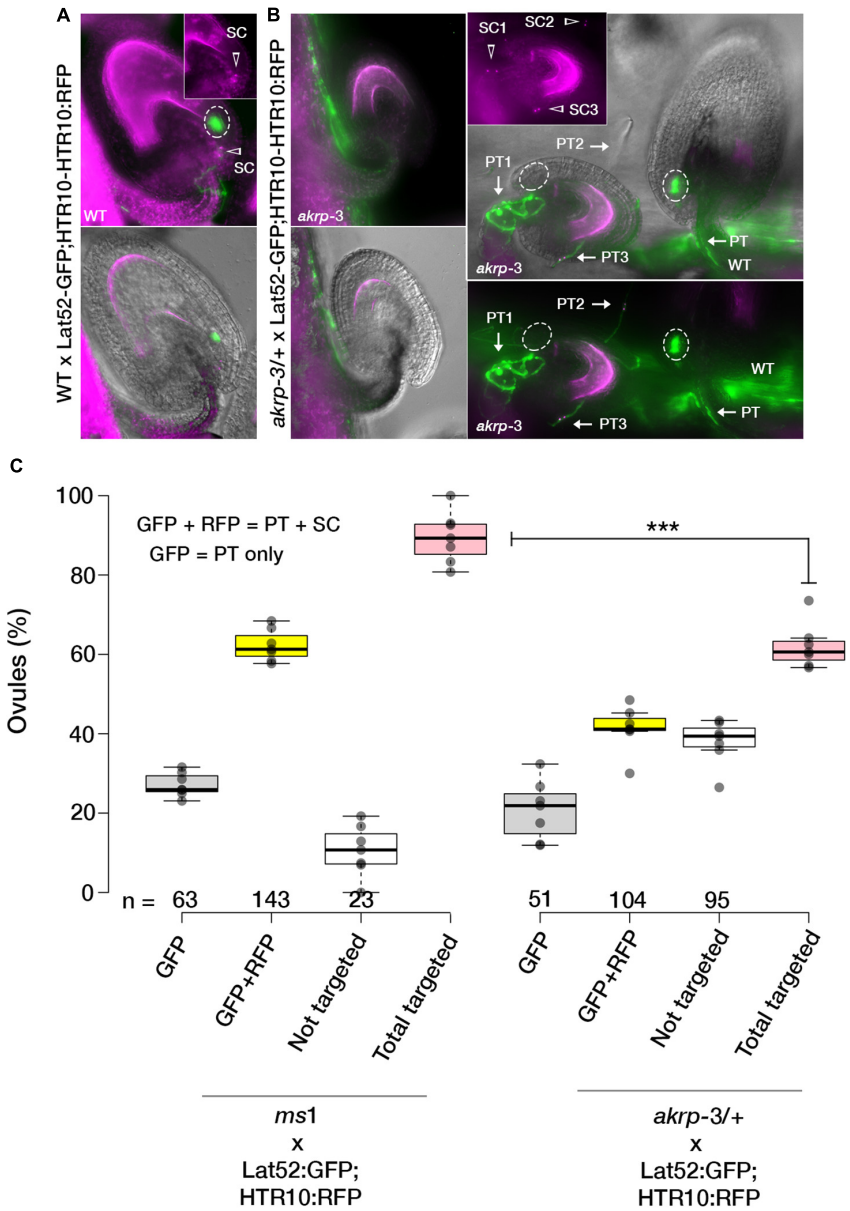

FIGURE 2 | The AKRP function in ovules is critical for pollen tube attraction. Double fertilization events in WT and *akrp*-3/+ pistils were observed after pollination with a double marker for sperm cells (pHTR10-HTR10:RFP) and vegetative cell (pLat52-GFP) 24 h after pollination. **(A)** Normal ovule targeting and reception are scored as a uniform GFP halo (ellipses) at the micropylar and presence of sperm cells (arrow head). **(B)** In *akrp*-3/+ pistil, a mixture of normal targeted and non-targeted ovules or with attraction/reception defects including up to three pollen tubes (arrows) without entry or display of GFP halo were observed. **(C)** Box plot quantification of attraction defects in respective crosses. Center lines represent the medians, and dots outside the quartile are outlier pistils, $n = 175$ and 166 ovules respectively. Statistics were conducted by two-sided non-parametric multiple comparisons with Dunnett contrast and logit approximation, $^{***}p < 0.0005$. PT, pollen tube; SC, sperm cells. Scale bar = 50 μm.

embryogenesis of Col-0 targeted mutant *akrp*-3 ovules (**Figure 3f** and **Supplementary Figure S4d**).

Arabidopsis Ankyrin Repeat Protein Post-fertilization Is Essential for Embryo Progression and Chlorophyll Synthesis

Self-pollinated *akrp*-3/+ generates, on average, 10% of homozygous *akrp* pale mutant seeds on top of the 44.2% average aborted ovule phenotype (**Figures 4A,B**). This suggests that mutant *akrp*-3 gametes from both gametophytes can get together and initiate an embryo in the aforementioned frequency. Isolation and dissection of the mutant pale seeds revealed that approximately 93% ($n = 173$) *akrp*-3 embryos are arrested at the globular stage, with the remaining 7% proceeding to late heart stage (**Figure 4C**), while the wild type segregant and Col-0 control had completed cotyledon development at similar time point (**Figure 4C**). Because of the

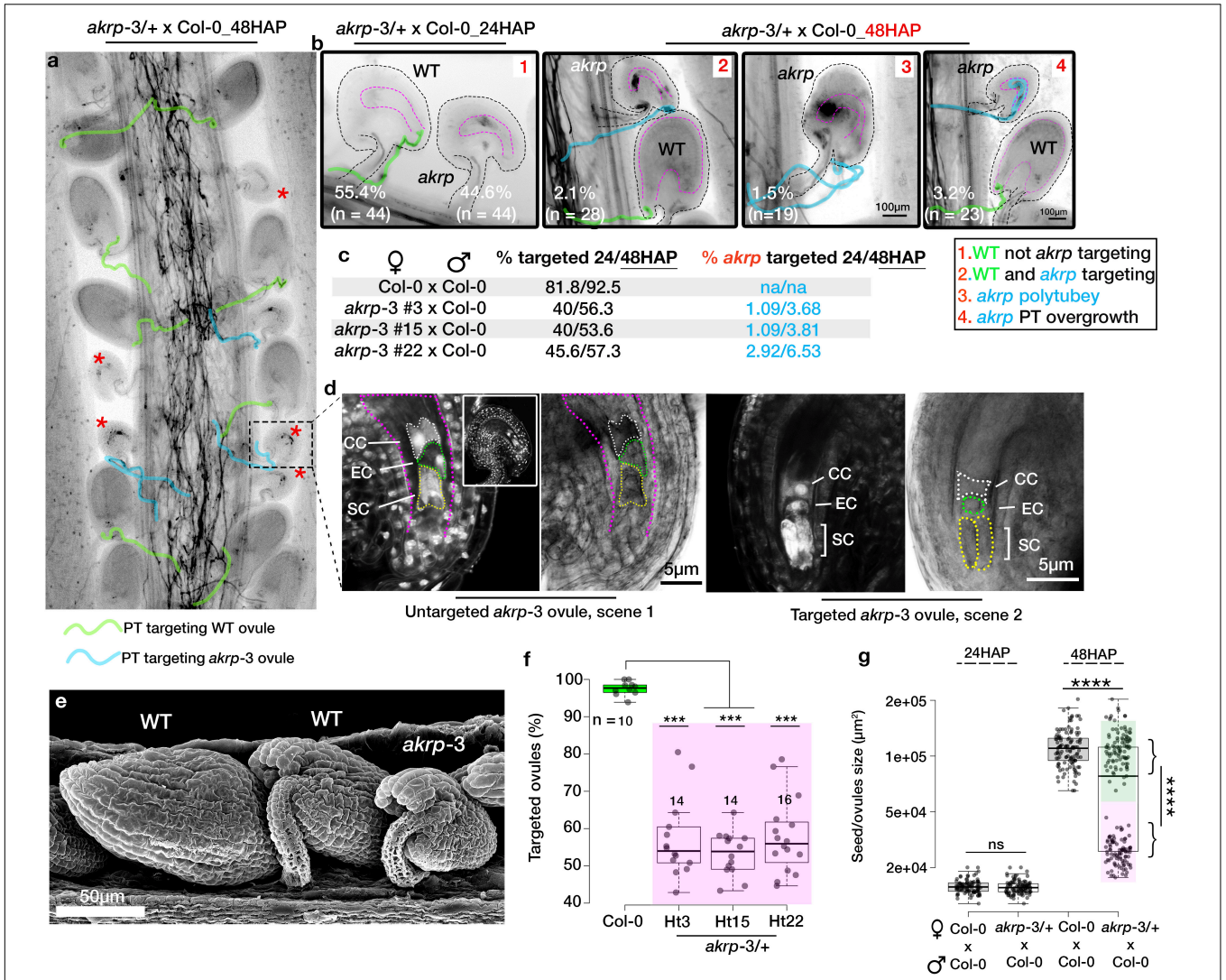

FIGURE 3 | Fraction of targeted *akrp* ovules fails to develop an embryo. *In vivo* pollen tube attraction between Col-0 × Col-0 and *akrp*-3/+ × Col-0 was assayed 24 and 48 h after pollination (HAP). **(a)** Representative pistil section from *akrp*-3/+ × Col-0 stained for callose showing wild-type (unmarked) and mutant ovules (red asterisks) and pollen tube traces (PT) targeting respective ovules. **(b)** Four phenotypic scenarios at 24 and 48 HAP were observed in *akrp*-3/+ × Col-0 pistil but not in wild-type pistil. n represents the number of pistils analyzed. **(c)** Quantification of total targeted ovules and a fraction of *akrp*-3 targeted ovules 24 and 48 HAP using both types of heterozygous *akrp*-3 with single or back-to-back insertion (**Figure 1C**). An increase in *akrp*-3 targeting can be seen 48 HAP. **(d)** Despite *akrp*-3 ovule targeting, the majority of the *akrp*-3 ovules do not produce an embryo, and the female gametophyte remains unfertilized. **(e)** Scanning electron microscopy images using secondary electron detector of *akrp*-3/+ pistil pollinated with Col-0 pollen 48 HAP demonstrated clear presence of underdeveloped *akrp*-3 seeds despite potential pollen tube targeting. **(f)** Variability in the frequency of ovule targeting as seen in individual pistils 48 HAP from respective genotypes. **(g)** Estimation of seed/ovule sizes 48 HAP clearly highlighting lack of fertilization and development of the majority of *akrp*-3 ovules. Statistics were conducted by two-sided non-parametric multiple comparisons with Dunnett contrast and logit approximation or by Student's *t*-test, ***/****$p < 0.0005/0.0001$. ns, not significant. PT, pollen tube; SC, synergid cell; EC, egg cell; CC, central cell.

genotyping variation we observed (**Figure 1C**), we investigated if this has an association with the *akrp*-3/+ silique phenotype. We dissected siliques from HT3, HT15, and HT22 (from **Figure 1C**) and observed the variable penetrance of pale seeds and unfertilized ovule phenotypes that were independent of genotypic origin (**Figures 4D,E**). Since mutant *akrp*-3 ovules are phenotypically without pigments (**Figure 4F**), we isolated mutant seeds and measured chlorophylls a and b, and total chlorophyll levels. All chlorophylls a and b levels as well as total chlorophyll were significantly depleted in the mutant *akrp*-3 seeds, suggesting lack of chlorophyll synthesis in the *akrp*-3 mutant seeds.

Arabidopsis Ankyrin Repeat Protein Localized to Proplastid in Gametophyte and in Isolated Chloroplast

A previous study colocalized 35S-spAKRP:GFP (first 50 amino acids from AKRP containing N-terminal transit peptide) with chlorophyll autofluorescence in transiently transformed

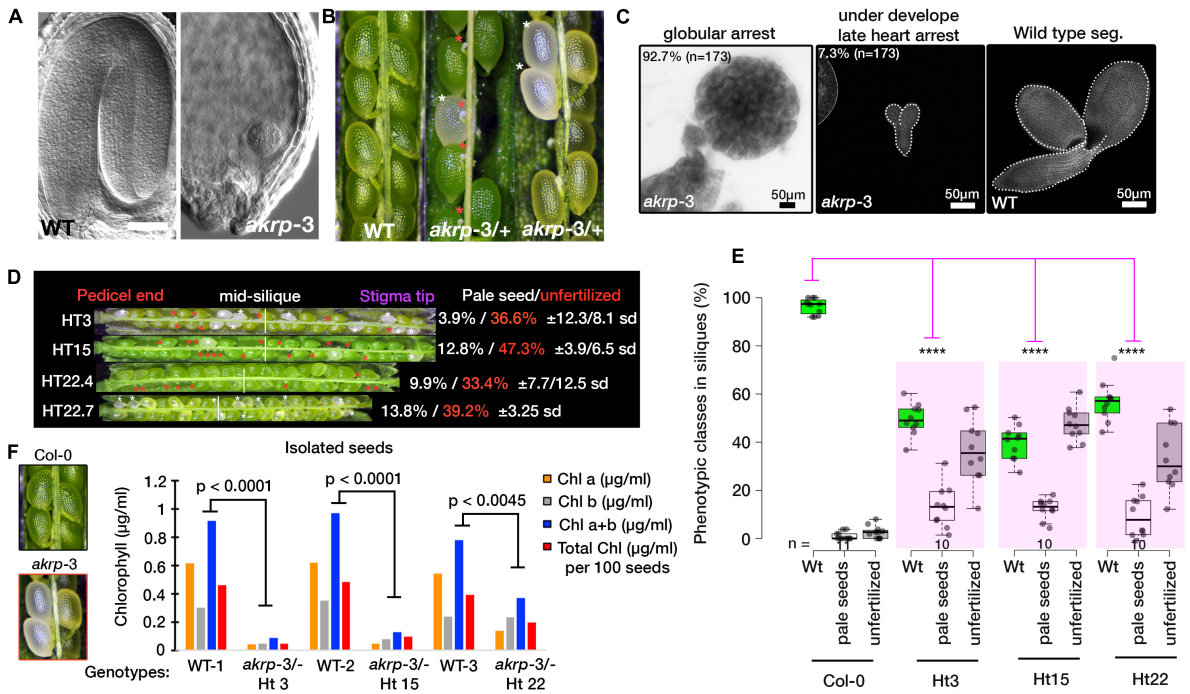

FIGURE 4 | Homozygous *akrp* arrests at globular embryo and is depleted of chlorophyll synthesis. **(A,B)** Fully developed seedlings of wild-type and globular arrested embryo of *akrp*-3 from cleared seeds of WT (green) and *akrp*-3 (pale, labeled with white asterisks, and red asterisks mark unfertilized *akrp*-3 ovules). Some siliques showed a more unfertilized phenotype over embryo arrest as quantified in panel **(D)**. **(C)** Although globular embryo arrest is a dominant *akrp*-3 embryo phenotype, some *akrp*-3 embryos halt their development in the later heart stage. **(D)** Phenotypic penetrance among *akrp*-3/+ hemizygous individuals from a common parent showing variation in the appearance of unfertilized ovules (red asterisks) and a pale embryo lethal phenotype (white asterisks). *N* = 15 siliques per genotype. **(E)** Measured frequency and variation of the *akrp*-3/+ seeds phenotype at silique maturity. **(F)** Chlorophyll measurements from isolated seeds of the respective genotypes. Data represent an average of pooled triplicates. Statistical analysis was performed by one-tail Student's *t*-test assuming unequal variance. ****$p < 0.0001$.

Nicotiana benthamiana guard cells but not the full length 35S-AKRP:GFP as proven deleterious to the chloroplast (Garcion et al., 2006). More recently, both EMB506 (STT1) and AKRP (STT2), under the control of their endogenous promoters, were reported to localize in a punctate pattern in the chloroplasts of an isolated protoplast (Ouyang et al., 2020). However, because of weakness of the *AKRP* promoter, we could not reliably detect any visible GFP signal in stable pAKRP-AKRP:GFP transformants. Nevertheless, the expression of AKRP under pLat52 (pollen vegetative cell-specific), egg cell specific EC1.1, or pDD1 (antipode-specific, AT1G36340, Steffen et al., 2007) promoters clearly localized the AKRP-GFP fusion protein into likely proplastids or differentiated elaioplasts in mature pollen, pollen tubes, the egg cell, and antipodal cells of the female gametophyte (**Figures 5A–C**). Only egg cell localization appeared less punctate and more cytoplasmically distributed (**Figure 5C**). We also isolated chloroplast from transiently transformed *Nicotiana benthamiana* leaves expressing a full-length AKRP-GFP and detected an AKRP localization in the chloroplast stroma (**Figure 5D**). To confirm AKRP-GFP plastid localization in pollen, we co-transformed pLat52-AKRP:GFP plants with a UBIQUITIN 10 promoter-driven pBINU-CHYA vector expressing 85 amino acids of the chloroplast NADPH-dependent thioredoxin reductase C (NTRC) destined to the chloroplast stroma fused to an aequorin calcium sensor and a YFP fluorophore (Mehlmer et al., 2012). Both fluorophores strongly colocalized in proplastids or differentiated elaioplasts of the pollen and pollen tubes, as supported by the GFP-YFP spectral overlap and online emission fingerprint (**Figures 5E–G**). These results confirmed AKRP-NTRC plastid co-localization (**Figure 5G**). Similar results from mature pollen were obtained by independent channel excitation (**Supplementary Figure S6**). Collectively, these data provide evidence that AKRP is likely to function in plastid differentiation and in chloroplast.

Cell-Type-Specific Complementation of *akrp-3* Revealed Timing of Arabidopsis Ankyrin Repeat Protein Function

To confirm the *akrp-3* unique gametophytic phenotype that was not observed in other alleles, we performed-complementation using a native AKRP promoter and cell type-specific promoters in an attempt to identify the developmental timing at which AKRP functions.

We fused the complete AKRP genomic fragment, including the 997-bp intergenic fragment, as a putative promoter region to N-terminal eGFP and transformed mutant *akrp*-3/+ plants. Intriguingly, the introduction of AKRP-GFP either complemented both male and female *akrp*-3 gametophytic

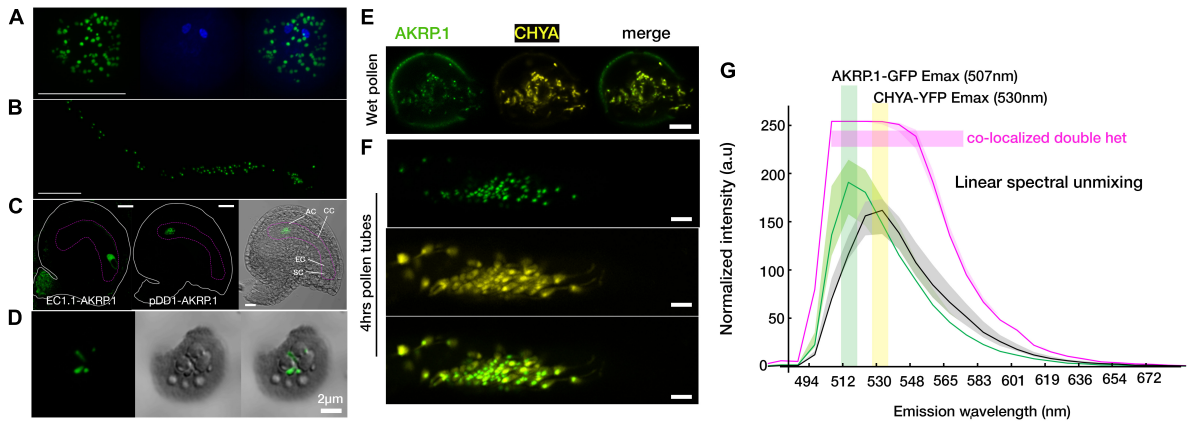

FIGURE 5 | Arabidopsis ankyrin repeat protein localized to the plastid in gametophyte and in an isolated chloroplast. **(A,B)** Punctate AKRP.1::GFP localization in pollen and *in vitro* pollen tubes expressed with the pollen-specific Lat52 promoter. **(C)** Under the egg cell promoter EC.1.1 (left panel) and an antipodal specific promoter DD1 (ubiquitin-conjugating enzyme 31, AT1G36340) (middle and right panels), AKRP.1::GFP punctate localization were observed specifically in the egg cell and antipodal cells of the wild-type embryo sac. **(D)** In isolated chloroplast, AKRP.1::GFP localized mainly in the stroma of the central chloroplast. **(E)** Co-expression of pLat52- AKRP::GFP with a plastid specific marker, pBINU-CHYA(K), in the pollen and **(F)** pollen tubes revealed strong co-localization and confirmed AKRP plastid localization in the gametophyte. **(G)** Representative linear unmixing spectra plot from double hemizygous pollen tubes for both constructs, *N* = 55 pollen tubes, ×32 ROI each. Quantification was performed with the ImageJ plug-in using fixed-size ROI. This panel is also supported by **Supplementary Figure S6**. Scale bar = 10 μm.

defects but not fully the embryo defect (lines 9, 11, and 26), or resulted in increased frequency of gametophytic defects and reduced embryo defects (lines 4, 7, and 10) (**Figure 6A**). In line 11, the complete rescue of both gametophytic *akrp* defects resulted in an increased average of pale *akrp*-3 homozygous mutant embryos, suggesting a possible uncoupling of gametophytic and embryogenic AKRP functions (**Figure 6A**). However, such individuals were underrepresented among the complemented lines.

Since AKRP encodes two splice isoforms, AKRP.1 and AKRP.2 (**Figures 1A,B** and **Supplementary Figure S1**), we tested both isoforms for their ability to complement the *akrp*-3/+ phenotype in a cell-specific manner. Using pLat52-AKRP.1/2::GFP constructs, we identified that only the longer isoform (AKRP.1) partially rescued the embryo-lethal phenotype but not the pollen phenotype, and that the gametophytes remained predominantly sterile (**Figure 6B**). This suggests that the time window for AKRP activity is much earlier during pollen maturation (as shown by the AKRP promoter activity) compared to the late onset of the Lat52 promoter activity (bicellular pollen), and that the shorter isoform is unlikely to function during the embryo development. Most of the Lat52-AKRP.1 rescued embryos were able to develop much further, forming complete cotyledons, compared to the original globular arrested *akrp-3* embryos (**Figures 6C–F**). The rescued embryos still exhibited cotyledons malformations and lacked the normal levels of chlorophyll; therefore, they remained white to pale green even during the vegetative phase in soil (**Figure 6G**). To establish how far the rescued embryos could develop, *akrp*-3/*akrp*-3 germinated seedlings were transferred into glass jars containing half MS medium and grown *in vitro* under 16-h/8-h light/dark cycle. Some of the complemented lines were able to produce flowers, although with long delays and high sterility (with only scarce seed set) compared to the control wild- type plants (**Figures 6H,I**).

To get a broader perspective of AKRP function, we complemented the *akrp-3*/+ plants with a CaMV 35S promoter-driven AKRP.1:GFP. Although the seeds remained pale, we again observed a partial 35S-AKRP.1 complementation of the pale seedlings, which later recovered the cotyledon chlorotic phenotype and produced viable flowering plants (**Supplementary Figures S5a–e**). While some of the lines retained a patchy white-green pattern on leaves, the others fully recovered and produced green organelles (**Supplementary Figures S5c,d**). A similar patchy appearance was observed when the 35S-AKRP:GFP construct was introduced into WT Col-0, suggesting that the observed phenotype was likely due to the nature of 35S overexpression-induced silencing.

To assess AKRP function in the female gametophyte, two promoters driving the expression of the longer *AKRP.1* isoform were used: an antipode-specific DD1 (AT3G36340) as a potential negative control for embryo sac cell-specific complementation and an egg cell-specific EC1.1 (AT1G76750) promoter. Intriguingly, the pEC1.1-driven AKRP complementation was not sufficient to rescue the embryo-lethal phenotype or the ovule-pollen tube attraction defect of *akrp*-3 (**Supplementary Figure S5f**). However, the pDD1-driven complementation construct was able to partially rescue the embryo developmental defects. Several lines were recovered with fully developed embryo; however, some had pale seeds that resembled the pLat52-AKRP:GFP-complemented lines (**Supplementary Figure S5g**). This suggests that the spatial-temporal DD1 promoter activity is sufficient to drive the AKRP embryo function.

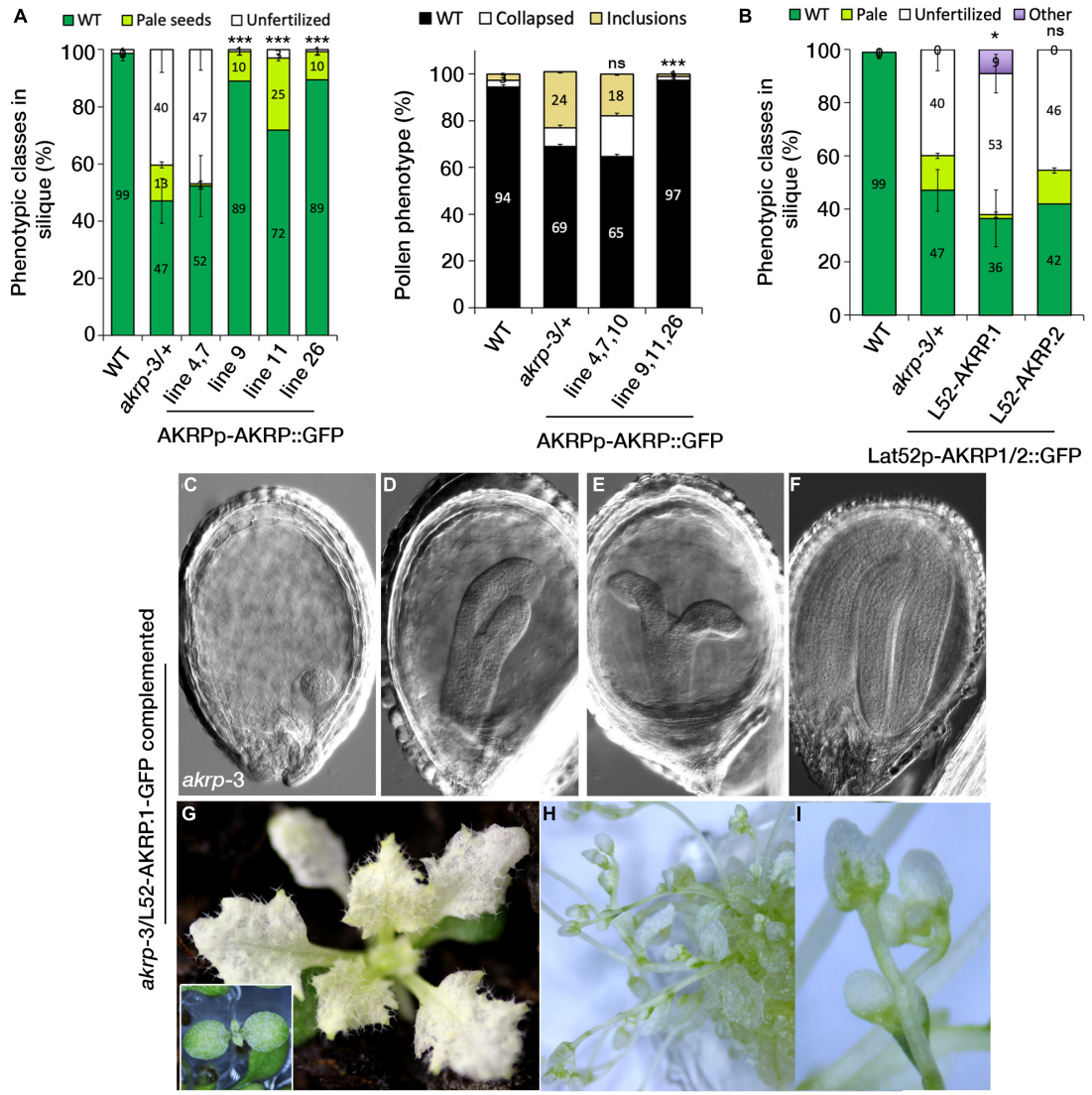

FIGURE 6 | Cell type-specific expression of *AKRP* longer isoform partially rescues embryo developmental perturbation and reveals the timing of AKRP function. **(A)** Native promoter-driven complementation resulted in two groups of complemented plants: those with reduced embryo phenotype but persistent gametophytic defects (lines 4, 7, and 10) and those with fully restored pollen defects (right panel) but with remnant pale seed embryo defects (lines 9, 11, and 26). **(B–I)** Complementation of *akrp*-3/+ with the pLat52-AKRP.1::GFP longer isoform partially complemented the *akrp-3* embryo defect ("other" category), producing rescued embryos beyond the globular arrested embryo of *akrp*-3. Some *akrp*-3 homozygote seeds were able to germinate and flower *in vitro*. Statistical tests were performed by Student's *t*-test assuming unequal variance, $*p < 0.05$, $***p < 0.001$; ns, not significant. Scale bar = 50 μm.

DISCUSSION

In this study, we have identified and functionally associated AKRP with a role in gametophyte competence to undergo fertilization. Previous studies highlighted the role of AKRP in embryonic development, but the alleles studied exhibited no gametophytic defects (Garcion et al., 2006; Meinke et al., 2008). The AKRP falls under the category of embryo-defective genes (EMB) where the fusion of two mutant gametes results in a lethal embryonic development. We show for the first time that AKRP functions earlier not only during embryonic development but also at the gametophytic level (**Figures 1–3**). In Arabidopsis, it is not yet clear how many EMB genes also have a role in the gametophyte, but 27% of the EMB genes exhibit embryo arrest in the globular stage, same stage as the *akrp*-3 mutant, whereas the others arrest earlier or later pass the globular stage, implying a differential timing of EMB gene function (Muralla et al., 2011; Meinke, 2019).

Putative Timing of Arabidopsis Ankyrin Repeat Protein Function in Gametophyte and Embryonic Development

An emerging role of plastids during pollen maturation, as assessed by transmission electron microscope, suggests an

essential role in carbohydrate storage that serves to provide energy and monomers for the construction of a PT wall. Moreover, in *Lolium perenne*, plastids store brassinosteroids during pollen maturation and later promote PT growth post pollination in stigmatic papillae and in transmitting tract tissues (Taylor et al., 1993). Therefore, the timing of genes associated with plastid biogenesis is crucial in the gametophyte and post fertilization.

The rescue of the *akrp*-3 embryo phenotype but not the pollen phenotype by the Lat52-AKRP:GFP construct is spatially intriguing. We suspect a possible inheritance of pollen-expressed AKRP: GFP post-fertilization. This possibility of sporophyte-to-gametophyte carryover inheritance (meiocytes to microspores in the male gametophyte), which masks the gametophytic phenotype, or gametophytic-to-diploid zygote carryover inheritance (ovule or pollen tube-to-zygote during double fertilization), which rescues early embryo defects, has been previously reported for several genes (Muralla et al., 2011; Nodine and Bartel, 2012; Meinke, 2019). The Lat52 promoter is known to be active only in pollen (Ursin et al., 1989; Twell et al., 1990); however, its activity was also reported in roots, as verified by protein gel blot analysis (Van Damme et al., 2006). Therefore, it is possible that the ectopic activity of the Lat52 promoter post-fertilization might be an alternative explanation over a pollen-originated AKRP transcript inheritance for the sufficient rescue of the *akrp-3* embryo phenotype. Partial complementation of the *akrp* embryo phenotype has also been previously reported by Garcion et al. (2006) using an embryo-specific promoter AB13, implying that the timing of AKRP expression is crucial for its function. Similar explanation could be hypothesized for the lack of *akrp*-3 pollen phenotype complementation by the pLat52-driven construct. The LAT52 promoter is active in vegetative cell from the bicellular stage (Brownfield et al., 2009a,b), whereas the AKRP promoter was most active in the earlier microspore stage and the tapetum (**Supplementary Figures S2c–f**), and the first defects in *akrp-3*/+ pollen morphology were already visible in the bicellular pollen stage. As such, Lat52-driven AKRP expression is far late to rescue the *akrp*-3 pollen phenotype, as supported by the lack of *akrp*-3 pollen complementation we observed (**Figure 6B**).

Interestingly, in the embryo sac, the antipodal cell-specific expression of AKRP.1 by the DD1 promoter, but not the egg cell-specific expression by EC1.1 promoter, partially complemented the *akrp*-3 globular arrest embryo phenotype (**Figures 4**, **6**). The antipodal-driven complementation of *akrp*-3 embryo arrest was unexpected because of the fact that antipodal cells degenerate post fertilization. We suspect that, perhaps, the window of expression by the DD1 promoter was sufficient to accumulate AKRP.1 transcripts to allow for AKRP.1 function post fertilization. On the other hand, the lack of *akrp*-3 complementation through egg cell-specific expression by the EC1.1 promoter can be explained by the fact that the EC1.1 promoter itself did not appear activated in *akrp*-3 ovules; therefore, the EC1.1-AKRP.1:GFP construct was not active in the *akrp*-3 egg cell (**Supplementary Figure S3g**). It will be informative in the future to express the AKRP.1, specifically in the egg cell, using a different promoter.

We also observed *akrp*-3 embryo complementation by 35S-AKRP: GFP. The construct seemed to improve pollen fitness in the rescued homozygous lines (**Supplementary Figure S4**). However, some of the rescued lines lacked pigmentation and developed deformation on leaves. The chlorotic patchiness in leaves might be the result of overexpression-induced silencing of AKRP in developing embryos. The AKRP-coding sequence contains a + 31-1,110-bp nonsense-mediated decay target sequence (Thierry-Mieg and Thierry-Mieg, 2006); therefore, its strong expression by the 35S promoter could likely induce silencing. A similar observation was reported by Zhang et al. (1992, 1994) from multiple transgenic lines with chlorotic phenotype after transformation with both sense and antisense AKRP constructs. A similar construct was also used to complement the *emb2036*-1 and generated homozygotes lines with a similar outcome (Garcion et al., 2006). In summary, our complementation analyses hinted that if the promoter used has a broader pattern of expression in either of the gametophytes (female proDD1 or male proLat52), it was sufficient to rescue the lethal embryo arrest phenotype. This is potentially substantiated through the inheritance of parental-originated macromolecules (transcripts or proteins) during double fertilization. The next step will be to structurally dissect isolated gametophytic plastids (predominantly from the vegetative cell of pollen and developing ovules) from *akrp*-3 mutant to evaluate their structures relative to those from the wild type. A similar analysis on developing embryos revealed a striking difference and assigned a role of AKRP in plastid differentiation (Garcion et al., 2006).

EMB-Defective Allele Non-canonical Penetrance

The two other mutant alleles of AKRP, *emb2036-1* and *emb2036-2*, are phenocopies, both showing 25% homozygous embryo arrest at the globular stage (Tzafrir et al., 2004; Meinke et al., 2008). Here, we have screened three alleles of *AKRP*, *emb2036-1*, *akrp-3,* and *akrp-4*. *emb2036-1,* with T-DNA inserted at the 5UTR showing no gametophytic defects, whereas *akrp-3* loss of function, with T-DNA inserted at the beginning of exon 1 exhibiting various pollen, ovule, and embryo defects (**Figures 1–3**). We suspect that these allelic variations might also be explained by T-DNA positional effect. The *AKRP* encodes two isoforms that we verified to be expressed in pollen, ovules, and seeds with the longer isoform up to three times more abundance (**Figure 1**). In pollen, only the longer isoform can complement the pollen defect, and in *akrp*-3 knockout, both isoforms are disrupted (**Figure 1**). It is unclear to us whether the *emb2036-1* and *emb2036-2* alleles that exhibit only the embryo phenotype result in the disruption of both isoforms. Because of the close proximity of AKRP with the neighboring AT5G66060 gene sharing the putative promoter region, our screening confirmed that none of the AT5G66060-associated T-DNA insertions exhibit any aberrant phenotypes. Together with the complementation of *akrp*-3 by the AKRP.1-GFP native construct, this confirms that the gametophytic phenotype we observed is linked to *akrp-3* loss of function.

Despite the substantial amount of aberrant pollen with altered cell fate and significant lack of pollen tube attraction leading

to an ovule abortion in *akrp*-3, there were no transmission defects through the male and only a reduced transmission (78%) through the female. This reduction does not correspond to the penetrance of the *akrp*-3 gametophytic phenotype (**Figures 1–3** and **Supplementary Figure S4**). A similar example of *akrp*-3 non-characteristic pattern of allele inheritance was observed in another plastidial isoform of NAD-MDH that produced NAD + required to generate ATP by glycolysis. Knockout plNAD-MDH is embryo-lethal and exhibits impaired pollen tube growth *in vitro,* which can be rescued by exogenous application of NADH-GOGAT substrates (Selinski and Scheibe, 2014). Just like *akrp*-3 pollen tubes, *plnad-mdh in vivo*-grown pollen tubes are functional and able to fully compete with the wild-type pollen tubes for fertilization (Selinski and Scheibe, 2014). This explains the normal transmission of the *plnad-mdh* mutant allele through the male despite the pollen and pollen tube phenotype. These results suggest that *in vivo*, female reproductive tissues play a key role in supporting semi-functional pollen tubes compromised by the knockout of some essential loci.

Allelic variation in *emb* mutants is also not uncommon. A T-DNA insertion in the GEX1 gene produces a truncated fragment sufficient to rescue a *gex1* gametophyte defect but not an embryo defect (Alandete-Saez et al., 2011). Similarly, a truncated fragment of ZAR1 receptor kinase results in dominant-negative effect on embryo development, a phenotype not visible in other *zar1* null alleles (Yu et al., 2016). A more similar example of *akrp*-3 allelic variation is disruption of geranylgeranyl diphosphate synthase required for isoprenoid biosynthesis that also encodes two isoforms, a short isoform and a longer isoform (Ruiz-Sola et al., 2016). A T-DNA disrupting only the longer isoform which is targeted to plastids shows a defect in seedling pigmentation, whereas disruption of the shorter isoform, exhibits embryo lethal phenotype (Ruiz-Sola et al., 2016).

Extensive screening of *emb*-defective genes by integrated multi-omics analysis has produced a consistent phenotypic profile that is transcription-linked to elaborate the behavior of *emb*-defective genes, including allelic variation, and their potential unusual inheritance (Muralla et al., 2011). Among *EMB* loci categories, those with functional male gametophyte but with pre-globular embryo arrest, 85% of the *EMB* genes in this category are maintained as heterozygous, and their transcripts are detected pre-meiosis in microsporocytes (pollen mother cell) and then in early microspores, suggesting a transcript inheritance from the microsporocytes to the microspores (Muralla et al., 2011; Meinke, 2019). By anthesis, their transcripts disappear. This is consistent with the masking of their gametophytic phenotype through a "maternal rescue," and they, instead, exhibit an onset of early embryo arrest phenotype. In other *EMB* genes with moderate-to-severe male gametophyte defect, their transcription tends to be throughout the pollen development with later onset of embryo arrest phenotype. *De novo* post-meiotic expression (over pre-meiotic transcript inheritance) is, therefore, likely essential for this category of *EMB* genes to allow sufficient levels for gene function throughout pollen ontogenesis. The profile of *akrp*-3 perfectly fits to the second category, exhibiting mild pollen phenotype yet functional to allow for normal transmission of the mutant *akrp*-3 allele. Transcripts of AKRP are detectable in microsporocytes and drastically decreased during pollen maturation, and the *akrp*-3 exhibits a pre-globular embryo arrest (**Figures 1**, **4**). The mild pollen phenotype also suggests that either *de novo* AKRP post-meiotic transcription is necessary for full AKRP function, or the *akrp*-3 allele that disrupts both isoforms of *AKRP* is a true null allele over the previously reported *emb2036*-1 and *emb2036*-2 alleles that did not exhibit the gametophytic phenotype. To summarize, RNA and/or protein storage in the gametophyte is emerging as a substantial element of sporophyte-gametophyte reinforced fitness in flowering plants to support the isolated gametophyte function for successful fertilization and sustain an early embryo development pre-zygotic gene activation. The complexity of an EMBRYO-DEFECTIVE gene (EMB) allelic variations and the non-canonical allelic inheritance patterns have recently been reviewed by the group of David W. Meinke, who initiated and characterized over 1,000 *emb* mutants more than 40 years ago. The resources presented in his review (Meinke, 2019) and the curated database, SeedGenes[2], exclusively documenting *emb* mutants, with gametophytic or embryo developmental role, are extremely valuable and are a must-explore data source.

Mechanistic Insight Into the Function of Arabidopsis Ankyrin Repeat Protein

Per cell, a chloroplast contains over 3,000 proteins; the majority of which are nuclear-encoded. These are synthesized in the cytosol with an N-terminal transit peptide and are subsequently translocated into chloroplasts (Jarvis and Loìpez-Juez, 2013; Lee et al., 2017). Chloroplasts constitute of multi-suborganellar membranes, outer envelope, inner envelope, and thylakoid membranes, and thus create three separate compartments, the intermembrane space, stroma, and the lumen (Ouyang et al., 2020). Therefore, nuclear-imported proteins need to be further resolved into subcellular organelles. The initial import into the stroma is done by the Toc/Tic import complex located in the outer/inner membrane of the chloroplast *via* N-terminal transit peptide recognition (Jarvis and Loìpez-Juez, 2013; Chen et al., 2018). To further sort nuclear-imported proteins, thylakoid membrane-destined proteins follow the chloroplast signal recognition particle pathway (RP), whereas thylakoid lumen proteins are sorted using an additional targeting signal at their N-terminal and enter either the chloroplast secretory (cpSec) or the chloroplast twin-arginine translocation (cpTat) pathway (Schuenemann et al., 1998; Yuan et al., 1994; Settles et al., 1997). Recently, AKRP (STT2) and EMB506 (STT1) were shown to be integral in the formation of liquid-liquid phase-separated droplets as a mechanistic novel mechanism of intra-chloroplast cargo sorting *via* the cpTat pathway to transport thylakoid membrane proteins (Ouyang et al., 2020). STT1-STT2 interacts to create a heterodimer and *via* N-terminal intrinsically disordered regions of the STT complex induces liquid-liquid phase

[2]https://seedgenes.org

separation (Ouyang et al., 2020). The RNAi silencing of either STT1 or STT2 led to a defective thylakoid membrane biogenesis and plastid morphogenesis, resulting in growth retardation, chlorotic leaves, and disrupted chlorophyll levels.

CONCLUSION

We report for the first time that the role of AKRP in intra-chloroplastic cargo protein sorting *via* a liquid-liquid phase translocon driven separation (Ouyang et al., 2020), plays a crucial role not only in pigmentation and embryonic development, but also in gametophytic-fertilization competence likely *via* plastidial morphogenetic function. Our data also suggest that this AKRP role is extended throughout plant development in sorting chloroplast import proteins from crowded stroma to thylakoid membranes, as partially rescued *akrp*-3 adult plants remain chlorotic with morphological distortion throughout plant development.

MATERIALS AND METHODS

Plant Material and Growth Conditions

Arabidopsis (*Arabidopsis thaliana* L. Heynh.) plants were grown at 22 and 60% humidity in Conviron PGC Flex growth chambers under 16-h light/8-h dark conditions. Seeds of Col-0 wild type (WT) and T-DNA lines of EMB2036/AKRP (At5g66055), and At5g66060 plants were obtained from The European *Arabidopsis* Stock Centre. Segregating T-DNA line Gabi-Kat GK_876D05, located in the first exon (in reverse orientation upstream of nucleotide 614) of AKRP was the main experimental material used in this study and herein referred to as *emb2036-3*. The second studied T-DNA line was SAIL_98_F02 (*emb2036-4*, located in 5′UTR). For At5g66060, located on chromosome 5 downstream of AKRP, three T-DNA insertion lines were grown (SALK_098611C, SAIL_595_H12, and SAIL_1262_D08). The T-DNA lines were genotyped using either Gabi-Kat o8474 or o8760, SALK LBb1.3, or SAIL LB2 primers in combination with gene-specific primers. Primer sequences are listed in **Supplementary Table S1**.

Phenotypic Screening

The T-DNA insertion lines were screened for defects in pollen and embryo development phenotypes. Mature pollen samples were screened in brightfield and UV on a Nikon TE-2000 microscope. Siliques in the cotyledon stage of embryo development were dissected and screened for the presence of pale white/transparent mutant seeds. The phenotypic screening was conducted on two subsequent generations.

Transmission Analysis

The *emb2036-3* heterozygous plants were back-crossed into Col-0 wild-type background to determine female transmission and crossed into male-sterile *ms1-/-* (Yang et al., 2007) to study male transmission. The progeny of these crosses was genotyped by PCR for presence of T-DNA insertion, and transmission efficiency (number of seedlings containing *emb2036-3* insertion/number of wild-type seedlings) was calculated. Siliques from the reciprocal crosses were screened for the presence of gametophytic or embryo phenotypes that could be caused by a single mutant parent.

Blue Dot Assay

Young buds of WT Col-0 and *emb2036-3/+* plants before dehiscence of stamens were emasculated and let to mature for 2-3 days until stigma papillae developed. The pistils were then pollinated with pollen containing the pLat52-GUS construct and collected 24 h after pollination. Fertilized pistils were dissected under a binocular dissection microscope (Leica, Germany), and the stripes of fertilized ovules attached to the septum were transferred to a GUS staining solution (view section Histochemical GUS staining). After 2 h of staining, fertilized ovules were observed under the Nikon TE-2000 microscope for the presence of a blue dot following pollen tube micropylar entry and burst.

Pollen Viability Stain and Aniline Blue Staining

Alexander staining was performed according to the protocol by Schoft et al. (2011). Stamens of WT and *akrp-3/+* plants were stained in a droplet of the solution. For aniline blue staining, pistils of 24-h self-pollinated WT Col-0 and *akrp-3/+* plants or cross-pollinated *ms1* plants with WT or *akrp-3/+* pollen (24-h growth *in vivo*) were stained for callose according to the protocol by Mori et al., 2006.

Pollen Tube Cultivation

In vitro pollen tube growth was performed according to the protocol by Boavida and McCormick (2007). After 8 h of *in vitro* growth, pollen germination rate and pollen tube length were measured using the NIS Elements software. For semi-*in vivo* pollen tube growth assay, sterile *ms1/-* pistils were pollinated with WT Col-0 or *akrp-3/+* pollen, and pistils were collected 1 h after pollination. The pistils were excised at the stigma shoulder with a needle and transferred to the growth medium (Palanivelu and Preuss, 2006) on a small Petri dish. The pistils were tilted to enable the pollen tubes to emerge on the surface of the solid medium and cultivated in a humidified growth chamber at 22°C for 24 h. Pollen tube length was measured using the NIS Elements software from the point where they emerged from the cut pistil.

Chloroplast Isolation and Chlorophyll Measurements

Six leaves of old *Nicotiana benthamiana* were infiltrated with0.4 O.D p35S-AKRP.1:GFP, as described in Billey et al., 2021. Two days post-infiltration (dpi), approximately 4g of transformed leaf segments were collected, rinsed with ddH2O, and ground with mortar and pestle in a 10-ml 1 × chloroplast isolation buffer (CIB):0.33M sorbitol,0.1M tris-Cl (pH 7.8), 5 mM MgCl2,

10 mM NaCl, and 2 mM EDTA supplemented with0.1% BSA. Here, all steps were performed on ice. Grounded leaves were passed through a 100-micron mesh filter into 15-ml falcon tubes and centrifuged at 1,000 × g for 3 min at 4oC. The supernatant were transferred to a sterile chilled 15-ml falcon tube and centrifuged for additional 7 min at 1,000 × *g*. The pellet was resuspended in 1 ml CIB with0.1% BSA. The mixture was gently loaded on a 40/80% percoll gradient (2.5 ml 80% and 5 ml 40%) in a 15-ml falcon tube. The gradient was centrifuged at 3,200 × *g* for 15 min at 4°C. Using a 1-ml cut tip, intact chloroplast from the gradient interface was transferred and suspended in 3 × volume CIB and centrifuged for 1 min at 1,700 × *g* table. Pelleted chloroplasts were resuspended in 50 ul CIB and aliquoted for live cell imaging or stored at −80°C for protein extraction.

For chlorophyll quantification, mature siliques from the wild-type Col-0 and *akrp*-3/+ plants were dissected, and wild-type green as well as mutant white *akrp*-3 seeds (100–200 seeds; see **Figure 6**) were collected in 1 ml dimethylformide (DMF) in triplicates: WT seeds: 200 seeds/replicate, Ht3: 200 seeds/replicate, Ht15: 133 seeds/replicate, and Ht22: 119 seeds/replicate. All the samples were incubated overnight at 4oC. Absorbance was measured at 664, 665, and 647 nm. The samples were diluted 3 × to fit the optical range and measured using a CLARIOstar microplate reader (BMG LABTECH, Ortenberg, Germany). The final amount (in ug/ml) of chlorophylls a and b, and total chlorophyll a + b was calculated according to Harris and Baulcombe (2015), as follows:

for chlorophyll a content (in μg/ml):
= (12 × A664.5) − (2.79 × A647),
for chlorophyll b content (in μg/ml):
= (20.78 × A647) − (4.88 × A664.5), and
for total chlorophyll content (in μg/ml): Chla + Chlb, later normalized to μg/ml per 100 ovules for each respective sample.

Histochemical GUS Staining

Stable transformants were screened for promoter-GUS activity in two subsequent generations. Selected plant organs were incubated in a GUS staining buffer:0.2 M Na_2HPO_4,0.2 M NaH_2PO_4, 10 mM EDTA„1% Triton X-100, 1 mM $K_3Fe(CN)_6$, and 2 mM X-Gluc, and stained for up to 48 h. Stained tissues were cleared from chlorophyll by bleaching in ethanol series (90, 70, and 50% (v/v)) prior to imaging.

Microscopy

For mutant embryo phenotypic screening, seeds were cleared in a solution of chloral hydrate. Samples were observed under the DIC optics on a Nikon TE-2000 microscope. Images were processed in the NIS Elements software (LIM). Confocal images were taken on a Nikon Eclipse Ti confocal microscope equipped with a CSU-X1 spinning disk module and an Andor iXon3 EMCCD camera, as well as with a Zeiss LSM880 confocal microscope, and captured with the ZEN 2.3v software. The images were analyzed and assembled with the ImageJ/Fiji[3][4], Adobe Photoshop CS6[5], Ink-scape[6], and NIS Elements (LIM) software. For colocalization study (based on a publication by Marcus and Raulet, 2013), a Zeiss LSM880 confocal microscope with these settings was used: 405-nm laser for excitation of GFP and 514-nm laser for excitation of YFP; emission was captured in a range of 481-508 nm for GFP and 552-561 nm for YFP.

Statistics

All the statistical analyses were performed using the Chi square test at $p < 0.01$ or as specified in respective sections.

RNA Extraction and qRT-PCR Analysis

Tissue samples were collected from the WT Col-0, *emb2036-3*/+ plants and complemented lines, and frozen in liquid nitrogen. The RNA was extracted using RNeasy Plant Mini Kit (Qiagen, Germany) and treated with RQ1 RNAse-free DNase I (Promega, Maryland, MD, United States). First-strand cDNA synthesis was conducted using a recombinant M-MLV reverse transcriptase (Promega, Maryland, MD, United States). Measurements of qRT-PCR were performed using a LightCycler 480 Instrument (Roche, Basel, Switzerland). Primers were designed to distinguish among splicing isoforms of AKRP. Translation initiation factor 1 alpha4 (AT560390G) was used as a reference gene. All the measurements were conducted in three biological and two technical replicates. A list of primers can be found in **Supplementary Table S1**.

Cloning Strategies

All the PCR reactions were performed using Phusion and Q5 Polymerase (New England Biolabs, Hitchin, United Kingdom) according to the instructions of the manufacturer. Primer sequences are listed in **Supplementary Table S1**. For the AKRP promoter, 997 bp upstream of the start codon was cloned into the pENTR/D-TOPO vector (Invitrogen, Thermo Fisher, Germany) and recombined into the destination vector pKGWFS7 (Karimi et al., 2002) bearing two reporter genes, GUS and GFP. For full-length AKRP, an AKRP putative promoter (997 bp) and a coding sequence with/without stop codon were amplified from gDNA, cloned into the pENTR/D-TOPO vector, and recombined into the destination vector pB7FWG,0 (Karimi et al., 2002) bearing the eGFP marker. For complementation under the control of different promoters (pEC1.1, pDD1, p35S, and pLat52), CDS was amplified from cDNA and recombined into the pENTR/D-TOPO vector. Complementation constructs were created using either only the longer isoform (p35S, pEC1.1, pDD1) or both isoforms (pLat52) *via* Multisite Gateway technology (Invitrogen, Thermo Fisher Scientific, Germany). The pB7m34GW, 0 backbone, and eGFP marker were used. These vectors were transformed into *Arabidopsis* WT Col-0 and/or *emb2036-3*/+ plants by floral dipping (Clough and Bent, 1998).

[3]http://imagej.net/
[4]http://fiji.sc/Fiji
[5]www.adobe.com
[6]www.inkscape.org

DATA AVAILABILITY STATEMENT

Theoriginal contributions presented in the study are included in the article/**Supplementary Material**, further inquiries can be directed to the corresponding author/s.

AUTHOR CONTRIBUTIONS

SH and KK designed the experiments. KK, SH, VK, and JP conducted the experiments and analyzed the data with supervision by SH. SH, KK, and DH wrote the manuscript. All the authors read and approved the manuscript.

FUNDING

We gratefully acknowledge Stefanie Sprunck for providing us the egg cell marker. This research was supported the Czech Science Foundation grants 21-15856S and 22-29717S and the Ministry of Education, Youth and Sports of the Czech Republic (projects LTAIN19030, and LTC20028). We acknowledge the Imaging Facility of the Institute of Experimental Botany AS CR supported by the MEYS CR (LM2018129 Czech-BioImaging) and IEB AS CR.

ACKNOWLEDGMENTS

We thank Laboratory of Electron Microscopy – IMCF Viničná, Faculty of Science, Charles University for assisting with scanning electron microscopy. We also thank Lenka Steinbachová and Jana Fecikova for help with genotyping, Christos Michaelidis for careful reading of the manuscript and Ivan Kulich for valuable comments and help throughout the study.

SUPPLEMENTARY MATERIAL

The Supplementary Material for this article can be found online at: https://www.frontiersin.org/articles/10.3389/fpls.2022.767339/full#supplementary-material

Supplementary Figure S1 | Protein alignment of two AKRP splice variants. The short isoform differs by one amino acid substitution and 75 amino acid deletion comprising two ankyrin repeats at the C-terminus. 1. Alignment was performed with Clustal Omega using HMM model and visualized in Jalview v2.9.0b2.

Supplementary Figure S2 | Profiling of AKRP promoter activity in various plant tissues. Detection of AKRP promoter activity in various tissues: cotyledons and stipules of 7-day old seedlings **(a,b)**, inflorescence **(c)**, uninucleate microspores **(d)**, bicellular pollen **(e)**, mature pollen **(f)**, immature **(g)**, and mature **(h)** ovules, and globular to cotyledon stage seeds and embryos **(i–k)**. Scale bar = 20 μm.

Supplementary Figure S3 | Gametophytic viability and pollen tube assays. **(a,b)** Alexander staining and quantification of pollen viability, (n = 664). **(c)** Comparative assessment of *in vitro* pollen germination. **(d)** Aniline blue staining of self-pollinated pistils 24 h after pollination revealed severe targeting defect (n = 953); this panel supports **Figure 2**. **(e)** Estimation of *in vitro* and semi-*in vivo* pollen tube length. **(f)** Confocal imaging of egg cell (EC1.1)-specific pEC1.1-H2B-mRFP (n = 2,511), vegetative cell-specific pLat52-GUS (n = 3,233) and a double marker for sperm cell (SC) pHTR10-HTR10:RFP (n = 4,342) and vegetative cell (VC) pLat52-GFP (n = 2,313). **(g)** Quantification of marker expression in *akrp-3*/+ and segregated WT plants. AC, antipodal cell expression of pDD1-AKRP.1::GFP.

Supplementary Figure S4 | The *akrp-3* transmission test and blue dot assay. **(a)** Segregation of self-fertilized *akrp-3*/+ on sulfadiazine antibiotic. **(b)** Transmission test of the *akrp-3* allele after reciprocal crosses. TE = transmission efficiency (Wt/Het × 100), χ^2 test: not significant at $p < 0.01$. **(c)** Blue dot assay to assess ovule attractivity following pollination with pLAT52-GUS-expressing pollen suggests a dramatic decrease in *akrp*-3 pollen tube attraction efficiency 24h after pollination (n = 824). This panel supports **Figure 2**. χ^2test, significant at $p < 0.01$. Scale bar = 50 μm. **(d)** Induction of aborted ovule phenotype through an *akrp*-3 female after reciprocal crosses.

Supplementary Figure S5 | Cell type-specific complementation of *akrp-3* mutation. **(a,b)** Complementation using a p35S promoter (35S-AKRP.1:GFP) yielded rescued homozygous plants already in the first generation. The complementation was not absolute, because some lines retained some levels of embryonic defects; **(c,d)** Chlorotic cotyledons that recovered in newly emerged true leaves and **(e)** lesions in rosette leaves. **(f)** Complementation with an egg cell-specific promoter (pEC1.1) was not sufficient to rescue *akrp*-3 fertilization or embryo-lethal phenotype (n = 11). **(g)** Complementation under an antipode-specific pDD1 promoter weakly rescued the embryo-lethal *akrp-3* phenotype (class labeled as "other," phenotypically similar to **Figure 6B** "other" category, n = 5).

Supplementary Figure S6 | AKRP.1 plastid co-localization in mature pollen. Analysis of double heterozygous Lat52-AKRP.1:GFP and pBINU-CHYA(K) marker in mature pollen by independent GFP and YFP channel excitation with Argon 488 laser in a Zeiss confocal microscope. Intensity values were plotted using the Prism software.

Supplementary Table S1 | List of primers used in this study.

REFERENCES

Ajjawi, I., Lu, Y., Savage, L. J., Bell, S. M., and Last, R. L. (2010). Large-scale reverse genetics in *Arabidopsis*: case studies from the Chloroplast 2010 Project. *Plant Physiol.* 152, 529–540. doi: 10.1104/pp.109.148494

Alandete-Saez, M., Ron, M., Leiboff, S., and McCormick, S. (2011). *Arabidopsis* thaliana GEX1 has dual functions in gametophyte development and early embryogenesis. *Plant J.* 68, 620–632. doi: 10.1111/j.1365-313X.2011.04713.x

Albert, S., Despres, B., Guilleminot, J., Bechtold, N., Pelletier, G., Delseny, M., et al. (1999). The EMB 506 gene encodes a novel ankyrin repeat containing protein that is essential for the normal development of *Arabidopsis* embryos. *Plant J.* 17, 169–179. doi: 10.1046/j.1365-313x.1999.00361.x

Allorent, G., Courtois, F., Chevalier, F., and Lerbs-Mache, S. (2013). Plastid gene expression during chloroplast differentiation and dedifferentiation into non-photosynthetic plastids during seed formation. *Plant Mol. Biol.* 82, 59–70. doi: 10.1007/s11103-013-0037-0

Beale, K. M., Leydon, A. R., and Johnson, M. A. (2012). Gamete fusion is required to block multiple pollen tubes from entering an *Arabidopsis* ovule. *Curr. Biol.* 22, 1090–1094. doi: 10.1016/j.cub.2012.04.041

Becerra, C., Jahrmann, T., Puigdomènech, P., and Vicient, C. M. (2004). Ankyrin repeat-containing proteins in *Arabidopsis*: characterization of a novel and abundant group of genes coding ankyrin-transmembrane proteins. *Gene* 340, 111–121. doi: 10.1016/j.gene.2004.06.006

Billey, E., Hafidh, S., Cruz-Gallardo, I., Litholdo, C. G., Jean, V. J., Carpentier, M. C., et al. (2021). LARP6C orchestrates posttranscriptional reprogramming of gene expression during hydration to promote pollen tube guidance. *Plant Cell* 33, 2637–2661. doi: 10.1093/plcell/koab131

Boavida, L. C., and McCormick, S. (2007). TECHNICAL ADVANCE: temperature as a determinant factor for increased and reproducible in vitro pollen germination in *Arabidopsis thaliana*. *Plant J.* 52, 570–582. doi: 10.1111/j.1365-313X.2007.03248.x

Brownfield, L., Hafidh, S., Borg, M., Sidorova, A., Mori, T., and Twell, D. (2009a). A plant germline-specific integrator of sperm specification and cell cycle progression. *PLoS Genet.* 5:e1000430. doi: 10.1371/journal.pgen.1000430

Brownfield, L., Hafidh, S., Durbarry, A., Khatab, H., Sidorova, A., Doerner, P., et al. (2009b). *Arabidopsis* DUO POLLEN3 is a key regulator of male germline development and embryogenesis. *Plant Cell* 21, 1940–1956. doi: 10.1105/tpc.109.066373

Bryant, N., Lloyd, J., Sweeney, C., Myouga, F., and Meinke, D. (2011). Identification of nuclear genes encoding chloroplast-localized proteins required for embryo development in *Arabidopsis*. *Plant Physiol.* 155, 1678–1689. doi: 10.1104/pp.110.168120

Chen, Y. L., Chen, L. J., Chu, C. C., Huang, P. K., Wen, J. R., and Li, H. M. (2018). TIC236 links the outer and inner membrane translocons of the chloroplast. *Nature* 564, 125–129. doi: 10.1038/s41586-018-0713-y

Chen, W., Yu, X. H., Zhang, K., Shi, J., De Oliveira, S., Schreiber, L., et al. (2011). Male Sterile2 encodes a plastid-localized fatty acyl carrier protein reductase required for pollen exine development in *Arabidopsis*. *Plant Physiol.* 157, 842–853. doi: 10.1104/pp.111.181693

Clément, C., and Pacini, E. (2001). Anther plastids in angiosperms. *Bot. Rev.* 67, 54–73. doi: 10.1007/BF02857849

Clough, S. J., and Bent, A. F. (1998). Floral dip: a simplified method forAgrobacterium-mediated transformation of*Arabidopsis thaliana*. *Plant J.* 16, 735–743. doi: 10.1046/j.1365-313x.1998.00343.x

Demarsy, E., Buhr, F., Lambert, E., and Lerbs-Mache, S. (2012). Characterization of the plastid-specific germination and seedling establishment transcriptional programme. *J. Exp. Bot.* 63, 925–939. doi: 10.1093/jxb/err322

Dickinson, H. G. (1973). The role of plastids in the formation of pollen grain coatings. Cytobios 8: 2 1981. The structure and chemistry ofplastid differentiation during male meiosis in Lilium heryi. *J. Cell Sci.* 52, 223–241. doi: 10.1242/jcs.52.1.223

Dickinson, H. G., and Lewis, D. (1973). The formation of tryphine coating the pollen grains of Raphanus and its properties relating to the self incompatibility system. *Proc. R. Soc. Lond B* 184, 149–156.

Garcion, C., Guilleminot, J., Kroj, T., Parcy, F., Giraudat, J., Devic, M., et al. (2006). AKRP and EMB506 are two ankyrin repeat proteins essential for plastid differentiation and plant development in *Arabidopsis*. *Plant J.* 48, 895–906. doi: 10.1111/j.1365-313X.2006.02922.x

Grossniklaus, U. (2017). Polyspermy produces tri-parental seeds in maize. *Curr. Biol.* 27, R1300–R1302. doi: 10.1016/j.cub.2017.10.059

Hafidh, S., and Honys, D. (2021). Reproduction multitasking - The male gametophyte. *Annu. Rev. Plant Biol.* 72, 581–614. doi: 10.1146/annurev-arplant-080620-021907

Harris, C. J., and Baulcombe, D. C. (2015). Chlorophyll Content Assay to Quantify the Level of Necrosis Induced by Different R Gene/Elicitor Combinations after Transient Expression. *Bio-Protoc.* 5:e1670. doi: 10.21769/BioProtoc.1670

Jarvis, P., and Loìpez-Juez, E. (2013). Biogenesis and homeostasis of chloroplasts and other plastids. *Nat. Rev. Mol. Cell Biol.* 14, 787–802. doi: 10.1038/nrm3702

Johnson, M. A., Harper, J. F., and Palanivelu, R. A. (2019). fruitful journey: pollen tube navigation from germination to fertilization. *Annu. Rev. Plant Biol.* 70, 809–837. doi: 10.1146/annurev-arplant-050718-100133

Julca, I., Ferrari, C., Flores-Tornero, M., Proost, S., Lindner, A.-C., Hackenberg, D., et al. (2021). Comparative transcriptomic analysis reveals conserved programmes underpinning organogenesis and reproduction in land plants. *Nat. Plants* 7, 1143–1159. doi: 10.1038/s41477-021-00958-2

Karimi, M., Inzé, D., and Depicker, A. (2002). GATEWAY vectors for Agrobacterium-mediated plant transformation. *Trends Plant Sci.* 7, 193–195. doi: 10.1016/S1360-1385(02)02251-3

Kleinboelting, N., Huep, G., Kloetgen, A., Viehoever, P., and Weisshaar, B. (2012). GABI-Kat SimpleSearch: new features of the *Arabidopsis thaliana* T-DNA mutant database. *Nucleic Acids Res.* 40, D1211–D1215. doi: 10.1093/nar/gkr1047

Kuai, X., MacLeod, B. J., and Després, C. (2015). Integrating data on the *Arabidopsis* NPR1/NPR3/NPR4 salicylic acid receptors; a differentiating argument. *Front. Plant Sci.* 6:235. doi: 10.3389/fpls.2015.00235

Lee, D. W., Lee, J., and Hwang, I. (2017). Sorting of nuclear-encoded chloroplast membrane proteins. *Curr. Opin. Plant Biol.* 40, 1–7. doi: 10.1016/j.pbi.2017.06.011

Liebers, M., Grübler, B., Chevalier, F., Lerbs-Mache, S., Merendino, L., Blanvillain, R., et al. (2017). Regulatory Shifts in Plastid Transcription Play a Key Role in Morphological Conversions of Plastids during Plant Development. *Front. Plant Sci.* 8:23. doi: 10.3389/fpls.2017.00023

Marcus, A., and Raulet, D. H. (2013). A simple and effective method for differentiating GFP and YFP by flow cytometry using the violet laser. *Cytometry A* 83, 973–974. doi: 10.1002/cyto.a.22347

Maruyama, D., Hamamura, Y., Takeuchi, H., Susaki, D., Nishimaki, M., Kurihara, D., et al. (2013). Independent control by each female gamete prevents the attraction of multiple pollen tubes. *Dev. Cell* 25, 317–323. doi: 10.1016/j.devcel.2013.03.013

Mehlmer, N., Parvin, N., Hurst, C. H., Knight, M. R., Teige, M., Vothknecht, U. C., et al. (2012). A toolset of aequorin expression vectors for in planta studies of subcellular calcium concentrations in *Arabidopsis thaliana*. *J. Exp. Bot.* 63, 1751–1761. doi: 10.1093/jxb/err406

Meinke, D. (2019). Genome-wide identification of EMBRYO- DEFECTIVE (EMB) genes required for growth and development in *Arabidopsis*. *New Phytol.* 226, 306–325. doi: 10.1111/nph.16071

Meinke, D., Muralla, R., Sweeney, C., and Dickerman, A. (2008). Identifying essential genes in *Arabidopsis thaliana*. *Trends Plant Sci.* 13, 483–491. doi: 10.1016/j.tplants.2008.06.003

Mori, T., Kuroiwa, H., Higashiyama, T., and Kuroiwa, T. (2006). GENERATIVE CELL SPECIFIC 1 is essential for angiosperm fertilization. *Nat. Cell Biol.* 8, 64–71. doi: 10.1038/ncb1345

Mosavi, L. K., Cammett, T. J., Desrosiers, D. C., and Peng, Z.-Y. (2004). The ankyrin repeat as molecular architecture for protein recognition. *Protein Sci.* 13, 1435–1448. doi: 10.1110/ps.03554604

Muñoz-Bertomeu, J., Cascales-Miñana, B., Irles-Segura, A., Mateu, I., Nunes-Nesi, A., Fernie, A. R., et al. (2010). The plastidial glyceraldehyde-3-phosphate dehydrogenase is critical for viable pollen development in *Arabidopsis*. *Plant Physiol.* 152, 1830–1841. doi: 10.1104/pp.109.150458

Muralla, R., Lloyd, J., and Meinke, D. (2011). Molecular Foundations of Reproductive Lethality in *Arabidopsis thaliana*. *PLoS One* 6:e28398. doi: 10.1371/journal.pone.0028398

Myouga, F., Akiyama, K., Motohashi, R., Kuromori, T., Ito, T., Iizumi, H., et al. (2010). The Chloroplast Function Database: a large-scale collection of *Arabidopsis Ds/Spm* - or T-DNA-tagged homozygous lines for nuclear-encoded chloroplast proteins, and their systematic phenotype analysis. *Plant J.* 61, 529–542. doi: 10.1111/j.1365-313X.2009.04074.x

Myouga, F., Akiyama, K., Tomonaga, Y., Kato, A., Sato, Y., Kobayashi, M., et al. (2013). The Chloroplast Function Database II: a Comprehensive Collection of Homozygous Mutants and Their Phenotypic/Genotypic Traits for Nuclear-Encoded Chloroplast Proteins. *Plant Cell Physiol.* 54:e2. doi: 10.1093/pcp/pcs171

Nagahara, S., Takeuchi, H., and Higashiyama, T. (2021). Polyspermy Block in the Central Cell During Double Fertilization of *Arabidopsis thaliana*. *Front. Plant Sci.* 11:588700. doi: 10.3389/fpls.2020.588700

Nodine, M. D., and Bartel, D. P. (2012). Maternal and paternal genomes contribute equally to the transcriptome of early plant embryos. *Nature* 482, 94–97. doi: 10.1038/nature10756

Ouyang, M., Li, X., Zhang, J., Feng, P., Pu, H., Kong, L., et al. (2020). Liquid-Liquid phase transition drives Intra-chloroplast cargo sorting. *Cell* 180, 1144–1159. doi: 10.1016/j.cell.2020.02.045

Pacini, E. (1994). "Cell biology of anther and pollen development," in *Genetic control of self-incompatibility and reproductive development in flowering plants*, eds E. G. Williams, A. E. Clarke, and R. B. Knox (Dordrecht, Netherlands: Kluwer Academic), 289–308. doi: 10.1007/978-94-017-1669-7_14

Pacini, E., and Juniper, B. E. (1979). The ultrastructure of pollen-grain development in the olive (Olea euro- pea), 2. Secretion by the tapetal cells. *New Phytol.* 83, 165–174. doi: 10.1111/j.1469-8137.1979.tb00738.x

Palanivelu, R., and Preuss, D. (2006). Distinct short-range ovule signals attract or repel *Arabidopsis thaliana* pollen tubes in vitro. *BMC Plant Biol.* 6:7. doi: 10.1186/1471-2229-6-7

Prabhakar, V., Löttgert, T., Geimer, S., Dörmann, P., Krüger, S., Vijayakumar, V., et al. (2010). Phosphoenolpyruvate provision to plastids is essential for gametophyte and sporophyte development in *Arabidopsis thaliana*. *Plant Cell* 22, 2594–2617. doi: 10.1105/tpc.109.073171

Ruiz-Sola, M. A., Barja, M. V., Manzano, D., Llorente, B., Schipper, B., Beekwilder, J., et al. (2016). A single *Arabidopsis* gene encodes two differentially targeted geranylgeranyl diphosphate synthase isoforms. *Plant Physiol.* 172, 1393–1402. doi: 10.1104/pp.16.01392

Schoft, V. K., Chumak, N., Choi, Y., Hannon, M., Garcia-Aguilar, M., Machlicova, A., et al. (2011). Function of the DEMETER DNA glycosylase in the *Arabidopsis thaliana* male gametophyte. *Proc. Natl. Acad. Sci. U. S. A.* 108, 8042–8047. doi: 10.1073/pnas.1105117108

Schuenemann, D., Gupta, S., Persello-Cartieaux, F., Klimyuk, V. I., Jones, J. D., Nussaume, L., et al. (1998). A novel signal recognition particle targets light-harvesting proteins to the thylakoid membranes. *Proc. Natl. Acad. Sci. U.S.A.* 95, 10312–10316. doi: 10.1073/pnas.95.17.10312

Settles, A. M., Yonetani, A., Baron, A., Bush, D. R., Cline, K., and Martienssen, R. (1997). Sec-independent protein translocation by the maize Hcf106 protein. *Science* 278, 1467–1470. doi: 10.1126/science.278.5342.1467

Selinski, J., and Scheibe, R. (2014). Pollen tube growth: where does the energy come from? *Plant Signal. Behav.* 9:e977200. doi: 10.4161/15592324.2014.977200

Steffen, J. G., Kang, H., Macfarlane, J., and Drew, G. N. (2007). Identification of genes expressed in the *Arabidopsis* female gametophyte. *Plant J.* 51, 281–292. doi: 10.1111/j.1365-313x.2007.03137.x

Taylor, P. E., Spuck, K., Smith, P. M., Sasse, J. M., Yokota, T., Griffiths, P. G., et al. (1993). Detection of brassinosteroids in pollen of Lolium perenne L. by immunocytochemistry. *Planta* 189, 91–100.

Thierry-Mieg, D., and Thierry-Mieg, J. (2006). AceView: a comprehensive cDNA-supported gene and transcripts annotation. *Genome Biol.* 7, S12.1–S12.14. doi: 10.1186/gb-2006-7-s1-s12

Ting, J. T. L., Wu, S. S. H., Ratnayake, C., and Huang, A. H. C. (1998). Constituents of tapetasomes and elaioplasts in Brassica campestris tapetum and their degradation and retention during microsporogenesis. *Plant J.* 16, 541–551. doi: 10.1046/j.1365-313x.1998.00325.x

Twell, D., Yamaguchi, J., and McCormick, S. (1990). Pollen-specific gene expression in transgenic plants: coordinate regulation of two different tomato gene promoters during microsporogenesis. *Development* 109, 705–713.

Tzafrir, I., Pena-Muralla, R., Dickerman, A., Berg, M., Rogers, R., Hutchens, S., et al. (2004). Identification of Genes Required for Embryo Development in *Arabidopsis*. *Plant Physiol.* 135, 1206–1220. doi: 10.1104/pp.104.045179. published

Ursin, V. M., Yamaguchi, J., and McCormick, S. (1989). Gametophytic and sporophytic expression of anther-specific genes in developing tomato anthers. *Plant Cell* 1, 727–736. doi: 10.1105/tpc.1.7.727

Van Damme, D., Coutuer, S., De Rycke, R., Bouget, F. Y., Inzé, D., Geelen, D., et al. (2006). Somatic cytokinesis and pollen maturation in *Arabidopsis* depend on TPLATE, which has domains similar to coat proteins. *Plant Cell* 18, 3502–3518. doi: 10.1105/tpc.106.040923

Yang, C., Vizcay-Barrena, G., Conner, K., and Wilson, Z. A. (2007). MALE STERILITY1 is required for tapetal development and pollen wall biosynthesis. *Plant Cell* 19, 3530–3548. doi: 10.1105/tpc.107.054981

Yu, F., Shi, J., Zhou, J., Gu, J., Chen, Q., Li, J., et al. (2010). ANK6, a mitochondrial ankyrin repeat protein, is required for male-female gamete recognition in *Arabidopsis thaliana*. *Proc. Natl. Acad. Sci. U. S. A.* 107, 22332–22337. doi: 10.1073/pnas.1015911107

Yu, T. Y., Shi, D. Q., Jia, P. F., Tang, J., Li, H. J., Liu, J., et al. (2016). The *Arabidopsis* receptor kinase ZAR1 is required for zygote asymmetric division and its daughter cell fate. *PLoS Genet.* 12:e1005933. doi: 10.1371/journal.pgen.1005933

Yuan, J., Henry, R., McCaffery, M., and Cline, K. (1994). SecA homolog in protein transport within chloroplasts: evidence for endosymbiont-derived sorting. *Science* 266, 796–798. doi: 10.1126/science.7973633

Zhang, H., Scheirer, D. C., Fowle, W. H., and Goodman, H. M. (1992). Expression of antisense or sense RNA of an ankyrin repeat-containing gene blocks chloroplast differentiation in *arabidopsis*. *Plant Cell* 4, 1575–1588. doi: 10.1105/tpc.4.12.1575

Zhang, H., Wang, J., and Goodman, H. M. (1994). Expression of the *Arabidopsis* Gene AKRP Coincides with Chloroplast Development. *Plant Physiol.* 106, 1261–1267.

Zhao, Z., and Assmann, S. M. (2011). The glycolytic enzyme, phosphoglycerate mutase, has critical roles in stomatal movement, vegetative growth, and pollen production in *Arabidopsis thaliana*. *J. Exp. Bot.* 62, 5179–5189. doi: 10.1093/jxb/err223

Conflict of Interest: The authors declare that the research was conducted in the absence of any commercial or financial relationships that could be construed as a potential conflict of interest.

Publisher's Note: All claims expressed in this article are solely those of the authors and do not necessarily represent those of their affiliated organizations, or those of the publisher, the editors and the reviewers. Any product that may be evaluated in this article, or claim that may be made by its manufacturer, is not guaranteed or endorsed by the publisher.

Copyright © 2022 Kulichová, Pieters, Kumar, Honys and Hafidh. This is an open-access article distributed under the terms of the Creative Commons Attribution License (CC BY). The use, distribution or reproduction in other forums is permitted, provided the original author(s) and the copyright owner(s) are credited and that the original publication in this journal is cited, in accordance with accepted academic practice. No use, distribution or reproduction is permitted which does not comply with these terms.

Supplementary Results

Supplementary Table S1

List of primers used in this study.

Primer list	
Name	**Sequence 5'-3'**
AT5G66055 genotyping primers	
GK_876D05_LP	CAGATCCAGTATCTGAAGCGC
GK_876D05_RP	AACCTCTCCGTCTCGTCTTTC
SAIL_98_F02 _LP	AACCGGGTAACAAAACCATTC
SAIL_98_F02 _RP	CATCTAATCTCTTAGCCCCGC
AT6G66060 genotyping primers	
SALK_098611C_LP	TTGGTTTCACAGACAACCCTC
SALK_098611C_RP	GCGAAGATGATTCAAAGAACG
SAIL_595_H12_LP	CCTCCTCAACATCTGATCTGC
SAIL_595_H12_RP	CGTGATTTTGATTCTTCTCGC
SAIL_1262_D08_LP	TGCTCTGCATGTTGTAGCATC
SAIL_1262_D08_RP	CTTCGCCGTATTGATCATGTC
qRT-PCR primers	
Reference gene	
EF1alpha4_LP	TGAGCACGCTCTTCTTGCTTTCA
EF1alpha4_RP	GGTGGTGGCATCCATCTTGTTACA
Long isoform	
QATE2036_F	ACCTGCTGAGGGAATCGGCAA
QATE2036_EXJU_R	CACCCGTCCCTGTCCTGAG
Short isoform	
QATE2036_F	ACCTGCTGAGGGAATCGGCAA
E20_SHORT_CDS_RP	TCATCCTACCCTGTCCTGAG
Cloning primers	
Sequencing primers	
E2_SEQ_1	TAGCGCAGGAGATGGAGTTCG
E2_SEQ_2	AACAGAAGCTCTGGGTTCCCA
E2_SEQ_3	AAGTAAGGCCCATTAGAAAGTGAG
E2_SEQ_4	AACCGATGTGGTATGTCTGAC
E2_SEQ_5	TCAGGACGGGTGGACTC
Promoter cloning	
proE2036_LP_DTOPO	CACCATTGAGTGAAAAGTATAAAAC
proE2036_RP_DTOPO	TATCGGAATAATCTTGAATAACGG
CDS cloning long isoform	
cdsE2036_LP_DTOPO	CACCATGCAGTCACTCTCCACC
cdsE2036_RPnostop_DTOPO	TCCTACCCTGTCCTGAGCGTT
CDS cloning short isoform	
cdsE2036_LP_DTOPO	CACCATGCAGTCACTCTCCACC
E20_SHORT_CDS_RP	TCATCCTACCCTGTCCTGAG
Genomic fragment cloning	
proE2036_LP_DTOPO	CACCATTGAGTGAAAAGTATAAAAC
cdsE2036_RPnostop_DTOPO	TCCTACCCTGTCCTGAGCGTT

Supplementary Figure S1

Protein alignment of two AKRP splice variants. The short isoform differs by one amino acid substitution and 75 amino acid deletion comprising two ankyrin repeats at the C-terminus. 1. Alignment was performed with Clustal Omega using HMM model and visualized in Jalview v2.9.0b2.

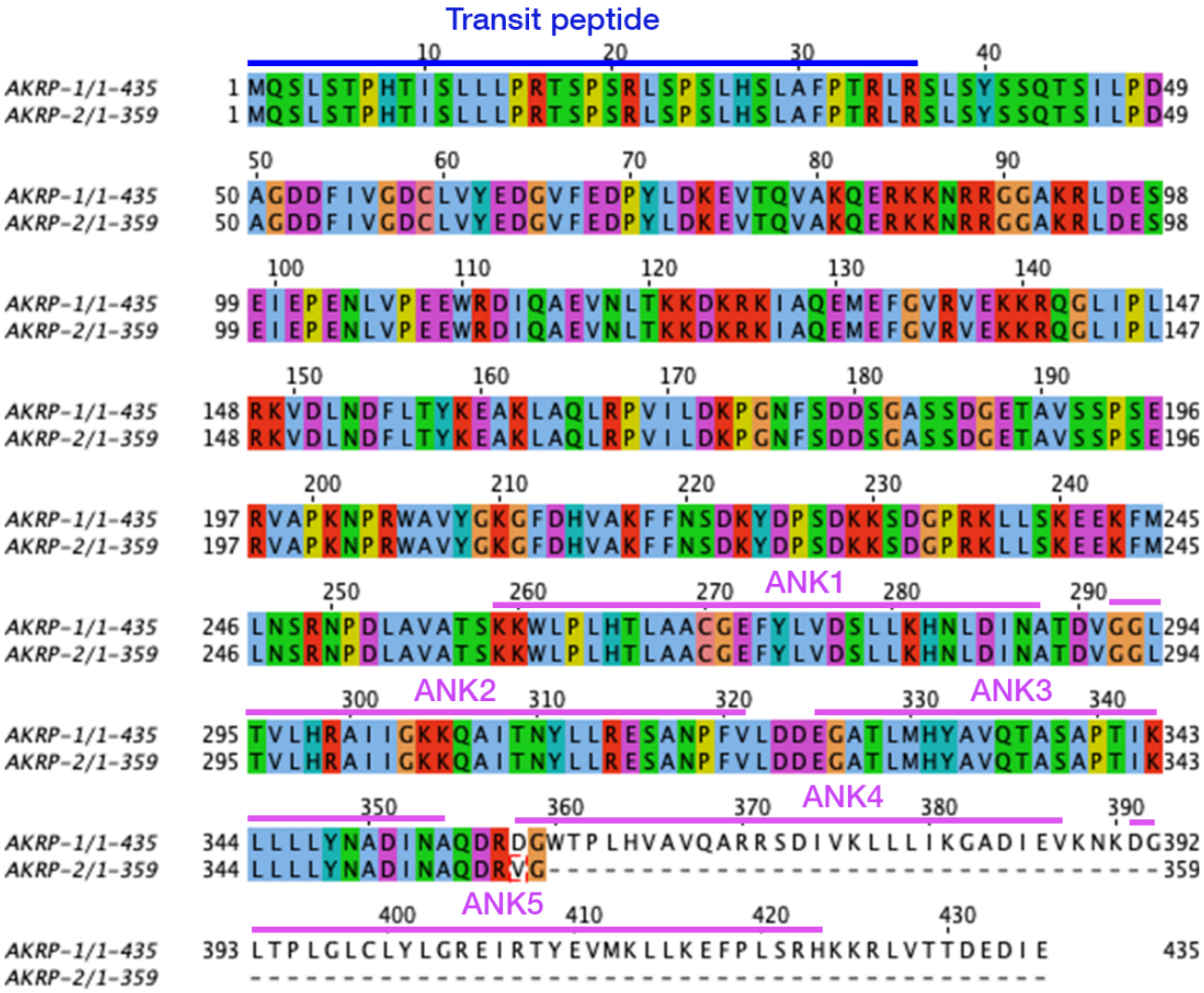

Supplementary Figure S2

Profiling of AKRP promoter activity in various plant tissues. Detection of AKRP promoter activity in various tissues: cotyledons and stipules of 7-day old seedlings (a, b), inflorescence (c), uninucleate microspores (d), bicellular pollen (e), mature pollen (f), immature (g), and mature (h) ovules, and globular to cotyledon stage seeds and embryos (i–k). Scale bar = 20 μm.

Figure S2

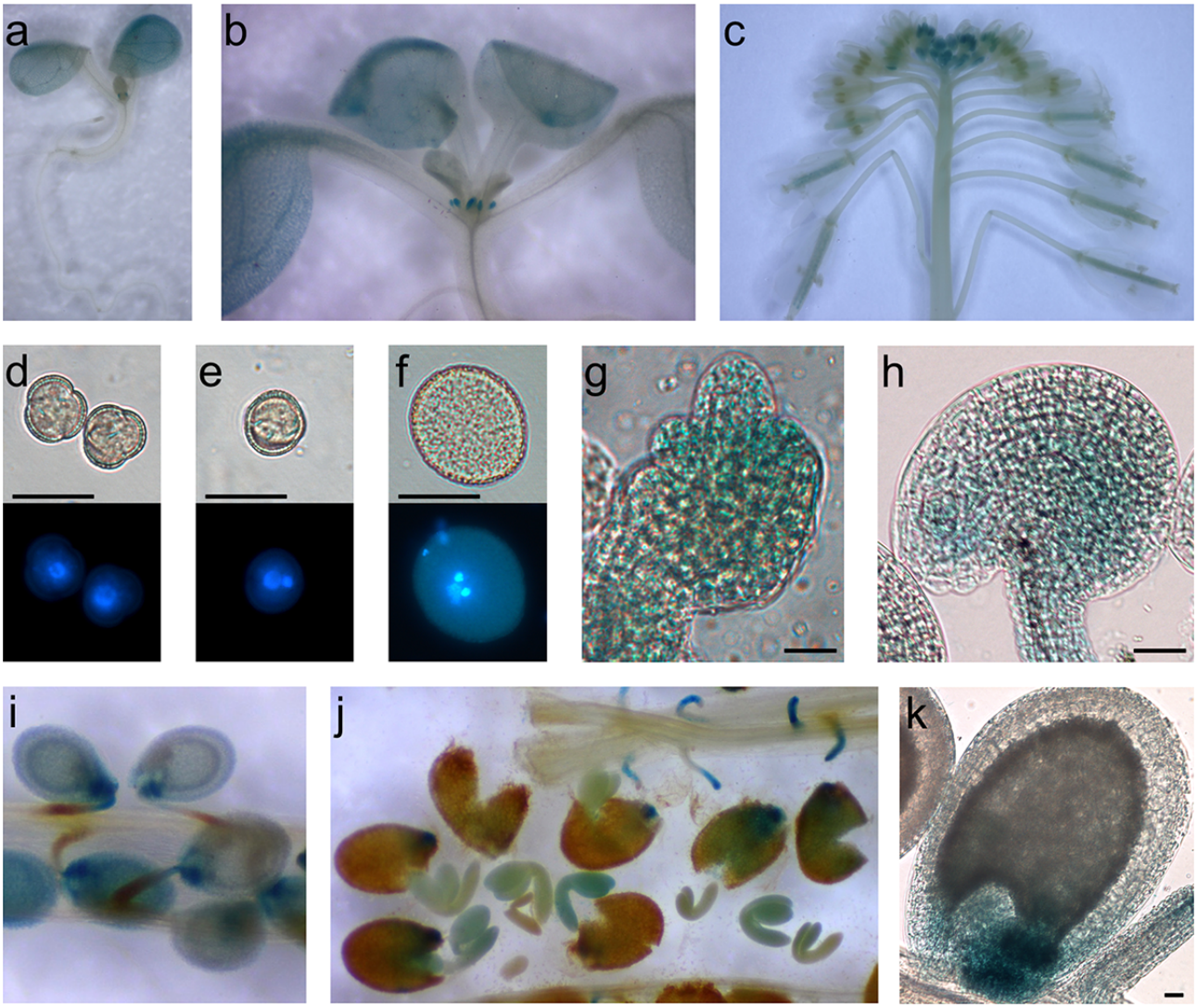

Supplementary Figure S3

Gametophytic viability and pollen tube assays. (a, b) Alexander staining and quantification of pollen viability, (n = 664). (c) Comparative assessment of in vitro pollen germination. (d) Aniline blue staining of self-pollinated pistils 24 h after pollination revealed severe targeting defect (n = 953); this panel supports Figure 2. (e) Estimation of in vitro and semi-in vivo pollen tube length. (f) Confocal imaging of egg cell (EC1.1)-specific pEC1.1-H2B-mRFP (n = 2,511), vegetative cell-specific pLat52-GUS (n = 3,233) and a double marker for sperm cell (SC) pHTR10-HTR10:RFP (n = 4,342) and vegetative cell (VC) pLat52-GFP (n = 2,313). (g) Quantification of marker expression in *akrp-3*/+ and segregated WT plants. AC, antipodal cell expression of pDD1-AKRP.1::GFP.

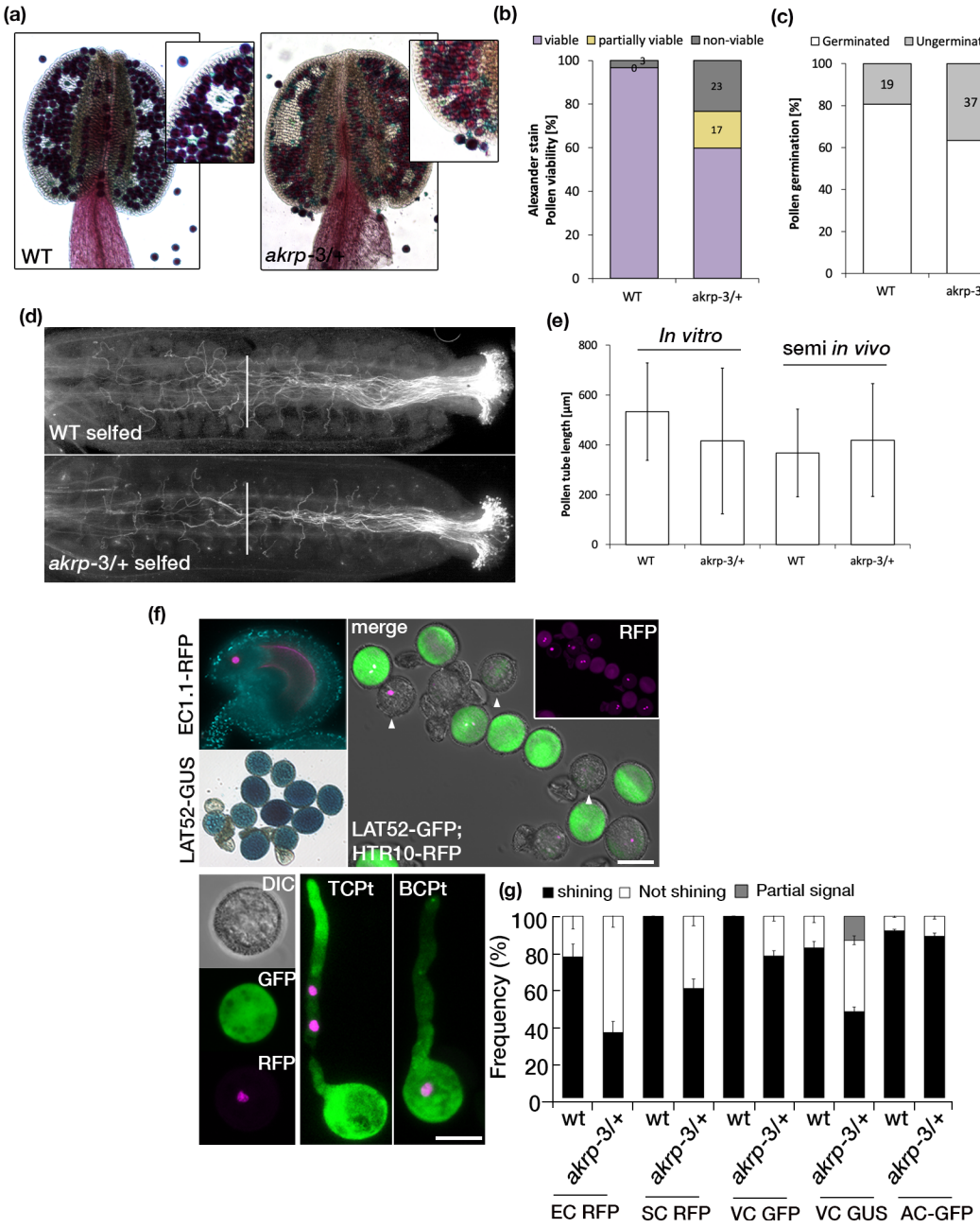

Supplementary Figure S4

The *akrp-3* transmission test and blue dot assay. (a) Segregation of self-fertilized *akrp-3*/+ on sulfadiazine antibiotic. (b) Transmission test of the *akrp-3* allele after reciprocal crosses. TE = transmission efficiency (Wt/Het × 100), $\chi 2$ test: not significant at $p < 0.01$. (c) Blue dot assay to assess ovule attractivity following pollination with pLAT52-GUS-expressing pollen suggests a dramatic decrease in *akrp-3* pollen tube attraction efficiency 24h after pollination (n = 824). This panel supports Figure 2. $\chi 2$test, significant at $p < 0.01$. Scale bar = 50 µm. (d) Induction of aborted ovule phenotype through an *akrp-3* female after reciprocal crosses.

Figure S4

(a)

Genotype	Resistent seedlings [%]	Sensitive seedlings [%]	N	Observed ratio (R:S)	$\chi 2$ test
akrp-3/+	68.5 ± 3.8	31.5 ± 3.8	3160	2.17 : 1 (3:1)*	0.057

expected ratio

(b)

Cross	Plant genotypes			Ratio WT/Het	TE (%)	χ2 test
	WT	Het	Total	Observed (Expected)		
♀ *akrp-3/+* x ♂ WT Col-0	309	243	552	1:0.78 (1:1)	78	NS
♀ *ms1/-* x ♂ *akrp-3/+*	470	457	927	1:0.97 (1:1)	97	NS

(c)

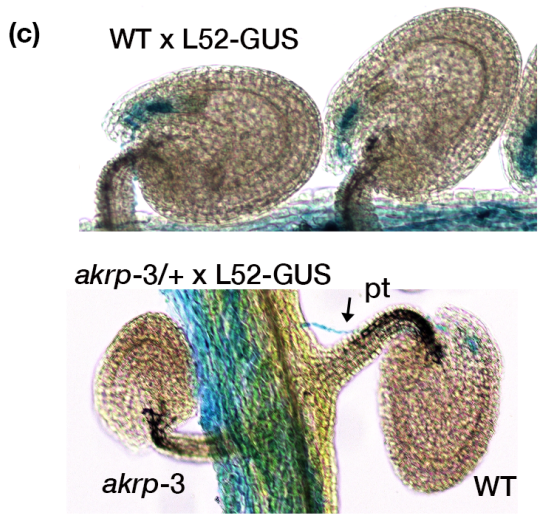

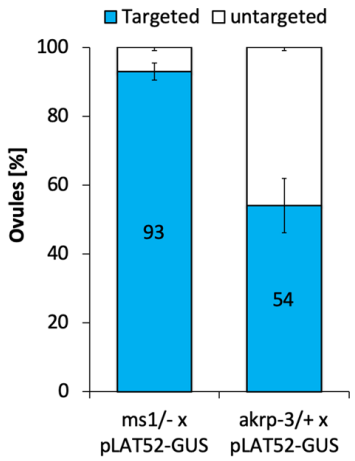

(d)

Cross	WT [%]	Unfertilized [%]	Pale seeds [%]
♀*akrp-3/+* x ♂WT Col-0	52	48	0
♀*ms1/-* x ♂*akrp-3/+*	99	1	0

Supplementary Figure S5

Cell type-specific complementation of *akrp-3* mutation. (a,b) Complementation using a p35S promoter (35S-AKRP.1:GFP) yielded rescued homozygous plants already in the first generation. The complementation was not absolute, because some lines retained some levels of embryonic defects; (c,d) Chlorotic cotyledons that recovered in newly emerged true leaves and (e) lesions in rosette leaves. (f) Complementation with an egg cell-specific promoter (pEC1.1) was not sufficient to rescue *akrp-3* fertilization or embryo-lethal phenotype (n = 11). (g) Complementation under an antipode-specific pDD1 promoter weakly rescued the embryo-lethal *akrp-3* phenotype (class labeled as "other," phenotypically similar to Figure 6B "other" category, n = 5).

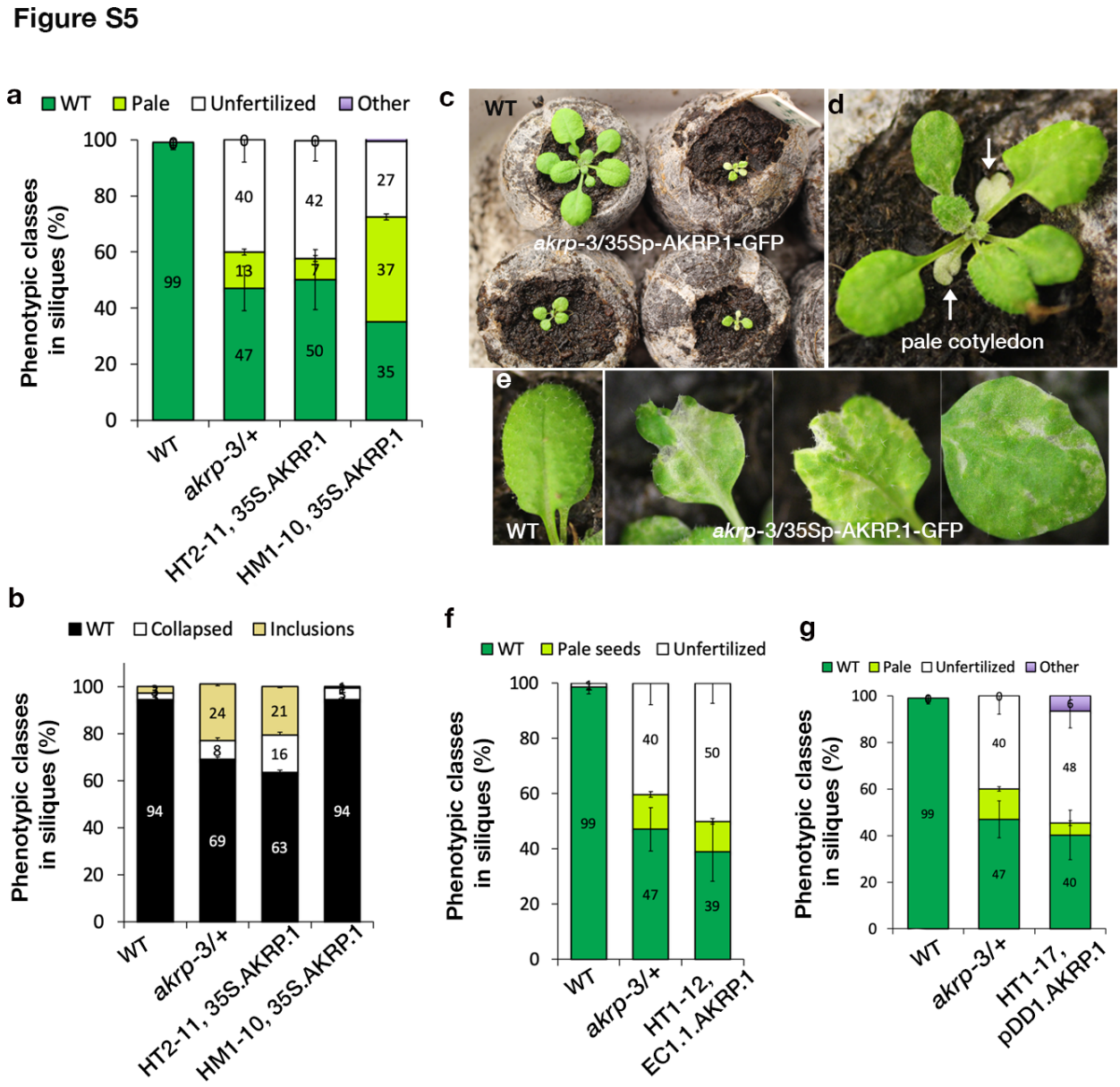

Supplementary Figure S6

AKRP.1 plastid co-localization in mature pollen. Analysis of double heterozygous Lat52-AKRP.1:GFP and pBINU-CHYA(K) marker in mature pollen by independent GFP and YFP channel excitation with Argon 488 laser in a Zeiss confocal microscope. Intensity values were plotted using the Prism software.

Figure S6

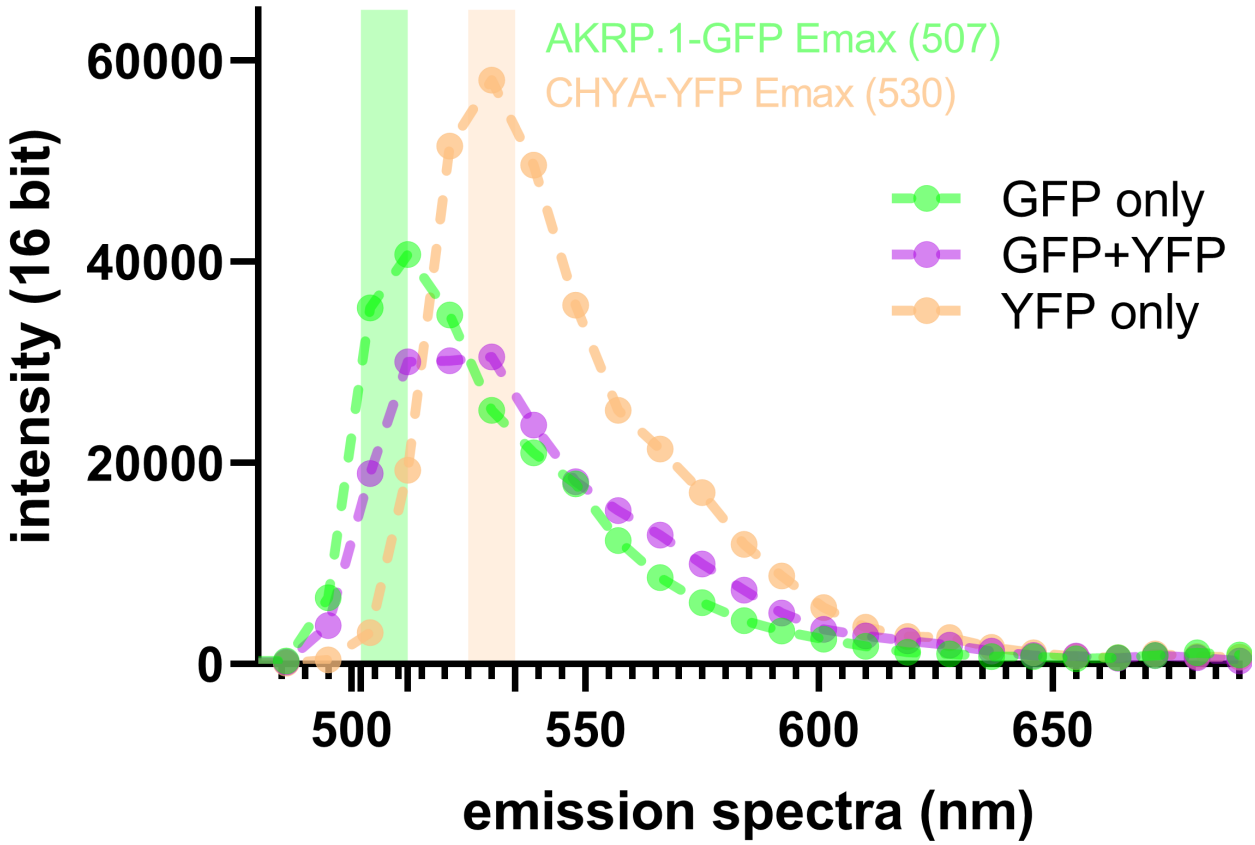

2.4. PRP8A and PRP8B spliceosome subunits act coordinately to control pollen tube attraction in Arabidopsis thaliana

Katarína Kulichová, Vinod Kumar, Lenka Steinbachová, Božena Klodová, Ljudmilla Timofejeva, Miloslav Juříček, David Honys and Said S. Hafidh (Kulichová and Hafidh are shared first authors)

Development (2020) 147, dev186742. doi:10.1242/dev.186742

My contribution: I selected the candidate gene based on transcriptomic data from our previous publications (Hafidh et al. 2012a, 2012b). Its transcripts were found to be stored in tobacco pollen tubes even after 24 hours of in vitro growth, making it an interesting candidate for studying RNA storage in pollen and its potential effects on gametogenesis and embryogenesis. I identified its homolog in Arabidopsis and screened several T-DNA lines for phenotypic defects, which were found to be embryo lethal. To study gametophytic and embryonic defects, transmission assay, pollen tube cultivation experiments, ovule and pistil staining, and crosses with marker lines were conducted. I also identified a second gene, an ortholog of PRP8a, named PRP8b. As the single mutant of PRP8a did not exhibit any issues with the female gametophyte, and the PRP8b T-DNA lines also showed no developmental issues, we decided to create a double mutant *prp8a/prp8b*. Knocking out two closely related genes had a severe impact on the splicing of many target genes, which resulted in morphological defects in both gametophytes, which were unable to produce a viable offspring. We then employed similar methods to study the defects in more detail and to determine the origin of the phenotypes. I did phenotypic screenings, pollen tube cultivation, crosses with markers, blue dot analysis and aniline blue staining. After I left for maternity leave, the results were expanded upon by Said Hafidh and other colleagues through additional experiments to quantify the extent of the observed phenotypes. I also noted an aberrant phenotype of the female ovules, which was later studied more in depth by my colleagues. I cloned and described PRP8a promoter activity in plant tissues through histochemical staining. I also did RT-PCR and qPCR measurements, PRP8a protein localisation and colocalisation with markers, and complementation of *prp8a* mutant by various constructs. The manuscript originally described only the single *prp8a* mutant, but has since evolved into a study of both PRP8a and PRP8b and their effects on splicing, gametophyte fitness, and morphology. Several experiments that focused on the role of PRP8a in early embryogenesis and inheritance of

transcripts had to be removed from the original manuscript versions due to reviewers comments and are currently presented in the following chapter in this dissertation thesis.

© 2020. Published by The Company of Biologists Ltd | Development (2020) 147, dev186742. doi:10.1242/dev.186742

RESEARCH ARTICLE

PRP8A and PRP8B spliceosome subunits act coordinately to control pollen tube attraction in *Arabidopsis thaliana*

Katarína Kulichová[1,*], Vinod Kumar[1], Lenka Steinbachová[1], Božena Klodová[1], Ljudmilla Timofejeva[1], Miloslav Juříček[1], David Honys[1,2] and Said S. Hafidh[1,*,‡]

ABSTRACT

Precise guided pollen tube growth by the female gametophyte is a prerequisite for successful sexual reproduction in flowering plants. Cysteine-rich proteins (CRPs) secreted from the embryo sac are known pollen tube attractants perceived by pollen tube receptor-like kinases. How pre-mRNA splicing facilitates this cell-to-cell communication is not understood. Here, we report a novel function of Pre-mRNA PROCESSING factor 8 paralogs, PRP8A and PRP8B, as regulators of pollen tube attraction. Double mutant *prp8a prp8b* ovules cannot attract pollen tubes, and *prp8a prp8b* pollen tubes fail to sense the ovule's attraction signals. Only 3% of ovule-expressed genes were misregulated in *prp8a prp8b*. Combination of RNA sequencing and the MYB98/LURE1.2-YFP reporter revealed that the expression of MYB98, LUREs and 49 other CRPs were downregulated, suggesting loss of synergid cell fate. Differential exon usage and intron retention analysis revealed autoregulation of PPR8A/PRP8B splicing. *In vivo*, PRP8A co-immunoprecipitates with splicing enhancer AtSF3A1, suggesting involvement of PRP8A in 3′-splice site selection. Our data hint that the PRP8A/PRP8B module exhibits spliceosome autoregulation to facilitate pollen tube attraction via transcriptional regulation of MYB98, CRPs and LURE pollen tube attractants.

KEY WORDS: Pre-mRNA PROCESSING factor 8, Splicing, Post-transcriptional regulation, Cell-to-cell signaling, Cysteine-rich proteins, Pollen tube attraction and reception, Sexual reproduction

INTRODUCTION

In flowering plants, two sperm cells are delivered to the female gametophyte for fertilization via a pollen tube after guided growth through the transmitting tract and the micropyle (Palanivelu et al., 2006; Dresselhaus and Franklin-Tong, 2013; Higashiyama and Yang, 2017). Both phases of pollen tube guidance rely on prelaid chemoattractants secreted by synergid cells and encoded by Cysteine-rich proteins (CRPs) and the Defensin-like subfamily of CRPs (DEFL) including LUREs (Márton et al., 2005, 2012; Okuda et al., 2009; Takeuchi and Higashiyama, 2012). Genes encoding the LURE family of proteins are specifically expressed in the synergid cells and their expression is under the control of MYB98 transcription factor, which is also synergid cell-specific (Kasahara et al., 2005). Intriguingly, expression of MYB98 is controlled by the central cell-specific RNA pol II component, Central Cell Guidance (CCG) and CCG Binding Protein 1 (CBP1), implying cell-to-cell pollen tube guidance control mediated by the central cell (Li et al., 2015). Pollen tube attraction and fertilization is inhibited in *ccg* and *cbp1*, suggesting an indispensable role of the central cell in pollen tube guidance (Li et al., 2015). Furthermore, several other secreted CRPs are expressed specifically from the central cell; however, their role is still unknown (Li et al., 2015). These relayed cell-to-cell signals between the two gametophytes are perceived by primary cell surface receptors at the micropyle and pollen tube tip, including female receptors such as LORELEI (Liu et al., 2016), LORELEI-LIKE GPI-anchored protein 1 (LLG1) and FERONIA, and male receptors such as COBRA GPI-anchored, MALE DISCOVERER1 (MDIS1) and MDIS2 from the LRR-VI subfamily, MDIS1-INTERACTING RECEPTOR LIKE KINASE 1 (MIK1) and MIK2 from LRR-XI and LRR-XII subfamilies, respectively, POLLEN RECEPTOR-LIKE KINASE 6 (PRK6) and palmitoylated LOSS IN POLLEN TUBE GUIDANCE 1 (LIP1) and LIP2 LURE receptors (Higashiyama and Yang, 2017). Collectively, the dominant feature of pollen tube guidance seems to rely on protein secretion and, thus, endomembrane and unconventional protein secretion mechanisms are likely to play fundamental roles in pollen tube attraction and guidance (Liu et al., 2015; Hafidh et al., 2016b).

In *Arabidopsis*, almost 90% of the genes are interrupted by introns and it is estimated that >60% of intron-containing genes undergo alternative splicing (AS) (Berget et al., 1977; Syed et al., 2012; Marquez et al., 2012; Reddy et al., 2013). Most frequently, 51% of the AS events utilize alternative 5′ or 3′ splice sites or exon skipping, influencing alternative protein coding sequences or aberrant mRNA production (McGlincy and Smith, 2008; Kalyna et al., 2012; Syed et al., 2012; Filichkin et al., 2015). Pre-mRNA splicing is mediated by the spliceosome complex, which catalyzes two sequential transesterification reactions to excise the interspaced intron (reviewed by Will and Lührmann, 2011). The spliceosome is composed of multiple subunits, the U2-dependent spliceosome type from U1, U2, U5 and U4/U6 small nuclear ribonucleoproteins (snRNPs) and numerous non-snRNP proteins. A few proteins remain as core components of the tri-snRNP complex, including Snu114, Brr2 and PRP8. PRP8A interacts with a preformed U4/U6.U5 tri-snRNP complex to form a larger catalytically active spliceosomal B complex (Maeder et al., 2009; Bartels et al., 2002). To select an alternative splice site, splicing factors bind to exonic/intron enhancer or suppressor sequence elements to influence recruitment of the spliceosome complex, resulting in alternative splicing (Staiger and Brown, 2013). Genetic screen of AtSF3A1a-U2-associated *ATROPOS* (Moll et al., 2008), U4/U6-associated LACHESIS (Gross-Hardt et al., 2007) and U5-associated

[1]Institute of Experimental Botany of the Czech Academy of Sciences, Rozvojová 263, 165 02 Prague 6, Czech Republic. [2]Department of Plant Experimental Biology, Faculty of Science, Charles University, Viničná 5, 128 44 Prague 2, Czech Republic. *These authors contributed equally to this work

‡Author for correspondence (hafidh@ueb.cas.cz)

K.K., 0000-0002-1115-9899; L.T., 0000-0002-1046-2001; D.H., 0000-0002-6848-4887; S.S.H., 0000-0002-3970-713X

Handling Editor: Ykä Helariutta
Received 25 November 2019; Accepted 14 April 2020

Development (2020) 147, dev186742. doi:10.1242/dev.186742

CLOTHO/GAMETOPHYTIC FACTOR 1 (Liu et al., 2009) revealed the crucial role of splicing factor proteins in the development and competence of the female gametophyte for fertilization; interestingly no effect has been reported for the male gametophyte (Tzafrir et al., 2004; Coury et al., 2007; Moll et al., 2008; Liu et al., 2009).

The *Arabidopsis* genome encodes two copies of PRP8: PRP8A (AT1G80070) and PRP8B (AT4G38780). An *abnormal suspensor* 2 (*sus2*) mutant defective in PRP8A is embryo lethal (Schwartz et al., 1994), whereas PRP8B function has not been investigated. A hypomorphic *prp8a*-6 allele was further identified to be involved in splicing of long noncoding antisense transcripts (COOLAIR) that are important for the regulation of FLOWERING LOCUS C activity and could complement the *prmt5* mutant of the NineTeen complex (NTC)/Prp19, a subcomplex of the spliceosome machinery (Marquardt et al., 2014; Deng et al., 2016).

Here, we report for the first time that double mutant *prp8a prp8b* has no striking female or male gametogenesis defects, but *prp8a prp8b* specifically impairs ovule competence for pollen tube attraction and the competence of the pollen tubes to navigate towards ovules. We propose that PRP8A/PRP8B associates with AtSF3A1 and functions in defining the competence of both gametophytes to facilitate female–male communication.

RESULTS

PRP8B is preferentially expressed in pollen

PRP8 is well conserved in all domains of life, including all land plants (Fig. 1A). In plants, the role of pre-mRNA splicing factor PRP8A in male or female gametophytes is unknown. Moreover, the role of PRP8B, a close paralog of PRP8A, has yet to be characterized (Fig. 1A). PRP8A shows 93% identity with PRP8B; however, they exhibit polymorphisms at the N-terminal PROCN domain and the C-terminal JAB domain, as predicted by PFAM (http://pfam.xfam.org) and InterProScan (https://www.ebi.ac.uk/interpro) EMBL-EBI databases (Fig. 1B). We initially identified PRP8A as a gene whose transcripts are mostly stored in tobacco pollen tubes as late as 24 h after pollen germination, and thus we hypothesized that they probably have a late function during pollen tube growth (Hafidh et al., 2018). Comparison of publicly deposited expression datasets (Zimmermann et al., 2004; Honys and Twell, 2004; Winter et al., 2007; Borges et al., 2008; Qin et al., 2009; Loraine et al., 2013) revealed over 30-fold elevated expression of PRP8B in pollen and semi-*in vivo* pollen tubes compared with PRP8A (Fig. 1C; Fig. S1A), whereas PRP8A dominates the expression during embryogenesis and seed development (Fig. S1A) (Belmonte et al., 2013). Real time RT-qPCR verified PRP8B dominant expression in pollen and a broader expression of PRP8A (Fig. 1D). In the embryo sac, both genes were classified as expressed in synergid cells, the egg cell and the central cell (Wuest et al., 2010). In agreement with public expression datasets, RT-qPCR verified negligible expression of PRP8B at the post-globular stage of embryo development relative to PRP8A (Fig. 1D).

To investigate localization of both subunits, we constructed PRP8Apro-PRP8A::GFP and PRP8Bpro-PRP8B::GFP and monitored their localization. Signal of PRP8A-GFP was detected in the nuclei of all female gametic cells and cells of the integuments in mature ovules, whereas PRP8B could only be reliably detected in the egg and the central cell of mature ovules (Fig. 1E). In the male gametophyte, both subunits localized in sperm cells and vegetative cell nuclei of pollen and pollen tubes; however, PRP8B was only reliably detected in hydrated pollen grains and we frequently observed vegetative cytosolic localization of PRP8B (Fig. 1E). Post-

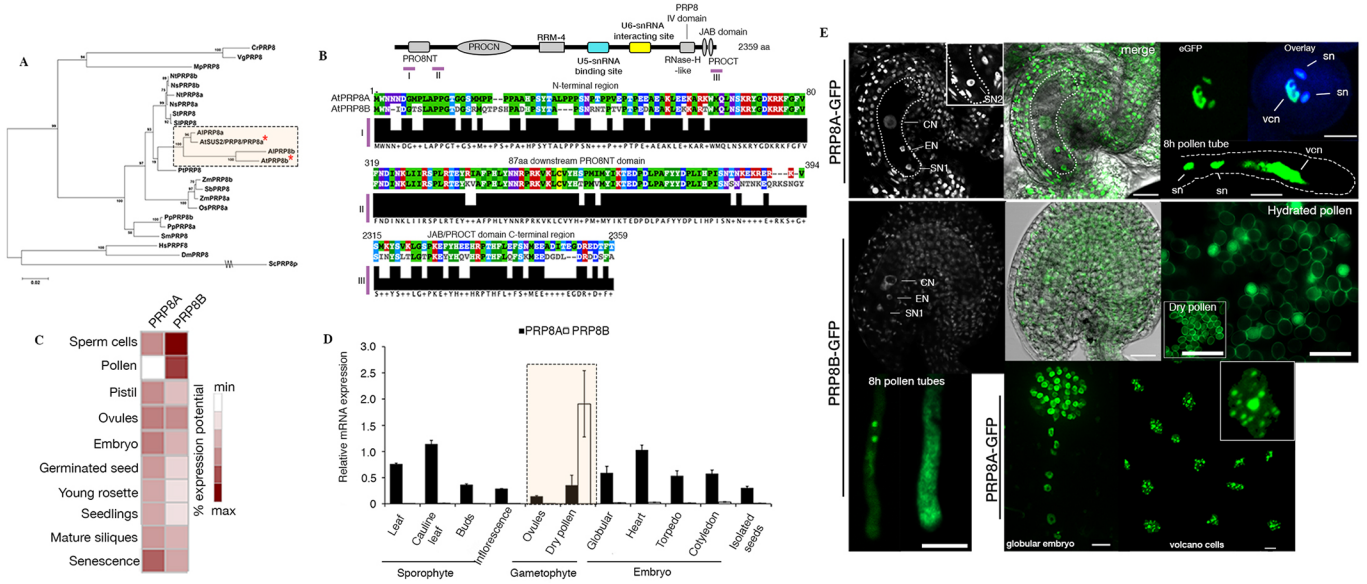

Fig. 1. PRP8B expression is dominant in pollen and in sperm cells. (A) Phylogeny of PRP8 orthologs in Archea, fungi, plants and animals. Asterisks indicate the two *Arabidopsis thaliana* paralogs. The scale bar indicates the rates of substitutions/site. (B) PRP8A and PRP8B are 93% identical but show polymorphisms at the PROCN and JAB domain regions. Alignment was performed with Clustal Omega and visualized with Jalview. (C) Comparative expression of *PRP8A* and *PPR8B*. Data were retrieved from Genevestigator (Zimmermann et al., 2004). This figure is extended to Fig. S1. (D) RT-qPCR verification of *PRP8A* and *PRP8B* steady-state transcript levels. Ct values of eIF4A1 were used as reference to compute relative expression. Data are mean±s.d. (E) Subcellular localization of PRP8Apro-PRP8A::GFP and PRP8Bpro-PRP8B::GFP in ovules, pollen, pollen tubes and developing globular stage embryo. Unlike PRP8A, PRP8B was not reliably detected in dry pollen and in addition to nuclear localization in pollen tubes, it also localized in the pollen tube cytoplasm. In mature ovules, PRP8B was only reliably detected in the central cell nucleus. Note the punctate subnuclear domains formed by PRP8A in epidermal cells of the seed with volcano-shaped columellae showing two distinct subpopulations. Dotted white lines highlight dominant expression of PRP8B in pollen. CN, central cell nucleus; EN, egg cell nucleus; sn, sperm cell nucleus; SN1/2, synergid cell 1 and 2 nuclei; vcn, vegetative cell nucleus. Scale bars: 40 µm.

Development (2020) 147, dev186742. doi:10.1242/dev.186742

fertilization, PRP8A localized in nuclei of developing embryo and suspensor cells and in heterogeneous nuclear speckles in volcano cells of mature seeds, whereas PRP8B was not reliably detectable.

Double mutant *prp8a prp8b* is female and male sterile

To assess PRP8A and PRP8B function, we characterized three transfer DNA (T-DNA) insertion alleles that disrupt the U6-snRNP interacting domain of PRP8A and PRP8B, designated *prp8a*-12, *prp8a*-13 and *prp8b*-1 (Fig. 2A). Two other *PRP8B* alleles, *prp8b*-2 and *prp8b*-3, were also screened (Fig. 2A). *prp8a*-12 is embryo lethal as previously reported from other *prp8a* alleles (Schwartz et al., 1994; Tzafrir et al., 2004; Meinke et al., 2008; Marquardt et al., 2014; Deng et al., 2016); therefore, heterozygous *PRP8Aa*-12 and homozygous *prp8bb*-1 plants were selected for further characterization. Henceforth, *prp8a*-12 and *prp8b*-1 mutant alleles will be referred to as *prp8a* and *prp8b*, respectively. RT-qPCR revealed that both *prp8a* and *prp8b* are knockdown alleles (Fig. 2B). Screen of heterozygous *PRP8Aa* and homozygous *prp8bb* mutant plants showed no developmental or gametophyte abnormalities, defects in pollen tube growth, gamete cell fate specification or any reduction in transmission of the mutant alleles (χ^2 test=1.53, 0.53; P>0.22) (Fig. S1B,C). Segregation of self-pollinated *PRP8Aa* plants confirmed the recessive homozygous embryo lethality of the *prp8a* allele (Fig. S1D). Our results implied a functional redundancy between PRP8A and PRP8B in both gametophytes. We therefore generated double mutant *prp8a prp8b* and investigated developmental phenotypic defects. No sporophytic defects could be observed throughout plant development (Fig. 2C). Instead, analysis of *PRP8Aa;Bb* and *PRP8Aa;bb* plants revealed that segregation and transmission of *prp8a prp8b* double mutant alleles was severely reduced through both the female and male gametophytes (female transmission efficiency 2.02%, male transmission efficiency 1.04%; P<0.001) (Fig. 2D,E). Rarely, in <4% of the cases in self-fertilized plants, *prp8a prp8b* alleles could be transmitted by either male or female gametophytes from the *PRP8Aa;bb* genotype plants (Fig. 2D). These results imply that the *prp8a prp8b* genotype is lethal in the gametophyte. In support, dissection of *PRP8Aa;bb* siliques revealed approximately 46% of unfertilized ovules (n=422/502) (Fig. 2F). To confirm the origin of this phenotype, we complemented *PRP8Aa;bb* plants with *PRP8A*pro-*PRP8A*-3UTR and *PRP8B*pro-*PRP8B*::*GFP* constructs. Both constructs fully complemented the unfertilized ovule phenotype, with the *PRP8*Apro-*PRP8A*-3UTR construct showing better complementation efficiency (Fig. 2F,G). Collectively, our results imply that PRP8A and PRP8B function redundantly in the gametophyte, and that PRP8A/PRP8B dual activities are essential for successful fertilization.

PRP8A and PRP8B act redundantly to control pollen tube attraction

The full penetrance of the *prp8a prp8b* aborted ovule phenotype suggested the possibility of a defect in pollen tube attraction, reception or fertilization. To investigate, we analyzed pollen tube attractiveness, receptivity and fertilization events in *prp8a prp8b* ovules *in vivo* using live cell imaging by pollinating *PRP8Aa;bb* pistils with pollen grains expressing double markers for vegetative and sperm cells (LAT52pro::GFP;HTR10pro-HTR10::RFP), respectively. Approximately 8 h after pollination (8 HAP), we observed accurate pollen tube attraction to the micropyle, pollen tube discharge and sperm cell release in approximately 81% (n=228/282) of ovules when wild-type pistils of *ms1* plants were pollinated with the double marker-expressing pollen grains (Fig. 3A). When *PRP8Aa;bb* pistils were pollinated with the same double marker pollen grains, only 49% (n=194/400) of the ovules were successfully targeted, referring to the *PRP8A;b* heterozygous ovule genotype (Fig. 3A). In contrast, 44% (n=175/400) of the adjacent *prp8a prp8b* double homozygous mutant ovules were defective in pollen tube attraction or no pollen tubes approached proximity to the ovules (Fig. 3A). Rarely, we noticed single or multiple pollen tube (polytubey) attraction by the *prp8a prp8b* ovules at the micropyle, but without detectable GFP discharge, suggesting a failure in correct pollen tube attraction or reception (Fig. 3A). Polytubey attraction into a single ovule results from pollen tube reception failure (Beale et al., 2012), thus supporting our observation on the lack of *prp8a prp8b* successful pollen tube reception. This was independently verified by the lack of female or male transmission of the *prp8a prp8b* genotype as well as by segregation distortion in the F2 siblings from *PRP8Aa;bb* selfing plants (Fig. 2E).

To test the pollen tube attraction defect of *prp8a prp8b* ovules independently, we stained callose of *in vivo* pollen tubes with aniline blue in self-pollinated *PRP8Aa;bb* plants or in an outcross of *PRP8Aa;bb* female pollinated with wild-type Col-0 pollen grains at 18 HAP to further emphasize the ovule phenotype of the *prp8a prp8b* double mutant (Fig. 3B). Almost 50% (n=276/541) of the ovules in *PRP8Aa;bb* pistils either failed in pollen tube attraction to the micropyle entry or no pollen tubes appeared near the mutant ovule micropyle entry in self-pollinated or in an outcross experiment (Fig. 3B). We classified the ovule phenotypes into four subtypes: type I, wild type-like ovule (*PRP8A;b*) with normal pollen tube reception; type II, double mutant *prp8a;b* ovule with normal pollen tube reception; type III, ovule with no pollen tubes nearby; and type IV, ovules with pollen tubes nearby but failed to attract pollen tubes into the micropyle (i.e. attraction defect) (Fig. 3B). In the progeny of *PRP8Aa;bb* self-pollinated plants, 39% were identified as type I, 8% as type II, 27% as type III ovules and 26% as type IV (Fig. 3B; Movies 1 and 2). In the progeny of *PRP8Aa;bb*×wild type crosses, 45% were type I, 6% were type II, 31% were type III ovules and 18% were type IV (Fig. 3B; Movies 1 and 2).

The *prp8a*-12 allele is a blue-SAIL T-DNA insertion containing a LAT52pro-GUS transgene that co-segregates with the T-DNA insertion of the mutant allele. We therefore took advantage and performed a blue dot histochemical assay (Palanivelu et al., 2006), by pollinating wild-type *ms*1 pistils and *PRP8Aa;bb* pistils with wild-type pollen grains or with pollen grains expressing LAT52pro-GUS (Fig. S2). Since *LAT52* promoter activity should be restricted to pollen only (Twell et al., 1990, 1991), we observed ectopic GUS staining in the *prp8a prp8b* embryo sac before fertilization that we did not observe in control plants (Fig. S2). However, this ectopic staining was distinguishable from GUS staining of ovules targeted with pollen tubes expressing LAT52pro-GUS (Fig. S2). Therefore, we proceeded with quantification by distinguishing the two populations in *PRP8Aa;bb* pistils. Quantification of targeted ovules supported our previous results that *prp8a prp8b* ovules fail in pollen tube attraction (Fig. S2). Collectively, our results suggest that simultaneous loss of *PRP8A* and *PRP8B* severely impairs pollen tube attraction, long-distance pollen tube guidance and fertilization in *Arabidopsis*.

PRP8A/PRP8B function is essential for pollen tube response to female attraction signals

The near-complete block of *prp8a prp8b* transmission through the male also hinted at a role of PRP8A/PRP8B in pollen tubes.

Development (2020) 147, dev186742. doi:10.1242/dev.186742

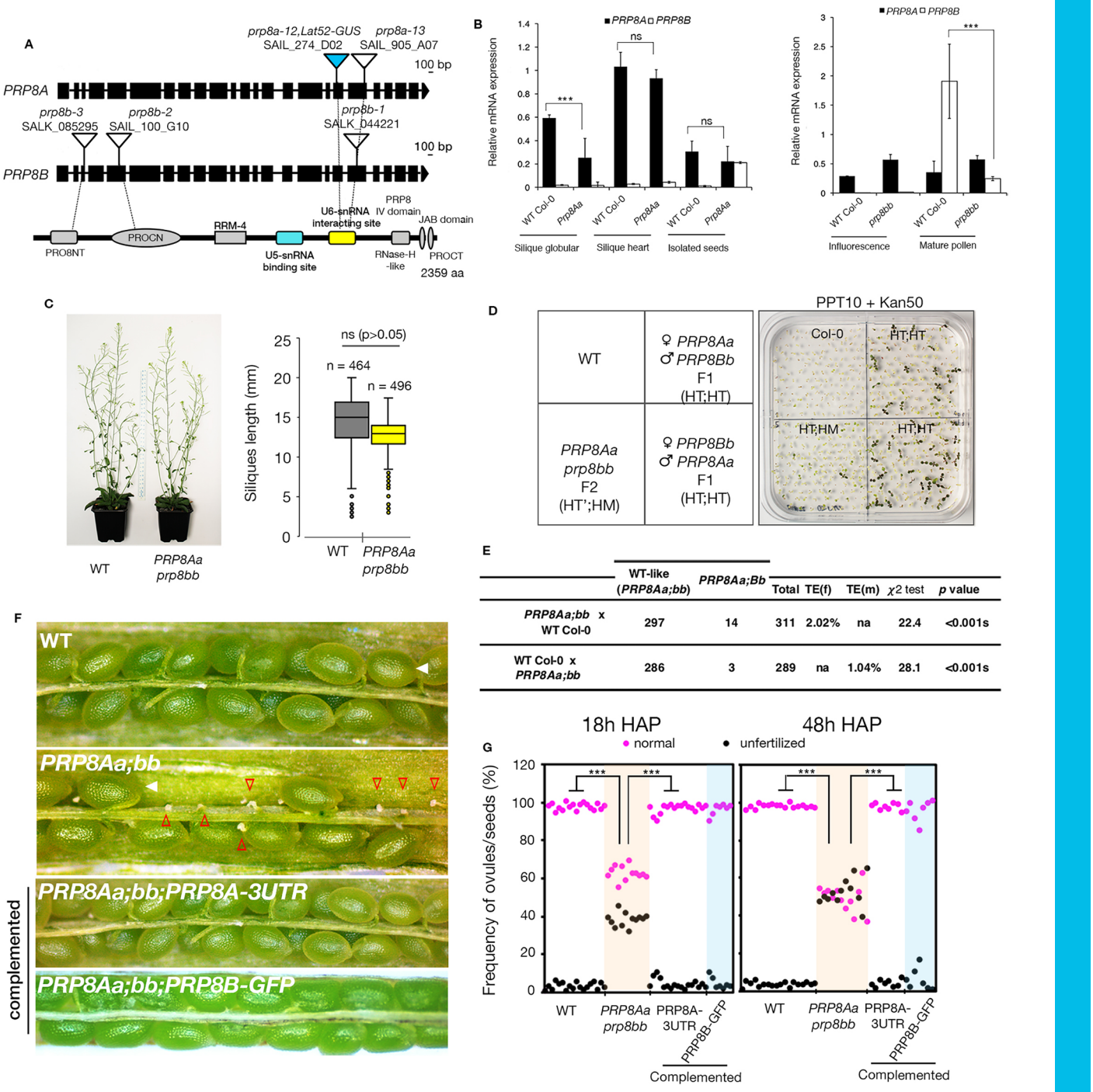

	WT-like (*PRP8Aa;bb*)	*PRP8Aa;Bb*	Total	TE(f)	TE(m)	χ2 test	*p* value
PRP8Aa;bb x **WT Col-0**	297	14	311	2.02%	na	22.4	<0.001s
WT Col-0 x ***PRP8Aa;bb***	286	3	289	na	1.04%	28.1	<0.001s

Fig. 2. Characterization of *prp8a*-12 *prp8b*-1 double mutant. (A) Schematic of *AtPRP8a* and *AtPRP8b* loci to scale with approximate positions of the T-DNA alleles, including the blue-sail SAIL allele analyzed. Dashed lines point to protein domains disrupted by the T-DNA insertion. Lower part is the scaled protein model with domains annotated according to PFAM and PROSITE databases. (B) RT-qPCR validation of *prp8a*-12 and *prp8b*-1 knockdown alleles. Relative expression between wild-type and mutant samples was determined by normalizing the Ct values with eIF4A1 as a reference. (C) Representative images of adult wild-type and *PRP8Aa;bb* plants and siliques showing normal sporophytic development. (D,E) Segregation and transmission of the *prp8a prp8b* mutant gametes through male and female. Seedlings from selfed *PRP8Aa;bb* plants were grown under double selection (Basta, *prp8a*-12; Kan50, prp8b-1) and genotypes of resistant seedlings were verified by PCR genotyping. Transmission data for the individual alleles are in Fig. S1. TE(f) female transmission efficiency; TE(m) male transmission efficiency. (F) Dissected siliques from wild-type and *PRP8Aa;bb* plants. Triangles with red borders indicate unfertilized ovules, white triangles indicate aborted seed development and filled white triangles mark fully developed wild-type seeds. (G) Quantification of ovule phenotype in *PRP8Aa;bb* plants at 18 and 48 HAP. Complementation was performed with PRP8A-3′UTR and PRP8B-GFP under their native promoters. Data are mean±s.d. (*n*=18). ns, not significant; ***P<0.01 (Student's *t*-test).

Viability testing and nuclear staining revealed that *prp8a prp8b* pollen grains are viable and morphologically normal. We then exploited the LAT52pro-GUS tagged T-DNA insertion of the *prp8a*-12 SAIL allele (Fig. 2A) to follow specifically *prp8a prp8b* mutant pollen tube growth *in vitro* as well as within the pistil by GUS staining. GUS staining revealed that *in vitro prp8a prp8b*

Development (2020) 147, dev186742. doi:10.1242/dev.186742

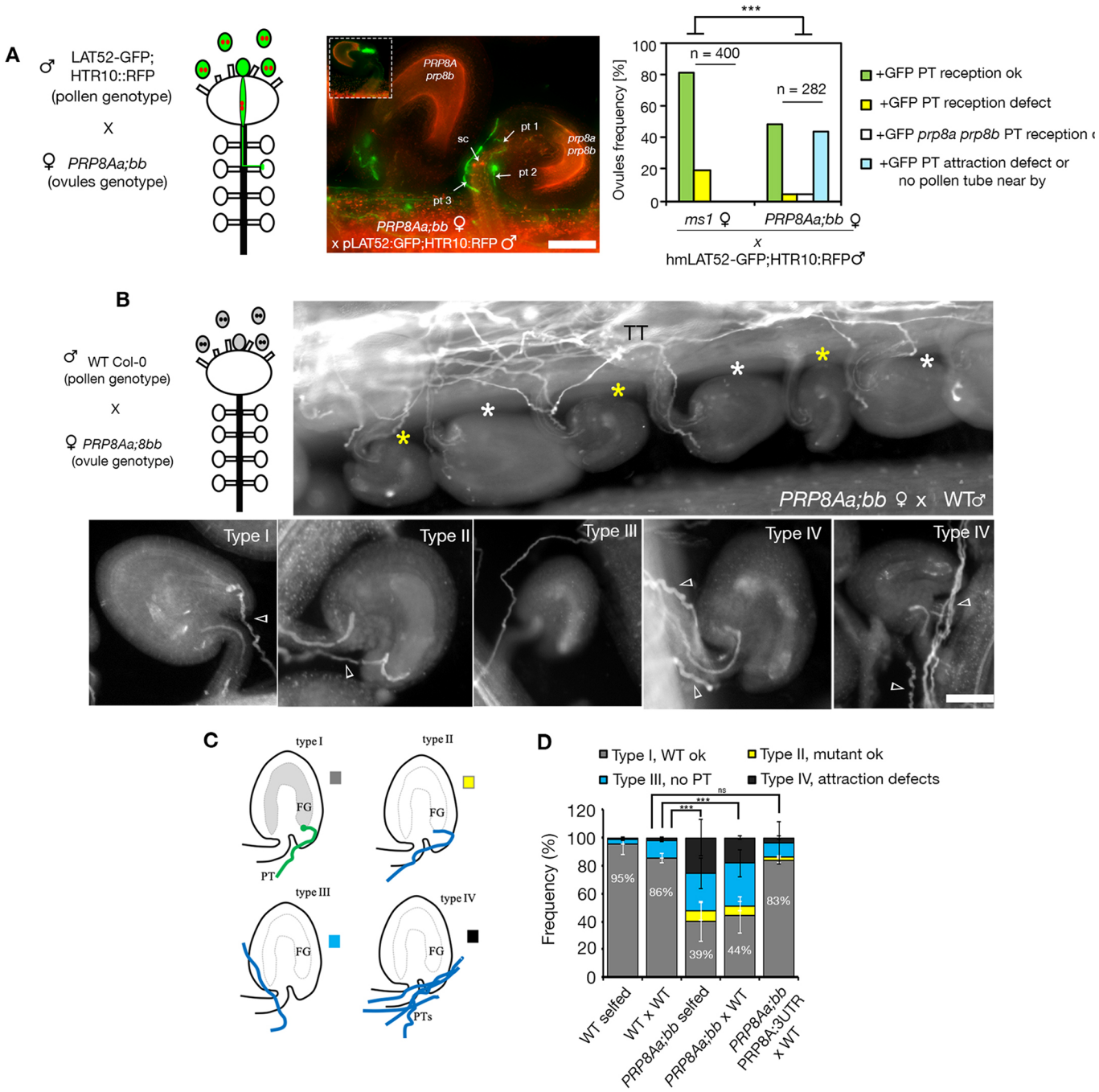

Fig. 3. PRP8A/PRP8B controls ovule competence for pollen tube attraction. (A) Live cell imaging of *prp8a prp8b* ovule fertilization using a dual pollen tube reporter. LAT52pro::GFP labeled the pollen tube cytosol and pHTR10-HTR10::RFP labeled sperm cells nuclei. Left ovule is wild-type-like (*PRP8A;8b* genotype), showing attraction and reception of pollen tube indicated by the GFP halo in the inset. On the right is a representative double mutant *prp8a prp8b* ovule showing attraction and a rare reception defect of multiple pollen tubes at 18 HAP. Bar chart is a quantification of ovule attraction efficiency of the respective genotypes crosses. Pt, pollen tube; sc, sperm cells. (B) *In vivo* quantification of *PRP8a;8b* pollen tube attraction defect. Top panel shows behavior of both genotypes *PRP8A;8b* (white asterisks) and *prp8a prp8b* (yellow asterisks) on pollen tube attraction and reception. Bottom panels show representative pictographs of type I-IV ovules. Type I-II, correct pollen tube reception; type III, no pollen tube within approximately 100 µm of the ovule; type IV, attraction defect (pollen tube nearby but failed to enter the micropyle). Triangles point to pollen tubes. TT, transmitting track. (C) Illustration of the *prp8a prp8b* ovules pollen tube attraction phenotype. (D) Frequency of the four types of phenotypes in each respective cross at 18 HAP. Data are mean±s.d. ns, not significant; ***P<0.01 (Student's t-test). Scale bars: 50 µm.

pollen tube growth is indistinguishable from that of wild-type pollen tubes (Fig. 4A). *In vivo*, double mutant *prp8a prp8b* pollen tube growth also appeared normal in the transmitting tract and the double mutant pollen tubes were able to reach the very bottom of the pistil, suggesting no growth or navigation defects in the transmitting tract (Fig. 4B). However, compared with control LAT52pro-GUS pollen tubes, the *prp8a prp8b* pollen tubes failed to turn towards the funiculus or target any ovules in wild-type pistils (0% targeted, n=0/391 ovules) (Fig. 4B). These results are in agreement with the blocked transmission of *prp8a prp8b* alleles through the male

Development (2020) 147, dev186742. doi:10.1242/dev.186742

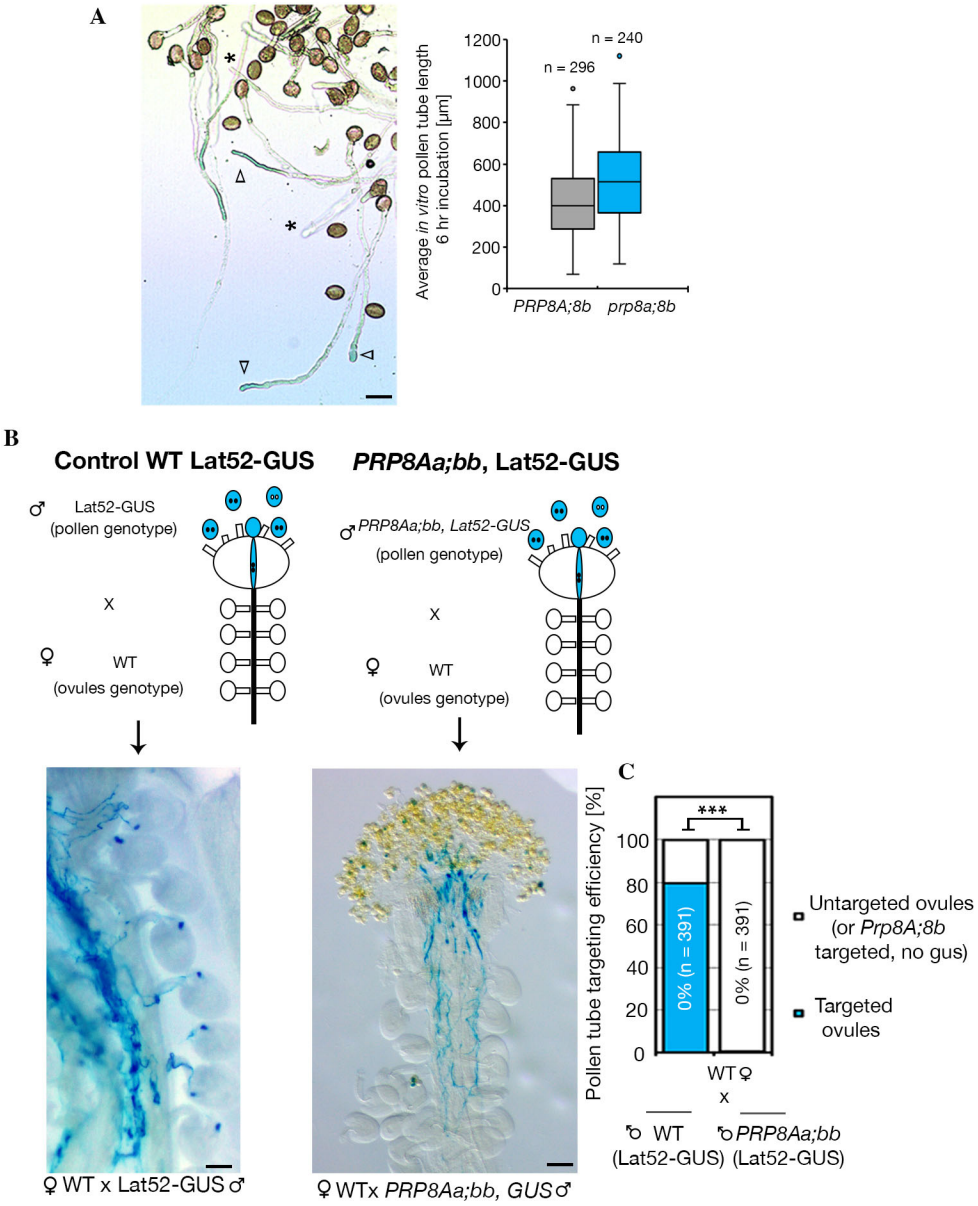

Fig. 4. PRP8A/PRP8B activity specifies pollen tube competence to target ovules for fertilization. (A) *In vitro prp8a prp8b* pollen tube growth is not affected. Empty triangles indicate double mutant pollen tubes stained with GUS; asterisks indicate wild-type-like (PRP8A;b) pollen tubes. The box plot shows pollen tube length distribution of the two genotypes. Middle bars are median values, boxes indicate the first to third interquatile ranges, whiskers indicate 1.5 of minimum and maximum interquartiles, and dots indicate outlier values. (B) *In vivo prp8a prp8b* pollen tube guidance towards wild-type ovules is defective. Blue dot assay of the wild-type pistil pollinated with control LAT52pro-GUS expressing pollen (left) or with *prp8a prp8b*-LAT52pro-GUS pollen (right). Note the normal growth of *prp8a prp8b*-Lat52GUS pollen tubes in the entire length of the pistil without ovule targeting or pollen tube burst at the micropyle entry. (C) Blue-dot assay quantification of *prp8a prp8b*-LAT52pro-GUS pollen tube ovule-targeting efficiency. ***P<0.001. Scale bars: 50 µm.

gametophyte. Together, our data suggest that PRP8A/PRP8B coordinately regulates pollen tube competence to respond to funiculus and/or micropylar attraction signals secreted by the ovules for pollen tube guidance.

prp8a prp8b double mutant ovules might exhibit abnormal embryo sac

To better understand the defects of *prp8a prp8b* ovules, we emasculated flowers from *PRP8Aa;bb* plants at stage 13-14 with fully developed embryo sacs (Christensen et al., 1997), and left them to mature for 48 h. DIC imaging revealed that mature *prp8a prp8b* double mutant ovules showed a probably malformed embryo sac morphology in ∼35% of the ovules (Fig. 5A-F). Morphologically, the characteristic conical projection associated with the wild-type embryo sac micropyle pole was not observed in *prp8a prp8b* ovules (Fig. 5B). Instead, the *prp8a prp8b* embryo sac appeared to protrude to the very close proximity of the micropyle entry site or be pressed against the inner integuments of the ovule maternal tissues (Fig. 5C,D). In other ovules, the *prp8a prp8b* embryo sac appeared either enlarged or collapsed (Fig. 5E,F). Compared with wild-type dissected ovules at the same stage, only 3% of the ovules showed unusual embryo sac morphology (Fig. 5G). Despite the abnormal embryo sac morphology of *prp8a prp8b* ovules, nuclear staining revealed no obvious defects in nuclear proliferation, nuclear fusion or cellularization (Fig. 5H,I).

To further assess the impact of *prp8a prp8b* on the female gametophyte, we monitored the expression of FGR7.0, an embryo sac triple cell marker for synergid cell-specific (LURE1.2pro-NLS::3×GFP, AT5G43510), egg cell-specific (EC1pro-NLS::3×mCherry) and central cell-specific expression (CRP defensin-like LCR80 DD22pro-NLS::YFP, AT5G38330) (Völz et al., 2013). Live cell imaging in the wild-type embryo sac revealed that 88.5±9% (n=357/403) of the ovules showed correct expression of FGR7.0 in all three cell types, with strong expression in the synergid and the egg cell and weak expression in the central cell (Fig. 5J,K). In contrast, only 50.4±3% (n=646/1288) of the ovules from *PRP8Aa;bb* dissected pistils correctly expressed the FGR7.0 marker (Fig. 5J,K). Instead, 44.8±4% (n=578/1288) of the embryo

Development (2020) 147, dev186742. doi:10.1242/dev.186742

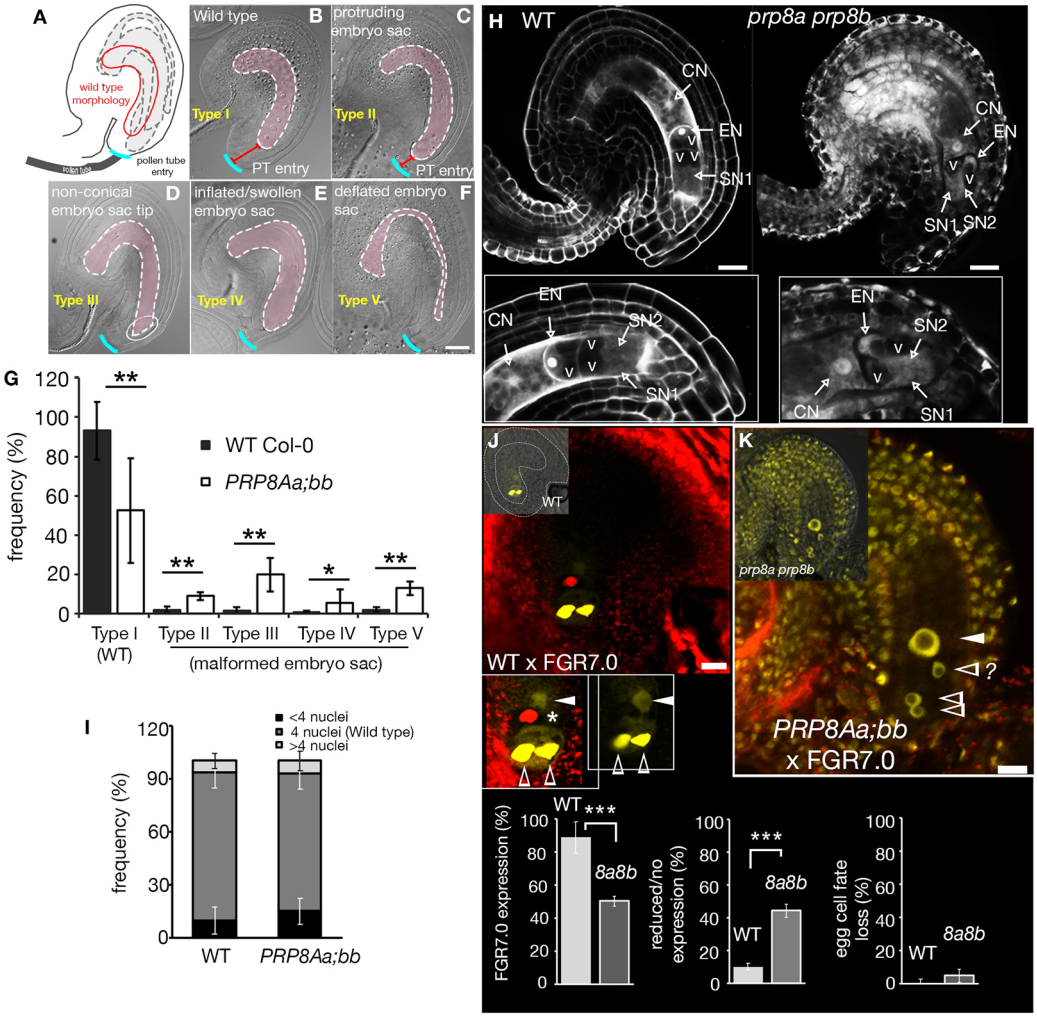

Fig. 5. Embryo sac morphology and expression of cell-fate markers is impaired in *prp8a prp8b* mutant ovules. (A) Superimposed cartoon summarizing the morphological defects of the *prp8a prp8b* embryo sac. (B-F) Representative DIC images of ovules dissected from wild-type and *PRP8Aa;bb* pistils at stage 13 of flower development. The embryo sac is highlighted in pink and its vicinity to the micropyle entry (turquoise) is marked by the red T-bone lines. Note the changes in morphology and distance of the embryo sac to micropyle entry. (G) Quantification of classes of defective embryo sac observed. (H) Optical sections from confocal laser scanning microscopy. Autofluorescent nuclei of each cell type of the female gametophyte are shown. Lower panels are at 3× magnification. (I) Frequencies of number of nuclei in wild-type and double mutant *prp8a prp8b* embryo sac at stage 13. (J) Representative expression of triple cell fate reporter markers FGR7.0 in wild-type mature ovules showing strong expression in synergid cells (open triangles), weak expression in the central cell (filled white triangles) and EC1-mCherry expression in the egg cell (asterisk). (K) In contrast, FGR7.0 expression is misregulated in *prp8a prp8b* ovules showing either no expression or stronger expression in the central cell and a loss of egg cell fate in some ovules. Graphs are quantification of FGR7.0 expression in control wild-type and double mutant *PRP8Aa;bb* genotypes. A question mark indicates unknown cell fate of the egg cell, expressing either the synergid or the central cell marker. Data are mean±s.d. (n=35). *P<0.05, **P<0.01, ***P<0.001 (Student's t-test). CN, central cell nucleus; EN, egg cell nucleus; m, micropyle; SN, synergid cell nucleus; V, vacuole. Scale bars: 50 µm.

sacs from *PRP8Aa;bb* pistils showed no or reduced expression in the synergid and egg cells (Fig. 5J,K). Remarkably, of the *prp8a prp8b* ovules with reduced FGR7.0 expression, 4.9±5% (n=64/1288) showed higher FGR7.0 expression in the central cell than in synergid cells, and the egg cell appeared to adopt the expression of either the synergid or the central cell marker and lost EC1-mCherry expression (Fig. 5K). These results imply that PRP8A and PRP8B could redundantly function in regulating gene expression and defining correct cell fate specification during ovule maturation.

RNA sequencing reveals splicing defects and deregulated gene expression in *prp8a prp8b* ovules

The fact that the *prp8a prp8b* double mutant did not show pleiotropic effects suggests that PRP8A and PRP8B are not strictly constitutive regulators of the splicing machinery. To unveil the extent of affected genes and define the molecular phenotype following *prp8a prp8b* knockdown, we isolated RNA from dissected ovules of *PRP8Aa;bb* pistils and conducted 150 bp paired-end RNA sequencing (RNA-seq) transcript profiling. We analyzed differential gene expression (DGE), intron retention (IR) and differential exon usage (DEU) relative to wild-type ovules. Pearson pairwise correlation clustering confirmed reproducibility of the replicates for individual RNA-seq libraries (Fig. 6A). Using DESeq2 R studio with a false-discovery rate (FDR) of <1%, RNA-seq data revealed that 764 genes (2.9%) were classified as downregulated and 779 genes (3%) were upregulated in *prp8a prp8b* ovules (Fig. 6B). At a Log2 fold change of >2 and P<0.05, 321 genes were considered downregulated and 163 genes were classified as upregulated in *prp8a prp8b* ovules (Fig. 6B; Tables S3, S4).

Development (2020) 147, dev186742. doi:10.1242/dev.186742

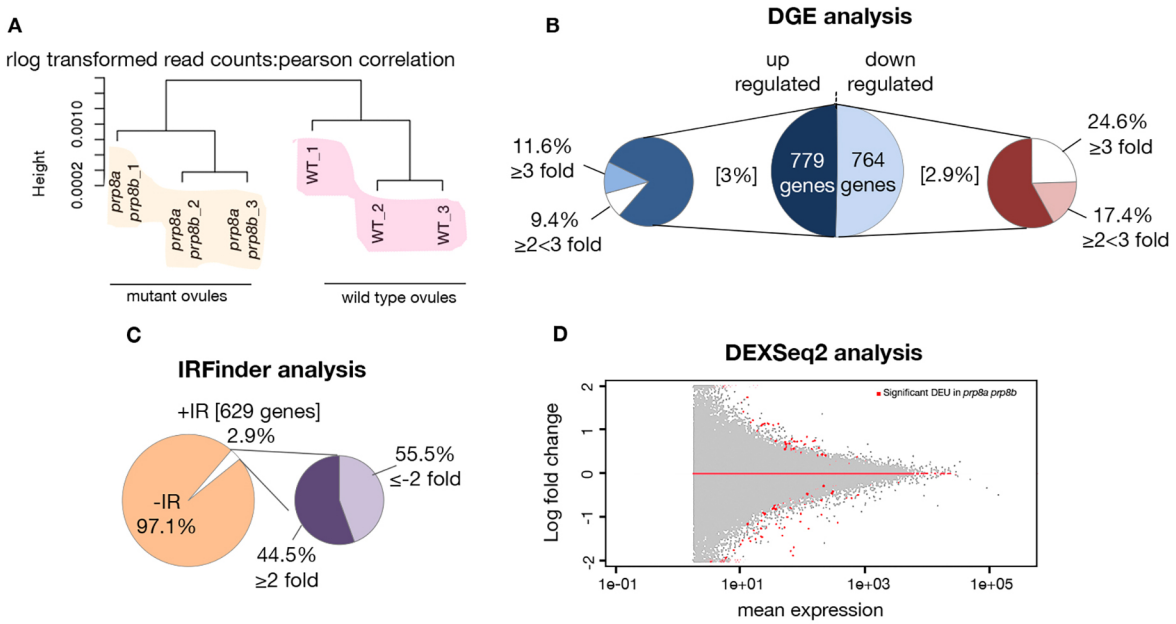

Fig. 6. *prp8a prp8b* molecular phenotype revealed by RNA-seq. (A) Clustering of the ovule transcriptome samples based on Pearson pairwise correlation. (B) DGE in *prp8a prp8b* mutant ovules analyzed using DESeq2 and independently complemented with edgeR analysis with $P<0.05$. (C) Frequency of IR in *prp8a prp8b* ovules assessed using IRFinder pipeline at FDR<5%. (D) MA plot of fold change of exon usage versus averaged normalized counts per exon. Red dots are exons with significant DEU at adjusted $P<0.1$.

Analysis of the RNA-seq data with the IRFinder platform identified 629 genes (2.9%) that showed >twofold significant IR in *prp8a prp8b* ovules compared with wild-type ovules (Fig. 6C). Of these, 55% showed reduced IR, whereas 45% showed increased IR events in *prp8a prp8b* ovules (Fig. 6B; Tables S5, S6). Analysis of DEU using DEXSeq R script (Anders et al., 2012) revealed 220 genes that showed significant DEU in *prp8a prp8b* ovules, indicating pre-mRNA mis-splicing in *prp8a prp8b* ovules (Fig. 6D, E; Tables S7-S9). Collectively, the RNA-seq data analyses suggest that PRP8A/PRP8B participates in the pre-mRNA splicing of only the subset of genes that are expressed in ovules.

PRP8A and PRP8B co-regulate expression of MYB98 and CRP genes

To investigate at the molecular level the likely cause of *prp8a prp8b* defects in pollen tube attraction, we analyzed the RNA-seq data for the expression of genes encoding CRPs, DEFLs, Rapid alkalinization factors (RALFs), MLO proteins and transcription factor MYB98, a family of genes that have been implicated to mediate pollen tube attraction and reception (Dresselhaus et al., 2016; Wang et al., 2017; Higashiyama and Yang, 2017; Leydon et al., 2017). In *prp8a prp8b* ovules, 55 genes belonging to the CRP family were mis-expressed, representing 11% of the total mis-expressed genes in *prp8a prp8b* ovules (Fig. 7A). Of these, 34 genes encode proteins belonging to the low molecular weight CRP subfamily and 21 encode the DEFL protein subfamily (Fig. 7A). Of the 34 mis-expressed low molecular weight CRPs, 8 genes (24%) were upregulated by up to fivefold and the remaining 26 genes (76%) were downregulated by up to sevenfold (Fig. 7A). Of the 21 DEFL subfamily genes, all were downregulated by up to sixfold in *prp8a prp8b* ovules ($P<0.05$, Fig. 7A). Of note, all of the LURE genes, *AtLURE1.1-1.5*, were downregulated in *prp8a prp8b* ovules (Fig. 7A). Similar analysis using edgeR (Robinson et al., 2010) consistently revealed downregulation of *LURE1.1* by 1.3 Log2 fold and *LURE1.2-1.5* by >2 Log2 fold ($P<0.05$) in *prp8a prp8b* ovules.

LURE gene expression is controlled by synergid cell-specific MYB98 transcription factor, which is itself under the regulation of central cell-specific CCG (Chen et al., 2007) and CBP1 (Li et al., 2015). Analysis of our RNA-seq data reliably detected downregulation of MYB98 and upregulation of CBP1 in *PRP8Aa;bb*-derived RNA-seq expression in all three replicates (Fig. 7C). To support this observation, we monitored the expression of MYB98pro-NLS::GFP and MYB98pro-PM::GFP decorating synergid cell nuclei and the plasma membrane, respectively, in *prp8a prp8b* ovules. In contrast to 90.2±5% (n=121/134) of positively expressing ovules in wild-type controls, live cell imaging revealed complete downregulation of MYB98pro-NLS:;GFP expression in the synergid cell nuclei of ∽46.9±4% (n=444/946) ovules from *PRP8Aa;bb* dissected pistils, representing the *prp8a prp8b* double mutant population (Fig. 7D). We obtained similar results using proMYB98pro-PM:;GFP. Mutants *myb98*, *ccg1* and *cbp1* all result in downregulation of CRPs including LURE gene expression (Okuda et al., 2009; Li et al., 2015). Furthermore, all members of the Egg Cell 1 family were also downregulated in *prp8a prp8b* ovules (Fig. 7C). These results suggest that downregulation of MYB98 is probably the reason why downregulation of LURE and other CRPs impacts pollen tube further circumventing *prp8a prp8b* ovules from any successful gamete fusion and fertilization.

The RALF gene family was recently shown to regulate pollen tube guidance and homeostasis (Mecchia et al., 2017; Ge et al., 2017). In *prp8a prp8b*, *RALF20* was more than fivefold upregulated, whereas *RALF21*, *RALF28* and *RALF29* were up to fivefold downregulated (Fig. 7A). Two *MLO* genes were also identified, *MLO6* was approximately fourfold upregulated and *MLO12* was twofold downregulated (Fig. 7A). However, the promoter activities of *MLO6* and *MLO12* were not active in ovules and were only detected in stigma and style, respectively (Davis et al., 2017).

We then tested whether *AtLURE1.1-1.6*, *FERONIA* (*FER*) and *LORELEI* (*LRE*) genes could be mis-spliced in *prp8a prp8b* ovules.

Development (2020) 147, dev186742. doi:10.1242/dev.186742

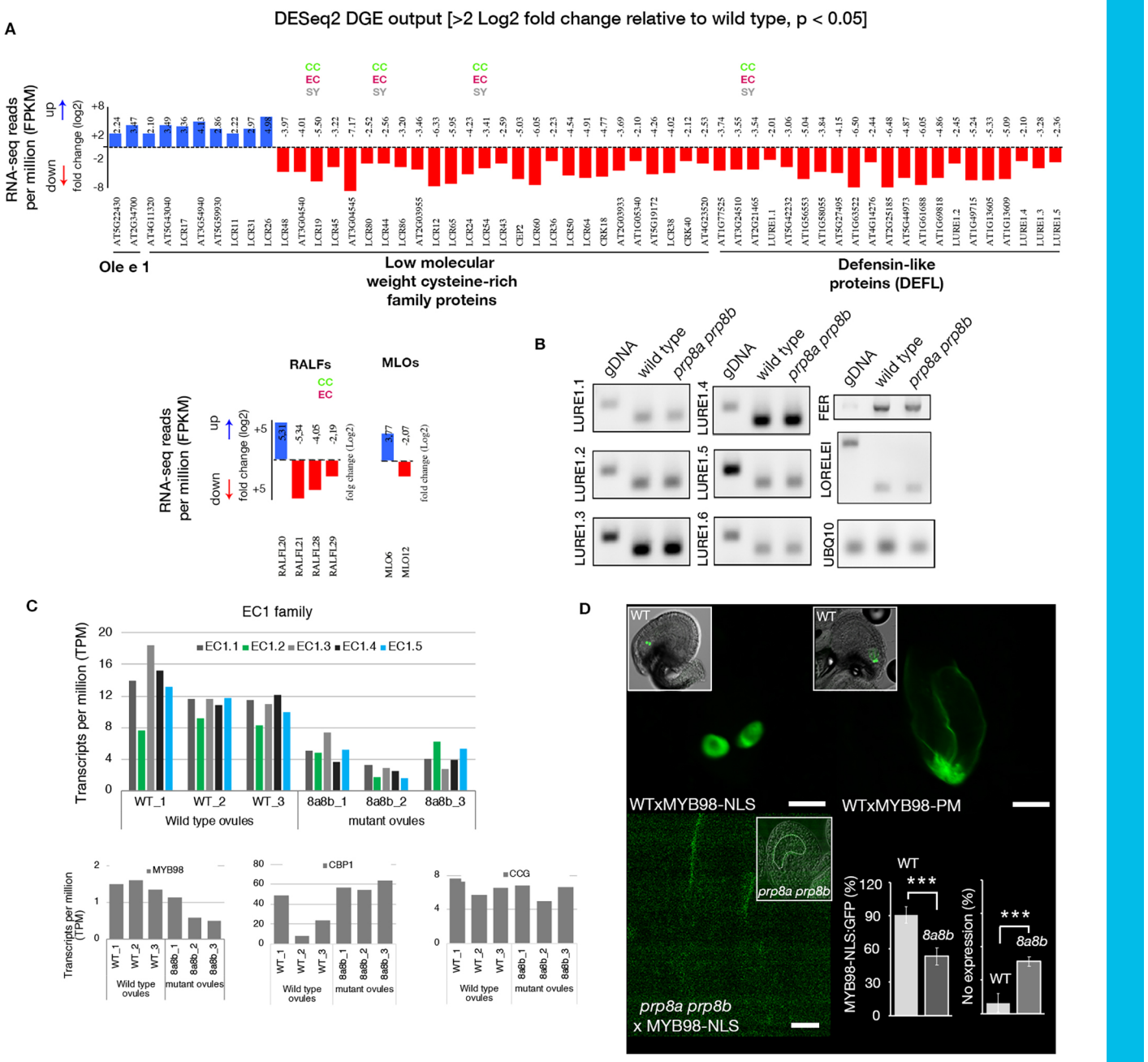

Fig. 7. MYB98, LUREs and several CRPs are downregulated in *prp8a prp8b* ovules. (A) DESeq2 differential gene expression RNA-seq analysis reveals several misregulated CRPs at Log2 >twofold, with FDR <5%. Note, however, only four of the CRP genes could be mapped to Wuest et al. (2010) embryo sac cell-specific transcriptome and are all expressed in all three cell types – central cell (CC), egg cell (EC) and synergid cells (SY). (B) Intron profiling by semi-qRT-PCR validated that PRP8A/PRP8B does not regulate splicing of *LURE* genes, *LORELEI* or *FER* in ovules. (C) Normalized ovule RNA-seq data reveals reduced expression of EC1 family members, MYB98 pollen tube attractant and overexpression of CBP1 in *prp8a prp8b* ovules. (D) Validation of *MYB98* mis-expression in *prp8a prp8b* ovules with MYB98pro-NL::GFP and MYB98pro-PM::GFP (plasma membrane). Insets show GFP-bright-field merged image. Graphs show frequency of ovules with GFP expression (left) and those with no detectable expression (right) in respective genotypes. Scale bars: 50 µm.

Intron profiling by semiRT-PCR and a test for the frequency of exon usage (DEU) and IR events revealed no significant alterations in pre-mRNA processing of LUREs, *FER* or *LRE* in *prp8a prp8b* ovules (Fig. 7B; Fig. S3).

It is also evident that protein secretion and the endomembrane system play pivotal roles in pollen tube guidance (von Besser et al., 2006; Li et al., 2011; Hafidh et al., 2016b). We therefore extended our RNA-seq analysis to include genes of the secretory pathways. Analysis of IR frequency revealed a plethora of secretory pathway genes to be aberrantly spliced in *prp8a prp8b* mutant ovules. Among them were genes involved in ER-Golgi transport (*GRIP*), Golgi-vacuole transport for sorting (*DRP2A* and *VSR-1*), Golgi-plasma membrane transport and exocytosis (*SFH3/SEC14* and *EXO70*) (Fig. S4). Additional secretory genes were identified as showing statistically significant DEU compared with wild-type controls, including *SFH3*, *Got1/SFT2*, DUF ER vesicle transporter (AT1G36050) and *AtRABC2b* (Fig. S4). In summary, our RNA-seq data revealed downregulation of upstream regulators of LURE gene expression and a plethora of other CRPs as well as aberrant splicing of key secretory pathway genes in *prp8a prp8b* ovules, which might

Development (2020) 147, dev186742. doi:10.1242/dev.186742

impair secretion of CRPs and therefore exacerbate the pollen tube attraction defects of *prp8a prp8b* ovules.

PRP8A/PRP8B splicing activity targets more central cell expressed genes

To investigate whether there is a cell-biased effect within the embryo sac following *prp8a prp8b* loss of function, we mapped all of the affected genes from IR, DGE and DEU to the female gametophyte RNA-seq transcriptome from Wuest et al. (2010). Of the 629 genes showing IR in *prp8a prp8b* ovules, 567 (90%) could be mapped to the female gametophyte transcriptome, of which 214 IR genes (34%) were classified as reliably expressed in all three replicates in at least one female gametophyte cell type – synergid cell, central cell or egg cell (Fig. 8A; Supplementary Dataset 2B). We observed that 79 genes (36.9%) with significant IR were central cell-specific, 38 genes (17.8%) were egg cell-specific and no genes with significant IR were identified to be synergid cell-specific (Fig. 8A; Supplementary Dataset 2B). This distribution implies that *prp8a prp8b* splicing defects impact central cell expressed genes twice as much as egg cell encoded genes. In comparison, of the 484 genes that showed significant DGE, 280 genes (58%) could be mapped to the female gametophyte transcriptome (Fig. 8A). Of these, 43 genes (8.9%) were reliably expressed in all three replicates in at least one female gametophyte cell type (Fig. 8A). Unlike IR events, DGE was less biased on cell type-specific deregulated expression (Fig. 8A). Similar results were also obtained with genes

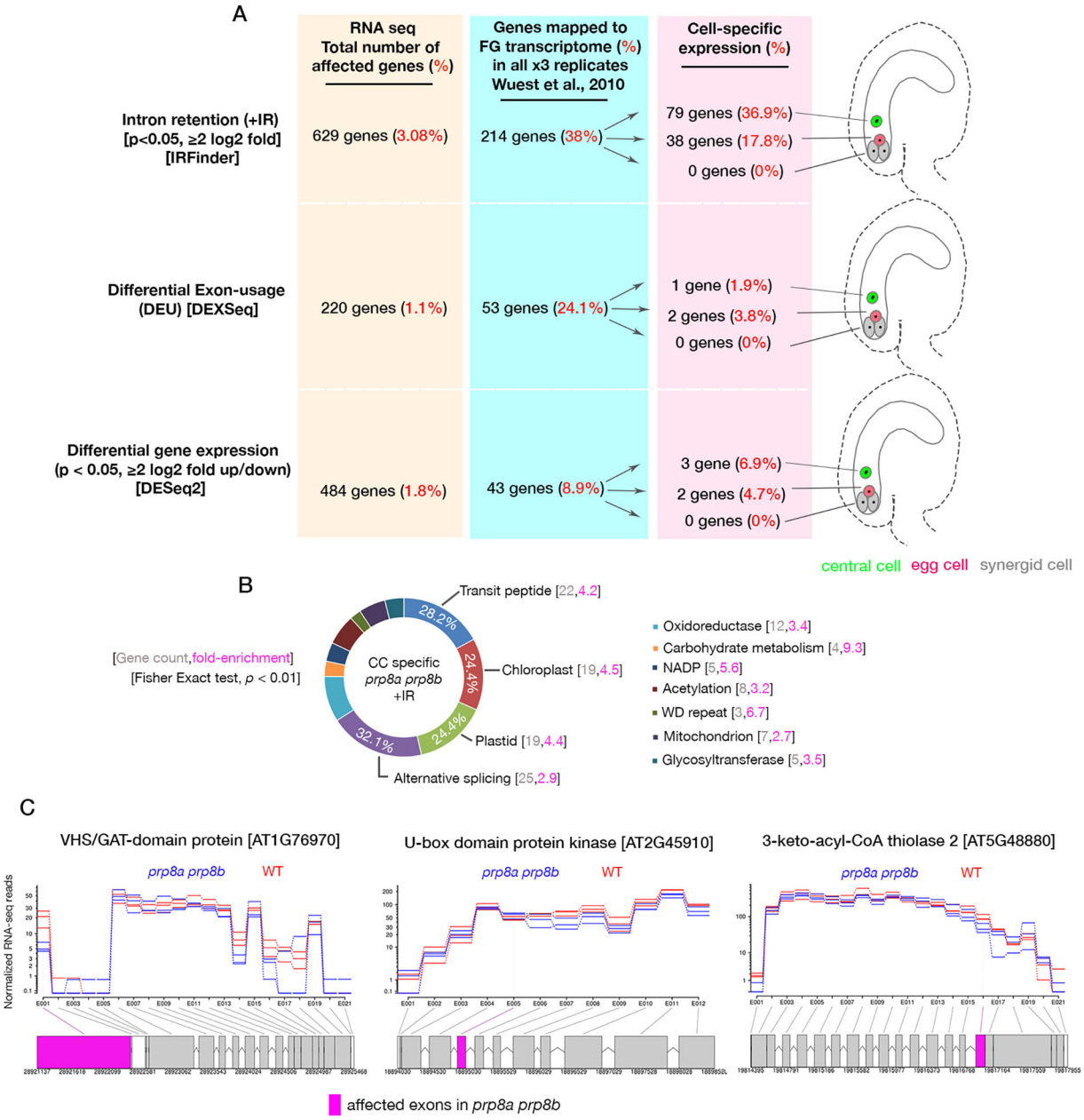

Fig. 8. *prp8a prp8b* intron retention effect impacts more central cell expressed genes. (A) Mapping of misregulated genes in *prp8a prp8b* ovules based on their cell type-specific expression according to Wuest et al. (2010) embryo sac cell-specific expression data. (B) Enriched keywords of the IR affected central cell genes, including the number of genes and fold enrichment for each category. (C) DEU of exemplified embryo sac-specific genes, highlighting affected exons in *prp8a prp8b* ovules.

Development (2020) 147, dev186742. doi:10.1242/dev.186742

showing DEU, in which 53 genes (24.1%) of the 220 genes that exhibited significant DEU were reliably expressed in the female gametophyte but showed no significant bias for cell type-specific effects (Fig. 8A). Keyword enrichment analysis (P<0.01) of central cell genes with significant IR highlighted genes involved in alternative splicing, transit peptide and chloroplast/plastid differentiation as among the predominantly affected genes (Fig. 8B). Of the genes showing DEU, the gene encoding VHS/GAT-domain protein was identified as central cell-specific, and genes encoding U-box domain protein kinase and 3-keto-acyl-coA thiolase were identified as egg cell-specific (Fig. 8B). These results imply that *prp8a prp8b* loss of function predominantly affects central cell expressed genes through IR as the most common molecular phenotype within the embryo sac.

Mutant *prp8a prp8b* ovules display differential exon usage of female gametophyte expressed genes and embryo sac developmental genes

To assess the possible molecular phenotype resulting in the *prp8a prp8b* embryo sac morphological defects, we searched the RNA-seq data with emphasis on mRNAs known to regulate embryo sac development (Pagnussat et al., 2005). Using DEXSeq analysis, genes of diverse subcellular roles were identified to show differential exon usage compared with their expression in wild-type ovules. Identified genes included those encoding plasma membrane signaling proteins (GPI-anchored protein), transcription factors and chromatin remodeling factors (DEIH-box helicase and COL13), metabolic enzymes (ATPHS2), splicing factors (PWI-domain splicing factor) and signaling kinases (CPK29) (Figs S5A and S6). More specifically, we identified 12 genes with a direct role in female gametophyte and embryo sac development to be differentially spliced, showing DEU, IR or changes in gene expression (Fig. S6). DEU-informed RNA-seq highlighted *EMBRYO SAC DEVELOPMENT ARREST 9* (*EDA9*, also known as *PGDH1*, AT4G34200), *EMBRYO SAC DEVELOPMENT ARREST 30* (*EDA30*, AT3G03810) and *MAP3K EPSILON PROTEIN KINASE 1* (*MAP3Kε1*, also known as *M3KE1*) to show statistically significant DEU in *prp8a prp8b* ovules (Fig. S5). EDA9 is a 3-phosphoglycerate dehydrogenase that is essential for embryo and pollen development, and *eda9* mutant ovules are arrested at the two-nuclei stage of embryo sac development (Pagnussat et al., 2005). EDA30 is a O-fucosyltransferase family protein that is essential for polar nuclei fusion (Pagnussat et al., 2005). MAP3Kε1 is expressed in developing ovules and the double mutant *map3kε1 map3kε2* displays plasma membrane irregularities in pollen grains, which result in pollen lethality (Chaiwongsar et al., 2012; Mithoe et al., 2016). Post fertilization, MAP3Kε1 is a downstream regulator of the YODA MAP kinase signaling pathway and is essential for the specification of suspensor cell fate at the 1-2 cell stage of zygote development (Bayer et al., 2009). IR and DGE analyses identified additional embryo sac developmental genes that showed either significant intron retention (±IR ≥twofold, P<0.05) or downregulation of their transcription in *prp8a prp8b* mutant ovules (≥twofold change, P<0.05) (Fig. S6).

PRP8A and PRP8B exhibit autonomous regulation of their pre-mRNA splicing and splicing of other spliceosome factors

Because PRP8A and PRP8B are subunits of the spliceosome machinery, we investigated whether the spliceosome complex is autonomously regulated by analyzing the RNA-seq data to compare the splicing patterns of *PRP8A* and *PRP8B* in *prp8a prp8b* ovules. DEU analysis revealed that exons 1-3 and 18-20 of *AtPRP8A* were differentially expressed in *prp8a prp8b* mutant ovules, suggesting defective splicing of PRP8A pre-mRNA (Fig. S5B), whereas *AtPRP8B* showed significant differential expression of exon 19 (Fig. S5B). DEXSeq also revealed differential expression of exon 10 of a PIWI domain-containing splicing factor (AT2G29210) (Fig. S5A). IRFinder further revealed mis-splicing of two genes encoding SER/ARG-rich protein splicing factor 34 (SRP34) and SRP34A in *prp8a prp8b* ovules, among other spliceosome subunits encoding genes (Fig. S5C). SRP34 regulates alternative splicing through binding in exonic enhancer and suppressor elements. Our results identified autoregulation of core subunits of the spliceosome machinery that probably culminate in the molecular phenotype of *prp8a prp8b* knockdown.

PRP8A co-immunoprecipitates with U2-associated SF3A1 splicing enhancer

In humans and yeast, the N terminus of PRP8 interacts with the core of the NineTeen Complex (Prp19/NTC) for activation of the spliceosome machinery, whereas the two domains at the C-terminal tail, the JAB1 (MPN) domain and the U6-RNaseH domain, interact with BRR2 U5-snRNP, U2-snRNPs such as the human homolog of SF3A1 (Tresini et al., 2015; Zhang et al., 2017), and human SLU7 step II factor for selection of the 3′-splice site junction (Zhang et al., 2017). Because the T-DNA insertions in both *prp8a*-12 and *prp8b*-1 interrupt the U6-RNaseH domain, resulting in female and male sterility, we tested whether the relationship between PRP8 and U2-snRNPs identified in human is also conserved in plants to get a hint on PRP8A/PRP8B mechanisms of action. We co-expressed pro*PRP8A-PRP8A*::GFP with *AtSF3A*1-mCherry (AT1G14650) in *Arabidopsis* roots. PRP8A-GFP colocalized with AtSF3A1-mCherry in a gradient-dependent manner within the nuclei of all cells at the root tip (Fig. 9A). Close observation of nuclear speckles confirmed that PRP8A and AtSF3A1 colocalized in some subdomains of the nuclei, but they also formed distinct subdomains within the nucleoplasm (Fig. 9A). Using these stable lines, we then performed *in vivo* co-immunoprecipitation (Co-IP) experiments using a nuclear-enriched proteome subfraction and a total cytosolic proteome from 7-day-old seedlings expressing pro*PRP8A-PRP8A::GFP* as a bait. Western dot blot analysis of PRP8A immunoprecipitated proteins revealed that the PRP8A-GFP complex strongly co-immunoprecipitated with AtSF3A1 in the nuclear-enriched and total fractions, suggesting that PRP8A associates with SF3A1 in *Arabidopsis* (Fig. 9B). We further observed similar affinity Co-IP of PRP8A with histone H3 variant (Fig. 9B). In humans, histone modifications, in particular H3K36me3 and H3K4me3, are strongly linked with alternative splicing through interaction of Histone adaptor (MRG15) and PTB-dependent exon inclusion (Luco et al., 2010, 2011), and recent reports have demonstrated association of several histone variants with splicing factors (Xu et al., 2018). A nuclear localized Translationally Controlled Tumor protein 1 (TCTP1), a non-spliceosome subunit from *Arabidopsis*, was used as a negative control to ensure Co-IP specificity (Fig. 9B). Our results revealed that AtPRP8A associates with U2-snRNP SF3A1 and histone H3 in *Arabidopsis*. We next investigated whether AtPRP8A associates with AtSF3A1 via direct interaction. We performed ratiometric biomolecular fluorescence complementation (rBiFC) (Grefen and Blatt, 2012) with AtPRP8A-nYFP and AtSF3A1-cYFP in *N. benthamiana* leaves. As a positive control, we included TCTP1-nYFP and CPN60-cYFP interaction. We observed no reconstitution of the YFP fluorophore when PRP8A-nYFP and SF3A1-cYFP were co-expressed (Fig. 9C). The lack of interaction indicates that in *Arabidopsis* PRP8A might be weakly or indirectly associated with SF3A1

Development (2020) 147, dev186742. doi:10.1242/dev.186742

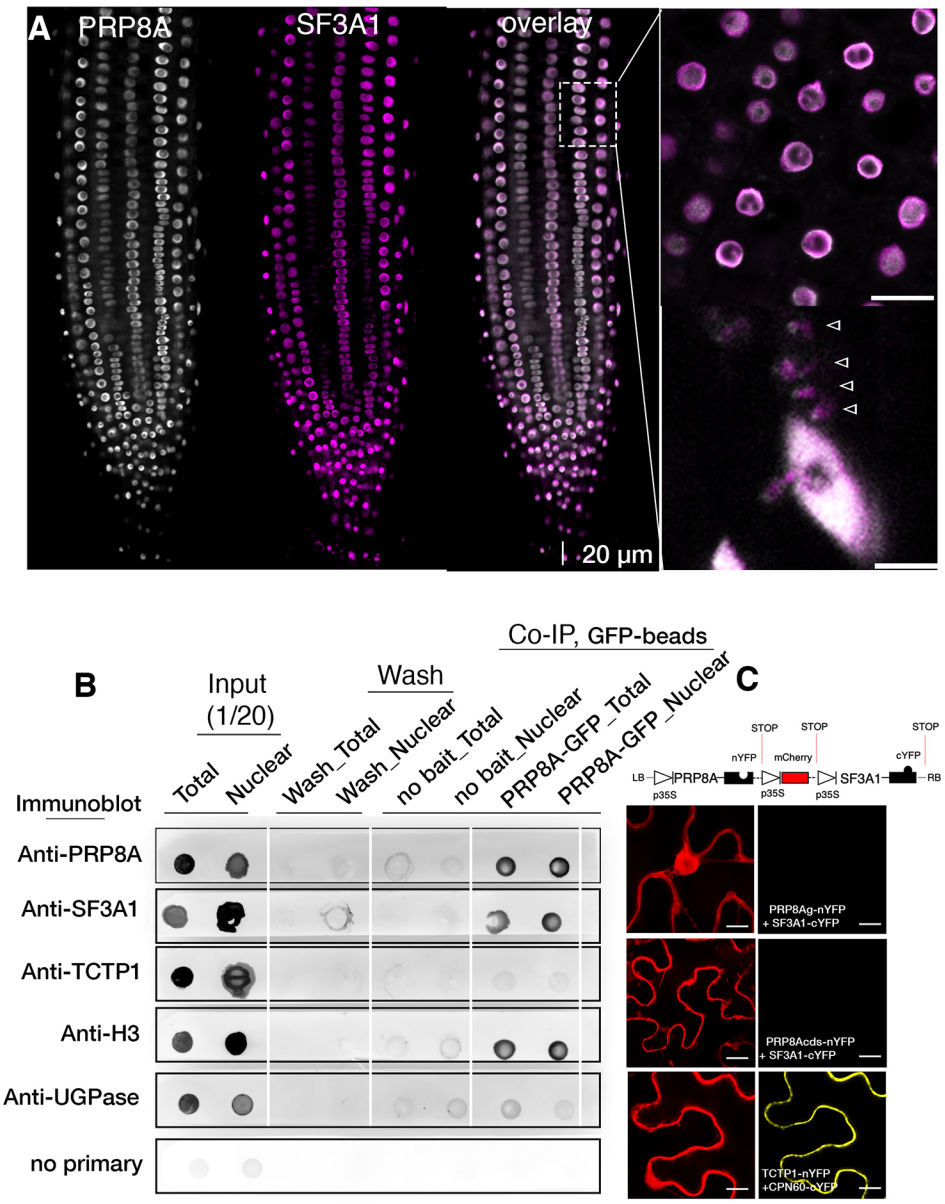

Fig. 9. PRP8A colocalizes and immunoprecipitates with SF3A1. (A) Colocalization of PRP8A-GFP with SF3A1-mCherry in 4-day-old *Arabidopsis* roots. Within the nuclear domain, PRP8A also localizes in unique subnuclear foci that do not colocalize with SF3A1 (indicated by triangles). Inset shows higher magnification of boxed area. (B) Western dot blot analysis of PRP8A-SF3A1 by *in vivo* Co-IP. SF3A1 was pulled down by PRP8A-GFP and detected by immunoblotting with anti-PRP8A, anti-SF3A1 and anti-Histone H3 antibodies. TCTP1 (AT3G16640) was used as a negative control. Histone H3 and UGPase antibodies served as nuclear and cytoplasmic markers, respectively. (C) Ratiometric BiFC assays reveals that PRP8A does not physically interact with SF3A1 in *N. benthamiana* leaves. PRP8A-nYFP, either as a full length genomic or full length cDNA, was co-expressed with SF3A1-cYFP in leaves of *N. benthamiana*. TCTP1-CPN60 interaction was used as a positive control for rBiFC. mCherry was used as a marker for monitoring successful expression. Scale bars: 40 µm (A); 5 µm (C).

DISCUSSION

The spliceosome complex required for pre-mRNA splicing functions uniquely in a tissue- and developmental-specific manner and some of its subunits have been genetically characterized as essential regulators of gamete development (Gross-Hardt et al., 2007; Moll et al., 2008; Staiger and Brown, 2013). In mice, alternative splicing of acrosomal matrix protein, preacrosin-binding protein (ACRBP), plays an essential role in the formation of secretory functional acrosome and competent sperm cells capable of fertilization (Kanemori et al., 2016). In *Drosophila*, a mutation in the NTC/Prp19 pre-spliceosome complex specifically impairs pre-mRNA splicing of early zygotic but not maternally encoded transcripts, suggesting spatiotemporal regulation of the spliceosome subcomplexes (Guilgur et al., 2014). In *Arabidopsis*, *lachesis* mutants (*lis*) with depleted U4/U6 splicing factor PRP4 are defective in lateral inhibition of accessory cell development, resulting in accessory cells with gametic cell fate identity (Gross-Hardt et al., 2007), whereas CLOTHO/GAMETOPHYTIC FACTOR 1 (CLO/GFA1), a U5 subunit of the spliceosome machinery and interactor of PRP8A (Liu et al., 2009), is specifically required for egg and central cell fate specification and tissue-specific expression of LIS (Moll et al., 2008). Similarly, *ATROPOS* (*ATO*, *SF3A60*) encodes a human homolog of SF3a60, a subunit of the SF3Aa-U2 complex. SF3Aa1 is a member of the SF3a-U2 complex and co-immunoprecipitates with PRP8A (Fig. 9). The *ato* (*sf3a60*) mutant is female gametophytic lethal and also shows severe reduction in male transmission with a maximum of 17.44% transmission efficiency (Moll et al., 2008). At ovule maturity, 20% of *ato* (*sf3a60)* embryo sac contained less than seven nuclei and the two female gametic-cell fate markers were deregulated (Moll et al., 2008). In this study, the *prp8a prp8b* double mutant embryo sac might have lost synergid and egg cell fates by not expressing MYB98, LURE1.2 and EC1 markers (Figs 5 and 7). Unlike *lis/gfa1* or *ato*, the *prp8a prp8b* double mutant does not show early gametophytic developmental defects. Even though GFA1 interacts with PRP8A (Liu et al., 2009) and both are components of the U4/U6.U5 tri-snRNP (Bartels et al., 2002; Staiger and Brown, 2013), the lack of direct phenocopy between

Development (2020) 147, dev186742. doi:10.1242/dev.186742

prp8a prp8b double mutant and the *gfa1*, *lis* or *ato* (*sf3a60*) mutants, exemplifies the complex regulation of the spliceosome individual subunits and non-universal role of the spliceosome machinery. The phenotype with closest resemblance to the *prp8a prp8b* double mutant phenotype is that of the *ato* (*sf3a60*) mutant, which might explain the close association of PRP8A with SF3aA1 (Fig. 9).

Moreover, PRP8A and PRP8B are fully redundant in their function in the gametophyte, as shown by the normal transmission of *prp8a* and *prp8b* single mutations and the finding that proPRP8A-PRP8A::3UTR and proPRP8B-PRP8B::GFP could fully complement *prp8a prp8b* fertilization defects (Fig. 2). However, this redundancy is restricted to the gametophyte, as *prp8a* alone is embryo lethal (Schwartz et al., 1994; Meinke et al., 2008). Our results suggest that PRP8A/PRP8B spliceosome subunits are selectively involved in splicing of subsets of pre-mRNAs with cell and developmental specific roles, and unlike other U4/U6.U5 tri-snRNP splicing subunits, PRP8A/PRP8B function might not be essential for early gametophyte development.

Intron mis-splicing predominates in central cell-expressed genes in *prp8a prp8b*

The post-transcriptional effect in *prp8a prp8b* ovules revealed a combined effect on intron splicing and DEU of approximately 4.18% (849 genes) compared with 1.8% (484 genes) on DGE at ≥twofold (Fig. 8). This observation suggests that PRP8A/PRP8B directly participates in intron splicing of ovule-expressed genes and that *prp8a prp8b* knockdown probably has an indirect effect on altered gene expression. In support, we have shown that PRP8A co-immunoprecipitates with a human homolog of SF3A1 as well as with histone H3 variant (Fig. 9). How histones influence splicing was not known until recently. In humans, histone modifications such as H3K4me3, H3K9me3, H3K36me3 and H3acetyl all positively influence recruitment of histone adaptor proteins MRG15, GCN5, CHD1 and HP1α that facilitate recruitment of splicing factors Polyuridine (polypyrimidine tract binding protein) binding proteins (PTB), U2 snRNP and hnRNPs to influence exon inclusion and alternative splicing (Luco et al., 2011). This was exemplified through splicing of two PTB-dependent mutually exclusive exons of human fibroblast growth factor receptor 2 (FGFR2) where two histone modifications, H3K36me3 and H3K4me1, act antagonistically to influence exon inclusion or exclusion, respectively. Moreover, crosslinking and immunoprecipitation experiments have demonstrated direct interaction of histone variants H1, H2A, H2B, H3 and H4 with splicing factors Rbfox2, Rbfox3 and proline- and glutamine-rich protein (SFPQ) (Kim et al., 2018). In plants, the direct link between alternative splicing and either chromatin structure or RNA Pol II elongation rates has yet to be demonstrated; however, recent studies in *Arabidopsis* have shown a positive correlation (Cui et al., 2017).

The observed biased effect on intron splicing over gene expression in the *prp8a prp8b* embryo sac extended to a cell type-specific origin in the female gametophyte. Assessment of the IR events of only genes expressed in all three replicates of the female gametophyte (214 genes of the 397 IR genes; Fig. 8) revealed that genes confined in the central cell are twice as affected on their intron splicing (79/214 genes, 36.9%) compared with those encoded by the egg cell (17.8%) (Fig. 8; Supplementary Dataset 2B). No affected genes were specific to the synergid cell; however, several genes expressed in the synergid cells were also mis-spliced (Fig. 8; Supplementary Dataset 2B). The central cell has a direct role in pollen tube attraction. Mutations in central cell-specific genes *ccg* (Chen et al., 2007), *cbp1* (Li et al., 2015), *maa3* (Shimizu et al., 2008) or *gex3* (Alandete-Saez et al., 2008) completely abolished pollen tube attraction. CCG (Chen et al., 2007) and CBP1 (Li et al., 2015) are thought to mediate pollen tube attraction by regulating transcription of synergid cell-specific MYB98 transcription factor, an upstream regulator of *LURE1* transcription (Okuda et al., 2009; Li et al., 2015). We propose that aberrant splicing of central cell-encoded genes, together with those affected in the synergid cells, might kick-start the molecular cascade leading to loss of *prp8a prp8b* ovule competence in pollen tube attraction. Although mis-splicing is the major event observed in *prp8a prp8b*, particularly in the central cell, it is difficult to draw a conclusion about whether this is the major factor (over changes in gene expression) leading to pollen tube attraction defects and lack in fertilization of *prp8a prp8b* ovules.

Downregulation of MYB98 and CRPs could be the hallmark cause of pollen tube attraction defects in *prp8a prp8b*

Although there was a prevalent effect on pre-mRNA splicing in *prp8a prp8b* double mutant ovules, transcripts encoding CRPs stood out the most, representing 20% (55/284 genes) of the total downregulated genes by ≥twofold (Fig. 7). Upstream of CRPs, our RNA-seq data supported by the MYB98pro-NLS::GFP reporter constructs revealed downregulation of MYB98 and upregulation of CBP1, both of which are essential transcriptional regulators of LURE CRPs and pollen tube attraction (Fig. 7) (Kasahara et al., 2005; Okuda et al., 2009; Li et al., 2015). CRPs are the major family of proteins that have been implicated to function directly in pollen tube attraction (Higashiyama and Yang, 2017). Among the downregulated CRPs, are all six members of the LURE subfamily expressed in the synergid cell (Fig. 7). Also, of significant note, three out of four of the central cell-specific CRPs that are also downregulated in *ccg* and *cbp1* pollen tube attraction mutants, DOWN-REGULATED IN *dif*22 (*DD22*, *LCR80*, At5g38330), *DD36* (At3g24510) and AT3G04540, were also downregulated by >2.5-fold in *prp8a prp8b* ovules (Fig. 7). In line with the misregulation of CRPs in *pr8a prp8b* ovules, we detected ectopic promoter activities of a pollen-specific CRP Ole e 1 subfamily gene LAT52, LAT52pro-GUS, initially in *prp8a prp8b* ovules and later confirmed in *prp8a* single mutant ovules (Fig. S2). LAT52 is secreted by pollen tubes and functions as a ligand perceived by pollen-specific receptor-like kinases (RLKs), PRK2 and PRK4, to regulate pollen tube growth by endocrine signaling (Tang et al., 2002; Muschietti et al., 1994; Hafidh et al., 2016a,b). The −572 bp LAT52 promoter fragment confers transcriptional regulatory elements that provide pollen (vegetative cell) specificity and enhanced transcriptional activity specifically in pollen (Twell et al., 1990, 1991). The ectopic activation of LAT52 expression in ovules culminates in the effect of the *prp8a prp8b* molecular phenotype on CRPs misregulation. It will be informative to further investigate which other male-specific expressed genes are ectopically activated in *prp8a prp8b* ovules. This will be key in defining the sexual identity and cell-fate specification of *prp8a prp8b* ovules. We propose that the downregulation of MYB98 and many CRPs is most likely the hallmark cause of the pollen tube attraction defects observed in *prp8a prp8b* ovules.

Conclusions

This work has uncovered a molecular signature through which PRP8A/PRP8B subunits act redundantly to define male-female signaling competence for successful pollen tube attraction in *Arabidopsis*. PRP8A/PRP8B facilitates pollen tube attraction by

Development (2020) 147, dev186742. doi:10.1242/dev.186742

controlling transcription of LURE pollen tube attractants and several other CRP genes via MYB98 transcriptional regulation as well as through splicing of predominantly central cell-expressed genes (Fig. S7). These defects in *prp8a prp8b* double mutants might be coupled with loss in female gametic cell fate specification at ovule maturity and thus could contribute to overall ovule incompetence for pollen tube attraction. It will be important to uncouple these two events and establish how PRP8A/PRP8B controls pollen tube pathfinding competence to achieve successful fertilization. Collectively, the results hint at a spliceosome autoregulation mechanism and provide a potential pathway to isolate upstream regulators for pollen tube attraction.

MATERIALS AND METHODS

Plant material and growth conditions

Arabidopsis thaliana plants were grown at 22°C and 60% humidity in Conviron PGC Flex growth chambers under 16 h light/8 h dark conditions. Seeds of Col-0 wild-type (WT), PRP8A (At1g80070) and PRP8B (At4g38780) plants were obtained from The European Arabidopsis Stock Centre. T-DNA insertion lines SAIL_274_D02 T-DNA (*prp8a*-12), SALK_085295C and SALK_085295 (*prp8b*-3), SALK_044221C and SALK_044221 (*prp8b*-1) and SAIL_100_G10 (*prp8b*-2) were used in this study. T-DNA insertion lines were genotyped using SALK LBb1.3 and SAIL LB2 oligonucleotides in combination with gene-specific oligonucleotides (Table S1). The exact positions of the T-DNA insertions were established by sequencing and are marked in Fig. 2A.

RNA-seq library construction and sequencing

Ovules were isolated by dissecting flowers from stage 13-14 (FG7) containing a fully developed embryo sac (Christensen et al., 1997) from *PRP8Aa;bb* double mutant plants and wild-type control plants. RNA extracted from three biological replicates of each was used for Next Generation (NGS) RNA Sequencing. Total RNA was isolated from dissected ovules using Qiagen Plant RNA extraction kit (Qiagen). Total RNA was treated with DNase (Ambion) and RNA integrity (RIN) analyzed using a bioanalyzer. RNA (800 ng) with RIN >7 was processed using TrueSeq stranded total RNA library with RiboZero plant prep kit (Illumina, San Diego, CA, USA) as per the manufacturer's protocol. Samples were run on HiSeq4000 2×100 bp paired-end run Illumina sequencing machine (Illumina, San Diego, CA, USA) by Macrogen (Geumcheon-gu, Seoul, South Korea).

mRNA-seq data analysis

The raw sequenced data were subjected to quality control and trimming using FastQC and Timmomatic (Bolger et al., 2014). Resulting reads were mapped to the TAIR 10 genome with STAR aligner, version 2.6 (Dobin et al., 2013) using default parameters. The Feature Count program from the subread package, version 1.6.2 (Liao et al., 2014) was used to generate the count matrix by following steps described in the documentation.

R programs DESeq2, version 1.22.1 (Love et al., 2014) was utilized to determine DGE and DEXSeq, version 1.28.0 (Anders et al., 2012) was used to determine DEU between wild-type and *prp8a prp8b* mutant plants. The count matrix was used as inputs in DESeq2. False discovery rates (FDR) were calculated for gene-specific *P*-values of <0.05 using the Benjamini–Hochberg method (Benjamini and Hochberg, 1990). Gene expression levels were then quantified using rlog normalized counts.

Counts, as input for DEXSeq, were prepared with included Python scripts. The generalized linear model (GLM) was used to detect DEU with FDR adjusted to the overall gene expression level with $P<0.1$. IRFinder (Middleton et al., 2017) with default parameters was applied to determine differentially retained introns between the wild-type and *prp8a prp8b* double mutant. Introns were considered differentially retained if the Benjamini–Hochberg adjusted *P*-value was <0.05 while the IR ratio was ≥2. All biostatistic analyses were implemented and performed using in-house scripts written in Unix shell and R. For graphical display, all genes identified to show statistically significant exon usage in *prp8a prp8b* ovules are presented in HTML interactive format (Table S7). The data discussed in this article have been deposited in GEO under accession number GSE151462.

In vivo co-immunoprecipitation with nuclei fraction

The full length coding sequences (CDSs) of PRP8A together with its native promoter (997 bp) were amplified and cloned into pB7FWG,0 to create proPRP8A-PRP8A::eGFP constructs. A 35S-AtSF3A1::mCherry construct was a donation from the Andreas Nebenfuhr laboratory (University of Tennessee). For detailed cloning information, see the next section. Stable *Arabidopsis* transformants were generated expressing both constructs. Total proteins from approximately 2 g of 4-day-old seedlings expressing proPRP8A-PRP8A::eGFP and 35Spro-AtSF3A1::mCherry constructs were isolated according to Deng et al. (2016) using Honda lysis buffer (25 mM Tris·HCl pH 7.4, 2.5% Ficoll 400, 5% dextran T40, 0.4 M sucrose, 10 mM $MgCl_2$, 5 mM DTT, and 1× complete protease inhibitor cocktail). The homogenate was filtered through 50 µm nylon mesh to clear larger fragments and Triton X-100 was added to a final concentration of 0.5%. For nuclei enrichment, the flow through was centrifuged at 1500×***g*** for 5 min at 4°C. The pellet was gently resuspended twice with nuclei resuspension buffer (10 mM Tris HCl pH 8.0, 0.25 M sucrose, 10 mM $MgCl_2$, 5 mM β-mercaptoethanol, 1% Triton X-100, 0.1 mM PMSF, protease inhibitors) and centrifuged at 1500×***g*** for 5 min at 4°C. Nuclei were then resuspended in ice-cold nuclei lysis buffer [200 mM $(NH_4)_2SO_4$, 20% glycogen, 25 mM HEPES pH 7.9, 5 mM DTT, 1 mM PMSF, protease inhibitors] and gently mixed for 2 h at 4°C to release the nuclear proteins. The nuclear fraction was centrifuged at 17,950×***g*** for 10 min to remove remaining debris. Total and nuclear-enriched proteomes were used immediately for Co-IP. GFP-Trap-A agarose (Chromotek) was used in subsequent Co-IP assays. The immunoprecipitates were detected by anti-PRP8A (1:1000; Abcam 79237), anti-SF3A1 (1:1000; Abcam 128898), anti-TCTP (1:500; Abcam 37506), anti-H3 (1:1000; Abcam 1791) and anti-UGPase (1:1500; Agrisera AS05086) antibodies. To monitor primary antibodies specificity, strips with omitted primary antibodies were used as negative controls. Appropriate alkaline phosphatase-conjugated anti-rabbit and anti-mouse secondary antibodies were used for detection using nitro-blue tetrazolium chloride (NBT) and 5-bromo-4-chloro-3′-indolyphosphate p-toluidine salt (BCIP) chemiluminescence detection.

Bimolecular fluorescence complementation analysis

To create ratiometric PRP8Agenomic-nYFP and AtSF3A1-cYFP constructs, a genomic fragment of PRP8A coding sequence and CDSs of SF3A1 from the cDNA of rosette leaves were cloned into the 35Spro:pBiFCt-2in1-CC vector to generate the PRP8Agenomic-nYFP SF3A1cds-cYFP co-expression construct (Grefen and Blatt., 2012). Similarly, CDSs of PRP8A were amplified from leaf cDNA and, together with SF3A1, were cloned into 35S:pBiFCt-2in1-CC vector to generate the PRP8Acds-nYFP SF3A1cds-cYFP co-expression construct. All cloning was performed using multisite gateway technology (Invitrogen). The specific oligonucleotides used are described in Table S1. These constructs were subsequently introduced into *Agrobacterium* strain GV3101 and used for infiltration into leaves of *N. benthamiana*. After transformation, plants were grown in light condition for 48 h before observation. The YFP fluorescence was observed using a Zeiss LSM880 microscope.

Constructs and plant transformation

All PCRs to amplify cloned fragments were performed using high-fidelity Phusion polymerase (New England Biolabs) according to the manufacturer's instructions. Oligonucleotide sequences are listed in Table S2. For the full-length PRP8A-GFP under native promoter, a fragment of 14,523 bp, including 997 bp of promoter and 5′UTR, was amplified with/without stop codon, cloned into the pENTR/D-TOPO vector and recombined into the destination vector pK7FWG,0 (Karimi et al., 2002) bearing the eGFP marker to generate the proPRP8A-PRP8A::eGFP construct. To generate proPRP8A-PRP8A-3′UTR, extended 3′-end oligonucleotides were used to incorporate the 498 bp 3′UTR and the entry clone was used in LR reaction with pH7FWG,0 backbone to generate the proPRP8A-PRP8A-3′UTR expression construct. Full-length proPRP8B-PRP8B::GFP was amplified and cloned using a similar approach. All constructs were transformed into *Arabidopsis* via floral dipping (Clough and Bent, 1998).

Development (2020) 147, dev186742. doi:10.1242/dev.186742

Transmission analysis

PRP8Aa heterozygous plants were back-crossed into Col-0 wild-type background for determining female transmission and crossed into male sterile *ms1*-/- (Yang et al., 2007) to study male transmission. To generate the *PRP8Aa;bb* double mutant plants, flowers of *PRP8Aa* were emasculated and pollinated with homozygous *prp8bb* pollen grains; inversely, *prp8bb* flowers were emasculated and pollinated with *PRP8Aa* pollen grains. For transmission analysis of the double mutant, *PRP8Aa;bb* flowers were emasculated and pollinated with Col-0 wild-type pollen grains and used to calculate female transmission efficiency. In addition, pollen grains from the *PRP8Aa;bb* double mutant plants were used to pollinate male sterile *ms1*-/- pistils and the resulting progeny used to calculate male transmission efficiency. Progeny of these crosses were genotyped by PCR for the presence of T-DNA insertion and the transmission efficiency calculated.

Imaging of embryo sacs

Stage 12a (FG1) and stage 13-14 (FG7) flowers (Christensten et al., 1997) were dissected on double-sided tape. The placentas bearing the developing ovule primordia were excised and placed immediately in chloral hydrate clearing solution. After 2 days, the fixative was removed and the placental strands mounted onto microscope slides in a 30% glycerol solution. During mounting, the two placental strands were separated and excess tissue was removed. Ovule primordia were observed under Zeiss AxioImager Apotome 2. Images were collected with a 40×/1.2 W C-Apochromat objective.

Live cell imaging of *prp8ab* ovules

Pistils from *PRP8Aa;bb* were emasculated and left to mature for 2 days. Emasculated pistils as well as control *ms1* pistils were pollinated with pollen expressing the LAT52pro::GFP;HTR10pro::RFP marker line. After 24 h, pollinated pistils were placed on double sided tape and the placentas bearing developing ovule primordia were excised with a 25 G needle and placed immediately on a microscope slide on a drop of 30% glycerol. Fertilization events were captured using a Zeiss LSM 880 confocal laser scanning microscope with C-Apochromat 40×/1.2 WI, excitation 514 nm, emission recorded 566-719 nm for the red channel and excitation 490 nm and emission recorded 509-520 nm for the green channel. Representative single slice confocal sections were used for presentation. Image processing was done using a Fiji application.

Analysis of ovule attractivity by aniline blue staining

Pistils were harvested at 18 HAP and subjected to aniline blue staining as described below. Samples were analyzed by Zeiss Axioimager Apotome2 and images captured with ZEN software.

Pollen viability stain and aniline blue staining

For aniline blue staining, pistils of self-pollinated wild-type and *PRP8Aa;bb* plants or cross-pollinated *ms1* plants with wild-type or *PRP8Aa;bb* pollen were stained for callose according to the protocol of Mori et al. (2006).

Confocal and DIC microscopy

For mutant embryo phenotypic screening, seeds were cleared in a solution of chloral hydrate. Overnight clearing was sufficient for all developmental stages. Samples were observed under the DIC optics on a Nikon TE-2000 microscope. Images were processed in the NIS Elements software (LIM). Confocal images were taken on a Nikon Eclipse Ti confocal microscope equipped with CSU-X1 spinning disk module and Andor iXon3 EMCCD camera, as well as with a Zeiss LSM880 confocal microscope, and captured with ZEN 2.3v software. Images were analyzed and assembled with ImageJ/Fiji (http://imagej.net/http://fiji.sc/Fiji), Adobe Photoshop CS6 (www.adobe.com), Ink-scape (www.inkscape.org) and NIS Elements (LIM) software.

Blue dot assay

Young buds of wild-type and *PRP8Aa;bb* plants before anther dehiscence were emasculated and let mature for 48 h until the stigma papillae fully developed. Pistils were then pollinated with pollen expressing the LAT52pro-GUS construct, pollen grains derived from *PRP8Aa;bb* plants or control wild-type pollen grains. Pistils were collected at 18-20 HAP. Fertilized pistils were dissected under the binocular dissection microscope (Leica) and strings of ovules attached to septum were transferred to GUS staining solution (0.2 M Na_2HPO_4, 0.2 M NaH_2PO_4, 10 mM EDTA, 0.1% Triton X-100, 1 mM $K_3Fe(CN)_6$, 2 mM X-Gluc). Samples were stained for between 2-48 h. Stained tissues were cleared of chlorophyll by bleaching in ethanol series of 90%, 70%, 50% and 0% (v/v) prior to imaging. Stained pistils were observed under the Nikon TE-2000 microscope equipped with DIC optics for the presence of a blue dot or with Zeiss binoculars containing a CCD camera for overall pollen tube growth through the pistil.

Pollen tube cultivation

In vitro pollen tube growth was performed according to the protocol of Boavida and McCormick (2007). Pollen tube length was measured after 8 h of *in vitro* growth using the NIS Elements software. For semi-*in vivo* pollen tube growth assay, sterile *ms1* pistils were pollinated with wild-type or *PRP8Aa;bb* pollen and pistils were collected at 1-2 HAP. Pistils were excised at the stigma shoulder with a needle and transferred to the growth medium (Palanivelu et al., 2006) on a small Petri dish. Pistils were tilted to enable the pollen tubes to emerge onto the solid medium surface and cultivated in a humidified growth chamber at 22°C for 24 h. Pollen tube length was measured using the NIS Elements software from the point where they emerged from the cut pistil.

Statistics

All statistical analysis was performed using Welch's analysis of unequal variances, Chi square test and Student's *t*-test where appropriate.

RNA extraction and qRT-PCR analysis

Tissue samples were collected and frozen in liquid nitrogen. RNA was extracted using RNeasy Plant Mini Kit (Qiagen) and treated with RQ1 RNAse-free DNase I (Promega). First strand cDNA synthesis was conducted using recombinant M-MLV reverse transcriptase (Promega). qRT-PCR measurements were obtained using LightCycler 480 Instrument (Roche). Relative expression quantification was obtained using the ΔΔCT method following the manufacturer's instructions. Oligonucleotides were designed to distinguish between *Arabidopsis PRP8A* and *PRP8B* genes. Specificity of the oligonucleotides was verified by sequencing of purified PCR products. All measurements were conducted in three biological and two technical replicates.

Sequences, alignment and phylogenetic analysis

Protein sequences of AtPRP8A and its homologs were downloaded from Phytozome v12.1 (www.phytozome.jgi.doe.gov) and NCBI (https://www.ncbi.nlm.nih.gov) databases. Multiple sequence alignment was carried out using T-Coffee algorithm (Notredame et al., 2000) or Clustal Omega and processed in Jalview alignment editor (Waterhouse et al., 2009). The phylogenetic tree shown in Fig. 1A was constructed using PhyML software (Guindon et al., 2010). Numbers at the nodes of the phylogenetic tree correspond to approximate likelihood ratio test with SH-like (Shimodaira–Hagesawa-like) support from maximum likelihood method. The phylogenetic tree was visualized and processed in Mega 6 software (Tamura et al., 2013). If multiple copies of PRP8 were present in one organism, they were labeled as 'a' or 'b' variants. Variants 'a' were sequentially more similar to AtPRP8A. This labeling does not reflect the phylogenetic relationship between homologs from different organisms.

Acknowledgements

We thank Daisuke Kurihara (Nagoya University), Gerd Jürgens (Max Planck Institute for Developmental Biology, Tübingen), Stefanie Sprunck (University of Regensburg), Mark Johnson (Brown University) and Rita Gross-Hardt (University of Bremen) for cell fate markers. We thank Christos Michaelidis and Kamil Růžička, (IEB ASCR, Prague), Ivan Kulich (University of Regensburg) and Roman Pleskot (Ghent University) for valuable discussion, and Zuzana Gadiou and Jana Fecikova for technical assistance. We acknowledge the Imaging Facility of the Institute of Experimental Botany CAS, which is supported by the MEYS CR (LM2018129

Czech-BioImaging and OPPK CZ.2.16/3.1.00/21519 projects), for providing microscope facilities; the SALK Institute for providing the sequence-indexed *Arabidopsis* T-DNA insertion lines and the Nottingham Arabidopsis Stock Centre for providing the lines.

Competing interests
The authors declare no competing or financial interests.

Author contributions
Conceptualization: S.S.H., D.H.; Methodology: S.S.H., K.K., V.K., L.S., B.K., L.T., M.J.; Software: S.S.H., B.K., M.J.; Validation: S.S.H., K.K.; Formal analysis: S.S.H., K.K., V.K., M.J.; Investigation: S.S.H., K.K., V.K.; Resources: S.S.H., L.S.; Data curation: S.S.H., K.K., V.K., B.K.; Writing - original draft: S.S.H.; Writing - review & editing: S.S.H., L.T., D.H.; Visualization: S.S.H., K.K., L.S., L.T.; Supervision: S.S.H.; Project administration: S.S.H.; Funding acquisition: S.S.H.

Funding
This work was financed by the Grantová agentura České republiky (17-23203S, 18-02448S and 19-01723S) and by the Ministerstvo školství, mládeže a tělovýchovy České republiky (LTAUSA18115). The work was also supported by a European Regional Development Fund project 'Centre for Experimental Plant Biology' (CZ.02.1.01/0.0/0.0/16_019/0000738). We also acknowledge Prague Structural Funds (CZ.2.16/3.1.00/21519).

Data availability
RNA-seq data have been deposited in GEO under accession number GSE151462.

Supplementary information
Supplementary information available online at
http://dev.biologists.org/lookup/doi/10.1242/dev.186742.supplemental

References
Alandete-Saez, M., Ron, M. and McCormick, S. (2008). GEX3, expressed in the male gametophyte and in the egg cell of Arabidopsis thaliana is essential for micropylar pollen tube guidance and plays a role during early embryogenesis. *Mol. Plant* **1**, 586-598. doi:10.1093/mp/ssn015

Anders, S., Reyes, A. and Huber, W. (2012). Detecting differential usage of exons from RNA-seq data. *Genome Res.* **22**, 2008-2017. doi:10.1101/gr.133744.111

Bartels, C., Klatt, C., Lührmann, R. and Fabrizio, P. (2002). The ribosomal translocase homologue Snu114p is involved in unwinding U4/U6 RNA during activation of the spliceosome. *EMBO Rep.* **3**, 875-880. doi:10.1093/embo-reports/kvf172

Bayer, M., Nawy, T., Giglione, C., Galli, M., Meinnel, T. and Lukowitz, W. (2009). Paternal control of embryonic patterning in Arabidopsis thaliana. *Science* **323**, 1485-1488. doi:10.1126/science.1167784

Beale, K. M., Leydon, A. R. and Johnson, M. A. (2012). Gamete fusion is required to block multiple pollen tubes from entering an Arabidopsis ovule. *Curr. Biol.* **22**, 1090-1094. doi:10.1016/j.cub.2012.04.041

Belmonte, M. F., Kirkbride, R. C., Stone, S. L., Pelletier, J. M., Bui, A. Q., Yeung, E. C., Hashimoto, M., Fei, J., Harada, C. M., Munoz, M. D. et al. (2013). Comprehensive developmental profiles of gene activity in regions and subregions of the Arabidopsis seed. *Proc. Natl. Acad. Sci. USA* **110**, E435-E444. doi:10.1073/pnas.1222061110

Benjamini, Y. and Hochberg, Y. (1990). Controlling the false discovery rate: a practical and powerful approach to multiple testing. *J. R. Stat. Soc.* **57**, 289-300. doi:10.1111/j.2517-6161.1995.tb02031.x

Berget, S. M., Moore, C. and Sharp, P. A. (1977). Spliced segments at the 5′ terminus of adenovirus 2 late mRNA. *Proc. Natl. Acad. Sci. USA* **74**, 3171-3175. doi:10.1073/pnas.74.8.3171

Boavida, L. C. and McCormick, S. (2007). TECHNICAL ADVANCE: temperature as a determinant factor for increased and reproducible in vitro pollen germination in Arabidopsis thaliana. *Plant J.* **52**, 570-582. doi:10.1111/j.1365-313X.2007.03248.x

Bolger, A. M., Lohse, M. and Usadel, B. (2014). Trimmomatic: a flexible trimmer for Illumina sequence data. *Bioinformatics* **30**, 2114-2120. doi:10.1093/bioinformatics/btu170

Borges, F., Gomes, G., Gardner, R., Moreno, N., McCormick, S., Feijó, J. A. and Becker, J. D. (2008). Comparative transcriptomics of Arabidopsis sperm cells. *Plant Physiol.* **148**, 1168-1181. doi:10.1104/pp.108.125229

Chaiwongsar, S., Strohm, A. K., Su, S.-H. and Krysan, P. J. (2012). Genetic analysis of the Arabidopsis protein kinases MAP3Kε1 and MAP3Kε2 indicates roles in cell expansion and embryo development. *Front. Plant Sci.* **3**, 228. doi:10.3389/fpls.2012.00228

Chen, Y.-H., Li, H.-J., Shi, D.-Q., Yuan, L., Liu, J., Sreenivasan, R., Baskar, R., Grossniklaus, U. and Yang, W.-C. (2007). The central cell plays a critical role in pollen tube guidance in Arabidopsis. *Plant Cell* **19**, 3563-3577. doi:10.1105/tpc.107.053967

Christensen, C. A., King, E. J., Jordan, J. R. and Drews, G. N. (1997). Megagametogenesis in Arabidopsis wild type and the Gf mutant. *Sex. Plant Reprod.* **10**, 49-64. doi:10.1007/s004970050067

Clough, S. J. and Bent, A. F. (1998). Floral dip: a simplified method for Agrobacterium-mediated transformation of Arabidopsis thaliana. *Plant J.* **16**, 735-743. doi:10.1046/j.1365-313x.1998.00343.x

Coury, D. A., Zhang, C., Ko, A., Skaggs, M. I., Christensen, C. A., Drews, G. N., Feldmann, K. A. and Yadegari, R. (2007). Segregation distortion in Arabidopsis gametophytic factor 1 (gfa1) mutants is caused by a deficiency of an essential RNA splicing factor. *Sex. Plant Reprod.* **20**, 87-97. doi:10.1007/s00497-007-0046-8

Cui, Z., Tong, A., Huo, Y., Yan, Z., Yang, W., Yang, X. and Wang, X.-X. (2017). SKIP controls flowering time via the alternative splicing of SEF pre-mRNA in Arabidopsis. *BMC Biol.* **15**, 80. doi:10.1186/s12915-017-0422-2

Davis, T. C., Jones, D. S., Dino, A. J., Cejda, N. I., Yuan, J., Willoughby, A. C. and Kessler, S. A. (2017). Arabidopsis thaliana MLO genes are expressed in discrete domains during reproductive development. *Plant Reprod.* **30**, 185-195. doi:10.1007/s00497-017-0313-2

Deng, X., Lu, T., Wang, L., Gu, L., Sun, J., Kong, X., Liu, C. and Cao, X. (2016). Recruitment of the NineTeen Complex to the activated spliceosome requires AtPRMT5. *Proc. Natl. Acad. Sci. USA* **113**, 5447-5452. doi:10.1073/pnas.1522458113

Dobin, A., Davis, C. A., Schlesinger, F., Drenkow, J., Zaleski, C., Jha, S., Batut, P., Chaisson, M. and Gingeras, T. R. (2013). STAR: ultrafast universal RNA-seq aligner. *Bioinformatics* **29**, 15-21. doi:10.1093/bioinformatics/bts635

Dresselhaus, T. and Franklin-Tong, N. (2013). Male-female crosstalk during pollen germination, tube growth and guidance, and double fertilization. *Mol. Plant* **6**, 1018-1036. doi:10.1093/mp/sst061

Dresselhaus, T., Sprunck, S. and Wessel, G. M. (2016). Fertilization mechanisms in flowering plants. *Curr. Biol.* **26**, R125-R139. doi:10.1016/j.cub.2015.12.032

Filichkin, S., Priest, H. D., Megraw, M. and Mockler, T. C. (2015). Alternative splicing in plants: directing traffic at the crossroads of adaptation and environmental stress. *Curr. Opin. Plant Biol.* **24**, 125-135. doi:10.1016/j.pbi.2015.02.008

Ge, Z., Bergonci, T., Zhao, Y., Zou, Y., Du, S., Liu, M.-C., Luo, X., Ruan, H., García-Valencia, L. E., Zhong, S. et al. (2017). *Arabidopsis* pollen tube integrity and sperm release are regulated by RALF-mediated signaling. *Science* **358**, 1596-1600. doi:10.1126/science.aao3642

Grefen, C. and Blatt, M. R. (2012). A 2in1 cloning system enables ratiometric bimolecular fluorescence complementation (rBiFC). *BioTechniques* **53**, 311-314. doi:10.2144/000113941

Gross-Hardt, R., Kägi, C., Baumann, N., Moore, J. M., Baskar, R., Gagliano, W. B., Jürgens, G. and Grossniklaus, U. (2007). LACHESIS restricts gametic cell fate in the female gametophyte of Arabidopsis. *PLoS Biol.* **5**, e47. doi:10.1371/journal.pbio.0050047

Guilgur, L. G., Prudêncio, P., Sobral, D., Liszekova, D., Rosa, A. and Martinho, R. G. (2014). Requirement for highly efficient pre-mRNA splicing during Drosophila early embryonic development. *eLife* **3**, e02181. doi:10.7554/eLife.02181

Guindon, S., Dufayard, J.-F., Lefort, V., Anisimova, M., Hordijk, W. and Gascuel, O. (2010). New algorithms and methods to estimate maximum-likelihood phylogenies: assessing the performance of PhyML 3.0. *Syst. Biol.* **59**, 307-321. doi:10.1093/sysbio/syq010

Hafidh, S., Fíla, J. and Honys, D. (2016a). Male gametophyte development and function in angiosperms: a general concept. *Plant Reprod.* **29**, 31-51. doi:10.1007/s00497-015-0272-4

Hafidh, S., Potěšil, D., Fíla, J., apková, V., Zdráhal, Z. and Honys, D. (2016b). Quantitative proteomics of the tobacco pollen tube secretome identifies novel pollen tube guidance proteins important for fertilization. *Genome Biol.* **17**, 81. doi:10.1186/s13059-016-0928-x

Hafidh, S., Potěšil, D., Müller, K., Fíla, J., Michailidis, C., Herrmannová, A., Feciková, J., Ischebeck,T., Valášek, L. S., Zdráhal, Z. et al. (2018). Dynamics of the pollen sequestrome defined by subcellular coupled omics. *Plant Physiol.* **178**, 258-282. doi:10.1104/pp.18.00648

Higashiyama, T. and Yang, W. (2017). Gametophytic pollen tube guidance: attractant peptides, gametic controls, and receptors. *Plant Physiol.* **173**, 112-121. doi:10.1104/pp.16.01571

Honys, D. and Twell, D. (2004). Transcriptome analysis of haploid male gametophyte development in Arabidopsis. *Genome Biol.* **5**, R85. doi:10.1186/gb-2004-5-11-r85

Kalyna, M., Simpson, C. G., Syed, N. H., Lewandowska, D., Marquez, Y., Kusenda, B., Marshall, J., Fuller, J., Cardle, L., McNicol, J. et al. (2012). Alternative splicing and nonsense-mediated decay modulate expression of important regulatory genes in Arabidopsis. *Nucleic Acids Res.* **40**, 2454-2469. doi:10.1093/nar/gkr932

Kanemori, Y., Koga, Y., Sudo, M., Kang, W., Kashiwabara, S., Ikawa, M., Hasuwa, H., Nagashima, K., Ishikawa, Y., Ogonuki, N. et al. (2016). Biogenesis of sperm acrosome is regulated by pre-mRNA alternative splicing of Acrbp in the mouse. *Proc. Natl. Acad. Sci. USA* **113**, E3696-E3705. doi:10.1073/pnas.1522333113

Karimi, M., Inzé, D. and Depicker, A. (2002). GATEWAY™ vectors for Agrobacterium-mediated plant transformation. *Trends Plant Sci.* **7**, 193-195. doi:10.1016/S1360-1385(02)02251-3

Kasahara, R. D., Portereiko, M. F., Sandaklie-Nikolova, L., Rabiger, D. S. and Drews, G. N. (2005). MYB98 is required for pollen tube guidance and synergid cell differentiation in Arabidopsis. *Plant Cell* **17**, 2981-2992. doi:10.1105/tpc.105.034603

Kim, Y.-E., Park, C., Kim, K. E. and Kim, K. K. (2018). Histone and RNA-binding protein interaction creates crosstalk network for regulation of alternative splicing. *Biochem. Biophys. Res. Commun.* **499**, 30-36. doi:10.1016/j.bbrc.2018.03.101

Leydon, A. R., Weinreb, C., Venable, E., Reinders, A., Ward, J. M. and Johnson, M. A. (2017). The molecular dialog between flowering plant reproductive partners defined by SNP-informed RNA-sequencing. *Plant Cell* **29**. 984-1006. doi:10.1105/tpc.16.00816

Li, H.-J., Xue, Y., Jia, D.-J., Wang, T., Hi, D.-Q., Liu, J., Cui, F., Xie, Q., Ye, D. and Yang, W.-C. (2011). POD1 regulates pollen tube guidance in response to micropylar female signaling and acts in early embryo patterning in Arabidopsis. *Plant Cell* **23**, 3288-3302. doi:10.1105/tpc.111.088914

Li, H.-J., Zhu, S.-S., Zhang, M.-X., Wang, T., Liang, L., Xue, Y., Shi, D.-Q., Liu, J. and Yang, W.-C. (2015). Arabidopsis CBP1 is a novel regulator of transcription initiation in central cell-mediated pollen tube guidance. *Plant Cell* **27**, 2880-2893. doi:10.1105/tpc.15.00370

Liao, Y., Smyth, G. K. and Shi, W. (2014). featureCounts: an efficient general purpose program for assigning sequence reads to genomic features. *Bioinformatics* **30**, 923-930. doi:10.1093/bioinformatics/btt656

Liu, M., Yuan, L., Liu, N.-Y., Shi, D.-Q., Liu, J. and Yang, W.-C. (2009). GAMETOPHYTIC FACTOR 1, involved in Pre-mRNA splicing, is essential for megagametogenesis and embryogenesis in arabidopsis. *J. Integr. Plant Biol.* **51**, 261-271. doi:10.1111/j.1744-7909.2008.00783.x

Liu, Y., Joly, V., Dorion, S., Rivoal, J. and Matton, D. P. (2015). The plant ovule secretome: a different view toward pollen-pistil interactions. *J. Proteome Res.* **14**, 4763-4775. doi:10.1021/acs.jproteome.5b00618

Liu, X., Castro, C., Wang, Y., Noble, J., Ponvert, N., Bundy, M., Hoel, C., Shpak, E. and Palanivelu, R. (2016). The role of LORELEI in pollen tube reception at the interface of the synergid cell and pollen tube requires the modified eight-cysteine motif and the receptor-like kinase FERONIA. *Plant Cell* **28**, 1035-1052. doi:10.1105/tpc.15.00703

Loraine, A. E., McCormick, S., Estrada, A., Patel, K. and Qin, P. (2013). RNA-seq of Arabidopsis pollen uncovers novel transcription and alternative splicing. *Plant Physiol.* **162**, 1092-1109. doi:10.1104/pp.112.211441

Love, M. I., Huber, W. and Anders, S. (2014). Moderated estimation of fold change and dispersion for RNA-seq data with DESeq2. *Genome Biol.* **15**, 550. doi:10.1186/s13059-014-0550-8

Luco, R. F., Pan, Q., Tominaga, K., Blencowe, B. J., Pereira-Smith, O. M. and Misteli, T. (2010). Regulation of alternative splicing by histone modifications. *Science* **327**, 996-1000. doi:10.1126/science.1184208

Luco, R. F., Allo, M., Schor, I. E., Kornblihtt, A. R. and Misteli, T. (2011). Epigenetics in alternative pre-mRNA splicing. *Cell* **144**, 16-26. doi:10.1016/j.cell.2010.11.056

Maeder, C., Kutach, A. K. and Guthrie, C. (2009). ATP-dependent unwinding of U4/U6 snRNAs by the Brr2 helicase requires the C terminus of PRP8. *Nat. Struct. Mol. Biol.* **16**, 42-48. doi:10.1038/nsmb.1535

Marquardt, S., Raitskin, O., Wu, Z., Liu, F., Sun, Q. and Dean, C. (2014). Functional consequences of splicing of the antisense transcript COOLAIR on FLC transcription. *Mol. Cell* **54**, 156-165. doi:10.1016/j.molcel.2014.03.026

Marquez, Y., Brown, J. W. S., Simpson, C., Barta, A. and Kalyna, M. (2012). Transcriptome survey reveals increased complexity of the alternative splicing landscape in Arabidopsis. *Genome Res.* **22**, 1184-1195. doi:10.1101/gr.134106.111

Márton, M. L., Cordts, S., Broadhvest, J. and Dresselhaus, T. (2005). Micropylar pollen tube guidance by egg apparatus 1 of maize. *Science* **307**, 573-576. doi:10.1126/science.1104954

Márton, M. L., Fastner, A., Uebler, S. and Dresselhaus, T. (2012). Overcoming hybridization barriers by the secretion of the maize pollen tube attractant ZmEA1 from Arabidopsis ovules. *Curr. Biol.* **22**, 1194-1198. doi:10.1016/j.cub.2012.04.061

McGlincy, N. J. and Smith, C. W. J. (2008). Alternative splicing resulting in nonsense-mediated mRNA decay: what is the meaning of nonsense? *Trends Biochem. Sci.* **33**, 385-393. doi:10.1016/j.tibs.2008.06.001

Mecchia, M. A., Santos-Fernandez, G., Duss, N. N., Somoza, S. C., Boisson-Dernier, A., Gagliardini, V., Martínez-Bernardini, A., Fabrice, T. N., Ringli, C., Muschietti, J. P. et al. (2017). RALF4/19 peptides interact with LRX proteins to control pollen tube growth in Arabidopsis. *Science* **358**, 1600-1603. doi:10.1126/science.aao5467

Meinke, D., Muralla, R., Sweeney, C. and Dickerman, A. (2008). Identifying essential genes in Arabidopsis thaliana. *Trends Plant Sci.* **13**, 483-491. doi:10.1016/j.tplants.2008.06.003

Middleton, R., Gao, D., Thomas, A., Singh, B., Au, A., Wong, J. J.-L., Bomane, A., Cosson, B., Eyras, E., Rasko, J. E. et al. (2017). IRFinder: assessing the impact of intron retention on mammalian gene expression. *Genome Biol.* **18**, 51. doi:10.1186/s13059-017-1184-4

Mithoe, S. C., Ludwig, C., Pel, M. J. C., Cucinotta, M., Casartelli, A., Mbengue, M., Sklenar, J., Derbyshire, P., Robatzek, S., Pieterse, C. M. J. et al. (2016). Attenuation of pattern recognition receptor signaling is mediated by a MAP kinase kinase kinase. *EMBO Rep.* **17**, 441-454. doi:10.15252/embr.201540806

Moll, C., Von Lyncker, L., Zimmermann, S., Kägi, C., Baumann, N., Twell, D., Grossniklaus, U. and Groß-Hardt, R. (2008). CLO/GFA1 and ATO are novel regulators of gametic cell fate in plants. *Plant J.* **56**, 913-921. doi:10.1111/j.1365-313X.2008.03650.x

Mori, T., Kuroiwa, H., Higashiyama, T. and Kuroiwa, T. (2006). GENERATIVE CELL SPECIFIC 1 is essential for angiosperm fertilization. *Nat. Cell Biol.* **8**, 64-71. doi:10.1038/ncb1345

Muschietti, J., Dircks, L., Vancanneyt, G. and McCormick, S. (1994). LAT52 protein is essential for tomato pollen development: pollen expressing antisense LAT52 RNA hydrates and germinates abnormally and cannot achieve fertilization. *Plant J.* **6**, 321-338. doi:10.1046/j.1365-313X.1994.06030321.x

Notredame, C., Higgins, D. G. and Heringa, J. (2000). T-coffee: a novel method for fast and accurate multiple sequence alignment. *J. Mol. Biol.* **302**, 205-217. doi:10.1006/jmbi.2000.4042

Okuda, S., Tsutsui, H., Shiina, K., Sprunck, S., Takeuchi, H., Yui, R., Kasahara, R. D., Hamamura, Y., Mizukami, A., Susaki, D. et al. (2009). Defensin-like polypeptide LUREs are pollen tube attractants secreted from synergid cells. *Nature* **458**, 357-361. doi:10.1038/nature07882

Pagnussat, G. C., Yu, H. J., Ngo, Q. A., Rajani, S., Mayalagu, S., Johnson, C. S., Capron, A., Xie, L. F., Ye, D. and Sundaresan, V. (2005). Genetic and molecular identification of genes required for female gametophyte development and function in Arabidopsis. *Development* **132**, 603-614. doi:10.1242/dev.01595

Palanivelu, R., Preuss, D., Weterings, K., Russell, S., Lord, E., Russell, S., Huck, N., Moore, J., Federer, M., Grossniklaus, U. et al. (2006). Distinct short-range ovule signals attract or repel Arabidopsis thaliana pollen tubes in vitro. *BMC Plant Biol.* **6**, 7. doi:10.1186/1471-2229-6-7

Qin, Y., Leydon, A. R., Manziello, A., Pandey, R., Mount, D., Denic, S., Vasic, B., Johnson, M. A. and Palanivelu, R. (2009). Penetration of the stigma and style elicits a novel transcriptome in pollen tubes, pointing to genes critical for growth in a pistil. *PLoS Genet.* **5**, e1000621. doi:10.1371/journal.pgen.1000621

Reddy, A. SN., Marquez, Y., Kalyna, M. and Barta, A. (2013). Complexity of the alternative splicing landscape in plants. *Plant Cell* **25**, 3657-3683. doi:10.1105/tpc.113.117523

Robinson, M. D., McCarthy, D. J. and Smyth, G. K. (2010). edgeR: a Bioconductor package for differential expression analysis of digital gene expression data. *Bioinformatics* **26**, 139-140. doi:10.1093/bioinformatics/btp616

Schwartz, B. W., Yeung, E. C. and Meinke, D. W. (1994). Disruption of morphogenesis and transformation of the suspensor in abnormal suspensor mutants of Arabidopsis. *Development* **120**, 3235-3245.

Shimizu, K. K., Ito, T., Ishiguro, S. and Okada, K. (2008). MAA3 (MAGATAMA3) helicase gene is required for female gametophyte development and pollen tube guidance in Arabidopsis thaliana. *Plant Cell Physiol.* **49**, 1478-1483. doi:10.1093/pcp/pcn130

Staiger, D. and Brown, J. W. S. (2013). Alternative splicing at the intersection of biological timing, development, and stress responses. *Plant Cell* **25**, 3640-3656. doi:10.1105/tpc.113.113803

Syed, N. H., Kalyna, M., Marquez, Y., Barta, A. and Brown, J. W. S. (2012). Alternative splicing in plants: coming of age. *Trends Plant Sci.* **17**, 616-623. doi:10.1016/j.tplants.2012.06.001

Takeuchi, H. and Higashiyama, T. (2012). A species-specific cluster of defensin-like genes encodes diffusible pollen tube attractants in Arabidopsis. *PLoS Biol.* **10**, e1001449. doi:10.1371/journal.pbio.1001449

Tamura, K., Stecher, G., Peterson, D., Filipski, A. and Kumar, S. (2013). MEGA6: molecular evolutionary genetics analysis version 6.0. *Mol. Biol. Evol.* **30**, 2725-2729. doi:10.1093/molbev/mst197

Tang, W., Ezcurra, I., Muschietti, J. and McCormick, S. (2002). A cysteine-rich extracellular protein, LAT52, interacts with the extracellular domain of the pollen receptor kinase LePRK2. *Plant Cell* **14**, 2277-2287. doi:10.1105/tpc.003103

Tresini, M., Warmerdam, D. O., Kolovos, P., Snijder, L., Vrouwe, M. G., Demmers, J. AA., van IJcken, W. FJ., Grosveld, F. G., Medema, R. H., Hoeijmakers, J. HJ. et al. (2015). The core spliceosome as target and effector of non-canonical ATM signalling. *Nature* **523**, 53-58. doi:10.1038/nature14512

Twell, D., Yamaguchi, J. and McCormick, S. (1990). Pollen specific gene expression in transgenic plants: coordinate regulation of two different tomato gene promoters during microsporogenesis. *Development* **109**, 705-713.

Twell, D., Yamaguchi, J., Wing, R. A., Ushiba, J. and McCormick, S. (1991). Promoter analysis of genes that are coordinately expressed during pollen development reveals pollen-specific enhancer sequences and shared regulatory elements. *Genes Dev.* **5**, 496-507. doi:10.1101/gad.5.3.496

Tzafrir, I., Pena-muralla, R., Dickerman, A., Berg, M., Rogers, R., Hutchens, S., Sweeney, T. C., Mcelver, J., Aux, G., Patton, D. et al. (2004). Identification of genes required for embryo development in arabidopsis. *Plant Physiol.* **135**, 1206-1220. doi:10.1104/pp.104.045179

Völz, R., Heydlauff, J., Ripper, D., von Lyncker, L. and Groß-Hardt, R. (2013). Ethylene signaling is required for synergid degeneration and the establishment of a pollen tube block. *Dev. Cell* **25**, 310-316. doi:10.1016/j.devcel.2013.04.001

von Besser, K., Frank, A. C., Johnson, M. A. and Preuss, D. (2006). Arabidopsis HAP2 (GCS1) is a sperm-specific gene required for pollen tube guidance and fertilization. *Development* **133**, 4761-4769. doi:10.1242/dev.02683

Wang, Y., Tsukamoto, T., Noble, J. A., Liu, X., Mosher, R. A. and Palanivelu, R. (2017). Arabidopsis LORELEI, a maternally expressed imprinted gene, promotes early seed development. *Plant Physiol.* **175**, 758-773. doi:10.1104/pp.17.00427

Waterhouse, A. M., Procter, J. B., Martin, D. MA., Clamp, M. and Barton, G. J. (2009). Jalview Version 2—a multiple sequence alignment editor and analysis workbench. *Bioinformatics* **25**, 1189-1191. doi:10.1093/bioinformatics/btp033

Will, C. L. and Lührmann, R. (2011). Spliceosome structure and function. *Cold Spring Harb. Perspect. Biol.* **3**, a003707. doi:10.1101/cshperspect.a003707

Winter, D., Vinegar, B., Nahal, H., Ammar, R., Wilson, G. V. and Provart, N. J. (2007). An "Electronic Fluorescent Pictograph" browser for exploring and analyzing large-scale biological data sets. *PLoS ONE* **2**, e718. doi:10.1371/journal.pone.0000718

Wuest, S. E., Vijverberg, K., Schmidt, A., Weiss, M., Gheyselinck, J., Lohr, M., Wellmer, F., Rahnenführer, J., von Mering, C. and Grossniklaus, U. (2010). Arabidopsis female gametophyte gene expression map reveals similarities between plant and animal gametes. *Curr. Biol.* **20**, 506-512. doi:10.1016/j.cub.2010.01.051

Xu, Y., Zhao, W., Olson, S. D., Prabhakara, K. S. and Zhou, X. (2018). Alternative splicing links histone modifications to stem cell fate decision. *Genome Biol.* **19**, 133. doi:10.1186/s13059-018-1512-3

Yang, C., Vizcay-Barrena, G., Conner, K. and Wilson, Z. A. (2007). MALE STERILITY1 is required for tapetal development and pollen wall biosynthesis. *Plant Cell* **19**, 3530-3548. doi:10.1105/tpc.107.054981

Zhang, X., Yan, C., Hang, J., Finci, L. I., Lei, J. and Shi, Y. (2017). An Atomic Structure of the Human Spliceosome. *Cell* **169**, 1-12. doi:10.1016/j.cell.2017.04.033

Zimmermann, P., Hirsch-Hoffmann, M., Hennig, L. and Gruissem, W. (2004). Genevestigator: arabidopsis microarray database and analysis toolbox. *Plant Biol.* **2004**, 186. doi:10.1104/pp.104.046367

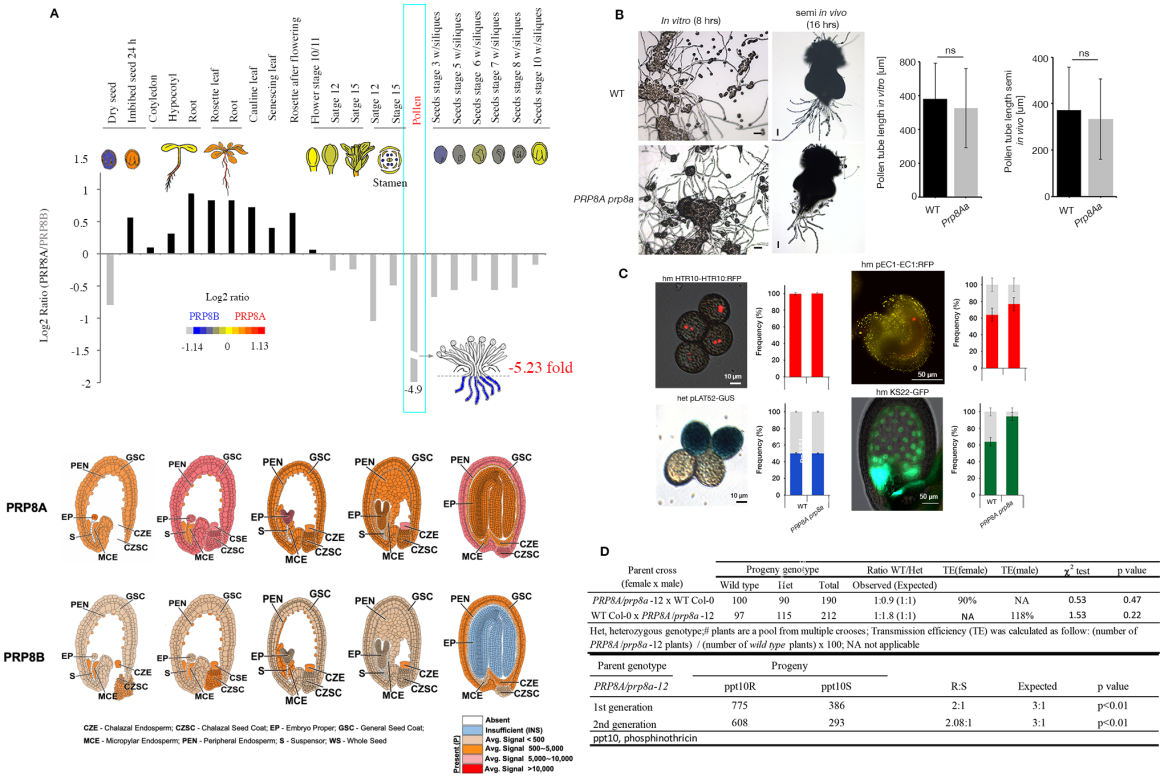

Parent cross (female x male)	Progeny genotype: Wild type	1/et	Total	Ratio WT/Het Observed (Expected)	TE(female)	TE(male)	χ^2 test	p value
PRP8A/prp8a -12 x WT Col-0	100	90	190	1:0.9 (1:1)	90%	NA	0.53	0.47
WT Col-0 x *PRP8A/prp8a* -12	97	115	212	1:1.8 (1:1)	NA	118%	1.53	0.22

Het, heterozygous genotype;# plants are a pool from multiple crooses; Transmission efficiency (TE) was calculated as follow: (number of *PRP8A/prp8a* -12 plants) / (number of *wild type* plants) x 100; NA not applicable

Parent genotype	Progeny: ppt10R	ppt10S	R:S	Expected	p value
PRP8A/prp8a-12					
1st generation	775	386	2:1	3:1	p<0.01
2nd generation	608	293	2.08:1	3:1	p<0.01

ppt10, phosphinothricin

Figure S1. Pollen Tube Growth and Gamete Cell Fate Specification is not Impaired in single mutant *prp8a*

(A) Comparative expression (in fold change) and domains specific expression of PRP8A and PRP8B during seed development. Data were retrieved from Arabidopsis eFP Browser and from the Bio-Analytic Resources for plant biology (http://bar.utoronto.ca/) (Winter et al., 2007) and from Gene Networks in Seed Development (http://seedgenenetwork.net) (Belmonte et al., 2013). (B) in vitro and semi in vivo pollen tube growth is normal in prp8a-12 single mutant. ns, not statistically significant difference based on one tail Student t test. (C) Gametophyte cell fate specification in prp8a-12 single mutant. Sperm cell-specific histone HTR10, vegetative cell-specific LAT52, egg cell-specific EC1 and an endosperm marker KS22 in mutant PRP8Aa plants. Ht and HM, heterozygous for the marker respectively. (D) Transmission and segregation of prp8a allele through male, female and in self-pollination. Presence of T-DNA was detected by PCR genotyping.

Development • Supplementary information

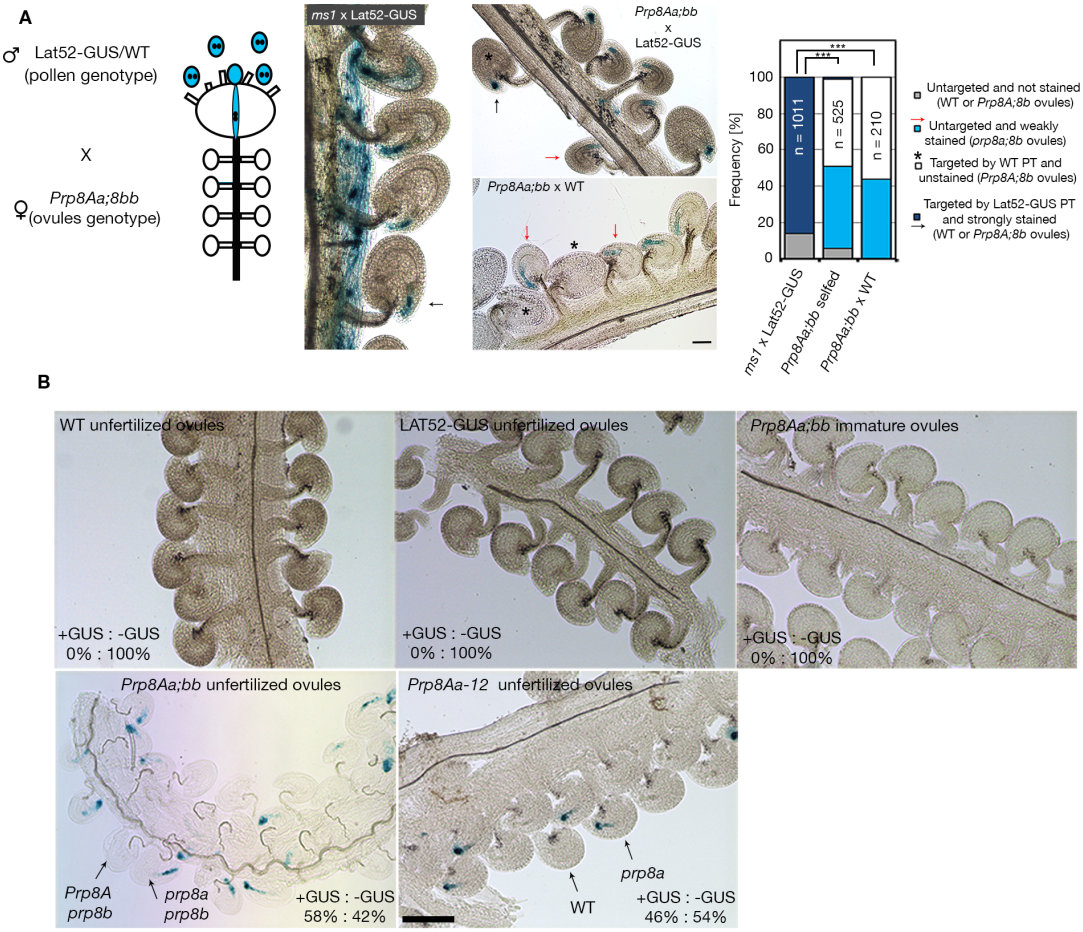

Figure S2. PRP8A/PRP8B are required for pollen tube attraction

(A) Blue dot assay recapitulated the lack of pollen tube attraction by *prp8a prp8b* ovules observed by live cell imaging and *in vivo* assay (Fig. 3). Black arrows are wild type ovules containing GUS discharge (blue dot) targeted by LAT52pro-GUS expressing pollen tubes, Red arrows indicate untargeted *prp8a prp8b* ovules with ectopic GUS expression without fertilization (elaborated in panel "B"), and asterisk are wild type-like ovules (*PRP8A prp8b* genotype) targeted by wild type pollen tubes without GUS expression. Note the larger size of the *PRP8A prp8b* ovules indicating embryo and endosperm development post fertilization. (B) Ectopic expression of pollen specific LAT52pro-GUS in *prp8a prp8b* embryo sac. Recognised ovules genotypes are labelled. Data are mean values ± SD. ***P < 0.01 (Student's t test). All scale bars = 50μm.

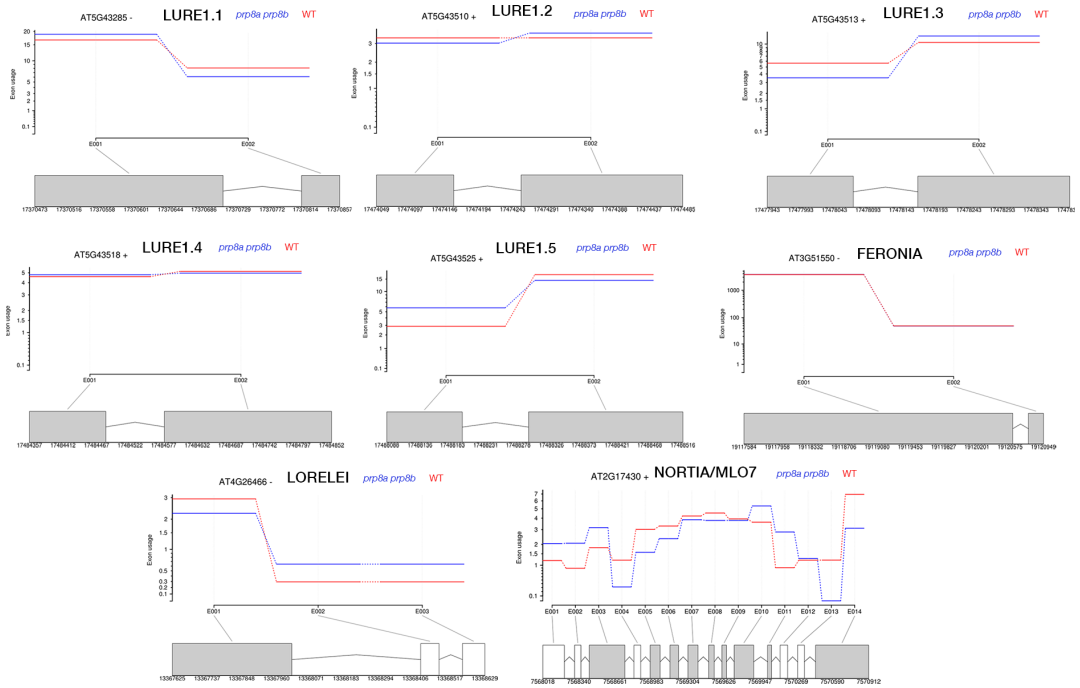

Figure S3. Splicing of LURE genes is Not Affected in *prp8a prp8b* Ovules

Exon usage in wild-type and *prp8a prp8b* ovules from normalized RNA-seq reads are shown over gene models.

A

Gene	Symbol	Intron	Chr:Intron coordinates:strand	+IR Log2 fold change	p-value	Description
AT5G37680	ARL8C	clean	5:14970149-14970248:-	3,54	3,23E-02	A member of ARF-like GTPase family
AT1G10290	DRP2A	clean	1:'-3371248-3371344:+	3,00	4,91E-02	Trans-Golgi to central vacuole transport
AT2G21540	SFH3	clean	2:'-9221960-9222038:-	-3,73	2,49E-02	SEC14 cytosolic factor of exocytosis
AT3G52850	VSR1	clean	3:19591290-19591382:+	3,75	1,26E-02	Vacuolar Sorting Receptor-1 (VSR-1)
AT5G11710	EPSIN1	clean	5:'-3773798-3773886:+	2,23	4,67E-02	Interact with gamma-ADR, VTI11, VSR1, and clathrin for vacuolar trafficking
AT1G75760		known-exon	1:28446988-28447116:-	-3,51	3,12E-02	ER lumen protein retaining receptor family protein
AT5G03540	ATEXO70A1	clean	5:'-893461-893553:+	3,54	4,63E-02	A member of EXO70 gene family, putative exocyst subunits
AT5G11980		clean	5:'-3871931-3872020:-	-3,20	3,23E-02	conserved oligomeric Golgi complex component-related (COG complex)
AT5G66030	GRIP	clean	2:12066022-12066110:+	3,43	3,73E-02	Golgi protein trafficking, directly associated with AtARL1 in a GTP-dependent manner
AT3G09900	RABE1E	clean	2:12066022-12066110:+	4,05	9,79E-03	AtRABE1e/AtRab8E (Arabidopsis Rab GTPase homolog E1e) for GTP binding
AT2G29020		clean	2:12066022-12066110:+	-3,80	1,44E-02	Rab5-interacting family protein

B

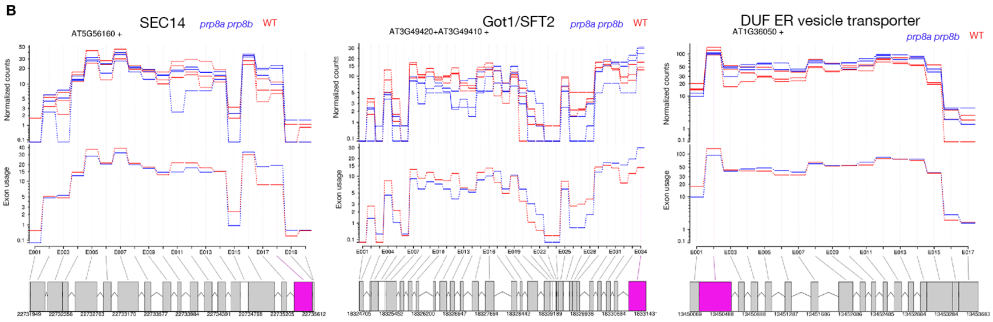

Figure S4. Several Secretory Pathway Genes are Mis-spliced in *prp8a prp8b* Ovules

(A) Significant Intron retention identified using IRFinder script. (B) A parallel analysis using DEXSeq script for differential exon usage. Charts showing both normalized counts from all three replicates (top) and exon usage from the mean of the counts.

Development • Supplementary information

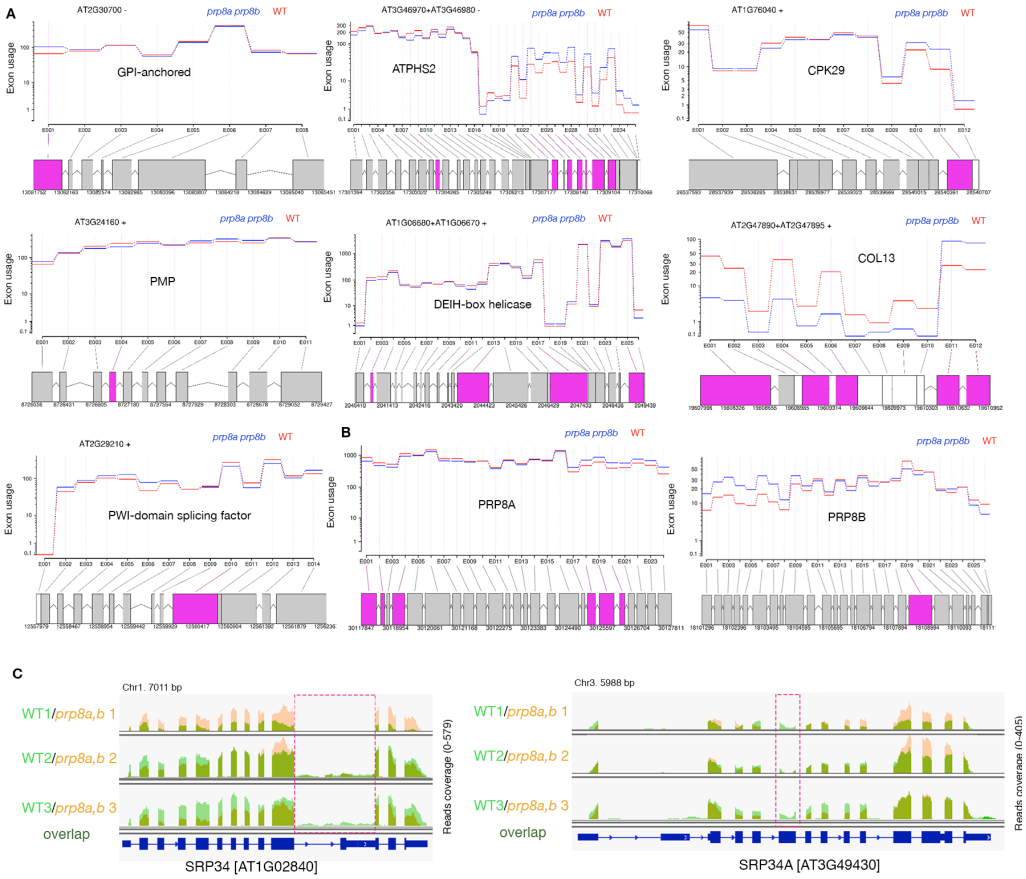

Figure S5. PRP8A and PRP8B Shows Autoregulation and Regulate Splicing of Other Spliceosome subunits

(A) Exemplified genes with significant DEU representing categories of plasma membrane signalling proteins, transcription factors and chromatin remodelling, metabolism, splicing factors and signalling kinases. (B) Significant DEU of PRP8A and PPR8B transcript isoforms in *prp8a prp8b* ovules relative to their expression in wild type ovules. (C) Selected mis-spliced core subunits of the spliceosome complex in *prp8a prp8b* ovules identified in IRFinder pipeline with >2 fold log2 difference. RNA-seq reads from wild type and mutant samples are color-coded and superimposed. Rectangles represent reduced/spliced-out gene sections in mutant samples.

A

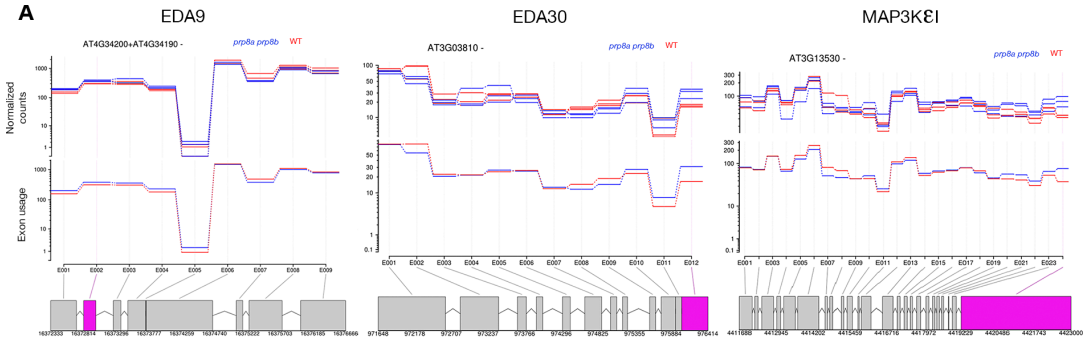

B

+IR (IRFinder) events relative to wild type control					
Gene ID	Symbol	Intron coordinates:strand	Log2 fold change	p-value	Pagnussat phenotype (Pagnussat et al., 2005)
AT4G34200	EDA9	Defect in DEU (Fig. 3M)	na	na	Arrested at two-nuclear stage
AT3G03810	EDA30	972619-972833:-	-4,04	0,02	Unfused polar nuclei
AT4G05450	EDA35/MFDX1	2759105- 2759305:+	2,39	0,04	Unfused polar nuclei
AT2G01620	ME11/SKIP28	278836- 278917:+	3,30	0,04	Arrested at one cell zygotic stage
AT2G35340	MEE29	14878939-14879012:+	-3,15	0,03	Arrested at one cell zygotic stage
AT3G13530	MAPK3E1	4413584-4413667:-	-3,37	0,04	Not represented
Differentially expressed (DESeq2) relative to wild type control					
Gene ID	Symbol	Description	Log2 fold change	p-value	Pagnussat phenotype (Pagnussat et al., 2005)
AT5G44700	GSO2/EDA23	LR repeat transmembrane protein kinase	-0,88	0,00016	Arrested during embro sac development
AT4G33050	EDA39	Calmodulin-binding protein	-0,81	3E-06	Unfused polar nuclei
AT4G00050	UNE10	bHLH DNA-binding protein	-1,07	2,5E-05	Unfertilized ovules but normal pollen tube attraction
AT4G13560	UNE15	Late embryogenesis abundant (LEA)	3,31	8,3E-17	Defects in pollen tube attraction
AT1G60870	MEE9	Maternal effect embryo arrest 9	-0,70	0,00277	Arrested at one cell zygotic stage
AT2G35210	RPA/MEE28	Root and Pollen ARFGAP	1,33	0,00028	Arrested at one cell zygotic stage

Figure S6. Genes With Direct Function in Embryo Sac Developmental are Mis-spliced in *prp8a prp8b* Ovules

(A) Exemplified output from DEXSeq analysis showing statistically differential exon usage of embryo sac developmental genes between wild type and double mutant *prp8a prp8b* ovules. (B) Additional embryo sac developmental genes identified with IRFinder pipeline and those that are differentially expressed from DESeq2 analysis.

Development • Supplementary information

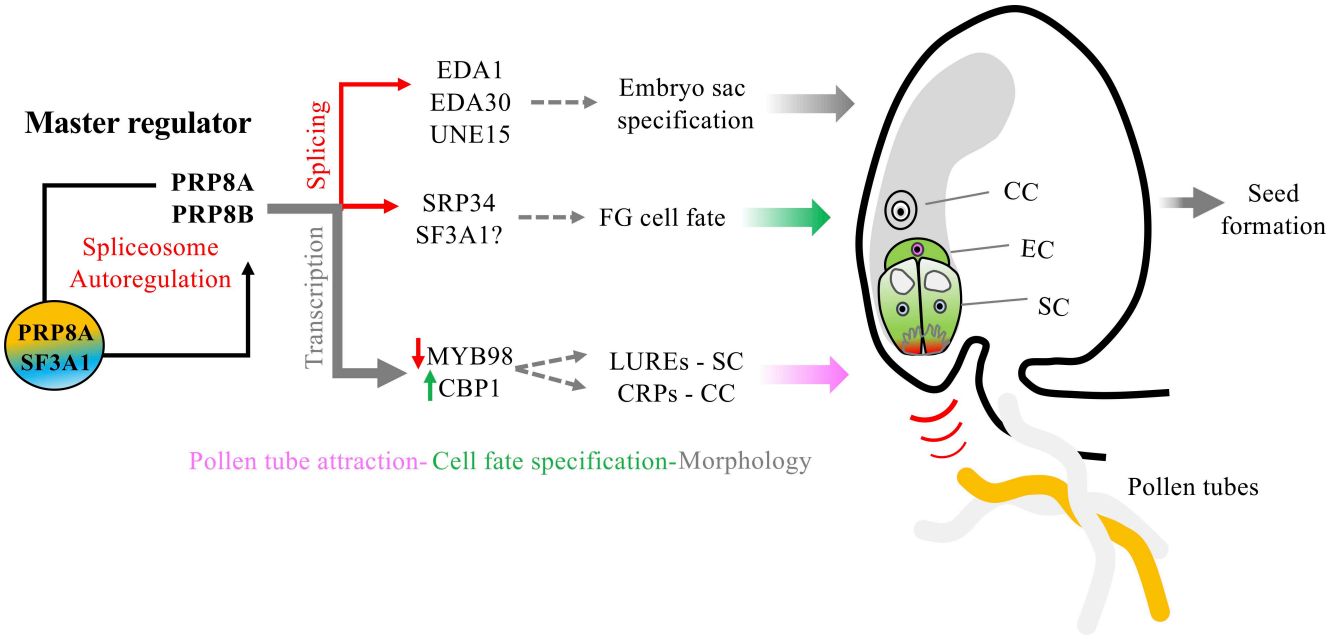

Figure S7. Proposed working model of PRP8A/PRP8B autoregulation and a dual function imposing pollen tube attraction and embryo sac specification.

Development • Supplementary information

Movie 1. Stained wild type pollen tubes in *PRP8A;bb* pistil showing all four-types of ovules phenotypes scored.

Development • Supplementary information

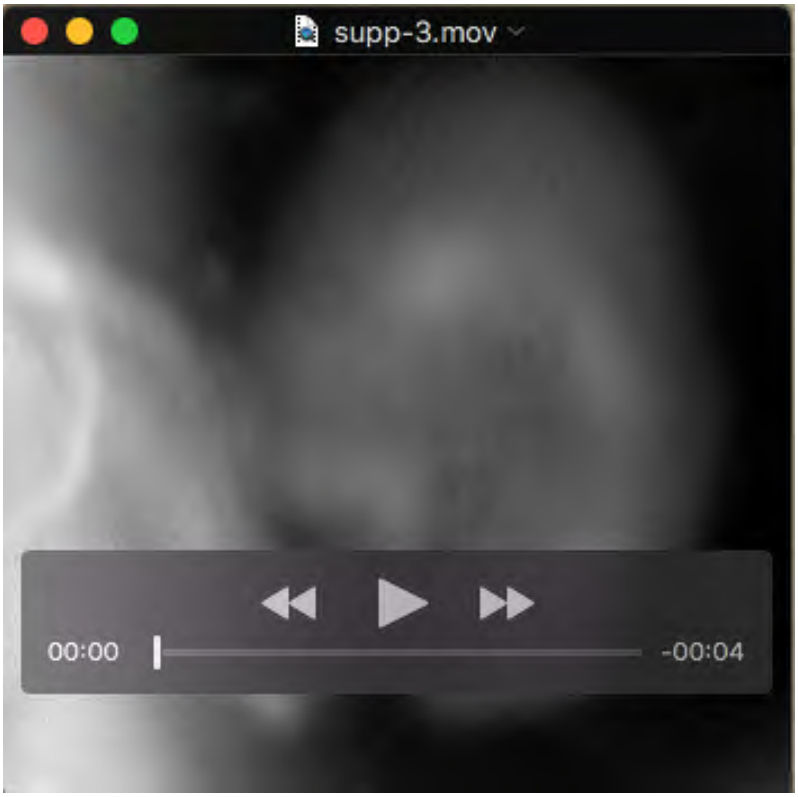

Movie 2. Close-up Z-stack series of the double mutant *prp8a prp8b* ovules showing pollen tube attraction defect (type IV ovules).

Development • Supplementary information

Table S1. List of primers used.

Click here to Download Table S1

Table S2. List of accessions used in this study

Click here to Download Table S2

Table S3. All 484 statistically differentially expressed genes (DEG), p value < 0.05 and ≥2 log2 fold change **up**/**down** identified by DESeq2 between WT and *prp8a;prp8b* double mutant ovules

Click here to Download Table S3

Table S4. Statistically differentially expressed genes (DEG) ≥2 fold **up**/**down** identified by DESeq2 between WT and *prp8a;prp8b* double mutant ovules and expressed in at least one of the three female gametophyte cell types [egg cell, central cell or synergid cell]. Wuest et al., 2010

Click here to Download Table S4

Table S5. Genes with significant Intron Retention (IR, p <0.05) in *prp8a prp8b* ovules. **+IR; -IR**

Click here to Download Table S5

Table S6. List of Female Gametophyte cell type specific genes with significant intron retention (+/-IR) (Data mapped to Wuest et al., 2010). EC; egg cell, CC; central cell, SY; synergid cell

Click here to Download Table S6

Development • Supplementary information

Table S7. List of FG cell type specific genes with significant intron retention (+IR)

Click here to Download Table S7

Table S8. Genes with significant differential Exon-usage (DEU) as identified by DEXSeq between WT and *prp8a;prp8b* double mutant ovules and their profile in the female gametophyte cell types [egg cell, central cell or synergid cell]. Mapped to Wuest et al., 2010.

Click here to Download Table S8

Table S9

Click here to Download Table S9

Development • Supplementary information

2.5. Unpublished chapter: Disruption of Arabidopsis Pre-mRNA Processing Factor PRP8a Affects Suspensor Cell Fate Specification and Embryogenesis

Katarína Kulichová, David Honys and Said Hafidh

My contribution: Initially, PRP8a was selected, because its transcripts are stored for a long time in tobacco pollen and growing pollen tubes (Hafidh et al. 2012a, 2012b). The gene annotation (abnormal suspensor SUS2) was intriguing, because it hinted at a gene with stored transcripts with a possible function in embryogenesis. Both of the gametophytes of the T-DNA line (described in the previous chapter about Kulichová et al. 2020) showed normal development and fitness. However, the embryo stopped properly developing at a late globular stage and wasn't viable. I performed screening of embryonic defects and quantification of transcripts by qRT-PCR in isolated translating/non-translating fractions from tobacco pollen tubes to verify our microarray data. I did crosses with pPRP8a-PRP8A::GFP and *ms1*/+ plants to detect inheritance of transcripts and protein after fertilisation. I also helped to prepare samples for *in situ* hybridisation, which was then performed by Said Hafidh. I cloned multiple vectors for complementation and did screening of the results and phenotypes induced by PRP8a imbalance. Together with Said we wrote the text of the chapter, which was originally part of a larger manuscript. However, due to reviewers comments and demands for further proof of our hypothesis and experiments, the chapter was excluded and remained unpublished so far. KK (Fig. 1A, B, D, E, F, G, Fig. 3), SH (Fig. 1 C, H, Fig. 2, Fig. 4., Fig. 5)

Abstract

The control of tissue specification and patterning during early stages of embryogenesis is highly under the influence of parental control. Here, we show that transcripts of the spliceosome subunit pre-mRNA processing factor 8a, PRP8a, are paternally inherited and regulate embryo development via splicing of key embryo developmental genes. PRP8a transcripts accumulate in pollen tubes, but are only moderately translated due to association with 80S monosomes and play no role in pollen ontogenesis or pollen tube growth. Instead, we show that paternally originated PRP8a-GFP transcripts are delivered to the zygote, suspensor and endosperm 1-2 days after pollination (DAP). To dissect the precise role of

PRP8a, we demonstrate that among others, PRP8a regulates embryo patterning by orchestrating splicing of WUSCHEL-related homeobox family of genes, DORNORSCHEN (ESR1); chloroplast TOC protein translocon complex TOC75 and rRNA processing factor, Ribonucleotide reductase 1 (RNR1); component of auxin efflux, PIN7; transcriptional repressor and apical embryo cell fate determinant TOPLESS-RELATED 2 (TPR2), as well as genes of the small RNA pathways, ARGONAUTE 1 (AGO1) and SHOOT REDIFFERENTIATION 2 (SRD2). Further, PRP8a regulates early suspensor cell fate specification through correct splicing of RING U Box zinc finger protein (AT5G42200). Our findings suggest that PRP8a is at the hub of embryo patterning, controlling splicing of early genes including those from *de novo* zygotic transcription, and its transcripts are delivered to early embryos via paternal inheritance providing essential backup on parental control over embryonic patterning and development.

Introduction

Parental control over early embryo development plays an important role in all multicellular organisms to ensure normal embryo development. In diverse animal species, maternally derived products are stored in the oocyte (Andeol 1994), constituting an astounding overrepresentation of 45% of all mouse genes (Evsikov et al. 2006, Wang et al. 2004) and 55% of all Drosophila genes (Tadros et al. 2007). In these animals, maternal control over embryogenesis is implicated to last in the range of 1-15 cell cycles (Baroux et al. 2008, Tadros and Lipshitz 2009). Transcriptional activation in the newly assembled zygotic genome is gradual, and relies on a large scale chromatin reprogramming and turnover of maternal products (Schier 2007, Tadros and Lipshitz 2009). This is simultaneously followed by a gradual increase in zygotic gene expression (Autran et al. 2012, Nodine and Bartel 2012).

In flowering plants on the other hand, the understanding of parental control and activation of zygotic gene expression is less clear. However, unprecedented progress with profound resolution has been achieved (Nodine and Bartel 2012, Autran et al. 2012). Plant embryos can progress to pre-globular stage in the absence of significant *de novo* zygotic activation following RNA polymerase II (PolII) knockdown (Pillot et al. 2010b). Two recent studies on plant embryogenesis have reported dissimilar maternal-to-paternal transcriptome contribution, with one study proposing maternally biased contribution (Autran et al. 2012), whereas the

second reported equal parental contribution and therefore immediate zygotic gene activation of both parental genomes (Nodine and Bartel 2012). Despite this, both studies have pointed to the likely enrichment of a small number of maternally/paternally-derived transcripts during early stages (1-2 cell stage) of embryogenesis (Nodine and Bartel 2012, Autran et al. 2012). The most effective parent-of-origin effect targets genes expressed in the endosperm, where maternal influence is enforced through imprinting of paternal alleles (Spillane et al. 2007). Therefore, it has been proposed that paternal transcript inheritance regulating suspensor development could provide an antagonistic solution over this tug-of-war and reinforces paternal influence (Bayer et al. 2009). To date, only one example in plants exist that demonstrates an exclusive paternally-derived temporal cue required for embryogenesis (Bayer et al. 2009). An interleukin-1 receptor–associated kinase (IRAK)/Pelle-like kinase gene SHORT SUSPENSOR (SSP) regulates YODA mitogen-activated protein kinase pathway. SSP is exclusively expressed in sperm cells without undergoing translation, and its transcripts are delivered post-fertilisation, where newly synthesised SSP protein promotes zygote and suspensor elongation (Bayer et al. 2009). In addition to MAPK cascade, RWP-RK Factor GROUNDED (GRD) was also shown to regulate cell fate specification of basal cell lineage through YDA MAP Kinase Signalling. Mutations of *GRD* resulted in partial loss of asymmetric zygote division and disappearance of the expression of suspensor marker gene *WOX8* in basal cell lineage. Since *GRD* is co-expressed with *YDA* in the apical and basal cell lineages, how its activity is only restricted to basal cell fate specification is still poorly understood (Jeong et al. 2011).

Here, we report that NtPRP8 transcripts are enriched in 80S monosomes RNA storing granules in pollen tubes, previously known as EPP (Honys et al. 2000, 2009, Hafidh et al. 2018). Polysome profiling analysis coupled with qRT-PCR demonstrated that nearly half of the PRP8a transcripts are associated with non-translating 80S monosomal fraction in pollen tubes. Translational repression of monosome-associated transcripts is well documented (Huntzinger and Izaurralde 2011, Rowe et al. 2014, Preissler et al. 2015, Castelli et al. 2015, Collier et al. 2015). Only transcripts containing short upstream reading frame (uORF), targets of non-sense mediated decay (NMD) and those encoding low abundant regulatory proteins, can be translated in 80S monosomal fraction in yeast (Heyer et al. 2016). PRP8a is

characterised by none of these features. We show that PRP8a is readily expressed in both gametophytes including sperm cells but plays no apparent role in pollen ontogenesis or during pollen tube growth (data presented in Kulichová et al. 2020). Instead, we show that PRP8a transcripts are delivered to newly formed embryos and endosperm and function in pre-mRNA processing including splicing of WUSCHEL-related homeobox genes and an array of other embryo developmental genes, linking parent-of-origin contribution over embryogenesis. Unlike the "exclusive" parent-of-origin temporal cue exerted with SSP on embryo development (Bayer et al. 2009), PRP8a seems to provide a "fail-safe" parent-of-origin mechanism, where both parents could participate from beginning to ensure correct embryo development.

Results

PRP8a translation is moderated in pollen tubes, and its transcripts are paternally transmitted to early embryos and endosperm

NtPRP8a (pre-*m*RNA processing factor 8a) was isolated as a candidate gene whose transcripts were predominantly associated with EPP particles as late as 24 hrs after *in vitro* pollen tube growth (Fig. 1A-B). Polysome profiling coupled with qRT-PCR analysis revealed a steady distribution of NtPRP8a transcripts to non-translating monosomes and in actively translating polysomes after 24 hrs of *in vitro* pollen tube growth (Fig. 1C).

To investigate whether paternally expressed PRP8a transcripts could be delivered to zygote post-fertilisation to regulate early embryogenesis, we pollinated wild type female flowers from male sterile plants (*ms1*-/-) with pollen grains expressing pPRP8a-PRP8a::GFP construct, and collected pistil samples one and two days after pollination (DAP). As a control, pistils were also pollinated with wild type pollen grains. Analysis by qRT-PCR revealed a reliable detection of PRP8a-GFP hybrid transcripts (PRP8a mRNA fusion with GFP mRNA fragment) upon fertilisation at 1 DAP (2-cell embryos) and 2 DAP (4-8-cell embryos) (Fig. 1D). At similar time point, no reliable signal could be detected from *ms1*/+ plants pollinated with wild type pollen grains (Fig. 1D).

Post fertilisation, deep RNA-sequencing profiling of 2-4 cells embryos revealed a dominant contribution of paternally derived PRP8a transcripts to newly formed zygote (Fig. 1H, data from Autran et al., 2012). This bulk paternal PRP8a transcript inheritance was not

affected in the imprinting allele *kryptonite* (*krp*) background (a SUVH4 histone methyltransferase that imposes epigenetic transcriptional silencing through dimethylation of histone H3 at lysine 9 (H3K9me2) in Arabidopsis (Jackson et al., 2002)), suggesting that the detected PRP8a transcripts in zygote at 1-2 DAP originated from the male gamete transcriptome and not from the *de novo* zygotic gene activation of paternally imprinted PRP8a allele (Autran et al., 2012). Independent dataset from Nodine and Bartel (2012) however showed only marginal differences of maternal-paternal derived PRP8a transcriptome in the newly formed embryos, suggesting an equal parental inheritance or *de novo* zygotic transcriptional activation (Nodine and Bartel, 2012).

Confocal analysis of fertilised ovules 1-2 DAP detected GFP signal in nuclei of developing embryo, suspensor cells as well as in syncytial endosperm, corroborated with the delivery of PRP8a-GFP transcripts in these cells (Fig. 1E-G).

Consistent with the qRT-PCR results, fluorescent whole mount *in situ* hybridisation (F-WISH, Bleckmann et al., 2015) of fertilised ovules from 1 and 2 DAP of pPRP8a-PRP8a::GFP pollinated pistils demonstrated a clear detection of pollen-originated PRP8a::GFP transcripts in the developing zygotic cells (proembryo), at the chalazal end as well as in the syncytial endosperm (Fig. 2 A-L). In contrast to the PRP8a::GFP transcript detection by the antisense RNA probe, PRP8a::GFP sense probe showed no signal at the corresponding stages of proembryo development confirming probe specificity (Fig. 2 H, J, L). Simultaneous *in situ* hybridisation of an egg cell specific gene, Egg Cell 1 (EC1, Bleckmann et al., 2015), was used as a positive control and as a reporter of embryo progression (Fig. 2 A, C, E). Collectively, our findings have demonstrated that prior to zygotic activation of gene expression, PRP8a transcripts are inherited via paternal gametes and likely function at the early stages of embryogenesis.

Imbalance in PRP8a gene expression induces embryonic defects

Overexpression of PRP8a induces embryonic defects

In an attempt to complement *prp8a-12* embryo lethal phenotype, we transformed heterozygous *+/prp8a-12* plants with native proPRP8a-PRP8a and proPRP8a-PRP8a::GFP fusion constructs and screened for rescue of the *prp8a* embryonic phenotype in two subsequent generations. Only a single line (line 11 [1/10]) was observed to show partial

complementation with detectable GFP expression. Instead, the remaining transformed lines exhibited an additive *prp8a-12* embryo phenotype showing increased amount of pale *prp8a-12*-like seeds up to 75% of mutant seed count in some instances (Fig. 4A-C). This loss-of-function phenotype was induced by both native and GFP-fused construct variants in transformed +/*prp8a-12* mutant plants as well as in wild type background suggesting a dominant negative effect. When observed under the DIC optics, mutant seeds showed developmental defects of various classes, some resembling original *prp8a-12* mutation (globular stage arrest), some having three cotyledons or having developed to normal size seeds but lacking chlorophyll (Fig. 3B). Five lines were selected for screening in T2 generation and all confirmed reoccurrence of the similar phenotypes (Fig. 4C). We then measured total PRP8a transcripts as well as PRP8a-GFP hybrid transcripts by qRT-PCR using tissues from rosette leaves. Our results revealed that insertion of proPRP8a-PRP8a::GFP transgene resulted in higher expression of total PRP8a transcript levels (native PRP8a plus PRP8a-GFP hybrid transcripts) relative to PRP8a wild type expression levels (Fig. 4D). Convincingly, the increased transcripts levels directly correlated with the increase in the frequency of mutant seeds (Fig. 4 C, D). This result implies that likely, a slight imbalance in PRP8a expression levels is lethal to embryo development. We propose that since PRP8a is associated with U5 in the tri-snRNP (U4/U6.U5) pre-catalytic spliceosome complex, the increased levels of PRP8a could disrupt the stoichiometry of the complex and result in a loss of function phenotype. Surprisingly, we did not observe any induced phenotype in mature pollen or during pollen tube growth were PRP8a is also expressed (data not shown). Perhaps this emphasises the minor role of PRP8 during male gametophyte ontogenesis as previously observed with the single and double mutant knockdown of PRP8a and PRP8b.

PRP8a loss-of-function causes widespread splicing defects of WUSCHEL-related homebox genes

The direct cause of embryo lethality in homozygous *prp8a-12* null mutation has remained unknown in plants. Unregulated alternative splicing could result in intron retention (IR), exon (ES) or multiple exon skipping (MES), use of cryptic intron with non-canonical donor and acceptor splice sites (AT-AC), all leading to aberrant mRNA production and frequently to nonsense mediated decay (NMD) of the invariant isoforms (Marquez et al., 2012 , Reddy et

al., 2013). *prp8a*-7 was shown to induce up to 6.7% of IR events in seedlings, affecting both major U2 and minor U12 type of introns (Sasaki et al., 2015). To test spliceosome activities directly in *prp8a-12* null mutant embryos, we have mapped splicing events of selected WUSCHEL-related homeobox family of genes (WOX), namely WOX2, WOX4, WOX8 (STIMPY-LIKE) and WOX9 (STIMPY). WUSCHEL-related homeobox genes are well known regulators of embryo development and patterning (Meinke et al., 2008). Strikingly, several WOX genes tested here showed aberrant splice isoforms in *prp8a-12* mutant embryos (Fig. 5A-C). These isoforms were either absent in wild type or dominated in the mutant embryos as opposed to dominant isoforms observed in wild type. Mapping of WOX2 produced two major transcript isoforms of equal abundance in wild type embryos, whereas multiple cryptic isoforms were prevalent in the mutant embryos without clear dominance of any isoform (Fig. 5B). WOX4 produced two major isoforms in wild type, with the shorter isoform being a dominant type (Fig. 5B). Conversely, in the mutant embryos, WOX4 pre-mRNA was processed to multiple isoforms including the two main isoforms observed in wild type, however, with the longer isoform being dominant in the *prp8a-12* mutant embryos (Fig. 5B). WOX8 on the other hand showed multiple isoforms in wild type with no clear dominance of either transcript variant (Fig. 5B). Similar splicing patterns were also observed in the mutant embryos with additional isoforms that were not present in wild type (Fig. 5B). The multiple isoforms observed in WOX8 could be partly attributed to lack of primer specificity as observed with genomic DNA (Fig. 5B). Lastly, WOX9 also produced multiple transcript isoforms with two major isoforms dominating the transcriptome (Fig. 5B). Comparable splice patterns were also present in the *prp8a-12* mutant embryos, however, with no apparent dominance (Fig. 5B). Further, the dominant WOX9 shorter isoform observed in wild type was completely missing in *prp8a-12* mutant embryos (Fig. 5B). Furthermore, DORNORSCHEN (DRN)/Enhancer of shoot regeneration 1 (ESR1), is another key regulator of apical embryo cell fate specification (Slane et al., 2014). Detection of its splice variants revealed several isoforms in wild type with two dominant isoforms of equal abundances (Fig. 5B). Strikingly, none of the DRN wild type splice variants were observed in the *prp8a-12* mutant embryos (Fig. 5B). What is even more intriguing and perhaps a novelty in autonomous feedback regulation, we identified that an interactor of PRP8a, a component of the U5-snRNP spliceosome complex, GFA1 (Coury et al., 2007), as well as an Exon Junction Complex

protein (EJC, MAGO/HAP1), were entirely mis-spliced showing none of the major isoforms observed in wild type (Fig. 5B,C).

PRP8a also regulates splicing of other essential embryo developmental genes

To investigate whether PRP8a role in splicing of embryo developmental genes was not confined to WUSCHEL-related genes, we incorporated additional subset of genes handpicked using a key word "embryogenesis" from The Arabidopsis Information Resource database (TAIR) [ref] and investigated their splicing patterns in wild type and in a null *prp8a-12* mutant seeds. For some genes (where present), primers were designed to span introns as well as within introns using RNA sequencing data from *atrft2-1* and *prp8a-7* mutant seedlings (Sasaki et al., 2015). Of the 16 genes tested, 12 showed defective splicing in *prp8a-12* mutant seeds, representing 75% positive occurrences (Fig. 6C). Among them were chloroplast functional genes including TOC protein translocon complex TOC75, FTsH protease (FTSH12) and chloroplast and mitochondrial rRNA processing factor, Ribonucleotide reductase 1 (RNR1); component of auxin efflux, PIN7; transcriptional repressor and apical embryo cell fate determinant TOPLESS-RELATED 2 (TPR2); as well as genes of the small RNA pathways including ARGONAUTE 1 (AGO1) and SHOOT REDIFFERENTIATION 2 (SRD2), a regulator of plasmodesmata intercellular movement of molecules (DLP1) and a homeobox protein required for polarity specification of adaxial/abaxial axis (PHABULOSA) (Fig. 6C). Our results hint that it is almost certain that PRP8a regulates splicing of an array of genes essential for embryogenesis.

Suspensor cell fate specification is altered in *prp8a*-deficient embryos

None of the studies that have reported PRP8a null alleles have dissected the origin of the *prp8a* embryo lethal phenotype. Whether proembryo cell fate or suspensor cell fate is affected and resulting in embryo lethality, or whether cell fate of both types are affected in *prp8a* mutant. We therefore crossed into *+/prp8a-12* mutant background a proembryo-specific marker, pDRN:n2xGFP:DRN 3'UTR (Slane et al., 2014), a suspensor-specific marker, pAT5G42200:n3xGFP RING/U-Box zinc finger protein (Slane et al., 2014), and a dual marker for both cell types, pWOX2-H2B::sGFP;pWOX2-::dTomato-LTI6b, with LTI6b labelling the plasma membrane (Gooh et al., 2013). Analysis of 1-cell to >16 cell-embryos

positive for the marker expression revealed that pDRN:n2xGFP:DRN 3'UTR expression in the *prp8a-12* mutant proembryos was not impaired (Fig. 6A-C, J). Contrarily, similar analysis with the suspensor cell specific marker, pAT5G42200:n3xGFP, revealed more than half of the *prp8a-12/+* embryo population were not expressing the suspensor cell fate marker (Fig. 6D-F, K). The expression of the double marker, pWOX2-H2B::sGFP;pWOX2-::dTomato-LTI6b in the proembryo, showed no significant differences between wild type and *prp8a-12/+* mutant embryo populations (Fig. 6G-I, L). Our results imply that *prp8a-12* mutation initially impacts more on suspensor development, which likely leads to embryo proper arrest at the globular-to-heart transition. Why WOX2 expression was not impacted similarly as pAT5G42200 in suspensor cells might be explained by the differential severity of mis-splicing (Fig. 5A, B) of different genes including transcriptional activators of the marker genes used here.

Discussion

This study has revealed a previously unknown role of PRP8a as a core subunit of the U4/U6.U5 tri-snRNP complex. Polysome profiling coupled with *in situ* hybridisation and qRT-PCR demonstrated that PRP8a transcripts reside in non-translating 80S monosomal fraction during pollen tube growth and that significant fraction of these transcripts is delivered to the zygote and central cells most likely via sperm cells. Unlike its interactors and modulators of the tri-snRNP complex, such as CLOTHO (CLO)/GAMETOPHYTIC FACTOR 1 (GFA1, Coury et al., 2007; Moll et al., 2008; Liu et al., 2009) and BRR2 (Liu et al., 2009), as well other core components of the spliceosome complex such as LACHESIS (LIS, Gross-Hardt et al., 2007) and ATROPOS (ATO, Moll et al., 2008), which all are gametophytic lethal, *prp8a-12* or a double mutant with its homolog, *prp8b-1,-2, or prp8b-3*, showed no significant gametophytic function (Kulichová et al. 2020). Collectively, these features hinted on a function of PRP8a post-fertilisation as previously reported (Schwartz et al. 1994, Bayer et al., 2009). Indeed, we verified that PRP8a is required for embryo patterning and development by regulating splicing of dozens of embryo related developmental genes (Fig. 5, Chapter 2.5). We have also shown that a slight imbalance in PRP8a expression levels is lethal for embryo patterning (Fig. 4, Chapter 2.5). The mechanism through which excess PRP8a levels affect embryogenesis is yet to be demonstrated. Furthermore, overexpression of PRP8a::GFP fusion under the 35S promoter caused even more severe seed phenotype, with only few seedlings

recovered from antibiotic selection. None of the resistant seedlings had detectable GFP signal in sporophytic or gametophytic tissues. This might be explained by post-transcriptional turnover of the PRP8a::GFP hybrid transcripts allowing only the translation of the antibiotic selection marker as a non-toxic unit. Such strong ectopic overexpression is probably even more toxic and caused embryo lethality of transformed plants.

Moreover, we have shown that PRP8a regulates correct splicing of several embryo developmental genes to regulate embryo patterning. It is almost certain that PRP8a regulates splicing of an array of other genes essential for embryogenesis. Therefore, a genome wide study with null mutant embryos at various developmental stages will provide a better insight on how PRP8a is recruited to impose embryo development and patterning. In light of this for instance, we have seen that DORNORSCHEN (a proembryo marker) and AT5G42200 RING/ U-box protein showed slight differences in severity on their splicing defects (Fig. 5B). This might explain the loss in suspensor cell fate over proembryo cell fate hypothetically. Why *prp8a-12* affected more suspensor cell fate and not proembryo cell fate (at least with respect to AT5G42200 RING/U-box protein expression) is not clear yet (Fig. 5). One possibility is, since suspensor cells inherit the bulk of parental-by-products after the first asymmetric division, this could lead to improper transcriptional activation of suspensor cell fate genes (directly or indirectly) including AT5G42200 RING/U-box expression. It will be interesting to compare the occurrence of the splice defects between suspensor-specific genes with those specifying proembryo cell fate in *prp8a* mutant. In parent-of-origin conflict, the paternal influence seems concerted towards suspensor development. We have shown here that PRP8a is delivered via paternal gametes and appears to contribute the bulk of the transcripts to developing embryo. Such a depletion of PRP8a would be expected to impact primarily suspensor development and consequently proembryo development.

Lastly, the clarity on when zygotic gene expression is initiated in plants seems not fully resolved. The study by Nodine and Bartel (2012) used the trans-activation system and performed reciprocal crosses which neatly demonstrated immediate activation of the reporter within few hours after fertilisation, supporting the bi-parental genome activation and equal maternal-to-paternal contribution. One questionable scenario in this result is that both promoters used to drive the expression of LhG4 transcription factor, RPS5A and UB13, are expressed in pollen and pollen tubes, with RPS5A showing extreme abundance; therefore

could it still be possible that the immediate activation of the reporter GFP post-fertilisation be due to (or at least partly) inherited LhG4 transcripts and/or proteins rather than its *de novo* zygotic activation? We certainly can not dismiss that the expression of paternally inherited PRP8a allele is simultaneously activated on top of the paternally inherited PRP8a transcripts to initiate spliceosome activities of newly transcribed genes in zygote (Fig. 2, Fig. 6, PRP8a unpublished chapter). Therefore, the paternally derived PRP8a-GFP transcripts we have detected at the 2-cell stage embryos and later could be a product of both events. The dataset from Autran et al., (2012) convincingly implies bulk paternally-derived PRP8a transcript inheritance post-fertilisation, whereas the dataset from Nodine and Bartel (2012) shows a slight underrepresentation of maternal contribution between 1-cell/2-cell stage and 8-cell stage embryos (Fig. 1H). The general trend observed by Nodine and Bartel (2012) was that majority of genes increased abundance >4-fold between 1-cell/2-cell stage and 8-cell stage embryos. If we eliminate technical variability and a probability that the trend observed with PRP8a expression happened by chance, PRP8a transcript abundance showed marginal paternal bias at the 8-cell stage embryos with a likely reduction in total transcripts levels (Fig. 1H). Considering the egg cell with its larger cytoplasm (favouring maternal PRP8a inheritance), this observation is unlikely to be by chance. An alternative view is, this also hints towards inconsistency if PRP8a expression was a *de novo* zygotic expression which is expected to increase at the 8-cell stage embryos as much as > 4-fold (Nodine and Bartel, 2012). Taking this into consideration, both datasets hint towards a likelihood of paternal PRP8a inheritance. To elaborate and precisely demonstrate the exact contribution of paternally inherited PRP8a transcripts over *de novo* PRP8a zygotic transcriptional activation, similar crosses should be performed with PRP8a expression driven by a pollen-specific promoter that is inactive post fertilisation and during embryogenesis. Nevertheless, as an exception (similar to SSP in this case), inheritance of PRP8a transcripts is almost a must as of our current knowledge. The reason being, since PRP8a role in spliceosome places it at the core of the RNA biosynthesis cascade and the beginning of cellular function, such type of regulators are likely of “inherited nature” essential to “kick start” the new life of the zygote, including processing of zygotic *de novo* transcriptional products. A plausible antagonistic argument would be to propose an exclusive/biased transcription of intron-less small genes

(that would allow efficient translation with minimal translation machinery) to "kick-start" cellular life without a need of spliceosome activities.

Figures

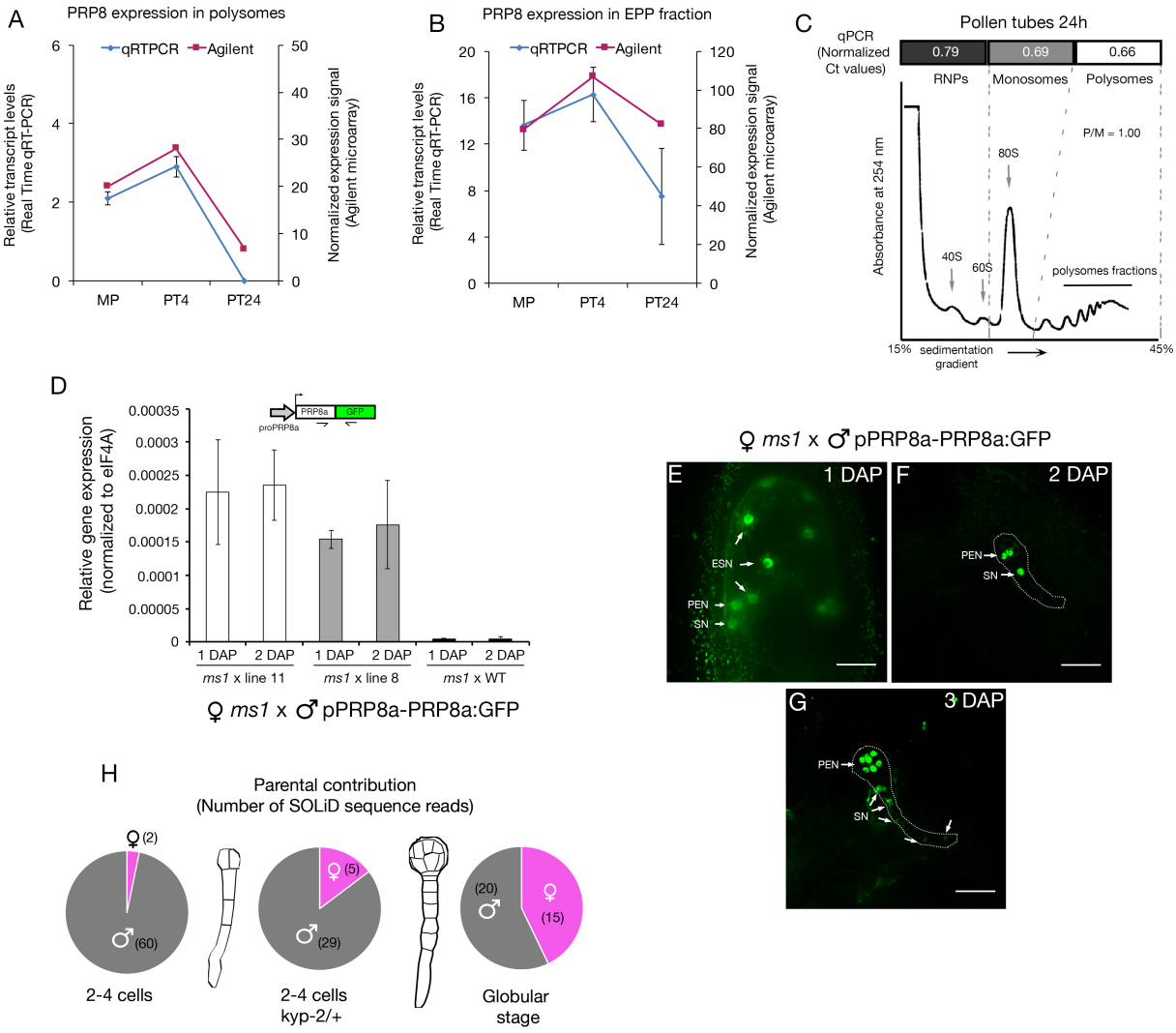

Figure 1. Subcellular distribution of PRP8a-transcripts between polysomes and monosomes (EPP) fractions and mRNA inheritance post fertilisation. (A-B) Predominant AtPRP8a homolog (NtPRP8) transcript abundance in tobacco, in monosomes (EPP) mRNA storage particles verified by quantitative RT-PCR. MP; mature pollen, PT4; 4 hrs *in vitro*-grown pollen tubes, PT24; 24 hrs *in vitro*-grown pollen tubes (C) Steady translation of pollen-stored NtPRP8 transcripts observed during *in vitro*-grown pollen tube growth by polysome profiling. The heatmap above the profiler shows qRT-PCR results from respective fractions with Ct values normalised to "TATAA spike" RNA. P/M is the ratio of translating polyribosomes to monosomes. (D) Hybrid transcripts (used primers are shown in a scheme above) were detected one and two days after pollination (1-2 DAP) with pollen grains expressing

pPRP8a-PRP8a::GFP fusion. *ms1/+* pollinated with WT Col-0 was used as a control. (E-G) Corresponding GFP signal was also visible in the 1-2 DAP nuclei of developing embryo proper (PEN), suspensor cells nuclei (SN) and nuclei of the endosperm (ESN). Two independent transgenic lines, line 8 and line 11, were used to perform the crosses. Confocal images are Z-projections of multiple optical sections. Scale bar = 30 m. SN, suspensor nuclei; PEN, proembryo nuclei; ESN, syncytium endosperm nuclei. (H) Venn diagrams of deep-sequencing based RNA profiling showing bulk paternal AtPRP8a transcript contribution to early embryo developmental stages according to Autran et al., 2012, consistently in wild type or in *kryptonite* epigenetic mutant embryos (*kyp,* an *SUVH4* histone methyltransferase imposing chromatin silencing and transcriptional repression).

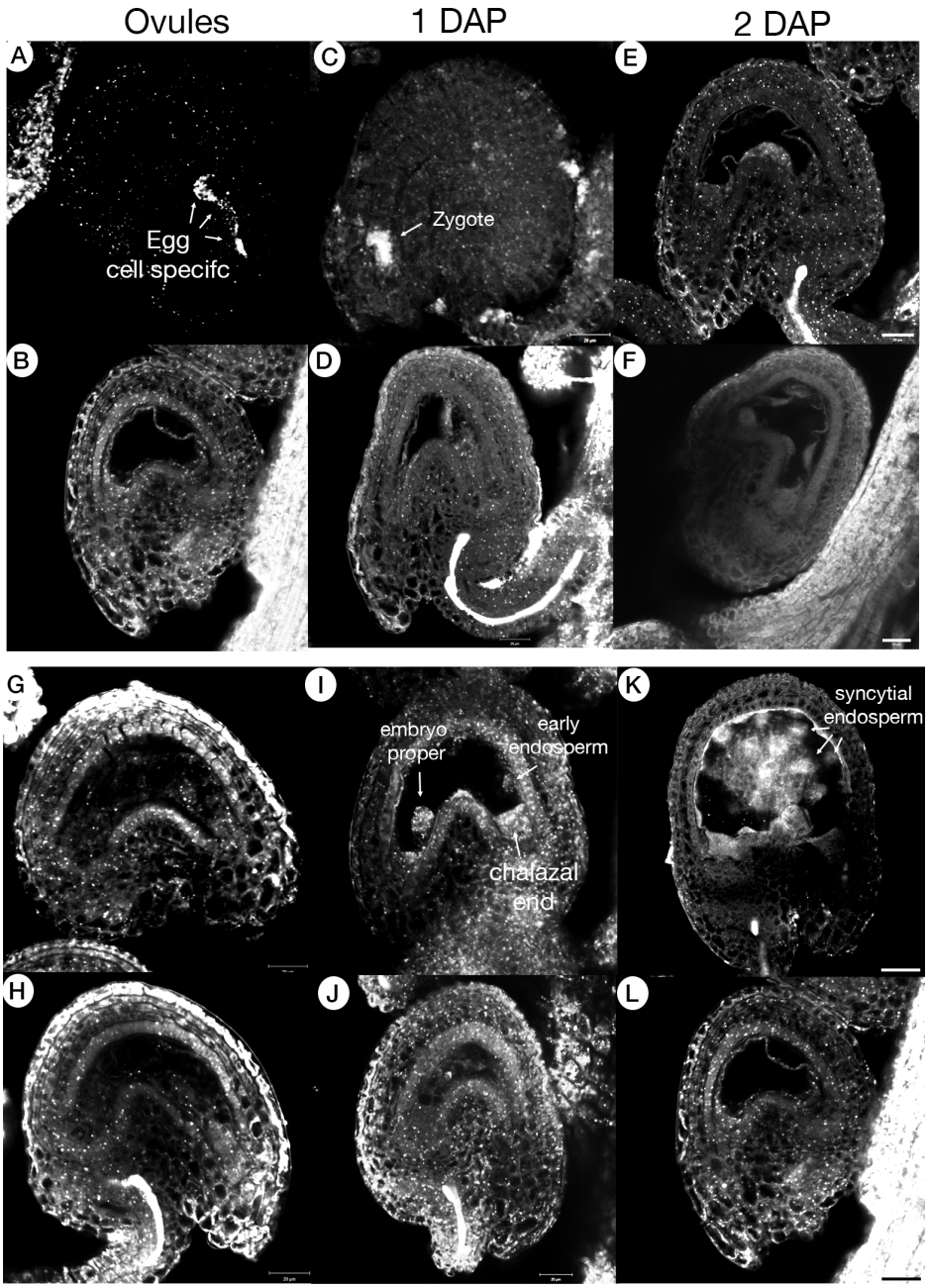

Figure 2. Detection of paternal PRP8a-GFP mRNA inheritance before and 1-2 days post pollination by *in situ* hybridisation. Expression pattern of PRP8a-GFP and native EC1.1 mRNA in seeds pollinated with pPRP8a-PRP8a:GFP expressing pollen grains. Approximately 500 bp probe spanning 3'-end of PRP8a 24th exon and the 5'-end of GFP (hybrid probe) was used for fluorescent whole mount *in situ* hybridisation and a 300bp probe for native EC1.1 detection. Egg cell specific 1 (EC1.1) was used as a marker to follow ontogeny of embryogenesis progression. (A, C) Detection of EC1.1 expression by the antisense probe in mature ovules specifically in the cytoplasm of the egg cell and 1 DAP likely in the newly formed zygote. (E) EC1.1 was undetectable 2 DAP in our conditions. (B, D, F) Corresponding EC1.1 detection at similar stages by sense probe as negative controls. (G, I and K) Contrary, paternally originated PRP8a-GFP transcripts were not detected in unfertilised ovules but

consistently detected from 1 DAP specifically in embryo proper, the chalazal end of the seed and in syncytial endosperm 2 DAP. (H, J, L) are corresponding PRP8a-GFP sense probes negative control. Scale bars = 20 m.

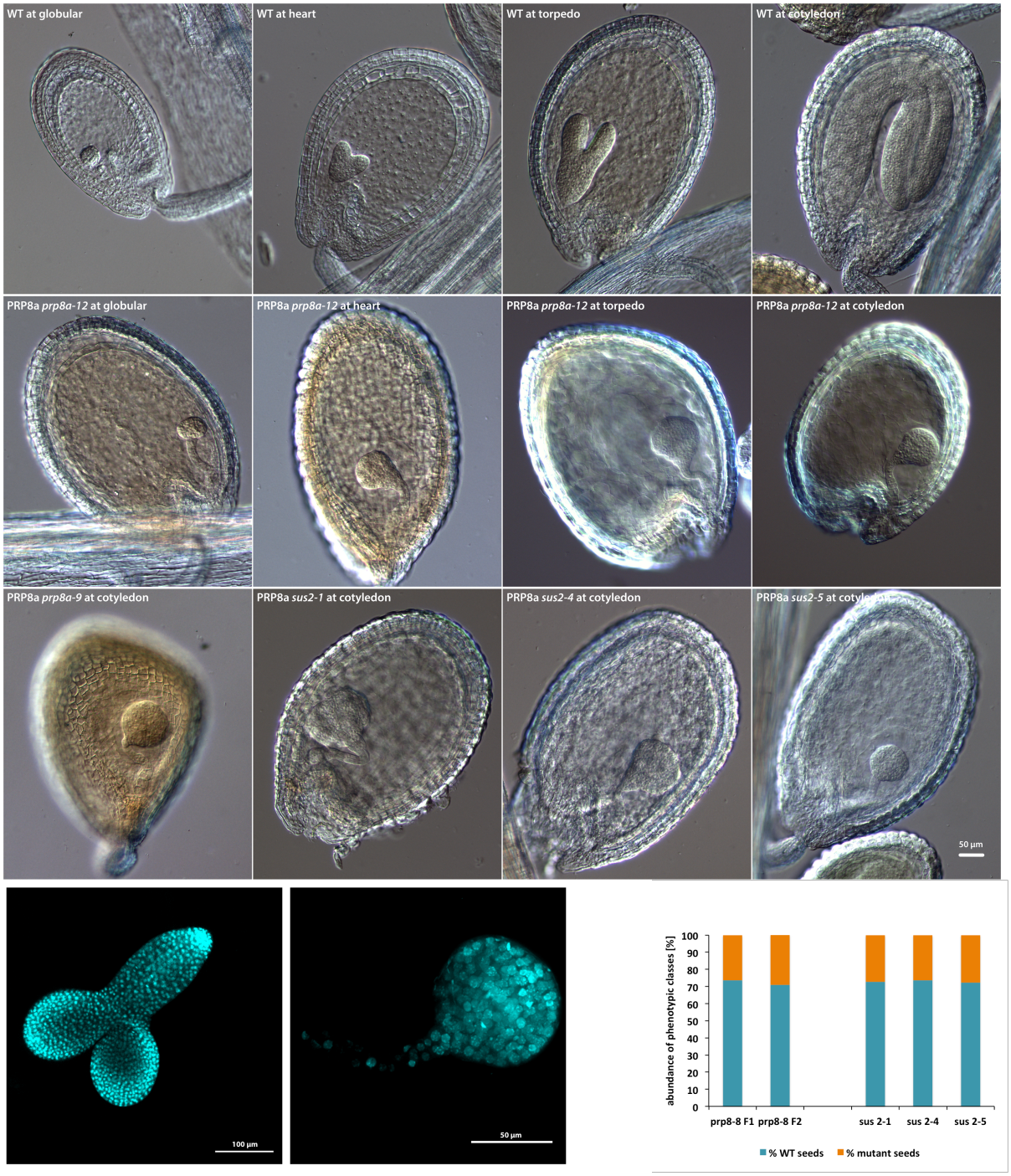

Figure 3. Embryo defects of *prp8a-12* observed at different stages of embryo development. Chart represents quantification of pale mutant seeds in two subsequent generations of *prp8a-12* alongside original three *prp8a* alleles (source: www.seedgenes.org). DAPI nuclear staining of WT Col-0 at torpedo stage embryo alongside the *prp8a-12* embryo.

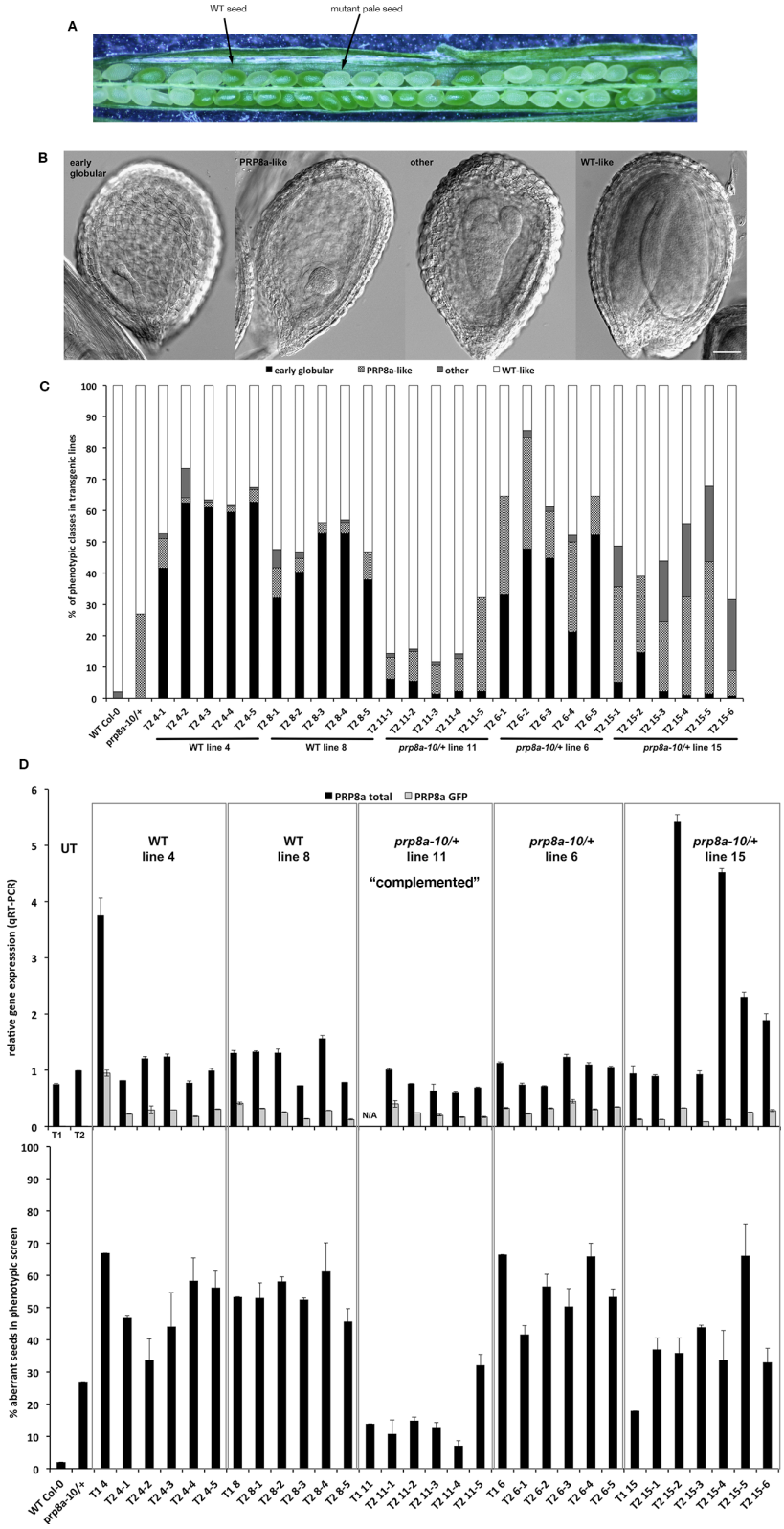

Figure 4. Imbalance of PRP8a expression levels induces a repertoire of embryonic defects. (**A**) Representative dissected silique showing average frequency of the mutants seeds observed in transgenic lines. (**B**) Embryo phenotypic classes induced following introduction of pPRP8a-PRP8a::GFP construct into wild type Col-0 and *prp8a-12*/+ lines for complementation. Category of

"other" phenotypes constitute three-cotyledon embryos and embryos of various developmental defects at the transition from heart to torpedo stage, N > 3000. (**C**) Charts depict quantification of individual phenotypic classes. (**D**) Correlation between total PRP8a transcripts levels (top chart) with the abundance of embryo-lethal phenotypes (bottom chart). qRT-PCR measurements were done in three biological and two technical replicates. Seed count, N> 4600; UT, untransformed WT Col-0; T1, transgenic parent lines; T2, progenies of T1 at the second generation.

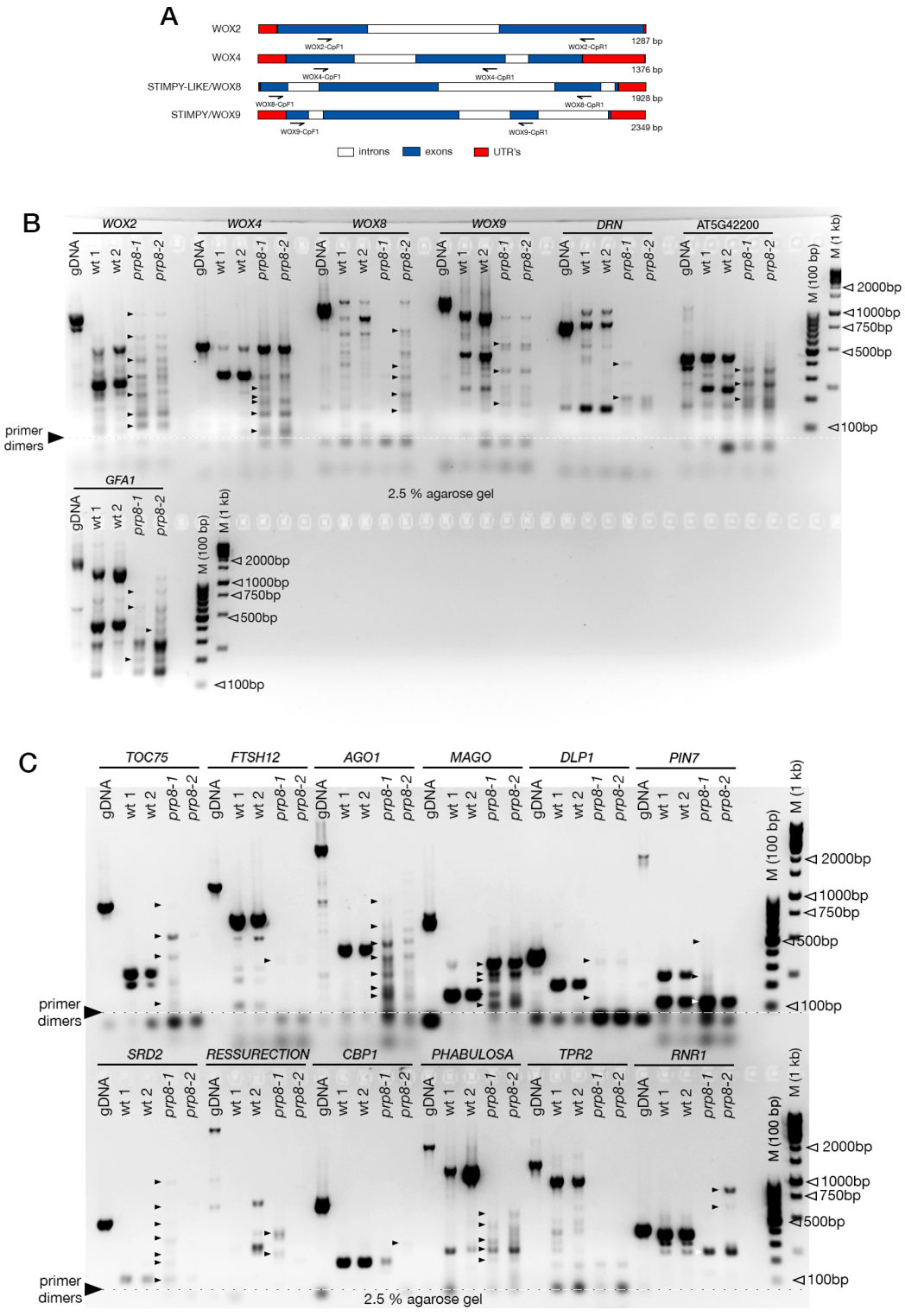

Figure 5. *prp8a-12* mutation causes widespread splicing defects of embryogenesis-related genes. (**A-B**) Schematic mapping of *prp8a-12* splice defects of WUSCHEL-related homeobox genes (WOX) in *prp8a* embryos arrested at globular-to-heart transition. Scheme shows primers gene span, arrowheads mark aberrant splice isoforms that were not observed in wild type at similar stage in biological replicates (**B-C**).

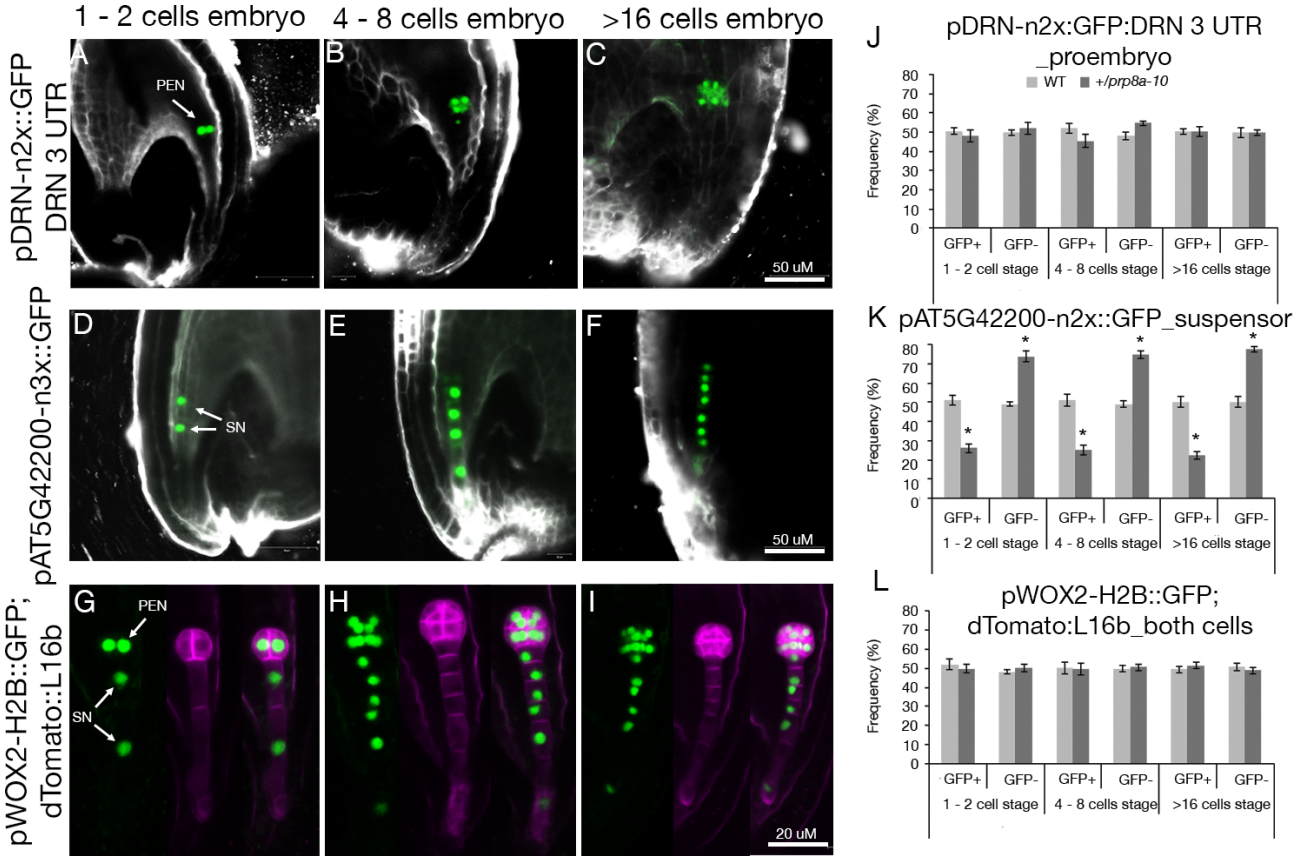

Figure 6. Suspensor cell fate is lost in *prp8a-12* mutant embryos. Defects in suspensor cell fate specification in *prp8a-12* mutant embryos identified using suspensor-specific E3 ubiquitin-protein ligase ATL23 (AT5G42200)-GFP marker. (**A-I**) Specificity of the cell fate markers used during embryogenesis obtained by showing confocal imaging of (**A-C**) proembryo (**D-F**) suspensor cell and (**G-I**) a double cell fate marker expression in dissected wild type embryos. The L16-dTomato marks plasma membrane of the developing embryo. (**J-L**) Quantification of cell fate specification in developing embryos of wild type and *prp8a*-12/+ mutant plants showing comparable expression of (**J**) proembryo and the double marker (**L**) but a reduction in expression of suspensor specific marker in *prp8a*-12/+ plants (**K**). Asterisks in (**K**) mark significant differences between mutant and wild type frequencies, Welch's unpaired t-test (*P < 0.01).

Materials and Methods

Cloning strategies

Full-length version of AtPRP8a containing promoter and coding sequence with/without stop codon was amplified using the Phusion polymerase (New England Biolabs) according to the manufacturer's instructions. The amplified fragment was cloned into the pENTR/D-TOPO vector (Invitrogen, Life Technologies) and after verification recombined into the destination vector pK7FWG,0 bearing the eGFP marker. This vector was transformed into Arabidopsis WT plants via floral dipping (Clough and Bent, 1998) to study protein localisation and into *prp8a-12/+* plants for mutant complementation. Both construct versions (with and without stop codon in PRP8a) were used for complementation. Plants were screened in two generations for the presence of embryo-lethal phenotype.

Polysome profiling

Polysomes from tobacco mature pollen grains and 4 hrs *in vitro*-cultivated pollen tubes were isolated with freshly prepared polysome extraction buffer (0.2M Tris-HCl, 0.2M KCL, 0.25M EGTA, 0.35M $MgCl_2$, detergent mix [20% Brij-35, 20% Triton X-100, 20% Igepal, 20% Tween 20], 1% deoxycholate, 1% PTE, 5uM DTT, 10ug/mL cycloheximide, 5ug/mL chloramphenicol, 1x MG132 (Sigma) and 10uL/mL enzymatic cocktail (Sigma). After pulverisation with a mortar and pestle, x3 volumes of polysome buffer was added to each sample and incubated on ice for 10 minutes. Samples were centrifuged at 17000g for 10 minutes at 4°C. Additional 10 minutes centrifugation was performed to clarify the samples. Polysomes were loaded on top of a 15-45% sucrose gradient prepared by BIOCOMP gradient master (BioComp instruments) containing (1.32M sucrose, 1x sucrose salts [0.04M Tris-HCl, pH 8.4, 0.02M KCl and 0.01M $MgCl_2$]), 5ug/mL chloramphenicol and 10ug/mL cycloheximide. Ultracentrifugation was performed with Beckman Optima XPN-80 at 30,000 RPM for 3.5 h at 4°C without brake. Fractions were collected using Brandel peristaltic pump (BRANDEL, UK) and Foxy R1 collector (Teledyne ISCO, USA) and polysome profiles were recorded using UA-6 UV/VIS detection system with 254nm filter (Teledyne ISCO). All fractions were flash frozen and stored at -80°C until use.

Microscopy

For mutant embryo phenotypic screening, seeds were cleared in a solution of chloral hydrate with glycerol and water. The length of clearing was optimised based on the age of seeds, but overnight clearing was sufficient for all developmental stages. Samples were observed under the DIC optics on a Nikon TE-2000 microscope. The images were processed in the NIS Elements software (LIM). Confocal images were taken on a Nikon Eclipse Ti confocal microscope equipped with with CSU-X1 spinning disk module and Andor iXon3 EMCCD camera. Images were analysed and assembled with ImageJ/Fiji (http://imagej.net/http://fiji.sc/Fiji), Adobe Photoshop CS6 (www.adobe.com), Ink-scape (www.inkscape.org) and NIS Elements (LIM) software.

Isolation of polysomes and EPP subcellular fractions

To fractionate polysomes and EPP complexes from *in vitro* cultivated pollen tubes, 150 mg of pollen tube pellets were homogenised with low salt (LS) buffer buffer (200 mM Tris-HCl pH 9, 25 mM KCl, 60 mM MgOAc, 2 mM DTT, 0.5 mM PMSF, 1% PTE, 1mM Cykloheximide, 250 mM Sucrose). The homogenates were centrifuged twice for 10 min and 15 min (Sigma, 2-16 K, 12141-H rotor, 400g followed by 20,000g respectively, 4 °C) to remove cellular debris. Post-mitochondrial supernatant was loaded on a 30% sucrose cushion with LS gradient buffer (40 mM Tris-HCl pH 8,5, 15 mM KCl, 30 mM MgOAc, 2 mM DTT, 0.5 mM PMSF, 1 mM Cykloheximide, 30% Sucrose) and centrifuged for 3h 20 min at 4 °C (Beckman Optima XPN-80 ultracentrifuge, 70.1 Ti rotor, 57 000 rpm). To separate polysomes and EPP complexes, the pelleted fraction was resuspended in a high salt EPP buffer (HSEP) (200 mM Tris-HCl, pH 9.0, 500 mM mM KCl, 2 mM MgOAc, 2 mM DTT, 0.5 mM PMSF, 1% PTE, 50 mM EDTA, pH 8.0, 0.2 mM puromycin, and 250 mM sucrose), loaded on a 30% sucrose cushion with HSEP gradient buffer (40 mM Tris-HCl pH 8.5, 200 mM KCl, 1 mM MgOAc, 2 mM DTT, 0.5 mM PMSF, 50 mM EDTA, pH 8.0, 0.2 mM Puromycin, 30% Sucrose) and centrifuged for 3h 20 min at 4 °C (Beckman Optima XPN-80 ultracentrifuge, 70.1 Ti rotor, 57 000 rpm). Sedimented pellet constitute of EPP complexes was collected, rinsed with RNAse free water and stored at -80 °C. The remaining supernatant containing lighter fraction was centrifuged further for 18 hr (Beckman Optima XPN-80 ultracentrifuge, 70.1 Ti rotor, 53 000

rpm). The obtained pellet constituted polysomes fraction was rinsed with RNAse free water and stored at -80 °C.

For total RNA isolation, three pellets of polysomes fraction were pooled and a single pellet from EPP complexes was used. Total RNA was isolated using the Qiagen RNeasy Plant Kit in accordance with the manufacturer's instructions (Qiagen, Valencia, CA). RNA was quantified using NanoDrop (Thermo Scientific, Wilmington, USA).

RNA extraction and qRT-PCR analysis

Tissue samples were collected from WT and prp8a-12/+ plants and frozen in liquid nitrogen. RNA was extracted using RNeasy Plant Mini Kit (Qiagen) and treated with RQ1 RNAse-free DNase I (Promega). For AtPRP8a expression profile in WT, first strand cDNA synthesis was conducted using ImPromII Reverse Transcription System (Promega). For use in quantitative RT-PCR, cDNA was synthesised using recombinant M-MLV reverse transcriptase (Promega) because of higher efficiency of the enzyme for long transcripts. qRT-PCR measurements were obtained using LightCycler 480 Instrument (Roche). Primers were designed to distinguish between Arabidopsis PRP8a and PRP8b genes. Specificity of the primers was verified by sequencing of purified PCR products. For tobacco PRP8, we could not design specific primers to distinguish the four gene copies. All measurements were conducted in three biological and two technical replicates. Polyubiquitin 10 (AT4G05320) was used as a reference for semi quantitative RT-PCR and elongation factor 1-alpha 4 (AT5G60390) was used as a reference for qRT-PCR.

For RNA extraction from polysome fractions, frozen samples were equilibrated to room temperature and universal spike RNA (TATAA Biocenter) was added to each sample. SDS was added to a final concentration of 1%. One volume of phenol/chloroform (2.5:1) was added and samples were incubated for 10 min at 65°C with occasional vortexing. Samples were cooled on ice for 5 min and spun at 14000 RPM for 5 min at 40°C. Aqueous layer was removed and the phenol/chloroform precipitation was repeated as above. The final aqueous layer was mixed with x1 volume of chloroform/isopropanol (25:1), vortexed for 1 min, incubated for 1 min at room temperature and spun for 2 min at 14000 RPM at 40°C. To the aqueous fractions, 300mM NaAoC and 2 uL Glycogen (Invitrogen) were added and mixed

with 2.5 volumes of 100% ethanol. RNA was precipitated overnight at -200°C. Samples were then spun for 45 min at 14000 RPM at 40°C. RNA pellets were washed with 75% ethanol. Dried pellets were resuspended in 20uL Tris pH8 and RNA concentrations were determined by Nanodrop (ThermoScientific). For quantitative RT-PCR analysis of each isolated fraction, total RNA was DNase treated (Ambion, Thermo Fischer Scientific) and first strand cDNA was synthesised using ImPromII Reverse Transcription System (Promega). qPCR measurements were obtained using LightCycler 480 Instrument (Roche). Ct values from each fraction were normalised with TATAA RNA spike crossing point.

Detection of paternally inherited PRP8a in developing embryo

For detection of PRP8a:GFP hybrid transcript and protein, two transgenic lines were crossed into *ms1* background. Line 8 was selected from GFP-localisation lines in WT Col-0 and Line 11 were WT plants segregated from complementation Line 11. Two lines were selected because of their differential abundance of PRP8a:GFP transcript levels and differential induction of embryo-lethal phenotypes (described in section about mutant complementation). Pollinated pistils were collected after 1 or 2 DAP (days after pollination) and frozen in liquid nitrogen for subsequent RNA extraction using RNeasy Plant Mini Kit (Qiagen). RNA samples were treated with RNase-free DNase 1 (Promega) and reverse-transcribed using M-MLV Reverse Transcriptase (Promega). qRT-PCR was measured on LightCycler 480 (Roche) in three biological and two technical replicas. Elongation factor 1alpha was used as a reference gene for data normalisation. For PRP8a::GFP protein detection, 1DAP and 2 DAP siliques were dissected and immature seeds mounted in water were used for imaging on Nikon Spinning Disc Confocal Microscope.

Probe synthesis

To detect paternal PRP8a-GFP transcript inheritance post-fertilisation, 500 bp fragment spanning 3'-end of PRP8a 24th exon and the 5'-end of GFP (hybrid probe) were amplified and cloned into the pCRTM-Blunt II-TOPO (ThermoFisher) vector. EC1.1 clone was a gift from Andrea Bleckmann (Regensburg university). Appropriate vectors were linearised and antisense and sense run-off transcripts were synthesised *in vitro* with SP6- and T7- RNA polymerases respectively. Digoxigenin labelled UTP (DIG-11-UTP) was used for labelling the

probes (DIG RNA Labeling Kit: Roche, cat. No. 11175025910). Synthesised probes were purified phenol:chloroform and precipitated in the presence of Glycogen for 3 h at -20 ^{0}C. The pellet was rinsed with 70% ethanol in RNAse-free water and resuspended in 50 L RNAse free water. Probes concentration was estimated with Nanodrop spectrophotometer (Thermosfisher) and quality controlled by agarose gel electrophoresis. Verified probes were stored at -80 ^{0}C.

Fluorescent whole mount *in situ* hybridisation (F-WISH)

Fluorescent in situ hybridisation was performed according to Bleckmann et al. (2015) with minor modifications. Pistils containing unfertilised ovules and ovules from pollinated pistils one and two days after pollination (1-2 DAP) were dissected with a 25 G needle. Whole transmitting tract with attached ovules were transferred to a medium well baskets and vacuum infiltrated with 1:1 fixative:n-Heptan (4% (w/v) Formaldehyde (freshly prepared from paraformaldehyde), 15% (v/v) DMSO and 0.1% (v/v) Tween 20 in PBS [0.13 M NaCl, 7.0 mM Na2HPO4, 3.0 mM NaH2PO4 (pH 7.4); 1% DEPC-treated]:n-heptan) for 10 min. Samples were incubated for 1 h at room temperature with gentle agitation. Fixed tissues were then rinsed in methanol (3x for 5 min) followed by 2x ethanol washes for 5 min each. Fixed tissues were stored in -20 ^{0}C until further processing. To degrade endogenous peroxidase, fixed tissues were incubated for 1 h in freshly prepared 3% (v/v) H_2O_2/methanol followed by two ethanol washing steps of 5 min each. To aid with probe permeabilisation and removal of chlorophyll, waxes and lipids, samples were incubated in a 1:1 mixture of ethanol:Histo-Clear (Sigma) for 30 min. Samples were then dehydrated in ethanol/PBS series with a 20 min intervals, re-fixed for 20 min with fixative and finally resuspended in PBST (PBS with 0.1% Tween 20). To expose target transcripts and aid with probe binding, tissues were digested with 150 µg/mL proteinase K in 0.1% Sodium dodecylsulfate (SDS) for 15 min at 37 ^{0}C. Proteinase K activities were terminated with 0.2% (w/v) glycine in PBS. Samples were then incubated in prehybridisation mixture (PHM) (50% (v/v) formamide, 5x SSC [0.75 M NaCl, 75 mM sodium citrate (pH 7.0); 1% DEPC-treated], 0.1% (v/v) Tween 20; 10% (v/v) heparin) for 1 h at 55 ^{0}C. Probe hybridisation was performed at 55 ^{0}C in hybridisation mixture (PHM, denatured and fragmented salmon sperm DNA at (1 mg/ml), digoxigenin (DIG) (Roche) labeled denatured RNA probe at 0.3 – 0.5 ng/mL) for 14 h. Excess probes were washed off

with wash solution 1 (50% (v/v) formamide, 2x SSC, 0.1% (v/v) Tween20) and incubated for 1 h, x2 with wash solution 2 (2x SSC, 0.1% (v/v) Tween 20) and x1 with wash solution 3 (0.2x SSC, 0.1% (v/v) Tween 20) at 20 min intervals. For Anti-digoxigenin antibody binding, samples were first rinsed x2 with TNT specimen buffer (0.1 M TRIS–HCl (pH 7.5), 0.15 M NaCl, 0.05% Tween 20), blocked in a blocking solution () for 1 h 30 min, and incubated with anti-DIG mixture (Anti-Digoxin-HRPO (1:1000) in 1% (w/v) BSA/PBS-T) for 10 h at room temperature. Unbound antibodies were washed off with TNT specimen buffer x8 at 10 min intervals. For signal detection and RNA localisation, samples were incubated in TSA Cy3 staining solution (TSA-Plus Stock Solution 1:50 in 1x Amplification Diluent (TSA-Plus-Cyanine3-Kit: PerkinElmer, cat. No. NEL744001KT) for 15 min at room temperature. Excess dye was rinsed x4 with TNT specimen buffer with 5 min intervals followed by x3 washes with 10 min intervals. Samples were mounted on 77% glycerol in PBS and analysed with Zeiss LSM 880 confocal microscope.

Detection of aberrant splice isoforms in *prp8a-12* embryos

To map splice defects events in the *prp8a*-12 mutant embryos, twenty siliques per sample from +/*prp8a*-12 plants were dissected and mutant seeds with embryos arrested at globular-heart transition were collected, flash frozen in liquid nitrogen and stored at -80 ^{0}C until RNA extraction. For wild type control, matured siliques were dissected first to estimate embryo developmental stage. Siliques from approximately 3 days after fertilisation (11-13 mm in length) contained majority of embryo at the globular-to-heart transitions were dissected and seeds were collected and stored at -80 ^{0}C. Total RNA was extracted (as above) from three biological replicates, DNAse treated for 45 minutes with RNase-free DNase 1 (Promega) and total cDNA library was generated using M-MLV Reverse Transcriptase (Promega). RT-PCR was performed using 1 l of 1/5 dilution of the cDNA library as a template for the PCR reaction. PCR conditions were as follow; 94 ^{0}C for 2 min followed by 35 cycles of 94 ^{0}C for 20 s, 55-58 ^{0}C for 30 s, and 72 ^{0}C for 1 m 30 s, and final 72 ^{0}C for 10 min. A set of WUSCHEL-related homeobox genes were selected based on literature search and use of publicly available seeds gene expression datasets. For the additional set of genes, a key word “embryogenesis” was used in the search at The Arabidopsis Information Resource database (TAIR). Obtained genes were handpicked based on functional categories and their expression

profiles to represent diverse functional categories. Final selection was drawn to represent genes with multiple spanning introns and literature search. Several primers were design per gene to span intron/s and different parts of the gene, 5'- and 3'- end with an average genomic fragment size of 1 kb. Primer pairs that positively mapped splice defects and were specific on genomic template were used to perform the final experiment.

Acknowledgements

We thank Andrea Bleckmann for F-WISH *in situ* protocol and discussion, Martina Laňková, Milada Čovanová and Jan Petrášek for assistance with Intavis InsituPro robot set up. We thank Gerd Jürgens (Max Planck Institute for Developmental Biology, Tübingen), Stefanie Sprunck (University of Regensburg), Daisuke Kurihara (Nagoya university) and Alexander Leydon (Brown university, Providence, RI) for cell fate markers. We thank Anna Heřmanová for assistance with polysome profiling (Institute of Microbiology ASCR, Prague), Karel Müller for help with qRT-PCR.

References

Andéol Y (1994) Early transcription in different animal species: implication for transition from maternal to zygotic control in development. Roux's Arch Dev Biol 204: 3–10

Autran D, Baroux C, Raissig MT, Lenormand T, Wittig M, Grob S, Steimer A, Barann M, Klostermeier UC, Leblanc O, et al (2011) Maternal Epigenetic Pathways Control Parental Contributions to Arabidopsis Early Embryogenesis. Cell 145: 707–719

Baroux C, Autran D, Gillmor CS, Grimanelli D, Grossniklaus U (2008) The maternal to zygotic transition in animals and plants. Cold Spring Harb Symp Quant Biol 73: 89–100

Bayer M, Nawy T, Giglione C, Galli M, Meinnel T, Lukowitz W (2009) Paternal control of embryonic patterning in Arabidopsis thaliana. Science 323: 1485–8

Bleckmann A, Alter S, Dresselhaus T (2014) The beginning of a seed: regulatory mechanisms of double fertilization. Front Plant Sci 5: 452

Bleckmann A, Dresselhaus T (2016) Fluorescent whole-mount RNA in situ hybridization (F-WISH) in plant germ cells and the fertilized ovule. Methods 98: 66–73

Castelli LM, Talavera D, Kershaw CJ, Mohammad-Qureshi SS, Costello JL, Rowe W, Sims PFG, Grant CM, Hubbard SJ, Ashe MP, et al (2015) The 4E-BP Caf20p Mediates Both eIF4E-Dependent and Independent Repression of Translation. PLoS Genet 11: e1005233

Clough SJ, Bent AF (1998) Floral dip: a simplified method forAgrobacterium-mediated transformation ofArabidopsis thaliana. Plant J 16: 735–743

Collier AE, Wek RC, Spandau DF (2015) Translational Repression Protects Human Keratinocytes from UVB-Induced Apoptosis through a Discordant eIF2 Kinase Stress Response. J Invest Dermatol 135: 2502–11

Coury DA, Zhang C, Ko A, Skaggs MI, Christensen CA, Drews GN, Feldmann KA, Yadegari R (2007) Segregation distortion in Arabidopsis gametophytic factor 1 (gfa1) mutants is caused by a deficiency of an essential RNA splicing factor. Sex Plant Reprod 20: 87–97

Evsikov A V., Graber JH, Brockman JM, Hampl A, Holbrook AE, Singh P, Eppig JJ, Solter D, Knowles BB (2006) Cracking the egg: molecular dynamics and evolutionary aspects of the transition from the fully grown oocyte to embryo. Genes Dev 20: 2713–2727

Gooh K, Ueda M, Aruga K, Park J, Arata H, Higashiyama T, Kurihara D (2015) Live-Cell Imaging and Optical Manipulation of Arabidopsis Early Embryogenesis. Dev Cell 34: 242–251

Groß-Hardt R, Kägi C, Baumann N, Moore JM, Baskar R, Gagliano WB, Jürgens G, Grossniklaus U (2007) LACHESIS restricts gametic cell fate in the female gametophyte of Arabidopsis. PLoS Biol 5: 0494–0500

Heyer EE, Moore MJ, Amrani N, Ganesan R, Kervestin S, Mangus DA, Ghosh S, Jacobson A, Arava Y, Wang Y, et al (2016) Redefining the Translational Status of 80S Monosomes. Cell 164: 757–69

Honys D, Combe JP, Twell D, Čapková V (2000) The translationally repressed pollen-specific ntp303 mRNA is stored in non-polysomal mRNPs during pollen maturation. Sex Plant Reprod 13: 135–144

Honys D, Reňák D, Feciková J, Jedelský PL, Nebesárová J, Dobrev P, Čapková V (2009) Cytoskeleton-associated large RNP complexes in tobacco male gametophyte (EPPs) are

associated with ribosomes and are involved in protein synthesis, processing, and localization. J Proteome Res 8: 2015–31

Huntzinger E, Izaurralde E (2011) Gene silencing by microRNAs: contributions of translational repression and mRNA decay. Nat Rev Genet 12: 99–110

Kulichová K, Kumar V, Steinbachová L, Klodová B, Timofejeva L, Juříček M, Honys D and Hafidh S (2020) PRP8a and PRP8b spliceosome subunits act coordinately to control pollen tube attraction in Arabidopsis thaliana. Development 147

Liu M, Yuan L, Liu N-Y, Shi D-Q, Liu J, Yang W-C (2009) GAMETOPHYTIC FACTOR 1 , Involved in Pre-mRNA Splicing, Is Essential for Megagametogenesis and Embryogenesis in Arabidopsis. J Integr Plant Biol 51: 261–271

Moll C, Von Lyncker L, Zimmermann S, Kägi C, Baumann N, Twell D, Grossniklaus U, Groß-Hardt R (2008) CLO/GFA1 and ATO are novel regulators of gametic cell fate in plants. Plant J 56: 913–921

Nodine MD and Bartel DP (2012) Maternal and paternal genomes contribute equally to the transcriptome of early plant embryos. Nature 482: 94–7

Pillot M, Baroux C, Vazquez MA, Autran D, Leblanc O, Vielle-Calzada JP, Grossniklaus U, Grimanelli D (2010) Embryo and endosperm inherit distinct chromatin and transcriptional states from the female gametes in Arabidopsis. Plant Cell 22: 307–20

Preissler S, Reuther J, Koch M, Scior A, Bruderek M, Frickey T, Deuerling E (2015) Not4-dependent translational repression is important for cellular protein homeostasis in yeast. EMBO J 34: 1905–1924

Rowe W, Kershaw CJ, Castelli LM, Costello JL, Ashe MP, Grant CM, Sims PFG, Pavitt GD, Hubbard SJ (2014) Puf3p induces translational repression of genes linked to oxidative stress. Nucleic Acids Res 42: 1026–41

Sasaki T, Kanno T, Liang S-C, Chen P-Y, Liao W-W, Lin W-D, Matzke AJM, Matzke M (2015) An Rtf2 Domain-Containing Protein Influences Pre-mRNA Splicing and Is Essential for Embryonic Development in Arabidopsis thaliana. Genetics 200: 523–35

Schier AF (2007) The maternal-zygotic transition: death and birth of RNAs. Science 316: 406–7

Schwartz BW, Yeung EC, Meinke DW (1994) Disruption of morphogenesis and transformation of the suspensor in abnormal suspensor mutants of Arabidopsis. Development 120: 3235–3245

Slane D, Kong J, Berendzen KW, Kilian J, Henschen A, Kolb M, Schmid M, Harter K, Mayer U, De Smet I, et al (2014) Cell type-specific transcriptome analysis in the early Arabidopsis thaliana embryo. Development 141: 4831–40

Spillane C, Schmid KJ, Laoueillé-Duprat S, Pien S, Escobar-Restrepo J-M, Baroux C, Gagliardini V, Page DR, Wolfe KH, Grossniklaus U (2007) Positive darwinian selection at the imprinted MEDEA locus in plants. Nature 448: 349–352

Tadros W, Goldman AL, Babak T, Menzies F, Vardy L, Orr-Weaver T, Hughes TR, Westwood JT, Smibert CA, Lipshitz HD (2007) SMAUG Is a Major Regulator of Maternal mRNA Destabilization in Drosophila and Its Translation Is Activated by the PAN GU Kinase. Dev Cell 12: 143–155

Tadros W, Lipshitz HD (2009) The maternal-to-zygotic transition: a play in two acts. Development 136: 3033–42

Wang QT, Piotrowska K, Ciemerych MA, Milenkovic L, Scott MP, Davis RW, Zernicka-Goetz M (2004) A Genome-Wide Study of Gene Activity Reveals Developmental Signaling Pathways in the Preimplantation Mouse Embryo. Dev Cell 6: 133–144

2.6. Unpublished chapter: EMB1441/AtNEMF has long-term stored transcripts in pollen and functions during embryogenesis

Katarína Kulichová, David Honys and Said Hafidh

My contribution: I have performed all of the experiments under the supervision of Said Hafidh, except for the EPP and polysome measurement, which was performed by Said Hafidh.

Abstract

Screening of tobacco microarray data for long-term stored transcripts in EPP particles (Hafidh et al. 2012a, 2012b) resulted in identification of a gene, whose homolog in Arabidopsis is annotated as EMBRYO DEFECTIVE 1441 (EMB1441, AT5G49930). Based on protein homology with human protein, EMB1441 is labelled as NEMF (nuclear export mediator factor) or NEMF-like in other plant species (here, we will address this gene as AtNEMF). AtNEMF, a single-copy gene in Arabidopsis, is well conserved among plant species and displays an embryo-lethal phenotype. However, it seems, that the SALK_090319 line of AtNEMF does not have gametophytic defects.

Introduction

Either errors occurring during gene expression or the action of damaging agents can lead to the synthesis of proteins with various forms of aberrations, from point mutations to truncations and extensions that are not coded by native open reading frames. Several quality-control machineries survey translation at multiple steps and handle defective proteins by mediating their folding, sequestration into compartments, or proteolysis via the ubiquitin-proteasome or autophagy pathways (reviewed in Filbeck et al. 2022). NEMF function has been described as a nuclear export mediator factor and a part of the ribosome quality control (RQC) complex. The substrates of RQC are ribosomes stalled during translation, specifically the dissociated large ribosomal subunits obstructed with a nascent-chain-tRNA conjugate that are recognized by the ribosome- and tRNA-binding protein NEMF and its orthologs in yeast and bacteria, Rqc2 and RqcH, respectively (Filbeck et al. 2022). Yeast Rqc2 binds to the inter-subunit surface of the 60S subunit in a manner that is mutually exclusive with the 40S

subunit, thereby specifically targeting free 60S particles while avoiding normally elongating ribosomes. Rqc2 also binds to the obstructing P-site tRNA, which stabilises the complex. Thus, the simultaneous binding of Rqc2 to the free 60S and P-tRNA informs that the 60S subunit is obstructed (Lyumkis et al. 2014). Once bound to the large subunit, eukaryotic NEMF orthologs promote proteolytic tagging by stabilising the binding of the Listerin (LTN1) E3 ubiquitin ligase to the ribosomal complex (Shao et al. 2015). Moreover, and more broadly across evolution, NEMF orthologs promote nascent-chain proteolysis by modifying them with C-terminal peptides (‘‘tails’’), with diverse functions having been described for the different organisms (reviewed in Filbeck et al. 2021). In eukaryotes, C-terminal tails have diversified their functions and, with the emergence of the ubiquitin system, work together with E3 ligases in signalling proteolysis. The best characterised in example is that of LTN1, which is an ancient E3 ligase found across eukaryotes. Eukaryotic NEMF orthologs have evolved an additional proteolytic function that is independent of C-terminal tailing but can nonetheless be stimulated by C-terminal tailing. This function is mediated by NEMF’s expanded M domain, which binds directly to LTN1 to stabilise its association with obstructed 60S subunits (Defenouillere et al. 2013, Shao et al. 2015, Shen et al. 2015).

Ahmed et al. (2021) identified the human NEMF gene as an important player in mammalian neuronal development, its mutation leading to central nervous system disorders. They further described that knock-down of NEMF led to impairment of axonal outgrowth and synapse development in cultured mouse primary cortical neurons.

Results

We have studied the T-DNA line SALK_090319 (Fig.1.) to assess the impact of NEMF mutation on Arabidopsis gametophyte development and embryogenesis. We found that these mutants show developmental arrest of embryos and unnatural proliferation of embryo proper cells at late globular stage resulting in embryo-lethal phenotype (Fig.2.). The abundance of aberrant seeds was 22-25% in two observed generations, which is similar to data obtained by D. Meinke from alleles *emb 1441-1* and *emb 1441-2* (22.7% and 27.2%, respectively, www.seedgenes.org). Transmission of the transgene is decreased through male to 77% and female to 75%, but the difference is not significantly different to expected efficiency (Fig.3.).

We studied viability of mature pollen grains and length of pollen tubes grown *in vitro* and in semi-*in vivo* conditions to test whether the mutation has impact on their fitness. We found no significant difference in phenotype, pollen viability or growth parameters compared to WT Col-0 plants (Fig.4.).

To address the ability of ovules to attract pollen tubes, *AtNEMF*/+ pistils were pollinated by pollen containing a pLAT52:GUS construct and stained for GUS activity 24 hrs after pollination. Targeting efficiency in AtNEMF was slightly decreased, but comparable to control *ms1*/+ plants (Fig.5.).

Aniline blue staining for detection of fertilised ovules was performed on self-pollinated *AtNEMF*/+ and WT Col-0 pistils and *ms1*/+ pistils pollinated by mutant and WT Col-0 pollen. Number of targeted ovules was calculated and showed no apparent difference in mutant compared to wild type controls (Fig. 5.). It seems, that the SALK_090319 line of AtNEMF does not have an impact on pollen or ovule fitness, or their ability to target and be targeted and fertilised.

Promoter of AtNEMF was fused with GUS marker to study gene expression in Arabidopsis (Fig.6.). Our observations are in concert with data from Arabidopsis eFP Browser (bar.utoronto.ca, Winter et al. 2007). In sporophytic tissues was the signal strongest in leaf hydatodes, tapetum of immature buds and in developing embryos and integuments. In gametophyte was the signal visible only in developing pollen grains, with the highest abundance in unicellular microspores and bicellular pollen, while in mature pollen grains the staining was barely detectable. This expression pattern hints at our hypothesis that AtNEMF could be transcribed and stored in EPP particles during pollen development and then later translated into protein, which can function during embryogenesis. Results from this experiment were confirmed by creating expression profile by semi-quantitative RT-PCR (Fig. 6.). Absence of the transcript in dissected mutant seeds of SALK_090319 line was confirmed by RT-PCR (Fig.7.). Our microarray data from tobacco subcellular fractions have been verified by qPCR (Fig.8.).

Conclusions

Our initial screen of transcriptomic data from tobacco mature pollen and pollen tubes (Hafidh et al. 2012a, 2012b) has shown few potential candidates with a specific profile of actively

translated vs stored transcripts. Several genes with annotated functions in embryogenesis had transcripts stored in EPP particles even after 24hrs of pollen tube growth *in vitro*. One of the promising candidates was EMB1441, which we later identified as AtNEMF due to its homology with known orthologs. Our gametophytic assays revealed normal fitness of both *AtNEMF*/+ gametophytes, including their growth and developmental parameters and ability to fertilise and produce offspring. However, when both alleles are missing, the embryo development is arrested at the globular stage and never develops further. These results suggest that the function of AtNEMF is essential for embryogenesis. The stored transcripts from pollen can be potentially delivered during the fertilisation to the ovule and can function in the very early stages of embryogenesis. However, the lack of new AtNEMF transcription after zygote formation leads to embryo arrest.

Figures

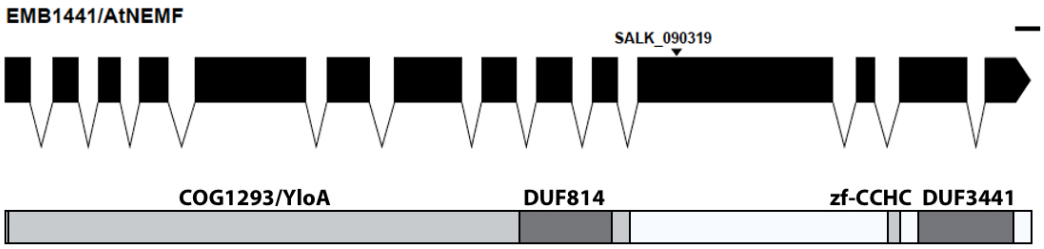

Figure 1. AtNEMF gene structure showing introns, exons and T-DNA line (arrow head) used for AtNEMF phenotypic screen. Below, a protein model depicting conserved domains (based on Pfam and COG prediction). Scale is 100 bp.

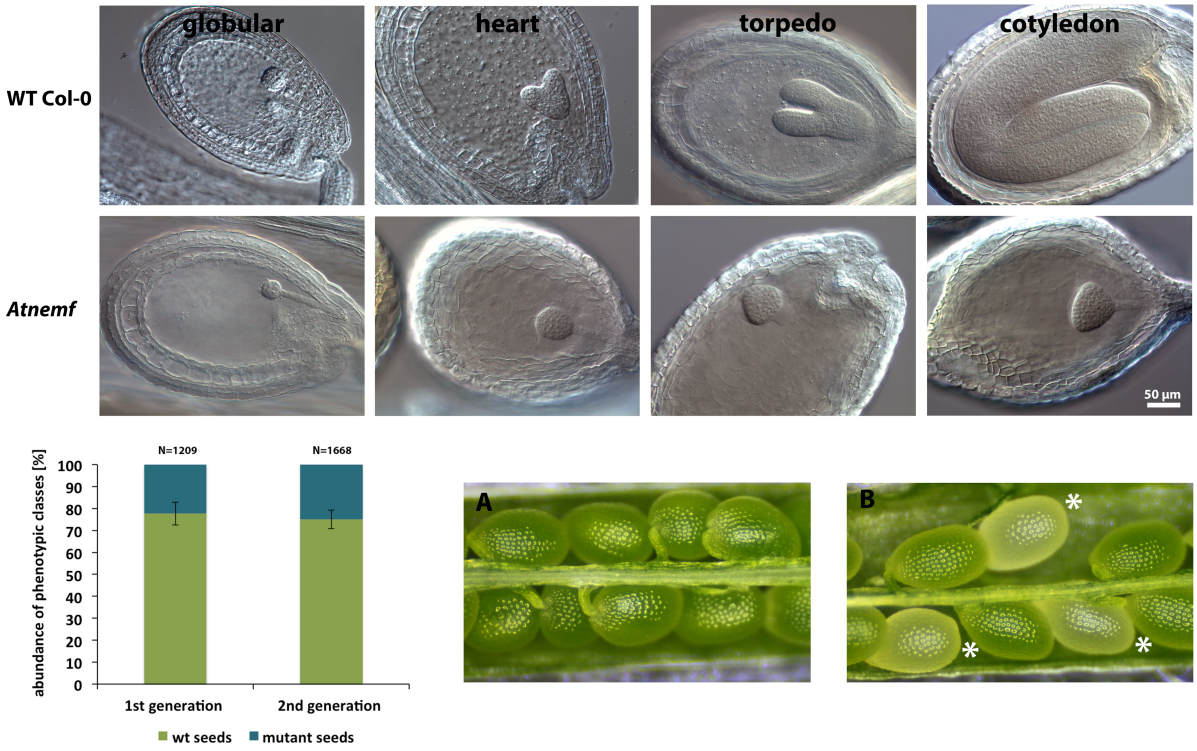

Figure 2. Embryo development in WT Col-0 and *Atnemf*/+ observed by DIC microscopy. A) WT seeds at cotyledon stage and B) seeds from heterozygous *Atnemf*/+ silique (mutants depicted by asterisk). Chart shows abundance of embryo-lethal phenotype in two observed generations. Bar represents 50 µm.

♀ WT x ♂ *AtNEMF/+*	total	ratio +/+:+/- (exp./obs.)	TEm	Chi-square	♀ *AtNEMF/+* x ♂ WT	total	ratio +/+:+/- (exp./obs.)	TEf	Chi-square
102 +/+ : 86 +/-	188	1:1/1:0.77	77%	NS	106 +/+ : 79 +/-	185	1:1/1:0.75	75%	NS

Figure 3. Transmission analysis of *Atnemf* mutant allele. The observed transmission efficiency of the T-DNA through male (TEm) and female (TEf) both are slightly decreased compared to expected ration 1:1, but the difference is not statistically significant. TE was calculated using formula: number of heterozygous (Nht)/number of wild type (Nwt) x 100.

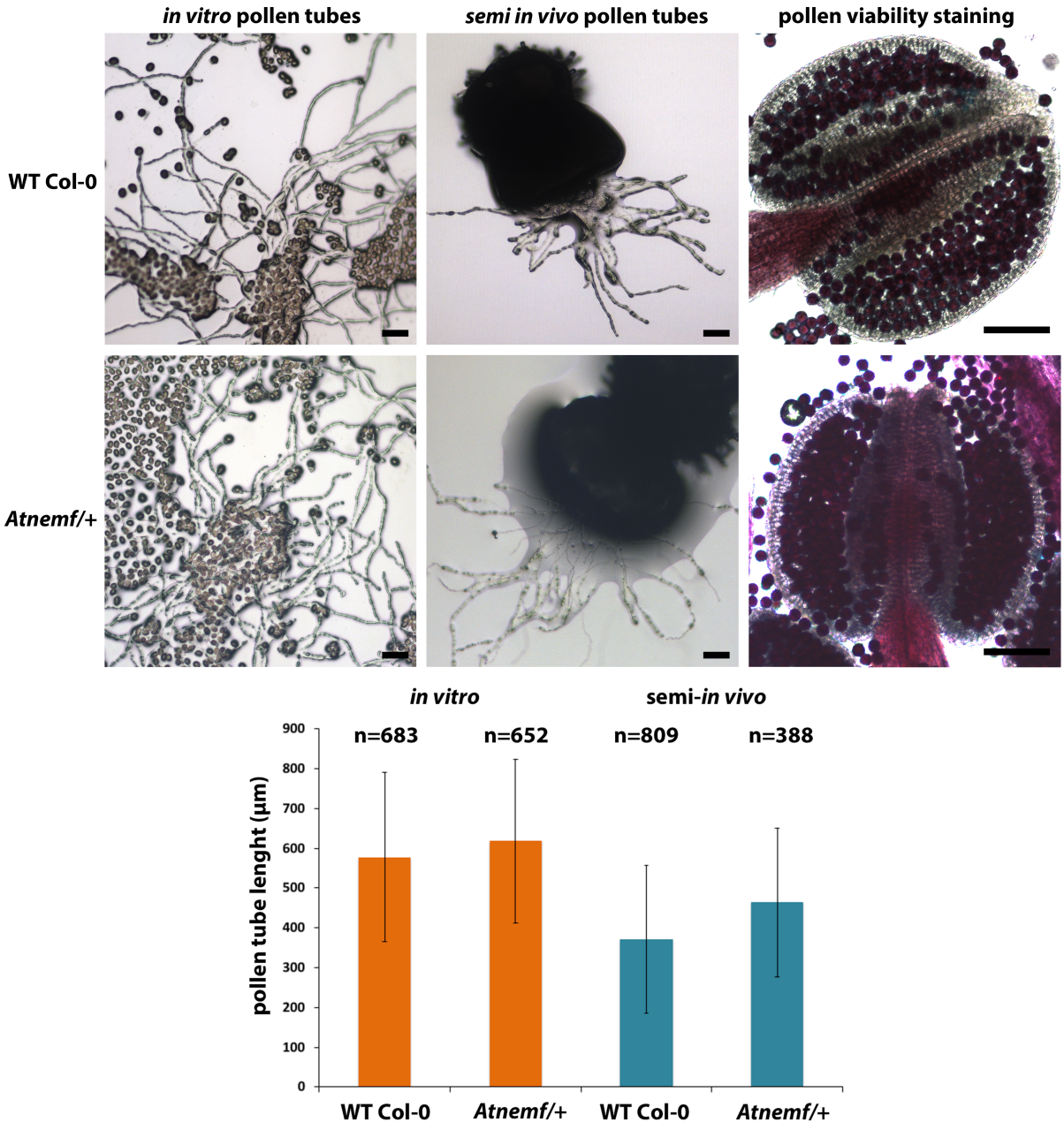

Figure 4. Pollen viability staining and pollen tube growth assays (i*n vitro*, semi-*in vivo*). Chart represents quantification of pollen tube growth measurements in WT Col-0 and *Atnemf/+* in both *in vitro* and semi-*in vivo* conditions.

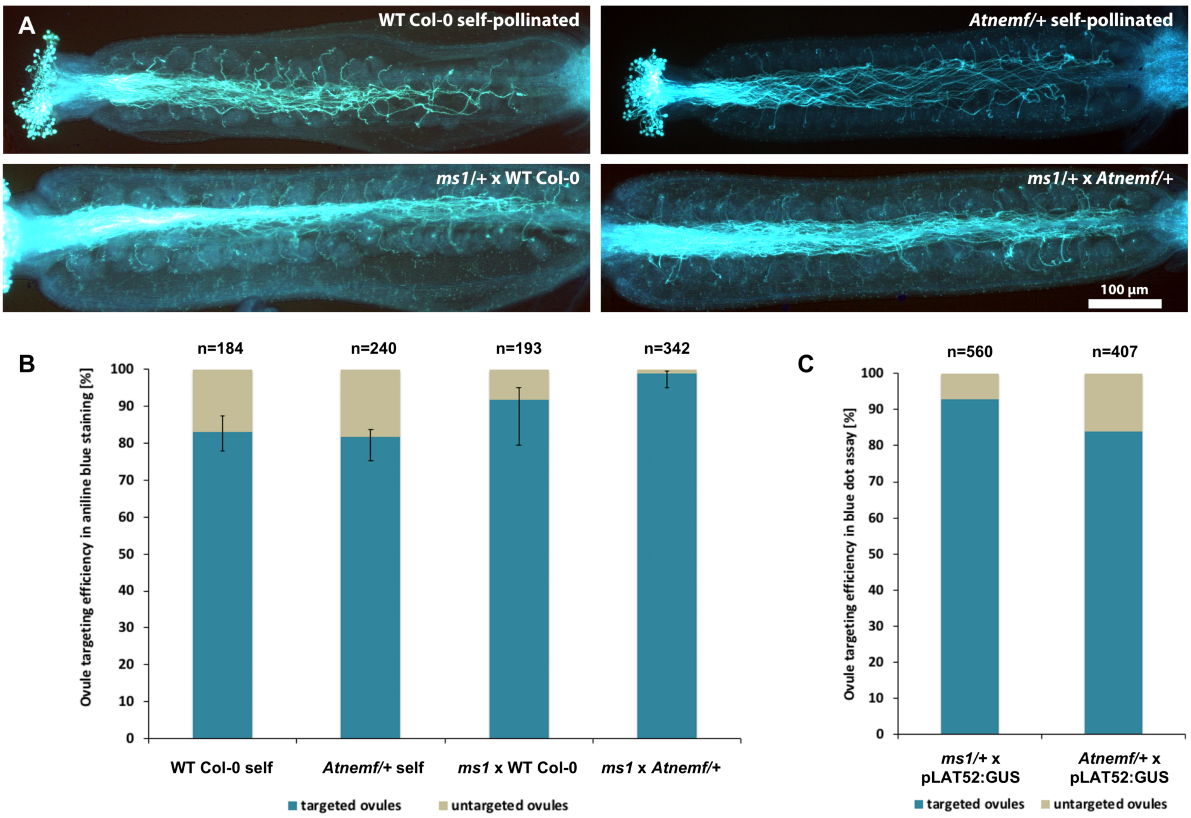

Figure 5. Aniline blue callose staining for detection of pollen tube reception by the ovules. A, B) Self-pollinated and *ms1/+* pistils pollinated with WT or *Atnemf/+* pollen were stained and the number of fertilised ovules was calculated. Bar represents 100 µm. C) Blue dot assay for detection of ovule attraction. Ovules were dissected from WT Col-0 and *Atnemf/+* pistils pollinated by pollen grains expressing pLAT52:GUS marker and stained for GUS activity. A targeted ovule is recognised by a blue dot, caused by release of blue vegetative nucleus and cytosol from the pollen tube after fertilisation.

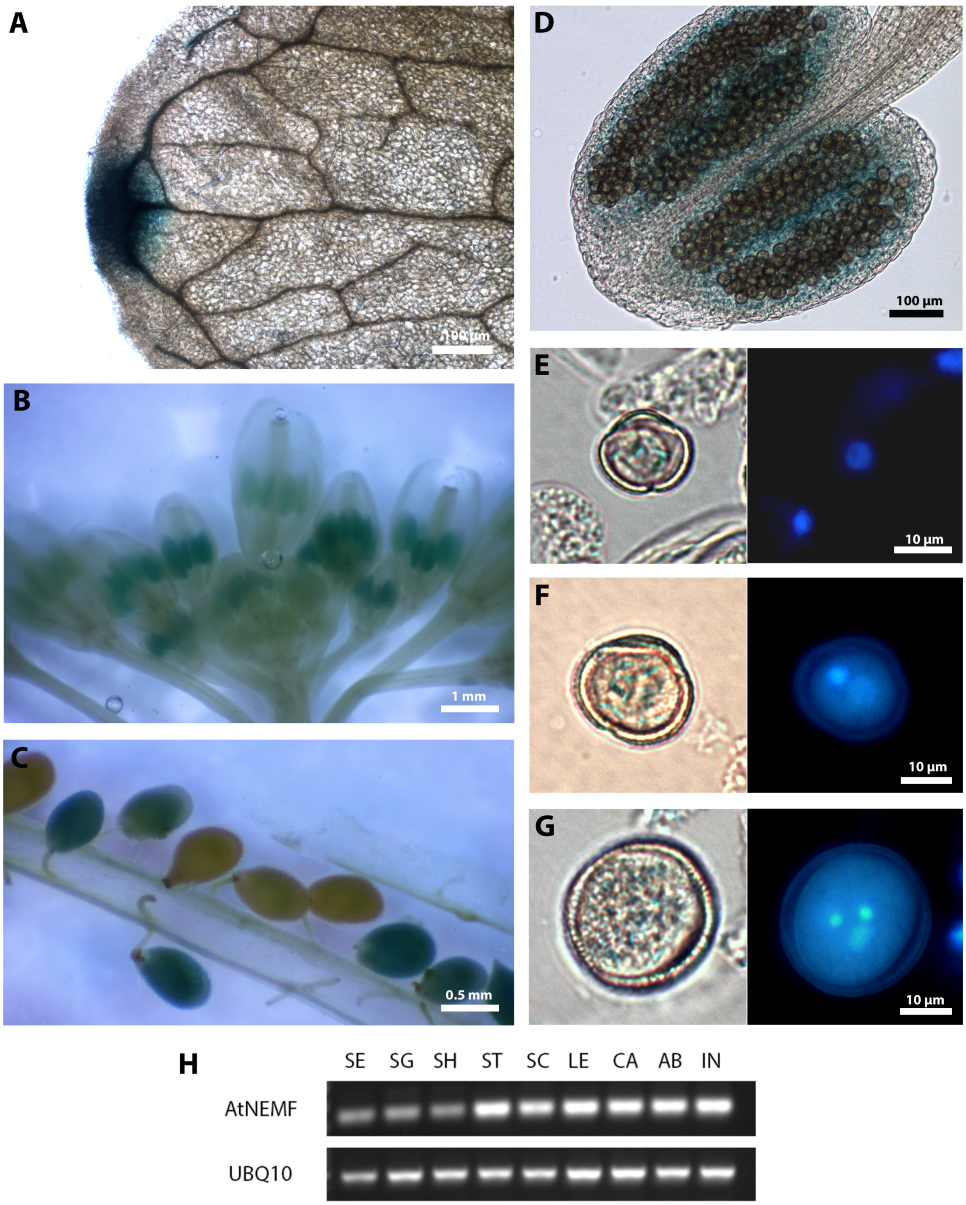

Figure 6. AtNEMF promoter activities assessed by GUS staining. 1kb upstream of ATG was fused with GUS reporter and expression was observed in two subsequent generations. AtNEMF promoter was found to be active in leaf and cauline leaf hydatodes (A), developing seeds (C, integuments and embryo proper), and anthers of immature buds (B) with the signal strongest in tapetum (D), unicellular microspores (E) and bicellular pollen (F) and lower signal in mature pollen grains (G). H) AtNEMF gene expression in WT Col-0 samples: (SE) dissected seeds with cotyledon stage embryo, (SG) silique with globular stage embryos, (SH) silique with heart stage embryos, (ST) silique with torpedo stage embryos, (SC) silique with cotyledon stage embryos, (LE) rosette leaf, (CA) cauline leaf, (AB) axillary buds, (IN) inflorescence. Ubiquitin 10 gene was used as a reference control.

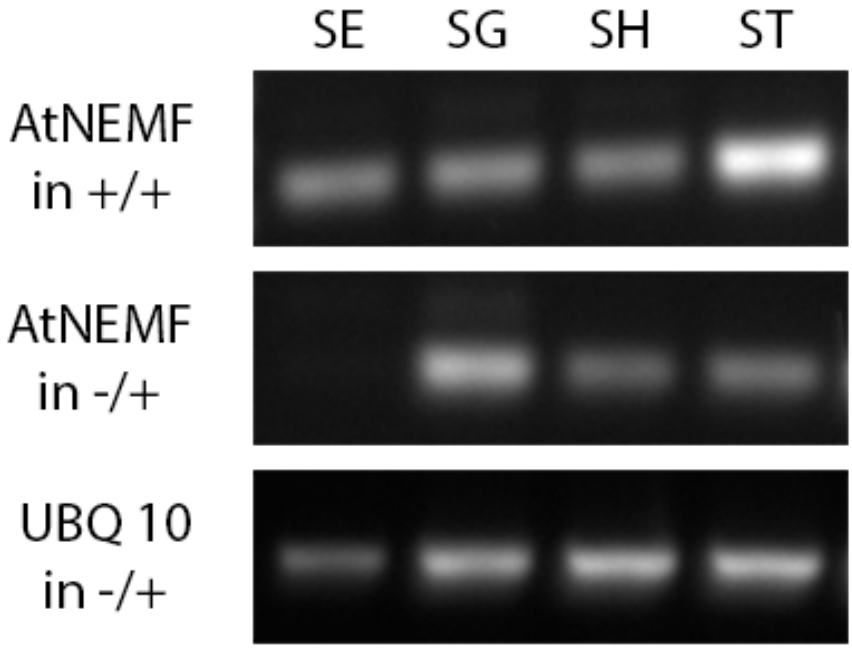

Figure 7. Detection of transcript presence in AtNEMF T-DNA line SALK_090319. Primers amplifying 254 bp product upstream of the T-DNA insertion were used. Arabidopsis ubiquitin 10 gene was used as a control. SE) dissected seeds with WT Col-0 cotyledon stage embryos or mutant homozygous embryos, SG) silique with globular stage embryos, SH) silique with heart stage embryos, ST) silique with torpedo stage embryos.

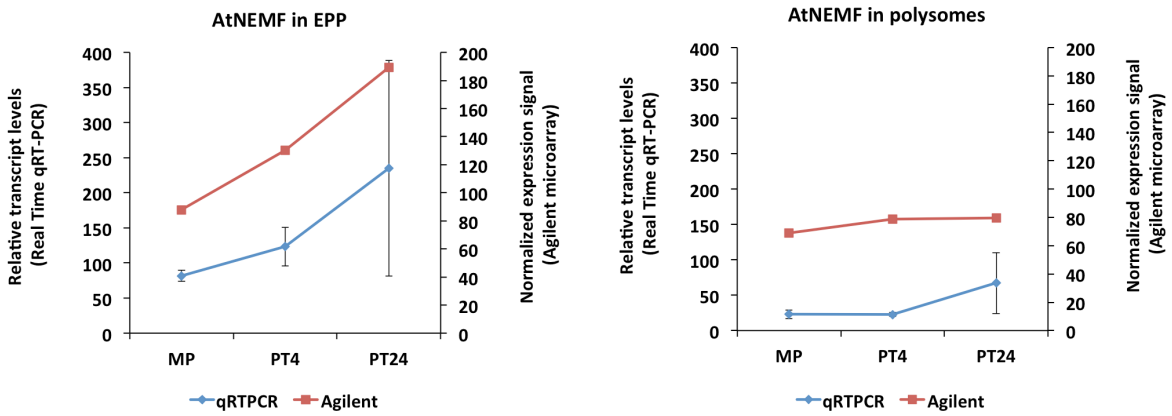

Figure 8. Quantification of tobacco AtNEMF homolog in polysomal (translated transcripts) and EPP (untranslated/stored transcripts) fraction in mature pollen (MP) and 4hrs- (PT4) and 24hrs-grown (PT24) *in vitro* tobacco pollen tubes.

Materials and Methods

Plant material and growth conditions

Arabidopsis (*Arabidopsis thaliana*) plants were grown at 25°C and 60% humidity in Conviron growth chambers under 16h light/8h dark conditions. Seeds of Col-0 wild type (WT) and EMB1441/AtNEMF SALK_090319 plants were obtained from The European Arabidopsis Stock Centre. T-DNA insertion line was genotyped using SALK LBb1.3 primer in combination with gene specific primers (left primer: 5'AGGAGAAGACTGTTTCTGCCC3', right primer: 5'TTACCATCAGCAGCTGTGTTG3'). Position of the T-DNA insertion was verified by sequencing the PCR product from genomic DNA gained by amplification with the T-DNA border primer and gene specific genotyping reverse primer.

Transmission analysis

EMB1441/NEMF-like heterozygous plants were back-crossed into WT Col-0 background, both through male and female. Progeny of these crosses was genotyped for the presence of T-DNA insertion and transmission coefficient was calculated as described in Fig. 3.

Cloning strategy

For AtNEMF promoter, 997 bp fragment upstream of the start codon was amplified using the Phusion polymerase (New England Biolabs) according to the manufacturer's instructions (forward primer: 5'CACCAAAGATATGGTAAAGTTCCTT3', reverse primer: 5'ATCTTAGTCTCTCTCGAAATTTCG3'). Fragment was cloned into the pENTR/D-TOPO vector (Invitrogen) and after verification recombined into the destination vector pKGWFS7 bearing GUS and GFP reporters.

pAtNEMF:GUS activity

Stable transformants were screened for GUS activity in two subsequent generations. Composition of the GUS staining buffer was as follows: 0.2 M Na_2HPO_4, 0.2 M NaH_2PO_4, 10 mM EDTA, 0,1% Triton X-100, 1mM $K_3Fe(CN)_6$, 2 mM X-Gluc. Various tissue types were

stained for up to 48 hrs and afterwards cleared with ethanol series (90%, 70%, 50%) prior to imaging. Representative 5 plants from the T1 generation and their progeny in T2 were used to investigate the AtNEMF promoter expression profile.

Microscopic techniques

For mutant embryos phenotypic screen, the seeds were cleared in a solution of chloral hydrate. Length of clearing was optimised based on the age of seeds, but overnight clearing was sufficient for all developmental stages. Samples were observed under the DIC optics on a Nikon TE-2000 microscope.

Pollen viability stain

Alexander's stain was used to distinguish viable mature pollen grains from non viable pollen grains. Composition of the staining solution was as follows: 10 ml of 95% ethanol, 1 ml of malachite green (1% in 95% ethanol), 5 ml of acid fuchsin (1% in water), 0,5 ml of Orange G (1% in water), 5 g of phenol, 5 g of chloral hydrate, 2 ml of glacial acetic acid, 25 ml of glycerol and 50 ml of distilled water. Stamens of flowers (WT Col-0 and *AtNEMF*/+) collected before and after anthesis were stained in a droplet of the solution for 5 min prior to imaging. To enhance staining, the glass slides were heated above a Bunsen burner for a few seconds.

Aniline blue staining

Pistils of 24-hrs self-pollinated WT Col-0 and AtNEMF plants or cross-pollinated *ms1*/+ plants with WT Col-0 or AtNEMF pollen (24 hrs pt growth *in vivo*) were stained for callose in pollen tube walls according to the protocol by Mori et al. (2006).

Blue dot assay

Young buds of WT Col-0 and *AtNEMF*/+ plants before dehiscence of stamens were emasculated and pistils were let to mature for 2-3 days until the stigma papillae fully developed. Pistils were then pollinated with pollen grains expressing pLAT52:GUS construct and collected 24 hrs after pollination. Fertilised pistils were dissected under the binocular dissection microscope and the stripes of immature seeds attached to septum were transferred

to GUS staining solution (for GUS buffer composition see section "Promoter:GUS activity" above). After 2 hrs of staining, the ovules were observed and imaged under the Nikon TE-2000 microscope equipped with DIC optics. Each fertilised ovule contained a blue dot after the release of pollen tube cytoplasmic content by the vegetative nucleus.

Pollen tube assays

In vitro

Open flowers after anthesis were taken and pollen was evenly spread out on top of an 0.8% low melting agarose pad. Three to five flowers were used per one pad. *AtNEMF*/+ pollen grains were grown alongside WT Col-0 grains. Pollen tube length was measured after 8 hrs of *in vitro* growth in the dark in a humidified chamber at 22°C using the NIS Elements software. Pollen germination medium composition was used according to Boavida and McCormick (2007).

Semi-*in vivo*

Sterile *ms1*/+ pistils were pollinated with WT Col-0 or *AtNEMF*/+ pollen, respectively, and after 1-2 hrs were removed from the plant. The upper segment of the pistil with stigma and up to 5 mm of tissue was cut with a sterile needle and transferred to the solid growth medium on a small Petri dish (1% low melting agarose in pollen germination media). Pistils were tilted to enable the pollen tubes to emerge onto the solid medium surface and cultivated in a humidified growth chamber at 22°C for 24 hrs. Pollen tube length was measured using the NIS Elements software from the point where they emerged from the pistil. Pollen germination medium composition was used according to Palanivelu and Preuss (2006).

Semi-quantitative RT-PCR

RNA from various tissues was extracted using RNeasy Plant Mini Kit (Qiagen) and DNase treated using DNase I (ThermoFisher). cDNA synthesis was performed using ImProm-II™ Reverse Transcription System (Promega). Same set of primers amplifying a 254 bp long fragment were used for detection of transcript presence in SALK_090319 line and for expression profile of AtNEMF in WT Col-0 plants (F primer: 5'ACTTTCGATGCGGCTTTAGA3', R primer: 5'CCTTTGCAAGTGCTACACGA3'). Ubiquitin 10 gene was used as an internal reference control (F primer:

5 ’ G A T C T T T G C C G G A A A A C A A T T G G A G G 3 ’ , R p r i m e r : 5’CGACTTGTCATTAGAAAGAAAGAGAT 3’).

References

Ahmed, A., Wang, M., Bergant, G., Maroofian, R., Zhao, R., Alfadhel, M., Nashabat, M., AlRifai, M. T., Eyaid, W., Alswaid, A., et al. (2021). Biallelic loss-of-function variants in NEMF cause central nervous system impairment and axonal polyneuropathy. Hum. Genet. 140, 579–592.

Boavida, L. C. and McCormick, S. (2007). TECHNICAL ADVANCE: Temperature as a determinant factor for increased and reproducible in vitro pollen germination in Arabidopsis thaliana. Plant J. 52, 570–582.

Defenouillère, Q., Yao, Y., Mouaikel, J., Namane, A., Galopier, A., Decourty, L., Doyen, A., Malabat, C., Saveanu, C., Jacquier, A., et al. (2013). Cdc48-associated complex bound to 60S particles is required for the clearance of aberrant translation products. Proc. Natl. Acad. Sci. U. S. A. 110, 5046–5051.

Filbeck, S., Cerullo, F., Paternoga, H., Tsaprailis, G., Joazeiro, C. A. P. and Pfeffer, S. (2021). Mimicry of Canonical Translation Elongation Underlies Alanine Tail Synthesis in RQC. Mol. Cell 81, 104-114.e6.

Filbeck, S., Cerullo, F., Pfeffer, S. and Joazeiro, C. A. P. (2022). Ribosome-associated quality-control mechanisms from bacteria to humans. Mol. Cell 82, 1451–1466.

Hafidh, S., Breznenová, K. and Honys, D. (2012). De novo post-pollen mitosis II tobacco pollen tube transcriptome. Plant Signal. Behav. 7, 918–921.

Hafidh, S., Breznenová, K., Růžička, P., Feciková, J., Čapková, V. and Honys, D. (2012). Comprehensive analysis of tobacco pollen transcriptome unveils common pathways in polar cell expansion and underlying heterochronic shift during spermatogenesis. BMC Plant Biol. 12, 24.

Lyumkis, D., Dos Passosb, D. O., Tahara, E. B., Webb, K., Bennett, E. J., Vinterbo, S., Potter, C. S., Carragher, B. and Joazeiro, C. A. P. (2014). Structural basis for translational

surveillance by the large ribosomal subunit-associated protein quality control complex. Proc. Natl. Acad. Sci. U. S. A. 111, 15981–15986.

Mori, T., Kuroiwa, H., Higashiyama, T. and Kuroiwa, T. (2006). GENERATIVE CELL SPECIFIC 1 is essential for angiosperm fertilization. Nat. Cell Biol. 8, 64–71.

Palanivelu, R. and Preuss, D. (2006). Distinct short-range ovule signals attract or repel Arabidopsis thaliana pollen tubes in vitro. BMC Plant Biol. 6, 7.

Shao, S., Brown, A., Santhanam, B. and Hegde, R. S. (2015). Structure and assembly pathway of the ribosome quality control complex. Mol. Cell 57, 433–444.

Shen, P. S., Park, J., Qin, Y., Li, X., Parsawar, K., Larson, M. H., Cox, J., Cheng, Y., Lambowitz, A. M., Weissman, J. S., et al. (2015). Rqc2p and 60S ribosomal subunits mediate mRNA-independent elongation of nascent chains. Science (80-.). 347, 75–78.

Winter, D., Vinegar, B., Nahal, H., Ammar, R., Wilson, G. V. and Provart, N. J. (2007). An “Electronic Fluorescent Pictograph” Browser for Exploring and Analyzing Large-Scale Biological Data Sets. PLoS One 2, e718.

2.7. LARP6C orchestrates posttranscriptional reprogramming of gene expression during hydration to promote pollen tube guidance

Elodie Billey, Said Hafidh, Isabel Cruz-Gallardo, Celso G Litholdo, Viviane Jean, Marie-Christine Carpentier, Claire Picart, Vinod Kumar, Katarina Kulichova, Eric Maréchal, David Honys, Maria R Conte, Jean-Marc Deragon and Cécile Bousquet-Antonelli

Plant Cell, 2021 Aug 31;33(8):2637-2661. doi: 10.1093/plcell/koab131

My contribution: During my stay in the Laboratory of Pollen Biology, David Honys and Said Hafidh started a collaboration with Cecile Bousquet-Antonelli from University of Perpignan, France. Her research focused on LARP6c, an RNA-binding protein with unknown specifics of its function. Based on data published in Hafidh et al. 2012a and 2012b, LARP6c was identified as an interesting gene found in RNA-storing EPP particles. PhD. student Elodie Billey came for a short term visit and I helped her to learn the specifics of working with pollen and pollen tubes, as the data suggested a possible role of LARP6c in pollen development. Moreover, I was given the task to examine pollen, pollen tubes and embryos of Arabidopsis LARP6c T-DNA lines over two subsequent generations. Even though my findings did not have a substantial value for the final manuscript, they were included as a starting point for the extensive studies later performed by Said Hafidh.

doi:10.1093/plcell/koab131

THE PLANT CELL

THE PLANT CELL 2021: 33: 2637–2661

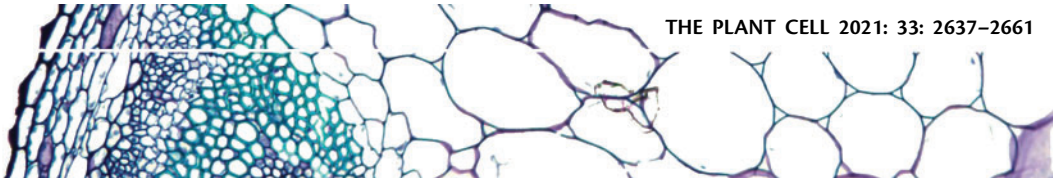

Research Article

LARP6C orchestrates posttranscriptional reprogramming of gene expression during hydration to promote pollen tube guidance

Elodie Billey ,[1,2,‡] Said Hafidh ,[3,*] Isabel Cruz-Gallardo ,[4,§] Celso G. Litholdo Jr, [1,2] Viviane Jean,[1,2] Marie-Christine Carpentier ,[1,2] Claire Picart,[1,2] Vinod Kumar ,[3] Katarina Kulichova,[3] Eric Maréchal,[5] David Honys ,[3] Maria R. Conte ,[4] Jean-Marc Deragon [1,2,6,*] and Cécile Bousquet-Antonelli [1,2,*,†]

1 Laboratoire Génome et Développement des Plantes, UMR5096, CNRS, 66860 Perpignan, France
2 Laboratoire Génome et Développement des Plantes, UMR5096, Université de Perpignan Via Domitia, 66860 Perpignan, France
3 Laboratory of Pollen Biology, Institute of Experimental Botany of the Czech Academy of Sciences, 16502 Prague 6, Czech Republic
4 Randall Centre for Cell and Molecular Biophysics, King's College London, London SE1 1UL, UK
5 Laboratoire de Physiologie Cellulaire et Végétale, UMR 5168 CNRS, CEA, INRAE, Université Grenoble Alpes, IRIG, CEA Grenoble, 38054 Grenoble, France
6 Institut Universitaire de France, 75231 Paris Cedex 5, France

*Author for correspondence: cecile.antonelli@univ-perp.fr (C.B.-A.), hafidh@ueb.cas.cz (S.H.), jean-marc.deragon@univ-perp.fr (J.-M.D.).
†Senior author.
‡Present address: TOTAL RC, 2 Place Jean Millier-Arche Nord Coupole/Regnault, 92078 Paris La Défense Cedex, France.
§Present address: Department of Chemistry, King's College London, Britannia House, 7 Trinity St, London SE1 1DB, UK.
These authors contributed equally (E.B., S.H.).

E.B. and S.H. performed the experiments and analyzed the data. C.P. helped E.B. with confocal microscopy analyses. V.J. helped E.B. with plant maintenance and reciprocal crossed. M.C.C. performed RNA-seq and RIP-seq bioinformatics. V.K. and K.K. assisted S.H. with in vitro pollen tube assays, and V.K. assisted S.H. with experiments presented in Figure 9. I.C.G. and M.R.C. designed and analyzed EMSA and ITCs; I.C.G. performed the experiments. C.G.L. Jr ran experiments from Figure 8. E.M. contributed his knowledge on lipid metabolism and suggested a role for MGD2 as cargo for TAGs. C.B.A. coordinated the work, designed the research, analyzed the data, and wrote the paper. J.M.D. helped with data analysis. E.B., S.H., M.R.C., J.M.D., and D.H. revised the manuscript.
The authors responsible for distribution of materials integral to the findings presented in this article in accordance with the policy described in the Instructions for Authors (https://academic.oup.com/plcell) are: Cécile Bousquet-Antonelli (cecile.antonelli@univ-perp.fr), Said Hafidh (hafidh@ueb.cas.cz), and Jean-Marc Deragon (jean-marc.deragon@univ-perp.fr).

Abstract

Increasing evidence suggests that posttranscriptional regulation is a key player in the transition between mature pollen and the progamic phase (from pollination to fertilization). Nonetheless, the actors in this messenger RNA (mRNA)-based gene expression reprogramming are poorly understood. We demonstrate that the evolutionarily conserved RNA-binding protein LARP6C is necessary for the transition from dry pollen to pollen tubes and the guided growth of pollen tubes towards the ovule in *Arabidopsis thaliana*. In dry pollen, LARP6C binds to transcripts encoding proteins that function in lipid synthesis and homeostasis, vesicular trafficking, and polarized cell growth. LARP6C also forms cytoplasmic granules that contain the poly(A) binding protein and possibly represent storage sites for translationally silent mRNAs. In pollen tubes, the loss of LARP6C negatively affects the quantities and distribution of storage lipids, as well as vesicular trafficking. In *Nicotiana benthamiana* leaf cells and in planta, analysis of reporter mRNAs designed from the LARP6C target *MGD2* provided evidence that LARP6C can shift from a repressor to an activator of translation when the pollen grain enters the

Received October 31, 2019. Accepted May 6, 2021. Advance access publication May 17, 2021
© American Society of Plant Biologists 2021. All rights reserved. For permissions, please email: journals.permissions@oup.com

Downloaded from https://academic.oup.com/plcell/article/33/8/2637/6276993 by Institute of Science and Technology Austria user on 22 August 2023

IN A NUTSHELL

Background: In flowering plants, pollen delivers male genetic material into the ovule, which is embedded in the pistil. When mature, the pollen dehydrates, turning "dormant", with most of its cellular activities shutdown. Upon landing on a pistil, the pollen rehydrates and "awakens"; it germinates and grows a protrusion, the pollen tube, which elongates and navigates into the pistil guided by ovule-emitted signals, a process known as "pollen tube guidance". Dormant pollen contains mRNAs encoding proteins stored as translationally silent. When the pollen "awakens", translation is reactivated, which is crucial for the emergence of pollen tubes and their penetration into the pistil.

Question: How are mRNAs chosen to be stored? How do they reenter translation? Which proteins are involved in this process? We previously proposed that *Arabidopsis thaliana* LARP6C regulates mRNAs through direct binding, but we did not know which mRNAs it controls, how this occurs, and what purpose it serves in plant development. Since LARP6C is a pollen-specific protein, we studied its roles in plant reproduction.

Findings: Using Arabidopsis mutants, we show that pollen deprived of LARP6C has delayed germination and guidance defects. By binding to and regulating a precise subset of mRNAs, LARP6C controls lipid biology and vesicular trafficking in pollen tubes. The misregulation of these processes in *larp6c*-depleted pollen is likely the basis of their germination and guidance defects. Exploring how LARP6C regulates its mRNA targets, we discovered that this two-faced protein acts as a translational repressor in dormant pollen and an activator when the pollen "awakens". However, things are not so simple as this: successful pollen tube guidance is seemingly dependent upon the two faced-nature that LARP6C retains in elongating pollen tubes.

Next steps: Next, we will seek to understand how LARP6C shifts from a repressor to an activator of translation when pollen exits its dormant state. This work also opens the possibility that the guidance process requires that some mRNAs are only reactivated translationally when they reach a precise subcellular location in the pollen tube. With LARP6C likely being part of this mechanism, we have a unique opportunity to explore this model.

progamic phase. We propose that LARP6C orchestrates the timely posttranscriptional regulation of a subset of mRNAs in pollen during the transition from the quiescent to active state and along the progamic phase to promote male fertilization in plants.

Introduction

In the cytoplasm, messenger RNAs (mRNAs) coated with RNA-binding proteins(RBPs) in the form of ribonucleoprotein particles (mRNPs) are in balance between translation, storage, and decay. Translationally silent mRNPs can be stored and protected from decay in cytosolic aggregates and released when their protein product is needed. In response to developmental or environmental cues, the fine-tuning between mRNA decay rate or storage will have a direct impact on translation and hence gene expression. RBPs play a crucial role in this fine-tuning, enabling gene-specific regulation through binding to their mRNA targets.

LA and related proteins (LARPs) form a large family of eukaryote RBPs that share the La motif (LAM), a structured RNA-binding domain. LARPs are classified into five distinct subfamilies, including the LARP6 group (Bousquet-Antonelli and Deragon, 2009). In most LARPs, an RNA recognition motif (RRM1) is found immediately after the LAM and forms a bipartite RNA-binding unit called the La-module (Maraia et al., 2017). Although the LAM is usually very well conserved between subfamilies, the RRM1s are specific to each subgroup (Bousquet-Antonelli and Deragon, 2009; Maraia et al., 2017). Members of the LARP6 subfamily are found in Stramenopiles, Chlorophytes, plants, invertebrates, and vertebrates and are characterized by the La-module and by a short conserved motif known as LAM and S1 Associated (LSA) at the C-terminus (Bousquet-Antonelli and Deragon, 2009) that mediates protein–protein interactions (Weng et al., 2009; Cai et al., 2010b; Vukmirovic et al., 2013; Manojlovic et al., 2017).

In mammals, one of the functions of LARP6 is to regulate the synthesis of type I collagen, a heterotrimer composed of two α1 and one α2 subunits whose assembly and correct secretion are dependent upon the coordinate translation of their transcripts at the endoplasmic reticulum (ER; Zhang and Stefanovic, 2016). The expression of type I collagen is primarily regulated by the binding of LARP6 through its La-module to a stem loop in their 5′-untranslated regions (UTRs; Cai et al., 2010a; Martino et al., 2015). LARP6 either stores or stabilizes the collagen mRNA transcripts in a translationally silent form by tethering them to vimentin filaments where they can further be activated for translation or subjected to decay (Challa and Stefanovic, 2011). Alternatively, LARP6 docks the mRNAs to nonmuscle

Downloaded from https://academic.oup.com/plcell/article/33/8/2637/6276993 by Institute of Science and Technology Austria user on 22 August 2023

myosin filaments (Cai et al., 2010b; Manojlovic et al., 2017) and either recruits serine threonine kinase receptor associated protein (Vukmirovic et al., 2013) or RNA helicase A via its LSA (Manojlovic et al., 2017), which respectively function as a repressor and activator of translation. Through this mechanism, LARP6 orchestrates the coordinated translation of α1 and α2 collagen transcripts at the ER. More recently, human LARP6 was found to regulate the localization and translation of ribosomal protein (RP) mRNAs to cell protrusions, enhancing RP synthesis, ribosome biogenesis, and overall protein synthesis in migratory cells (Dermit et al., 2020). Furthermore, in zebrafish (*Danio rerio*), both *LARP6* paralogs are required for normal oocyte development, chorion formation, and egg activation (Hau et al., 2020).

While LARP6 proteins are generally encoded by a single gene, vascular plant proteins are encoded by three to six genes and are of three evolutionary types named 6A, 6B, and 6C (Merret et al., 2013b). While the members of 6A subgroup most closely resemble LARP6 from other eukaryotes, in addition to a reorganized La-module, B- and C-type orthologs carry a poly(A) binding protein (PABP)-interacting motif 2 (PAM2). *Arabidopsis thaliana* has three *AtLARP6* genes, one of each type, which we will refer to as *LARP6A*, *B*, and *C* throughout this manuscript.

We previously demonstrated that LARP6C directly associates with the PABP in plants, which is consistent with the presence of a PAM2 motif and that the finding that its La-module binds to oligo(U_{20}) homopolymers in vitro. In addition, in onion (*Allium cepa*) epidermis, LARP6C accumulates in the cytoplasm, the nucleoplasm, and the nucleolus. Strikingly, LARP6C redistributes to stress granules upon hypoxia, where it associates with mRNP aggregates (Merret et al., 2013b). These data support the view that Arabidopsis LARP6C is an RBP that is likely involved in mRNA posttranscriptional regulation.

In flowering plants, the haploid male gamete (pollen grain) consists of a vegetative cell that encases two sperm cells, which are connected (through a so-called cytoplasmic connexion) with the vegetative cell nucleus to form the male germ unit. A characteristic feature of angiosperm sexual reproduction is that sperm cells are nonmotile and must be carried simultaneously to the ovule by a pollen tube (Johnson and Preuss, 2002). Upon adhesion to the stigma, the male vegetative cell hydrates, germinates, and grows into a tube that delivers the two sperm cells to the ovule. The pollen tube is a highly polarized and fast tip-growing cell whose growth directionality is determined by various perceived cues. It is first guided in the gynoeceum by female sporophytic tissue in the pistil (preovular guidance) and then, upon exit from the transmitting tract, it navigates in gametophytic tissues guided by ovule-emitted signals (ovular guidance). Ovular cues guide the pollen tube alongside the funiculus to the micropyle. Upon reaching the ovule, the pollen tube stops growing and bursts to free the sperm cells that will fuse respectively with the egg cell (to form the embryo) and the central cell (to form the endosperm), hence completing the fertilization process (Higashiyama and Takeuchi, 2015).

In the pollen tube, upon reception and transduction of extracellular female signals, a complex cellular process targets the cell wall synthesis machinery at the site of perception, hence, permitting the delivery of macromolecules at site of extension and the directional growth of the tube. This requires tip-localized receptors, the flow of ions, intracellular trafficking of signaling molecules and proteins, and also vesicular trafficking, cytoskeleton-dependent transport, and novel cell wall formation through exocytosis (Hafidh et al., 2014; Higashiyama and Takeuchi, 2015; Feng et al., 2018). Pollen tube growth also requires changes in the pattern of gene expression that at least in part rely on posttranscriptional mechanisms. Several studies have suggested that all mRNAs required for germination and pollen tube growth are already present in the mature pollen grain and maintained in a translationally silent state until the progamic phase (Honys et al., 2000; Honys and Twell, 2004; Scarpin et al., 2017; Hafidh et al., 2018). Nonetheless, how male gene expression is posttranscriptionally regulated to permit correct pollen guidance is largely unknown, and the mRNA-regulating factors required for proper ovular guidance of pollen are currently unclear.

In the present study, we further explored the role of LARP6C and determined that it is a pollen-specific factor required for male fertility during the progamic phase. We provide evidence that the loss of LARP6C affects lipid synthesis and homeostasis as well as vesicular trafficking. Moreover, our experimental results support the notion that LARP6C orchestrates the balance between the translation, storage, and decay of its mRNA clients through direct binding, thus intervening in the guided growth of the pollen tube.

Results

LARP6C and its RNA-binding domain are required for male fertility at the pollen tube guidance step

Immunoblotting and high-throughput transcriptomic analyses (Klepikova et al., 2015) showed that, unlike LARP6A and 6B, LARP6C is almost exclusively expressed in pollen grains and pollen tubes (Figure 1A; Supplemental Figure S1). We therefore investigated its role in male fertility using two Arabidopsis T-DNA insertion mutants, *larp6c-3* and *larp6c-4*. Immunoblotting showed that both alleles are loss-of-function (lof) mutants (Figure 1B). To establish whether *larp6c* is a gametophytic mutation, we monitored the transmission efficiency (TE) through the female (TE^f) and the male (TE^m) gametophytes by reciprocal crosses with the wild-type (WT) and heterozygous *larp6c-3*/+ or *larp6c-4*/+ mutants (Figure 1C). Both alleles were transmitted normally through the female gametophyte (TE^f *6c-3* = 100% and *6c-4* = 96.7%), whereas their transmission through the male was significantly reduced, with *6c-3* showing TE^m = 74.1% and *6c-4* TE^m = 68.2% (Figure 1C). This suggests that male but not female fertility is compromised by the loss of LARP6C function.

There are different stages at which the male gametophyte could be deficient, including pollen development,

Downloaded from https://academic.oup.com/plcell/article/33/8/2637/6276993 by Institute of Science and Technology Austria user on 22 August 2023

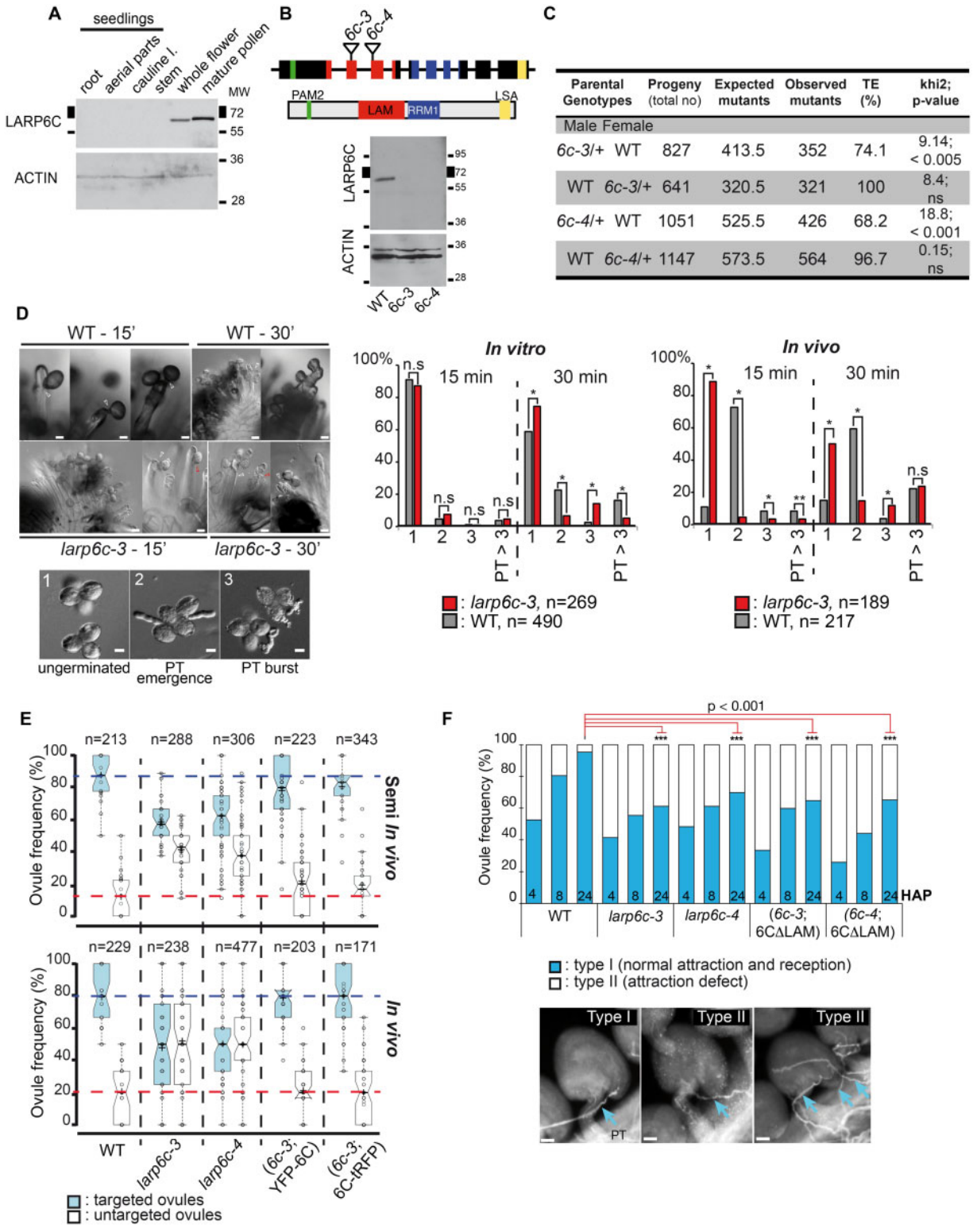

Figure 1 LARP6C is required for pollen tube guidance. A, Immunoblot analysis of steady-state LARP6C protein accumulation. The same blot was probed with antibodies against LARP6C or ACTIN as a loading control. B, *larp6c-3* and *larp6c-4* alleles are lof mutants. Top panel: schematic representation of the *LARP6C* gene and LARP6C protein. Plain boxes represent exons and lines represent introns. The color code for exons is identical to that for the conserved protein domains. The insertion sites of the T-DNAs in *larp6c-3* and *6c-4* mutants are reported. Bottom panel: immunoblot analysis of LARP6C accumulation in flowers from the WT, *larp6c-3* and *6c-4* lines. ACTIN was used as a loading control. C, Transmission efficiencies of *larp6c-3 and 6c-4* mutant alleles. TE was calculated as: ((([No. of mutant]/[No. of WT]) × 100). ns: the number of mutant seedlings in the progeny is not significantly different from the expected number of mutant seedlings. D, Scoring of germination rate, pollen tube bursting, and elongation in vitro and in vivo. Left panels show representative images of in vivo (upper part) and in vitro (lower part) experiments. On the right,

Downloaded from https://academic.oup.com/plcell/article/33/8/2637/6276993 by Institute of Science and Technology Austria user on 22 August 2023

germination, pollen tube growth or guidance, and sperm delivery (Johnson and Preuss, 2002). We monitored these pollen stages in *larp6c-3*, *6c-4*, and WT plants (Figure 1, D–F; Supplemental Figure S2, A–E). Assessment of male gametophyte maturation by DAPI staining revealed that 10% of the *6c-3* and *6c-4* mutant pollen grains did not complete their maturation and were arrested at the bicellular stage, compared to less than 3% in the WT (Supplemental Figure S2A).

We next monitored germination and pollen tube growth during the early and late steps after hydration (in vitro) or pollination (in vivo and semi in vivo [SIV]; Palanivelu and Preuss, (2006); and "Methods" section; Figure 1D; Supplemental Figure S2). In vitro, *larp6c-3* showed some defects in germination, with over 70% of ungerminated pollen grains after 30 min incubation versus 60% for the WT and an increased frequency of pollen tube burst. Moreover, at 30 min, *larp6c-3* showed less than 5% elongated pollen tubes versus 20% in the WT, for example, pollen tubes with lengths over three times that of mature pollen grains. In vivo, the situation appeared more dramatic, with a very high levels of ungerminated *larp6c-3* pollen at 15 and 30 min after pollination of over 80% and 50%, respectively, compared to the WT pollen, which showed less than 10% ungerminated pollen after 15 min incubation. Moreover, in vivo, at 30 min, *larp6c-3* pollen tubes seemed to be more prone to bursting than the WT (Figure 1D). These germination and pollen tube growth defects were likely due to delays rather than full arrest, since 7 and 24 h after pollination (HAP; Supplemental Figure S2, B, C, and E) or 4 h after hydration (Supplemental Figure S2D), the density and length of *larp6c* pollen tubes were similar to those of the WT.

We next investigated the requirement for LARP6C for pollen tube guidance and ovule targeting competence (Johnson and Preuss, 2002). We set up SIV experiments using pistils from *ms1* plants, a male-sterile mutant with normal pistil function (van der Veen and Wirtz, 1968), to assess the ability of *larp6c*-deficient pollen tubes to be guided through the pistil tissues towards the WT ovules for fertilization (Figure 1E, top panel; Supplemental Figure S3A). Whereas the WT pollen targeted 80% to 100% of the ovules (with a median value of around 90%), both *larp6c-3* and *6c-4* pollen showed a significant reduction, targeting 50%–70% of the WT ovules (with a median value of 60%). This failed pollen tube guidance phenotype was rescued by the N- and C-terminal LARP6C fusion constructs (YFP-LARP6C and LARP6C-tRFP; Figure 1E; Supplemental Figure S3, B–C). In competition assays, irrespective of the order of pollination or the side of the stigma in which the pollen grains were dusted on, *larp6c-3* and *6c-4* pollen also showed a clear deficiency in ovule targeting, with a maximum targeting efficiency of 20% compared with the expected 50% rate (Supplemental Figure S3, A and D). This further supports the notion that the observed guidance phenotype directly relates to *larp6c* deficiency.

We next monitored the ability of the *larp6c* and *larp6c*-complemented pollen to target ovules in planta (Figure 1, E and F; Supplemental Figure S2E). We hand pollinated *ms1* pistils and following aniline blue staining, scored the number of targeted and nontargeted ovules. Aniline blue stains callose-like polysaccharides contained in pollen tube walls, and after exposure to UV emits yellow-green fluorescence that allows visualization of pollen tubes even after penetration in the ovule. Here, again the *larp6c* deficient pollen tubes displayed only 60% ovule targeting efficiency versus the 80% average observed in the WT pollinated pistils (Figure 1E, bottom panel). The targeting efficiency by the (*larp6c-3*; LARP6C-tRFP) and (*larp6c-3*; YFP-LARP6C) complemented lines recovered to a WT frequency (Figure 1E). Considering that 4 HAP, the density and length of mutant pollen tubes were similar to those of the WT (Supplemental Figure S2E), it appears unlikely that the ovule targeting deficiency of *larp6c* pollen was due to delays in germination or pollen tube elongation. Nonetheless, to completely rule out this possibility, we monitored the type of ovule targeting defects at 4, 8, and 24 HAP in vivo. We observed and scored two types of behavior: type I: if pollen tube attraction and reception were normal and type II: if pollen tube attraction was defective. We did not observe a situation where attraction was normal but reception defective. Consistent with previous experiments, we found that *larp6c*-deficient pollen tubes showed a significant increase in type II behavior compared to the WT (Figure 1F). At 24 HAP, while some 40% of the ovules remain unfertilized in pistils pollinated with *larp6c-3* or *4* mutant pollen due to attraction defects, only 5% of the ovules were not fertilized when pollination was conducted with the WT pollen (Figure 1F).

Considering that *LARP6A* mRNA is highly expressed in pollen (three to four times more than *LARP6C* mRNA in

graphs report the frequency of ungerminated pollen (1), PT emergence (2), PT burst (3), and PT longer than three lengths of the pollen grain (PT > 3) 15 or 30 min after pollination. *n* represents the number of scored pollen grains. E, SIV (upper panel) and in vivo (bottom panel) pollen tube guidance assays. For SIV assays, the WT ovules were arranged around homozygous *ms1* pistil explants pollinated with pollen from various homozygous backgrounds. For in vivo assays, homozygous *ms1* pistils were pollinated in planta with pollen from various homozygous genotypes. For each type of experiment, the numbers of targeted (blue boxes) and nontargeted (white boxes) ovules were scored and results represented as whisker notched boxplots. The genotypes of the pollen used for fertilization are recorded below the graphs and *n* is the total number of ovules scored in each experiment. The dotted lines respectively show the WT mean values of targeted (blue) and nontargeted (dark red) ovules by the WT pollen. F, In vivo scoring of pollen tube behaviors. The WT pistils were pollinated in planta with pollen from various homozygous genotypes (recorded below the graph) and the behavior of pollen tubes monitored and scored over a time course: 4, 8, and 24 HAP. Type I (blue bars): targeting and reception are normal, type II (white bars): attraction (targeting) is defective. Below the graph are representative images of the type of behaviors observed. Scale bars correspond to 10 μm. The table below the graphs reports the numbers of scored ovules (*n*). *P*-values were calculated with an unpaired Student's *t* test. ns, not significant; $^{*}P \leq 0.05$, $^{**}P \leq 0.01$, $^{***}P \leq 0.001$.

Downloaded from https://academic.oup.com/plcell/article/33/8/2637/6276993 by Institute of Science and Technology Austria user on 22 August 2023

mature pollen grain, Supplemental Figure S1A), we wondered whether LARP6A and LARP6C could at least partially act redundantly. In backcross experiments, *larp6a-1* lof pollen (Supplemental Figure S3F) displayed over 95% TE, and the TE of (*larp6c-3; larp6a-1*) was not significantly different from that of single *larp6c-3* mutant pollen (82.7%; Supplemental Figure S3F). We also ran in vivo pollination assays with the WT, *larp6c-3*, or (*larp6c-3; larp6a-1*) pollen and scored fertilization behaviors (Supplemental Figure S3G). Consistent with the results of backcross experiments, the absence of LARP6A did not affect fertilization in the WT or *larp6c* null background.

Finally, to confirm that *larp6c* lof specifically affects male fertility, we examined the capability of *larp6c-3* and *6c-4* mutant ovules to attract the WT pollen tubes by SIV and in vivo assays and found no significant difference from the WT (Supplemental Figure S4). A detailed description of these experiments can be found in the legend of Supplemental Figure S4.

We previously demonstrated that LARP6C is an RBP and that its La-module is sufficient to bind RNA homopolymers in vitro (Merret et al., 2013b). We hence wondered whether the RNA-binding function of LARP6C is necessary for its role in pollen tube guidance. As for LARPs, including human LARP6, which carry a bipartite La-Module, the LAM is absolutely necessary to bind RNA both in vitro and in vivo (Cai et al., 2010a; Martino et al., 2015), we constructed a truncated *LARP6C* deleted of its LAM (*LARP6CΔ-LAM*). We then stably expressed this deletion mutant construct in the *larp6c-3* and *larp6c-4* backgrounds under the control of the *LARP6C* native promoter (Supplemental Figure S3C). In vivo fertilization assays showed that pollen expressing LARP6CΔLAM had the same pollen tube guidance defects as *larp6c* lof pollen, suggesting that *LARP6CΔ-LAM* cannot complement the *larp6c-3* lof phenotype and that the La-Module RNA-binding motif is essential for LARP6C function in pollen tube guidance (Figure 1F).

In summary, our results support the notion that LARP6C is required for male fertility at least in part at the progamic phase through its function in pollen germination and during pollen tube guidance and does not appear to act redundantly with LARP6A. Moreover, LARP6C function in pollen tube guidance requires an intact La-Module, supporting the notion that this physiological role involves the RNA-binding activity of LARP6C.

LARP6C forms dynamic cytoplasmic granules in mature pollen grains and in pollen tubes

To better understand the cellular roles of LARP6C, we monitored its subcellular distribution across pollen maturation and during pollen tube growth (Figure 2A; Supplemental Figure S5). In microspores, LARP6C was only detected in the nucleolus. At the bicellular stage, LARP6C was much more generally distributed in the cytoplasm of the vegetative cell, as well as in the vegetative and generative cell nuclei. At the tricellular stage, the subcellular distribution of LARP6C was similar to that at the bicellular stage, with possibly reduced amounts of LARP6C in the sperm cell nucleus compared to other subcellular compartments. In mature pollen grain, LARP6C displayed a complex localization pattern. It was clearly present in vegetative cell cytoplasm but transitioned from a diffuse pattern to a granular, aggregate-like pattern (Figure 2A; Supplemental Figure S5). In addition to this granular distribution, LARP6C appeared to concentrate around the membrane surrounding the vegetative cell nucleus, the sperm cells and the cytoplasmic connection linking the sperm cell 1 to the vegetative cell nucleus.

To determine more precisely the distribution of LARP6C in mature pollen grains, we performed colocalization experiments between LARP6C-tRFP and various markers (Figure 2B). The histone H2B-GFP fusion protein, expressed under the control of the tomato (*Solanum lycopersicum*) pollen-specific *LAT52* promoter (Twell et al., 1989), was used to label the vegetative cell nucleus, thereby demonstrating the absence of LARP6C in this compartment. GEX2 is a sperm cell-expressed transmembrane protein (Mori et al., 2014) that labels the sperm cell membranes and the cytoplasmic connection between sperm cell 1 and the vegetative cell nucleus (Brownfield et al., 2009; McCue et al., 2011; Mori et al., 2014). Confocal analyses showed that LARP6C and GEX2 displayed distinct distributions (Figure 2B). The tRFP signal surrounded the GFP-GEX2 signal decorating the outer membrane of the male germ unit but not the membrane connecting the two sperm cells (the inner membrane), supporting the notion that LARP6C is excluded from the sperm cells and therefore only resides in the vegetative cell cytoplasm in mature pollen.

We next inquired on the nature of LARP6C cytoplasmic foci (Figure 2B). Eukaryotic cells contain many types of membrane-less cytoplasmic aggregates composed of translationally silent mRNAs and RBPs (Buchan, 2014). So far, only two types of mRNP granules have been identified in plant cells: processing bodies (p-bodies) and stress granules (Weber et al., 2008). Plant p-bodies are—as in other eukaryotes—characterized by the presence of actors of the general mRNA turnover process, such as the DCP1/DCP2 decapping holoenzyme, the XRN4 exoribonuclease, or the deadenylation complex. Stress granules, on the contrary, contain factors belonging to the translational machinery, including the PABP (Weber et al., 2008). First clues on the nature of LARP6C aggregates observed in mature pollen were derived by colocalization experiments with specific markers of p-bodies and stress granules, namely DCP1 and PABP, respectively. We used a YFP-tagged DCP1 protein expressed from its own upstream genomic sequences (Merret et al., 2013a). Although YFP-DCP1 displayed a punctuate distribution in the vegetative cell cytoplasm, similar to LARP6C, no obvious colocalization of DCP1 and LARP6C was observed. Of note, DCP1 accumulation appeared to be restricted to the vegetative cell cytoplasm, at least in mature pollen, and contrary to

Downloaded from https://academic.oup.com/plcell/article/33/8/2637/6276993 by Institute of Science and Technology Austria user on 22 August 2023

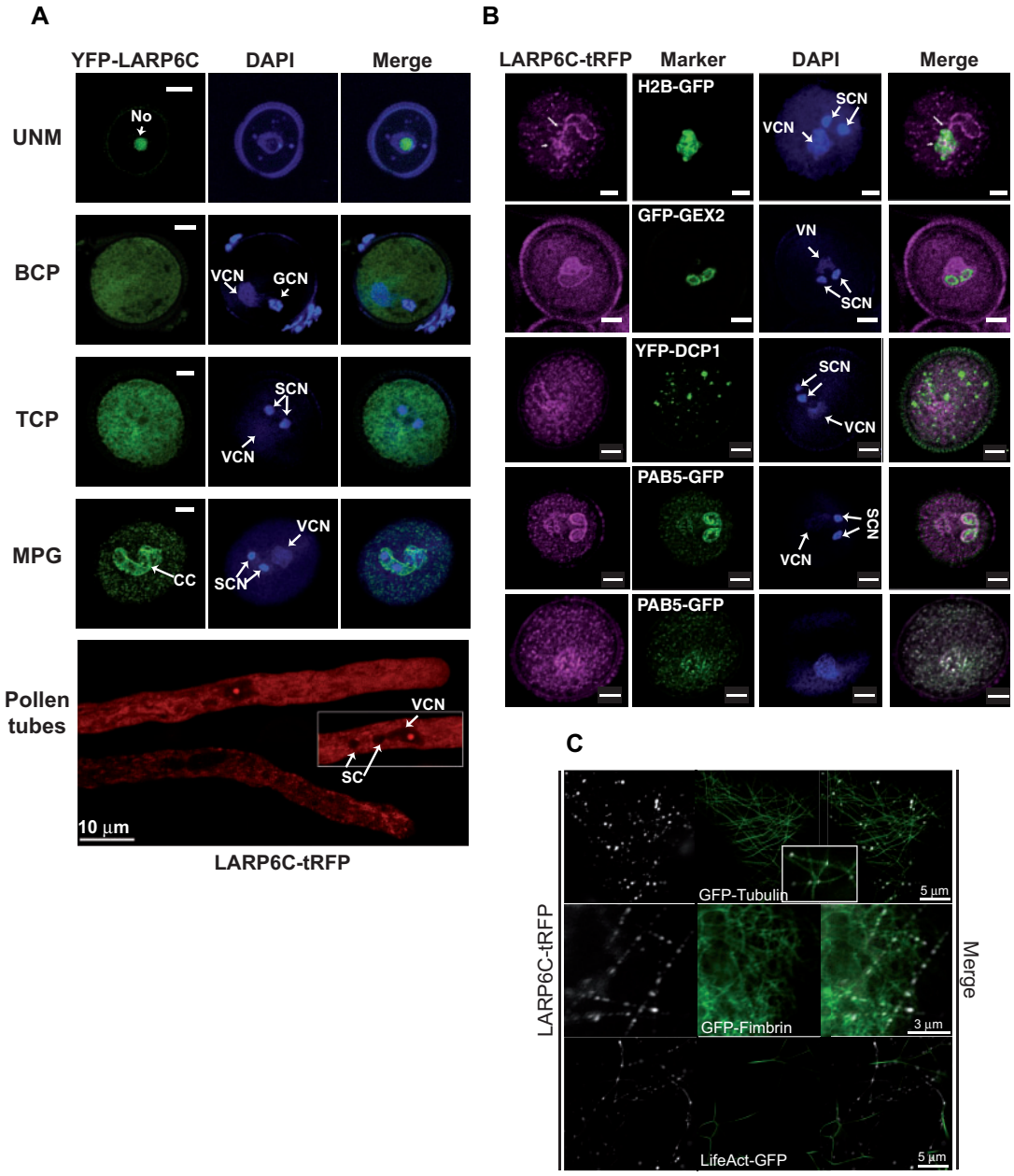

Figure 2 Subcellular distribution of LARP6C across pollen development and pollen tubes. A, Subcellular localization of fluorescently tagged YFP-LARP6C by confocal microscopy at different stages of pollen maturation. UNM, uninucleate microspore; BCP, bicellular pollen; TCP, tricellular pollen; MPG, mature pollen grain and pollen tube. Scale bars correspond to 5 μm for pollen and 10 μm for pollen tube images. Representative images of LARP6C fused at its C-terminus with a tagRFP reporter are shown in Supplemental Figure S5A. B, Confocal observation of mature pollen grains that stably coexpress the LARP6C-tRFP fusion and the H2B-GFP fusion, the GFP-GEX2 fusion, the YFP-DCP1 fusion, or the PAB5-GFP fusion. Except for the H2B-GFP marker, which is expressed from the tomato *LAT52* promoter, all marker genes are expressed from their own upstream genomic sequences. Scale bars correspond to 5 μm. In (A) and (B), arrows indicate the position of the nucleolus (No), generative cell nucleus (GCN), vegetative nucleus (VCN), sperm cell nucleus (SCN), and cytoplasmic connection (CC). C, Confocal observation of *N. benthamiana* epidermis cells transiently expressing the LARP6C-tRFP fusion coexpressed with microtubule-binding GFP-AtTUB6 and two actin-binding GFP-FABD2 or LifeAct-GFP reporters. $n = 20$ cells from three independent infiltration repeats.

LARP6C, it did not localize at the periphery of the sperm cells or the vegetative nucleus (Figure 2B).

The Arabidopsis genome contains seven genes (*PAB2* to *8*) encoding canonical PABPs, including *PAB3*, *5*, *6*, and *7* (Belostotsky and Meagher, 1996; Belostotsky, 2003; Honys and Twell, 2004), whose transcripts accumulation is restricted to pollen. We fused the genomic sequence of the *PAB5* gene (the most highly expressed of the pollen specific *PABP* genes) to a YFP tag under the control of its own upstream sequences. In the vegetative cell cytoplasm, the YFP-PAB5 protein displayed a pattern identical to that of the LARP6C protein in that it accumulated in foci

Downloaded from https://academic.oup.com/plcell/article/33/8/2637/6276993 by Institute of Science and Technology Austria user on 22 August 2023

surrounding the sperm cells and was excluded from the vegetative nucleus, but contrary to LARP6C, it was also present in the cytoplasm of sperm cells.

Finally, in pollen tubes, LARP6C was clearly excluded from the sperm cells and restricted to vegetative cell cytoplasm. In the cytoplasm, LARP6C signals showed various degrees of aggregate patterns, with foci appearing to be organized along a longitudinal string-like structure (Figure 2A; Supplemental Figure S5C). To explore the possibility that LARP6C foci could bind to the cytoskeleton structure, we coexpressed LARP6C-tRFP with GFP-AtTUB6 (which labels microtubules) in *Nicotiana benthamiana* epidermis cells (Ambrose and Cyr, 2007), GFP-FABD2 (Voigt et al., 2005), or LifeACT-GFP (Cvrčková and Oulehlová, 2017); which label actin microfilaments (Figure 2C; Supplemental Movie S1). While LARP6C did not significantly colocalize with actin microfilament markers, it colocalized with GFP-tubulin (Figure 2C; Supplemental Movie S1). Not only did the strings formed by LARP6C foci overlap with tubulin filaments, but LARP6C foci also appeared to move along microtubules, as revealed by time series observations (Supplemental Movie S1).

Finally, as an additional exploration of possible redundancy, we ran colocalization experiments between LARP6C and LARP6A (Supplemental Figure S5, B and C). We previously showed that, when transiently expressed in onion epidermis cells, LARP6C localized to stress granules (together with PABP), while LARP6A did not. Consistently, in mature pollen grain, we observed that LARP6C formed foci, while LARP6A did not (Supplemental Figure S5C). Additionally, LARP6A and 6C showed distinct subcellular distributions in pollen tubes, with 6A mainly accumulating in sperm cell cytoplasm while 6C was excluded from the sperm cells (Supplemental Figure S5C).

In summary, our data indicate that LARP6C shows a dynamic subcellular distribution across pollen maturation. We found that in mature pollen and pollen tubes, LARP6C is restricted to the vegetative cell cytoplasm and is present in aggregates that could possibly associate with microtubules.

RIP-seq pulldown reveals LARP6C mRNA targets in mature pollen grain

The presence of LARP6C in cytoplasmic aggregates, which contain the PABP, together with our previously published data (Merret et al., 2013b), strongly support the notion that at the cellular level, LARP6C likely acts to control mRNA fate in pollen. In addition, since its RNA-binding domain is necessary to fulfill its role in pollen tube guidance, we reasoned that the identification of its mRNA clients would help reveal how LARP6C controls male fertilization at the molecular level. We hence sought to identify its mRNA targets using an unbiased RNA immunoprecipitation and sequencing (RIP-seq) strategy. We conducted the RIP procedure from complemented *larp6c-3* lof mature pollen grains expressing a PRO_{6C}:LARP6C-FlagHA tagged version (6C-FH hereafter; Supplemental Figure S3, B and C) and from the WT pollen grains as a negative control. After assessing the efficiency of the immunoprecipitation through immunoblotting (Supplemental Figure S6A), RNAs were extracted from the input and eluate fractions and subjected to RNA-seq. After mapping and filtering of the data set (see Supplemental Methods), a read per kilobase per million mapped reads (RPKM) value was calculated for each protein-coding gene. The replicates were found to be reproducible (Supplemental Figure S6B), enabling us to build a table with a mean normalized value per gene and filter out those with less than 1 RPKM value in one of the four samples (input or eluate from the WT or 6C-FH; Supplemental Data Set S1). Using such criteria, we retained a list of 7,356 expressed transcripts.

We first filtered out transcripts based on input fraction values, retaining mRNAs that are not differentially expressed (DE) and show a fold change between 6C-FH and WT < 1.2 in order to select for transcripts whose levels did not vary between control and 6C-FH inputs. Then, from this trimmed list, we selected mRNAs that are DE (False Discovery Rate: FDR 0.01) and accumulated to a higher extent in the eluate fraction of 6C-FH compared to the WT (Figure 3A). Next, we selected mRNAs that were enriched by the immunoprecipitation procedure, by selecting those with a $RE_{6C\text{-}FH}$ (RE is the eluate over input ratio) value > 1. To further increase stringency and reveal mRNAs that are most likely to be direct targets of LARP6C, we compared the RE_{WT} to the $RE_{6C\text{-}FH}$ and, based on the repartition of the values (Supplemental Figure S6, C and D) selected transcripts with an ($RE_{6C\text{-}FH}/RE_{WT}$) value of 3 or more (Figure 3B). Through the above series of filters, we identified a high-confidence list of 115 genes encoding direct or indirect mRNA targets of LARP6C (Supplemental Data Set S1).

No gene ontology term was found to be significantly enriched amongst the 115 mRNAs identified as potential LARP6C targets. Nonetheless, a gene-to-gene analysis shows that the majority of LARP6C targets encode factors likely to be involved in polarized cell growth and male fertilization. This includes protein involved in endomembrane system trafficking and synthesis, signalling factors, and kinases (Samaj et al., 2006; Grebnev et al., 2017) and most strikingly proteins involved in lipid metabolism and homeostasis control (Ischebeck, 2016; Figure 3C; Supplemental Data Set S1). Also, we found that some LARP6C targets are known actors of pollen gametogenesis, pollen germination, pollen tube growth and guidance, or tip-polarized growth, such as the growth of roots or neurons (Supplemental Data Set S1).

Loss of LARP6C affects lipid metabolism and the endomembrane system during pollen tube growth

In angiosperms, lipids are crucial for male fertilization. Pollen tube elongation depends on lipids synthesized and stored in pollen grain before desiccation or produced on the way from pistil to ovule (Ischebeck, 2016). Amongst the list of LARP6C targets are actors involved in fatty acid synthesis, di- and triacylglycerol (TAG) synthesis and homeostasis,

Downloaded from https://academic.oup.com/plcell/article/33/8/2637/6276993 by Institute of Science and Technology Austria user on 22 August 2023

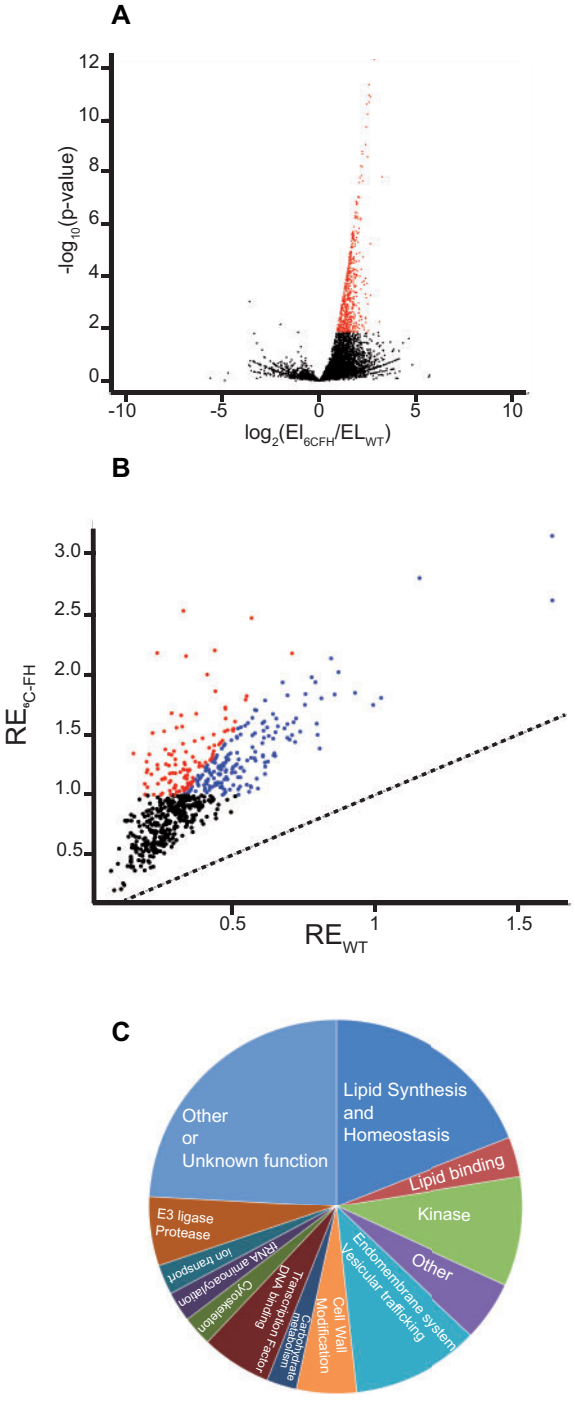

Figure 3 RIP-Seq identification of LARP6C mRNA targets. A, Volcano plot repartition of the log2 of fold changes between values in the eluate fractions of LARP6C-FH and WT for mRNAs found in the LARP6C-FH eluate fraction, according to their *P*-values obtained through the DESeq2 pipeline. Red dots represent mRNAs that are significantly more represented in LARP6C-FH eluates. A $P \leq 0.01$ and FC ≥ 1 was used as significance criteria. B, Plotting the RE (Eluate-RPM/Input-RPM) values in LARP6C-FH against the RE values in the WT for the 635 mRNAs highlighted in graph A. mRNAs with a RE6c-FH $\geq$ 3RE-WT are labeled as blue dots. See Supplemental Figure S6C for a detailed description of the RIP-seq pipeline. C, Pie chart representation of the number of LARP6C targets within the various functional categories identified.

whose control were previously found to be necessary for correct pollen tube growth (Botté et al., 2011; Pleskot et al., 2012; Zheng et al., 2018). This includes genes encoding fatty acid synthesis factors (FAD2 (Botella et al., 2016), ACX4 (Khan et al., 2012), and AtLPEAT2 (Stålberg et al., 2009)); DGAT1, which catalyzes the first step of TAG synthesis (Zhang et al., 2009); DYRKP-2A (Schulz-Raffelt et al., 2016); and MPK6 kinases, which regulate TAG production (Zheng et al., 2018); SDP1, a TAG lipase involved in membrane lipid homeostasis control (Kelly et al., 2013); and MGD2, which catalyzes the synthesis of monogalactosyldiacylglycerol (MGDG; Botté et al., 2011).

Considering that LARP6C might control the expression of genes encoding proteins involved in glycerolipid metabolism and homeostasis at the posttranscriptional level, we tested lipid accumulation and synthesis in the absence of LARP6C in mature pollen grains and pollen tubes (Figure 4). First, we visualized lipid droplets (LDs), which consist of a phospholipid monolayer surrounding a core of neutral lipids, such as TAG and fatty acid steryl esters, by staining with Bodipy 505/515 (which stains neutral lipids) and Nile Red (which stains nonpolar and neutral lipids; Figure 4, A and B). In *larp6c-3* mature pollen grain, we did not detect any significant difference in staining compared to the WT grains (Figure 4A). We then germinated and grew WT and *larp6c-3* pollen tubes in vitro and visualized LD accumulation at 2 and 4 h post germination (Figure 4B). At 2 h after germination, 77 out 132 (58%) observed pollen tubes showed fewer LDs compared to the WT, and at 4 h, 84% ($n = 100/119$) of pollen tubes showed an abnormal distribution of LDs. In 72% of the cases, LDs were absent from apical and subapical regions and were only detected in the shank, and 12% showed an overaccumulation and aggregation of lipids at the tip. Such aberrant distribution was never observed amongst the WT pollen tubes ($n = 109$). This phenomenon was even more pronounced when pollen tubes were grown through a pistil explant, with 100% of *larp6c-3* pollen tubes showing an atypical distribution of LDs (Figure 4C, SIV). These results support the notion that lipid synthesis and/or distribution in pollen tubes is perturbed in the absence of LARP6C.

We next explored the impact of the downregulation of lipid synthesis on pollen tube guidance in the absence of LARP6C. Amongst the LARP6C mRNA targets, *MGD2* encodes a pollen specific (our data and Qin et al. (2009)) MGDG synthase (Botté et al., 2011). In situ labeling of Arabidopsis pollen tube membranes previously showed the presence of digalactosyldiacylglycerol (DGDG, which are synthesized from MGDG), and the chemical inhibition of the MGD enzymatic pathway with galvestine-1 reduces MGDG content and downregulates pollen tube elongation rates (Botté et al., 2011), supporting a role for MGD in male fertilization.

We reasoned that if one of the molecular bases of the guidance defect of *larp6c* relates to the misregulation of *MGD2* mRNA fate and expression, the specific inhibition of its enzymatic activity and downregulation of MGDG/DGDG

Downloaded from https://academic.oup.com/plcell/article/33/8/2637/6276993 by Institute of Science and Technology Austria user on 22 August 2023

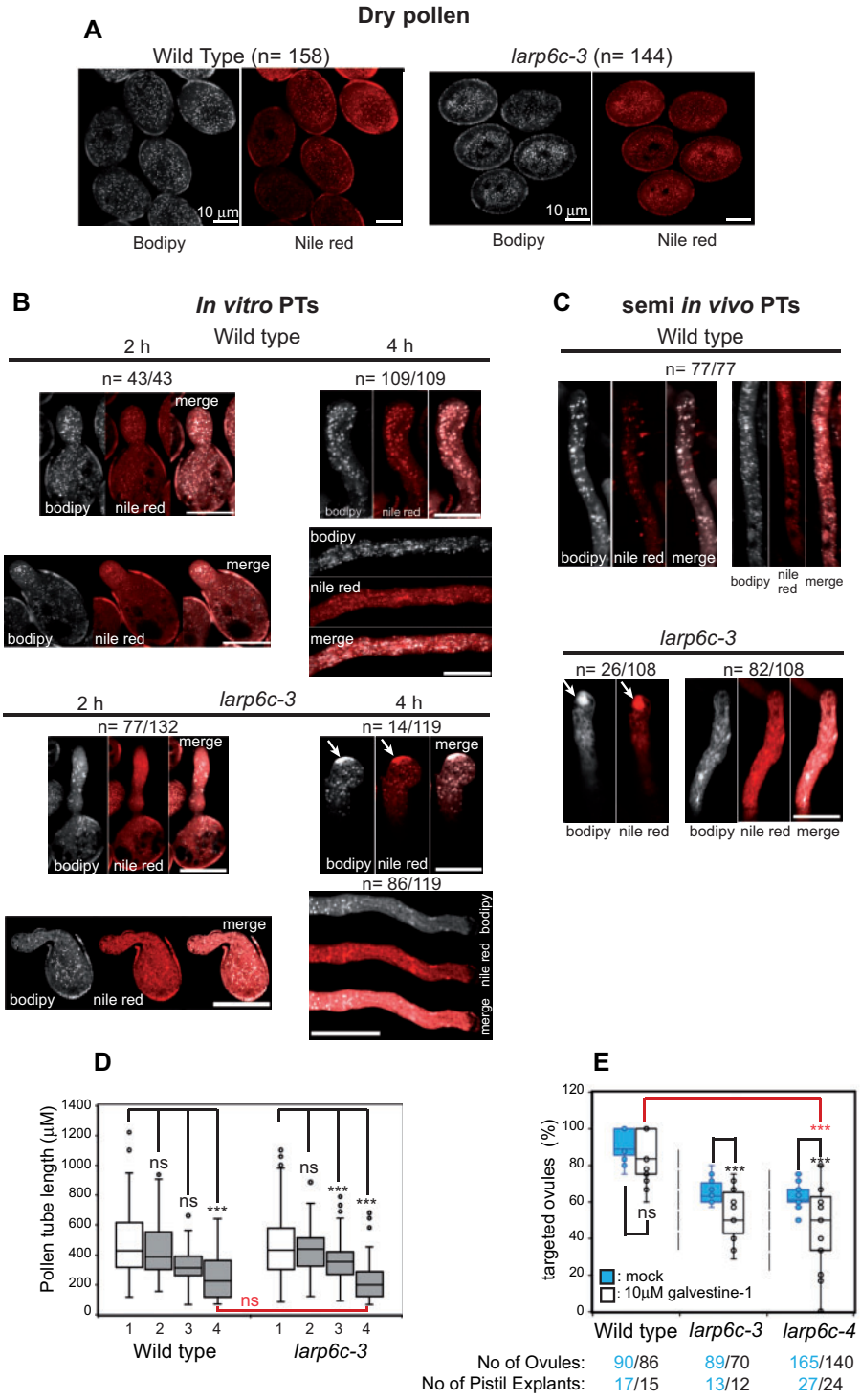

Figure 4 The loss of LARP6C function affects lipid homeostasis in pollen tubes. The WT and *larp6c-3* pollen grains were stained with Bodipy 505/515 and Nile red at the mature pollen stage (MPG; A) or in pollen tubes (PTs; B and C). In (B) PTs were germinated and grown in vitro. PTs were collected at 2 h and 4 h after activation for staining. Representative images are shown. In (C) PTs grown SIV were collected 7 h following pollination (4 hap, pistils are cut at shoulder, placed on plate with ovules, and further incubated 3 h before scoring). *n* represents the number of pollen tubes with LDs distributed as on the presented image over the total number of observed pollen grains. Scale bars correspond to 10 µm in (A) and to 5 µm in (B, C). D, Monitoring of pollen tube growth in the presence of galvestine-1. Whisker boxplot representation of the length of the WT or *larp6c-3* pollen tubes grown in vitro for 4 h in the presence or absence of galvestine-1. 1: untreated, 2: mock (1% DMSO), 3 and 4: 5 µM and 10 µM galvestine-1. E, SIV pollen tube guidance assays. Assays were conducted either in the presence of 1% DMSO (untreated) or in the presence of 10 μM of galvestine-1. Results are represented as whisker boxplots. *P*-values were obtained through an unpaired Student's *t* test; ns, not significant; ***$P \leq 0.001$.

Downloaded from https://academic.oup.com/plcell/article/33/8/2637/6276993 by Institute of Science and Technology Austria user on 22 August 2023

production with galvestine-1 should alleviate or aggravate the *larp6c* lof phenotype. We hence monitored pollen tube elongation rates and pollen tube guidance in the presence of galvestine-1 by SIV assays (Figure 4, D and E). Consistent with a previous report (Botté et al., 2011), we observed that galvestine-1 application reduced pollen tube elongation in the WT pollen as well as *larp6c-3* mutant pollen (Figure 4D). However, when we monitored pollen tube guidance efficiency, the WT pollen tubes were only slightly or not affected at all, whereas pollen tubes of *larp6c* mutants showed a considerable decrease in ovule targeting in the presence of galvestine-1 (Figure 4E). Under these conditions, only 30%–60% of ovules were targeted by *larp6c*-pollen tubes, whereas the mock-treated samples showed 60%–70% targeting. In some pistil explants, *larp6c* pollen tubes showed no ovule targeting at all in the presence of the MGD inhibitor, a situation that was never observed with *larp6c-3* pollen tubes in the absence of the MGD inhibitor (Figures 1, E and F; 4E). Collectively, these results support a synergic effect between the lof of LARP6C and the pharmacological inhibition of MGD2 synthase activity on pollen tube guidance but not on pollen tube elongation.

LARP6C also binds mRNA encoding factors involved in endosome functioning and vesicular trafficking. Brefeldin A (BFA) is a fungal toxin known to perturb endomembrane system trafficking, particularly at the level of retrograde

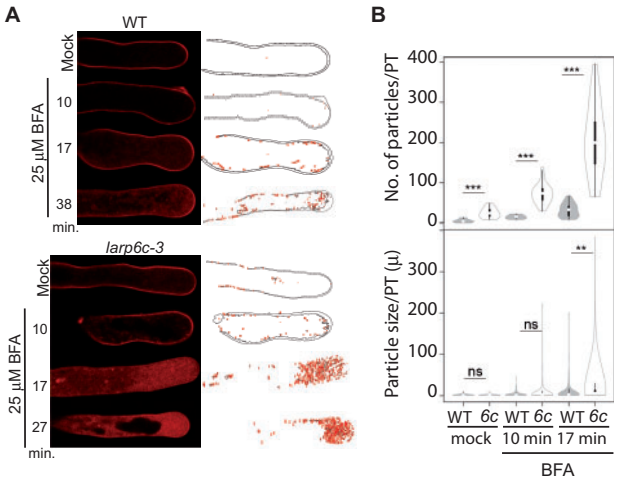

Figure 5 Pollen tubes deprived of LARP6C are hypersensitive to BFA. Pollen grains were germinated in vitro and after 1 h activation on germination medium, pollen tubes were incubated with mock (DMSO) or 25-µM BFA. A, Representative images of FM4-64 staining captured at the respective times or the WT and *larp6c-3* PTs treated with mock or BFA. Sketched outline of the PTs with red dots (counts) describing the appearance of the particle frequency and size, as detected by the ImageJ particle analysis plug in. B, Following FM 4-64 staining, the number (top panel) and size (bottom panel) of BFA bodies was scored over a time course and represented as violin plots. Number of PTs observed to score particle number: WT: mock: 23, 10 min: 14, 17 min: 30; *larp6c-3*: mock: 32, 10 min: 35, 17 min: 25. Number of PTs observed to score particle size: WT: mock: 59, 10 min: 62, 17 min: 95; *larp6c-3*: mock: 61, 10 min: 115, 17 min: 189. *P*-values were obtained with an unpaired Student's *t* test. ns, not significant; $^{**}P \leq 0.01$, $^{***}P \leq 0.001$.

Golgi to ER trafficking and to induce ectopic ER–Golgi fusions known as BFA bodies (Tse et al., 2006). We therefore monitored *larp6c-3* pollen tube sensitivity to BFA compared to the WT (Figure 5). After 1 h activation on germination medium, the pollen tubes were exposed to BFA and the number and size of BFA bodies scored over time through FM 4-64 staining. As soon as 10 min after exposure to BFA, *6c-3* pollen tubes showed increased number of BFA bodies and a dramatic increase in size compared to the WT 17 min after treatment. At this time point, ectopic BFA-particles were also bigger in the mutant than in the WT. These results indicate that pollen tubes deprived of LARP6C are hypersensitive to pharmacological perturbation of endosomal trafficking.

LARP6C directly binds to the 5′-UTRs of its mRNA targets

We next sought to understand how LARP6C recognizes and influences the fate of its mRNA targets through binding. RBPs often bind to primary sequence motifs shared between their mRNA targets to regulate their fate. Considering that cis regulatory elements are mostly located in the 5′- and/or 3′-UTRs of transcripts, we looked for primary sequence motif(s) shared between the UTRs of the putative LARP6C targets. Using the Araport database, we found and retrieved the 5′- and 3′-UTRs for 112 mRNAs and ran a discriminative motif search using a MEME search (at the MEME suite portal (https://meme-suite.org/)). Whereas no significant motif could be detected in the 3′-UTRs of LARP6C mRNA targets, we identified two regions we named A-box (E^{value}: $5.5E^{-99}$) and B-box (E^{value}: $9.3E^{-91}$) motifs that are highly enriched in the 5′-UTRs of LARP6C mRNA targets (Figure 6A). As a control, we ran an identical motif search using a set of 112 randomly chosen 5′- and 3′-UTRs from genes expressed in pollen according to our transcriptomic analyses. We found no significant enrichment for an A- or a B-type region, supporting the idea that these sequence motifs are specific for mRNAs that are in a complex with LARP6C.

The A motif is a purine-rich 21 nt sequence with a clear dominance of A over G nucleotides, while the B motif is a pyrimidine-rich 21 nt sequence with a majority of U (T in DNA) over C repeats (Figure 6A; Supplemental Data Set S1). A closer examination of sequences that contain the A and/or B consensus sequence revealed two major categories for each box type. In particular, sequences harboring the A motif are mainly composed of either A or AG/AAG repeats, whilst sequences sharing the B consensus motif contain either U or UC/UUC repeats (Supplemental Data Set S1). Amongst the 112 identified 5′-UTRs, 70 (62.5%) bear the A motif, 74 (66%) the B motif, and 49 (43.7%) carry both (Supplemental Figure S6E).

The presence of motifs shared by transcripts that coimmunoprecipitated with LARP6C in vivo suggests that one or both of these boxes mediate the direct binding of LARP6C. To explore this hypothesis, we tested the RNA-binding unit of LARP6C, the La-module, for its ability to interact with

Downloaded from https://academic.oup.com/plcell/article/33/8/2637/6276993 by Institute of Science and Technology Austria user on 22 August 2023

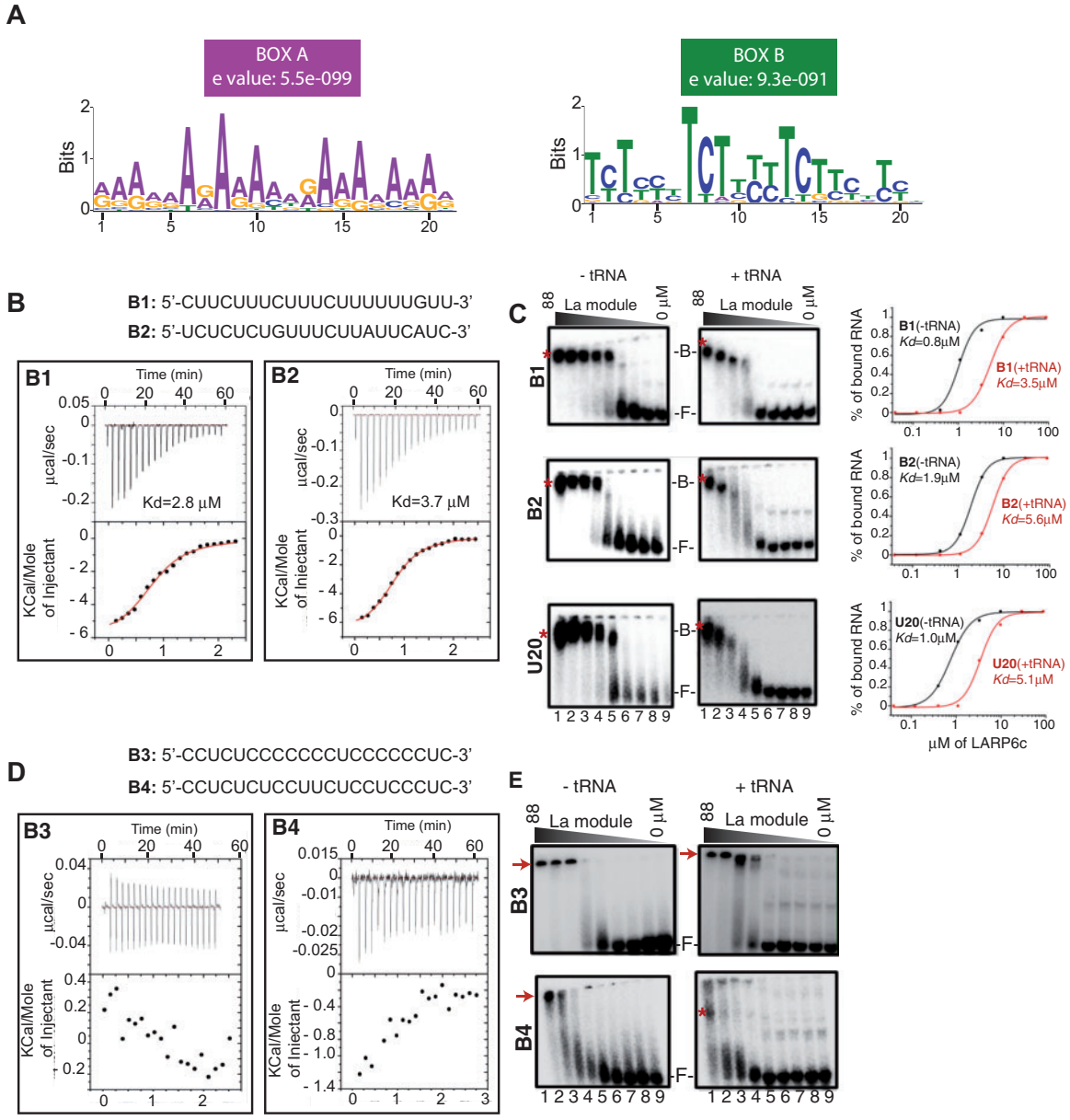

Figure 6 The LARP6C La-module binds to B-type RNA boxes. A, Consensus sequences of the conserved motifs within the 5′-UTRs of LARP6C-bound mRNAs. Calorimetric (B, D) and EMSA (C, E) analyses of the interaction between the LARP6C La-module (encompassing residues 137–332) and oligos B1, B2 (B, C), U_{20} (C), B3 and B4 (D, E). In (B) and (D) for each graph, the upper panel corresponds to the raw titration data showing the thermal effect of injecting an RNA oligo solution into a calorimetric cell containing the recombinant LARP6C La-module. The lower panels show the normalized heat per injection values obtained by integrating the raw data and subtracting the heat value of the RNA dilution. The red lines in the graphs for oligos B1 and B2 (B) represent the best fit derived by a nonlinear best-square procedure based on an independent binding site model. The dissociation constants (Kd) are indicated for the B1 and B2 oligos; the thermodynamic parameters are shown in Supplemental Table S1. C, E, EMSAs of LARP6C La-module binding to: B1, B2 or oligo U_{20} (C), B3 or B4 (E). Decreasing concentrations (µM; 88 [lane 1], 29.3 [lane 2], 9.8 [lane 3], 3.3 [lane 4], 1.1 [lane 5], 0.4 [lane 6], 0.12 [lane 7], 0.04 [lane 8], and 0 [lane 9]) of the recombinant LARP6C La-module were mixed with 3 nM of 5′-labeled oligos. B stands for Bound, F for Free, red asterisks mark the RNA-protein complex, and the red arrows on (E) shows samples retained into the gel wells. Experiments were conducted in the absence (-tRNA) or presence (+tRNA) of unlabeled competitor (tRNAmix of *E. coli* MRE 600 at 0.01 mg·mL^{-1} concentration). Graphs in (C) show the quantification of the bound RNA fraction versus the protein concentration in the absence (black lines) or presence (red lines) of tRNA competitor. The values of the dissociation constants are reported. Kd values reported for the EMSA experiments were calculated out of three independent replicates with the following standard deviations: LARP6C-B1 (−tRNA): 0.8 ±0.1; LARP6C-B1 (+tRNA): 3.5 ± 0.3; LARP6C-B2 (−tRNA): 1.9 ± 0.3; LARP6C-B2 (+tRNA): 5.6 ± 0.2.

these boxes in vitro (Figure 6, B–E; Supplemental Figure S7). We designed two oligonucleotide sequences for the A motifs called A1 and A2, representing the "A-rich" and the "AG/AAG-rich" types, respectively (Supplemental Figure S7A). Analogously, B1 and B2 were designed for the B motifs exemplifying the "U-rich" and "UC/UUC-rich" types,

Downloaded from https://academic.oup.com/plcell/article/33/8/2637/6276993 by Institute of Science and Technology Austria user on 22 August 2023

respectively (Figure 6B). As a control, we designed oligos B3 and B4, representing C- or CU/CCU-rich sequences, respectively. A recombinant version of the LARP6C La-module, identical to the one used in Merret et al. (2013b), was expressed in *E. coli* as previously described and its ability to bind the A- and B-type oligo RNAs was quantified by isothermal titration calorimetry (ITC) and electrophoretic mobility shift assay (EMSA; Figure 6, B–E; Supplemental Figure S7). In the ITC experiments, serial titration of LARP6C La-module with RNA oligos B1 and B2 generated (in both cases) a profile that could be fitted to a sigmoid-shaped binding curve centered around a 1:1 stoichiometry, with a dissociation constant in the low micromolar range (Kds of 2.8 and 3.7 μM, respectively, indicating direct binding of LARP6C La-module to B1- and B2-type motifs (Figure 6B; Supplemental Table S1). The binding mode of LARP6C La-module for the B1 and B2 oligos is similar (but with higher affinity) to that previously observed for an U20 homopolymer (Supplemental Table S1; Merret et al. (2013b)). On the contrary, no binding of oligos B3, B4, A1, or A2 to the recombinant LARP6C domain was detected by ITC under the same experimental conditions (Figure 6D; Supplemental Figure S7A; Table S1).

To confirm the ITC results, parallel EMSAs were performed using RNA oligos labeled at the 5′ end with γ-^{32}P to monitor RNA-protein complex formation by native gel electrophoresis. Experiments were conducted in the presence or absence of tRNA competitor. For oligos showing the ability to form a complex with La-module, the fraction of bound RNA was plotted against the protein concentration and the dissociation constant determined (Figure 6C). In agreement with the ITC results, EMSA confirmed that B1 and B2 oligos associate with the LARP6C La-module, with estimated dissociation constants in the low micromolar range (Kds of 0.8 and 1.9 μM, respectively), again suggesting a high affinity of LARP6C La-module towards B1 and B2 oligos (Figure 6C). The binding behavior of B2 oligo was very similar to what we observed for an oligo(U_{20}; Merret et al., 2013b), whereas B1 showed a slightly higher binding affinity. Assays with oligos A1, A2, B3, oligo(C_{20}) and to a lesser extent with B4 were hindered by samples being retained in the wells of the gel at high protein concentration (Figure 6E; Supplemental Figure S7B), an issue most likely linked to protein and/or protein/RNA nonspecific aggregation (Hellman and Fried, 2007). Despite changing various experimental conditions, this issue could not be overcome. The presence of a tRNA competitor marginally helped in the case of B4, albeit association with LARP6C was observable only at high protein concentrations and a Kd could not be calculated, as the binding curve did not reach a plateau (Figure 6E).

Collectively, these experiments demonstrate that LARP6C La-module binds to oligos B1 and B2 with high affinity and with a similar association mechanism observed with oligo(U_{20}). B1, which contains three stretches of U residues, one of which is six uridines long, appeared to bind slightly more tightly than B2 and U_{20}. Altogether, these results indicate that the LARP6C La-module strongly binds to B-type motifs and does not associate with A-type motifs, at least in vitro, and that it displays low affinity for B4.

We hence propose that in vivo, LARP6C directly binds (at least) to mRNAs that carry a B1- or B2-type box in their 5′-UTRs to execute posttranscriptional regulation on its mRNA targets.

LARP6C is not required for the accumulation of its mRNA targets in mature pollen grain

To gain a global view of the role of LARP6C in the accumulation of its mRNA targets, we monitored the polyadenylated transcriptome of mature pollen grains in the absence of LARP6C. Pollen grains were collected from the WT and *larp6c-3* plants grown together in a greenhouse (see "Supplemental methods"), total RNAs were extracted from the pollen, and the polyadenylated fraction was subjected to next generation sequencing. Following mapping and filtering of the reads (see "Supplemental methods"), we retained a list of 7,399 transcripts with at least 1 RPKM as reliably expressed from both Col-0 and *larp6c-3* (Supplemental Figure S8 and Supplemental Data Set S2). We then used a DE-seq pipeline (FDR 0.05) to find genes whose transcripts differentially accumulate in the mutant background and retained those with a fold change of at least 1.5 between the WT and *larp6c-3*. We found 2,174 genes that were upregulated or downregulated in *larp6c-3* pollen compared to the WT (Figure 7A). Monitoring the fold changes of these transcripts between the WT and (*larp6c-3*; 6C-FH) in the input fraction of the RIP-seq samples, we observed that they are centered around 1 (Figure 7B). This suggests that the expression of the *LARP6C-FlagHA* transgene in the *larp6c-3* background fully complemented the *larp6c-3* mutation and restored a WT expression level, demonstrating that the LARP6C-FlagHA translational fusion is functional and that the misregulation of the *larp6c-3* pollen transcriptome is biologically significant and a direct consequence of the loss of LARP6C function. We then asked if the steady-state levels of LARP6C-bound mRNAs are affected in *larp6c-3* pollen grains. Of the 115 targets, 96 were detected in the RNA-seq data, and only 15 of these differentially accumulated in the *larp6c-3* background (Figure 7C; Supplemental Data Set S2). Of these, 10 were downregulated by 1.5- to 2.8-fold and five were upregulated by 1.5- to 1.7-folds in *larp6c-3* (Figure 7D). These observations suggest that, at least in dry pollen, LARP6C is not required for maintaining steady-state levels of its mRNA targets.

LARP6C controls the expression of a reporter transcript containing a functional 5′-UTR B-box motif

To gain a mechanistic insight into the impact of LARP6C binding to its mRNA targets, we performed transient assays to monitor the expression of a *YFP* reporter gene under the

Downloaded from https://academic.oup.com/plcell/article/33/8/2637/6276993 by Institute of Science and Technology Austria user on 22 August 2023

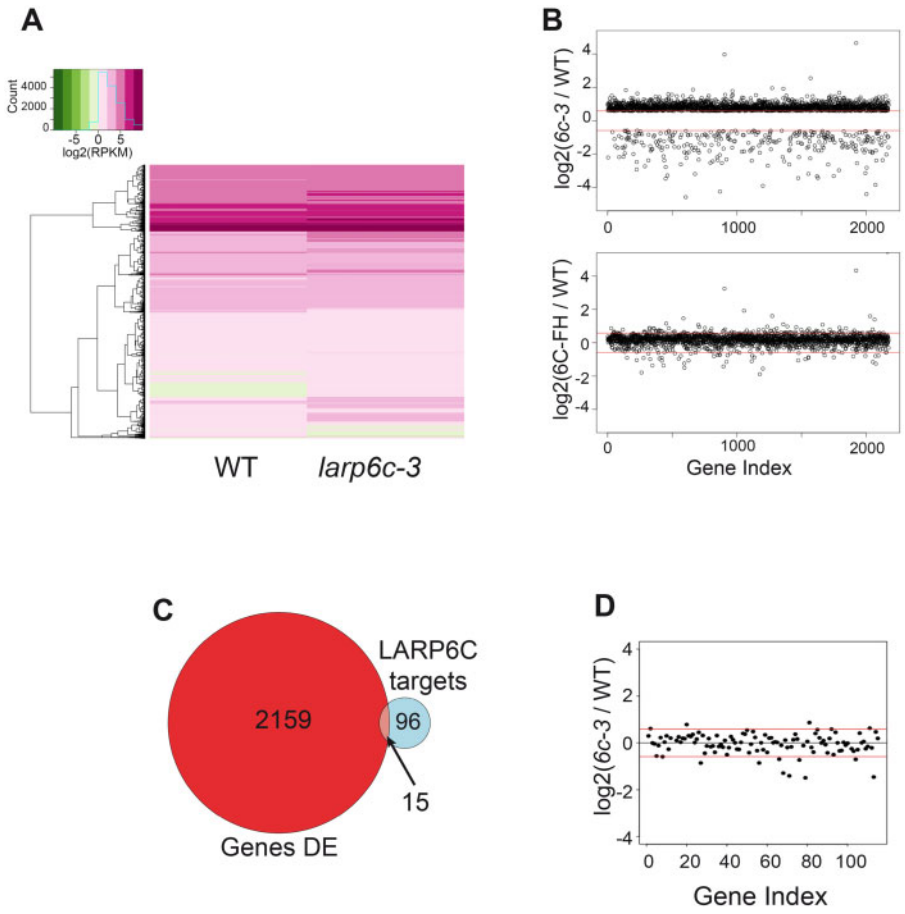

Figure 7 *larp6c* lof does not affect the steady-state transcript levels of its target in dry pollen. A, Heat map representation of the $\log_2$(RPKM) values of genes that are DE between the WT and *larp6c-3* plants. The heat map was built from the list of DE genes with log2(RPKM) values between −2 and +10 (2,142 genes: 98.5% of the DE genes). B, Plot representation of the log2 values of the ratios: (*larp6c-3*/WT; upper panel) and log2(6C-FH/WT; lower panel) for the 2,174 genes found to be DE in *larp6c-3* mutant pollen. Red lines mark the cut off value (log2(1.5) and log2(1/1.5)). C, Venn diagram representation of the number of transcripts that are DE in *larp6c-3* and/or immunoprecipitated by 6C-FH. Note that of the 115 RIP targets, 19 were not present in the transcriptomic data from RNA-seq. D, plot representation of the log2(*larp6c-3*/WT) for mRNAs identified by RIP-seq. Red lines mark the cut off value (log2(1.5) and log2(1/1.5)).

control of a modified 5′-UTR belonging to *MGD2*, a LARP6C mRNA target that carries a potential bona fide B-box and no A-box motif (Supplemental Data Set S1). We then respectively replaced the native B-box by two sequences that we demonstrated in vitro are strongly bound (B1-box) or not bound at all (B3-box) by the LARP6C La-module (Figure 6). We inserted the modified 5′-UTR sequences downstream of the CaMV35S promoter and fused to coding sequence of YFP (*B1-YFP* and *B3-YFP*) in a plant binary vector (Figure 8A). These YFP-containing plasmids were transiently expressed in *N. benthamiana* leaves individually or coinfiltrated with a plant binary vector expressing a tRFP-tagged LARP6C also under the control of the CaMV35S promoter. Three days post infiltration, leaves were collected and YFP mRNA and protein levels assessed (Figure 8, B and C). Quantitative analyses showed that when the LARP6C protein was present, *B1-YFP* transcript levels increased by two-fold (Figure 8B). Conversely, the coexpression of LARP6C with the *B3-YFP* construct did not significantly affect *B3-YFP* mRNA levels (Figure 8B). Remarkably, the presence of LARP6C significantly reduced YFP protein accumulation when expressed from the B1 but not the B3 construct (Figure 8C). We also monitored the subcellular distribution of the tRFP-LARP6C fusion protein following agroinfiltration. Similar to findings for mature pollen grains (Figure 2) and onion epidermis cells following stress exposure, LARP6C formed foci in the cytoplasm of *N. benthamiana* leaves (Figure 8D). As in pollen grains and onion epidermis cells, LARP6C foci contained the PABP, we reason that LARP6C also likely aggregates into mRNP granules in *N. benthamiana*.

LARP6C controls native MGD2 protein levels and distribution in pollen tubes

We next asked whether LARP6C controls the mRNA and proteins levels of their target genes using *MGD2* mRNA as an example. We cloned the *MGD2* genomic locus (starting at position −579 from ATG) including its native B-box motif in fusion with the YFP coding region that we placed at the C-terminus and transformed this chimeric gene into the

Downloaded from https://academic.oup.com/plcell/article/33/8/2637/6276993 by Institute of Science and Technology Austria user on 22 August 2023

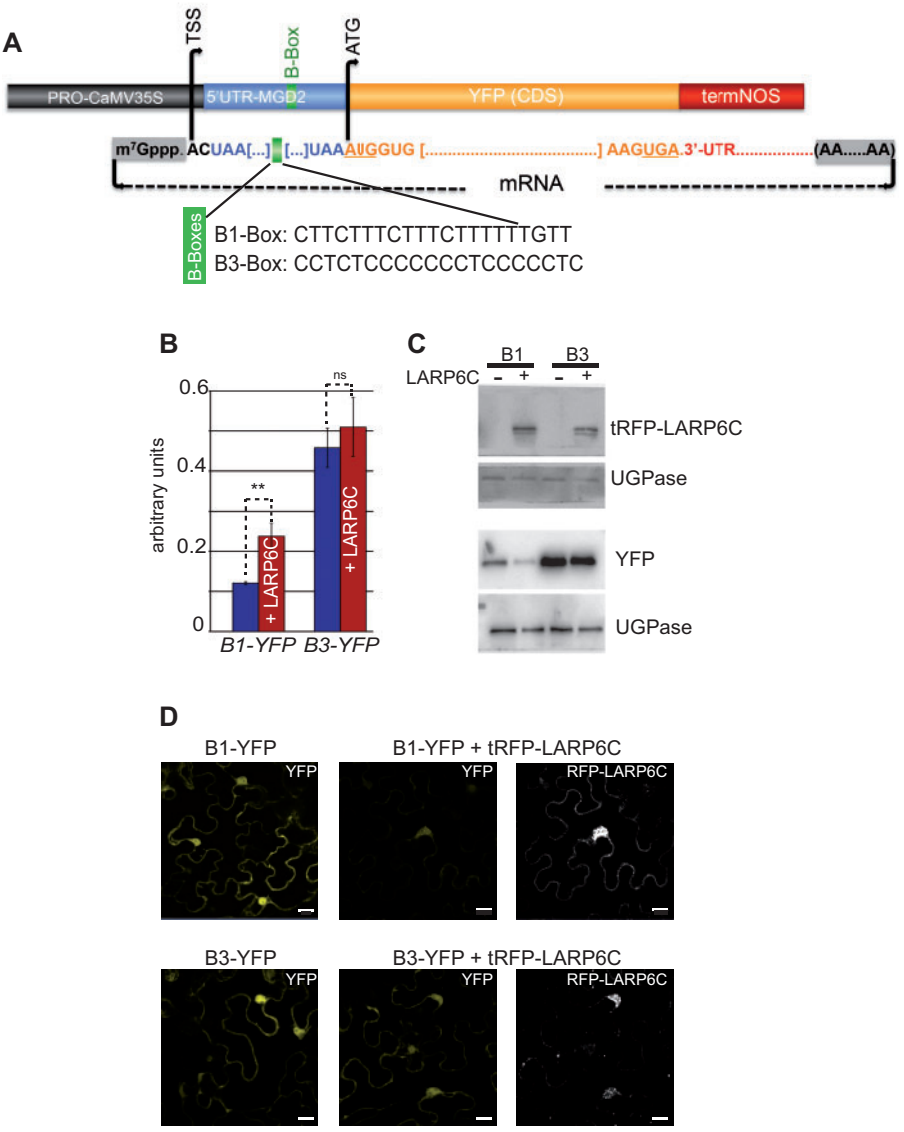

Figure 8 LARP6C binding at the 5′-UTR of a reporter construct reduces protein and increases mRNA levels. A, Schematic representation of the YFP reporter constructs, B, RT-qPCR monitoring of *YFP* mRNA levels. To normalize *YFP* mRNA levels to transformation efficiency, we used the levels of *HPTII* mRNA encoded by the *HPTII* gene carried by the YFP binary plasmid but not the tRFP-LARP6C one. SDS were calculated from three biological replicates. *P*-value was obtained using a Student's *t* test. $^{**}P < 0.005$; ns, not significant. C, Immunoblot analysis of tRFP-LARP6C and YFP protein levels. Two immunoblots were prepared and respectively hybridized with anti-LARP6C or GFP antibodies. Levels of UGPase were used as the loading control. Representative images of three replicates are shown. D, Confocal imaging of YFP from leaves not transformed with tRFP-LARP6C (left panels) and of YFP and tRFP-LARP6C distribution (right panels). Scale bars represent 20 µm. Leaves that were observed are different from those used to prepare total RNA and protein extracts. Representative images of three biological replicates are shown

WT background. We then screened pollen and pollen tubes from 22 primary transformants and selected line 6, which we crossed to *larp6c-3* homozygous plants. In the F2 generation, we selected plant homozygous for the *larp6c-3* allele that expressed heterozygous *MGD2-YFP*. We then performed microscopic observations of the WT and *larp6c-3* pollen that was heterozygous for the *MGD2-YFP* transgene. Pollen grains were placed on in vitro pollen germination agarose pad medium and YFP signals monitored in mature pollen grain (dry pollen), pollen at 15 and 30 min after hydration (Figure 9A), and pollen tubes at the 4 h time point (Figure 9B). Strikingly, both in the WT and *larp6c-3*, mature pollen grains show very low levels of YFP signal, which intensified over time upon hydration and in pollen tubes.

To confirm this finding and to assess the role of LARP6C in MGD2 protein accumulation, we quantified fluorescence intensity in dry pollen and at 1 and 4 h after activation. As shown in Figure 9C, MGD2-YFP levels drastically increased in pollen tubes 1 h after activation in both the WT and mutant. Nonetheless, compared to the WT, *larp6c-3* dry pollen showed higher levels of fluorescence, a situation opposite that observed in 1 h pollen tubes, which showed reduced

Downloaded from https://academic.oup.com/plcell/article/33/8/2637/6276993 by Institute of Science and Technology Austria user on 22 August 2023

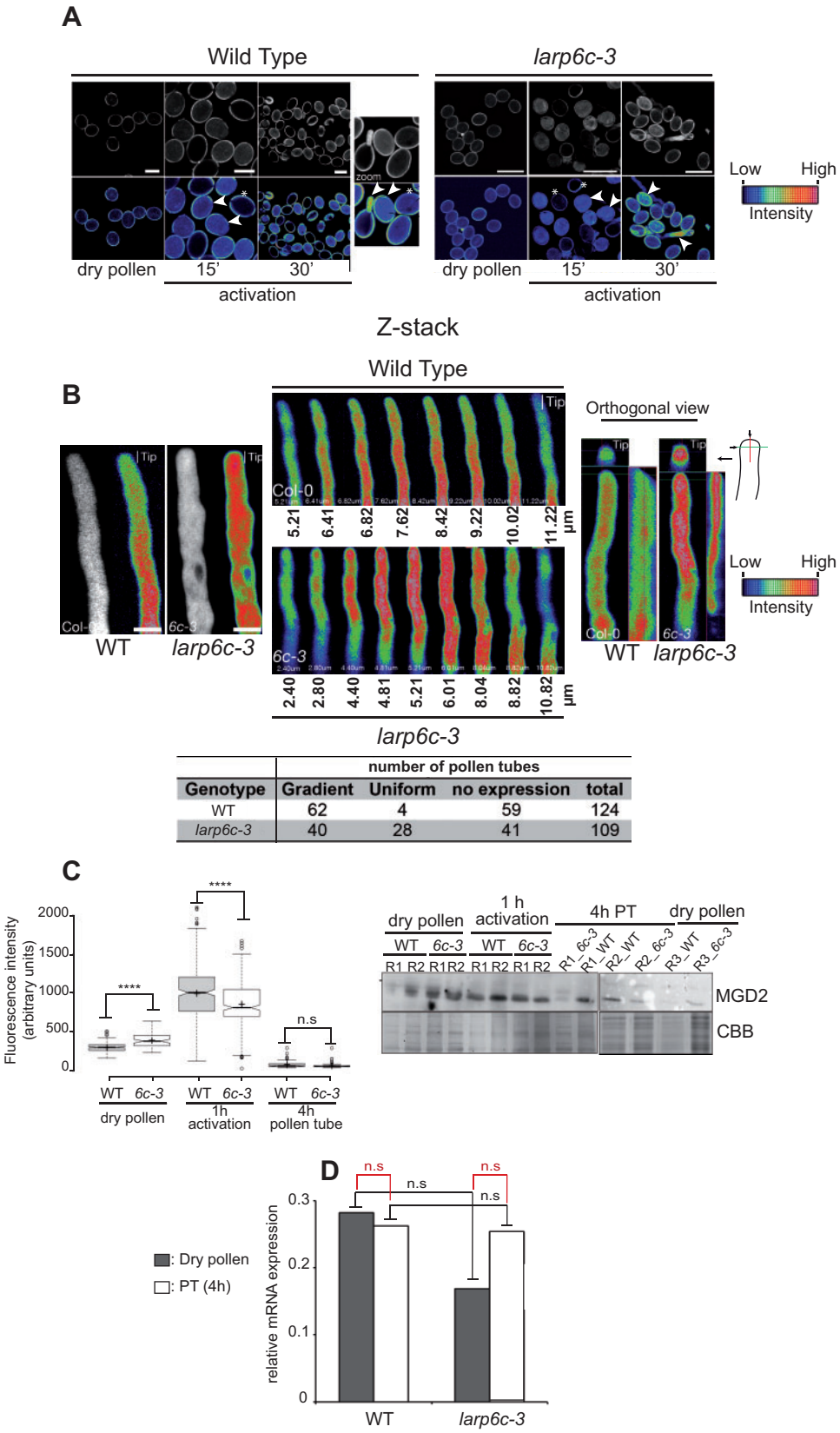

larp6c-3

Genotype	number of pollen tubes			
	Gradient	Uniform	no expression	total
WT	62	4	59	124
larp6c-3	40	28	41	109

Figure 9 LARP6C is involved in the dynamic fine-tuning of MGD2 protein accumulation in vivo. Monitoring of the levels of MGD2-YFP fusion protein expressed from the *MGD2* native promoter (PRO_{MGD2}:*MGD2-YFP*) and endogenous MGD2 in the WT and *larp6c-3* plants. A, Representative images of YFP signal in heterozygous mature pollen grains at activation: 0, 15, and 30 min after incubation on in vitro germination medium. Bottom panels show images in pseudo color with the associated scale bar representing the intensity of the YFP signal. White arrows and asterisks respectively point to segregation pollen grains expressing or not expressing the translational fusion. B, Live cell imaging of MGD2-YFP

Downloaded from https://academic.oup.com/plcell/article/33/8/2637/6276993 by Institute of Science and Technology Austria user on 22 August 2023

MGD2-YFP signals in the absence of LARP6C. Using specific antibodies (Awai et al., 2001), we made similar observations for endogenous MGD2 accumulation, finding significantly more protein in pollen tubes than in dry pollen. Moreover, the loss of LARP6C function induced the overaccumulation of MGD2 in mature pollen and underaccumulation in pollen tubes compared to the WT (Figure 9C, right panel). Next, quantitative reverse transcription polymerase chain reaction (RT-qPCR) assays revealed that the mRNA levels of *MGD2-YFP* and endogenous *MGD2* did not significantly vary before and after pollen hydration and that the lof of LARP6C did not affect mRNA levels (Figure 9D). This is consistent with previously published transcriptomic data showing that endogenous *MGD2* mRNA levels did not significantly vary between dry pollen and pollen tubes after 30 min or at 4 h activation in vitro (Qin et al., 2009).

Beyond an impact on protein levels, the loss of LARP6C function also appeared to affect MGD2-YFP distribution along the pollen tube (Figure 9B). In the WT, MGD2-YFP signal showed a diffuse cytosolic pattern, with the signal intensity distributed along a gradient decreasing from the shank toward the tip in almost 94% ($n = 124$) of the pollen tubes. In the absence of LARP6C, the gradient distribution of MGD2-YFP was lost in 59% ($n = 109$) of the observed pollen tubes, which showed a uniform distribution of the signal that also reached the pollen tube tip.

Discussion

We report here that LARP6C, an evolutionarily conserved RBP, is essential for male fertility, acting during gametogenesis and germination and especially during the progamic phase, during which it is necessary for the directional growth of pollen tubes.

The role of LARP6C in vesicular trafficking during male fertilization

The anisotropic growth of the pollen tube, which takes place exclusively at the apical dome, requires vast amounts of secretory vesicles delivered at the tip via cytoplasmic streaming. Golgi-derived secretory vesicles supply cell wall material as well as material for plasma membrane extension at the site of growth. Vesicles also deliver transmembrane proteins, such as receptor kinases, which are inserted into the apical plasma membrane through exocytosis (Grebnev et al., 2017). Indeed, the exocyst secretory complex was found to be essential for the specification of plasma membrane nanodomains that define sites for the directional growth of pollen tubes (Synek et al., 2006, 2017; Li et al., 2010; Vukašinović and Žárský, 2016). We found that *larp6c*-pollen tubes are hypersensitive to BFA and identified several transcripts encoding components of the vesicular system as LARP6C mRNA clients, including factors involved in the trafficking of ER vesicles, constituents of the vacuolar trafficking system HOPS (Takemoto et al., 2018), components and regulators of the endosomal sorting complex required for transport (Reyes et al., 2014), and a subunit of the exocyst complex (Supplemental Data Set S1). We hence propose that the pollen tube guidance defects of *larp6c* mutants are in part the consequence of abnormal vesicular trafficking.

LARP6C is necessary for lipid homeostasis during male fertilization

To optimize polar tip growth, pollen has evolved a unique lipid composition. In particular, pollen grains produce extraplastidial glycerolipids and store fatty acids and TAGs in LDs (Ischebeck, 2016). LDs are necessary for gametogenesis, pollen grain maturation, viability, and germination. They also might be required for pollen tube guided growth, as supported by the finding that MPK6 is a regulator of their synthesis involved in pollen tube guidance (Zhang et al., 2009, 2018). The exact role of LDs in pollen tubes is not currently clear, but it has been proposed that TAGs could be synthesized in the shank of the pollen tube and transported to the tip in the form of LDs to deliver membrane components (Ischebeck, 2016). In line with this idea, we report that LDs are distributed from shank to tip in the WT pollen tubes (Figure 4). Hence, the role of LARP6C in pollen tube guidance could also involve maintaining adequate LD levels, distribution, and possibly composition, as it can specifically bind mRNAs encoding fatty acid, TAG, phospho-, and glycerolipid synthases (FAD2, ACX4, TAG1, LPEAT2, MGD2) for lipases, such as SDP1, which is involved in storage lipid breakdown (Kelly et al., 2013), and for regulators of their synthesis, such as DYRKP-2A (Schulz-Raffelt et al., 2016) and MPK6 kinases (Zheng et al., 2018).

MGD2 is one of the three Arabidopsis synthases that catalyze the last step of MGDG synthesis. Consistent with the finding that galactolipids are unique and major constituents of plastid membranes, MGD1 and MGD3 were previously found to localize inside chloroplasts and at the periphery of plastids, respectively, which are consistent with a protein embedded in the outer envelope membrane. The subcellular

distribution in pollen tubes. The numbers of pollen tubes with gradient MGD2 distribution toward the tip, uniform (lost gradient), or no expression of MGD2-YFP are reported in the table below. Scale bars correspond to 10 μm. C, Left panel: fluorescence quantification of MGD2-YFP in the WT and *larp6c-3* (*6c-3*) pollen and during the progamic phase (1 and 4 h). $n = 3$ biological replicates at each time point, a Student's *t* test for two independent samples/two-tailed test was conducted, with ns, not significant; ****$P \leq 0.0001$. Right panel: immunoblot analysis of endogenous levels of MGD2 in pollen and during progamic phase in the WT and *larp6c-3*. Experiments were conducted in two or three independent replicates labeled R1, R2, and R3. D, RT-qPCR analysis of *MGD2* mRNA levels originating from the *MGD2-YFP* transgene and endogenous *MGD2* gene in dry pollen and 4 h pollen tubes. Experiments were conducted in three independent replicates, and *TUBULIN8* mRNA was used as a control. An unpaired Student's *t* test was conducted, with ns, not significant. Both the WT and *larp6c-3* express MGD2-YFP from the same primary transformant (line 6). In (A) and (B), the MGD2-YFP transgene is in the heterozygous state and the *larp6c-3* allele is homozygous. In (C) and (D), the WT and *larp6c-3* carry the MGD2-YFP transgene in the homozygous state

Downloaded from https://academic.oup.com/plcell/article/33/8/2637/6276993 by Institute of Science and Technology Austria user on 22 August 2023

distribution of MGD2 was more difficult to interpret than that of its two counterparts, as it was detected in the cytosol (Awai et al., 2001). Here, in the absence of any plastid, we also report that MGD2 is present in the cytosol of the pollen tube and that it is distributed from shank to tip along a decreasing gradient that is lost in the absence of LARP6C. These observations uncover an unsuspected role for cytosolic MGD2, which could have the ability to produce MGDG outside plastids and possibly transport its substrate DAG to the site of MGDG synthesis. As MGDG is the substrate for DGDG, which was detected at the periphery of pollen tubes (Botté et al., 2011), MGD2 could participate to pollen tube membrane expansion. Alternatively, as DAG is also a substrate for TAG production, MGD2 may also transport this substrate to the sites of LD production and therefore participate to the guidance process. The changes in MGD2 protein levels and distribution along pollen tubes could hence be another reason for the observed guidance defect of the *larp6c* mutants.

On top of vesicular trafficking and lipid dynamics, LARP6C likely controls other cellular processes required for the directed growth of pollen tubes. Indeed, several LARP6C targets encode actors in processes involved in pollen tube elongation and guidance, such as signaling factors and kinases, cell wall modification players, or ion transporters. Moreover, some LARP6C clients were experimentally found to be involved in anisotropic cell elongation. These include, the transcription factor TFIIB1, which controls guided pollen tube growth (Zhou et al., 2013); TUB4, a structural microtubule component required for normal hypocotyl guidance and elongation (Yu et al., 2015); or the α/β hydrolase-domain protein WAV2, which is involved in directional root growth (Mochizuki et al., 2005; Supplemental Data Set S1).

Molecular functions of LARP6C during male fertilization

LARP6C is an RBP that physically interacts with PABP, a master regulator of mRNA translation and decay (Merret et al., 2013b). Here we demonstrated that LARP6C at least in part colocalizes with PABP in mature pollen grain. Furthermore, a LARP6C protein deficient in its RNA-binding domain (La-module) was unable to restore LARP6C's function in pollen tube guidance. We hence propose that LARP6C acts at the molecular level to control gene expression by regulating mRNA fate in the cytoplasm.

We provided strong evidence that LARP6C directly interacts with mRNAs harboring B-boxes of the B1 or B2 type in their 5′-UTRs (i.e. at least 52 of the 115 transcripts identified by RIP-seq; Supplemental Data Set S1). For some transcripts, only A-boxes were identified in the 5′-UTR. This might have occurred because we were only able to retrieve a partial 5′-UTR sequence, and inadvertently missed sequence regions that could contain the B-box, but it is also possible that some LARP6C RIP targets are in complex with this RBP but not through direct binding.

In *N. benthamiana* leaf epidermis, LARP6C appeared to control the levels of its mRNA targets as well as the amount of the corresponding translated proteins. LARP6C promoted the overaccumulation of *YFP* mRNA that carried its recognition sequence, specifically a B1-type B-box motif (Figure 6). We propose that at least in somatic cells, this overaccumulation is the result of LARP6C-mediated protection from cytoplasmic decay, rather than an action at the transcriptional level. Surprisingly, our results also show that this increase in mRNA levels is associated with a decrease in the corresponding YFP protein levels (Figure 8). This suggests that LARP6C could, while protecting its mRNA targets, dampen their translation. Alternatively, LARP6C could control protein stability, but since it is unlikely to interact with the reporter YFP protein (the only protein encoded by the reporter gene we designed), we deem this hypothesis unlikely. In eukaryotic cells, one common feature of mRNP granules is that they contain translationally silent mRNAs that are capable of (re)-entering translation in response to the appropriate signals and protect these mRNAs from decay (Buchan, 2014). Hence, the presence of LARP6C in foci that we propose are mRNP storage granules also rather favors the first hypothesis.

The mRNA stabilization effect of LARP6C binding observed in transient *N. benthamiana* assays is in contrast with the observation that in pollen grains, LARP6C does not seem to control its targets' steady-state levels. In pollen, as in animal gametes, mRNAs are highly stable, suggesting that in the male gametophyte, the mRNA decay machineries, as well as the translational apparatus, have poor activity (Ylstra and McCormick, 1999; Hafidh et al., 2018). This assumption is consistent with our observation that DCP1, a core constituent of the mRNA decapping complex, localizes to foci in mature pollen grains and that this localization is thought to be linked to quenched DCP1 activities. Indeed, work conducted in animal cells proposed that when components of the mRNA decay machineries are present in p-bodies, they are catalytically inactive (Hubstenberger et al., 2017). The discrepancies between the results from transient assays in *N. benthamiana* leaf cells and RNA-seq of pollen grains could hence be the consequence of differences in how the mRNA decay complex operates between sporophytic and reproductive cells.

In vivo, we propose that LARP6C plays a dual role in controlling of the levels of translated proteins encoded by its targets' transcripts. Using *MGD2* mRNA as a model, we indeed showed that whilst antagonizing MGD2 protein accumulation in mature pollen grains, LARP6C promotes its translation after germination without affecting *MGD2* mRNA levels (Figure 9). Although the possibility that LARP6C regulates the amount of MGD2 protein posttranslationally cannot be ruled out at this stage, we believe that it is unlikely, as discussed for the YFP reporter protein. This implies that LARP6C shifts from a repressor to an activator role in translation. This could be the result of a differential pattern of posttranslation modifications that might allow LARP6C to recruit different sets of accessory proteins to its

Downloaded from https://academic.oup.com/plcell/article/33/8/2637/6276993 by Institute of Science and Technology Austria user on 22 August 2023

target mRNAs before and after pollen hydration, resulting in a mode switch from repression to activation.

Scarpin et al. (2017) reported that like *MGD2* mRNA, *SK14* mRNA is translationally silent in mature pollen grain and reactivated at germination. They also found that *SK14* mRNA aggregates in subcytoplasmic bodies that also contain the p-body component DCP1 (Scarpin et al., 2017). Here, we also demonstrated the existence of foci in mature pollen grain containing proteins that function in mRNA regulation (LARP6C and PAB5), which we believe also contain mRNAs. mRNP granules exist in most eukaryotes and in many cell types and are of different types based on their protein content. However, a common feature is that they store and protect translationally silent mRNPs until their protein product is needed. We therefore propose that a large portion of mRNAs whose expression is necessary for male fertilization are stored in mature pollen grains in the form of mRNP aggregates until their protein products are required during the progamic phase, as supported by previous findings (Hafidh et al., 2018), and that LARP6C is one of the trans-acting factors that orchestrate this process (see Supplemental Figure S9 for a summary model).

An intriguing observation from the current study is that LARP6C appears to be required for the distribution of the protein encoded by one of its client mRNAs, *MGD2*, along the pollen tube. We presently have no conclusive proof that LARP6C does not act at the protein level to participate in this gradient distribution. Nonetheless, considering that LARP6C is an mRNA-binding protein, we hypothesize that the defective distribution of MGD2 in *larp6c* is the consequence of the aberrant regulation of its mRNA. We propose that LARP6C transports the translationally silent mRNAs present in mRNP granules to the appropriate cytoplasmic location where the protein is then translated and required. The existence of such localized translation events following the transport of silent mRNAs is a conserved and widespread feature of eukaryotes, including plants, where few examples of mRNAs targeted to the surface of the ER, chloroplasts, or mitochondria have been reported (Tian et al., 2020). In the vast majority of cases, mRNAs are transported by cytoskeletal motors in the form of silent mRNPs (Bullock, 2011; Eliscovich and Singer, 2017). Consistent with a possible role in mRNA delivery, our data support the notion that LARP6C, in association with mRNP granules, likely navigates along microtubules in growing pollen tubes. Considering the phenotypes of *larp6c*-pollen, we propose that mRNA movement and localized translation are necessary for the polarized growth of pollen tubes and hence plant reproduction.

The role of LARP6 proteins in mRNA control might be evolutionarily conserved

Interestingly, a recent study by Dermit et al. demonstrated that human LARP6 acts in migrating cells to navigate mRNAs encoding RPs along microtubules to transport them from the cell body to protrusions; these cellular migrating fronts act as translation hotspots. This function of human LARP6 in the spatiotemporal control of RP mRNA translation is necessary for cell proliferation and migration (Dermit et al., 2020). The physiological roles of zebrafish LARP6 differ from that of Arabidopsis LARP6C, as it participates in oocyte development, chorion formation, and egg activation whilst it is not involved in male fertilization. Nevertheless, the authors suggest that zebrafish LARP6 could function in chorion formation by regulating mRNA metabolism in microvilli, that is, fine cell protrusions extending from both the developing oocytes and granulosa cells (Hau et al., 2020). It is interesting that LARP6 proteins, which are highly conserved eukaryotic RBPs, seem to have acquired distinct physiological roles during eukaryote evolution but could have retained their molecular mode of action in mRNA transport and translational control.

Materials and methods

Plant material and growth conditions

Arabidopsis thaliana ecotype Columbia-0 (Col-0) was used as the WT reference. The *larp6c-3* (SAIL_268E02; McElver et al., 2001) and *larp6c-4* (WiscDsLox293-296invG4; Woody et al., 2007) lines were respectively ordered from the NASC and ABRC stock centers. Genotyping primers are shown in Supplemental Table S2. Stable transgenic lines were obtained using the *Agrobacterium tumefaciens*-based floral dip technique (Clough and Bent, 1998). For in vitro culture, surface sterilized seeds were sown on synthetic Murashige & Skoog (MS) medium at 2.20 $g{\cdot}L^{-1}$ (1/2 MS) with 0.8% agar and stored for 48 h at 4°C in the dark before being grown under continuous light (50–60 $\mu E{\cdot}m^{-2}{\cdot}s^{-1}$) at 20°C. Plants in soil cultures were grown in growth chambers under a 16 h light (100 $\mu E{\cdot}m^{-2}{\cdot}s^{-1}$)/8 h dark cycle at 20°C with approximately 75% humidity. See "Supplemental methods" for growth conditions used to collect mature pollen for RNA-seq and RIP-seq experiments.

Cloning and plasmids

All LARP6C-containing fusion proteins (YFP, TagRFP, and FLAGHA) were expressed under the control of the upstream genomic sequences (spanning region −1181 to −1 from ATG) of the *LARP6C* gene (*AT3G19090* locus). To obtain the LARP6C-tRFP and LARP6C-FLAGHA fusions, we isolated total genomic DNA from Col-0 and PCR amplified the *LARP6C* genomic region starting from nucleotide −1181 from the ATG to the last nucleotide before the stop codon using primers 543 and 544 (Supplemental Table S2). The PCR product was inserted at sites *KpnI* and *NheI* upstream of either the tagRFP or FLAG-HA tag into a pCAMBIA (1300-based plant binary vector expressing the *HPTII* (hygromycin) resistance gene, giving rise to vectors pEB16 and pEB13. To obtain the YFP-LARP6C expressing binary vector, the genomic region spanning nucleotides −1181 to −1 from the ATG of the *LARP6C* gene was PCR amplified with primers 974 and 975 from vector pEB13 and cloned at sites *SacI* and *KpnI* upstream of a Gateway entry cassette into a pPZP221-based (Hajdukiewicz et al., 1994) plant

Downloaded from https://academic.oup.com/plcell/article/33/8/2637/6276993 by Institute of Science and Technology Austria user on 22 August 2023

binary vector carrying the *AAC1* (gentamycin) resistance gene, giving rise to vector p788. The *LARP6C* coding genomic region was PCR amplified from total genomic DNA with primers 976–977 and cloned at sites *Spe*I-*Eco*RV downstream of the YFP tag located between the AttL1 and L2 Gateway donor sites, giving rise to plasmid p793. The plant binary vector p795 was obtained through a Gateway cloning reaction between p788 and 793. The *PAB5* genomic sequence (−1966 from the ATG to the last nucleotide before the stop codon) was PCR amplified from total genomic DNA with primers eb3 and eb4 and cloned using the restriction endonucleases *Xba*I and *BamH*I into vector CTL579 (pCAMBIA-1300) upstream of the GFP tag, giving rise to plasmid pEB3. To prepare transgenic lines expressing the YFP-LARP6CΔLAM protein, we transformed *larp6c-3* or *larp6c-4* plants with plasmid p844. The *LARP6CΔLAM* CDS codes for a LARP6C protein deleted of the region spanning amino acids 137–227 were obtained as follows. We PCR amplified the regions of the coding sequence from +1 to + 411 from ATG (primers 1197 and 1198) with primer 1198, which also adds a 3′-tail extension of 20 nt complementary to region 684–704 of the CDS (located just downstream to the LAM). A second PCR product was generated with primers 1199–1200, starting from position 684 to the stop codon. To fuse both products, we ran a third PCR amplification with primers 1201–1200 and an equimolar mixture of products 1 and 2 as a matrix. The resulting fragment corresponds to the full-length *LARP6C* CDS deleted of its LAM and carrying *Xba*I and *Eco*RV restriction sites at its 5′ and 3′ ends, respectively. This fragment was inserted downstream of the *YFP* sequence into a Gateway donor vector through enzymatic restriction and ligation (p843). The *YFP-LARP6CΔLAM* fusion construct was transferred into a plant binary vector under the control of the *LARP6C* native promoter through Gateway cloning between p843 and p788 (p844).

The binary vector pGEX2-GEX2GFP was obtained from Mori et al. (2014). Binary plasmids for transient assays were prepared as follow. DNA fragments encompassing a basal CaMV35S promoter without enhancer sequences (Töpfer et al., 1987), modified *MGD2* 5′-UTRs, and the YFP CDS were ordered from GeneCust (http://www.genecust.com/fr) and subcloned into a Gateway donor vector. DNA cassettes were then introduced into a plant binary vector containing the *HPTII* (hygromycin) resistance gene (vector CTL575, a derivative of pCAMBIA-1300). The *LARP6C* coding sequence was fused downstream of the tagRFP fluorescent reporter and placed under the control of a strong CaMV35S promoter by Gateway recombination with the plant binary entry vector p-SITE-6C1 (Martin et al., 2009).

To prepare a translational MGD2-YFP fusion, we amplified the *MGD2* genomic region starting from nucleotide −579 from the ATG to the last nucleotide before the stop codon using primers 31 and 32 (Supplemental Table S2). The complete PCR product was cloned into pDONR221 via the TOPOisomerase cloning technique to generate entry vector pDONR221-MGD2no-stop. To generate the plant expression vector, LR Clonase was used to recombine pDONR221-MGD2no-stop into the pB7FWG,0 Gateway binary vector in frame with C-terminal YFP. Primary transformants were selected using BASTA selection.

Pollen phenotyping

Pollen transmission tests were conducted through hand pollination of the WT pistils with pollen from mutant and complemented homozygous plants. The number of offspring carrying the mutation was scored either by PCR-based genotyping or by selection of antibiotic/herbicide-resistant seedlings. The number of mutant seedlings was expressed as a percentage over the total number of seedlings and TE of the mutant gametophyte calculated $\text{asTE} = \left(\left(\frac{\text{No.ofmutant}}{\text{No.ofWT}}\right) \times 100\right)$.Experiments were conducted in triplicate. Pollen tube guidance efficiency was scored either by SIV (Palanivelu and Preuss, 2006) or in vivo assays by observing pistils hand pollinated with the mutant pollen of interest and stained with aniline blue (Mori et al., 2006). Emasculated pistils were from *ms1* (male sterility 1) heterozygous plants. This guaranteed that the pistils were not contaminated with the WT pollen, as the *ms1-1* mutant is male sterile (van der Veen and Wirtz, 1968; Ito et al., 2007). Monitoring of pollen tube guidance in the presence of galvestine-1 was conducted through SIV assays on plates containing 1% DMSO for mock treatment or 5 or 10 μM of galvestine-1 with a final concentration of 1% DMSO. For all pollen tube guidance assays, in vivo aniline blue staining and SIV as well as in vivo blue dot assays were performed according to Kulichová et al. (2020).

Pollen and pollen tube collection for total RNA and protein extraction

Approximately 250 μL equivalent of open flowers were collected in 1.5-mL Eppendorf tubes for each respective genotype. To collect mature pollen, flowers were vigorously and briefly vortexed with 500 μL of RIPA extraction buffer for protein extraction or with pollen germination medium for RNA extraction and spun in a benchtop centrifuge for 1 min. Media were removed and pellets stored at −80°C until extraction. For pollen activation/germination, the pollen pellet was resuspended in liquid pollen germination medium and incubated for 1 h at 22°C. One biological replicate corresponds to one sample of 250 μL equivalent of open flowers.

Microscopy

Subcellular localization experiments in pollen grain and pollen tubes were conducted with an LSM700 confocal microscope (Zeiss) using emission/excitation wavelengths: 405 nM/420–480 nM for DAPI, 555 nM/600–700 nM for tRFP, and 488 nM/490–555 nM for YFP and GFP. Mature pollen grains were collected by dipping open flowers into a drop of DAPI solution (1× PBS pH 7, 0.5% Triton-X100, 1 $\mu g \cdot mL^{-1}$

Downloaded from https://academic.oup.com/plcell/article/33/8/2637/6276993 by Institute of Science and Technology Austria user on 22 August 2023

4′,6-diamino-2-phenylindole) on a glass slide. To collect immature pollen grains at the microspore, bicellular and tricellular stages, anthers were collected from unopened buds, placed in a drop of DAPI solution on a glass slide, and gently crushed to free the pollen grains from pollen sacs. Pollen tubes germinated and grown as described in the Supplemental Methods were directly observed from the germination slide. For cytoskeleton colocalization, PRO_{LARP6C}:tRFP:LARP6C was coinfiltrated in *N. benthamiana* leaves with either p35S:GFP-AtTUB6, p35S:GFP-FABD2, or pUBQ-LifeAct:GFP. Confocal images were taken under a Nikon Eclipse Ti confocal microscope equipped with a CSU-X1 spinning disk module and Andor iXon3 EMCCD camera, as well as with a Zeiss LSM880 confocal microscope, and captured with ZEN 2.3v software. Images were analyzed and assembled with ImageJ/Fiji (http://imagej.net/http://fiji.sc/Fiji), Adobe Photoshop CS6 (www. adobe.com), Ink-scape (www.inkscape.org), and NIS Elements (LIM) software. For YFP quantification in pollen tubes, MGD2-YFP signals in the respective genotypes were captured under a Zeiss LSM880 confocal microscope using an Argon 488 laser and detected with GasP detector with fixed configurations. Zen (blue edition) software was used to quantify pixel intensity, and data were processed in Excel.

Pharmacological treatment

For the galvestine-1 inhibition assay, pollen tubes were grown on solid pollen germination medium containing 1% DMSO for mock treatment or 5 or 10 μM of galvestine-1 at a final concentration of 1% DMSO. For BFA A treatment, Arabidopsis pollen tubes were grown for 1 h in vitro and stained by incubating with 1-μM FM4-64 (Thermo Fisher Scientific, https://www.thermofisher.com) concomitantly with BFA at 25 μM (Sigma, www.sigmaaldrich.com, BFA stock solution at 50 mM in DMSO) in liquid pollen germination medium for 5 and 10 min. To visualize LDs, Bodipy stain (505/515) at a final concentration of 2 μM and Nile red stain (552/636) at a final concentration of (0.1 $\mu g \cdot mL^{-1}$) were simultaneously added to germinated pollen tubes and incubated for 3 min prior to imaging.

Total RNA extraction and RT-qPCR

For RNA-sequencing purpose, total RNA was purified from mature pollen grain as follow. Around 0.5–3 mg of dry pollen was ground with a Silamat S6 mixing device (Ivolcar Vivadent, Schaan, Liechtenstein) in 500 μL of GuHCl buffer (8-M GuHCl, 20-mM MES, 20-mM EDTA, at pH 7, 50-mM β-mercaptoethanol) and with five glass beads. Following 1 min vortexing at full speed and 10 min incubation on ice, RNAs were separated from proteins via two consecutive phenol–chloroform–isoamyl alcohol (IAA, 25:24:1) extractions, followed by one extraction with chloroform–IAA (24:1), consisting of 1 min vortexing at full speed and 10-min centrifugation at 16°C, 14,000*g*. RNAs are then precipitated in the presence of 0.7 vol. isopropanol, 1/20th CH_3COOH at 1 M for 20 min at −20°C. Following 20-min centrifugation at 4°C, 14,000*g*, the RNA pellet was washed in 90% EtOH and resuspended in RNAse free water. The average efficiency of pollen RNA extraction was 5–6 μg of RNA per mg of dry pollen. To measure *MGD2* (*YFP-MGD2* and endogenous *MGD2*) mRNA levels, total RNA was extracted from 5 mg of dry pollen and 250 μL equivalent of flowers used to grow pollen tubes for 4 h in vitro from (MGD2-YFP; *LARP6C*) and (MGD2-YFP; *larp6c*-3) homozygous lines. One biological replicate corresponds to 5 mg of dry pollen and 250 μL equivalent flowers for pollen tubes. A total of three biological and six technical replicates were generated. *MGD2* native primers and *TUB8* were used for measurement and normalization, respectively. Relative expression was computed as above.

To quantify *YFP* mRNA levels in *N. benthamiana* transient assays, total RNA was isolated from the samples using a Monarch Total RNA Miniprep Kit (New England Biolabs), and genomic DNA was eliminated using gDNA removal columns and on-column DNaseI-treated (New England Biolabs). Five micrograms of total RNA were reverse transcribed with a SuperScript IV kit (Life Technology) using an oligodT_{18} primer. qPCR was conducted on a LightCycler 480 Multiwell Plates 384-well themocycler (Roche Applied Sciences) with the following amplification program: 5 min 95°C, 40 cycles of 15 s at 95°C, and 1 min at 60°C. After amplification, melting curve analysis was performed with a temperature gradient of $0.1°C \cdot s^{-1}$ from 60°C to 95°C. The PCR mixture contained Takyon qPCR master mix (Eurogentec), 500-nM gene-specific primers, and 1-μL cDNA in a total reaction volume of 10 μL. Primer efficiencies were determined using standard curves, with 10-fold serial dilution series ranging from 1×10^1 to 1×10^6 of the cDNA samples. Relative quantification was performed by the $\Delta\Delta C_T$ method (Livak and Schmittgen, 2001), with *YFP* and *HPTII* used as the target and reference gene, respectively. The sequences of the primers used for RT- and qPCR are shown in Supplemental Table S2.

RNA-seq, RIP-seq, bioinformatics

Techniques related to large-scale analyses (RNA-seq and RIP-seq), as well as the bioinformatic analyses, are detailed in the "Supplemental methods."

Protein-related techniques

Total protein extracts were separated by sodium dodecyl sulphate–polyacrylamide gel electrophoresis (SDS–PAGE) on an acrylamide gel before being electrotransferred onto a PVDF membrane (0.45 μM, Merck Millipore). After saturation in a (1× TBS – 0.1% tween – 5% fat-free dry milk) solution, the membranes were incubated with the appropriate primary then secondary antibodies, washed three times with a 1× TBS – 0.1% Tween solution, and chemiluminescence revealed with an EMD Millipore Immobilon Western Chemiluminescent HRP Substrate kit. Antibodies against the LARP6C protein were custom made (at Agro-Bio, La Ferté St Aubin, France) through immunization of rabbits with the peptide "KRTSQFTDRDREELGQ" (amino acids 220–235). Anti-LARP6C antibodies are utilized at 1/1,000 dilution in a

Downloaded from https://academic.oup.com/plcell/article/33/8/2637/6276993 by Institute of Science and Technology Austria user on 22 August 2023

(1× TBS – 0.1% Tween – 5% fat-free dry milk) solution and incubated overnight at 4°C with gentle shaking. Secondary antibodies were anti-rabbit HRP (Bio-Rad) and used at a 1/5,000 dilution. Anti-ACTIN antibodies were from Affinity Bio Reagents (Golden, CO, USA) and used at 1/15,000 dilution. Secondary antibodies were anti-mouse HRP (Bio-Rad) used at a 1/10,000 dilution. For transient assays, the YFP protein was detected using the GFP antibody (Clontech) at 1/5,000 and the UGPase antibody (Agrisera) at 1/7,500 dilution, both incubated overnight at 4°C. Secondary antibodies anti-mouse HRP (Bio-Rad) used at a 1/2,000 dilution and anti-rabbit HRP (Bio-Rad) used at a 1/5,000 dilution were incubated for YFP and UGPase detection, respectively, for 1h at room temperature. To detect endogenous MGD2, proteins were extracted from 5 mg of dry pollen and 250 µL equivalent of flowers used to germinate pollen tubes in vitro for 1h or 4h from (MGD2-YFP; LARP6C) and (MGD2-YFP; *larp6c*-3) homozygous lines. One biological replicate corresponds to 5 mg of pollen grain, and 250 µL equivalent open flowers for pollen tubes. A total of three replicates for dry pollen and 1 h activated pollen, and two replicates for 4 h pollen tubes were generated. After SDS–PAGE separation, membrane blocking was performed with 5% milk for 30 min at room temperature. The membrane was incubated with antibodies against MGD2 (a gift from Eric Maréchal [LPCV, Grenoble]; Awai et al., 2001), at 1/500 dilution, overnight at 4°C. Secondary anti-Rabbit HRP (Agrisera) was used at 1/10,000 dilution and incubated for 1 h at room temperature prior to membrane development.

For RNA-protein binding in vitro assays, the LARP6C La-module (amino acids 137–223) was recombinantly expressed as in Merret et al. (2013b). The hexahistidine tag (His-tag) was removed by proteolysis via incubation at 4°C overnight with HRV 3C Protease in a buffer containing 50-mM Tris-HCl, pH 7.25, 100-mM KCl, 0.2-mM EDTA, 1-mM DTT, 10% glycerol. The cleaved His-Tag and the protease were separated from the La-module through retention onto a Ni-NTA column. The protein was then subjected to heparin column purification and dialysis in a final buffer as in Merret et al. (2013b).

ITC and EMSA

RNA oligos were custom made from IBA-Lifescience GmbH (Göttingen, Germany) at a 1-µ Molar scale and HPLC purified. The lyophilized RNAs were resuspended in RNAse free water (DEPC treated) at concentrations ranging from 2.5 to 3 mM. The ITC experiments were performed as in Merret et al. (2013b) on an iTC200 microcalorimenter (Malvern). Here, 20 injections of 2-µL RNA solutions at 200–320 µM concentration were added to protein solutions (LARP6C La-module) at 20–30 µM with a computer-controlled 40-µL syringe. Control titrations of RNA into buffer alone and into protein solution without the His-tag were performed. The heat per injection normalized per mole of injectant versus molecular ratio was analyzed with the MicroCal-Origin 7.0 software package and fitted using a nonlinear least-square minimization algorithm using a theoretical single-site binding model. ΔH (reaction enthalpy change in kcal·mol^{-1}), K_b (binding constant equal to 1/Kd), and n (molar ratio between the two proteins in the complex) were the fitting parameters. The reaction entropy was calculated using the equations $\Delta G = -RT\ln Kb$ ($R = 1.986$ cal·mol^{-1} K^{-1}; $T = 298$ K) and $\Delta G = \Delta H - T\Delta S$. All ITC experiments were repeated at least three times, and a detailed analysis of the thermodynamic parameters and errors calculated as the standard deviation from the mean value are reported in Supplemental Table S1. For EMSA, RNAs were 5′-labeled with γ-^{32}P-ATP using T4 polynucleotide kinase. Recombinant protein and RNA were mixed and incubated for 15 min at room temperature in 20-mM Tris, pH 7.25, 200-mM KCl, 5% of glycerol, 1-mM DTT, 0.1 mg·mL^{-1} of BSA and 0.7 units of RNase inhibitors (RNaseOUT, Invitrogen). Each reaction mixture (22 µL) contained 3 nM of labeled RNA oligo and varying amounts of LARP6C La-module (3-fold serial dilutions from an 88-µM sample). The experiments were performed in the absence or presence of unlabeled mixed tRNAs from *E. coli* MRE 600 (0.01 mg·mL^{-1}). After the addition of 2 µL of 30% Ficoll, the samples were loaded on a 9% native polyacrylamide gel prerun at 100 mV for 1 h at 4°C in 0.5× Tris-borate-EDTA buffer. A typical EMSA experiment was run at 4°C for 1 h at 125 mV. Gels were dried onto 3MM chromatography paper, exposed to a phosphoimaging plate overnight, analyzed on a Typhoon Trio phosphoimager, and quantified with Image Quant TL software. The fraction of bound RNA was plotted versus the protein concentrations. To determine the dissociation constants, the data were fitted with Origin 8.0 to a modified Hill equation (Ryder et al., 2008) using nonlinear least squares methods and assuming a 1:1 stoichiometry.

Nicotiana benthamiana transient assays

Plasmids B1-YFP, B3-YFP, and RFP-LARP6C were respectively transformed into *A. tumefaciens* strain LB4404. Transformed bacteria were cultivated until they reached OD 0.8 and used to infiltrate fully expanded leaves from 8-week-old *N. benthamina* plants using a needless syringe as described in Ruiz et al. (1998). When double transformations were performed (B1-YFP and RFP-LARP6C or B3-YFP and RFP-LARP6C), an equimolar mixture of *Agrobacterium* cultures (OD 0.4) was used for transformation. For each transformation, we also used an *Agrobacterium* culture carrying a plasmid (OD 0.2) allowing the expression of the P19 suppressor of RNA silencing (Lasierra and Prat, 2018).Three days postinfiltration (dpi), transformed leaf segments were collected, flash frozen, and total RNA or protein extracted. Alternatively, at 3 dpi transformed leaves were observed by confocal microscopy to monitor YFP and tRFP signals.

Accession numbers

Sequence data in this study can be found under the following accession numbers: Bioproject PRJNA557669. RNA-Seq-Col0-Rep 1: SRR9887494; RNA-Seq-Col0-Rep 1: SRR9887493; RNA-Seq-*larp6c-3*-Rep 1; SRR9887496; RNA-Seq-*larp6c-3*-Rep 2

Downloaded from https://academic.oup.com/plcell/article/33/8/2637/6276993 by Institute of Science and Technology Austria user on 22 August 2023

SRR9887495; RIP-Col0-Input-Rep 1: SRR9887498; RIP-Col0-Eluate-Rep 1: SRR9887500; RIP-Col0-Input-Rep 2: SRR9887497; RIP-Col0-Eluate-Rep 2: SRR9887499; RIP-LARP6C-Input-Rep 1: SRR9887490; RIP-LARP6C-Eluate-Rep 1: SRR9887492; RIP-LARP6C-Input-Rep 2: SRR9887489; RIP-LARP6C-Eluate-Rep 2: SRR9887491.

Supplemental data

The following materials are available in the online version of this article.

Supplemental Figure S1. Expression profiles of *LARP6A*, *6B*, and *6C* mRNAs across development.

Supplemental Figure S2. Pollen maturation, germination, and pollen tube growth of *larp6c* lof mutants.

Supplemental Figure S3. Schematic representation of *LARP6C* transgenes, immunoblotting analyses of their accumulation, SIV pollen tube guidance competition assays, and analysis of LARP6A function in male fertilization.

Supplemental Figure S4. Pollen attraction competence of *larp6c*-3 and *6c4* ovules.

Supplemental Figure S5. Confocal analyses of LARP6C-tRFP and/LARP6A-GFP in pollen.

Supplemental Figure S6. Reproducibility of the RIP-seq data, RIP-seq filtering workflow, representation of the position of A and/or B boxes on the 5′-UTRs of LARP6C targets.

Supplemental Figure S7. ITC and EMSA assessment of LARP6C La-module binding to A-type oligos.

Supplemental Figure S8. Reproducibility of the RNA-seq data.

Supplemental Figure S9. Model of the molecular functions of LARP6C in male fertilization.

Supplemental Table S1. Thermodynamic parameters of the calorimetric analyses shown in Figure 4, B and D; Supplemental Figure 6A.

Supplemental Table S2. List and sequences of primers used for q-PCR, genotyping, and cloning.

Supplemental Methods

Supplemental Data Set S1. Results of RIP-seq experiment.

Supplemental Data Set S2. Results of RNA-Seq experiment.

Supplemental Movie S1. LARP6C foci move along microtubules.

Acknowledgments

We thank David Twell group (Leicester University) for sharing LAT52:H2B-GFP marker, Martin Potoský (Cell Biology, IEB Prague), Eva Kollárová, and Fatima Cvrčková (Faculty of Science, Charles University, Prague) for the cytoskeleton constructs. The authors would like to thank Eric Maréchal (LPCV, Grenoble) for sharing MGD2 antibodies and galvestine-1, as well as for fruitful discussions on LARP6C targets' functions, in particular those involved in lipid biology.

Funding

This work was funded by the CNRS, The University of Perpignan (UPVD), the Agence Nationale pour la Recherche (ANR) grant Heat-EpiRNA (grant no. ANR-17-CE20-007-01); a Bonus Quality Research (BQR) funded by the University of Perpignan; a Collaborative PICS Project (LARP&STRESS, grant no. 6170) funded by CNRS; Grantová agentura České republiky (GACR; grant nos. 17-23203S and 18-02448S), European Regional Development Fund-Project "Centre for Experimental Plant Biology" (No. CZ.02.1.01/0.0/0.0/16_019/0000738) and the Royal Society Newton International fellowship (ref. NF140482). This study is set within the framework of the "Laboratoires d'Excellence (LABEX)" TULIP (ANR-10-LABX-41). E.B. was the recipient of a PhD grant from the UPVD, Doctoral School ED305. C.G.L. Jr is the recipient of a short-term contract supported by the ANR Heat-EpiRNA (ANR-17-CE20-007-01). S.H., K.K., and D.H. are supported by GACR (grant nos. 17-23203S and 18-02448S). S.H. is also supported by European Regional Development Fund-Project "Centre for Experimental Plant Biology" (grant no. CZ.02.1.01/0.0/0.0/16_019/0000738). I.C.G. was supported by a Royal Society Newton International fellowship (ref. NF140482). I.G.C. and M.R.C. thank the Centre for Biomolecular Spectroscopy at King's College London funded by a capital award from the Wellcome Trust.

Conflict of interest statement. None declared.

References

Ambrose JC, Cyr R (2007) The Kinesin ATK5 functions in early spindle assembly in Arabidopsis. Plant Cell **19**: 226–236

Awai K, Maréchal E, Block MA, Brun D, Masuda T, Shimada H, Takamiya K, Ohta H, Joyard J (2001) Two types of MGDG synthase genes, found widely in both 16:3 and 18:3 plants, differentially mediate galactolipid syntheses in photosynthetic and non-photosynthetic tissues in Arabidopsis thaliana. Proc Natl Acad Sci USA **98**: 10960–10965

Belostotsky DA (2003) Unexpected complexity of poly(A)-binding protein gene families in flowering plants: three conserved lineages that are at least 200 million years old and possible auto- and cross-regulation. Genetics **163**: 311–319

Belostotsky DA, Meagher RB (1996) A pollen-, ovule-, and early embryo-specific poly(A) binding protein from Arabidopsis complements essential functions in yeast. Plant Cell **8**: 1261–1275

Botella C, Sautron E, Boudiere L, Michaud M, Dubots E, Yamaryo-Botté Y, Albrieux C, Marechal E, Block MA, Jouhet J (2016) ALA10, a phospholipid flippase, controls FAD2/FAD3 desaturation of phosphatidylcholine in the ER and affects chloroplast lipid composition in Arabidopsis thaliana. Plant Physiol **170**: 1300–1314

Botté CY, Deligny M, Roccia A, Bonneau A-L, Saïdani N, Hardré H, Aci S, Yamaryo-Botté Y, Jouhet J, Dubots E, et al. (2011) Chemical inhibitors of monogalactosyldiacylglycerol synthases in Arabidopsis thaliana. Nat Chem Biol **7**: 834–842

Bousquet-Antonelli C, Deragon J-M (2009) A comprehensive analysis of the La-motif protein superfamily. RNA **15**: 750–764

Brownfield L, Hafidh S, Borg M, Sidorova A, Mori T, Twell D (2009) A plant germline-specific integrator of sperm specification and cell cycle progression. PLoS Genet **5**: e1000430

Buchan JR (2014) mRNP granules. Assembly, function, and connections with disease. RNA Biol **11**: 1019–1030

Downloaded from https://academic.oup.com/plcell/article/33/8/2637/6276993 by Institute of Science and Technology Austria user on 22 August 2023

Bullock SL (2011) Messengers, motors and mysteries: sorting of eukaryotic mRNAs by cytoskeletal transport. Biochem Soc Trans **39**: 1161–1165

Cai L, Fritz D, Stefanovic L, Stefanovic B (2010a) Binding of LARP6 to the conserved 5′ stem-loop regulates translation of mRNAs encoding type I collagen. J Mol Biol **395**: 309–326

Cai L, Fritz D, Stefanovic L, Stefanovic B (2010b) Nonmuscle myosin-dependent synthesis of type I collagen. J Mol Biol **401**: 564–578

Challa AA, Stefanovic B (2011) A novel role of vimentin filaments: binding and stabilization of collagen mRNAs. Mol Cell Biol **31**: 3773–3789

Clough SJ, Bent AF (1998) Floral dip: a simplified method for Agrobacterium-mediated transformation of Arabidopsis thaliana. Plant J **16**: 735–743

Cvrčková F, Oulehlová D (2017) A new kymogram-based method reveals unexpected effects of marker protein expression and spatial anisotropy of cytoskeletal dynamics in plant cell cortex. Plant Methods **13**: 19

Dermit M, Dodel M, Lee FCY, Azman MS, Schwenzer H, Jones JL, Blagden SP, Ule J, Mardakheh FK (2020) Subcellular mRNA localization regulates ribosome biogenesis in migrating cells. Dev Cell **55**: 298–313.e10

Eliscovich C, Singer RH (2017) RNP transport in cell biology: the long and winding road. Curr Opin Cell Biol **45**: 38–46

Feng Q-N, Liang X, Li S, Zhang Y (2018) The ADAPTOR PROTEIN-3 complex mediates pollen tube growth by coordinating vacuolar targeting and organization. Plant Physiol **177**: 216–225

Grebnev G, Ntefidou M, Kost B (2017) Secretion and endocytosis in pollen tubes: models of tip growth in the spot light. Front Plant Sci **8**: 154

Hafidh S, Potěšil D, Fíla J, Feciková J, Čapková V, Zdráhal Z, Honys D (2014) In search of ligands and receptors of the pollen tube: the missing link in pollen tube perception. Biochem Soc Trans **42**: 388–394

Hafidh S, Potěšil D, Müller K, Fíla J, Michailidis C, Herrmannová A, Feciková J, Ischebeck T, Valášek LS, Zdráhal Z, et al. (2018) Dynamics of the pollen sequestrome defined by subcellular coupled omics. Plant Physiol **178**: 258–282

Hajdukiewicz, P., Svab, Z., and Maliga, P. (1994) The small, versatile pPZP family of Agrobacterium binary vectors for plant transformation. Plant Mol. Biol. **25**: 989–94

Hau HTA, Ogundele O, Hibbert AH, Monfries CAL, Exelby K, Wood NJ, Nevarez-Mejia J, Carbajal MA, Fleck RA, Dermit M, et al. (2020) Maternal Larp6 controls oocyte development, chorion formation and elevation. Development **147**: dev187385

Hellman LM, Fried MG (2007) Electrophoretic mobility shift assay (EMSA) for detecting protein–nucleic acid interactions. Nat Protoc **2**: 1849–1861

Higashiyama T, Takeuchi H (2015) The mechanism and key molecules involved in pollen tube guidance. Annu Rev Plant Biol **66**: 393–413

Honys D, Combe JP, Twell D, Capková V (2000) The translationally repressed pollen-specific ntp303 mRNA is stored in non-polysomal mRNPs during pollen maturation. Sex Plant Reprod **13**: 135–144

Honys D, Twell D (2004) Transcriptome analysis of haploid male gametophyte development in Arabidopsis. Genome Biol **5**: R85

Hubstenberger A, Courel M, Bénard M, Souquere S, Ernoult-Lange M, Chouaib R, Yi Z, Morlot JB, Munier A, Benard M, et al. (2017) P-body purification reveals the condensation of repressed mRNA regulons. Mol Cell **68**: 144–157.e5

Ischebeck T (2016) Lipids in pollen—they are different. Biochim Biophys Acta **1861**: 1315–1328

Ito T, Nagata N, Yoshiba Y, Ohme-Takagi M, Ma H, Shinozaki K (2007) Arabidopsis MALE STERILITY1 encodes a PHD-type transcription factor and regulates pollen and tapetum development. Plant Cell **19**: 3549–3562

Johnson MA, Preuss D (2002) Plotting a course: multiple signals guide pollen tubes to their targets. Dev Cell **2**: 273–281

Kelly AA, van Erp H, Quettier A-L, Shaw E, Menard G, Kurup S, Eastmond PJ (2013) The SUGAR-DEPENDENT1 lipase limits triacylglycerol accumulation in vegetative tissues of Arabidopsis. Plant Physiol **162**: 1282–1289

Khan BR, Adham AR, Zolman BK (2012) Peroxisomal acyl-CoA oxidase 4 activity differs between Arabidopsis accessions. Plant Mol Biol **78**: 45–58

Klepikova AV, Logacheva MD, Dmitriev SE, Penin AA (2015) RNA-seq analysis of an apical meristem time series reveals a critical point in Arabidopsis thaliana flower initiation. BMC Genomics **16**: 466

Kulichová K, Kumar V, Steinbachová L, Klodová B, Timofejeva L, Juříček M, Honys D, Hafidh SS (2020) PRP8A and PRP8B spliceosome subunits act coordinately to control pollen tube attraction in Arabidopsis thaliana. Development **147**: dev186742

Lasierra P, Prat S (2018) Transient transactivation studies in Nicotiana benthamiana leaves. Methods Mol Biol **1794**: 311–322

Li S, van Os GMA, Ren S, Yu D, Ketelaar T, Emons AMC, Liu C-M (2010) Expression and functional analyses of EXO70 genes in Arabidopsis implicate their roles in regulating cell type-specific exocytosis. Plant Physiol **154**: 1819–1830

Livak KJ, Schmittgen TD (2001) Analysis of relative gene expression data using real-time quantitative PCR and the $2-\Delta\Delta$CT method. Methods **25**: 402–408

Manojlovic Z, Earwood R, Kato A, Perez D, Cabrera OA, Didier R, Megraw TL, Stefanovic B, Kato Y (2017) LA-related protein 6 controls ciliated cell differentiation. Cilia **6**: 4

Maraia RJ, Mattijssen S, Cruz-Gallardo I, Conte MR (2017) The La and related RNA-binding proteins (LARPs): structures, functions, and evolving perspectives. Wiley Interdiscip Rev RNA **8**: e1430

Martin K, Kopperud K, Chakrabarty R, Banerjee R, Brooks R, Goodin MM (2009) Transient expression in Nicotiana benthamiana fluorescent marker lines provides enhanced definition of protein localization, movement and interactions in planta. Plant J **59**: 150–162

Martino L, Pennell S, Kelly G, Busi B, Brown P, Atkinson RA, Salisbury NJ, Ooi ZH, See KW, Smerdon SJ, et al. (2015). Synergic interplay of the La motif, RRM1 and the interdomain linker of LARP6 in the recognition of collagen mRNA expands the RNA binding repertoire of the La module. Nucleic Acids Res **43**: 645–660

McCue AD, Cresti M, Feijó JA, Slotkin RK (2011) Cytoplasmic connection of sperm cells to the pollen vegetative cell nucleus: potential roles of the male germ unit revisited. J Exp Bot **62**: 1621–1631

McElver J, Tzafrir I, Aux G, Rogers R, Ashby C, Smith K, Thomas C, Schetter A, Zhou Q, Cushman MA, et al. (2001). Insertional mutagenesis of genes required for seed development in Arabidopsis thaliana. Genetics **159**: 1751–63.

Merret R, Descombin J, Juan Y-T, Favory J-J, Carpentier M-C, Chaparro C, Charng Y-Y, Deragon J-M, Bousquet-Antonelli C (2013a). XRN4 and LARP1 are required for a heat-triggered mRNA decay pathway involved in plant acclimation and survival during thermal stress. Cell Rep **5**:1279–1293

Merret R, Martino L, Bousquet-Antonelli C, Fneich S, Descombin J, Billey É, Conte MR, Deragon J-M (2013b) The association of a La module with the PABP-interacting motif PAM2 is a recurrent evolutionary process that led to the neofunctionalization of la-related proteins. RNA **19**: 36–50

Mochizuki S, Harada A, Inada S, Sugimoto-Shirasu K, Stacey N, Wada T, Ishiguro S, Okada K, Sakai T (2005) The Arabidopsis WAVY GROWTH 2 protein modulates root bending in response to environmental stimuli. Plant Cell **17**: 537–547

Mori T, Igawa T, Tamiya G, Miyagishima S-Y, Berger F (2014) Gamete attachment requires GEX2 for successful fertilization in Arabidopsis. Curr Biol **24**: 170–175

Mori T, Kuroiwa H, Higashiyama T, Kuroiwa T (2006) GENERATIVE CELL SPECIFIC 1 is essential for angiosperm fertilization. Nat Cell Biol **8**: 64–71

Downloaded from https://academic.oup.com/plcell/article/33/8/2637/6276993 by Institute of Science and Technology Austria user on 22 August 2023

Palanivelu R, Preuss D (2006) Distinct short-range ovule signals attract or repel Arabidopsis thaliana pollen tubes in vitro. BMC Plant Biol **6**: 7

Pleskot R, Pejchar P, Bezvoda R, Lichtscheidl IK, Wolters-Arts M, Marc J, Zárský V, Potocký M (2012) Turnover of phosphatidic acid through distinct signaling pathways affects multiple aspects of pollen tube growth in tobacco. Front Plant Sci **3**: 54

Qin Y, Leydon AR, Manziello A, Pandey R, Mount D, Denic S, Vasic B, Johnson MA, Palanivelu R (2009) Penetration of the stigma and style elicits a novel transcriptome in pollen tubes, pointing to genes critical for growth in a pistil. PLoS Genet **5**: e1000621

Reyes FC, Buono RA, Roschzttardtz H, Di Rubbo S, Yeun LH, Russinova E, Otegui MS (2014) A novel endosomal sorting complex required for transport (ESCRT) component in Arabidopsis thaliana controls cell expansion and development. J Biol Chem **289**: 4980–4988

Ruiz MT, Voinnet O, Baulcombe DC (1998) Initiation and maintenance of virus-induced gene silencing. Plant Cell **10**: 937–946

Ryder SP, Recht MI, Williamson JR (2008) Quantitative analysis of protein-RNA interactions by gel mobility shift. Methods Mol Biol **488**: 99–115

Samaj J, Müller J, Beck M, Böhm N, Menzel D (2006) Vesicular trafficking, cytoskeleton and signalling in root hairs and pollen tubes. Trends Plant Sci **11**: 594–600

Scarpin MR, Sigaut L, Temprana SG, Boccaccio GL, Pietrasanta LI, Muschietti JP (2017) Two Arabidopsis late pollen transcripts are detected in cytoplasmic granules. Plant Direct **1**: e00012

Schulz-Raffelt M, Chochois V, Auroy P, Cuiné S, Billon E, Dauvillée D, Li-Beisson Y, Peltier G (2016) Hyper-accumulation of starch and oil in a Chlamydomonas mutant affected in a plant-specific DYRK kinase. Biotechnol Biofuels **9**: 55

Stålberg K, Ståhl U, Stymne S, Ohlrogge J (2009) Characterization of two Arabidopsis thaliana acyltransferases with preference for lysophosphatidylethanolamine. BMC Plant Biol **9**: 60

Synek L, Schlager N, Eliáš M, Quentin M, Hauser M-T, Žárský V (2006) AtEXO70A1, a member of a family of putative exocyst subunits specifically expanded in land plants, is important for polar growth and plant development. Plant J **48**: 54–72

Synek L, Vukašinović N, Kulich I, Hála M, Aldorfová K, Fendrych M, Žárský V (2017) EXO70C2 is a key regulatory factor for optimal tip growth of pollen. Plant Physiol **174**: 223–240

Takemoto K, Ebine K, Askani JC, Krüger F, Gonzalez ZA, Ito E, Goh T, Schumacher K, Nakano A, Ueda T (2018) Distinct sets of tethering complexes, SNARE complexes, and Rab GTPases mediate membrane fusion at the vacuole in Arabidopsis. Proc Natl Acad Sci USA **115**: E2457–E2466

Tian L, Chou H-L, Fukuda M, Kumamaru T, Okita TW (2020) mRNA localization in plant cells. Plant Physiol **182**: 97–109

Töpfer R, Matzeit V, Gronenborn B, Schell J, Steinbiss HH (1987) A set of plant expression vectors for transcriptional and translational fusions. Nucleic Acids Res **15**: 5890

Tse YC, Lo SW, Hillmer S, Dupree P, Jiang L (2006) Dynamic response of prevacuolar compartments to brefeldin a in plant cells. Plant Physiol **142**: 1442–1459

Twell D, Wing R, Yamaguchi J, McCormick S (1989) Isolation and expression of an anther-specific gene from tomato. Mol Gen Genet **217**: 240–245

van der Veen JH, Wirtz P (1968) EMS-induced genic male sterility in Arabidopsis thaliana: a model selection experiment. Euphytica **17**: 371–377

Voigt B, Timmers ACJ, Samaj J, Müller J, Baluska F, Menzel D (2005) GFP-FABD2 fusion construct allows in vivo visualization of the dynamic actin cytoskeleton in all cells of Arabidopsis seedlings. Eur J Cell Biol **84**: 595–608

Vukašinović N, Žárský V (2016) Tethering complexes in the Arabidopsis endomembrane system. Front Cell Dev Biol **4**: 46

Vukmirovic M, Manojlovic Z, Stefanovic B (2013) Serine-threonine kinase receptor-associated protein (STRAP) regulates translation of type I collagen mRNAs. Mol Cell Biol **33**: 3893–3906

Weber C, Nover L, Fauth M (2008) Plant stress granules and mRNA processing bodies are distinct from heat stress granules. Plant J **56**: 517–530

Weng H, Kim C, Valavanis C, Wang Z, Schwartz LM (2009) Acheron, an novel LA antigen family member, binds to CASK and forms a complex with Id transcription factors. Cell Mol Biol Lett **14**: 273–287

Woody ST, Austin-Phillips S, Amasino RM, Krysan PJ (2007) The WiscDsLox T-DNA collection: an arabidopsis community resource generated by using an improved high-throughput T-DNA sequencing pipeline. J Plant Res **120**: 157–165

Ylstra B, McCormick S (1999) Analysis of mRNA stabilities during pollen development and in BY2 cells. Plant J **20**: 101–108

Yu J, Qiu H, Liu X, Wang M, Gao Y, Chory J, Tao Y (2015) Characterization of tub4(P287L), a β-tubulin mutant, revealed new aspects of microtubule regulation in shade. J Integr Plant Biol **57**: 757–769

Zhang M, Fan J, Taylor DC, Ohlrogge JB (2009) DGAT1 and PDAT1 acyltransferases have overlapping functions in Arabidopsis triacylglycerol biosynthesis and are essential for normal pollen and seed development. Plant Cell **21**: 3885–3901

Zhang Y, Stefanovic B (2016) LARP6 meets collagen mRNA: specific regulation of type I collagen expression. Int J Mol Sci **17**: 419

Zheng Y, Deng X, Qu A, Zhang M, Tao Y, Yang L, Liu Y, Xu J, Zhang S (2018) Regulation of pollen lipid body biogenesis by MAP kinases and downstream WRKY transcription factors in Arabidopsis. PLoS Genet **14**: e1007880

Zhou J-J, Liang Y, Niu Q-K, Chen L-Q, Zhang X-Q, Ye D (2013) The Arabidopsis general transcription factor TFIIB1 (AtTFIIB1) is required for pollen tube growth and endosperm development. J Exp Bot **64**: 2205–2218

Downloaded from https://academic.oup.com/plcell/article/33/8/2637/6276993 by Institute of Science and Technology Austria user on 22 August 2023

Supplemental data. Billey, Hafidh et al. (2021). LARP6C orchestrates post-transcriptional reprogramming of gene expression during hydration to promote pollen tube guidance. Plant Cell.

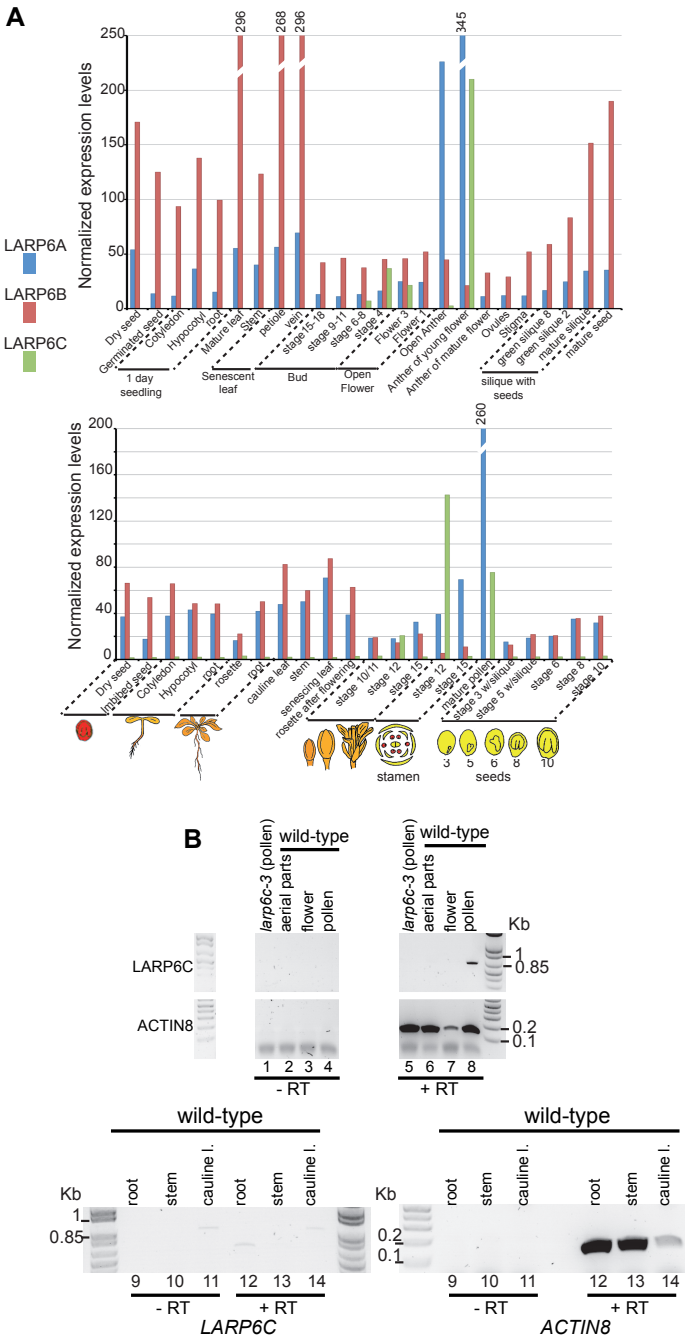

Supplemental Figure S1: ***Expression profiles of LARP6A, 6B and 6C mRNAs across development***. (Supports Figure 1A). (**A**), Expression profiles of the *LARP6A (AT5g46250)*, *6B* (*AT2g43970*) and *6C* (*AT3g19090*) mRNA across Arabidopsis development. Data were retrieved from the TraVa database of gene expression profiles monitored by RNA-seq (http://travadb.org/) (Klepikova et al., 2015) (upper graph) and from the Arabidopsis eFP Browser from the Bio-Analytic Resources for plant biology (http://bar.utoronto.ca/) (Winter et al., 2007) and are represented as histograms. The normalized expression values are arbitrary units. (**B**) RT-PCR analysis of steady-state *LARP6C* mRNA levels in various tissues from wild-type plants. Specificity of the PCR reactions was verified by omitting the reverse transcription step (no RT, lanes 1-4; 9-11). RNAs from *larp6c-3* pollen grains were utilized as negative controls (lanes 1 and 5). RNAs extracted from: seedling aerial parts (lanes 2, 6), whole flower (lanes 3, 7), mature pollen grains (lanes 4, 8), seedling roots (lanes 9, 12), stem (lanes 10, 13) and cauline leaves (lanes 11, 14) were tested. The *ACTIN8* transcript was used as a positive control.

Supplemental data. Billey, Hafidh et al. (2021). LARP6C orchestrates post-transcriptional reprogramming of gene expression during hydration to promote pollen tube guidance. Plant Cell.

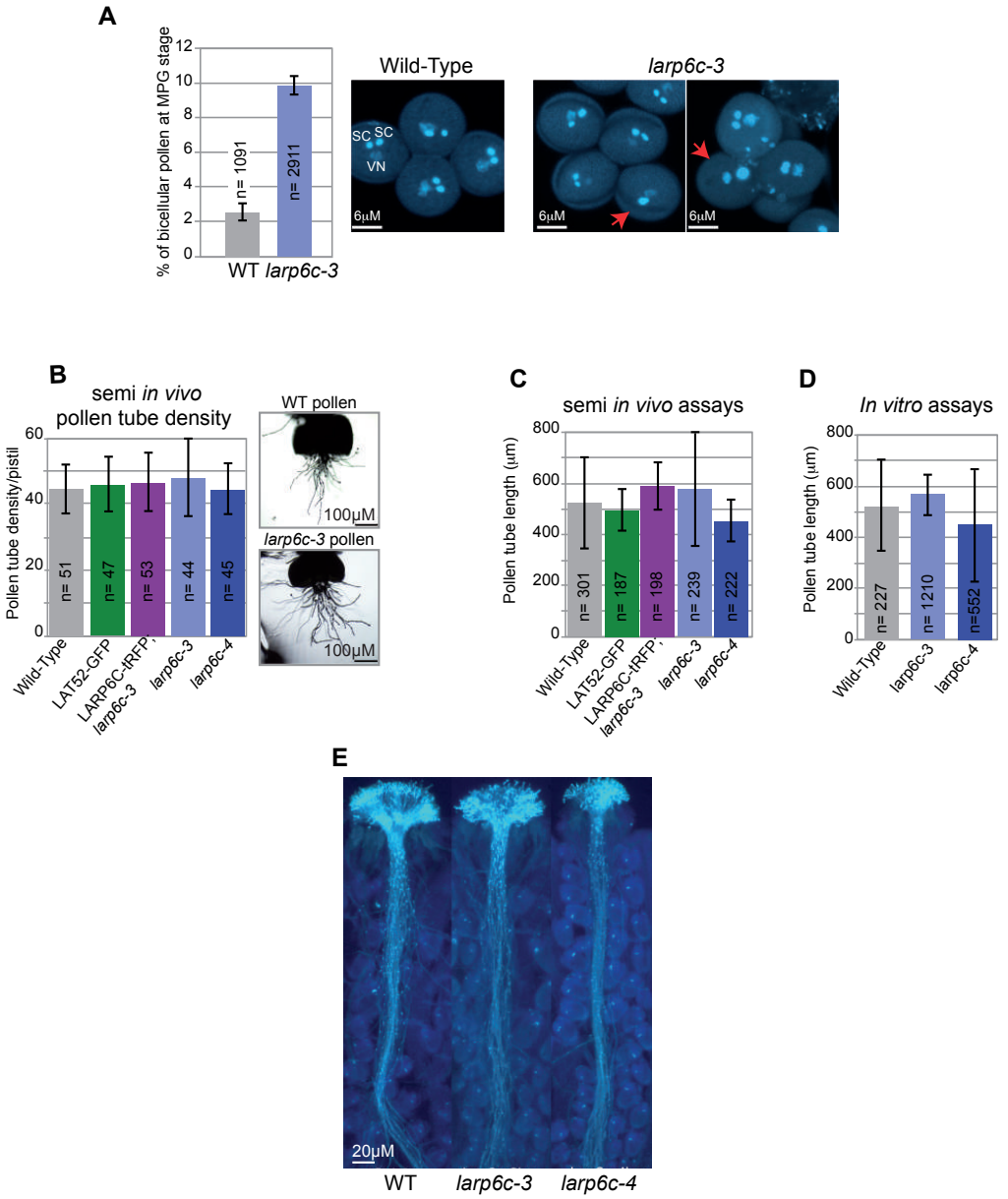

Supplemental Figure S2: Pollen maturation, germination, and pollen tube growth of larp6c loss-of-function mutants. (Supports Figure 1). **(A)**, *larp6c* loss-of-function induces a slight pollen maturation deficiency. Mature Pollen Grain (MPG) from wild type (WT) or *larp6c-3* homozygous in quartet (*qrt-/-*) mutant plants were collected and observed following DAPI staining. The number of bicellular pollen grains was scored over the total number of observed MPGs. The results are presented as histograms and correspond to mean values of three replicates ± SD and "n" is a total number of pollen grains examined. On the right are representative fluorescence micrographs of wild-type and *larp6c-3* pollen grains stained with DAPI. Red arrows point to mature pollen grains in which the generative cell remained undivided and appeared as binucleate. Scale bars correspond to 6 µm. **(B)**, Mean germination rates (± SD) of pollen tubes emerged per pistil in a semi *in vivo* assay. The total number of observed pistils is reported as "n" from three biological replicates. Transgenic LAT52-GFP pollen grains were used as a control. **(C)**, Pollen tube length derived from the semi *in vivo* assay. No significant difference was observed between wild-type and mutant pollen tubes (Student *t* test $p > 0.05$) calculated from pooled replicates. **(D)**, *In vitro* pollen tube length measurements. The total number of pollen tubes measured is reported on the histogram as "n". (**E**) *In vivo* aniline blue staining of pollen tubes after fertilization with wild-type (WT), *larp6c-3* or *larp6c-4* pollen. n = 10, 16 and 21 pistils respectively. In the semi *in vivo* assays, scoring was conducted 7 hours after pollination (hap) (4 hap pistils were cut at the shoulder, placed on a plate, and further incubated 3 hours before scoring). In the *in vitro* assays, scoring was conducted 4 hours after activation on germination medium. In the *in vivo* assays, scoring was performed 24 hap.

Supplemental data. Billey, Hafidh et al. (2021). LARP6C orchestrates post-transcriptional reprogramming of gene expression during hydration to promote pollen tube guidance. Plant Cell.

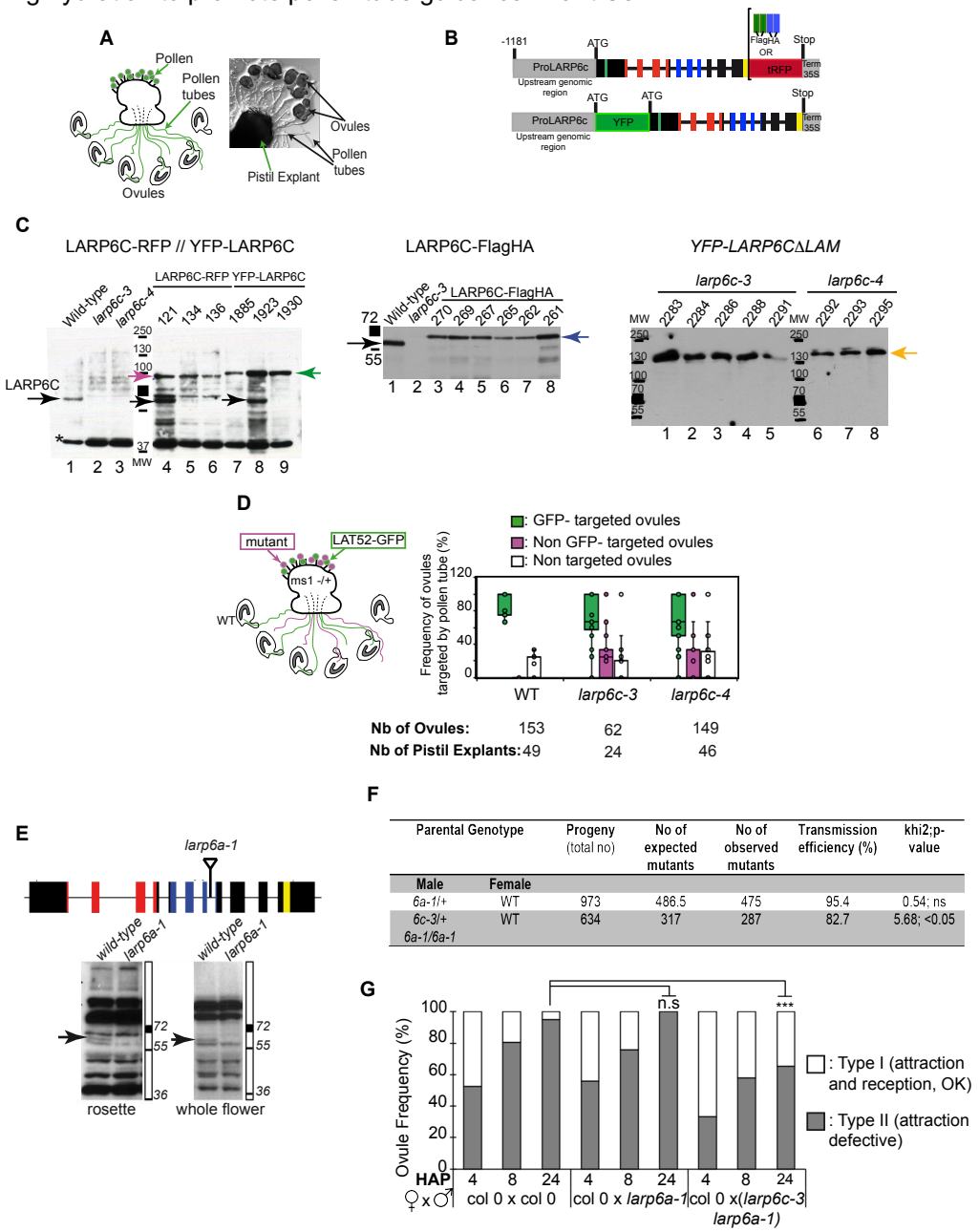

Parental Genotype		Progeny (total no)	No of expected mutants	No of observed mutants	Transmission efficiency (%)	khi2;p-value
Male	**Female**					
6a-1/+	WT	973	486.5	475	95.4	0.54; ns
6c-3/+ 6a-1/6a-1	WT	634	317	287	82.7	5.68; <0.05

Supplemental Figure S3: Schematic representation of LARP6C transgenes and immunoblotting analyses of their accumulation. Semi *in vivo* pollen tube guidance competition assays. Analysis of LARP6A function in male fertilization. (Supports Figures 1 to 3). **(A)** Representation of the setting of a semi *in vivo* guidance assay. (**B**) Schematic representation of the transgenes utilized to stably express tagged versions of LARP6C protein in mature pollen. The drawing and color codes are as in Figure 1B. **(C)** Immunoblot analysis of the expression of tagged LARP6C transgenic proteins. Total proteins were extracted from whole flowers, and blots were probed with anti-LARP6C antibodies. Left panel: expression levels of LARP6C-tRFP and YFP-LARP6C in the wild type (lanes 4 and 8), *larp6c-3 (lanes 5, 6, 9)* and/or *larp6c-4* (lane 7) backgrounds. Confocal analyses presented in Figure 2 were conducted with pollen from: lines 1885 (UNM), 1930 (BCP and TCP), 1923 (MPG) and 136 (pollen tubes). Line 134 was used to co-express the various markers presented in Figure 3. Lines 134 and 1930 were used as complemented lines for pollen experiments reported in Figures 1D and E and Supplemental Figure 2. Black arrows point to endogenous LARP6C, red arrows to LARP6C-tRFP, green arrows to YFP-LARP6C and black asterisk to non-specific signal. Middle panel: steady-state levels of the LARP6C-FlagHA (6C-FH) fusion from six distinct transformants (lanes 3 to 8). 6C-FH was expressed in *larp6c-3* knockout plants. Mature pollen from line number 267 (lane 5) was used for the RIP-seq experiment. Right Panel: expression levels of YFP-LARP6C-ΔLAM expressed in the *larp6c-3* (lanes 1-5) or *larp6c-4* (lanes 6-8) backgrounds. Complementation assays presented in Figure 1F were conducted with lines 2291 (lane 5) and 2293 (lane 7). (**D**) Semi *in vivo* pollen tube guidance competition assays. On the left, a cartoon representation of the pollen tube guidance assay. Unfertilized wild-type ovules were arranged around an *ms1* pistil pollinated with both mutant *larp6c* and LAT52-GFP pollen. A limited pollination was performed with pollen from wild-type plants homozygous for LAT52-GFP reporter (hmLAT52-GFP) (labeled "WT"), with hmLAT52-GFP and *larp6c-3* pollen (labeled "*larp6c-3*") or with hmLAT52-GFP and larp6c-4 pollen (labeled "*larp6c-4*"). Ovules were scored as: GFP positive (targeted by LAT52-GFP pollen), non-GFP ovules (targeted by mutant pollen) or non-targeted. The results are presented as whisker boxplots. **(E)** Top panel: Schematic representation of the LARP6A genomic locus; the color code is identical to that of Figure 1B. The position of *larp6a-1* (SK39668) T-DNA is reported. Bottom panel: immunoblot analysis of LARP6A steady-state levels in the wild-type and *larp6a-1* backgrounds. (**F**) Male transmission efficiencies of *larp6a-1* and *(larp6c-3+/-; larp6a-1)* mutants. Transmission Efficiency (TE) was calculated as: (([No of mutant] / [No of wild type]) x 100). ns: the number

of mutant seedlings in the progeny is not significantly different from the expected number of mutant seedlings. (**G**) *In vivo* scoring of pollen tube behaviors. Wild-type pistils were pollinated *in planta* with pollen from various homozygous genotypes and the behavior of pollen tubes monitored and scored over a time course: 4h, 8h and 24h after pollination (HAP). Type I (white bars): targeting and reception are normal, Type II (grey bars): targeting is defective (see Supplemental Figure S3D). The numbers of scored ovules are reported as "n'" in the table below the graphs. p-values were calculated with a t-test, unpaired, ns: non significative, ***, p-value <0.001.

Supplemental data. Billey, Hafidh et al. (2021). LARP6C orchestrates post-transcriptional reprogramming of gene expression during hydration to promote pollen tube guidance. Plant Cell.

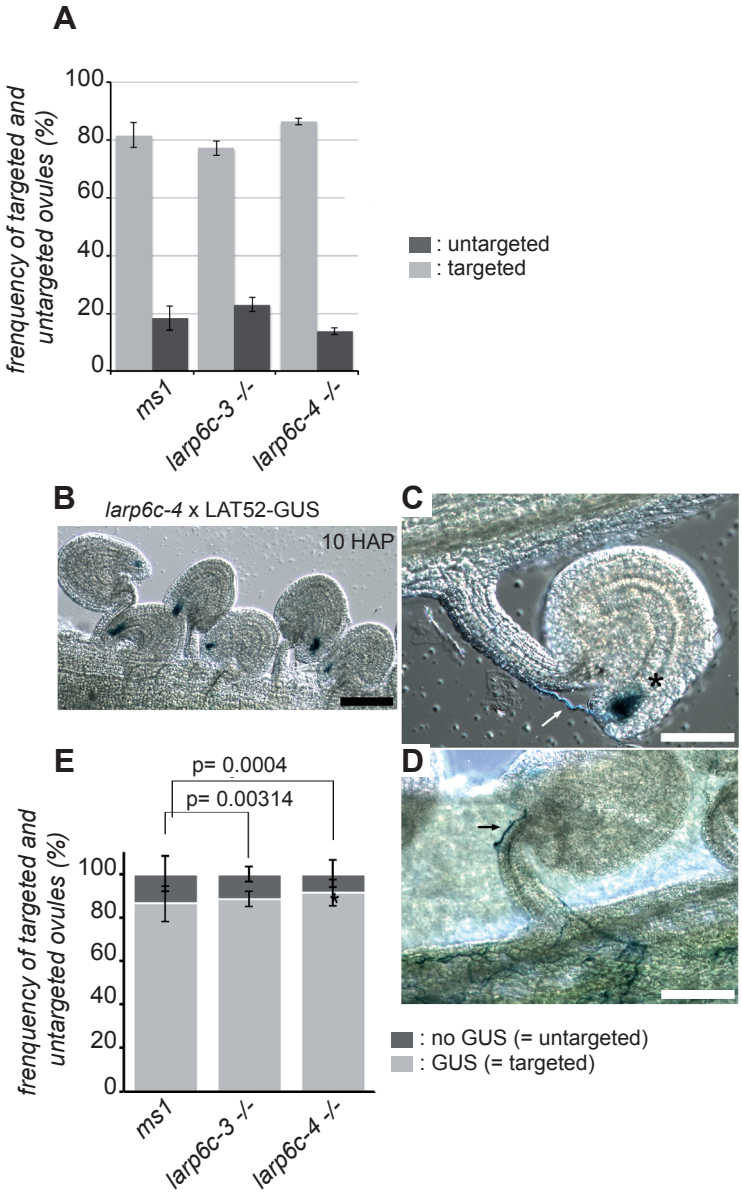

Supplemental Figure S4: Pollen attraction competence of *larp6c*-3 and *6c4* ovules. (Supports Figure 1C-F). **(A)**, Semi *in vivo* assays using wild-type (WT) (Col 0 ecotype) or *larp6c* (from *larp6c-3* or *larp6c-4* homozygous plants) mutant ovules for wild-type (WT) pollen tube attraction. The histograms report the frequency of targeted/untargeted ovules for each ovule genotype. Error bars are standard deviations calculated from 2 biological replicates with n= 150 ovules (contained in 25 pistil explants) tested for each replicate and each genotype. **(B-E)**, *In vivo* ovule attraction competence assays. Pollen tube targeting events were scored as successful attraction. *ms1*, *larp6c-3* or *larp6c-4* homozygous pistils were pollinated with pollen grains expressing the GUS transgene under the control of the *LAT52* promoter. Ovules showing positive GUS staining were scored as competent. **(B-D)**, representative micrographs of pollinated *larp6c-4* mutant ovules. Arrows point to pollen tubes (C, D) and asterisks to pollen tube penetration and burst (C). Scale bars correspond to 20 µm. **(E)**, Histogram representation of ovule attraction frequency. The minus GUS (dark grey) corresponds to frequency of untargeted ovules and the plus GUS (light grey) to the frequency of targeted ovules. Error bars are standard deviations calculated from 2 biological replicates. The total number of ovules scored in replicate 1 (n_1) and 2 (n_2) are: *ms1* (n_1=802 from 24 pistils; n_2= 975 from 29 pistils), *larp6c-3* (n_1= 1063 from 31 pistils; n_2= 869 from 28 pistils) and *larp6c-4* (n_1=860 from 26 pistils, n_2= 912 from 29 pistils).

Supplemental data. Billey, Hafidh et al. (2021). LARP6C orchestrates post-transcriptional reprogramming of gene expression during hydration to promote pollen tube guidance. Plant Cell.

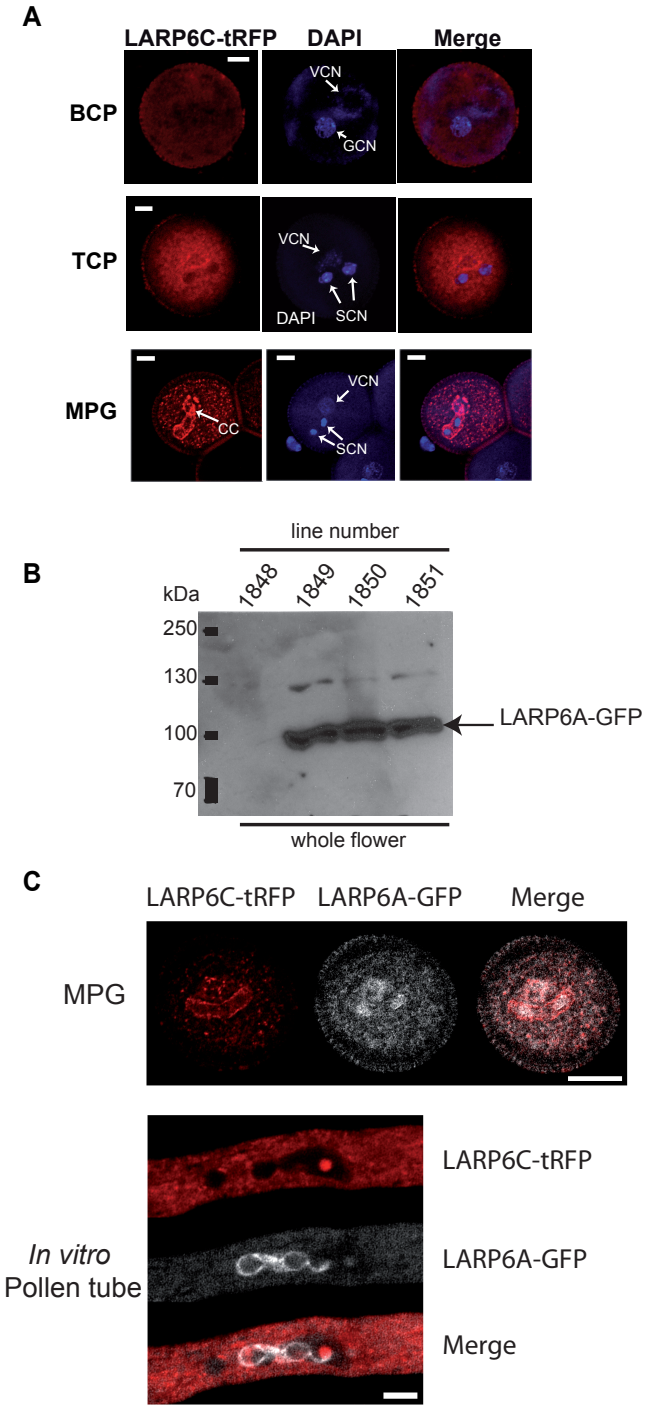

Supplemental Figure S5: Confocal analyses of LARP6C-tRFP and/or LARP6A-GFP in pollen. (Supports Figure 2). **(A)** Confocal analyses of LARP6C-tRFP distribution in bicellular pollen (BCP), tricellular pollen (TCP), and mature pollen grain (MPG). Line 134 was used to monitor LARP6C-tRFP subcellular distribution. White arrows point to the cytoplasmic connexion (CC), the generative and vegetative cell nuclei (GCN and VCN), and the sperm cell nuclei (SCN). Scale bars correspond to 5µm. (**B**) Immunoblot analysis of LARP6A-GFP expression in four independent transgenic lines. The *LARP6A* whole genomic region (including promoter and introns) was fused at its C-terminus with the GFP CDS and expressed in the wild-type background. Line 1850 was crossed with line 134 (LARP6C-tRFP) to monitor LARP6A and 6C co-localization. (**C**) Confocal analysis of LARP6A-GFP and LARP6C-tRFP localization in mature pollen grain (MPG) and *in vitro* grown pollen tubes. Scale bars correspond to 10 µm.

Supplemental data. Billey, Hafidh et al. (2021). LARP6C orchestrates post-transcriptional reprogramming of gene expression during hydration to promote pollen tube guidance. Plant Cell.

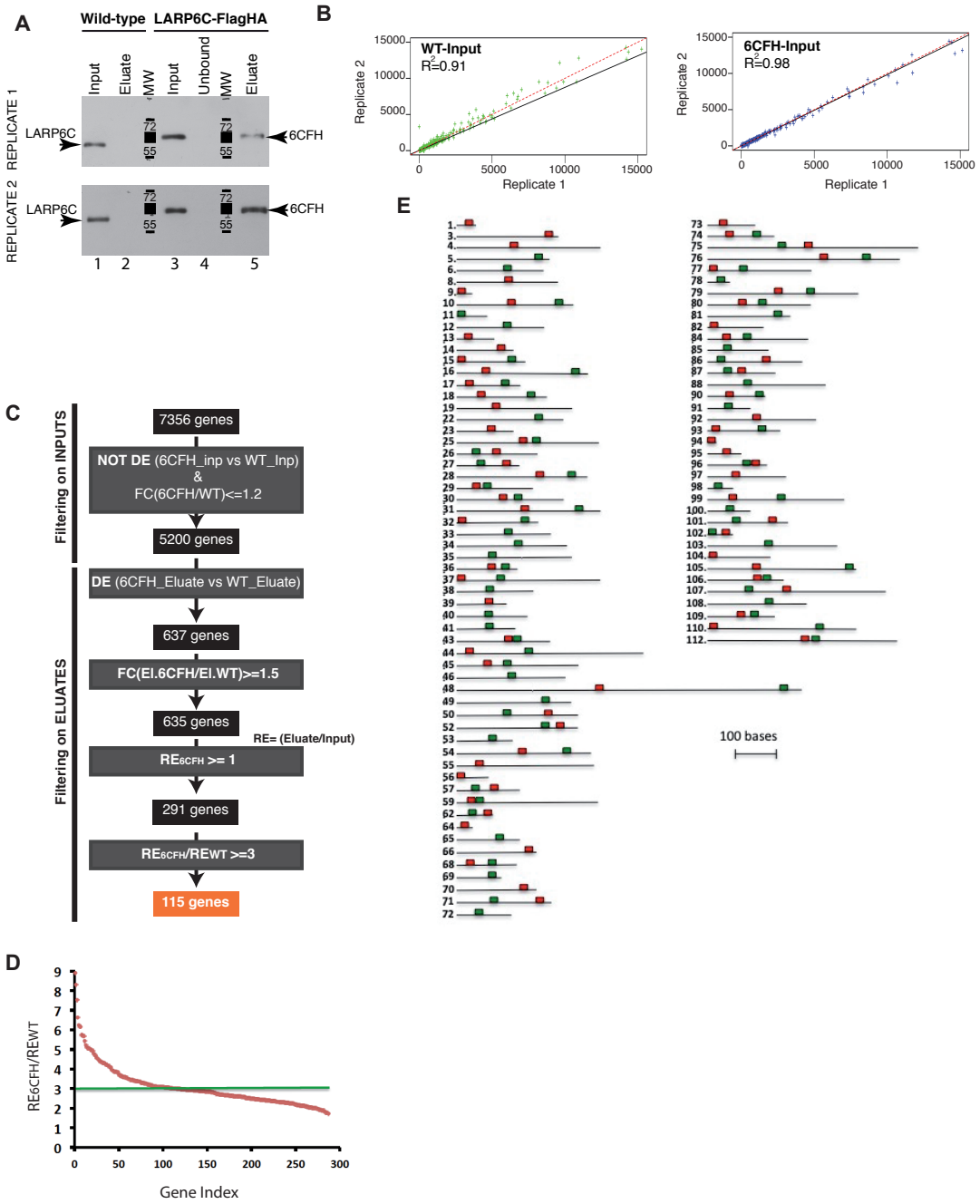

Supplemental Figure S6: Reproducibility of the RIP-seq data, RIP-seq filtering workflow, representation of the position of A and/or B boxes on the 5'-UTRs of LARP6C targets. **(**Supports Figure 3**). (A)**, Immunoblot analysis of the input (lanes 1, 3), unbound (lane 4), and eluate fractions (lanes 2, 5) of the RIP samples. 0.3% (15 µL) of the input and unbound and 3% (7.5 µL) of the eluate fractions were analyzed. The blots were probed with the anti-LARP6C antibody. **(B)**, Comparison of the two biological replicates for the inputs of the RIP-Seq analysis. Correlation of expression levels between replicates of the inputs from wild-type (Col 0) (left panel) or complemented *larp6c-3* ((LARP6C-FlagHA; *larp6c-3*), labelled 6C-FH) (right panel) lines. The X and Y axes correspond to read counts in RPKM respectively for replicates 1 and 2. The expected correlation line for a correlation coefficient of 1 is represented by a red dotted line and the actual correlation line is in black. Correlation coefficients are reported as R^2 on each graph. **(C)**, Representation of the workflow utilized to identify the putative mRNA targets of the LARP6C protein in mature pollen grains. The filtering process was conducted with the weighted average values calculated between replicates, and with the list of genes that displayed at least 1 RPKM value in one of the four conditions (inputs, wild type and 6C-FH and eluates, wild type, and 6C-FH) (see Supplemental Data Set S1). To identify Differentially Expressed (DE) genes between wild type and 6C-FH, respectively, in the input and eluate fractions, we used the Cuffdiff suite. The first filtering step consisted of the elimination of all DE genes in the input. To increase stringency, in the first step, we also filtered out genes non-DE but having Fold Change (FC) values over 1.2, calculated as the ratios between 6C-FH and WT inputs. The second filtering step selects DE genes between the eluate fractions that present a FC of 1.5 or more, calculated as the ratios between 6C-FH and WT eluates. The third filtering step is based on the Enrichment Ratio (RE) calculated as the ratio between eluate and input values and initially selected genes with a RE6CFH≥1. We then calculated the ratio between RE6C-FH and REWT values, whose distribution is represented in **D** and retained genes with a ratio ≥ 3. The target gene list is shown in Supplemental Data Set S1. **(E)**, Schematic representation of the 5'-UTRs of Box A and/or Box B containing mRNAs identified as putative LARP6C baits. The positions of the A (red boxes) and B (green boxes) motifs are shown. Correspondence between numbers on the left hand-side and gene accession numbers are reported in Supplemental Data Set S1.

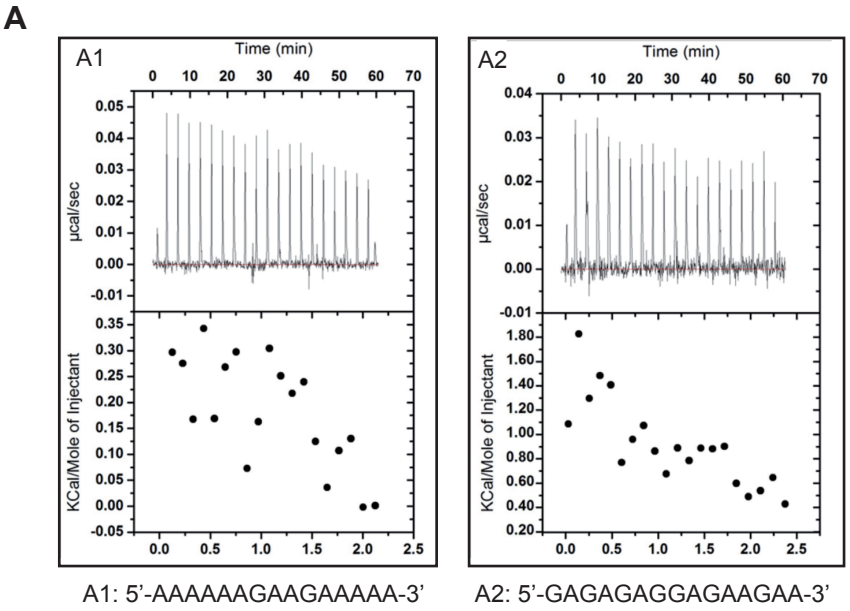

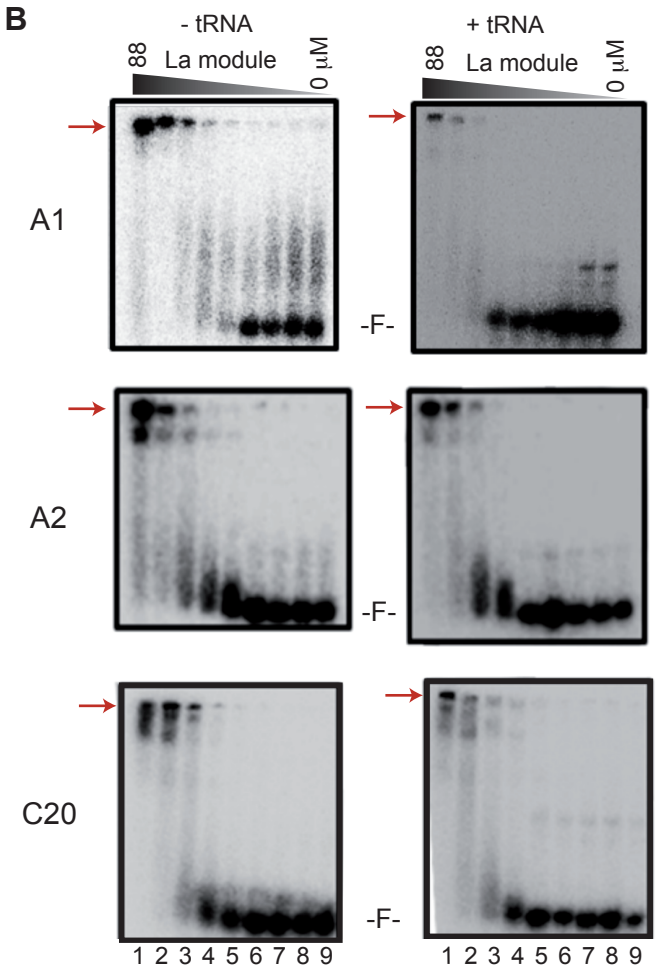

Supplemental Figure S7: ITC and EMSA assessment of LARP6C La-module binding to A type oligos. (Supports Figure 4). **(A)**, Calorimetric analysis of the interaction between the LARP6C La-module (encompassing residues 137-332) and two A-type oligos (A1 and A2) whose sequences are reported below the graphs. For each graph, the upper panel corresponds to the raw titration data showing the thermal effect of injecting an RNA oligos solution into a calorimetric cell containing the recombinant LARP6C La-module. The lower panels show the normalized heat value for the titrations obtained by integrating the raw data and subtracting the heat value of the RNA dilution. **(B)**, EMSAs of the LARP6C La-module binding to A1, A2, or C20 oligos. Decreasing concentrations (µM) 88 (lane 1), 29.3 (lane 2), 9.8 (lane 3), 3.3 (lane 4), 1.1 (lane 5), 0.4 (lane 6), 0.12 (lane 7), 0.04 (lane 8) and 0 (lane 9) of the recombinant La-module were mixed with 3 nM of 5'-labelled oligos. F stands for Free RNA and the red arrows show samples that were retained in the wells of the gel. Experiments were conducted in the absence (-tRNA) or presence (+tRNA) of unlabelled competitor (tRNAmix of *E. coli* MRE 600 at 0.01 mg/mL concentration).

Supplemental data. Billey, Hafidh et al. (2021). LARP6C orchestrates post-transcriptional reprogramming of gene expression during hydration to promote pollen tube guidance. Plant Cell.

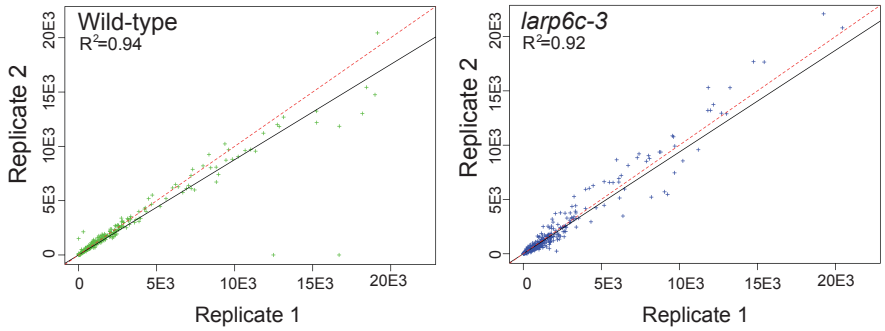

Supplemental Figure S8: Reproducibility of the RNA-seq data. (Supports Figure 7) Comparison of the two biological replicates used for the RNA-seq analyses. Correlation of expression levels between replicates of the RNA-seq data from wild-type (Col 0) (left panel) or from *larp6c-3* (right panel) lines. The X and Y axes correspond to read counts in RPKM respectively for replicates 1 and 2. The expected correlation line for a correlation coefficient of 1 is represented by a red dotted line and the actual correlation line is in black. Correlation coefficients are reported as R^2 on each graph.

Supplemental data. Billey, Hafidh et al. (2021). LARP6C orchestrates post-transcriptional reprogramming of gene expression during hydration to promote pollen tube guidance. Plant Cell.

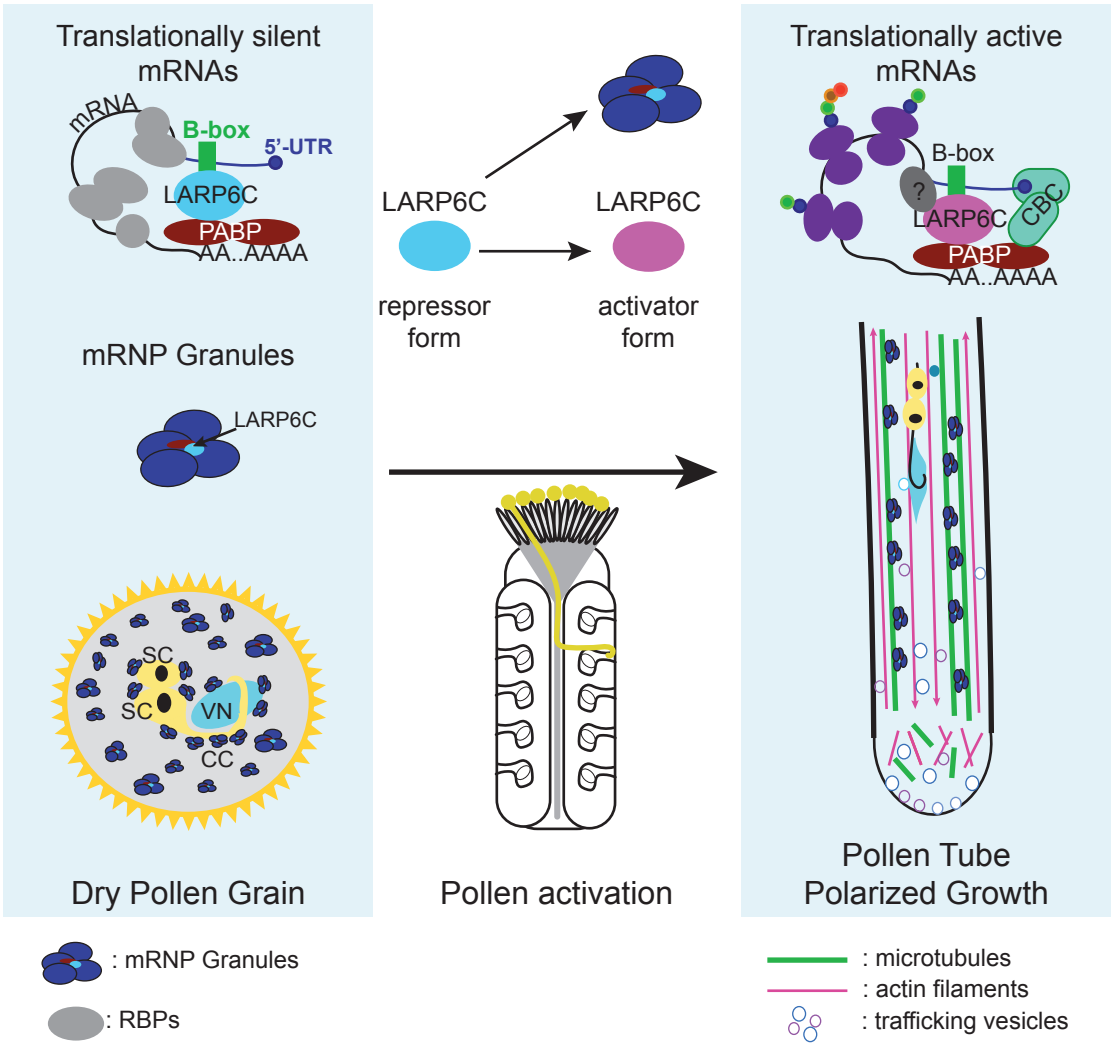

Supplemental Figure S9: Model of the molecular functions of LARP6C in male fertilization. In mature dry pollen grain, LARP6C is part of mRNP granules and acts as s repressor of translation of its target transcripts. During pollen hydration and along the progamic phase, LARP6C shifts from a repressor to an activator of translation. In growing pollen tubes, we postulate that LARP6C could also participate in the transport of at least some of its target transcripts, navigating them along the cytoskeleton as translationally silent to their site of translation.

Experiment Syringe: Cell	n	K_b M^{-1}	K_d µM	ΔH kcal/mol	-TΔS kcal/mol	ΔG kcal/mol
B1:La module 6C	0.8 +/- 0.01	(2.8 +/-0.4)xE^5	3.5+/-0.5	-6.6+/-0.1	-1.3+/-0.1	-7.4+/-0.1
B2:La module 6C	0.9 +/- 0.1	(3.7 +/-0.9)xE^5	2.8+/-0.4	-6.6+/-0.3	-1.0+/-0.3	-7.6+/-0.1
B3:La module 6C	na	na	na	na	na	na
B4:La module 6C	na	na	na	na	na	na
U_{20}:La module 6C*	1.1 +/- 0.1	(5.8 +/-0.3)xE^5	1.7+/-0.1	-3.1+/-0.1	-4.7+/-0.7	-7.8+/-1.0
A1:La module 6C	na	na	na	na	na	na
A2:La module 6C	na	na	na	na	na	na
C_{20}:La module 6C	na	na	na	na	na	na

Every value is averaged over three experiments and the errors are obtained as the standard deviation from the mean value. *: The values for oligo(U_{20}) are those previously reported in (Merret et al. RNA, 2013). na: not attributed.

Supplemental Table S1: Thermodynamic parameters of the calorimetric analyses shown in Figure 4B, 4D and Supplemental Figure 6A.

Supplemental data. Billey, Hafidh et al. (2021). LARP6C orchestrates post-transcriptional reprogramming of gene expression during hydration to promote pollen tube guidance. Plant Cell.

qPCR PRIMERS						
Primer Name	**Gene**	**5'-3' sequence**	**Primer Tm (°C)**	**Amplicon Tm (°C)**	**Amplicon lenght (nt)**	**Primer pair Efficiency (%)**
YFP-F	YFP	TAAACGGCCACAAGTTCAGC	59.05	86.91	87	99.85
YFP-R		CGGTGGTGCAGATGAACTTC	59.20			
Hyg-F	Hygromycin	CGTGGTTGGCTTGTATGGAG	58.91	86.91	156	97.9
Hyg-R		CCCAAGCTGCATCATCGAAA	58.90			
MGD2-F	YFP-MGD2 & MGD2	TGTGACTGCATCATCACAAAAG				
MGDR		GGCTGAGCTAGTTTACGTGCAT				
TUBULIN 8-R	TUBULIN 8	CTTCGTATTTGGTCAATCCGGTGC				
TUBULIN 8-F		GAACATGGCTGAGGCTGTCAAGTA				

Cloning & Genotyping Primers		
Primer Name	5'-3' sequence	Purpose
31	CACCtcacactttcaagtctcatt	MGD2 genomic region cloning (-579 to last nt before stop codon)
32	AACTAAACTGGCAAAAGAAGAG	
543	CCCCGGTACCGTGCTTTCTGATTTAAGAGAGGCAAAGGA	LARP6C genomic region (-1181 to Stop codon) cloning
544	CCCCGCTAGCGAGATTGTTAGGTGAGAGTGAGATGGAA	
974	CCCCGAGCTCGTGCTTTCTGATTTAAGAGAGGCAAAGGA	ProLARP6C genomic region (-1181 to -1) cloning
975	CCCCGGTACCTTTCCTCTCACTACTCTGAAAAAATCTCTAAC	
976	CCCCCACTAGTATGGCGCAGATGCAGCGAGAAG	Cloning of genomic LARP6C from ATG to STOP codon
977	CCCCCGATATCTTAGAGATTGTTAGGTGAGAGTGAGATGG	
eb3	CCCCTCTAGACTCGAGCTAGAAAGAGAACCAGGGACTTCT	Cloning of genomic PAB5 from ATG to STOP codon
eb4	CCCCGGATCCCTCGGATGAGGATAGAGCAAACTGGTCATC	
1197	GCAGGCTGCGGCCGCTCTAG	Construction of LARP6CDLAM CDS (underlined sequence is complementary to the 20 first nt of pcr product 2, obtained with primers 1198 and 1200)
1198	GCAATTCCTCTCTGTCTCTCTTCGACGAAGAAGACGAGTTCTGA	

1199	AGAGACAGAGAGGAATTGCA	Construction of LARP6CDLAM CDS
1200	TATCGATAAGCTTGATATCGA	
1201	GCTCTAGAATGGCGCAGAT	
488	GAAGTAGAGTCCGTCACGACG	*larp6c-3* LP primer
489	TTTCTTGCCGTCTTCACTCAC	*larp6c-3* RP primer
491	TAGCATCTGAATTTCATAACCAATCTCGATACAC	SAIL-LB2
999	GTTCAAATTCAACGCTCAAGC	*larp6c-4* LP primer
1000	AATTCTCTGCAACGACAGTCC	*larp6c-4* RP primer
483	AACGTCCGCAATGTGTTATTAAGTTGTC	DsLox-p745-LB
475	AAGCTGGAAGGTAGGCTATGG	*larp6a-1 RP primer*
476	GACGCTTTGAGACCTCAACAG	*larp6a-1 LP primer*
474	ATACGACGGATCGTAATTTGTCG	*Saskatoon-3*

Supplemental table S2: List and sequences of primers used for qPCR analyses, genotyping and cloning.

SUPPLEMENTAL METHODS

Plant material and plasmid construction

The *larp6a-1* (SK39668) line from the Saskatoon Arabidopsis T-DNA population collection (Robinson et al., 2009) was obtained from the NASC stock center. Genotyping primer sequences are listed in Supplemental Table S2. To determine whether this insertion line was loss-of-function, we ordered a custom-made antibody through immunization of rabbits with peptide "EESEKGGKKENFIRTR" (Agro-Bio (La Ferté St Aubin, France)). Anti-LARP6A antibodies were used at 1/5,000 dilution. To obtain the LARP6A-GFP fusion, we PCR amplified the whole genomic locus *AT5G46250* from position -1498 up to the last nucleotide before the stop codon with primers 959 and 960 and inserted the DNA fragment following *Kpn*I-*Sac*I digestion upstream of the *GFP*, into a pCAMBIA1300-based plant binary vector expressing the *HPTII* (hygromycin) resistance gene, giving rise to plasmid p791. A stable transgenic line was prepared through agroinfiltration of plasmid p791 into wild-type Col-0. To monitor co-localization of LARP6A and LARP6C, we transferred the LARP6A-GFP transgene (line 1850) into a LARP6C-tRFP expressing line (line 134) through crossing.

Growth conditions and pollen collection technique for RNA-Seq and RIP-Seq assays

Mature pollen materials for RNA-seq and RIP-seq were obtained from plants sown, grown and harvested under the exact same conditions. Wild type (Col-0), *larp6c-3* and (*larp6c-3*; PRO_{6C}-LARP6CFLAGHA) (abbreviated as 6C-FH) were sown on 1/2 MS - 0.8% agar in duplicate and cultivated for 15 days *in vitro* at 20°C, with 24 h light (50-60 $mE^{-1}m^{-2}$-s^{-1}). Seedlings were then transferred to soil treated with the nematode *Steinernema feltiae* (at 5000 / soil Liter) and cultivated in a greenhouse with approximately 16 h day at 22°C night and day (greenhouse conditions, July 2013 Gif/Yvette France) for 5 weeks. Wild type Col-0, *larp6c-3* and 6C-FH (transformant number 267 (see Supplemental Figure S3C for an immunoblot analysis of LARP6C-FLAGHA protein accumulation)) plants were grown together in the same compartment of the greenhouse in large plates, each containing 96 plants. Two sets (Col-0, *larp6c-3*, 6C-FH) of plants were grown to produce two replicates. For each replicate, 15 Col-0, 3 *larp6c-3* and 15 6C-FH plates were prepared. The plates of each replicate were respectively installed on two distinct growth shelves inside a same compartment and each genotype interspersed inside each replicate. To avoid the effects of cooling air efflux and temperature gradients and to obtain homogeneous growth between genotypes inside each replicate, the plates were rotated along their respective shelf every 2 weeks. Mature pollen grains were collected using a homemade pollen collector as described in (Johnson-Brousseau and McCormick, 2004). Briefly, mature pollen was collected by aspiration with a vacuum cleaner equipped with three successive filters

of 140, 60 and 10 μm diameter. Pollen grains were scraped from the 10 μm filter into an Eppendorf tube, weighed, flash frozen in liquid nitrogen, and stored at -80°C.

RNA sequencing

Total RNAs were extracted from 5 mg of wild-type and *larp6c-3* mature pollen grains as described in the Methods section of the main text. RNA quality was verified by gel electrophoresis and staining with Gel-red (Biotium). DNase treatment was conducted as for RT-PCR assays. The reaction was stopped and DNase extracted with phenol/chloroform/IAA before RNA was precipitated and resuspended in RNase-free water. The quality of DNase-treated RNA was assessed with a Bio-Analyser. Library preparation (with a True seq Stranded mRNA kit from Illumina) and sequencing were subcontracted to Fasteris (Switzerland). Single-end (101bp read length) sequencing was performed on the HiSeq 2000 platform with a depth of 31 to 60 M reads. Experiments were conducted in duplicate for each genotype.

RNA Immunoprecipitation and sequencing (RIP-Seq)

After pollen collection, crude extracts (Inputs) were prepared from identical amounts of wild-type and 6C-FH expressing pollen grains. Twenty-five mg of mature pollen was resuspended in 250 volumes of extraction buffer (50 mM Tris HCl pH 7.4, 10% glycerol, 100 mM NaCl, 5 mM $MgCl_2$, 80 units / ml RNAsin® Plus RNAse Inhibitor (Promega), 1X mg132, 1% protease inhibitor cocktail for plant extract (Sigma)) and ground using a Silamat S6 before extracts were cleared by centrifugation (4°C, 14.000 g for 10 min). 700 and 40 μL of Input fraction were saved to purify total RNA (Input RNA) and total protein (Input Protein) to respectively conduct RNA-sequencing and immunoblotting. For each sample (Col0-Replicate 1, Col0-Replicate 2, 6C-FH-Replicate 1 and 6C-FH-Replicate 2), the immunoprecipitation step was conducted with 5 mL of crude extract. For each sample, 250 μL of Anti-Flag M2 (Sigma) magnetic beads were thoroughly washed with 10 volumes of extraction buffer and evenly divided between the 5 tubes. After removing the supernatant, 1 mL of crude extract (approximately 300 μg of total protein) were added to each tube and rotated for 1 h at 4°C on a wheel at 10 rpms. The unbound fractions were collected, pooled, and 700 and 60 μL stored for RNA and protein analyses. The beads were washed once with 5 vol of washing buffer (50 mM Tris HCl pH 7.4, 10 % Glycerol, 150 mM NaCl, 3 mM $MgCl_2$, 80 units / ml RNAsin® Plus RNAse Inhibitor (Promega), 1X Mg132, 1% protease inhibitor cocktail for plant extract (Sigma), 0.1% Triton™ (Sigma)) before being transferred to a new tube, pooled, and washed twice more in 2 vol of washing buffer. The elution step was conducted as follow: 6% of the beads (15 μL) were resuspended in 1X Laemmli buffer, heated for 10 min at 100°C, and

the supernatant used to run immunoblot analysis to monitor the efficiency of immunoprecipitation of the 6C-FH protein. The remaining 94% of the beads were resuspended into 400 μL of guanidium hydrochloride buffer, incubated for 10 min at RT, the supernatant collected and separated from proteins with two phenol/chloroform/IAA extractions before the RNA was precipitated in the presence of 80 μg of glycogen and resuspended into 10 μL of RNase-free water. RNAs in the eluate fractions were quantified with a NanoDrop and their quality verified with a Bio-Analyzer system. The library preparation and sequencing (Input RNA and Eluate RNA) were subcontracted to Fasteris (Switzerland). The libraries constructed with the input RNAs were prepared from poly(A) purified RNAs using a True seq Stranded mRNA kit from Illumina and the libraries prepared from the eluate fractions were constructed from unpurified RNAs. Sequencing was performed as single-end 101 bp and with a depth of 42 to 64 M reads for the inputs and 25 to 40 M reads for the eluates.

Bioinformatics

For each RNA-seq and RIP-seq sample and replicate, read quality was first verified with FastQCsoftware (http://www.bioinformatics.babraham.ac.uk/projects.fastqc) and clusters with a Qscore below 30 filtered out. 95-96% of the RNA-seq clusters and 92-94% of the RIP-seq clusters had a Qscore of at least 30 (please see Supplemental Data Set S1 and S2 for the sequencing depth and quality scores of each sample). In the second step, non-nuclear genomic and ribosomal RNA sequences were filtered out against the TAIR10 database using Bowtie2 (Langmead and Salzberg, 2012) and the remaining clusters aligned against TAIR10 (TAIR10_genes_transposons.gtf) with TopHat2 (Kim et al., 2013) . After filtering, more than 99% of the clusters were retained for the RNA-seq samples and inputs of the RIP-seq. For the eluates, 5% of the Col-0 clusters and 15% of the 6C-FH clusters were retained, because of the high contamination with ribosomal RNAs. For the RNA-seq and RIP-seq assays, genes that did not display at least 1 RPKM (read per kilobase per million mapped reads) value in one of the conditions were filtered out. Normalized mean values were attributed to each gene, and differentially expressed genes were identified with the Cufflinks, Cuffmerge and Cuffdiff suite (Trapnell et al., 2010) with an FDR of 0.05 for RNA-seq and 0.01 for RIP-seq and $|\log2(FC)| \leq 0.585$ as cut-off for total RNA-seq and $\log2(FC) \geq 0.585$ for eluate values of RIP-Seq. To search for a motif shared by putative targets of LARP6C, we looked at the Araport database (https://www.araport.org/) for their 5' and 3'-UTR sequences and retrieved sequences for 112 out of 115 putative targets. We then ran MEME searches (at the MEME suite portal (http://meme-

suite.org/)) using, as control sequences, a set of 112 randomly chosen 5'- and 3'-UTR sequences from genes expressed in pollen according to our transcriptomic analysis.

Pollen phenotyping: pollen maturation, pollen tube germination and growth

To monitor pollen maturation defects, mature pollen grains were collected from wild-type and *larp6c* homozygous plants, deposited on a DAPI solution (1X PBS pH7, 0.5% Triton, 1 μg/mL 4',6-diamidino-2-phenylindole (DAPI)) and the number of mutant pollen grains with undivided generative cells determined using confocal microscopy. Pollen tube germination and growth defects were monitored *in vitro* or through semi *in vivo* assays. To grow pollen tubes *in vitro*, we used a modified version of the protocol from (Boavida and McCormick, 2007). Freshly prepared pollen tube growth medium (0.01% boric acid, 5 mM $CaCl_2$, 5 mM KCl, 1 mM $MgSO_4$, 10% sucrose, pH 7.5 (KOH), 1.5% Phytagel) was directly poured onto a microscope slide. Mature pollen was deposited on the solid medium and slides incubated for 8 h in a humid chamber at 20-22°C in the dark. Pollen tubes were photographed (with a Hamamatsu camera (Sunayama-cho, Shizuoka, Japan)) and pollen tube lengths measured with NIS-element software from Nikon (Nikon Instruments, Melville, NY USA). Pollen tube density and length were also determined through semi *in vivo* analyses. Following hand pollination with wild-type or *larp6c* homozygous mutant pollen, the pistils were excised at the shoulder and incubated for 16 h on a plate containing pollen tube solid growth medium. Pistil explants and pollen tubes were photographed and images analyzed with the plugin Bio-format (Open microscopy environment) from Image J software (Rasband, W.S. ImageJ, NIH, Bethesda USA) (Abràmoff et al., 2004) to determine pollen tube length and density per pistil.

Ovule attraction assays

larp6c-3 or *larp6c-4* pistils were emasculated at stage 12C and left to mature for 2 days. Limited pollination was performed on day 3 using LAT52-GUS homozygous pollen grains in the *qrt-/-* background alongside *ms1-/-* pistils as the control. Eighteen hours after pollination, pollinated pistils were collected and gently dissected with a 25G needle to expose fertilized ovules. Dissected pistils were stained for GUS activity in GUS staining buffer (50 mM PBS, pH7, 0.2% Triton-X100, 10 mM potassium ferrocyanide and 1 mM X-Glu). Pistils were vacuum infiltrated for 10 min and stained o/n at 37°C. For microscopy analyses, stained pistils were cleared using an ethanol series (70%-30%), mounted on 30% glycerol, and analyzed with a Nikon TE2000 equipped with DIC modulation contrast and NIS-element software. Images were processed with ImageJ.

SUPPLEMENTAL REFERENCES

Abràmoff, M., Magalhaes, P., and Ram, S. (2004). Image processing with ImageJ. Biophotonics Int. **11**: 36–41.

Boavida, L.C. and McCormick, S. (2007). TECHNICAL ADVANCE: Temperature as a determinant factor for increased and reproducible in vitro pollen germination in Arabidopsis thaliana. Plant J. **52**: 570–582.

Johnson-Brousseau, S.A. and McCormick, S. (2004). A compendium of methods useful for characterizing Arabidopsis pollen mutants and gametophytically- expressed genes. Plant J. **39**: 761–775.

Kim, D., Pertea, G., Trapnell, C., Pimentel, H., Kelley, R., and Salzberg, S.L. (2013). TopHat2: accurate alignment of transcriptomes in the presence of insertions, deletions and gene fusions. Genome Biol. **14**: R36.

Klepikova, A. V, Logacheva, M.D., Dmitriev, S.E., and Penin, A.A. (2015). RNA-seq analysis of an apical meristem time series reveals a critical point in Arabidopsis thaliana flower initiation. BMC Genomics **16**: 466.

Langmead, B. and Salzberg, S.L. (2012). Fast gapped-read alignment with Bowtie 2. Nat. Methods **9**: 357–359.

Robinson, S.J. et al. (2009). An archived activation tagged population of Arabidopsis thaliana to facilitate forward genetics approaches. BMC Plant Biol. **9**: 101.

Trapnell, C., Williams, B.A., Pertea, G., Mortazavi, A., Kwan, G., van Baren, M.J., Salzberg, S.L., Wold, B.J., and Pachter, L. (2010). Transcript assembly and quantification by RNA-Seq reveals unannotated transcripts and isoform switching during cell differentiation. Nat. Biotechnol. **28**: 511–515.

Winter, D., Vinegar, B., Nahal, H., Ammar, R., Wilson, G. V., and Provart, N.J. (2007). An “Electronic Fluorescent Pictograph” Browser for Exploring and Analyzing Large-Scale Biological Data Sets. PLoS One **2**: e718.

3. DISCUSSION

When I joined the Laboratory of Pollen Biology at the Institute of Experimental Botany, the research was focused on transcriptomic and translatomic regulation in tobacco and Arabidopsis pollen. In order to understand the RNA dynamics during pollen development and maturation, the group focused on creating a transcriptomic profile from unicellular microspores through mature pollen up to the 24 hrs-grown pollen tubes. My task was to identify transcripts that were preferentially stored in specialised EPP particles (stalled monosomes) during the pollen development. The hypothesis behind RNA storage in pollen was that transcripts are stored (either gradually, or continuously) during pollen maturation to serve as a reservoir for rapid translation initiation and protein production during the fast pollen tube growth. Strikingly, few of the transcripts that were preferentially stored in the EPP particles even after 24 hrs of pollen tube growth, were annotated as genes with embryo-defective mutants in their Arabidopsis homologs. This intrigued observation prompted us to follow three of these candidate genes (EMB1441/AtNEMF, EMB 2036/AKRP and SUS2/ PRP8A) and to study them in more detail. Why do genes involved in embryogenesis have their transcripts stored in pollen and pollen tubes? Could the transcripts that are stored in pollen have roles during fertilisation or at the early stages of zygotic development? When could the pollen-stored transcripts be activated and translated? These questions opened another chapter of research in the Laboratory of Pollen Biology, as these topics were beyond the previous scope.

My research started with identification of tobacco candidate homologs in Arabidopsis of the three candidate genes and a selection of multiple T-DNA lines. The lines were simultaneously screened for pollen, ovule and embryo phenotypic defects and led to a more limited selection of mutant lines. Alongside the phenotypic screens, I was cloning multiple constructs to study promoter activity, protein localisation and for mutant complementation. Out of the three studied candidate genes, EMB1441/AtNEMF showed no convincing gametophytic defects, instead, *emb1441* mutants possessed embryos with malformations during the early stages of embryonic development. Due to the substantial amount of work dedicated to each gene, we decided to focus only on EMB2036 and more importantly SUS2/PRP8A.

3.1. AnKyrin Repeat Protein (AKRP)

Chloroplasts contain ~3,000 proteins, and only a small fraction of these proteins are encoded by the chloroplast genome. Most of the nuclear-encoded chloroplast proteins are synthesised in the cytoplasm as precursors with an N-terminal targeting signal called transit peptide and are subsequently translocated into chloroplasts (Jarvis and López-Juez, 2013, Lee et al. 2017). Nuclear-encoded chloroplast proteins are imported across the chloroplast envelope into the stroma by a common import apparatus, namely the Toc/Tic (translocon at the outer/inner envelope of chloroplasts) complex (Jarvis and López-Juez 2013, Lee et al. 2017, Chen et al. 2018). Once a preprotein reaches the stromal side of the chloroplast envelope and its transit peptide has been cleaved off by the stromal processing peptidase, in many cases, the protein is further targeted to its correct sub-compartment within the chloroplast (Schleiff and Becker 2011). Thylakoid lumen proteins usually carry further targeting information at their N-terminal end, which guides them via the chloroplast secretory (cpSec) or the chloroplast twin arginine translocation (cpTat) pathways (Yuan et al. 1994, Settles et al. 1997). AKRP, previously labelled as EMB2036 is a single copy gene with five ankyrin repeats (ANK, Zhang et al. 1992), which are protein-protein interaction domains. Study by Ouyang et al. (2020) described a mechanistic role of AKRP (therein labelled as STT2) as essential in the sorting of chloroplast twin-arginine translocation (Tat) pathway proteins into thylakoid membranes. The twin-arginine translocation pathway is a protein export system present in bacteria, archaea, and chloroplasts that moves folded proteins across a lipid membrane bilayer. The Tat pathway differs from the Sec pathway, which transports proteins in an unfolded state. Tat substrates include redox enzymes that require cofactor insertion in the cytoplasm, multimeric proteins that assemble into a complex prior to export, specific membrane proteins, and proteins with folding requirements that are incompatible with Sec export.

Down-regulation of STT1 or STT2 by RNAi led to retarded growth, pale green leaves, as well as to reduced chlorophyll levels and abnormal plastids that lack stacked thylakoid membranes (Ouyang et al. 2020). These results suggest that STT1 and STT2, which form a heterodimer,

play important roles in thylakoid membrane biogenesis during plastid development and are in agreement with our published results. The authors also observed reduced accumulation of PsaA/B and D1 proteins in both STT1 and STT2 RNAi lines. This was consistent with previous reports that deficiencies of cpTat pathway substrates lead to reduced accumulation of photosystem core proteins (Settles et al. 1997, Motohashi et al. 2001).

Similar phenotypes can be observed with loss of chloroplast translation machinery in Arabidopsis, which results in embryo lethality and seed abortion, whereas in maize, dependent upon genetic background, it leads to embryo lethality with normal endosperm development, or to albino seedlings or variegated leaf sectors (Parker et al. 2014). Similarly, two candidate genes (*ycf1* and *ycf2*) known to be essential for plant growth (Drescher et al., 2000) have been shown to encode components of chloroplast protein import complexes (Kikuchi et al. 2013, 2018). The importance of these proteins for embryo development is confirmed by the knockout phenotypes of EMB genes encoding other components of the same complexes (Meinke et al. 2020). Taken together, failure of multiple core plastid components results in embryo lethality and was often linked to the defect of chloroplast biogenesis.

In addition to the well established embryonic phenotypes, we have shown that T-DNA insertion in *akrp-3*/+ allele caused aberrant changes in the male gametophyte, such as mature pollen grains with inclusion bodies, presence of binucleate pollen instead of trinucleate mature grains and loss of pollen gametic cell fate. Cell fate of the egg cells was also compromised, leading to a drastic decline in targeting by pollen tubes and in fertilisation. The small percentage of ovules that were still capable of being fertilised produced malformed pale embryos arrested at the early stage of development. Tissue- and time-specific complementations were performed to understand the importance of AKRP during the plant life. The critical time points for AKRP activity seem to be at the early developmental stages of both pollen grains and the embryo. AKRP also plays an important role in the ovule, affecting its viability and attractivity. Since all of these time points are critical in forming the viable plastid types necessary for photosynthesis and proper tissue formation, loss of AKRP function in transporting proteins into their subcompartment plastid location results in severe

phenotypic defects. The important role of AKRP in plants thus seems to be constitutive, with its loss causing a cascade of phenotypes caused by the mis-localisation and reduced accumulation of essential proteins (Kulichová et al. 2022).

While pollen tubes do not form chloroplasts, plastids are indeed required for their growth. During pollen germination, some plastids migrate throughout the pollen tube. Pollen plastids play a role in transforming carbon and energy from sugars into fatty acids to achieve rapid pollen tube growth. The synthesis of FA in pollen plastids consumes a large amount of ATP, NADPH, NADH, and acetyl coenzyme A (Liu et al. 2022). The newly identified T-DNA insertion *akrp-3*/+ allele displayed not only embryo malformation, but also morphological and developmental defects in both gametophytes. This observation extends AKRP function beyond chloroplast biogenesis and shows likely importance for development of other types of plastids as well. This is consistent with its essential role in the protein transport across plastid membranes.

3.2. Pre-mRNA Processing Protein 8 (PRP8)

Based on sequence homology, in this thesis work, we identified not only PRP8A, but also PRP8B in Arabidopsis. PRP8A (SUS2) was initially only described as an embryo-defective mutant with abnormal suspensor growth (Schwartz et al. 1994). Both proteins are subunits of an important splicing machinery in plants and animals, the spliceosome, affecting the proper splicing of a myriad of downstream target transcripts. Pre-mRNA splicing is a co-transcriptional, high-fidelity process consisting of two sequential trans-esterification reactions carried out by the spliceosome complex, resulting in the excision of an intron and the ligation of its flanking exons. These reactions depend on conserved intronic and exonic sequences: the branch-point sequence (BPS) and the 5 splice site (5 SS) and 3 SS. Mutations that damage genuine SSs or create novel SSs frequently produce a mixture of wild-type and aberrant mature mRNAs from a single pre-mRNA. These mutations are a major cause of several rare human diseases, including inherited mental disorders and several plant growth and developmental defects (Cabezas-Fuster et al. 2022).

We initially studied PRP8 T-DNA single mutants, focusing on a description of morphological and developmental defects in both the embryo and the male and female gametophytes. Neither PRP8A, nor PRP8B, single mutants showed any gametophytic abnormalities, however, when we generated *prp8a/prp8b* double mutant, we observed a severe ovule targeting and fertilisation defects (Kulichová et al. 2020). The transmission through both male and female gametophytes was severely perturbed and we were not able to retrieve double homozygous plants (Kulichová et al. 2020). Follow up experiments showed that a simultaneous loss of PRP8A and PR8PB impairs pollen tube attraction, long-distance pollen tube guidance and fertilisation. Double homozygous pollen grains and pollen tubes appeared morphologically normal and their growth was not impaired, however, they failed at targeting the wild type ovules, hinting at a loss of a receptiveness towards the female-derived attraction signals (Kulichová et al. 2020).

Even though both PRP8 proteins are core subunits of the general splicosome complex, knockdown of both genes did not result in pleiotropic effects on splicing during the plant life. RNA sequencing of mutant ovules showed a low percentage of down- (2.9%) and up-regulated (3%) genes compared to wild type ovules. Detailed analysis of alternative splicing events showed that intron retention was the most common occurrence (2.9% total: 55% reduced IR, 45% increased IR events), followed by different exon usage (Kulichova et al. 2020). Our results also identified auto-regulation of core subunits of the spliceosome complex that can exacerbate the phenotype of *prp8a/prp8b* mutants. Assessment of the IR events of only genes expressed in all three replicates of the female gametophyte revealed that genes confined in the central cell were twice as affected on their intron splicing compared to those encoded by the egg cell (Kulichova et al. 2020).

Low frequency of mis-spliced genes in *prp8a/b* mutants is indeed an interesting observation. Spliceosome is highly conserved across eukaryotes, with yeast and Arabidopsis PRP8 showing 62% identical amino acids. Furthermore, plants and animals have comparable consensus sequences for the 5′ splice site (5′SS), 3′ splice site (3′SS), and branch point (BP), suggesting that core splicing factors act similarly in both groups (Reddy et al 2013). While spliceosomes are responsible for cca 90% splicing in both yeast and animals (Grainger and Beggs 2005), it is only ~3% in plants *prp8a/b* double mutant (Kulichova et al. 2020). Both

homologs were interrupted by T-DNA in the U6-RNP binding region, which is essential for the PRP8 function as well as for the function of the spliceosome complex (Turner et al. 2006).

In line with this, exploration of the available RNA-seq data for mutants of various RNA processing factors revealed that depletion of some core spliceosomal components (*luc7*, *gemin2*, *lsm8*, and *rbm25*) had a strong effect specifically on ES (exon skipping) and IR (intron retention) events regulated by abiotic stress conditions. In particular, loss-of- function mutations in *gemin2* and *lsm8*, which are important for multiple steps of spliceosomal assembly, caused both increased IR and ES, with these changes tightly mimicking the AS patterns observed under abiotic stress. In the case of *luc7* and *rbm25*, which are specifically associated with the U1 snRNP and 5′ splice site recognition, their disruption caused mainly ES, likely by compromising exon definition (Martin et al. 2021).

Efficient splicing requires a balance between high-fidelity sequence selection and speed. Structural analysis has revealed two alternative conformations of PRP8: one promotes fidelity over catalytic efficiency and the other promotes efficient, error-prone splicing. Indeed, some mis-sense alleles of PRP8 suppress mis-splicing of pre-mRNAs carrying mutations that damage SSs, which are not efficiently recognised by the spliceosome. The *mas5* mutations belong to an unusual class of mis-splicing suppressors that increase splicing fidelity without causing a dramatic global increase in mis-splicing (Cabezas-Fuster et al. 2022). Point mutations at the 5 SSs or 3 SSs may abolish or reduce their recognition by the spliceosome, which then recognises a cryptic site close to the genuine, mutated SS. Numerous prp8 alleles have been described to act as mis-splicing suppressors, mainly in S. *cerevisiae*. Most of these mutations promote changes in SS choice by the spliceosome, increasing the frequency of proper, in-frame splicing of pre-mRNAs. Null alleles of genes encoding components of the spliceosome, or its associated factors, can cause global missplicing and lethality, as is the case of PRP8. The *mas5-1* and *mas5-3* mutations do not cause global defects in splicing, since only a few missplicing events were detected. Most of these mis-splicing events are increased IR events, corresponding to 0.17% (201 events) and 0.1% (117 events) of the introns analysed in *mas5-1* and *mas5-3*, respectively, which are minimal compared to those found in the *prp8-7* mutant (8,124 events, corresponding to 6.7% of total introns), which exhibits a very weak morphological phenotype (Cabezas-Fuster et al. 2022).

Two of the previously described viable *prp8a* missense alleles, *prp8a-6* and *prp8a-7*, are hypomorphs that are late flowering and display increased intron retention (Marquardt et al. 2014, Sasaki et al. 2015). The developmental impacts of other *prp8a* missense mutations (*prp8a-8*, *prp8a-9*, *prp8a-10*, and *prp8a-11*) have not been reported. The viable *prp8a* missense *prp8a-14* mutant exhibits pleiotropic defects, including reduced fertility and small stature. In addition to loss-of-function alleles, gain-of-function *prp8* alleles have been identified in Arabidopsis and in yeast *Saccharomyces cerevisiae*. These gain-of-function *prp8* mutations were isolated using suppression screens for secondary mutations that improved splicing in an original mutant with defective splicing. For example, spliceosome assembly is impaired in an Arabidopsis protein arginine methyltransferase5 (*prmt5*) mutant, and the *prp8a-8* and *prp8a-9* missense alleles restore splicing in *prmt5* by improving *prp8a* association with a stabilising protein complex, thus restoring spliceosome assembly and function (Deng et al., 2016).

In another example, Llinas et al. (2022) used *pex14-6,* a peroxisome-defective mutant with reduced protein accumulation as a result of mis-splicing of the first exon, in a suppression screen for restored peroxisome function. They recovered a point mutation in the PRP8A splicing factor (mutation in exon 13 changes the conserved Gly1326 to Arg in the Thumb/X domain) that corrected *pex14-6* splicing, restored pex14 protein accumulation, and improved peroxisome function. Global analysis of mRNA splicing in *prp8a-14* seedlings showed significant differences from WT at only a small subset of splicing junctions. Strikingly, they did not detect alternative splicing events in *prp8a-14* that were not also detected in WT This result indicated that *prp8a-14* did not markedly reduce splicing efficiency, which would presumably increase intron retention and/or exon skipping. Instead, the alternatively spliced junctions that were altered in *prp8a-14* were enriched for those showing differential splicing of 5’ and 3'-splice sites. Among these differentially spliced junctions, *prp8a-14* often favoured the site closest to the branch site, thus shortening the intron in both the 5’ and 3'-splice sites (Llinas et al. 2022).

3.3. RNA inheritance

Even though our results with AKRP and PRP8 clearly indicate that proteins, which are present in pollen and pollen tubes can have important functions also in ovule development, ovule attraction, targeting and subsequent fertilisation and embryogenesis, we were still not sure what is the origin of the phenotypes. The initial question was whether the specific transcripts that are stored in pollen and pollen tubes could potentially be inherited and required to function on target tissues and therefore their lack of causing the phenotypes, or if the phenotype originated from the lack of the transcripts/proteins caused by the T-DNA insertion within the target tissue. Providing evidence for such a hypothesis proved to be more complex than we anticipated.

Parental control and activation of zygotic gene expression is not well understood in flowering plants. (Nodine and Bartel, 2012, Autran et al., 2012). Plant embryos can progress to the pre-globular stage in the absence of significant *de novo* zygotic activation following RNA polymerase II (PolII) knockdown (Pillot et al., 2010b). Two studies on plant embryogenesis have reported dissimilar maternal-to-paternal transcriptome contribution, with one proposing maternally biased contribution (Autran et al., 2012), whereas the second reported equal parental contribution and therefore immediate zygotic gene activation of both parental genomes (Nodine and Bartel, 2012). Despite this, both studies have pointed to the likely enrichment of a small number of maternally/paternally-derived transcripts during early stages (1-2 cell stage) of embryogenesis (Nodine and Bartel, 2012; Autran et al., 2012). To date, only one example in plants exist that demonstrates an exclusive paternally-derived temporal cue required for embryogenesis (Bayer et al., 2009). An interleukin-1 receptor–associated kinase (IRAK)/Pelle-like kinase gene SHORT SUSPENSOR (SSP) regulates YODA mitogen-activated protein kinase pathway. SSP is exclusively expressed in sperm cells without undergoing translation, and its transcripts are delivered post-fertilisation, where newly synthesised SSP protein promotes zygote and suspensor elongation (Bayer et al., 2009).

Even though the principle for the selection of all studied candidate genes was the same, i.e. they should encode tranships that are long-term stored as translationally-silenced RNA in pollen tubes after 24 hrs of *in vitro* germination, due to time constraints and technical difficulties, we were tested the RNA inheritance hypothesis only with PRP8A. Both AtNEMF and AKRP native promoters showed weak activities, thus they were unsuitable for this experiment. PRP8A under its native promoter localised into the sperm cells and the vegetative nucleus in pollen and pollen tubes and were able to detect the GFP signal both 1 and 2 days after pollination (DAP) in the developing zygote after reciprocal crosses (see chapter 2 on unpublished PRP8 results). Fluorescent whole mount *in situ* hybridisation (F-WISH) of fertilised ovules from 1 and 2 DAP of pPRP8a-PRP8a::GFP pollinated pistils demonstrated a clear detection of pollen-originated PRP8a-GFP transcripts of the developing zygotic cells (proembryo), at the chalazal end as well as in the syncytial endosperm (Chapter 2.5., Fig. 1, Fig.2). Both experiments showed presence of PRP8a-GFP transcripts and protein, which originated in the male. However, we cannot prove that these transcripts were stored in the 80S stalled monosomes in the sperm cells. They could and probably do originate from the sperm cells that clearly contain the GFP-tagged products and can be transferred to the female gametophyte upon fertilisation, similar to SSP inherited transcripts (Bayer et al. 2009). It is still not clear where in the pollen and pollen tubes the 80S stalled RMA-storing monosomes reside. If they were present only in the vegetative cell and not the sperm cells, the inheritance of such transcripts could be disputed, even though it is not clear how much the vegetative cytosolic contents is able to affect zygotic development. While it has been proven that the pollen tube content after burst can induce ovule enlargement and promote seed coat development even without fertilisation (Kasahara et al. 2016), it is unclear how much of the content could possibly get inside the egg cell, as this is surrounded by a membrane that fuses with the peri-germ cell membrane of the pollen tube upon fertilisation (Sugi et al. 2024).

4. CONCLUSIONS

The study of pollen and its RNA metabolism has been one of the major topics of research in the Laboratory of Pollen Biology at the Institute of Experimental Botany CAS. One of the major findings was the description of mRNA storage in mature pollen and pollen tubes, initially described in tobacco as EPP particles (Honys, Reňák et al. 2009) and later refined as stalled monosomes (Hafidh et al. 2018). Transcriptomic data (Hafidh et al. 2012a, 2012b) and their classification into actively translated and stored transcripts served as a starting point for the selection of interesting candidate genes for further study. Three genes with transcripts stored even after 24hrs of pollen tube growth were selected and their Arabidopsis homologs were studied in this thesis (namely EMB1441/AtNEMF, EMB2036/AKRP and SUS2/PRP8a). The focus was on the description of morphological defects in the gametophytes and the developing embryo, together with a characterisation of molecular aspects for the phenotypic malformations. The major findings from this thesis are:

1) Pollen prepares for a rapid response needed for the germination of the pollen tube by synthesising and sequestering mRNA transcripts, that are further kept in storage granules, accompanied by RNA-binding proteins and monosomes (Billey et al. 2019). Translation of these mRNAs can be quickly reactivated when needed and a mass production of proteins can start at an appropriate time point during pollen germination and the pollen tube growth. Some transcripts can be stored for a prolonged time (even up to 24 hrs of PT growth) and could function during the fertilisation and embryogenesis (Hafidh et al. 2012a, 2012b, 2018, Kulichova et al. 2020, 2022, Hafidh et al. 2021).
2) EMB1441/AtNEMF is a nuclear export mediator factor and was one of the three genes I studied. We found that *Atnemf* mutant showed perturbed proliferation of the embryo proper cells at late globular stage resulting in embryo-lethal phenotype. However, the mutation did not affect pollen morphology, fitness, growth or ovule targeting efficiency (Chapter 2.6.).
3) EMB2036/AKRP, the second candidate gene, has a function in plastid biogenesis and serves as a part of a sorting mechanism for the twin-arginine translocation system into thylakoids. The loss of function leads to an arrested globular embryo and is thus lethal. Moreover, the T-DNA used in our study showed additional phenotypes in pollen, pollen

tubes and ovules, severely impacting their morphology, fitness and attractivity. Colocalisation study confirmed AKRP presence in the plastids, whereas embryo sac cell specific complementations demonstrated the importance of proper timing and transcriptional balance for precise function of AKRP in plastid development (Kulichova et al. 2022).

4) PRP8a, the third and most studied candidate gene, plays an important role in mRNA splicing. It is a large core subunit of the spliceosome and its loss of function led to embryo arrest at the globular stage (Chapter 2.5.). Together with its paralog, PRP8b, their dual loss of function double mutant *prp8a/prp8b* led to a specific loss in pollen tube guidance in the male gametophyte and ovule targeting competence in *prp8a/prp8b* female gametes, but showed no male or female gametogenesis defects (Kulichová et al., 2020). Moreover, double homozygous *prp8a/-prp8b/-* plants could not be recovered. The RNA-seq data analysis suggested that PRP8A/PRP8B participates in the pre-mRNA splicing of core genes with direct roles in the secretion of female ovule attractants, the specification of egg cell, central cell and synergid cell fates (Kulichová et al. 2020).

Overall, we have identified several candidate genes with pollen-stored transcripts that play key role pre-fertilisation during pollen-pistil interaction and post-fertilisation by promoting early stages of embryogenesis. Despite our attempted work and previous reports (Nodine et al. 2012, Autran et al. 2012), it still remains unclear in plants, whether the male-derived transcripts can be delivered to the female during fertilisation and play a role there. Even though it has been proven that the cytosolic content of the pollen tube can induce enlargement of the embryo sac even without fertilisation (Kasahara et al. 2016), the peri-germ cell membrane poses a barrier for the cytosolic content of the pollen tube. Can there be RNA inheritance beyond the sperm cells? Are there any mechanism how the cytosolic mRNA/ proteins can affect embryogenesis? The precise localisation of the stalled monosomes is still unclear. If they reside only in the vegetative cell and not the sperm cells, their content could be functionally limited up to the fertilisation process. If the monosomes are present also in the sperm cells, the transcripts could be delivered to the female, the proteins could be quickly made and function in the very early and crucial steps of zygote formation, even before the

onset of zygotic expression. These questions remain to be elucidated and pose interesting questions for further research.

5. LITERATURE

Abe, S. and Davies, E. (1995). Chapter 16 Methods for Isolation and Analysis of the Cytoskeleton. Methods Cell Biol. - METHOD CELL BIOL 50, 223–236.

Alon, U. (2007). Network motifs: theory and experimental approaches. Nat. Rev. Genet. 8, 450–461.

Anderson, S. N., Johnson, C. S., Jones, D. S., Conrad, L. J., Gou, X., Russell, S. D. and Sundaresan, V. (2013). Transcriptomes of isolated Oryza sativa gametes characterized by deep sequencing: evidence for distinct sex-dependent chromatin and epigenetic states before fertilization. Plant J. 76, 729–741.

Anderson, S., Johnson, C., Chesnut, J., Jones, D., Khanday, I., Woodhouse, M., Li, C., Conrad, L., Russell, S. and Sundaresan, V. (2017). The Zygotic Transition Is Initiated in Unicellular Plant Zygotes with Asymmetric Activation of Parental Genomes. Dev. Cell 43, 349-358.e4.

Ariizumi, T. and Toriyama, K. (2011). Genetic regulation of sporopollenin synthesis and pollen exine development. Annu. Rev. Plant Biol. 62, 437–460.

Armenta-Medina, A. and Gillmor, C. S. (2019). Genetic, molecular and parent-of-origin regulation of early embryogenesis in flowering plants. Curr. Top. Dev. Biol. 131, 497–543.

Armenta-Medina, A., Gillmor, C. S., Gao, P., Mora-Macias, J., Kochian, L. V, Xiang, D. and Datla, R. (2021). Developmental and genomic architecture of plant embryogenesis: from model plant to crops. Plant Commun. 2, 100136.

Autran, D., Baroux, C., Raissig, M. T., Lenormand, T., Wittig, M., Grob, S., Steimer, A., Barann, M., Klostermeier, U. C., Leblanc, O., et al. (2011). Maternal epigenetic pathways control parental contributions to Arabidopsis early embryogenesis. Cell 145, 707–719.

Babu, Y., Musielak, T., Henschen, A. and Bayer, M. (2013). Suspensor length determines developmental progression of the embryo in Arabidopsis. Plant Physiol. 162, 1448–58.

Bai, B., Peviani, A., van der Horst, S., Gamm, M., Snel, Berend, Bentsink, L. and Hanson, J. (2017). Extensive translational regulation during seed germination revealed by polysomal profiling. New Phytol. 214, 233–244.

Bai, B., van der Horst, S., Cordewener, J. H. G., America, T. A. H. P., Hanson, J. and Bentsink, L. (2020). Seed-Stored mRNAs that Are Specifically Associated to Monosomes Are Translationally Regulated during Germination. Plant Physiol. 182, 378–392.

Bailey-Serres, J., Sorenson, R. and Juntawong, P. (2009). Getting the message across: cytoplasmic ribonucleoprotein complexes. Trends Plant Sci. 14, 443–453.

Bartels, C., Klatt, C., Lührmann, R. and Fabrizio, P. (2002). The ribosomal translocase homologue Snu114p is involved in unwinding U4/U6 RNA during activation of the spliceosome. EMBO Rep. 3, 875–880.

Basbouss-Serhal, I., Soubigou-Taconnat, L., Bailly, C. and Leymarie, J. (2015). Germination Potential of Dormant and Nondormant Arabidopsis Seeds Is Driven by Distinct Recruitment of Messenger RNAs to Polysomes. Plant Physiol. 168, 1049–1065.

Baud, S. and Lepiniec, L. (2010). Physiological and developmental regulation of seed oil production. Prog. Lipid Res. 49, 235–249.

Bayer, M., Nawy, T., Giglione, C., Galli, M., Meinnel, T. and Lukowitz, W. (2009). Paternal control of embryonic patterning in Arabidopsis thaliana. Science 323, 1485–1488.

Beale, K. M., Leydon, A. R. and Johnson, M. A. (2012). Gamete fusion is required to block multiple pollen tubes from entering an Arabidopsis ovule. Curr. Biol. 22, 1090–1094.

Becker, D., Boavida, L. C., Carneiro, J., Haury, M. and Feijo, a (2003). Transcriptional Profiling of Arabidopsis Tissues. Society 133, 713–725.

Bemer, M., Wolters-Arts, M., Grossniklaus, U. and Angenent, G. C. (2008). The MADS domain protein DIANA acts together with AGAMOUS-LIKE80 to specify the central cell in Arabidopsis ovules. Plant Cell 20, 2088–2101.

Benina, M., Ribeiro, D. M., Gechev, T. S., Mueller-Roeber, B. and Schippers, J. O. S. H. M. (2015). A cell type-specific view on the translation of mRNAs from ROS-responsive genes upon paraquat treatment of Arabidopsis thaliana leaves. Plant. Cell Environ. 38, 349–363.

Boisson-Dernier, A., Roy, S., Kritsas, K., Grobei, M. A., Jaciubek, M., Schroeder, J. I. and Grossniklaus, U. (2009). Disruption of the pollen-expressed FERONIA homologs ANXUR1 and ANXUR2 triggers pollen tube discharge. Development 136, 3279–3288.

Borg, M., Brownfield, L. and Twell, D. (2009). Male gametophyte development: A molecular perspective. J. Exp. Bot. 60, 1465–1478.

Borg, M., Jacob, Y., Susaki, D., LeBlanc, C., Buendía, D., Axelsson, E., Kawashima, T., Voigt, P., Boavida, L., Becker, J., et al. (2020). Targeted reprogramming of H3K27me3 resets epigenetic memory in plant paternal chromatin. Nat. Cell Biol. 22, 621–629.

Borges, F., Gomes, G., Gardner, R., Moreno, N., McCormick, S., Feijó, J. A. and Becker, J. D. (2008). Comparative transcriptomics of Arabidopsis sperm cells. Plant Physiol. 148, 1168–1181.

Brownfield, L., Hafidh, S., Durbarry, A., Khatab, H., Sidorova, A., Doerner, P. and Twell, D. (2009). Arabidopsis DUO POLLEN3 is a key regulator of male germline development and embryogenesis. Plant Cell 21, 1940–1956.

Browning, K. S. and Bailey-Serres, J. (2015). Mechanism of Cytoplasmic mRNA Translation. https://doi.org/10.1199/tab.0176 2015, e0176.

Burri, J. T., Vogler, H., Läubli, N. F., Hu, C., Grossniklaus, U. and Nelson, B. J. (2018). Feeling the force: how pollen tubes deal with obstacles. New Phytol. 220, 187–195.

Cabezas-Fuster, A., Micol-Ponce, R., Fontcuberta-Cervera, S. and Ponce, M. R. (2022). Missplicing suppressor alleles of Arabidopsis PRE-MRNA PROCESSING FACTOR 8 increase splicing fidelity by reducing the use of novel splice sites. Nucleic Acids Res. 50, 5513–5527.

Capron, A., Gourgues, M., Neiva, L. S., Faure, J.-E., Berger, F., Pagnussat, G., Krishnan, A., Alvarez-Mejia, C., Vielle-Calzada, J.-P., Lee, Y.-R., et al. (2008). Maternal control of male-gamete delivery in Arabidopsis involves a putative GPI-anchored protein encoded by the LORELEI gene. Plant Cell 20, 3038–3049.

Chantarachot, T. and Bailey-Serres, J. (2018). Polysomes, Stress Granules, and Processing Bodies: A Dynamic Triumvirate Controlling Cytoplasmic mRNA Fate and Function. Plant Physiol. 176, 254–269.

Chaudhary, S., Khokhar, W., Jabre, I., Reddy, A. S. N., Byrne, L. J., Wilson, C. M. and Syed, N. H. (2019). Alternative Splicing and Protein Diversity: Plants Versus Animals. Front. Plant Sci. 10,.

Chebli, Y. and Geitmann, A. (2007). Mechanical principles governing pollen tube growth. Funct. Plant Sci. Biotechnol. 1,.

Chehab, E. W., Eich, E. and Braam, J. (2009). Thigmomorphogenesis: a complex plant response to mechano-stimulation. J. Exp. Bot. 60, 43–56.

Chen, J., Strieder, N., Krohn, N. G., Cyprys, P., Sprunck, S., Engelmann, J. C. and Dresselhaus, T. (2017). Zygotic Genome Activation Occurs Shortly after Fertilization in Maize. Plant Cell 29, 2106–2125.

Chen, Y.-H., Li, H.-J., Shi, D.-Q., Yuan, L., Liu, J., Sreenivasan, R., Baskar, R., Grossniklaus, U. and Yang, W.-C. (2007). The central cell plays a critical role in pollen tube guidance in Arabidopsis. Plant Cell 19, 3563–77.

Chen, Y.-L., Chen, L.-J., Chu, C.-C., Huang, P.-K., Wen, J.-R. and Li, H. (2018). TIC236 links the outer and inner membrane translocons of the chloroplast. Nature 564, 125–129.

Cho, H., Cho, H. S. and Hwang, I. (2019). Emerging roles of RNA-binding proteins in plant development. Curr. Opin. Plant Biol. 51, 51–57.

Choi, Y., Gehring, M., Johnson, L., Hannon, M., Harada, J. J., Goldberg, R. B., Jacobsen, S. E. and Fischer, R. L. (2002). DEMETER, a DNA glycosylase domain protein, is required for endosperm gene imprinting and seed viability in arabidopsis. Cell 110, 33–42.

Christensen, C. A., King, E. J., Jordan, J. R. and Drews, G. N. (1997). Megagametogenesis in Arabidopsis wild type and the Gf mutant. Sex. Plant Reprod. 10, 49–64.

Creasey, K. M., Zhai, J., Borges, F., Van Ex, F., Regulski, M., Meyers, B. C. and Martienssen, R. A. (2014). miRNAs trigger widespread epigenetically activated siRNAs from transposons in Arabidopsis. Nature 508, 411–415.

Cruz, J. A. and Westhof, E. (2009). The dynamic landscapes of RNA architecture. Cell 136, 604–609.

Cucinotta, M., Cavalleri, A., Guazzotti, A., Astori, C., Manrique, S., Bombarely, A., Oliveto, S., Biffo, S., Weijers, D., Kater, M. M., et al. (2021). Alternative Splicing Generates a MONOPTEROS Isoform Required for Ovule Development. Curr. Biol. 31, 892-899.e3.

Cyprys, P., Lindemeier, M. and Sprunck, S. (2019). Gamete fusion is facilitated by two sperm cell-expressed DUF679 membrane proteins. Nat. plants 5, 253–257.

Davies, E. and Abe, S. (1995). Chapter 15 Methods for Isolation and Analysis of Polyribosomes. Methods Cell Biol. - METHOD CELL BIOL 50, 209–222.

Davies, E., Stankovic, B., Vian, A. and Wood, A. (2012). Where has all the message gone? Plant Sci. 185–186, 23–32.

Dean, P. J., Siwiec, T., Waterworth, W. M., Schlögelhofer, P., Armstrong, S. J. and West, C. E. (2009). A novel ATM-dependent X-ray-inducible gene is essential for both plant meiosis and gametogenesis. Plant J. 58, 791–802.

Del Toro-De León, G., García-Aguilar, M. and Gillmor, C. S. (2014). Non-equivalent contributions of maternal and paternal genomes to early plant embryogenesis. Nature 514, 624–627.

Del Toro-De León, G., Lepe-Soltero, D. and Gillmor, C. S. (2016). Zygotic genome activation in isogenic and hybrid plant embryos. Curr. Opin. Plant Biol. 29, 148–153.

Deng, X., Lu, T., Wang, L., Gu, L., Sun, J., Kong, X., Liu, C. and Cao, X. (2016). Recruitment of the NineTeen Complex to the activated spliceosome requires AtPRMT5. Proc. Natl. Acad. Sci. U. S. A. 113, 5447–52.

Denninger, P., Bleckmann, A., Lausser, A., Vogler, F., Ott, T., Ehrhardt, D. W., Frommer, W. B., Sprunck, S., Dresselhaus, T. and Grossmann, G. (2014). Male-female communication triggers calcium signatures during fertilization in Arabidopsis. Nat. Commun. 5, 4645.

Dickinson, H. G. and Heslop-Harrison, J. (1977). Ribosomes, membranes and organelles during meiosis in angiosperms. Philos. Trans. R. Soc. London. Ser. B, Biol. Sci. 277, 327–342.

Drechsel, G., Kahles, A., Kesarwani, A. K., Stauffer, E., Behr, J., Drewe, P., Rätsch, G. and Wachter, A. (2013). Nonsense-mediated decay of alternative precursor mRNA splicing variants is a major determinant of the Arabidopsis steady state transcriptome. Plant Cell 25, 3726–3742.

Drescher, A., Ruf, S., Calsa, T. J., Carrer, H. and Bock, R. (2000). The two largest chloroplast genome-encoded open reading frames of higher plants are essential genes. Plant J. 22, 97–104.

Drews, G. N. and Koltunow, A. M. G. (2011). The female gametophyte. Arab. B. 9, e0155.

Dure, L. and Waters, L. (1965). Long-Lived Messenger RNA: Evidence from Cotton Seed Germination. Science (80-.). 147, 410–412.

Erdem, M., Cicek, M. and Erson-Bensan, A. E. (2023). Versatile RNA: overlooked gems of the transcriptome. FEBS J. 290, 4843–4851.

Escobar-Restrepo, J.-M., Huck, N., Kessler, S., Gagliardini, V., Gheyselinck, J., Yang, W.-C. and Grossniklaus, U. (2007). The FERONIA receptor-like kinase mediates male-female interactions during pollen tube reception. Science 317, 656–660.

Evans and Grossniklaus, U. (2008). 4 . The Maize Megagametophyte. In J. Bennetzen & S. Hake (Eds.), (pp. 79–104). Springer. doi:10.1007/978-0-387-79418-1_5

Fédry, J., Liu, Y., Péhau-Arnaudet, G., Pei, J., Li, W., Tortorici, M. A., Traincard, F., Meola, A., Bricogne, G., Grishin, N. V, et al. (2017). The Ancient Gamete Fusogen HAP2 Is a Eukaryotic Class II Fusion Protein. Cell 168, 904-915.e10.

Filichkin, S., Priest, H. D., Megraw, M. and Mockler, T. C. (2015). Alternative splicing in plants: directing traffic at the crossroads of adaptation and environmental stress. Curr. Opin. Plant Biol. 24, 125–35.

Frank, A. C. and Johnson, M. A. (2009). Expressing the diphtheria toxin A subunit from the HAP2(GCS1) promoter blocks sperm maturation and produces single sperm-like cells capable of fertilization. Plant Physiol. 151, 1390–1400.

Friml, J., Vieten, A., Sauer, M., Weijers, D., Schwarz, H., Hamann, T., Offringa, R. and Jürgens, G. (2003). Efflux-dependent auxin gradients establish the apical-basal axis of Arabidopsis. Nature 426, 147–153.

Galland, M., Huguet, R., Arc, E., Cueff, G., Job, D. and Rajjou, L. (2014). Dynamic Proteomics Emphasizes the Importance of Selective mRNA Translation and Protein Turnover during Arabidopsis Seed Germination*. Mol. Cell. Proteomics 13, 252–268.

Ge, Z., Bergonci, T., Zhao, Y., Zou, Y., Du, S., Liu, M.-C., Luo, X., Ruan, H., García-Valencia, L. E., Zhong, S., et al. (2017). Arabidopsis pollen tube integrity and sperm release are regulated by RALF-mediated signaling. Science 358, 1596–1600.

Ge, Z., Zhao, Y., Liu, M.-C., Zhou, L.-Z., Wang, L., Zhong, S., Hou, S., Jiang, J., Liu, T., Huang, Q., et al. (2019). LLG2/3 Are Co-receptors in BUPS/ANX-RALF Signaling to Regulate Arabidopsis Pollen Tube Integrity. Curr. Biol. 29, 3256-3265.e5.

Glisovic, T., Bachorik, J. L., Yong, J. and Dreyfuss, G. (2008). RNA-binding proteins and post-transcriptional gene regulation. FEBS Lett. 582, 1977–1986.

Glöckle, B., Urban, W. J., Nagahara, S., Andersen, E. D., Higashiyama, T., Grini, P. E. and Schnittger, A. (2018). Pollen differentiation as well as pollen tube guidance and discharge are independent of the presence of gametes. Development 145,.

Golicz, A. A., Allu, A. D., Li, W., Lohani, N., Singh, M. B. and Bhalla, P. L. (2021). A dynamic intron retention program regulates the expression of several hundred genes during pollen meiosis. Plant Reprod. 34, 225–242.

Grainger, R. J. and Beggs, J. D. (2005). Prp8 protein: at the heart of the spliceosome. RNA 11, 533–557.

Grau-Bové, X., Ruiz-Trillo, I. and Irimia, M. (2018). Origin of exon skipping-rich transcriptomes in animals driven by evolution of gene architecture. Genome Biol. 19, 135.

Groß-Hardt, R., Kägi, C., Baumann, N., Moore, J. M., Baskar, R., Gagliano, W. B., Jürgens, G. and Grossniklaus, U. (2007). LACHESIS restricts gametic cell fate in the female gametophyte of Arabidopsis. PLoS Biol. 5, 0494–0500.

Guan, Y., Lu, J., Xu, J., McClure, B. and Zhang, S. (2014). Two Mitogen-Activated Protein Kinases, MPK3 and MPK6, Are Required for Funicular Guidance of Pollen Tubes in Arabidopsis. Plant Physiol. 165, 528–533.

Gusti, A., Baumberger, N., Nowack, M., Pusch, S., Eisler, H., Potuschak, T., De Veylder, L., Schnittger, A. and Genschik, P. (2009). The Arabidopsis thaliana F-box protein FBL17 is essential for progression through the second mitosis during pollen development. PLoS One 4, e4780.

Haecker, A., Gross-Hardt, R., Geiges, B., Sarkar, A., Breuninger, H., Herrmann, M. and Laux, T. (2004). Expression dynamics of WOX genes mark cell fate decisions during early embryonic patterning in Arabidopsis thaliana. Development 131, 657–668.

Hafidh, S., Breznenová, K. and Honys, D. (2012). De novo post-pollen mitosis II tobacco pollen tube transcriptome. Plant Signal. Behav. 7, 918–921.

Hafidh, S., Breznenová, K., Růžička, P., Feciková, J., Čapková, V. and Honys, D. (2012). Comprehensive analysis of tobacco pollen transcriptome unveils common pathways in polar cell expansion and underlying heterochronic shift during spermatogenesis. BMC Plant Biol. 12, 24.

Hafidh, S., Fíla, J. and Honys, D. (2016). Male gametophyte development and function in angiosperms: a general concept. Plant Reprod. 29, 31–51.

Hafidh, S. and Honys, D. (2021). Reproduction Multitasking: The Male Gametophyte. Annu. Rev. Plant Biol. 72, 581–614.

Hafidh, S., Potěšil, D., Müller, K., Fíla, J., Michailidis, C., Herrmannová, A., Feciková, J., Ischebeck, T., Valášek, L. S., Zdráhal, Z., et al. (2018). Dynamics of the Pollen Sequestrome Defined by Subcellular Coupled Omics. Plant Physiol. 178, 258–282.

Hamamura, Y., Nishimaki, M., Takeuchi, H., Geitmann, A., Kurihara, D. and Higashiyama, T. (2014). Live imaging of calcium spikes during double fertilization in Arabidopsis. Nat. Commun. 5, 4722.

Hamamura, Y., Saito, C., Awai, C., Kurihara, D., Miyawaki, A., Nakagawa, T., Kanaoka, M. M., Sasaki, N., Nakano, A., Berger, F., et al. (2011). Live-cell imaging reveals the dynamics of two sperm cells during double fertilization in Arabidopsis thaliana. Curr. Biol. 21, 497–502.

Hartmann, L., Wießner, T. and Wachter, A. (2018). Subcellular Compartmentation of Alternatively Spliced Transcripts Defines SERINE/ARGININE-RICH PROTEIN30 Expression . Plant Physiol. 176, 2886–2903.

Haruta, M., Sabat, G., Stecker, K., Minkoff, B. B. and Sussman, M. R. (2014). A peptide hormone and its receptor protein kinase regulate plant cell expansion. Science 343, 408–411.

Hater, F., Nakel, T. and Groß-Hardt, R. (2020). Reproductive Multitasking: The Female Gametophyte. Annu. Rev. Plant Biol. 71, 517–546.

Hernández-Lagana, E., Rodríguez-Leal, D., Lúa, J. and Vielle-Calzada, J.-P. (2016). A Multigenic Network of ARGONAUTE4 Clade Members Controls Early Megaspore Formation in Arabidopsis. Genetics 204, 1045–1056.

Herridge, R. P., Dolata, J., Migliori, V., de Santis Alves, C., Borges, F., Schorn, A. J., van Ex, F., Lin, A., Bajczyk, M., Parent, J.-S., et al. (2025). Pseudouridine guides germline small RNA transport and epigenetic inheritance. Nat. Struct. Mol. Biol. 32, 277–286.

Heydlauff, J. and Groß-Hardt, R. (2014). Love is a battlefield: programmed cell death during fertilization. J. Exp. Bot. 65, 1323–1330.

Higashiyama, T., Yabe, S., Sasaki, N., Nishimura, Y., Miyagishima, S., Kuroiwa, H. and Kuroiwa, T. (2001). Pollen tube attraction by the synergid cell. Science 293, 1480–1483.

Higashiyama, T., Kuroiwa, H., Kawano, S. and Kuroiwa, T. (1998). Guidance in vitro of the Pollen Tube to the Naked Embryo Sac of Torenia fournieri. Plant Cell 10, 2019–2031.

Higashiyama, T. and Yang, W. C. (2017). Gametophytic pollen tube guidance: Attractant peptides, gametic controls, and receptors. Plant Physiol. 173, 112–121.

Hisanaga, T., Okahashi, K., Yamaoka, S., Kajiwara, T., Nishihama, R., Shimamura, M., Yamato, K. T., Bowman, J. L., Kohchi, T. and Nakajima, K. (2019). A cis-acting bidirectional transcription switch controls sexual dimorphism in the liverwort. EMBO J. 38,.

Hong, E. M., Ingemarsdotter, C. K. and Lever, A. M. L. (2020). Therapeutic applications of trans-splicing. Br. Med. Bull. 136, 4–20.

Honys, D., Combe, J. P., Twell, D. and Capková, V. (2000). The translationally repressed pollen-specific ntp303 mRNA is stored in non-polysomal mRNPs during pollen maturation. Sex. Plant Reprod. 13, 135–144.

Honys, D., Rěnák, D., Feciková, J., Jedelský, P. L., Nebesárová, J., Dobrev, P. and Capková, V. (2009). Cytoskeleton-associated large RNP complexes in tobacco male gametophyte (EPPs) are associated with ribosomes and are involved in protein synthesis, processing, and localization. J. Proteome Res. 8, 2015–31.

Honys, D. and Twell, D. (2004). Transcriptome analysis of haploid male gametophyte development in Arabidopsis. Genome Biol. 5, R85.

Honys, D. and Twell, D. (2003). Comparative Analysis of the Arabidopsis Pollen Transcriptome . Plant Physiol. 132, 640–652.

Huang, B.-Q. and Russell, S. D. (1992). Female Germ Unit: Organization, Isolation, and Function. In (ed. Russell, S. D.) and Dumas, C.), pp. 233–293. Academic Press.

Huang, J., Dong, J. and Qu, L.-J. (2021). From birth to function: Male gametophyte development in flowering plants. Curr. Opin. Plant Biol. 63, 102118.

Huang, J., Ju, Y., Wang, X., Zhang, Q. and Sodmergen (2015). A one-step rectification of sperm cell targeting ensures the success of double fertilization. J. Integr. Plant Biol. 57, 496–503.

Huck, N., Moore, J. M., Federer, M. and Grossniklaus, U. (2003). The Arabidopsis mutant feronia disrupts the female gametophytic control of pollen tube reception. Development 130, 2149–2159.

Irimia, M. and Blencowe, B. J. (2012). Alternative splicing: decoding an expansive regulatory layer. Curr. Opin. Cell Biol. 24, 323–332.

Ishibashi, N., Yamauchi, D. and Minamikawa, T. (1990). Stored mRNA in cotyledons of Vigna unguiculata seeds: nucleotide sequence of cloned cDNA for a stored mRNA and induction of its synthesis by precocious germination. Plant Mol. Biol. 15, 59–64.

Iwakawa, H., Shinmyo, A. and Sekine, M. (2006). Arabidopsis CDKA;1, a cdc2 homologue, controls proliferation of generative cells in male gametogenesis. Plant J. 45, 819–831.

Iwano, M., Ngo, Q. A., Entani, T., Shiba, H., Nagai, T., Miyawaki, A., Isogai, A., Grossniklaus, U. and Takayama, S. (2012). Cytoplasmic Ca2+ changes dynamically during the interaction of the pollen tube with synergid cells. Development 139, 4202–4209.

Iwano, M., Shiba, H., Miwa, T., Che, F.-S., Takayama, S., Nagai, T., Miyawaki, A. and Isogai, A. (2004). Ca2+ dynamics in a pollen grain and papilla cell during pollination of Arabidopsis. Plant Physiol. 136, 3562–3571.

Jabre, I., Reddy, A. S. N., Kalyna, M., Chaudhary, S., Khokhar, W., Byrne, L. J., Wilson, C. M. and Syed, N. H. (2019). Does co-transcriptional regulation of alternative splicing mediate plant stress responses? Nucleic Acids Res. 47, 2716–2726.

Jangi, M. and Sharp, P. A. (2014). Building Robust Transcriptomes with Master Splicing Factors. Cell 159, 487–498.

Jarvis, P. and López-Juez, E. (2013). Biogenesis and homeostasis of chloroplasts and other plastids. Nat. Rev. Mol. Cell Biol. 14, 787–802.

Jeong, S., Palmer, T. M. and Lukowitz, W. (2011). The RWP-RK Factor GROUNDED Promotes Embryonic Polarity by Facilitating YODA MAP Kinase Signaling. Curr. Biol. 21, 1268–1276.

Johnson, M. A., Harper, J. F. and Palanivelu, R. (2019). A Fruitful Journey: Pollen Tube Navigation from Germination to Fertilization. Annu. Rev. Plant Biol. 70, 809–837.

Jones, D. S., Yuan, J., Smith, B. E., Willoughby, A. C., Kumimoto, E. L. and Kessler, S. A. (2017). MILDEW RESISTANCE LOCUS O Function in Pollen Tube Reception Is Linked to Its Oligomerization and Subcellular Distribution. Plant Physiol. 175, 172–185.

Julca, I., Ferrari, C., Flores-Tornero, M., Proost, S., Lindner, A.-C., Hackenberg, D., Steinbachová, L., Michaelidis, C., Gomes Pereira, S., Misra, C. S., et al. (2021). Comparative transcriptomic analysis reveals conserved programmes underpinning organogenesis and reproduction in land plants. Nat. plants 7, 1143–1159.

Juntawong, P., Girke, T., Bazin, J. and Bailey-Serres, J. (2014). Translational dynamics revealed by genome-wide profiling of ribosome footprints in Arabidopsis. Proc. Natl. Acad. Sci. U. S. A. 111,.

Kägi, C., Baumann, N., Nielsen, N., Stierhof, Y.-D. and Groß-Hardt, R. (2010). The gametic central cell of Arabidopsis determines the lifespan of adjacent accessory cells. Proc. Natl. Acad. Sci. 107, 22350–22355.

Kalyna, M., Simpson, C. G., Syed, N. H., Lewandowska, D., Marquez, Y., Kusenda, B., Marshall, J., Fuller, J., Cardle, L., McNicol, J., et al. (2012). Alternative splicing and nonsense-mediated decay modulate expression of important regulatory genes in Arabidopsis. Nucleic Acids Res. 40, 2454–69.

Kao, P. and Nodine, M. D. (2019). Transcriptional Activation of Arabidopsis Zygotes Is Required for Initial Cell Divisions. Sci. Rep. 9, 17159.

Kasahara, R. D., Maruyama, D., Hamamura, Y., Sakakibara, T., Twell, D. and Higashiyama, T. (2012). Fertilization recovery after defective sperm cell release in Arabidopsis. Curr. Biol. 22, 1084–1089.

Kasahara, R. D., Notaguchi, M., Nagahara, S., Suzuki, T., Susaki, D., Honma, Y., Maruyama, D. and Higashiyama, T. (2016). Pollen tube contents initiate ovule enlargement and enhance seed coat development without fertilization. Sci. Adv. 2, e1600554.

Kasahara, R. D., Portereiko, M. F., Sandaklie-Nikolova, L., Rabiger, D. S. and Drews, G. N. (2005). MYB98 is required for pollen tube guidance and synergid cell differentiation in Arabidopsis. Plant Cell 17, 2981–2992.

Kashkan I, Hrtyan M, Retzer K, Humpolíčková J, Jayasree A, Filepová R, Vondráková Z, Simon S, Rombaut D, Jacobs TB, Frilander MJ, Hejátko J, Friml J, Petrášek J, Růžička K. Mutually opposing activity of PIN7 splicing isoforms is required for auxin-mediated tropic responses in Arabidopsis thaliana. New Phytol. 2022 Jan;233(1):329-343. doi: 10.1111/nph. 17792. Epub 2021 Nov 5. PMID: 34637542.

Kelemen, O., Convertini, P., Zhang, Z., Wen, Y., Shen, M., Falaleeva, M. and Stamm, S. (2013). Function of alternative splicing. Gene 514, 1–30.

Keller, M., Hu, Y., Mesihovic, A., Fragkostefanakis, S., Schleiff, E. and Simm, S. (2017). Alternative splicing in tomato pollen in response to heat stress†. DNA Res. 24, 205–217.

Kessler, S. A., Shimosato-Asano, H., Keinath, N. F., Wuest, S. E., Ingram, G., Panstruga, R. and Grossniklaus, U. (2010). Conserved molecular components for pollen tube reception and fungal invasion. Science 330, 968–971.

Kikuchi, S., Asakura, Y., Imai, M., Nakahira, Y., Kotani, Y., Hashiguchi, Y., Nakai, Y., Takafuji, K., Bédard, J., Hirabayashi-Ishioka, Y., et al. (2018). A Ycf2-FtsHi Heteromeric AAA-ATPase Complex Is Required for Chloroplast Protein Import. Plant Cell 30, 2677–2703.

Kikuchi, S., Bédard, J., Hirano, M., Hirabayashi, Y., Oishi, M., Imai, M., Takase, M., Ide, T. and Nakai, M. (2013). Uncovering the protein translocon at the chloroplast inner envelope membrane. Science 339, 571–574.

Kim, H. J., Oh, S. A., Brownfield, L., Hong, S. H., Ryu, H., Hwang, I., Twell, D. and Nam, H. G. (2008). Control of plant germline proliferation by SCF(FBL17) degradation of cell cycle inhibitors. Nature 455, 1134–1137.

Kim, M. Y., Ono, A., Scholten, S., Kinoshita, T., Zilberman, D., Okamoto, T. and Fischer, R. L. (2019). DNA demethylation by ROS1a in rice vegetative cells promotes methylation in sperm. Proc. Natl. Acad. Sci. U. S. A. 116, 9652–9657.

Kinoshita, T., Yadegari, R., Harada, J. J., Goldberg, R. B. and Fischer, R. L. (1999). Imprinting of the MEDEA polycomb gene in the Arabidopsis endosperm. Plant Cell 11, 1945–1952.

Klepikova, A. V, Kasianov, A. S., Gerasimov, E. S., Logacheva, M. D. and Penin, A. A. (2016). A high resolution map of the Arabidopsis thaliana developmental transcriptome based on RNA-seq profiling. Plant J. 88, 1058–1070.

Klodová, B., Potěšil, D., Steinbachová, L., Michailidis, C., Lindner, A.-C., Hackenberg, D., Becker, J. D., Zdráhal, Z., Twell, D. and Honys, D. (2023). Regulatory dynamics of gene expression in the developing male gametophyte of Arabidopsis. Plant Reprod. 36, 213–241.

Köhler, C., Wolff, P. and Spillane, C. (2012). Epigenetic mechanisms underlying genomic imprinting in plants. Annu. Rev. Plant Biol. 63, 331–352.

Koi, S., Hisanaga, T., Sato, K., Shimamura, M., Yamato, K. T., Ishizaki, K., Kohchi, T. and Nakajima, K. (2016). An Evolutionarily Conserved Plant RKD Factor Controls Germ Cell Differentiation. Curr. Biol. 26, 1775–1781.

Koncz, C., Dejong, F., Villacorta, N., Szakonyi, D. and Koncz, Z. (2012). The spliceosome-activating complex: molecular mechanisms underlying the function of a pleiotropic regulator. Front. Plant Sci. 3, 9.

Köster, T., Marondedze, C., Meyer, K. and Staiger, D. (2017). RNA-Binding Proteins Revisited – The Emerging Arabidopsis mRNA Interactome. Trends Plant Sci. 22, 512–526.

Kőszegi, D., Johnston, A. J., Rutten, T., Czihal, A., Altschmied, L., Kumlehn, J., Wüst, S. E. J., Kirioukhova, O., Gheyselinck, J., Grossniklaus, U., et al. (2011). Members of the RKD transcription factor family induce an egg cell-like gene expression program. Plant J. 67, 280–291.

Kulichová, K., Kumar, V., Steinbachová, L., Klodová, B., Timofejeva, L., Juříček, M., Honys, D. and Hafidh, S. S. (2020). PRP8A and PRP8B spliceosome subunits act coordinately to control pollen tube attraction in Arabidopsis thaliana. Development 147, dev186742.

Kuligowski, J., Ferrand, M. and Chenou, E. (1991). Stored mRNA in early embryos of a fern Marsilea vestita: A paternal and maternal origin. Mol. Reprod. Dev. 30, 27–33.

Łabno, A., Tomecki, R. and Dziembowski, A. (2016). Cytoplasmic RNA decay pathways - Enzymes and mechanisms. Biochim. Biophys. Acta 1863, 3125–3147.

Lancelle, S. A. and Hepler, P. K. (1992). Ultrastructure of freeze-substituted pollen tubes ofLilium longiflorum. Protoplasma 167, 215–230.

Lawit, S. J., Chamberlin, M. A., Agee, A., Caswell, E. S. and Albertsen, M. C. (2013). Transgenic manipulation of plant embryo sacs tracked through cell-type-specific fluorescent markers: cell labeling, cell ablation, and adventitious embryos. Plant Reprod. 26, 125–137.

Layat, E., Leymarie, J., El-Maarouf-Bouteau, H., Caius, J., Langlade, N. and Bailly, C. (2014). Translatome profiling in dormant and nondormant sunflower (Helianthus annuus) seeds highlights post-transcriptional regulation of germination. New Phytol. 204, 864–872.

Lee, D. W., Lee, J. and Hwang, I. (2017). Sorting of nuclear-encoded chloroplast membrane proteins. Curr. Opin. Plant Biol. 40, 1–7.

Lee, J. H., Ryu, H.-S., Chung, K. S., Posé, D., Kim, S., Schmid, M. and Ahn, J. H. (2013). Regulation of temperature-responsive flowering by MADS-box transcription factor repressors. Science 342, 628–632.

Lee, J.-Y. and Lee, D.-H. (2003). Use of Serial Analysis of Gene Expression Technology to Reveal Changes in Gene Expression in Arabidopsis Pollen Undergoing Cold Stress . Plant Physiol. 132, 517–529.

Lei, L., Shi, J., Chen, J., Zhang, M., Sun, S., Xie, S., Li, X., Zeng, B., Peng, L., Hauck, A., et al. (2015). Ribosome profiling reveals dynamic translational landscape in maize seedlings under drought stress. Plant J. 84, 1206–1218.

Leprince, O., Pellizzaro, A., Berriri, S. and Buitink, J. (2017). Late seed maturation: drying without dying. J. Exp. Bot. 68, 827–841.

Leshem, Y., Johnson, C. and Sundaresan, V. (2013). Pollen tube entry into the synergid cell of Arabidopsis is observed at a site distinct from the filiform apparatus. Plant Reprod. 26, 93–99.

Lewis, B. P., Green, R. E. and Brenner, S. E. (2003). Evidence for the widespread coupling of alternative splicing and nonsense-mediated mRNA decay in humans. Proc. Natl. Acad. Sci. U. S. A. 100, 189–192.

Leydon, A. R., Tsukamoto, T., Dunatunga, D., Qin, Y., Johnson, M. A. and Palanivelu, R. (2015). Pollen Tube Discharge Completes the Process of Synergid Degeneration That Is Initiated by Pollen Tube-Synergid Interaction in Arabidopsis. Plant Physiol. 169, 485–496.

Li, C., Wu, H.-M. and Cheung, A. Y. (2016). FERONIA and Her Pals: Functions and Mechanisms. Plant Physiol. 171, 2379–2392.

Li, H. J., Zhu, S. S., Zhang, M. X., Wang, T., Liang, L., Xue, Y., Shi, D. Q., Liu, J. and Yang, W. C. (2015). Arabidopsis CBP1 is a novel regulator of transcription initiation in central cell-mediated pollen tube guidance. Plant Cell 27, 2880–2893.

Li, L., Zheng, P. and Dean, J. (2010). Maternal control of early mouse development. Development 137, 859–870.

Li, S., Gu, Y., Yan, A., Lord, E. and Yang, Z.-B. (2008). RIP1 (ROP Interactive Partner 1)/ICR1 Marks Pollen Germination Sites and May Act in the ROP1 Pathway in the Control of Polarized Pollen Growth. Mol. Plant 1, 1021–1035.

Li, Y., Tan, X., Wang, M., Li, B., Zhao, Y., Wu, C., Rui, Q., Wang, J., Liu, Z. and Bao, Y. (2017). Exocyst subunit SEC3A marks the germination site and is essential for pollen germination in Arabidopsis thaliana. Sci. Rep. 7, 40279.

Liang, X. and Zhou, J.-M. (2018). The secret of fertilization in flowering plants unveiled. Sci. Bull. 63, 408–410.

Ling, Z., Brockmöller, T., Baldwin, I. T. and Xu, S. (2019). Evolution of Alternative Splicing in Eudicots. Front. Plant Sci. 10,.

Listerman, I., Sapra, A. K. and Neugebauer, K. M. (2006). Cotranscriptional coupling of splicing factor recruitment and precursor messenger RNA splicing in mammalian cells. Nat. Struct. Mol. Biol. 13, 815–822.

Lituiev, D. S. and Grossniklaus, U. (2014). Patterning of the angiosperm female gametophyte through the prism of theoretical paradigms. Biochem. Soc. Trans. 42, 332–339.

Liu, J., Lim, S.-L., Zhong, J. Y. and Lim, B. L. (2022). Bioenergetics of pollen tube growth in Arabidopsis thaliana revealed by ratiometric genetically encoded biosensors. Nat. Commun. 13, 7822.

Liu, L., Lu, Y., Wei, L., Yu, H., Cao, Y., Li, Y., Yang, N., Song, Y., Liang, C. and Wang, T. (2018). Transcriptomics analyses reveal the molecular roadmap and long non-coding RNA landscape of sperm cell lineage development. Plant J. 96, 421–437.

Liu, M., Yuan, L., Liu, N.-Y., Shi, D.-Q., Liu, J. and Yang, W.-C. (2009). GAMETOPHYTIC FACTOR 1 , Involved in Pre-mRNA Splicing, Is Essential for Megagametogenesis and Embryogenesis in Arabidopsis. J. Integr. Plant Biol. 51, 261–271.

Liu, X., Adhikari, P. B. and Kasahara, R. D. (2019). Pollen tube contents from failed fertilization contribute to seed coat initiation in Arabidopsis. F1000Research 8, 348.

Llinas, R. J., Xiong, J. Q., Clark, N. M., Burkhart, S. E. and Bartel, B. (2022). An Arabidopsis pre-RNA processing8a (prp8a) missense allele restores splicing of a subset of mis-spliced mRNAs. Plant Physiol. 189, 2175–2192.

Long, J., Walker, J., She, W., Aldridge, B., Gao, H., Deans, S., Vickers, M. and Feng, X. (2021). Nurse cell--derived small RNAs define paternal epigenetic inheritance in Arabidopsis. Science 373,.

Loraine, A., McCormick, S., Estrada, A., Patel, K. and Qin, P. (2013). High-throughput sequencing of Arabidopsis thaliana pollen cDNA uncovers novel transcription and alternative splicing. Plant Physiol. 162, 1092–1109.

Luo, M., Bilodeau, P., Dennis, E. S., Peacock, W. J. and Chaudhury, A. (2000). Expression and parent-of-origin effects for FIS2, MEA, and FIE in the endosperm and embryo of developing Arabidopsis seeds. Proc. Natl. Acad. Sci. U. S. A. 97, 10637–10642.

Maeder, C., Kutach, A. K. and Guthrie, C. (2009). ATP-dependent unwinding of U4/U6 snRNAs by the Brr2 helicase requires the C terminus of Prp8. Nat. Struct. Mol. Biol. 16, 42–48.

Marquardt, S., Raitskin, O., Wu, Z., Liu, F., Sun, Q. and Dean, C. (2014). Functional consequences of splicing of the antisense transcript COOLAIR on FLC transcription. Mol. Cell 54, 156–165.

Marquez, Y., Brown, J. W. S., Simpson, C., Barta, A. and Kalyna, M. (2012). Transcriptome survey reveals increased complexity of the alternative splicing landscape in Arabidopsis. Genome Res. 22, 1184–95.

Martín, G., Márquez, Y., Mantica, F., Duque, P. and Irimia, M. (2021). Alternative splicing landscapes in Arabidopsis thaliana across tissues and stress conditions highlight major functional differences with animals. Genome Biol. 22, 35.

Martínez, G., Panda, K., Köhler, C. and Slotkin, R. K. (2016). Silencing in sperm cells is directed by RNA movement from the surrounding nurse cell. Nat. plants 2, 16030.

Márton, M. L., Cordts, S., Broadhvest, J. and Dresselhaus, T. (2005). Micropylar pollen tube guidance by egg apparatus 1 of maize. Science (80-.). 307, 573–576.

Maruyama, D., Hamamura, Y., Takeuchi, H., Susaki, D., Nishimaki, M., Kurihara, D., Kasahara, R. D. and Higashiyama, T. (2013). Independent Control by Each Female Gamete Prevents the Attraction of Multiple Pollen Tubes. Dev. Cell 25, 317–323.

Maruyama, D., Völz, R., Takeuchi, H., Mori, T., Igawa, T., Kurihara, D., Kawashima, T., Ueda, M., Ito, M., Umeda, M., et al. (2015). Rapid Elimination of the Persistent Synergid through a Cell Fusion Mechanism. Cell 161, 907–918.

Mascarenhas, J. P. (1993). Molecular Mechanisms of Pollen Tube Growth and Differentiation. Plant Cell 5, 1303–1314.

Mascarenhas, J. P. (1990). Gene Activity During Pollen Development. Annu. Rev. Plant Physiol. Plant Mol. Biol. 41, 317–338.

Matera, A. G. and Wang, Z. (2014). A day in the life of the spliceosome. Nat. Rev. Mol. Cell Biol. 15, 108–121.

Matsuura, H., Ishibashi, Y., Shinmyo, A., Kanaya, S. and Kato, K. (2010). Genome-Wide Analyses of Early Translational Responses to Elevated Temperature and High Salinity in Arabidopsis thaliana. Plant Cell Physiol. 51, 448–462.

Matsuura, H., Takenami, S., Kubo, Y., Ueda, K., Ueda, A., Yamaguchi, M., Hirata, K., Demura, T., Kanaya, S. and Kato, K. (2013). A Computational and Experimental Approach Reveals that the 5′-Proximal Region of the 5′-UTR has a Cis-Regulatory Signature Responsible for Heat Stress-Regulated mRNA Translation in Arabidopsis. Plant Cell Physiol. 54, 474–483.

McCue, A. D., Cresti, M., Feijó, J. A. and Slotkin, R. K. (2011). Cytoplasmic connection of sperm cells to the pollen vegetative cell nucleus: potential roles of the male germ unit revisited. J. Exp. Bot. 62, 1621–1631.

McGuire, A. M., Pearson, M. D., Neafsey, D. E. and Galagan, J. E. (2008). Cross-kingdom patterns of alternative splicing and splice recognition. Genome Biol. 9, R50.

Meinke, D. W. (2020). Genome-wide identification of EMBRYO-DEFECTIVE (EMB) genes required for growth and development in Arabidopsis. New Phytol. 226, 306–325.

Merret, R., Nagarajan, V. K., Carpentier, M.-C., Park, S., Favory, J.-J., Descombin, J., Picart, C., Charng, Y., Green, P. J., Deragon, J.-M., et al. (2015). Heat-induced ribosome pausing triggers mRNA co-translational decay in Arabidopsis thaliana. Nucleic Acids Res. 43, 4121–4132.

Michard, E., Simon, A. A., Tavares, B., Wudick, M. M. and Feijó, J. A. (2017). Signaling with Ions: The Keystone for Apical Cell Growth and Morphogenesis in Pollen Tubes. Plant Physiol. 173, 91–111.

Michlewski, G. and Cáceres, J. F. (2019). Post-transcriptional control of miRNA biogenesis. Rna 25, 1–16.

Minich, W. and Ovchinnikov, L. P. (1992). Role of cytoplasmic mRNP proteins in translation. Biochimie 74, 477–483.

Misra, C. S., Sousa, A. G. G., Barros, P. M., Kermanov, A. and Becker, J. D. (2023). Cell-type-specific alternative splicing in the Arabidopsis germline. Plant Physiol. 192, 85–101.

Miyazaki, S., Murata, T., Sakurai-Ozato, N., Kubo, M., Demura, T., Fukuda, H. and Hasebe, M. (2009). ANXUR1 and 2, sister genes to FERONIA/SIRENE, are male factors for coordinated fertilization. Curr. Biol. 19, 1327–1331.

Mizuta, Y. and Higashiyama, T. (2018). Chemical signaling for pollen tube guidance at a glance. J. Cell Sci. 131, jcs208447.

Moll, C., Von Lyncker, L., Zimmermann, S., Kägi, C., Baumann, N., Twell, D., Grossniklaus, U. and Groß-Hardt, R. (2008). CLO/GFA1 and ATO are novel regulators of gametic cell fate in plants. Plant J. 56, 913–921.

Mori, T., Igawa, T., Tamiya, G., Miyagishima, S. and Berger, F. (2014). Gamete Attachment Requires GEX2 for Successful Fertilization in Arabidopsis. Curr. Biol. 24, 170–175.

Morin, R. D., O'Connor, M. D., Griffith, M., Kuchenbauer, F., Delaney, A., Prabhu, A.-L., Zhao, Y., McDonald, H., Zeng, T., Hirst, M., et al. (2008). Application of massively parallel sequencing to microRNA profiling and discovery in human embryonic stem cells. Genome Res. 18, 610–621.

Motohashi, R., Yamazaki, T., Myouga, F., Ito, T., Ito, K., Satou, M., Kobayashi, M., Nagata, N., Yoshida, S., Nagashima, A., et al. (2007). Chloroplast ribosome release factor 1 (AtcpRF1) is essential for chloroplast development. Plant Mol. Biol. 64, 481–497.

Murgia, M., Huang, B.-Q., Tucker, S. C. and Musgrave, M. E. (1993). EMBRYO SAC LACKING ANTIPODAL CELLS IN ARABIDOPSIS THALIANA (BRASSICACEAE). Am. J. Bot. 80, 824–838.

Nakabayashi, K., Okamoto, M., Koshiba, T., Kamiya, Y. and Nambara, E. (2005). Genome-wide profiling of stored mRNA in Arabidopsis thaliana seed germination: Epigenetic and genetic regulation of transcription in seed. Plant J. 41, 697–709.

Nakajima, K. (2018). Be my baby: patterning toward plant germ cells. Curr. Opin. Plant Biol. 41, 110–115.

Nelms, B. and Walbot, V. (2022). Gametophyte genome activation occurs at pollen mitosis I in maize. Science 375, 424–429.

Nelms, B. and Walbot, V. (2019). Defining the developmental program leading to meiosis in maize. Science 364, 52–56.

Ner-Gaon, H., Halachmi, R., Savaldi-Goldstein, S., Rubin, E., Ophir, R. and Fluhr, R. (2004). Intron retention is a major phenomenon in alternative splicing in Arabidopsis. Plant J. 39, 877–885.

Neve, J., Patel, R., Wang, Z., Louey, A. and Furger, A. M. (2017). Cleavage and polyadenylation: Ending the message expands gene regulation. RNA Biol. 14, 865–890.

Ngo, Q. A., Baroux, C., Guthörl, D., Mozerov, P., Collinge, M. A., Sundaresan, V. and Grossniklaus, U. (2012). The Armadillo repeat gene ZAK IXIK promotes Arabidopsis early embryo and endosperm development through a distinctive gametophytic maternal effect. Plant Cell 24, 4026–4043.

Ngo, Q. A., Vogler, H., Lituiev, D. S., Nestorova, A. and Grossniklaus, U. (2014). A calcium dialog mediated by the FERONIA signal transduction pathway controls plant sperm delivery. Dev. Cell 29, 491–500.

Nodine, M. D. and Bartel, D. P. (2012). Maternal and paternal genomes contribute equally to the transcriptome of early plant embryos. Nature 482, 94–97.

Nowack, M. K., Grini, P. E., Jakoby, M. J., Lafos, M., Koncz, C. and Schnittger, A. (2006). A positive signal from the fertilization of the egg cell sets off endosperm proliferation in angiosperm embryogenesis. Nat. Genet. 38, 63–67.

Okuda, S., Tsutsui, H., Shiina, K., Sprunck, S., Takeuchi, H., Yui, R., Kasahara, R. D., Hamamura, Y., Mizukami, A., Susaki, D., et al. (2009). Defensin-like polypeptide LUREs are pollen tube attractants secreted from synergid cells. Nature 458, 357–61.

Olsen, O.-A. (2004). Nuclear endosperm development in cereals and Arabidopsis thaliana. Plant Cell 16 Suppl, S214-27.

Onelli, E., Idilli, A. I. and Moscatelli, A. (2015). Emerging roles for microtubules in angiosperm pollen tube growth highlight new research cues. Front. Plant Sci. 6,.

Ouyang, M., Li, X., Zhang, J., Feng, P., Pu, H., Kong, L., Bai, Z., Rong, L., Xu, X., Chi, W., et al. (2020). Liquid-Liquid Phase Transition Drives Intra-chloroplast Cargo Sorting. Cell 180, 1144-1159.e20.

Owen, H. A. and Makaroff, C. A. (1995). Ultrastructure of microsporogenesis and microgametogenesis inArabidopsis thaliana (L.) Heynh. ecotype Wassilewskija (Brassicaceae). Protoplasma 185, 7–21.

Pagnussat, G. C., Yu, H.-J. and Sundaresan, V. (2007). Cell-fate switch of synergid to egg cell in Arabidopsis eostre mutant embryo sacs arises from misexpression of the BEL1-like homeodomain gene BLH1. Plant Cell 19, 3578–3592.

Palanivelu, R. and Preuss, D. (2006). Distinct short-range ovule signals attract or repel Arabidopsis thaliana pollen tubes in vitro. BMC Plant Biol. 6, 7.

Parker, N., Wang, Y. and Meinke, D. (2014). Natural Variation in Sensitivity to a Loss of Chloroplast Translation in Arabidopsis . Plant Physiol. 166, 2013–2027.

Pereira, A. M., Lopes, A. L. and Coimbra, S. (2016). JAGGER, an AGP essential for persistent synergid degeneration and polytubey block in Arabidopsis. Plant Signal. Behav. 11, e1209616.

Pérez Di Giorgio, J. A., Barberini, M. L., Amodeo, G. and Muschietti, J. P. (2016). Pollen aquaporins: What are they there for? Plant Signal. Behav. 11, e1217375.

Pillot, M., Baroux, C., Vazquez, M. A., Autran, D., Leblanc, O., Vielle-Calzada, J. P., Grossniklaus, U. and Grimanelli, D. (2010). Embryo and endosperm inherit distinct chromatin and transcriptional states from the female gametes in Arabidopsis. Plant Cell 22, 307–20.

Pina, C., Pinto, F., Feijo, J. A. and Becker, J. D. (2005). Gene family analysis of the Arabidopsis pollen transcriptome reveals biological implications for cell growth, division control, and gene expression regulation. Plant Physiol. 138, 744–756.

Portereiko, M. F., Sandaklie-Nikolova, L., Lloyd, A., Dever, C. A., Otsuga, D. and Drews, G. N. (2006). Nuclear Fusion Defective1 Encodes the Arabidopsis RPL21M Protein and Is Required for Karyogamy during Female Gametophyte Development and Fertilization. Plant Physiol. 141, 957–965.

Posé, D., Verhage, L., Ott, F., Yant, L., Mathieu, J., Angenent, G. C., Immink, R. G. H. and Schmid, M. (2013). Temperature-dependent regulation of flowering by antagonistic FLM variants. Nature 503, 414–417.

Protter, D. S. W. and Parker, R. (2016). Principles and Properties of Stress Granules. Trends Cell Biol. 26, 668–679.

Punwani, J. A., Rabiger, D. S., Lloyd, A. and Drews, G. N. (2008). The MYB98 subcircuit of the synergid gene regulatory network includes genes directly and indirectly regulated by MYB98. Plant J. 55, 406–414.

Quesada, V., Macknight, R., Dean, C. and Simpson, G. G. (2003). Autoregulation of FCA pre‐mRNA processing controls Arabidopsis flowering time. EMBO J. 22, 3142–3152.

Radoeva, T., Vaddepalli, P., Zhang, Z. and Weijers, D. (2019). Evolution, Initiation, and Diversity in Early Plant Embryogenesis. Dev. Cell 50, 533–543.

Ray, D., Kazan, H., Cook, K. B., Weirauch, M. T., Najafabadi, H. S., Li, X., Gueroussov, S., Albu, M., Zheng, H., Yang, A., et al. (2013). A compendium of RNA-binding motifs for decoding gene regulation. Nature 499, 172–177.

Reddy, A. S. N. (2007). Alternative splicing of pre-messenger RNAs in plants in the genomic era. Annu. Rev. Plant Biol. 58, 267–294.

Reddy, A. S. N., Marquez, Y., Kalyna, M. and Barta, A. (2013). Complexity of the Alternative Splicing Landscape in Plants . Plant Cell 25, 3657–3683.

Reimann, R., Kah, D., Mark, C., Dettmer, J., Reimann, T. M., Gerum, R. C., Geitmann, A., Fabry, B., Dietrich, P. and Kost, B. (2020). Durotropic Growth of Pollen Tubes. Plant Physiol. 183, 558–569.

Reiser, L. and Fischer, R. L. (1993). The Ovule and the Embryo Sac. Plant Cell 5, 1291–1301.

Robert, H. S., Park, C., Gutièrrez, C. L., Wójcikowska, B., Pěnčík, A., Novák, O., Chen, J., Grunewald, W., Dresselhaus, T., Friml, J., et al. (2018). Maternal auxin supply contributes to early embryo patterning in Arabidopsis. Nat. plants 4, 548–553.

Rodriguez, J. M., Pozo, F., di Domenico, T., Vazquez, J. and Tress, M. L. (2020). An analysis of tissue-specific alternative splicing at the protein level. PLOS Comput. Biol. 16, e1008287.

Romagnoli, S., Cai, G., Faleri, C., Yokota, E., Shimmen, T. and Cresti, M. (2007). Microtubule- and actin filament-dependent motors are distributed on pollen tube mitochondria and contribute differently to their movement. Plant Cell Physiol. 48, 345–361.

Ron, M., Alandete Saez, M., Eshed Williams, L., Fletcher, J. C. and McCormick, S. (2010). Proper regulation of a sperm-specific cis-nat-siRNA is essential for double fertilization in Arabidopsis. Genes Dev. 24, 1010–1021.

Rotman, N., Rozier, F., Boavida, L., Dumas, C., Berger, F. and Faure, J.-E. (2003). Female control of male gamete delivery during fertilization in Arabidopsis thaliana. Curr. Biol. 13, 432–436.

Rövekamp, M., Bowman, J. L. and Grossniklaus, U. (2016). Marchantia MpRKD Regulates the Gametophyte-Sporophyte Transition by Keeping Egg Cells Quiescent in the Absence of Fertilization. Curr. Biol. 26, 1782–1789.

Russell, S. D. and Jones, D. S. (2015). The male germline of angiosperms: repertoire of an inconspicuous but important cell lineage. Front. Plant Sci. 6, 173.

Sachs, A. B. (1993). Messenger RNA degradation in eukaryotes. Cell 74, 413–421.

Sajeev, N., Bai, B. and Bentsink, L. (2019). Seeds: A Unique System to Study Translational Regulation. Trends Plant Sci. 24, 487–495.

Sandaklie-Nikolova, L., Palanivelu, R., King, E. J., Copenhaver, G. P. and Drews, G. N. (2007). Synergid Cell Death in Arabidopsis Is Triggered following Direct Interaction with the Pollen Tube. Plant Physiol. 144, 1753–1762.

Sano, N., Permana, H., Kumada, R., Shinozaki, Y., Tanabata, T., Yamada, T., Hirasawa, T. and Kanekatsu, M. (2012). Proteomic Analysis of Embryonic Proteins Synthesized from Long-Lived mRNAs During Germination of Rice Seeds. Plant Cell Physiol. 53, 687–698.

Sasaki, T., Kanno, T., Liang, S.-C., Chen, P.-Y., Liao, W.-W., Lin, W.-D., Matzke, A. J. M. and Matzke, M. (2015). An Rtf2 Domain-Containing Protein Influences Pre-mRNA Splicing and Is Essential for Embryonic Development in Arabidopsis thaliana. Genetics 200, 523–35.

Scheible, N. and McCubbin, A. (2019). Signaling in Pollen Tube Growth: Beyond the Tip of the Polarity Iceberg. Plants (Basel, Switzerland) 8,.

Schleiff, E. and Becker, T. (2011). Common ground for protein translocation: access control for mitochondria and chloroplasts. Nat. Rev. Mol. Cell Biol. 12, 48–59.

Schneitz, K., Hülskamp, M. and Pruitt, R. E. (1995). Wild−type ovule development in Arabidopsis thaliana : a light microscope study of cleared whole−mount tissue . Plant J. 7, 731–749.

Schoenaers, S., Balcerowicz, D., Breen, G., Hill, K., Zdanio, M., Mouille, G., Holman, T. J., Oh, J., Wilson, M. H., Nikonorova, N., et al. (2018). The Auxin-Regulated

CrRLK1L Kinase ERULUS Controls Cell Wall Composition during Root Hair Tip Growth. Curr. Biol. 28, 722-732.e6.

Schöning, J. C., Streitner, C., Meyer, I. M., Gao, Y. and Staiger, D. (2008). Reciprocal regulation of glycine-rich RNA-binding proteins via an interlocked feedback loop coupling alternative splicing to nonsense-mediated decay in Arabidopsis. Nucleic Acids Res. 36, 6977–6987.

Schwartz, B., Yeung, E. and Meinke, D. (1994). Disruption of morphogenesis and transformation of the suspensor in abnormal suspensor mutants of Arabidopsis. Development 120, 3235–3245.

Scott, R. J., Spielman, M. and Dickinson, H. G. (2004). Stamen Structure and Function. Plant Cell 16, S46–S60.

Seo, P. J., Hong, S.-Y., Kim, S.-G. and Park, C.-M. (2011). Competitive inhibition of transcription factors by small interfering peptides. Trends Plant Sci. 16, 541–549.

Settles, A. M., Yonetani, A., Baron, A., Bush, D. R., Cline, K. and Martienssen, R. (1997). Sec-Independent Protein Translocation by the Maize Hcf106 Protein. Science (80-.). 278, 1467–1470.

Shi, Y. and Manley, J. L. (2015). The end of the message: multiple protein-RNA interactions define the mRNA polyadenylation site. Genes Dev. 29, 889–897.

Silverman, I. M., Li, F. and Gregory, B. D. (2013). Genomic era analyses of RNA secondary structure and RNA-binding proteins reveal their significance to post-transcriptional regulation in plants. Plant Sci. 205–206, 55–62.

Skinner DJ, Sundaresan V. Recent advances in understanding female gametophyte development. F1000Res. 2018 Jun 20;7:F1000 Faculty Rev-804. doi: 10.12688/f1000research.14508.1. PMID: 29983913; PMCID: PMC6013762.

Slane, D., Lee, C. H., Kolb, M., Dent, C., Miao, Y., Franz-Wachtel, M., Lau, S., Maček, B., Balasubramanian, S., Bayer, M., et al. (2020). The integral spliceosomal component CWC15 is required for development in Arabidopsis. Sci. Rep. 10, 13336.

Slotkin, R. K., Vaughn, M., Borges, F., Tanurdzić, M., Becker, J. D., Feijó, J. A. and Martienssen, R. A. (2009). Epigenetic reprogramming and small RNA silencing of transposable elements in pollen. Cell 136, 461–472.

Song, X., Yuan, L. and Sundaresan, V. (2014). Antipodal cells persist through fertilization in the female gametophyte of Arabidopsis. Plant Reprod. 27, 197–203.

Sorenson, R. and Bailey-Serres, J. (2014). Selective mRNA sequestration by OLIGOURIDYLATEBINDING PROTEIN 1 contributes to translational control during hypoxia in Arabidopsis. Proc. Natl. Acad. Sci. U. S. A. 111, 2373–2378.

Sprunck, S. (2020). Twice the fun, double the trouble: gamete interactions in flowering plants. Curr. Opin. Plant Biol. 53, 106–116.

Sprunck, S. and Gross-Hardt, R. (2011). Nuclear behavior, cell polarity, and cell specification in the female gametophyte. Sex. Plant Reprod. 24, 123–136.

Sprunck, S., Rademacher, S., Vogler, F., Gheyselinck, J., Grossniklaus, U. and Dresselhaus, T. (2012). Egg cell-secreted EC1 triggers sperm cell activation during double fertilization. Science 338, 1093–1097.

Staiger, C. J., Poulter, N. S., Henty, J. L., Franklin-Tong, V. E. and Blanchoin, L. (2010). Regulation of actin dynamics by actin-binding proteins in pollen. J. Exp. Bot. 61, 1969–1986.

Steffen, J. G., Kang, I.-H., Portereiko, M. F., Lloyd, A. and Drews, G. N. (2008). AGL61 Interacts with AGL80 and Is Required for Central Cell Development in Arabidopsis . Plant Physiol. 148, 259–268.

Stegmann, M., Monaghan, J., Smakowska-Luzan, E., Rovenich, H., Lehner, A., Holton, N., Belkhadir, Y. and Zipfel, C. (2017). The receptor kinase FER is a RALF-regulated scaffold controlling plant immune signaling. Science 355, 287–289.

Štorchová, H., Čapková, V. and Tupý, J. (1994). A Nicotiana tabacum mRNA encoding a 69-kDa glycoprotein occurring abundantly in pollen tubes is transcribed but not translated during pollen development in the anthers. Planta 192, 441–445.

Sugi, N., Calhau, A. R. M., Jacquier, N. M. A., Millan-Blanquez, M., Becker, J. D., Begcy, K., Berger, F., Bousquet-Antonelli, C., Bouyer, D., Cai, G., et al. (2024). The peri-germ cell membrane: poorly characterized but key interface for plant reproduction. Nat. plants 10, 1607–1609.

Suñé-Pou, M., Prieto-Sánchez, S., Boyero-Corral, S., Moreno-Castro, C., El Yousfi, Y., Suñé-Negre, J. M., Hernández-Munain, C. and Suñé, C. (2017). Targeting Splicing in the Treatment of Human Disease. Genes (Basel). 8,.

Susaki, D., Takeuchi, H., Tsutsui, H., Kurihara, D. and Higashiyama, T. (2015). Live Imaging and Laser Disruption Reveal the Dynamics and Cell-Cell Communication During Torenia fournieri Female Gametophyte Development. Plant Cell Physiol. 56, 1031–1041.

Tafuri, S. R., Familari, M. and Wolffe, A. P. (1993). A mouse Y box protein, MSY1, is associated with paternal mRNA in spermatocytes. J. Biol. Chem. 268, 12213–12220.

Takeuchi, H. and Higashiyama, T. (2012). A Species-Specific Cluster of Defensin-Like Genes Encodes Diffusible Pollen Tube Attractants in Arabidopsis. PLoS Biol. 10,.

Takeuchi, H. and Higashiyama, T. (2016). Tip-localized receptors control pollen tube growth and LURE sensing in Arabidopsis. Nature 531, 245–248.

Tedeschi, F., Rizzo, P., Rutten, T., Altschmied, L. and Bäumlein, H. (2017). RWP-RK domain-containing transcription factors control cell differentiation during female gametophyte development in Arabidopsis. New Phytol. 213, 1909–1924.

Tian, B., Pan, Z. and Lee, J. Y. (2007). Widespread mRNA polyadenylation events in introns indicate dynamic interplay between polyadenylation and splicing. Genome Res. 17, 156–165.

Timofeyenko, K., Kanavalau, D., Alexiou, P., Kalyna, M. and Růžička, K. (2023). Catsnap: a user-friendly algorithm for determining the conservation of protein variants reveals extensive parallelisms in the evolution of alternative splicing. New Phytol. 238, 1722–1732.

Tognacca, R. S., Rodríguez, F. S., Aballay, F. E., Cartagena, C. M., Servi, L. and Petrillo, E. (2023). Alternative splicing in plants: current knowledge and future directions for assessing the biological relevance of splice variants. J. Exp. Bot. 74, 2251–2272.

Turner, I. A., Norman, C. M., Churcher, M. J. and Newman, A. J. (2006). Dissection of Prp8 protein defines multiple interactions with crucial RNA sequences in the catalytic core of the spliceosome. RNA 12, 375–386.

Twell, D. (1995). Diphtheria toxin-mediated cell ablation in developing pollen: Vegetative cell ablation blocks generative cell migration. Protoplasma 187, 144–154.

Twell, D., Oh, S. A. and Honys, D. (2006). Pollen development, a genetic and transcriptomic view. Plant Cell Monogr. 3, 15–45.

Ueda, M., Aichinger, E., Gong, W., Groot, E., Verstraeten, I., Vu, L. D., De Smet, I., Higashiyama, T., Umeda, M. and Laux, T. (2017). Transcriptional integration of paternal and maternal factors in the Arabidopsis zygote. Genes Dev. 31, 617–627.

Ueda, M., Zhang, Z. and Laux, T. (2011). Transcriptional Activation of Arabidopsis Axis Patterning Genes WOX8/9 Links Zygote Polarity to Embryo Development. Dev. Cell 20, 264–270.

Vaneechoutte, D., Estrada, A. R., Lin, Y.-C., Loraine, A. E. and Vandepoele, K. (2017). Genome-wide characterization of differential transcript usage in Arabidopsis thaliana. Plant J. 92, 1218–1231.

Verma, S., Attuluri, V. P. S. and Robert, H. S. (2021). An Essential Function for Auxin in Embryo Development. Cold Spring Harb. Perspect. Biol. 13,.

Völz, R., von Lyncker, L., Baumann, N., Dresselhaus, T., Sprunck, S. and Gross-Hardt, R. (2012). LACHESIS-dependent egg-cell signaling regulates the development of female gametophytic cells. Development 139, 498–502.

von Besser, K., Frank, A. C., Johnson, M. A. and Preuss, D. (2006). Arabidopsis HAP2 (GCS1) is a sperm-specific gene required for pollen tube guidance and fertilization. Development 133, 4761–9.

Wahl, M. C., Will, C. L. and Lührmann, R. (2009). The spliceosome: design principles of a dynamic RNP machine. Cell 136, 701–718.

Wang, B.-B. and Brendel, V. (2006). Genomewide comparative analysis of alternative splicing in plants. Proc. Natl. Acad. Sci. 103, 7175–7180.

Wang, J., Ma, X., Hu, Y., Feng, G., Guo, C., Zhang, X. and Ma, H. (2024). Regulation of micro- and small-exon retention and other splicing processes by GRP20 for flower development. Nat. Plants 10, 66–85.

Wang, Y., Tsukamoto, T., Noble, J. A., Liu, X., Mosher, R. A. and Palanivelu, R. (2017). Arabidopsis LORELEI, a Maternally Expressed Imprinted Gene, Promotes Early Seed Development. Plant Physiol. 175, 758–773.

Weber, C., Nover, L. and Fauth, M. (2008). Plant stress granules and mRNA processing bodies are distinct from heat stress granules. Plant J. 56, 517–530.

Will, C. L. and Lührmann, R. (2011). Spliceosome structure and function. Cold Spring Harb. Perspect. Biol. 3, 1–2.

Willemse, M. T. M. and van Went, J. L. (1984). The Female Gametophyte. In Embryology of Angiosperms (ed. Johri, B. M.), pp. 159–196. Berlin, Heidelberg: Springer Berlin Heidelberg.

Williams, J. H. and Reese, J. B. (2019). Evolution of development of pollen performance. Curr. Top. Dev. Biol. 131, 299–336.

Wolffe, A. P. (1994). Structural and functional properties of the evolutionarily ancient Y-box family of nucleic acid binding proteins. BioEssays 16, 245–251.

Xiong, F., Ren, J.-J., Yu, Q., Wang, Y.-Y., Kong, L.-J., Otegui, M. S. and Wang, X.-L. (2019). AtBUD13 affects pre-mRNA splicing and is essential for embryo development in Arabidopsis. Plant J. 98, 714–726.

Xu, T., Wu, X., Wong, C. E., Fan, S., Zhang, Y., Zhang, S., Liang, Z., Yu, H. and Shen, L. (2022). FIONA1-Mediated m6A Modification Regulates the Floral Transition in Arabidopsis. Adv. Sci. 9, 2103628.

Yadegari, R., Kinoshita, T., Lotan, O., Cohen, G., Katz, A., Choi, Y., Katz, A., Nakashima, K., Harada, J. J., Goldberg, R. B., et al. (2000). Mutations in the FIE and MEA genes that encode interacting polycomb proteins cause parent-of-origin effects on seed development by distinct mechanisms. Plant Cell 12, 2367–2382.

Yang, X., Coulombe-Huntington, J., Kang, S., Sheynkman, G. M., Hao, T., Richardson, A., Sun, S., Yang, F., Shen, Y. A., Murray, R. R., et al. (2016). Widespread Expansion of Protein Interaction Capabilities by Alternative Splicing. Cell 164, 805–817.

Ylstra, B. and McCormick, S. (1999). Analysis of mRNA stabilities during pollen development and in BY2 cells. Plant J. 20, 101–108.

Yu, L., Rege, M., Peterson, C. L. and Volkert, M. R. (2016). RNA polymerase II depletion promotes transcription of alternative mRNA species. BMC Mol. Biol. 17, 20.

Yuan, J., Henry, R., McCaffery, M. and Cline, K. (1994). SecA Homolog in Protein Transport Within Chloroplasts: Evidence for Endosymbiont-Derived Sorting. Science (80-.). 266, 796–798.

Zhang, D., Shi, J. and Yang, X. (2016). Role of Lipid Metabolism in Plant Pollen Exine Development. Subcell. Biochem. 86, 315–337.

Zhang, H., Scheirer, D. C., Fowle, W. H. and Goodman, H. M. (1992). Expression of antisense or sense RNA of an ankyrin repeat-containing gene blocks chloroplast differentiation in arabidopsis. Plant Cell 4, 1575–1588.

Zhang, M., Wu, H., Su, J., Wang, H., Zhu, Q., Liu, Y., Xu, J., Lukowitz, W. and Zhang, S. (2017). Maternal control of embryogenesis by MPK6 and its upstream MKK4/ MKK5 in Arabidopsis. Plant J. 92, 1005–1019.

Zhang, Y., Zhang, X., Shi, J., Tuorto, F., Li, X., Liu, Y., Liebers, R., Zhang, L., Qu, Y., Qian, J., et al. (2018). Dnmt2 mediates intergenerational transmission of paternally acquired metabolic disorders through sperm small non-coding RNAs. Nat. Cell Biol. 20, 535–540.

Zhao, P., Zhou, X., Shen, K., Liu, Z., Cheng, T., Liu, D., Cheng, Y., Peng, X. and Sun, M.-X. (2019). Two-Step Maternal-to-Zygotic Transition with Two-Phase Parental Genome Contributions. Dev. Cell 49, 882-893.e5.

Zhao, Y., Wang, S., Wu, W., Li, L., Jiang, T. and Zheng, B. (2018). Clearance of maternal barriers by paternal miR159 to initiate endosperm nuclear division in Arabidopsis. Nat. Commun. 9, 5011.

Zheng, R. H., Su, S. D., Xiao, H. and Tian, H. Q. (2019). Calcium: A Critical Factor in Pollen Germination and Tube Elongation. Int. J. Mol. Sci. 20,.

Zhong, S. and Qu, L.-J. (2019). Peptide/receptor-like kinase-mediated signaling involved in male–female interactions. Curr. Opin. Plant Biol. 51, 7–14.

Zhong, S., Zhang, J. and Qu, L.-J. (2017). The signals to trigger the initiation of ovule enlargement are from the pollen tubes: The direct evidence. J. Integr. Plant Biol. 59, 600–603.

Zhu, F.-Y., Chen, M.-X., Ye, N.-H., Shi, L., Ma, K.-L., Yang, J.-F., Cao, Y.-Y., Zhang, Y., Yoshida, T., Fernie, A. R., et al. (2017). Proteogenomic analysis reveals alternative splicing and translation as part of the abscisic acid response in Arabidopsis seedlings. Plant J. 91, 518–533.